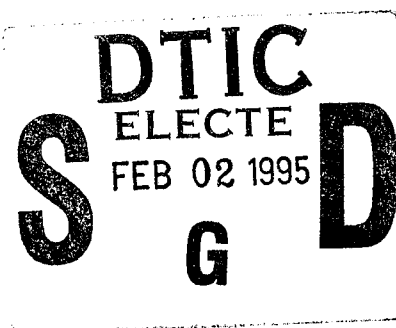


Development of Continuous Visible Chemical Laser Amplifiers and
Oscillators from the $\text{Na}_3\text{-X}(\text{Cl}, \text{Br}, \text{I})$ Reactions and Their Analogs
and Energy Transfer Pumping from Efficiently Produced Metastable States

A report submitted to AFOSR-SDIO

(Final Report June 1, 1990 - October 31, 1994)

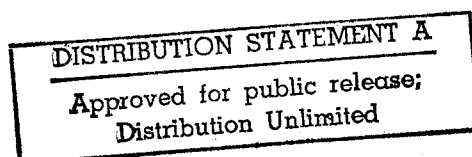
by James L. Gole
High Temperature Laboratory
and
School of Physics
Georgia Institute of Technology
Atlanta, Georgia 30332



Visible chemical laser amplifiers have been generated employing the highly efficient and selective formation of sodium dimer electronically excited states from the sodium trimer-halogen atom ($\text{X} = \text{Cl}, \text{Br}, \text{I}$) reactions. Optical gain through stimulated emission has been demonstrated in select regions close to 527, 492, and 460 nm. With a focus to increasing amplifier gain length and amplifying medium concentration, a newly configured device creates intersecting alkali and halogen sheaths which form the basis for the creation of visible chemical laser oscillators. This device has now revealed the first Raman pumping due purely to chemical reaction in the absence of an external light source. Extrapolations on the $\text{Na}_3\text{-X}$ amplifier concept involving Group IIA metal - F, Cl reactions are considered. Very near resonant energy transfers from selectively formed metastable states of SiO and GeO to receptor alkali atoms form sodium or potassium atom laser amplifiers and a gain condition at $\lambda = 569, 616, 819, \text{ and } 581 \text{ nm}$. These results form the basis for full cavity oscillation in the Na system at 569 nm. Silane based thermolysis - discharge and thermolysis - photolysis sources of SiO metastables are under development. The efficient energy transfer pumping of potential amplifying transitions in the lead (Pb), copper (Cu), and tin (Sn) systems is outlined.

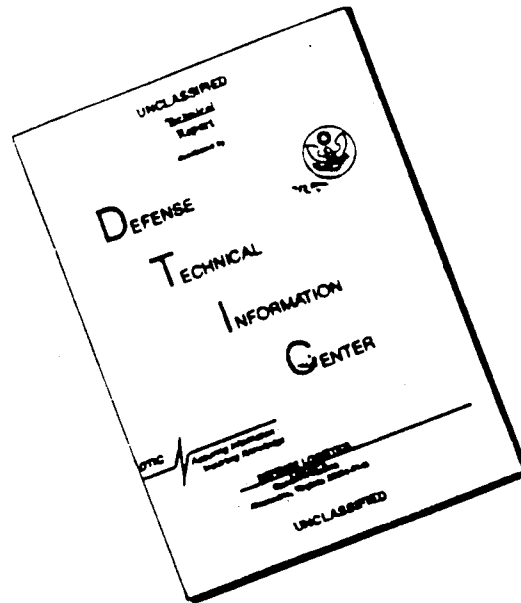
DTIC QUALITY INSPECTED 3

19950130 086



REPORT DOCUMENTATION PAGE			Form Approved OMB No. 0704-0188	
Public reporting burden for this collection of information is estimated to average 1 hour per response, including the time for reviewing instructions, searching existing data sources, gathering and maintaining the data needed, and completing and reviewing the collection of information. Send comments regarding this burden estimate or any other aspect of this collection of information, including suggestions for reducing this burden to Washington Headquarters Services, Directorate for Information Operations and Reports, 1215 Jefferson Davis Highway, Suite 1204, Arlington, VA 22202-4302, and to the Office of Management and Budget, Paperwork Reduction Project (0704-0188), Washington, DC 20503				
1. AGENCY USE ONLY (Leave Blank)	2. REPORT DATE December 1994	3. REPORT TYPE AND DATES COVERED Final - June 1, 1990 - October 31, 1994		
4. TITLE AND SUBTITLE Development of Continuous Visible Chemical Laser Amplifiers and Oscillators from the Na ₃ -X(Cl,Br,I) Reactions and Their Analogs and Energy Transfer Pumping		5. FUNDING NUMBERS G-AFOSR-90-0285 1601/08 63218C		
6. AUTHOR(S) James L. Gole		7. PERFORMING ORGANIZATION REPORT NUMBER Deliverable No. 12		
7. PERFORMING ORGANIZATION NAME(S) AND ADDRESS(ES) Georgia Tech Research Corporation Georgia Institute of Technology Office of Contract Administration Atlanta, GA 30332-0430		8. PERFORMING ORGANIZATION REPORT NUMBER		
9. SPONSORING/MONITORING AGENCY NAME(S) AND ADDRESS(ES) AFOSR/N E /PKA 110 Duncan Avenue, Suite B115 Bolling AFB, DC 20332-0001 Dr. Berman		10. SPONSORING/MONITORING AGENCY REPORT NUMBER		
11. SUPPLEMENTARY NOTES COR: To be published in Journal of Quantum Electronics, Journal of Chemical Physics, Proceedings of 10th Conference on Gas Flow and Chemical Lasers				
12a. DISTRIBUTION/AVAILABILITY STATEMENT UNRESTRICTED		12b. DISTRIBUTION CODE		
Visible chemical laser amplifiers have been generated employing the highly efficient and selective formation of sodium dimer electronically excited states from the sodium trimer-halogen atom (X = Cl,Br,I) reactions. Optical gain through stimulated emission has been demonstrated in select regions close to 527, 492, and 460 nm. With a focus to increasing amplifier gain length and amplifying medium concentration, a newly configured device creates intersecting alkali and halogen sheaths which form the basis for the creation of visible chemical laser oscillators. This device has now revealed the first Raman pumping due purely to chemical reaction in the absence of an external light source. Extrapolations on the Na ₃ -X amplifier concept involving Group IIA metal - F,Cl reactions are considered. Very near resonant energy transfers from selectively formed metastable states of SiO and GeO to receptor alkali atoms form sodium or potassium atom laser amplifiers and a gain condition at = 569, 616, 819, and 581 nm. These results form the basis for full cavity oscillation in the Na system at 569 nm. Silane based thermolysis - discharge and thermolysis - photolysis sources of SiO metastables are under development. The efficient energy transfer pumping of potential amplifying transitions in the lead (Pb), copper (Cu), and tin (Sn) systems is outlined.				
14. SUBJECT TERMS Chemical Lasers, Visible Chemical Lasers, Fast Energy Transfer Metastable Storage States, Selective Reactions		15. NUMBER OF PAGES		
		16. PRICE CODE		
17. SECURITY CLASSIFICATION OF REPORT UNCLASSIFIED	18. SECURITY CLASSIFICATION OF THIS PAGE UNCLASSIFIED	19. SECURITY CLASSIFICATION OF ABSTRACT UNCLASSIFIED	20. LIMITATION OF ABSTRACT SAR	

DISCLAIMER NOTICE



THIS DOCUMENT IS BEST QUALITY AVAILABLE. THE COPY FURNISHED TO DTIC CONTAINED A SIGNIFICANT NUMBER OF PAGES WHICH DO NOT REPRODUCE LEGIBLY.

TABLE OF CONTENTS

	page
1. FOREWORD.	1
2. CURVE CROSSINGS, ELECTRONIC ENERGY TRANSFER COLLISIONS, AND EFFICIENT CHEMICAL PUMPING.	4
3. A HIGHLY EFFICIENT AND SELECTIVE ELECTRON JUMP-HARPOON PROCESS. . .	4
4. EFFICIENT, FAST, INTRA- AND INTERMOLECULAR ENERGY TRANSFER PUMPING.	4
5. CONTINUOUS CHEMICAL LASER AMPLIFIERS IN THE VISIBLE REGION BASED ON HIGHLY EFFICIENT AND SELECTIVE REACTIONS	6
- Formation of Amplifiers (Oscillators) Through Direct Chemical Reaction.	6
- Electronically Inverted Na ₂ Produced from the Na ₃ -X(Cl,Br,I) Reactions	6
- Development of an Extended Path Length Na ₃ -X(Cl,Br,I) Reaction Amplification Zone.	8
- Raman Pumping in the Absence of an External Light Source.	10
- Extension of the Na ₃ -X(Cl,Br,I) Amplifier Concept	13
- Long Range Collisional Stabilization and the Symmetry Constrained Dynamics of High Temperature Complex Formation.	14
6. NEAR RESONANT ENERGY TRANSFER FROM METASTABLE ENERGY STORAGE STATES OF SiO AND GeO TO FORM ATOM BASED LASER AMPLIFIERS.	16
- Full Cavity Measurements.	18
- Improvement of the Energy Transfer Based Configuration - Ultimate Goals	19
A. Concentric Reactant Mixing.	19
B. Considering Self Absorption and Self Quenching.	20
C. Nitrogen vs. Argon Entrainment.	20
D. Output Coupling	21
- System Modeling	21
- Extension of Near Resonant Intermolecular Energy Transfer Concept to Additional Energy Transfer Pumped Atomic Receptors	22
- Improving the Si Atom and SiO Metastable Source Configurations. .	24
REFERENCES.	27
PUBLICATIONS.	32
INVITED TALKS ON AFOSR SPONSORED RESEARCH	34
SCIENTIFIC PERSONNEL SUPPORTED BY THIS PROJECT (DEGREES AWARDED). .	36

Dist	Avail and/or Special
A-1	

- APPENDIX I - A Chemically Driven Visible Laser Transition Using Fast Near-Resonant Energy Transfer to Group IIIA Metals
- APPENDIX II - Chemically Driven Pulsed and Continuous Visible Laser Amplifiers and Oscillators
- APPENDIX III - An Approach to Visible Chemical Laser Development Using Fast Near Resonant Energy Transfer
- APPENDIX IVA - On the BiF Bond Dissociation Energy and the Evaluation of the BiF Red Emission Band Systems
- APPENDIX IVB - Fluorine Hot Atom Oxidation of Bismuth Vapor. A Comment on the Evaluation of the BiF Bond Energy
- APPENDIX V - Toward the Modeling of the Oxidation of Small Metal and Metalloid Molecules
- APPENDIX VI - The Unique Nature of Metal Cluster Oxidation
- APPENDIX VII - Chemically Driven Pulsed and Continuous Visible Laser Amplifiers and Oscillators
- APPENDIX VIII - Evidence for Continuous Visible Chemical Lasing From the Fast Near Resonant Energy Transfer Pumping of Atomic Sodium
- APPENDIX IX - Visible Chemical Lasers from Alkali Based Electronic Inversions
- APPENDIX X - Chemically Driven Continuous Visible Laser Amplifiers and Oscillators Based on Metal Molecule - Halogen Atom Reactions
- APPENDIX XI - Chemically Driven Visible Laser Amplifiers and Oscillators Based on Fast Electronic Energy Transfer
- APPENDIX XII - Laser Induced Fluorescence and Radiative Lifetimes of the Low-Lying Electronic States of Gaseous AgF
- APPENDIX XIII - A Chemiluminescent and Laser Induced Fluorescent Probe of A New Low-Lying $A^1\Omega_1$ State of Gaseous AgF
- APPENDIX XIV - Raman Pumping in the Absence of an External Light Source
- APPENDIX XV - The Expansion of Small Molecule Configuration Space: Highly Efficient Long Range Stabilization and Energy Transfer Involving Electronically Excited States
- APPENDIX XVI - Chemically Induced Processes Evidencing Raman Gain
- APPENDIX XVII - Highly Efficient Collisional Stabilization and the Symmetry Constrained Dynamics of High Temperature Complex Formation
- APPENDIX XVIII - Confirmation of Long-Range Collision Complex Stabilization Through The Controlled Relaxation of High Internal Excitation

Foreword

We have developed a wealth of evidence to suggest that surprisingly efficient collision induced energy transfers and collisional stabilization can be ascribed to small molecules and atoms present at elevated energies in high stress non-equilibrium environments. Apparent energy transfer and stabilization rates, which in some cases would appear to defy conventional kinetic models, are far in excess of those normally associated with the lowest vibrational-rotational levels of molecules and systems in their lowest or ground states at room temperature. This project has attempted to take advantage of these characteristics with a focus toward the development of the first visible chemical laser amplifiers and oscillators. Two novel approaches to form electronically inverted molecular diatomic and atomic configurations making use of (1) highly efficient and selective fast "electron jump" reactive encounters, and (2) highly efficient near resonant electronic energy transfer, have been employed to produce amplification and oscillation and to reveal several unusual characteristics of high temperature environments.

A primary approach to continuous visible chemical laser development has been signaled by the successful production of visible chemical laser amplifiers using the highly efficient and selective formation of alkali dimer, ($M_2 = Na_2, (K_2)$), excited states from the fast alkali trimer-halogen atom ($M_3 - X(Cl, Br, I)$) reactions. These chemical laser amplifiers have employed the extremely high cross section Na_n ($n=2,3$)- $X(Cl, Br, I)$ reactions to create a continuous electronic population inversion based on the chemical pumping of sodium dimer (Na_2). Optical gain through stimulated emission has been demonstrated in select regions close to 527, 492, and 460 nm. A model, under development, which evokes the vibrational and rotational selectivity inherent to a dissociative ionic recombination process ($Na_3^+ + X^- \rightarrow Na_2 + NaX$) in correlation with the coupling between select sodium dimer excited states, appears to provide a semiquantitative explanation of the observed behavior.

An assessment of the manner in which gain is generated in these fast reactive encounters has suggested that a considerable enhancement of the amplification can be obtained with a versatile long-path length source configuration. The considered amplifiers are therefore being optimized with a focus to increasing amplifier gain length and amplifying medium concentration using an upscaled device which has been designed to allow the ready movement of extended path length alkali trimer and halogen atom slit sources relative

to each other by creating adjustable intersecting reactive alkali and halogen atom flows. The controlled intersection of these reacting sheaths forms an extended reaction - amplification zone. It is this extended gain zone which we are employing to convert the created amplifiers to visible chemical laser oscillators. With this focus to the development of a long path length amplifying medium employing the trimer reactions, we have observed the first resonance Raman pumping of Na_2 in the absence of an external light source. Here, the Na D-line emission which results from the Na_2 -Br reaction is scattered by sodium dimers cooled, in supersonic expansion, to the lowest vibrational levels of the Na_2 ground electronic state. An initial analysis suggests that we have observed resonance Raman progressions, however, the time scale for the Raman process may be considerably shorter than anticipated. This suggests a further long range interaction of the excited Na^2P atoms with those Na_2 molecules which are Raman pumped. We are beginning to observe the manifestation of significant and surprising interactions. In concert with observations made on several additional systems, these observations suggest that the Na_n -X reaction systems may also behave in response to the highly efficient funneling of energy via a diffuse electron density and that their study can serve as a model for more complex systems.

This report also suggests and begins to demonstrate extrapolations on the sodium trimer halogen atom systems including the potential excimer forming M_3 ($\text{M}=\text{Mg}, \text{Ca}, \text{Sr}, \text{Ba}$) - F (Cl) reactions. Initial results reported for the Mg_x ($x=2,3$) - F atom reactions are reported. Further, the course of these studies has also lead to a remarkable discovery concerning the stabilization of high temperature complexes. Through a combination of single and multiple collision chemiluminescence (CL) and laser induced fluorescence (LIF) spectroscopy, we have demonstrated the astonishing efficiency with which a high temperature reaction complex can be stabilized. We have obtained clear evidence for the stabilization of Group IIA MX_2 ($\text{M}=\text{Ca}, \text{Sr}, \text{Ba}, \text{X}=\text{Cl}, \text{Br}, \text{I}$) dihalide complexes, formed in concert with direct $\text{M} + \text{X}_2 \rightarrow \text{MX}_2^*$ reactive encounters, through extremely long range interaction with an additional halogen molecule. The onset of the monitored R3BR process at 1×10^{-6} Torr signals an enormous stabilization cross section ($\sigma > 5000 \text{ \AA}^2$). The demonstrated efficiency is certainly not explained within an RRKM framework, again suggesting that new models, which focus on long range energy flow as opposed to fragmentation, may be necessary to explain these efficient interactions. The data from this

study begins to reveal a much broader range of interaction than has typically been associated with the collisional stabilization process. The enhanced interaction range of these dihalide complexes may also result from the influence of a diffuse electron density. The current results focus attention on the potential importance of collisionally stabilized radiative or non-radiative complexation processes at elevated temperatures. These efficient processes may influence gas-surface depositions which are strongly dependent upon formation of the gas phase constituency.

We also present the results of studies in which we have used a very near resonant energy transfer from selectively formed metastable states of SiO and GeO ($a^3\Sigma^+$, $b^3\Pi$) to select metal atoms in order to form thallium, gallium, sodium, and potassium atom based laser amplifiers at $\lambda = 535, 417, 569, 616, 819,$ and 581 nm. The metastable triplet states are generated in high yield from a select group (Ge-O₃, Si-N₂O, Si-NO₂) of oxidation reactions. The energy stored in these generated triplet states is transferred in a highly efficient electronic energy transfer process to pump ground state Tl, Ga, Na, and K atoms to select excited states. So efficient are these transfers that they have been used to produce superfluorescence from Tl and Ga atoms at 535 and 417 nm (Appendix I) and amplified spontaneous emission (ASE) from Na atoms at 569, 616, and 819 nm (Appendices VIII and IX). Adopting a pumping sequence in which a premixed Group IVA metalloid-receptor atom combination is oxidized we have demonstrated full cavity oscillation in the Tl (535 nm - Appendix I) and Na (569 nm - Appendices VIII and IX) systems. The concepts employed to create amplification and oscillation in these systems also appear applicable to the efficient energy transfer pumping of potential amplifying transitions in the lead (Pb), copper (Cu - analog of Cu vapor laser), and tin (Sn) receptor atoms.

The outlined results, obtained with an oven based source of the Group IVA metalloid, require high source operating temperatures so as to obtain substantial Si or Ge atomic fluxes. In order to (1) greatly alleviate the temperature requirement and (2) generate higher metalloid concentrations for the pumping of appropriate atomic receptors, we have also been concerned with the development of considerably lower temperature silane (SiH₄) based thermolysis-discharge and thermolysis-photolysis combination sources as a means of generating atomic silicon. These partially successful efforts are also summarized in this report.

Curve Crossings, Electronic Energy Transfer Collisions, and Efficient Chemical Pumping

"A Highly Efficient and Selective Electron-Jump-Harpoon Process"

The collision dynamics of processes proceeding on electronically excited surfaces is fundamental to the attainment of population inversions based on electronic transitions in the visible spectral region.^{1,2} A particular subgroup of these electronic energy transfer processes involves metal atoms or molecules of low ionization potential. These species react very efficiently with atoms or molecules of significant electron affinity via what is termed the electron jump-harpoon process. It is this process, specifically involving the reaction of metal trimers and forming the product metal dimer and metal halide, that may represent one of the few direct chemical routes to produce electronically inverted products. The alkali trimer molecule, Na_3 , readily provides an electron to harpoon a hungry halogen atom, X , producing a switch from the interaction of two neutral species to that of two ions ($\text{Na}_3^+ + \text{X}^-$). The convergence, crossing, and interaction of the two potentials describing the neutral (covalent) and ionic (coulombic) constituencies allows an effective switch of the reactants (curve crossing). For Na_3 , with its low ionization potential, the curve crossing occurs at very long range ($> 10\text{\AA}$) leading to a high cross section for product Na_2 formation. Based upon the experimental results obtained thusfar in our laboratory, the sodium trimer reactions show not only vibrational but also rotational selectivity as they create electronic population inversions in the product Na_2 . Theoretical considerations (see also following sections) would suggest that these trimer reactions and their analogs represent key processes to yield electronically inverted products in direct chemical reaction.^{1,2}

"Efficient, Fast, Intra- and Intermolecular Energy Transfer Pumping"

The energy transfer based approach which we have used to develop the first visible chemical laser amplifiers and oscillators has relied on our belief that the majority of successful electronic transition chemical lasers will require a two-step approach.^{3,4} Chemical energy must be produced and stored in a first step and then transferred in a collision induced process to

an appropriate lasing medium in a second step. Following this scheme, we can attempt to produce inversions using (1) "ultrafast" intramolecular energy transfer among the excited electronic states of small diatomic molecules⁵⁻⁸ or (2) intermolecular transfer from electronically excited metastable storage states to readily lasing atomic receptors. Both processes inherently involve the curve crossing of electronic states which is basic to the creation of a highly efficient energy transfer route.

Electronically and highly vibrationally excited molecules, with their inherently diffuse electron density and large amplitude vibrational motions simply interact more effectively than do ground state molecules in their lowest vibrational-rotational levels. We have determined that several diatomic metal monoxides including silicon and germanium oxide display collision induced electronic-to-electronic (E-E)⁵⁻⁹ and vibrational-to-electronic (V-E)¹⁰ intermolecular energy transfers which proceed at rates comparable to or far in excess of gas kinetic. Transfers from metastable to shorter lived excited states may proceed at rates which approach 500 times gas kinetic (cross sections in excess of 4000 \AA^2). The low-lying electronic states of several simple high temperature molecules (the products of metal oxidation) interact with a collision partner which induces energy transfer with a much larger impact parameter than would have been previously anticipated on the basis of studies involving the lowest vibrational-rotational levels of their ground states. In a sense, we are dealing with "pseudo-macromolecules" which display many of the characteristics inherent to Rydberg states¹¹ with their large transfer and relaxation cross sections. In several cases the rates for the observed transfers may be comparable to the radiative lifetimes associated with the usually shorter lived and potentially useful upper levels in which the intramolecular transfer terminates.¹² Rates of this magnitude, properly employed, can be competitive with optical pumping!

At some point, the distinction between fast intramolecular energy transfer processes, correlating with electronic state couplings and the periods of molecular vibrations (rotations), and intermolecular energy transfer governed by the duration of collisions with electronically excited states is indistinguishable.^{1,2} We have demonstrated that it is reasonable to expect certain near resonant intermolecular energy transfers to proceed with extremely high cross sections.¹³ One might consider that an electronically excited molecule, with its diffuse electron density, has the ability to send

out more feelers or interaction lines as it influences reaction and collision partners. The increased interaction rates which several experiments now suggest are most encouraging for the development of visible chemical lasers from energy transfer processes. It is precisely these very exciting results which we have already made use of in the initial development of several systems.

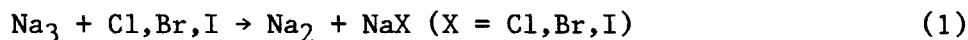
CONTINUOUS CHEMICAL LASER AMPLIFIERS IN THE VISIBLE REGION BASED ON HIGHLY EFFICIENT AND SELECTIVE CHEMICAL REACTIONS

Formation of Amplifiers (Oscillators) Through Direct Chemical Reaction

Na_2 chemical laser amplifiers have been developed¹⁴⁻¹⁶ in our laboratory employing the high cross section Na_n ($n = 2, 3$) - $\text{X}(\text{Cl}, \text{Br}, \text{I})$ electron jump reactions to create a continuous electronic population inversion based on the chemical pumping of sodium dimer (Na_2). Sodium trimer molecules produced in supersonic expansion (see Appendices II, V, VI) are reacted with halogen atoms to create the inversions on electronic transitions in Na_2 . Optical gain through stimulated emission has been demonstrated in select regions close to 527, 492, and 460 nm with potential extension to the ~ 395 , ~ 365 , and ~ 350 nm regions. The observed gain (max. of 4% at ~ 527 nm corres. to $8 \times 10^{-3}/\text{cm}$ for individual rotational levels (see following)) can be enhanced considerably with a more versatile long path length source configuration. The development of this source configuration has been a major focus of our efforts over the last three years.

Electronically Inverted Na_2 Produced from the Na_3 - $\text{X}(\text{Cl}, \text{Br}, \text{I})$ Reactions

Efficient chemical laser oscillators should be developed from the high cross section, highly exothermic Na_3 - $\text{X}(\text{Cl}, \text{Br}, \text{I})$ reactions which selectively form Na_2^* in a limited number of its excited electronic states (Fig. 1(a)). The optical signatures for the processes



encompass emission from a limited number of Na_2 band systems. Surprisingly,

Figure 1(a) Approximate potential curves for select states of Na_2 .

Figure 1(b) Chemiluminescent emission resulting from the reaction $\text{Na}_3 + \text{X} \rightarrow \text{Na}_2 + \text{NaX}$ with $\text{X} = \text{Br}, \text{I}$. The spectra display sharp fluorescence features in the visible at 527, 492, and 460.5 nm superimposed on a broader Na_2 background emission.

Figure 1(c) Comparison of (a) observed and (b) calculated emission spectra for the Na_2 B-X emission system. The experimental spectrum corresponds to the chemiluminescence from the Na_2 -Br reaction. The calculated spectrum, which was obtained for a rotational temperature, $T_{\text{rot}} \approx 1000\text{K}$, represents an estimate of effective rotational temperatures in a system operated under single collision conditions and therefore not at equilibrium. Relative vibrational populations input for Na_2 B-X, $v' = 0.6$ were in the ratio 1.00:1.17:1.33:1.50:1.67:1.54.

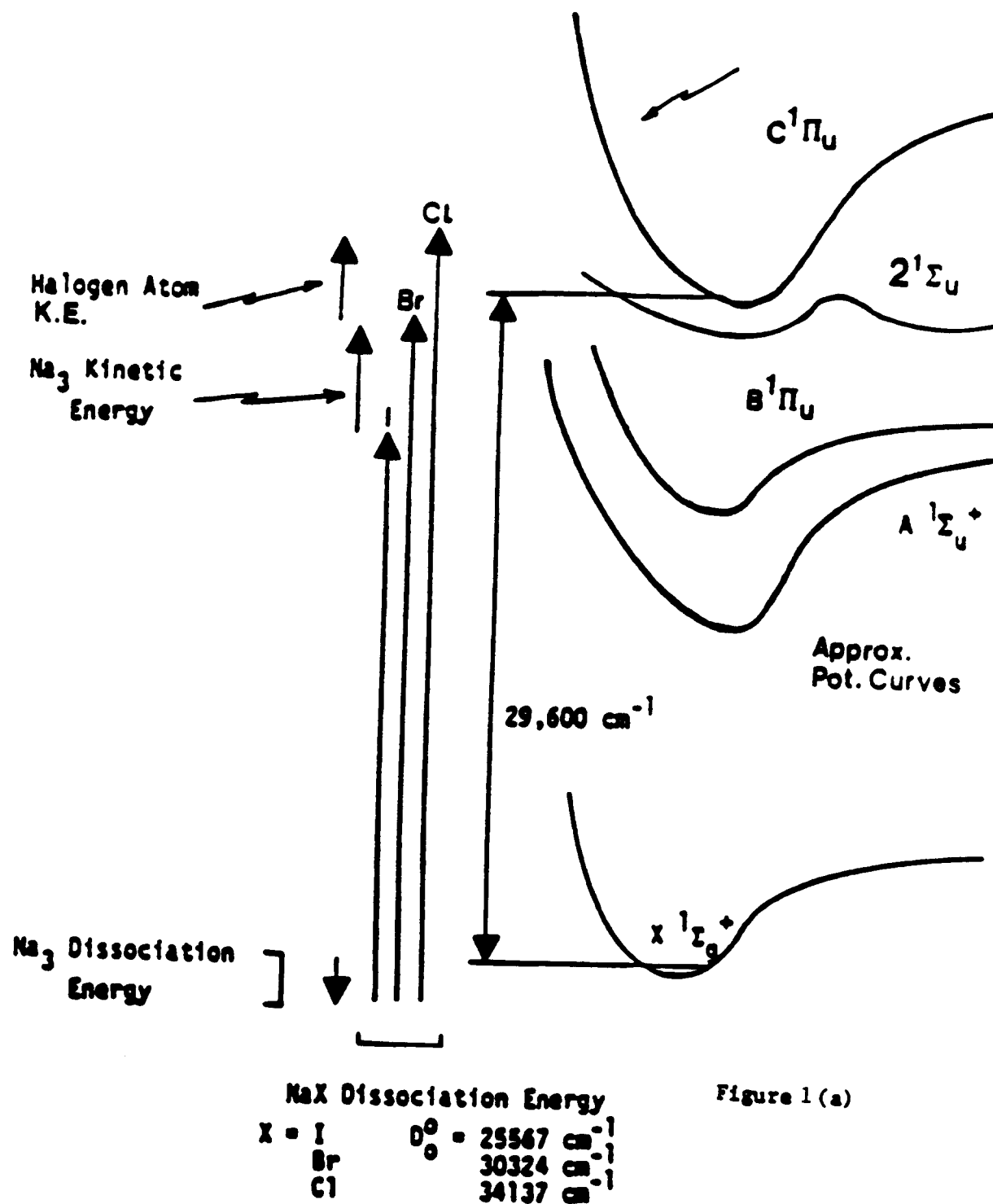


Figure 1(a)

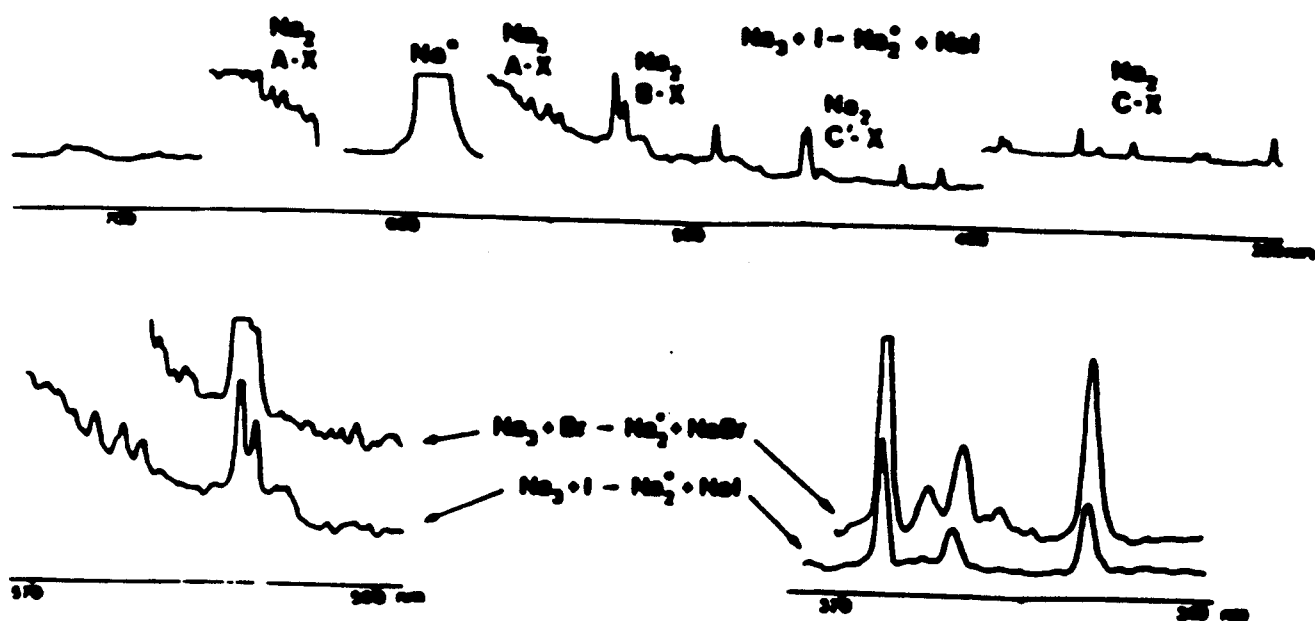


Figure 1(b)

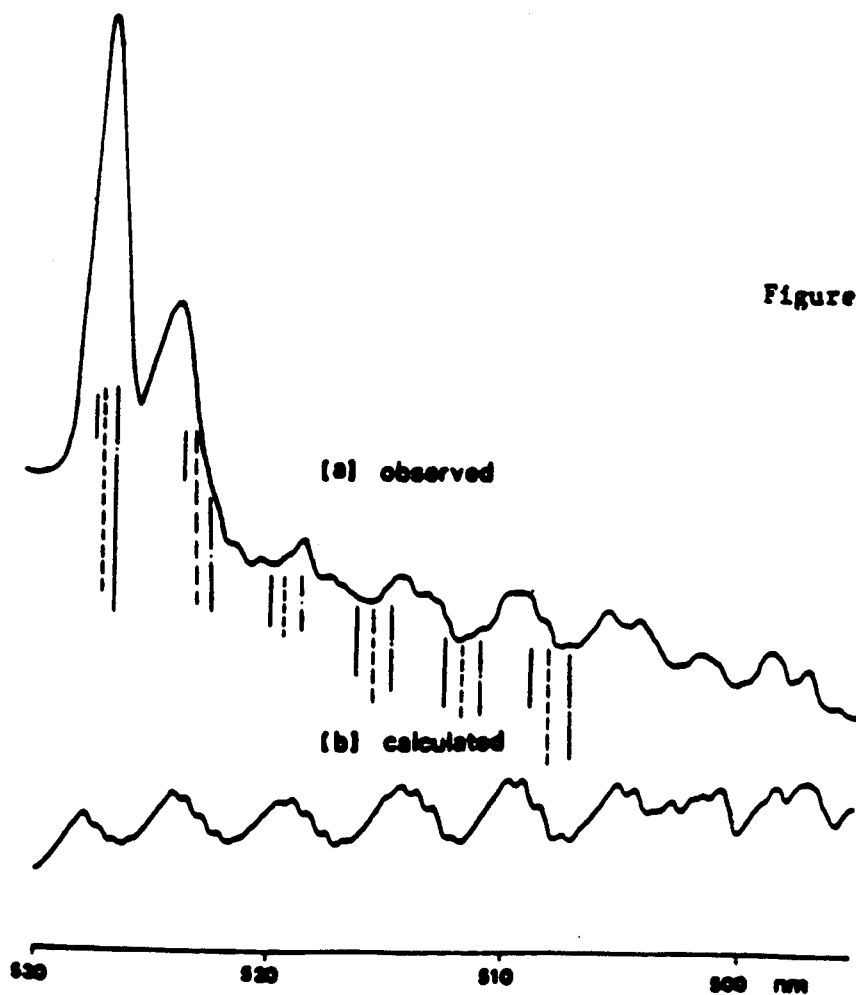


Figure 1(c)

the observed emission is characterized by sharp well defined emission regions (Figs. 1(b), 1(c)) superimposed on a much weaker but perceptible and analyzable Na_2 background fluorescence. As Fig. 1(c) demonstrates, these sharp emission features are not readily explained by invoking a purely fluorescent process.

The sharp nature of several of the B-X, C-X, and C'-X Na_2 fluorescence features (Figs. 1(b), 1(c)), their correlation in certain regions to the emission characteristic of optically pumped Na_2 laser systems¹⁷ (ex: 528.2 nm (v',v'') = (6,14) B-X), and the near exponential growth of these features relative to the background Na_2 fluorescence spectrum with increasing Na_3 concentration, suggests that stimulated emission might be associated with certain of the emitting Na_2 reaction products. Laser gain measurements were carried out to assess this possibility.

In order to do these gain studies, we further developed (Fig. 2(a)) a unique source configuration which allows the supersonic expansion of pure sodium vapor to create a Na_3 concentration not previously attained in a reaction-amplification zone. Using argon ion laser pumped dye lasers to study the $\text{Na}_3 + \text{Br}$ reaction we have scanned (Fig. 2(b)) the entire wavelength region from 420 to 600 nm (Figure 1(b)) in ~ 3 nm intervals at 0.5 cm^{-1} resolution (FWHM) and the regions around 527 nm and 460 nm (Fig. 1(c)) at 0.007 cm^{-1} resolution.¹²⁻¹⁶ We find that laser gain and hence amplification is associated with very limited regions of the spectrum. The observations suggest that several of the sharp emission features apparent in Figure 1 correspond to a stimulated emission process and the establishment of a population inversion. Optical gain through stimulated emission (0.5 cm^{-1} resolution) in the regions close to 527 nm (1%), 492 nm (0.3%), and 460.5 nm (0.8% gain) correlates precisely with the reactive process and the relative intensities of those features observed while monitoring the light emitted from the $\text{Na}_3\text{-Br}$ and $\text{Na}_3\text{-I}$ reactions. High resolution ring dye laser scans in the 527 nm region indicate that the gain for the system is a minimum of 3.8% for an individual rovibronic transition with approximately four to seven individual rotational transitions showing gain. At 459.8 nm, we have measured an 2.3% gain for an individual rotational transition. The results demonstrate the continuous amplifying medium for a visible chemical laser in at least three wavelength regions.¹⁴⁻¹⁶ At no other scanned wavelengths have we observed gain. In fact, in scanning the 420-600 nm region, we generally

Figure 2: Schematic of (a) apparatus for the study of the chemiluminescent Na_3 - X reactions and (b) the arrangement of the experimental configuration for measuring gain from the Na_3 - X metathesis.

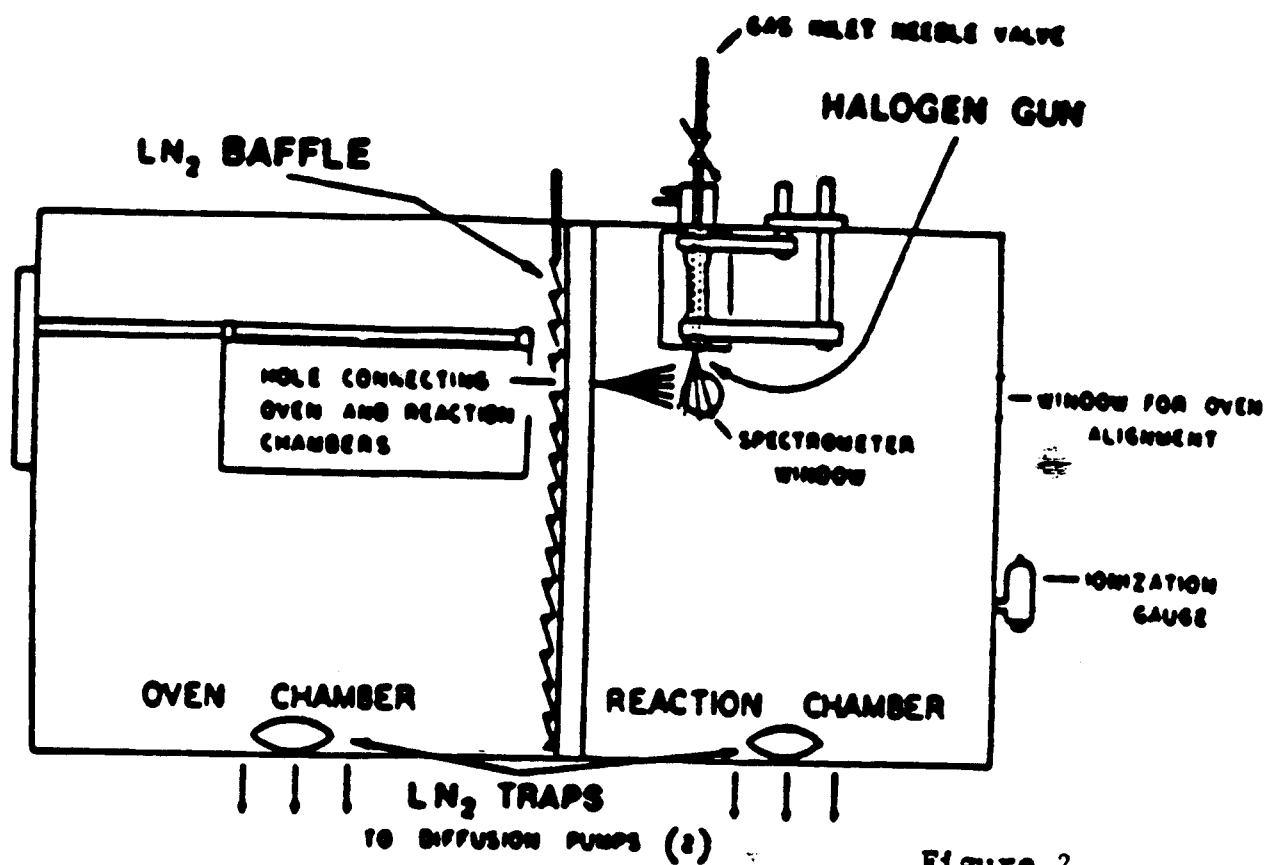
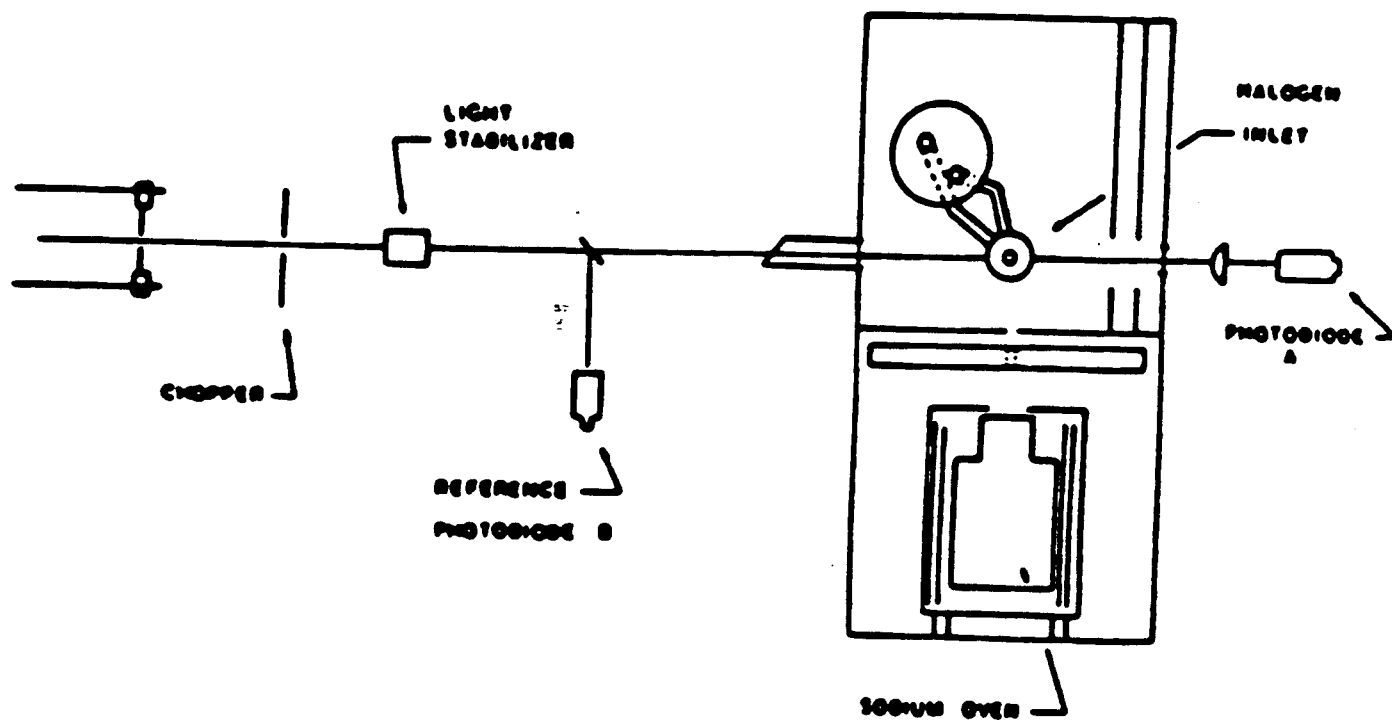


Figure 2



b

observe losses of the laser photon flux due primarily to scattering (to only a negligible extent, absorption) on transit through the $\text{Na}_3\text{-Br}$ reaction zone. In the region of the sodium D-line, a substantial absorption and hence loss is monitored as a function of the trimer-halogen atom reaction.¹⁴⁻¹⁶

Because of the low Na_3 ionization potential and the high halogen electron affinities,¹⁸ the Na_3 -halogen atom reactions are expected to proceed via an electron jump mechanism with extremely high cross sections,¹⁹ producing substantial Na_2 excited state populations. The question of why the $\text{Na}_3\text{-X}$ reactions appear to demonstrate vibrational and rotational selectivity associated with certain wavelength regions may be dealt with by invoking a model for the dissociative ionic recombination, $\text{Na}_3^+ + \text{X}^- \rightarrow \text{Na}_2^* + \text{NaX}$, and the curve crossings which influence the distribution of product molecules for this process.²⁰ This model, coupled with an analysis of the electronic coupling between select sodium dimer excited states, may provide a semi-quantitative explanation for the created population inversions.

The population inversions monitored thusfar are thought to be sustained (1) by the large number of free halogen atoms reacting with Na_2 molecules in those ground state levels on which the transitions emanating from the Na_2 excited states terminate and (2) collisional relaxation of the ground state sodium dimer molecules. The cross section for reaction of vibrationally excited ground state Na_2 is expected to be at least comparable to the cross section for collision induced vibrational deactivation of the Na_2 manifold. Extremely efficient reactions greatly assist the depletion of the lower state levels in this system allowing one to sustain a continuous population inversion.

Development of an Extended Path Length $\text{Na}_3\text{-X}$ (Cl,Br,I) Reaction - Amplification Zone

A major focus of our efforts has been to considerably improve the magnitude of the amplification demonstrated for the sodium dimer amplifiers at ~ 527 , ~ 492 , and ~ 460 nm. The apparatus depicted in Figure 2 now produces a substantial Na_3 concentration ($\geq 10^{13}/\text{cc}$) albeit in a limited reaction-amplification zone. In order to demonstrate continuous chemical laser oscillation, however, it is desirable to create an enhanced sodium trimer-halogen atom reaction zone not only in terms of reactant concentration but

also with respect to the amplification zone path length. The overall apparatus design which we are developing, depicted in part schematically in Figures 3-5 and discussed in detail in Appendices VII, IX, and X is meant to accomodate high intersecting reactant flows from both sodium trimer and (dual rotatable) halogen atom sources in order to produce an enhanced concentration of Na_2 amplifiers over a significantly extended path length.

The apparatus outlined in Figs. 3-5 attempts to increase the Na_3 reaction - amplification zone concentration by repositioning the trimer and halogen atom sources relative to each other and facilitating the halogenation process much closer to the alkali nozzle itself, in a gas dynamic configuration. We also have incorporated the facility for the in-situ adjustment of the alkali and halogen source positions. This includes the ability to rotate the dual alkali-trimer-flow-encompassing halogen atom slit sources (Figs. 3(b)) so as to optimize flow mixing. Further, as a means of increasing the reaction zone and gain length, we have developed and continue to test several continuous flow slit sources (Appendix X for more detailed discussion).

In a pure sodium supersonic expansion, the Na_3 constituency is dominated by a much larger atom and cold dimer concentration.²¹ These constituencies do not absorb at the Na_2 amplifier wavelengths characteristic of the Na_3 -halogen atom reaction systems. However, it is desireable to minimize the atom and dimer while increasing the trimer concentration. The trimer concentration must be altered and improved through an appropriate adjustment of the supersonic expansion conditions shifting the distribution to higher sodium polymers. By seeding the expansion with helium, argon, or other noble gas atoms, several researchers²² have demonstrated that the atom and dimer concentrations can be made quite small relative to the much larger sodium polymers.²² Our ultimate goal is to develop a system which does not operate at these extreme expansion conditions but, rather, we seek a middle ground which will allow us to produce primarily the trimer and a few larger clusters.²³ This condition should be achieved through the appropriate adjustment of parameters which can be manipulated in the expansion including (1) the rear oven stagnation pressure (argon or helium + sodium), (2) the frontal nozzle temperature, and (3) the ratio of the supersonic expansion source pressure to the overall expansion chamber pressure.

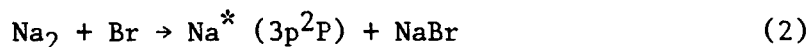
The sodium slit source is positioned relative to the dual halogen slit sources located above and below what can be envisioned as the position of an

alkali sheath created upon expansion from the alkali slit source. The reaction zone-cavity configuration is designed to allow for 1) short transit of the reactants Na_3 and $\text{X} = \text{Cl}, \text{Br}, \text{I}$ to the reaction - amplification zone, 2) flexible movement of these sources with respect to each other and with respect to the flow patterns created in the system and 3) minimal interaction of these reactants with laser cavity windows. To insure this minimal interaction, self-cleaning optical windows²⁴ are used.

We have now carried out several experiments using the extended amplification zone device depicted in Figure 3. These studies are outlined in more detail in Appendices X and XIV-XVI, however, it is important to note the most important observations which we have made in these initial efforts. These include 1) what appears to be the first observation of Raman pumping in a purely chemical environment with the attendant measurement of gain associated with the Stokes scattering and 2) excited state chemical pumping which is the equivalent of that obtained with a substantial $2\text{W}/\text{cm}^2$ laser pump of sodium vapor (Na_x @ 0.344 mm/Hg - see Appendix X). Thus, while we have not yet reached the necessary Na_3 concentrations in our reactive zone to produce the inverted Na_2 B-X features (Figs. 3-5), we have already observed an unusual and unexpected behavior associated with the longer path length configuration.

Raman Pumping in the Absence of an External Light Source

Using the configuration described in Figures 3-5 (Appendices X, XIV-XVI for additional detail) we have observed the first resonance Raman pumping generated in a purely chemical reactive environment in the absence of an external light source. The observations made in the present study bear a close analogy to those of Wellegehausen¹⁷ and Bergmann and coworkers²⁵⁻²⁶ in their analysis of optically pumped sodium dimer lasers operative on a stimulated Raman scattering process. Here, as Fig. 6 demonstrates, we observe a series of Raman-like Stokes and anti-Stokes features which are (1) associated primarily with the lowest vibrational levels of Na_2 , (2) correlate strongly with a scattering process involving the Na D-line components ($\text{Na } 3p^2P_{3/2,1/2} - 3s^2S_{1/2}$), clearly evident in Fig. 7, and created in the chemical reaction sequence



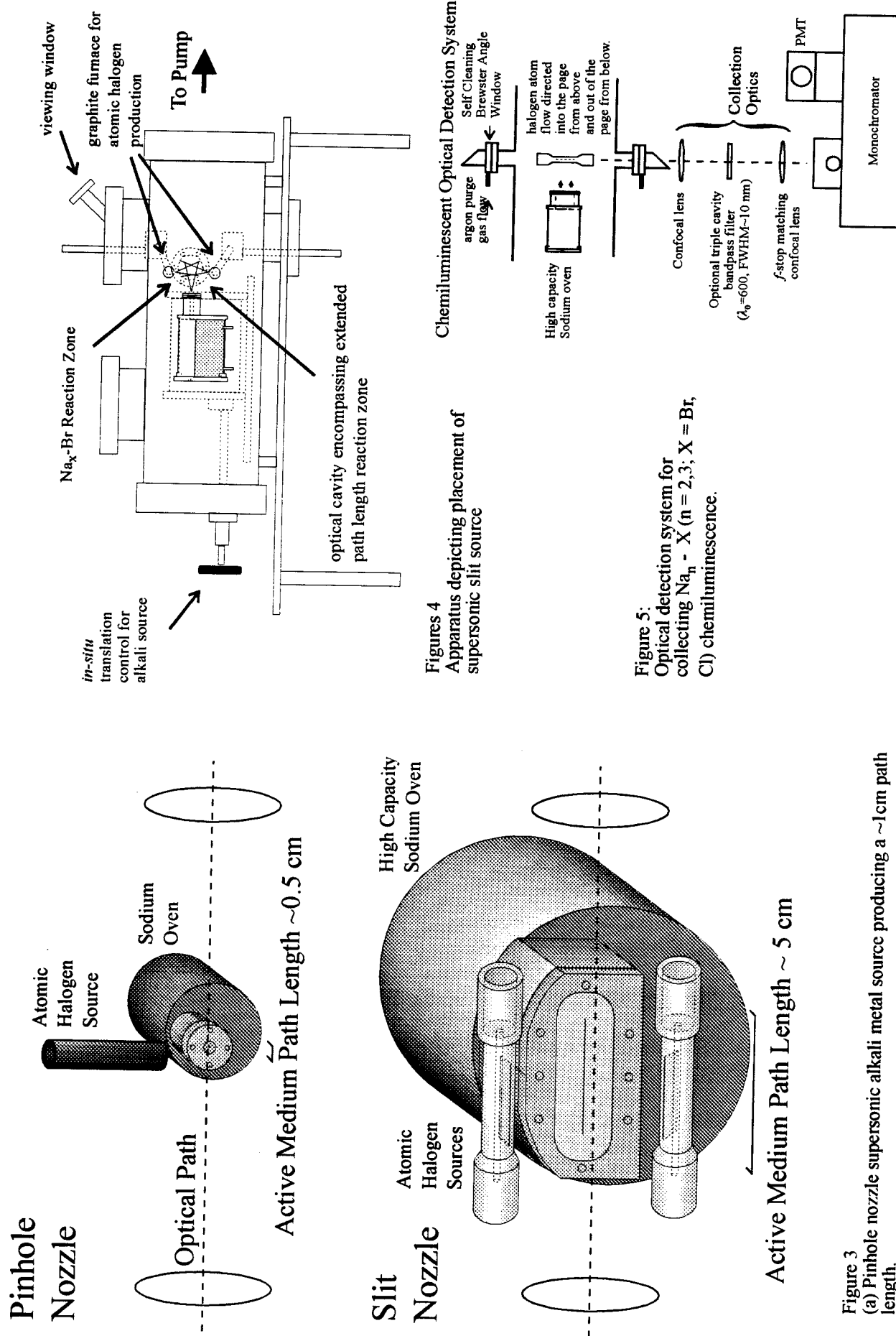
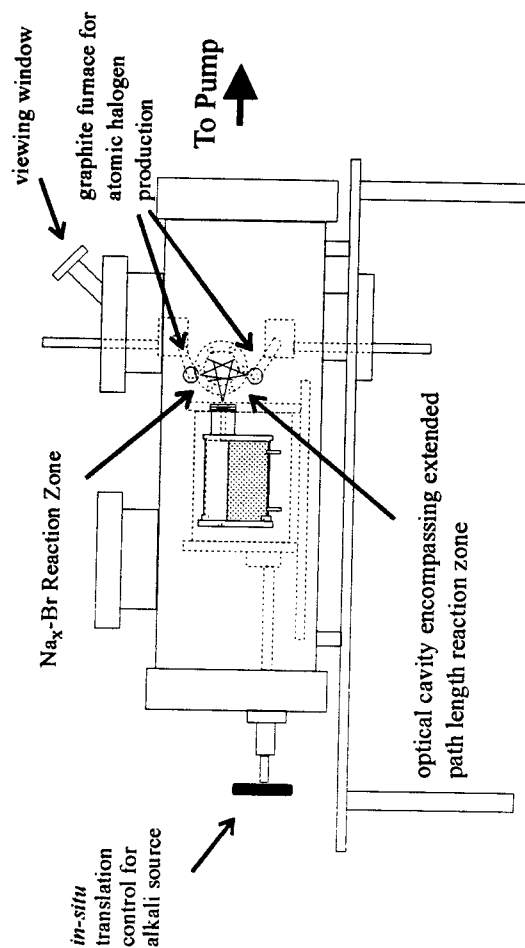


Figure 3
 (a) Pinhole nozzle supersonic alkali metal source producing a ~ 1 cm path length.
 (b) Slit nozzle supersonic source producing an extended path length reaction zone.



Figures 4
 Apparatus depicting placement of supersonic slit source

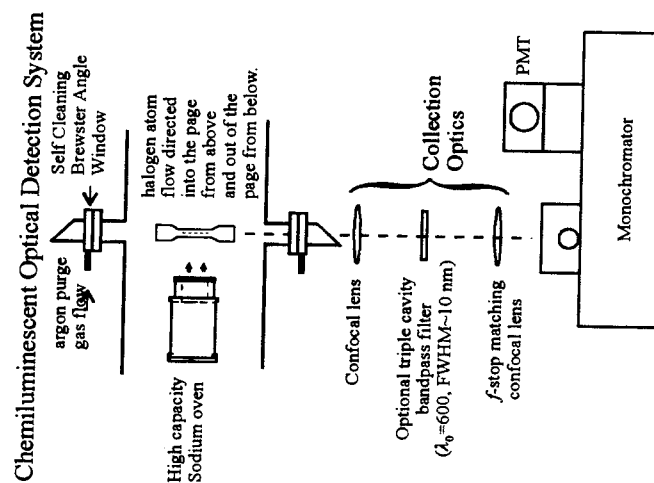


Figure 5:
 Optical detection system for collecting $\text{Na}_n - \text{X}$ ($n = 2, 3$; $\text{X} = \text{Br}, \text{Cl}$) chemiluminescence.

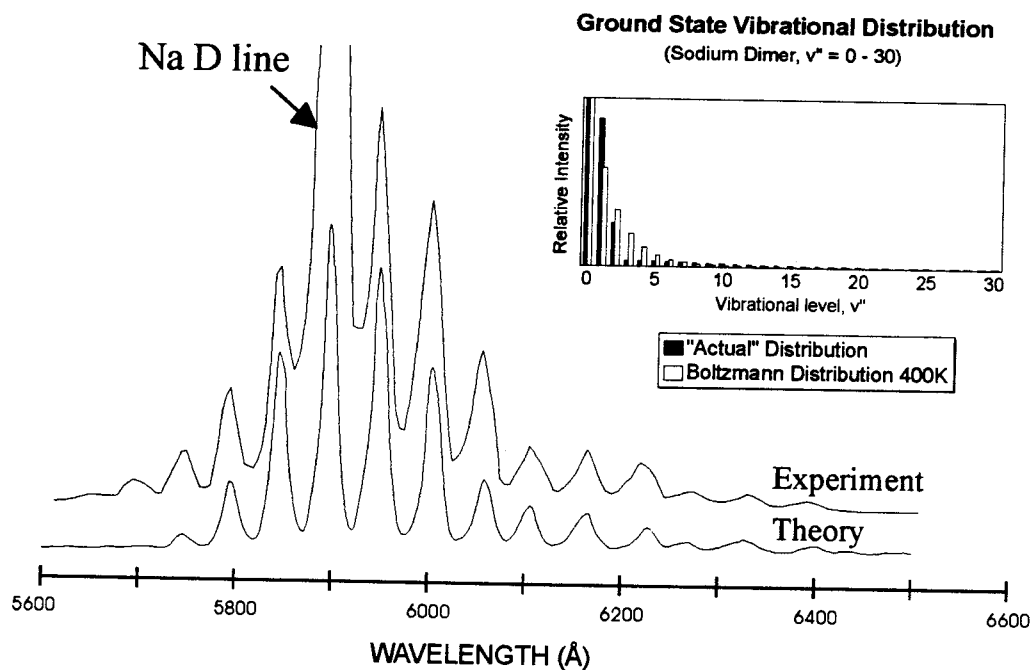


Figure 6
Comparison of experimental spectrum with computer modelled distribution (res. $\sim 5 \text{ \AA}$, $T_{\text{oven}} \sim 875\text{K}$, $T_{\text{nozzle}} \sim 935\text{K}$). Optimum agreement between calculation and experiment was found for the slightly nonthermal distribution depicted in the upper righthand corner of the figure. A Boltzmann distribution at 400K is included for comparison. See text for discussion.

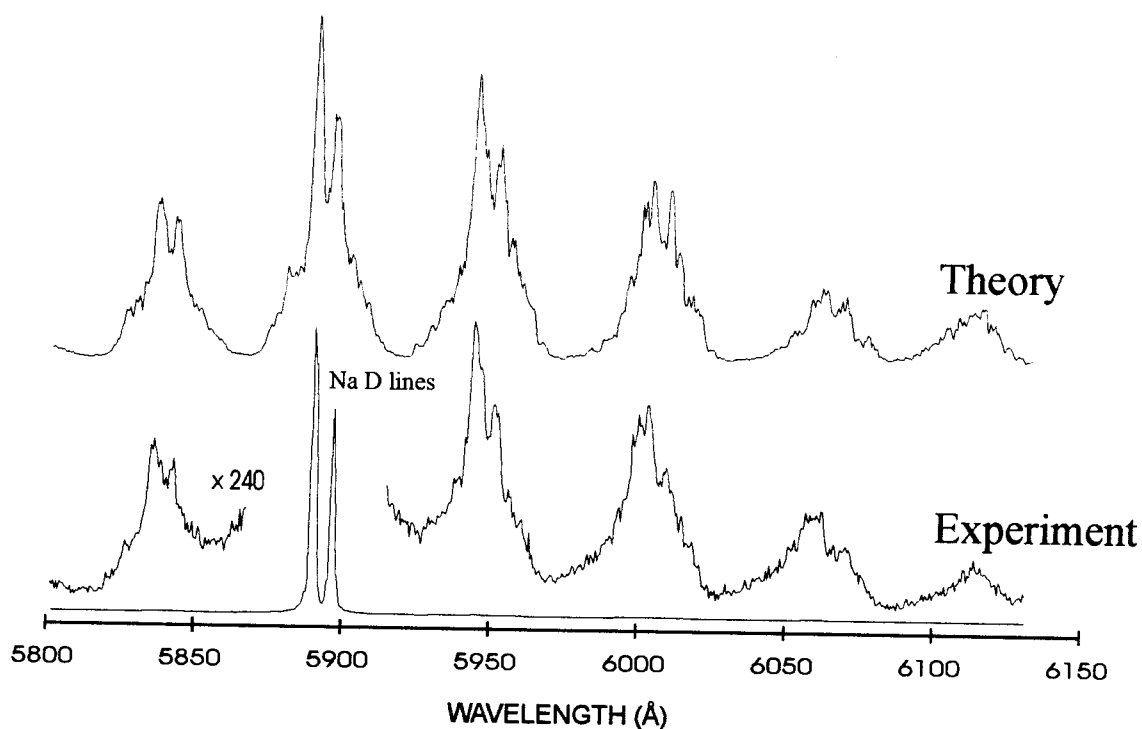
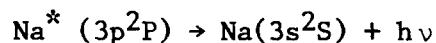


Figure 7
Raman-like spectrum taken at a resolution of $\sim 1.5 \text{ \AA}$ ($T_{\text{oven}} \sim 875\text{K}$, $T_{\text{nozzle}} \sim 935\text{K}$) depicting the two Na D-line components and the satellite Raman structure. The spin-orbit frequency difference of the two Na D-line components is reproduced in the scattered radiation. A simulated spectrum is presented for comparison ($T_{\text{ROT}} \sim 400\text{K}$, $\Gamma = 4 \text{ cm}^{-1}$). See text for discussion.



The Raman features depicted in Figures 6 and 7 are not readily generated by light from an external laser (Appendices XIV, XVI) tuned to the Na D-line resonance and appear to be enhanced by the environment of the reaction zone itself.

Any attempt to fit the observed structure (symmetric about the Na D-line) to a resonance fluorescent series appropriate to the experimental conditions fails completely. The D-line emission is scattered by cooled sodium dimers (Na_2) generating multiple Stokes and anti-Stokes features. These are assigned as resonance Raman progressions and, as Figures 6 and 7 indicate, are well simulated on the basis of the resonance Raman theory outlined by Rousseau and Williams²⁷ and others.²⁸ Here, except at very low reactant concentrations, the intensity of the Raman scattering overwhelms any normal chemiluminescent emission from the reaction zone.

The results of initial gain studies (in which amplification has been observed on many of the Stokes and anti-Stokes components of the Raman spectrum) are suggestive of a stimulated Raman scattering process similar to that associated with optically pumped alkali dimer lasers. However, as Figure 8 demonstrates, the scattering linewidth, Γ , determined from a higher resolution fit ($\sim 0.5 \text{ \AA}$) of the resonance Raman intensity expression (see Appendix XIV for definitions)

$$I_s(v_G, J_G; \nu_F, J_F) = \frac{32\pi^3 \omega_i^4 I_P}{9c^4 h^2} M(\xi_0)^4 e^{-BJ_G(J_G+1)hc/kT} N(v_G) \times \sum_{q, J_1} \left(3S_{J_{G1}} S_{J_{F1}} \frac{|\langle v_F | v_1 \rangle \langle v_1 | v_G \rangle|^2}{(\omega_{G1} - \omega_{F1})^2 + \Gamma^2} + 2S_{J_{G2}} S_{J_{F2}} \frac{|\langle v_F | v_1 \rangle \langle v_1 | v_G \rangle|^2}{(\omega_{G1} - \omega_{F2})^2 + \Gamma^2} \right) \quad (3)$$

associated with the present process appears to be close to 4 cm^{-1} . This result suggests that we have observed more than a "simple" Raman-like scattering process. In order to address this result we might consider a further long range interaction of the electronically excited sodium $3p^2P$ atoms with those Na_2 molecules which are Raman pumped, an interaction of the Na_2 molecules with the Br atoms that induces a time varying enhancement of the dimer polarizability (hyperpolarizability), or (less likely) the presence of a

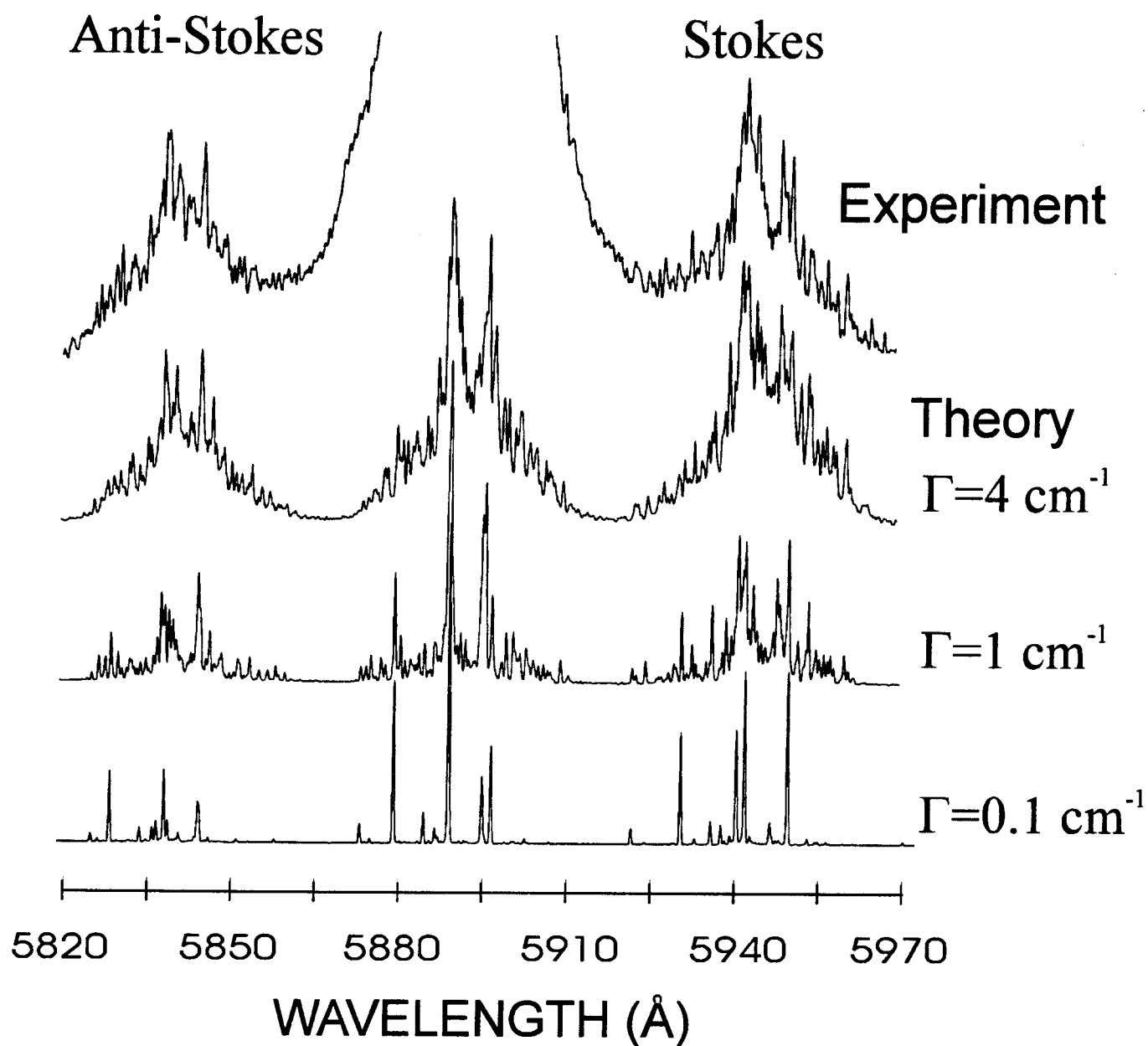


Figure 8

High resolution spectrum ($\sim 0.5 \text{ Å}$) and simulated spectra for $\Gamma = 0.1, 1, \text{ and } 4 \text{ cm}^{-1}$ demonstrating the marked improvement in the fit to the experimental Raman-like features for increasing values of Γ . See text for discussion

large electric field created due to the reactive environment in the vicinity of the reaction zone. It would appear that this interaction leads to a much more efficient Raman-like scattering process which also appears to be chemically enhanced.

While further experiments will be necessary to clarify the mechanism for the scattering process, the long path length reaction zone employed in these experiments appears to have revealed the manifestation of a significant cooperative phenomena. The moderate Rydberg character of the Na $3p^2P$ excited state, with its diffuse electron density, may lend itself to a considerable long range interaction inducing cooperative effects. The assessment of these surprising cooperative effects should be the subject of continued study.

The intense "Raman" features depicted in Figures 6-8 have prompted preliminary experiments (Appendix XVI) to assess whether a stimulated Raman process might be operative. The path length of the active medium is in excess of 5 cm (considerably longer than most gas phase chemical reaction zones) and since the very intense D-line pumping is distributed virtually throughout the entire extent of this area, we attempted to assess the possible existence of a gain condition on any of the suspected Raman features (most likely the first Stokes line). It should be noted that gain would be predicted on the basis of the nonlinear treatment of the stimulated Raman effect, however, the gain condition might also be achieved for certain levels of the Na₂ A-X transition through the resonance Raman effect if the Na₂ ground state temperature is sufficiently low.

The layout of the gain measurement configuration used to conduct several preliminary gain measurements is depicted in Figure 9. In this experiment, a laser beam (HeNe laser) originating ~15 ft from the expansion zone is directed through a small adjustable aperture and the reaction zone. The beam is subsequently reflected back through the aperture, thus insuring that the normal of the reflector is perfectly parallel to the reaction zone. A light gathering lens is placed intermediary to the reaction zone and the adjustable aperture so that light from the HeNe laser is reflected from the back mirror and focused onto the aperture. Establishing the geometry in this manner insures that the optical system rejects off-axis light rays and accepts only radiation parallel to the optic axis. Consequently, observed output light intensities measured when the high reflector is blocked can be compared with intensities measured with the same reflector open to the reaction zone.

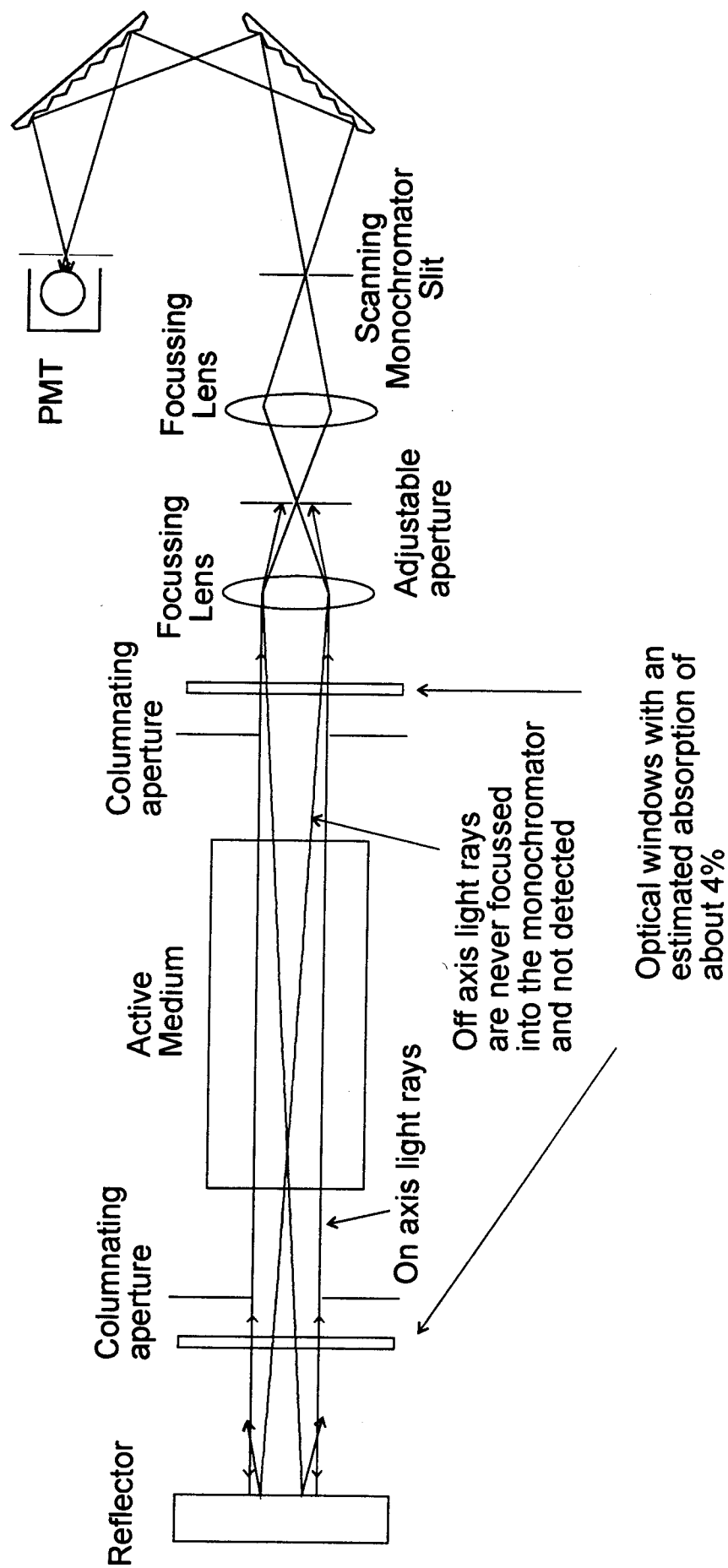


Figure 9

Schematic of gain measurement configuration. Intensities monitored with the PMT are measured with the high reflector blocked and unblocked. In the absence of gain or loss, the maximum ratio of those intensities that can be monitored can be no greater than two. The condition that we accept only light travelling parallel to the optical axis is necessary for the case in which the gain medium may not be uniform.

Assuming that only on-axis radiation can be reflected from the mirror and subsequently detected, the maximum intensity ratio for the unblocked mirror (I_u) to that observed with a blocked mirror (I_b) can be no greater than two (neglecting the effects of gain and absorption in the reactive medium). The detection of a ratio (I_u/I_b) greater than two is suggestive of the development of enough gain in the reactive medium to overcome any losses due to absorption or scattering. Although explicit measurements have not yet been performed, our glass optical windows typically absorb about 4% of the incident radiation per pass. Typically the distance between the mirror and the aperture is 1m, with the aperture narrowed to about 1 mm in diameter. The focal length of the lens was about 12 cm.

The described gain configuration was used to make several measurements at the Stokes frequency ($\sim 16830 \text{ cm}^{-1}$). The ratio, I_u/I_b , was consistently found to be in excess of 2.3. The measurements, performed on the remaining satellite peaks suggested ratios of order slightly greater than 2. Similar measurements performed on the Na D line components and several peaks of the thermally relaxed Na_2 B-X emission system (Figure 5 - Appendix X) showed intensity ratios much less than 2, the maximum intensity ratio monitored at the D-line being 1.3. Further discussion of the gain measurements can be found in Appendix XVI.²⁹

Extension of the Na_3 - X(Cl,Br,I) Amplifier Concept

The Na_2 amplifiers which we have characterized in the visible region operate on bound-bound transitions. It is not difficult to envision an extrapolation on the Na_3 -X reaction concept which involves the alkaline earth metal trimers and the formation of excited state dimers which can undergo bound-free excimer transitions. With this focus, we are attempting to generate the M_2 excimer analogs of the Na_2 laser amplifiers discussed previously. The ground electronic state of Mg_2 is very weakly bound.³⁰ However, detailed calculations suggest the Mg_2 - Mg bond strength may be on the order of 0.6 eV,³¹ quite comparable to that of Na_3 . We are now forming magnesium molecules, specifically Mg_2 and Mg_3 , and observing the excited state products of their oxidation with F and Cl atoms. A halogen atom discharge source which we have developed to study the $\text{Bi}_2 + \text{F}$ reaction³² (see also Appendix IV) is being used to investigate the Mg_2 -F, Mg_3 -F, Mg_2 -Cl, and

Mg₃-Cl reactions.³³ These studies will soon be extrapolated to the heavier alkaline earths, Ca_x - Ba_x. To date, we have not observed strong Mg₂ emission from the Mg₃ - F, Cl reactions, however, surprisingly, preliminary results on this system signal the formation of excited state Mg_xF and Mg_xCl charge transfer complexes where x is most likely two (Appendices VI, X). Although we have not yet demonstrated the potential for forming an Mg₂^{*} based excimer amplifier laser system, the creation of a long-lived Mg_xF complex suggests that, with some modification, this may be feasible.

Long Range Collisional Stabilization and the Symmetry Constrained Dynamics of High Temperature Complex Formation

As an off-shoot of our study of Group IIA cluster halogen atom reactions, in a study of Group IIA metal-halogen molecule reactions, we have now clearly demonstrated the highly efficient collisional stabilization of high temperature complexes of some considerable spatial extent.³⁴ In a series of near single collision and well-defined multiple collision CL and LIF studies extending over six decades of pressure (Appendices XVII, XVIII), we demonstrate the stabilization of electronically excited Group IIA dihalide collision complexes via a radiative three body recombination (R3BR) process operative at microTorr pressures. Over the pressure range 1×10^{-6} - 5×10^{-4} Torr, a comparative study of the emission from M (M = Ca, Sr, Ba) - X₂(Cl₂, Br₂, I₂) and M-XY(ICl, IBr) reactive encounters identifies a symmetry constrained dynamics associated with the formation of the dihalide complexes (along a C_{2v} reaction coordinate) as they are stabilized by interaction with an additional halogen molecule. The symmetry constraint, indicated by a much weaker emission from the mixed halogen reactions (especially of barium and strontium), signals the dominance of an efficient collisional stabilization. The onset of the monitored R3BR process at 1×10^{-6} Torr defines an extremely large stabilization cross section which cannot be readily explained within an RRKM framework.

By relaxing the near continuous emissions (exemplified for Sr reactions in Figure 10) observed for the complex formation under near single collision conditions, controlled multiple collision experiments establish the previously challenged stabilization mechanism³⁵ and show that the low pressure continua result from the overlap of a closely spaced, highly excited, rovibronic

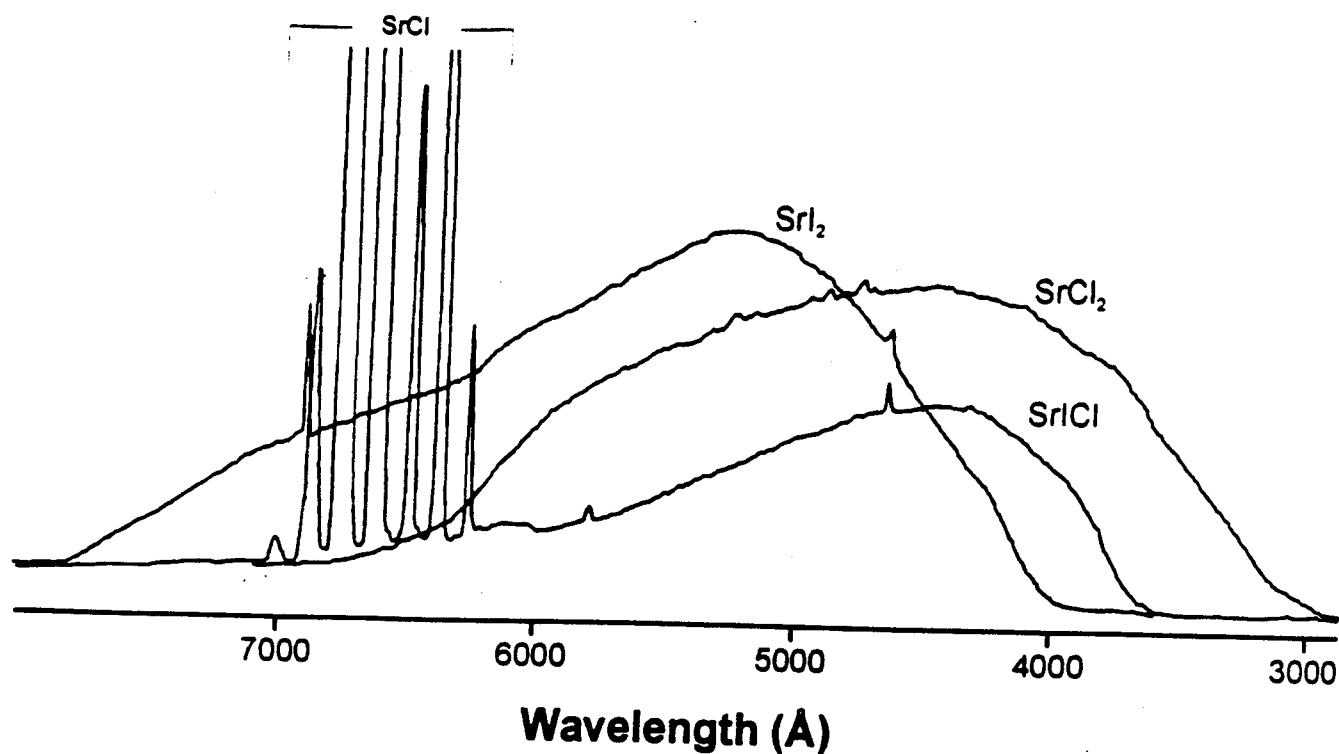


Figure 10

Continuum emission associated with the Strontium dihalides

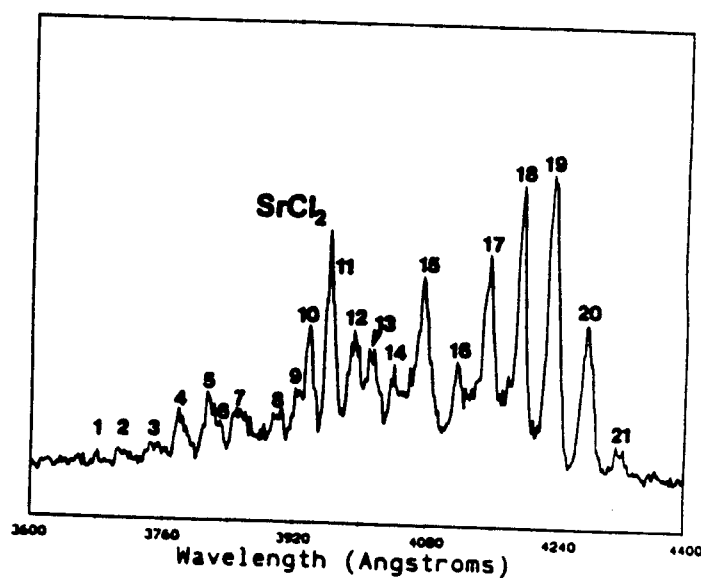
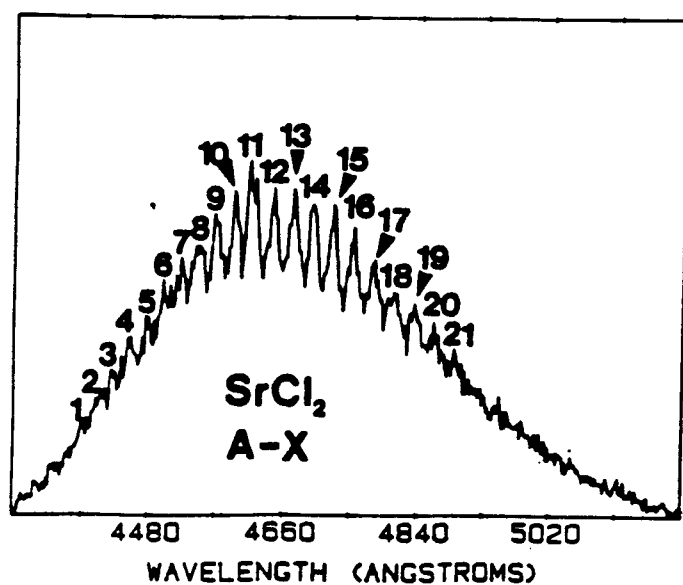
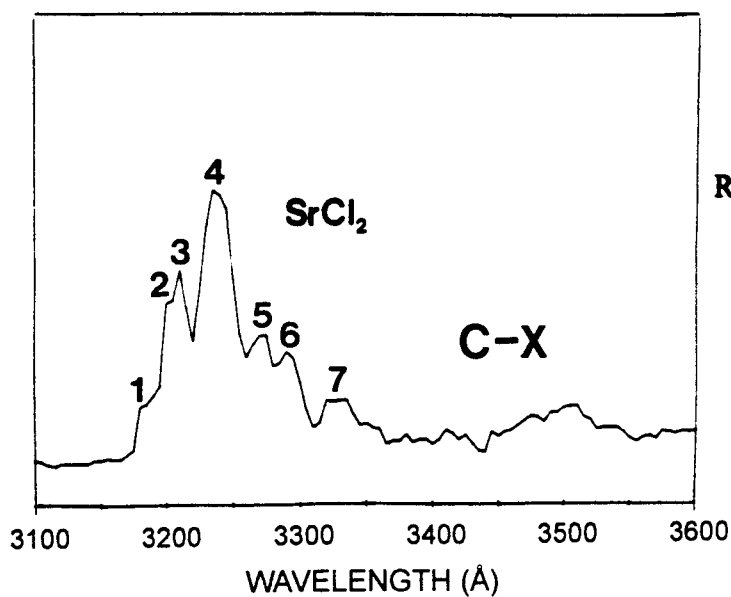


Figure 11

Resolved SrCl_2 emission for the A-X, B-X, and C-X systems



distribution. Further, as we demonstrate for the Sr-Cl_2 reaction in Figure 11, these multiple collision studies reveal the first vibronically resolved electronic emission for the dihalides. Comparative studies on several systems of the resolved vibronic emission from the multiple collision experiments (Appendix V) provide strong confirmation of the highly efficient collisional stabilization.

The observation of an R3BR process at pressures as low as 1×10^{-6} Torr is surprising. A steady-state treatment of the most reasonable mechanism for dihalide formation via collisional stabilization (within the RRKM framework) which models the chemiluminescence signal as a function of halogen concentration can be shown to be consistent with (1) an enormous stabilization cross section of order $\sigma \sim 3000\text{-}5000 \text{ \AA}^2$ ³⁶ and (2) an extremely long excited state radiative lifetime, $\tau \sim 10^{-2}$ seconds. Within an RRKM framework, the collisional stabilization mechanism requires a radiative lifetime well in excess of 10^{-5} seconds in order that emission from the complex compete favorably with the excited state dihalide loss mechanisms. Experiments indicate that the process appears to be operative for much shorter lived excited states.

If we eliminate the requirement for a long-lived excited state, we must require a considerably larger stabilization cross-section and an extremely long range interaction involving the forming Group IIA dihalide excited states and their relaxing collision partner. It is clear that the stabilization process competes favorably with unimolecular decomposition for which RRKM calculations suggest a unimolecular lifetime (averaged over the distribution of energy and angular momentum) on the order of $\tau \sim 10^{-7}$ seconds. These factors raise the question of whether association processes in these systems can be treated in a satisfactory fashion by employing some variant of unimolecular rate theory. A key question must be whether dissociative processes (well characterized by RRKM theory) or highly efficient energy transfer dominates these high temperature environments. We suggest that some answers to this question can be obtained by monitoring the pressure dependence of the chemiluminescence over pressure ranges extending from the near single collision regime (e.g., Fig. 10) to the relaxed multiple collision regime (e.g., Fig. 11).

An expansion of the studies we have outlined, using a combination of CL and LIF techniques, can be employed to carefully define the periodicity of

complex formation, and the importance of electronically induced pathways for energy flow. In the final analysis, these effects are associated with dihalide molecular electronic structure and its attendant effect on the dynamics of halide formation. They should, however, be manifest in all high temperature environments. A demonstrated collisional stabilization not readily explained within the RRKM framework suggests that new or highly modified models will be necessary to explain the efficient interaction of electronically excited states as well as highly vibrationally excited ground states. The data from this study now begin to provide important information on the efficient stabilization of excited state intermediate complexes, defining a much broader range of interaction than has typically been associated with collisional stabilization phenomena. The demonstrated interaction range of the dihalides (and the enhanced interaction of high temperature molecules in general) has direct implication for the understanding of molecular formation and energy transfer in those environments which characterize systems operating under extreme conditions. A neglect of these phenomena in models of chemical lasing, combustion, propulsion, or shock driven phenomena renders these descriptions unrealistic.

NEAR RESONANT ENERGY TRANSFER FROM METASTABLE ENERGY STORAGE STATES OF SiO AND GeO TO FORM ATOM BASED LASER AMPLIFIERS

We have found that certain near resonant intermolecular energy transfers proceed with extremely high cross sections. We have discovered an exciting family of reactions that efficiently transfer energy from the metastable triplet states of SiO^* and GeO^* to pump select excited states of several atoms. So efficient are these transfers that they have been used to produce superfluorescence from Tl^{37} and $\text{Ga}^{37,38}$ atoms at 535 and 417 nm and amplified spontaneous emission (ASE) from Na atoms³⁷ at 569, 616, and 819 nm (Appendices VIII, IX) and K atoms at 581 nm. The energy stored in the metastable triplet states, formed from the $\text{Si}(^3\text{P}) + \text{NO}_2$, $\text{N}_2\text{O}^{39,40}$ and $\text{Ge}(^3\text{P}) + \text{O}_3^{41}$ reactions, is transferred to pump (Fig. 12) $\text{X}^2\text{P}_{1/2}$ Tl atoms to their lowest lying $^2\text{S}_{1/2}$ state³⁷ and (Fig. 13) $\text{X}^2\text{S}_{1/2}$ Na atoms³⁷ to their excited $3\text{d}^2\text{D}$, $4\text{d}^2\text{D}$, and $5\text{s}^2\text{S}$ states. Adopting a pumping sequence in which a premixed Group IVA metalloid-receptor atom combination is oxidized, we observe a system temporal behavior which suggests the creation of a population inversion and gain condition in

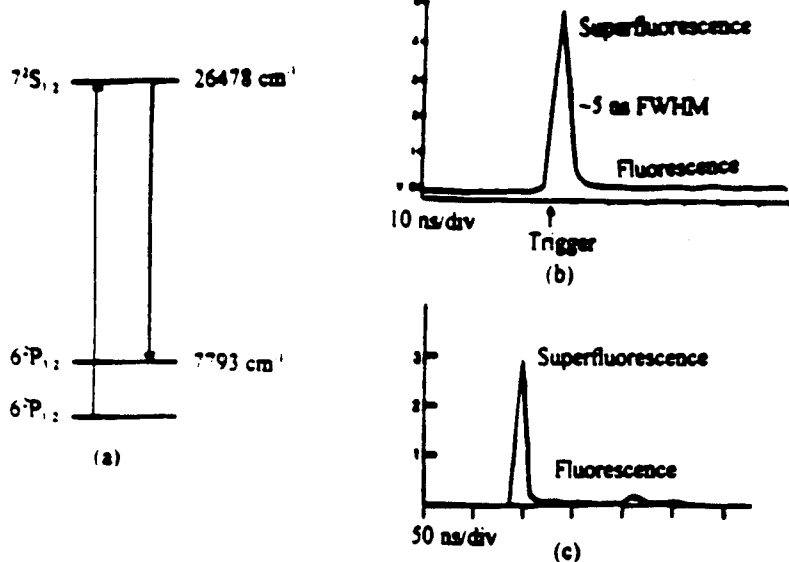


Figure 12

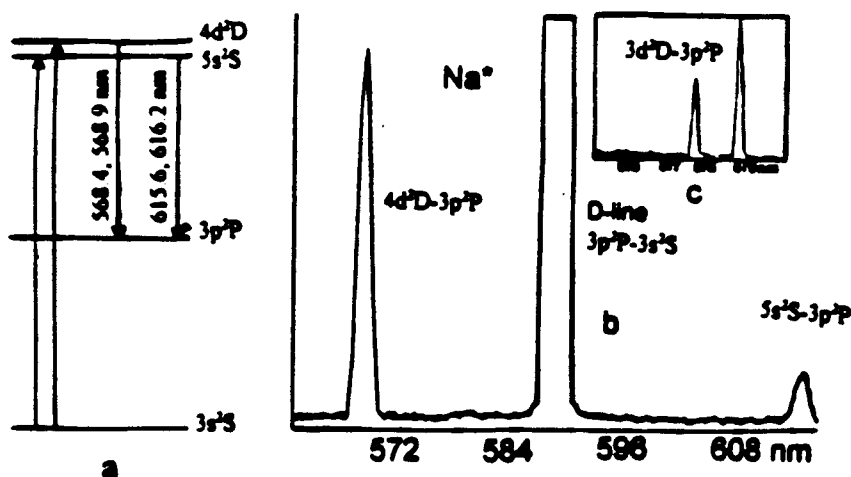


Figure 13

Figure 12(a): Tl atom energy levels.

Figure 12(b): Tl $7^2S_{1/2} - 6^2P_{3/2}$ (535 nm) superfluorescence observed at a signal trigger level of 0.2V (fluorescent level ~ 0.45V). The measured FWHM is < 5 ns (compared to $\tau \sim 7.5$ ns, the radiative lifetime of the $7^2S_{1/2}$ level. A return to the fluorescence level is seen subsequent to the superfluorescence pulse. No superfluorescent pulse is associated with the Tl $7^2S_{1/2} - 6^2P_{1/2}$ (377 nm) transition.

Figure 12(c): Tl $7^2S_{1/2} - 6^2P_{3/2}$ (535 nm) superfluorescent oscillation observed with full laser cavity configuration. The superfluorescence/fluorescence ratio (fluorescence following termination of lasing action) is in excess of 100.

Figure 13(a): Na atom energy level scheme and pumping cycles to produce $4d^2D$ and $5s^2S$ excited states.

Figure 13(b): Typical energy transfer pumping spectrum for Na $4d^2D - 3p^2P$ and $5s^2S - 3p^2P$ transitions and $3p^2P - 3s^2S$ sodium D-line emission. The D-line emission results both from direct energy transfer pumping from ground state N_2O and from fluorescence to the $3p^2P$ level.

Figure 13(c): Energy transfer pumping spectrum corresponding to the Na $3d^2D - 3p^2P$ transition.

Figure 13(d): Full cavity output created with ~0.2% output coupling for the continuous Si-SiO (Si-N₂O) - Na amplifier at 569 nm. The full cavity output is compared to that obtained with both a blocked high reflector and with the entire cavity isolated from the signal detection system. The ratio of the output obtained for the full cavity to that obtained with a blocked high reflector exceeds $10^3/1$.

the Tl and Na systems, forming the basis for short pulse full cavity oscillation on the Tl $7^2S_{1/2} - 6^2P_{3/2}$ transition at 535 nm (Appendix I) and continuous oscillation on the Na $4d^2D - 3p^2P$ transition at 569 nm. The continuous oscillation associated with the sodium system (Appendices VIII, IX), in particular, demonstrates an astounding energy transfer efficiency.

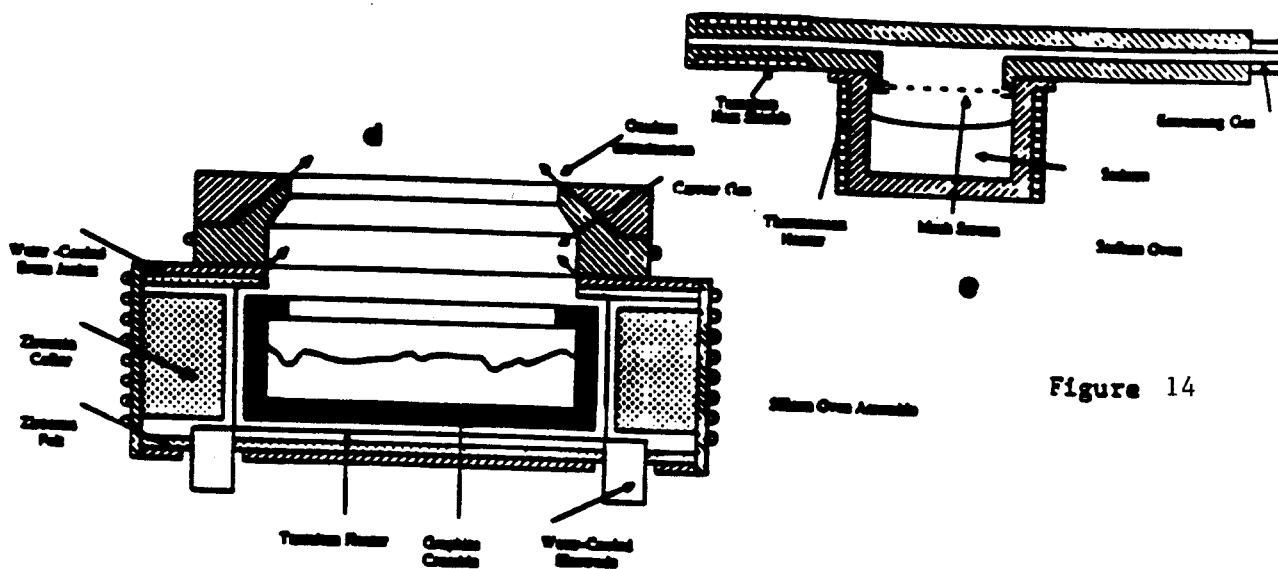
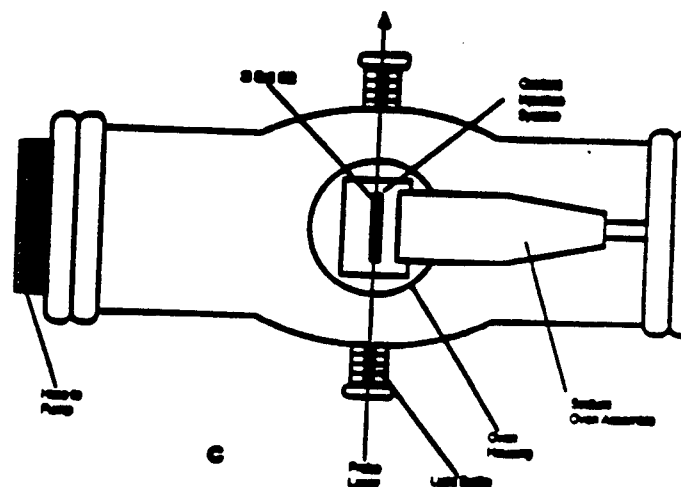
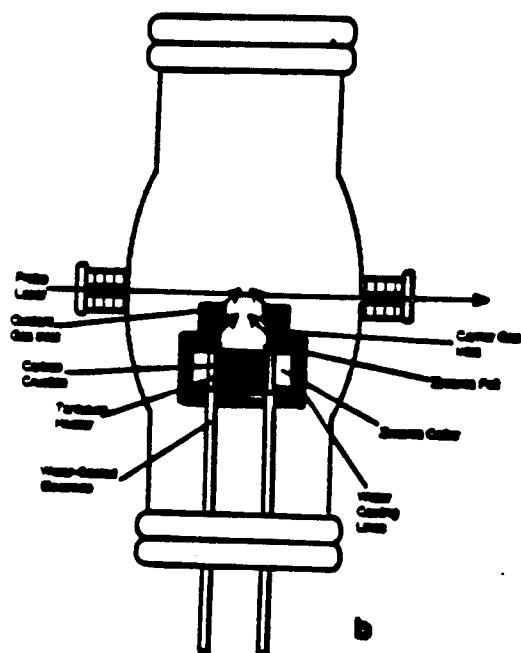
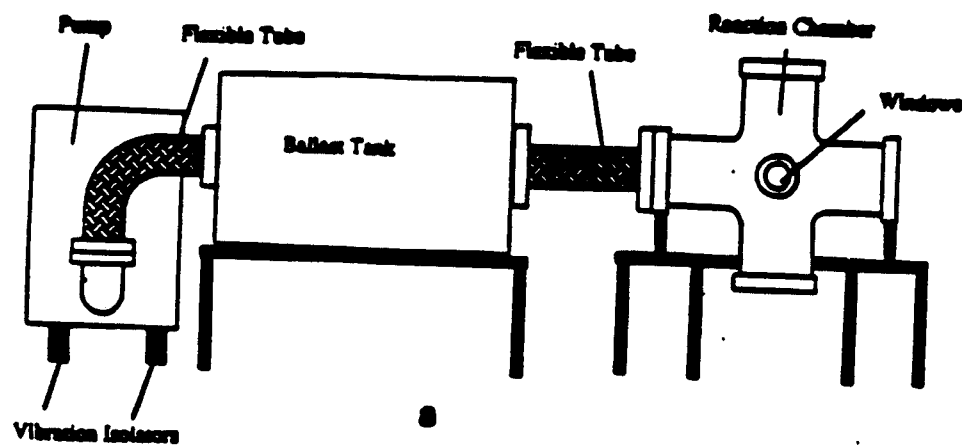
One might envision the SiO and GeO " $a^3\Sigma^+$ " and " $b^3\Pi$ " states forming a combined metastable triplet state reservoir which is, at best, weakly coupled to the ground electronic $X^1\Sigma^+$ state (minimal nonradiative transfer). This reservoir can be maintained and can transfer its energy to pump the atom of interest if a near resonant energy transfer is feasible. This approach is outlined in more detail in Appendices I, VI, IX, and XI.

We have used SiO metastables formed in the Si-N₂O reaction, to successfully energy transfer pump Na atoms to their low-lying $5s^2S$ and $4d^2D$ levels from which they subsequently emit radiation at $\lambda \approx 616$ nm and 569 nm as they undergo transition to the $3p^2P$ levels. The accessed Na cycle with its 50^{42} ($4d^2D - 3p^2P$) to ~ 100 nanosecond upper state radiative lifetimes (vs. for example Tl $2^2S_{1/2}$ at $\sim 7_{\text{nsec}}$.⁴³) and short-lived terminal laser level would appear ideally suited to obtain higher duty cycle laser amplifiers and oscillators. We also obtain evidence for the energy transfer pump of the Na $3d^2D$ level with which is associated an atomic emission at $\lambda \approx 819$ nm ascribed to the Na $3d^2D - 3p^2P$ transition.

In order to study amplification in the sodium and potassium systems, we have constructed a relatively versatile device (Fig. 14) (see also Appendices VI, IX, XI) which allows us to obtain a moderately long amplification path length.¹⁶ This construction can take advantage of three entrainment flow configurations for silicon or germanium in the cycle producing SiO and GeO metastables, one of which is depicted in Fig. 14. These flow configurations produce one of the longest path length SiO metastable flames (5 + cm) yet obtained. The entrainment flow configuration must be designed to create large concentrations of SiO (GeO) metastables which are intersected at $\sim 90^\circ$, in subsonic flow, by a high concentration of sodium or potassium atoms. The entrained (argon, helium, nitrogen) silicon and sodium flows can also be moved in-situ relative to each other and hence with respect to the reaction - energy transfer - amplification zone to optimize conditions for formation of the gain medium.

The entrainment flow device depicted in Figure 14 can be surrounded by a

Figure 14: (a) Schematic of reaction chamber and windows defining optical train, ballast tank to moderate pumping fluctuations, and pumping configuration, for extended path lengths Si-SiO (Si-N₂O)-Na reaction amplification zone. (b),(c) Side and overhead views of reaction chamber showing positioning of Si oven source, relative locations of Si and Na oven sources, oxidant injection system, and relative positions of these devices with respect to the optical train. (d),(e) Closeup view of silicon and sodium oven assemblies. (f) Schematic overview of reaction chamber-amplification zone, ballast, and pump for extended path length Si-SiO(Si-N₂O)-Na gain medium. The figure indicates the course alignment path (~ 15 ft) for the HeNa laser and its correlation with the optical train surrounding the reaction zone and terminating at the monochromator.



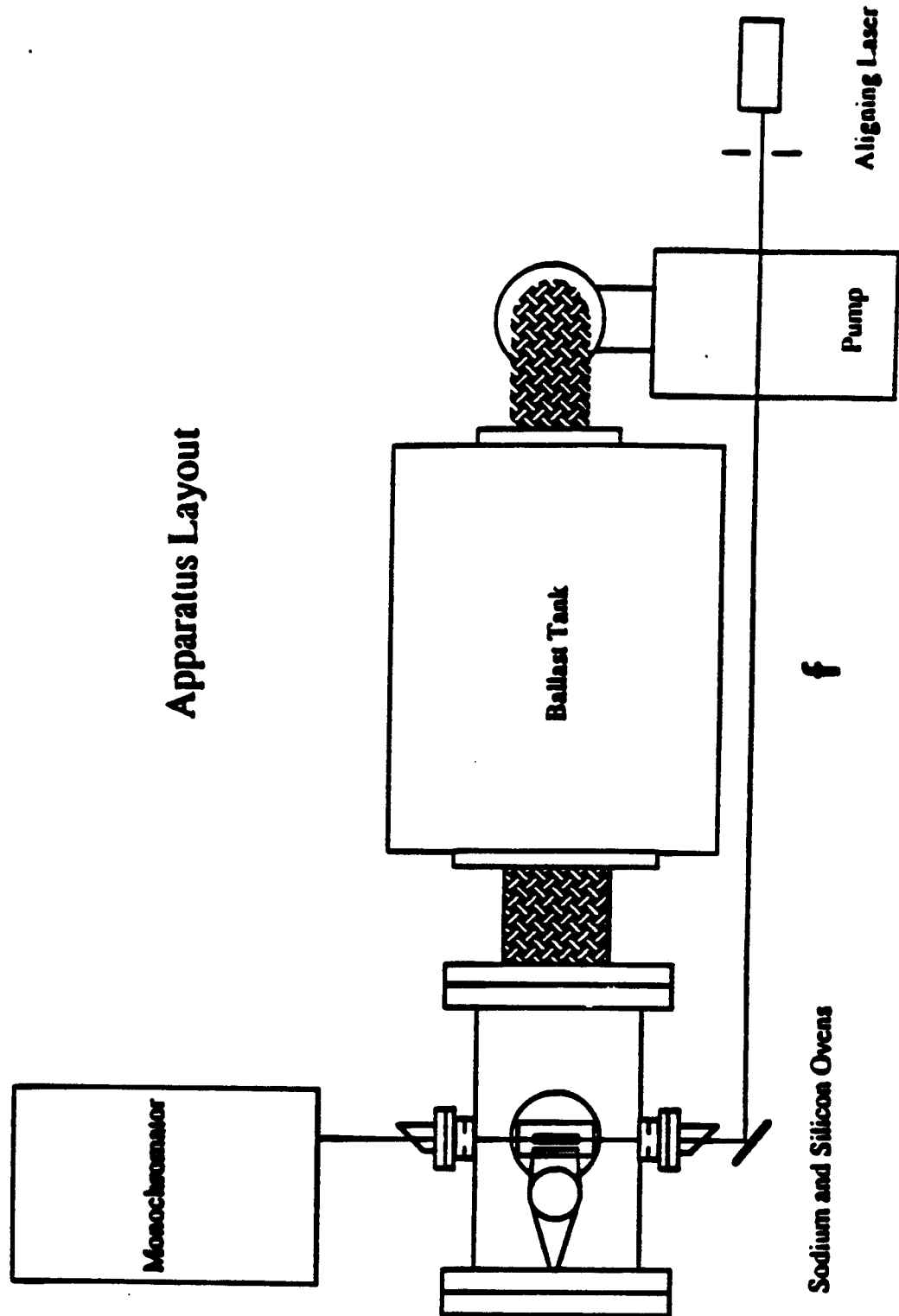


Figure 14

variety of optical trains to measure gain and lasing in the Si-SiO-Na system. These are discussed in detail in Appendices VIII and XI. The three sodium atom transitions at $\lambda \approx 569$ nm ($\alpha \approx 0.1-0.15/\text{cm}$), $\lambda \approx 616$ nm ($\alpha \approx 0.03-0.05/\text{cm}$), and $\lambda \approx 819$ nm ($\alpha \approx 0.02-0.03$) demonstrate continuous gain, although optimal gain on each line is monitored under slightly different mixing in the amplification zone (App. VIII). The gain has been measured (Appendices VIII, XI) at all three wavelengths using the ingenious design of Roll and Mentel.⁴⁴ We compare the (paraxial) single vs. double pass amplified spontaneous emission emanating from the 5 cm amplification zone of Fig. 14. Further, at 569 nm, two additional gain measurements have been performed (Detailed - Appendix VIII), one deducing the amplification of the $4d^2D - 3p^2P$ transition from a sodium discharge lamp and a second employing a scanning single-mode ring dye laser. Preliminary measurements at 616 nm using the sodium discharge lamp also demonstrate a continuous gain condition.

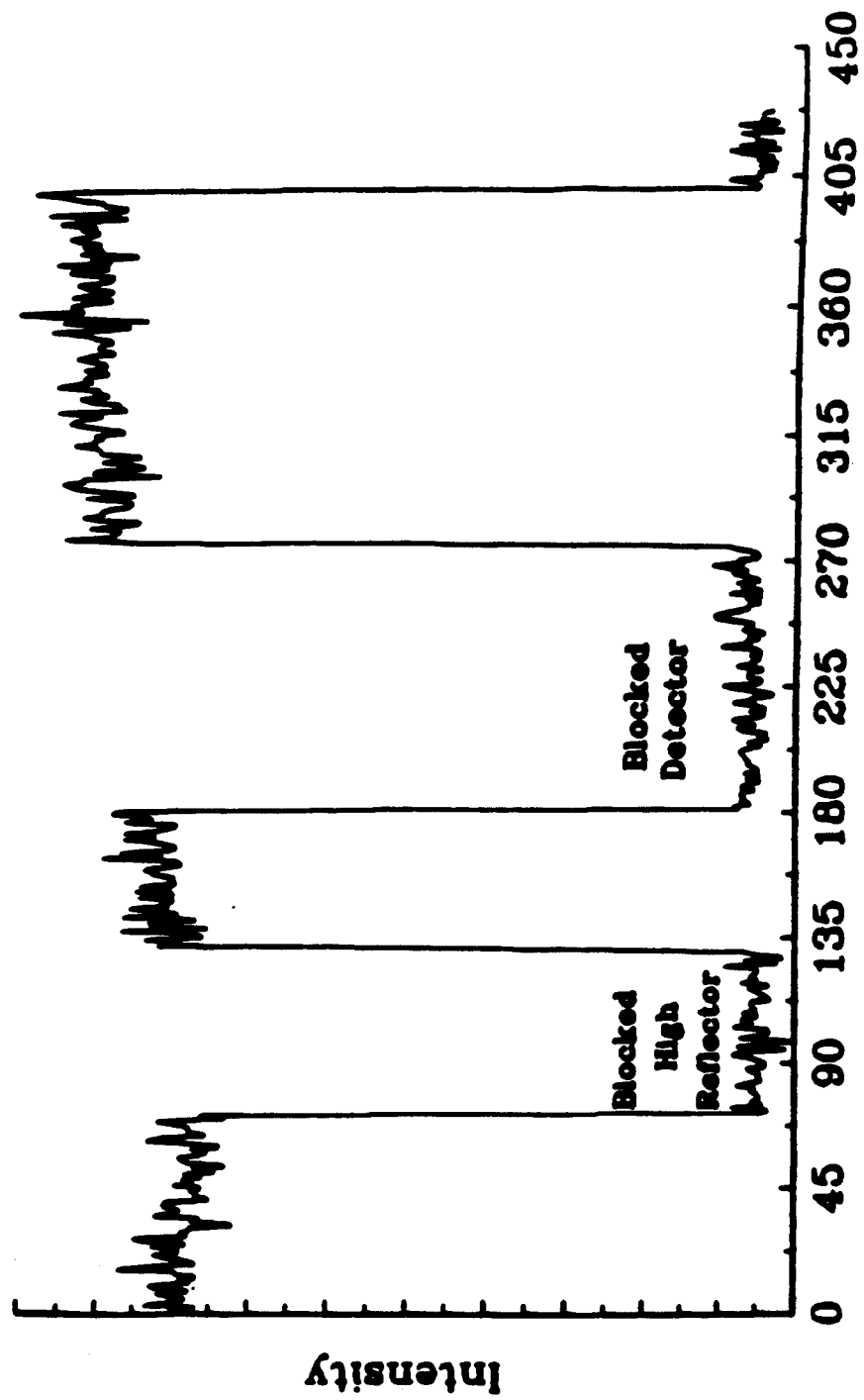
"Full Cavity Measurements"

Full cavity measurements (detailed in Appendices VIII, IX) have also been made on the sodium system. The results of these measurements at 569 nm for a 0.2% output coupled stable cavity configuration are shown in Figure 15. We find that the ratio of the output for full cavity operation to that obtained with a blocked high reflector easily exceeds 10^3 . Compare also the signal level observed with the blocked high reflector and that monitored with a completely blocked detector. The corresponding ratio obtained operating the full cavity below threshold using the 0.2% output coupled cavity was slightly greater than 1.8 for the Na D-line. These results clearly indicate continuous laser oscillation in the sodium system.

The value slightly greater than 1.8 for the Na D-line should be compared to a maximum of 1.2 for a much more lossy 4.5% output coupled device ($g_{1g2} \approx 0.56$). In fact, a maximum (full cavity/blocked reflector) ratio of order 1.9-1.95 is typical for all those wavelengths considered ($\lambda \approx 569, 616$, Na D-line) when conditions in the reaction-amplification zone are such that no gain is monitored. We have also observed intermediate behavior associated with the establishment of moderate but not optimal gain conditions.

Figure 15: Full cavity output created with $\sim 0.2\%$ output coupling for the continuous Si-SiO(Si-N₂O)-Na amplifier at $\lambda = 569$ nm. These measurements were taken in continuous flow with the cavity configuration depicted in Fig. 3(b). The full cavity output is compared to that obtained with both a blocked high reflector and with the entire cavity isolated from the signal detection system. The ratio of the output obtained for the full cavity to that obtained with a blocked high reflector exceeds $10^3/1$.

Resonant Cavity



Time (arbitrary unit)

Improvement of the Energy Transfer Based Configuration - Ultimate Goals

A. Concentric Reactant Mixing

While the outlined configurations have been used to demonstrate lasing action in the visible region, this should be substantially enhanced with several improvements in the manner in which the lasing medium is created and the laser output is extracted from the cavity. The mixing zone depicted in Figure 14 is greatly stabilized by the moderate sized (~ 15 cubic feet) ballast separating the 150 cfm pump and reaction chamber. While this insures that the 90° intersection of the SiO and sodium atom flows can be used to establish a continuous lasing action, the 90° reactant intersection is by no means optimal. It remains to increase both the rate limiting silicon and sodium atom concentrations in the reaction zone while maintaining atomization. A logical way to approach this problem involves the conversion of the intersecting flow configuration of Figure 14 to a concentric interaction configuration. We are currently testing and modifying the two designs depicted in Figure 16 (see also Appendices IX and X) as a means of attaining higher reactant - amplifying medium concentrations. These two designs attempt to create a more efficient mixing of those constituents forming the amplifying medium. In both designs, the sodium source is now placed directly above the silicon source, however, the designs differ in the sequence in which they introduce the reactants. One design (Fig. 16(a)) first creates the SiO metastables through the Si-N₂O reaction and subsequently interacts the entrained metastables with an entrained Na flow. In a slightly modified design (Fig. 16(b)) we attempt to premix concentric entrained flows of silicon and sodium, oxidizing the mixture with N₂O. The two designs both result in a substantial enhancement of reactant concentration and mixing as evidenced by the significant ~ 100 fold increase in light emission from the reaction zone as monitored through a side-angle viewing port. However, they also produce a significant increase in particulate matter and gas phase condensibles for which the current pumping system does not appear to be well suited. These condensibles have the attendant affect of degrading cavity windows, substantially increasing loss elements in the optical train. With some modification of the pumping system, the realignment of entrainment flows, the modification of entrainment gases to best suit the chemistry of the system, and the adjustment of window protecting flows, these problems should be

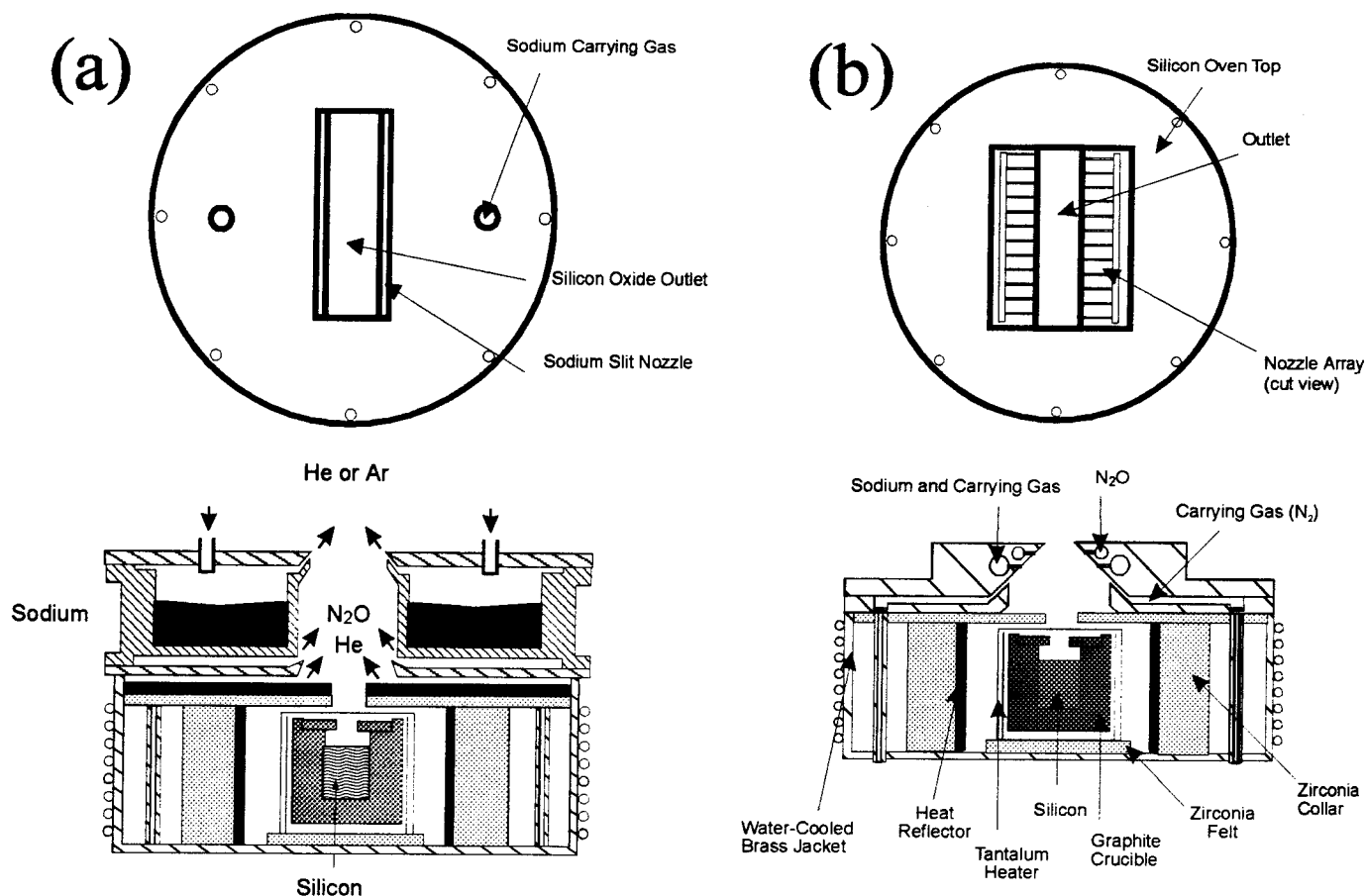


Figure 16(a):

Concentric configuration for energy transfer pumping. The sodium oven is placed above the silicon oven. The oxidant N_2O is introduced into the silicon flow to form SiO^* which then interacts with sodium vapor. The energy transfer zone is approximately 1" above the silicon oven.

Figure 16(b):

Concentric configuration for energy transfer pumping with a sodium and N_2O injector nozzle array placed above the silicon oven. In this configuration the sodium and silicon are mixed before the oxidant is introduced to initiate the energy transfer process.

Sodium Atomic Emission SiO-Na Energy Transfer

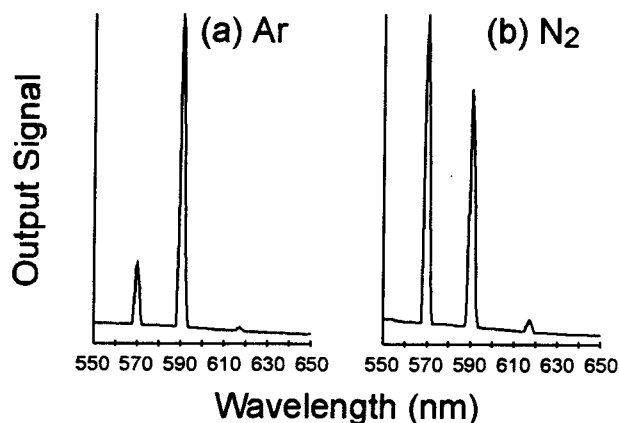


Figure 17:

Energy transfer pumping spectra obtained for (a) Ar and (b) N_2 entrainment. The observed Na $4d^2D - 3p^2P$ emission feature (~ 569 nm) is seen to increase precipitously in intensity relative to the Na $3p^2P - 3s^2S$ D-line (~ 590 nm) with change of entrainment gas from Ar to N_2 .

greatly alleviated.

B. Considering Self Absorption and Self Quenching

The increase of reactant concentrations may lead to a leveling off and eventual loss of the gain condition if self-absorption on the Na D-line transitions becomes a dominant factor or SiO triplet self-quenching begins to play a deleterious role. Evidence is obtained for some self-absorption at the highest sodium concentrations when the alkali atom production dominates the concomitant SiO metastable production. With our sodium atom source operated, in the absence of interacting silicon or N₂O, at the temperature which we have employed to produce the highest flux densities in the amplification zone, we have measured the attenuation of the Na D-line emission from a sodium discharge lamp. We find an attenuation which is much less than 50%. In combination with the cross section for self absorption, $4 \times 10^{-14} \text{ cm}^2$, as measured by Ermin et al.,⁴⁵ this suggests a sodium atom concentration close to that estimated for the system (Appendices VIII, IX, XI). Of course, in the presence of the N₂O and silicon reactants, the attenuation due to self absorption, while evidenced, is considerably diminished ($\sim 5 - 10\%$).

Although concern with the possible deleterious effect which a pumping of the Na D-line might have on transitions terminating in the 3p²P level is somewhat alleviated in the present system by the sodium discharge experiments of Tribilov and Shukhtin,⁴⁶ and the 0.01 second duration laser pulse for the Na 4s²S - 3p²P infrared transition observed by Mishakov and Tkachenko⁴⁷ as quasicontinuous lasing, it must eventually limit the size of the laser systems. However, this might be forestalled to great degree if we take advantage of the efficient quenching of Na 3p²P atoms which Tanarro et al.⁴⁸ have demonstrated for N₂ and CO. In fact, as demonstrated in Figure 17, if we replace the Si-SiO and Na entraining argon or helium gases with N₂, we observe a pronounced effect on the energy transfer spectrum taken for an intermediate sodium flux.

C. Nitrogen vs. Argon Entrainment

While the 569 nm feature is dominated by the Na D-line emission when argon is used as an entrainment gas, its intensity can be made to exceed that

of the D-line when N_2 is used. This result, obtained and repeated for successive scans taken during the same experimental run, suggests the possibility for a considerable enhancement of the 569 nm output. This improvement might well result from the quenching of $Na\ 3p^2P$, however, it might also result from an increased inhibition of the $Na + N_2O \rightarrow NaO + N_2$ reaction as the equilibrium is forced toward reactants.⁴⁹

D. Output Coupling

The experiments conducted thusfar have made use of two distinct output coupling configurations. As well as improving reactant concentrations the optimum output coupling for the current cavity remains to be evaluated. We have constructed a modification which will allow removal of the cavity windows that represent significant loss elements. With these improvements and further collaboration in both cavity and output coupling design with Professor Lee Sentman and his group at the University of Illinois,⁵⁰ the output from our full cavity configuration should be substantially enhanced.

System Modeling

Recently, Smith et al.⁵¹ carried out a laser chemistry modeling effort on the SiO-Na system. Starting with the initial concentrations of the reactants Na, Si, and N_2O which are achievable in the present system these authors have used a model which includes the 10 possible processes

1. $Si + N_2O \rightarrow SiO^* + N_2$ - metastable excited state formation.
2. $Si + N_2O \rightarrow SiO + N_2$ - ground state formation - power depleting.
3. $SiO^* + Na \rightarrow SiO + Na^* (4d^2D)$ - upper state amplifying transition.
4. $SiO^* + Na \rightarrow SiO + Na^* (3p^2P)$ - terminal level amplifying transition.
5. $SiO^* + SiO^* \rightarrow SiO + SiO$ - self quenching of SiO metastables.
6. $Na^* (4d^2D) \rightarrow Na^* (3p^2P) + h\nu (569\text{ nm})$ - spontaneous emission.
7. $Na^* (4d^2D) + h\nu (569\text{ nm}) \rightarrow Na^* (3p^2P) + 2h (569\text{ nm})$ stimulated emission.
8. $Na^* (3p^2P) + h\nu (569\text{ nm}) \rightarrow Na^* (4d^2D)$ - optical pumping.
9. $Na^* (3p^2P) \rightarrow Na^* (3s^2S) + h\nu (569\text{ nm})$ - spontaneous emission.
10. $h\nu (569\text{ nm}) \rightarrow h\nu (569\text{ nm})$ outcoupling fraction for 569 nm photons (laser cavity 5 cm in length - mirror reflectivities 99.99 and 99.80%.

Using known kinetic rates, variable initial concentrations, reasonable

and variable rates for those processes which have not been directly measured, and assuming a closed reaction in which the reactants are not replenished, Smith et al.⁵¹ have deduced temporal profiles for the Na concentration, 569 nm photon concentration, energy density, and power density. They conclude that order of magnitude increases in the initial concentration of Si or N₂O have a profound effect on the system (power density increase) whereas significant changes in the Na concentration have relatively little effect. This signals the rate limiting nature of the silicon concentration and the importance of the branching into the metastable triplet states. It is also to be noted that a significant increase in power density may be muted by SiO* self quenching, the rate of which certainly must be established for these systems. For the diversity of initial reactant concentrations and rates used in their model, Smith et al.⁵¹ predict output power densities peaking between 100 (strong SiO* self quenching) and 7000 mW/cc. These results are quite encouraging.

Extension of Near Resonant Intermolecular Energy Transfer Concept to Additional Energy Transfer Pumped Atomic Receptors

While we have emphasized the results obtained thusfar for the sodium system based on an SiO metastable pump, it is also feasible to use GeO metastables. In fact, we have obtained evidence that the energy transfer pumping of the sodium analog potassium based amplifiers associated with the $5d^2D - 4p^2P$ ($\lambda = 581, 583$ nm), $4d^2D - 4p^2P$ ($\lambda = 694, 697$ nm), and $6s^2S - 4p^2P$ ($\lambda = 691, 694$ nm) potassium atom transitions might best be accomplished with pumping by GeO metastables.

We have also successfully energy transfer pumped potential amplifying transitions in lead (Pb), copper (Cu), and tin (Sn) receptor atoms. Two of these systems are particularly intriguing. Figure 18 demonstrates the results we have obtained when interacting SiO metastables (Si-N₂O) with lead receptor atoms (see also Tables III and IV - Appendix XI). Observed Pb transitions are indicated to the right of the figure. First, we notice that self absorption involving ground state Pb atoms is so dominant that no emission to the X ³P₀ ground state is observed. Second, we find significant pumping of both the ¹S₀ and ¹D₂ levels. The corresponding transitions from the ¹S₀ level terminate in the lowest X ³P₂ (531.2 nm) and X ³P₁ (462 nm) levels. It is thought that

Figure 18: Comparison of lead - SiO ($A^3\Sigma^+, b^3\Pi$) near resonant energy transfer spectra. Metastable SiO molecules were created in the reaction $\text{Si} + \text{N}_2\text{O} \rightarrow \text{SiO}^* + \text{N}_2$. (a) The spectrum corresponds to a portion of the SiO metastable emission spectrum before lead atoms are brought into the reaction zone. (b) Spectrum recorded with high Pb flux (\sim torr vapor pressure) showing the manifestation of energy transfer pumping to produce electronically excited $^3\text{P}^0$, $^1\text{S}_0$ and $^1\text{D}_2$ levels of the lead atom. (c) Energy levels for the lead atom with observed transitions as indicated in (b).

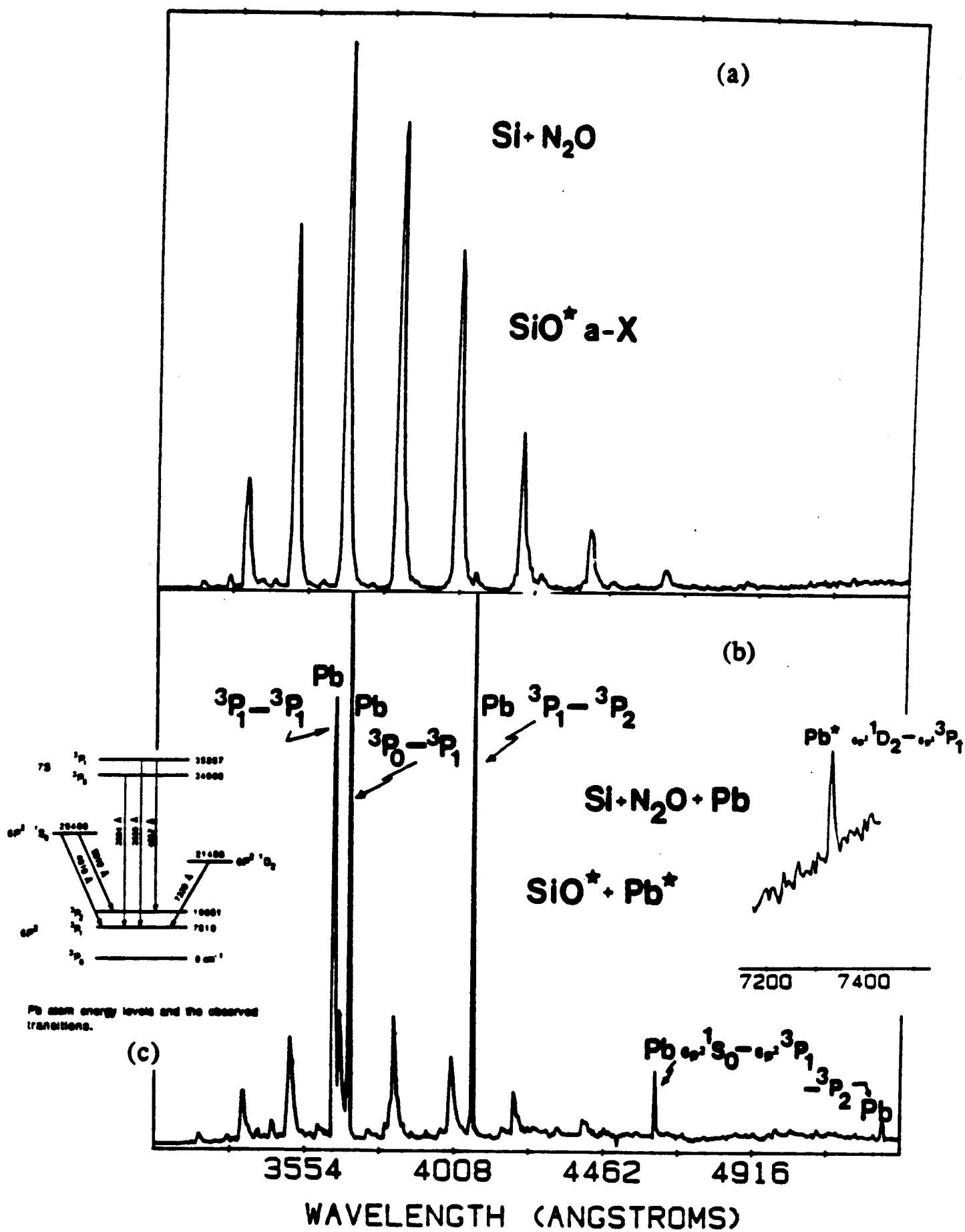


Figure 18

collisional quenching and relaxation of the 1S_0 level will be minimal relative to that of the X 3P manifold.⁵² This may lead to potential inversions and amplification at $\lambda = 462, 531 \text{ nm}$.⁵³ The well known lead laser transition at $\lambda = 723 \text{ nm}$ ⁴⁶ with an A value $\sim 10^6 \text{ sec}^{-1}$ terminates on the 1D_2 level.

Surprisingly, we find no evidence for this transition which emanates from the upper $^3P^0$ level (Fig. 18). We do find evidence for the $^3P_1^0 - X \ ^3P_1$ and $^3P_1^0 - X \ ^3P_2$ transitions and for the $^1D_2 - ^3P_1$ transition at 733 nm .⁵⁴ This suggests that the $^3P_1 - ^1D_2$ transition may be self-absorbed due to a significant 1D_2 population. If we have observed the manifestation of a substantial 1D_2 population, does this result from direct energy transfer pumping or is the 1D_2 state populated by the 723 nm transition at times considerably shorter than the time scale for the present observations? This must be assessed in future experiments. The results obtained for the energy transfer pumping of lead atoms certainly suggest the possibility of additional amplifier systems. It is particularly encouraging that some of these may represent four level systems which obviate the self absorption bottleneck that may plague the Si-SiO-Na system at high Na concentration.

The near resonant energy transfer pumping of copper vapor is of interest not only because of the close analogy which it bears to the sodium and potassium systems but also, as Figure 19 indicates, because it is possible to energy transfer pump the copper vapor laser transitions⁵⁵ (see also Table IV - Appendix XI) using metastable SiO (Si-SiO-Cu system). However, it is also of interest that the results demonstrated in Figure 19 were obtained using an approach which represents a significant extrapolation from the configuration in which a "premixed" Tl/Ge mixture has been used to obtain pulsed amplification on the Tl $^2S_{1/2} - ^2P_{3/2}$ transition.⁴³ Here, Si and Cu were premixed and co-vaporized from a single crucible. The resulting mixture was then oxidized to yield the observed energy transfer pumping spectrum depicted in Figure 19. (It is worth noting that N_2O , used as the oxidant, produces a dark reaction with copper vapor.)

The results presented in Figures 18 and 19 clearly demonstrate that there are intriguing variations on the sodium based system. In fact the level structure depicted suggest that the three level excitation scheme may offer a considerable range of radiative configurations (lifetimes) which can be accessed in near resonant pumping.

Figure 19: Copper - SiO ($a^3\Sigma^+, b^3\Pi$) near resonant energy transfer spectra generated from a "premixed" Si-Cu mixture subsequently oxidized with N_2O . (a) Spectrum showing a portion of the SiO metastable emission, the Cu $2P_{3/2} - {}^2D_{5/2}$ blue green emission line (copper vapor laser) and the Cu $2P_{3/2,1/2} - {}^2D_{3/2}$ yellow-orange emission features. (b) Energy levels for the copper atom.

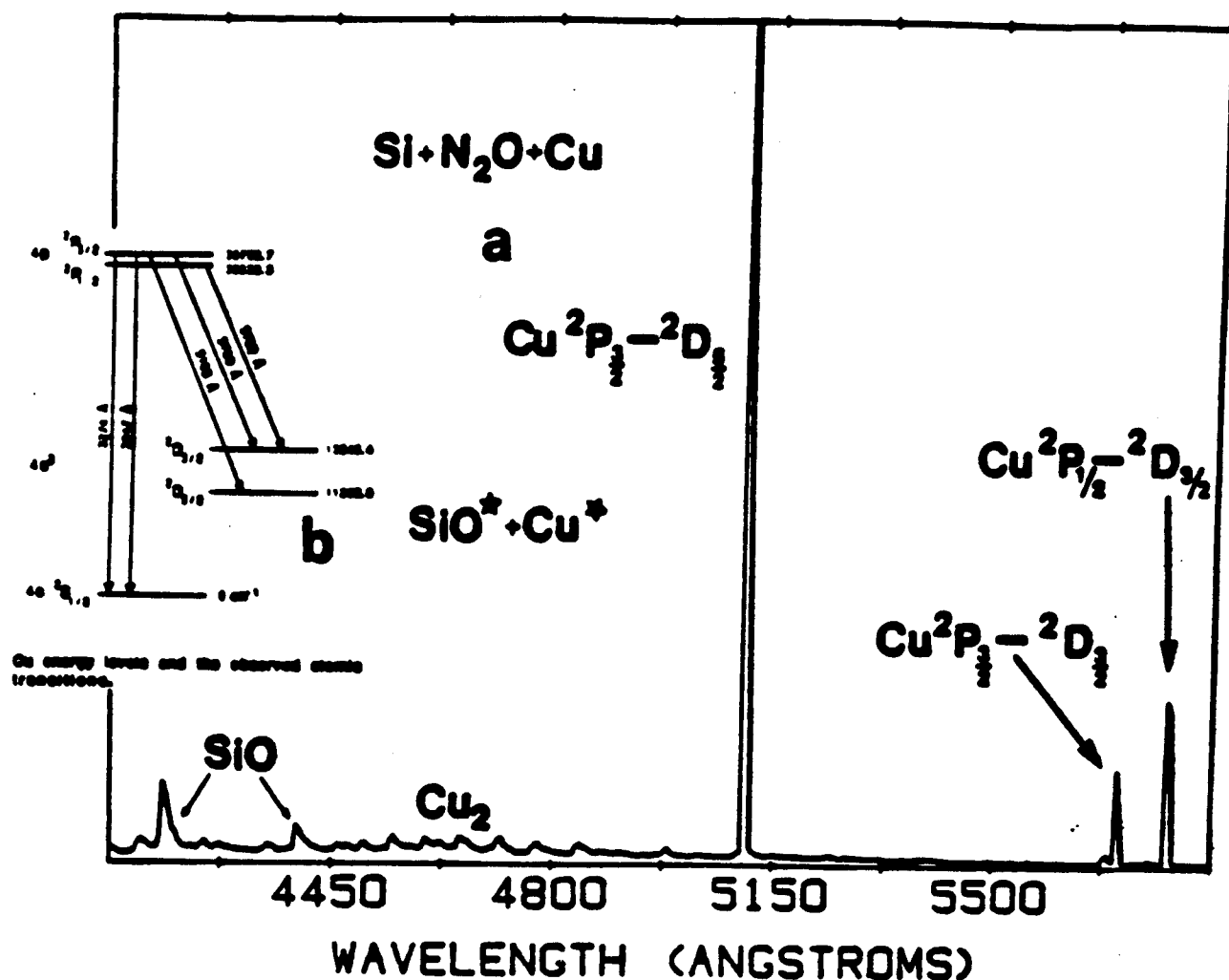
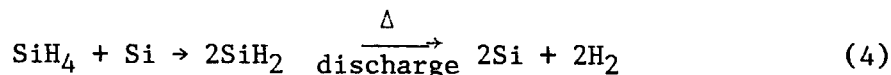


Figure 19 Copper - SiO ($a^3\Sigma^+$, $b^3\Pi$) near resonant energy transfer spectra generated from a "premixed" Si-Cu mixture subsequently oxidized with N_2O . (a) Spectrum showing a portion of the SiO metastable emission, the $\text{Cu}^2\text{P}_{3/2} - ^2\text{D}_{5/2}$ blue green emission line (copper vapor laser) and the $\text{Cu}^2\text{P}_{3/2, 1/2} - ^2\text{D}_{3/2}$ yellow-orange emission features. (b) Energy levels for the copper atom with observed transitions as indicated in (a). See text for discussion.

Improving the Si Atom and SiO Metastable Source Configurations

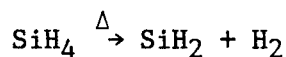
In order to obviate the need for a high temperature source technology to generate the silicon atoms which are subsequently oxidized to form metastable SiO, we have been concerned with the conversion of gaseous silane (SiH_4) in high yield to atomic silicon. The development of a successful device for the generation of silicon atoms and SiO_x species in large yield might also prove useful to the microelectronics industry. The sources which we have constructed and tested can be categorized into three groups involving low temperature thermolysis + subsequent discharge through the products of thermal decomposition, low and elevated temperature thermolysis followed by photolysis, and a hybrid approach which involves the thermolysis of silane over bulk silicon viz.



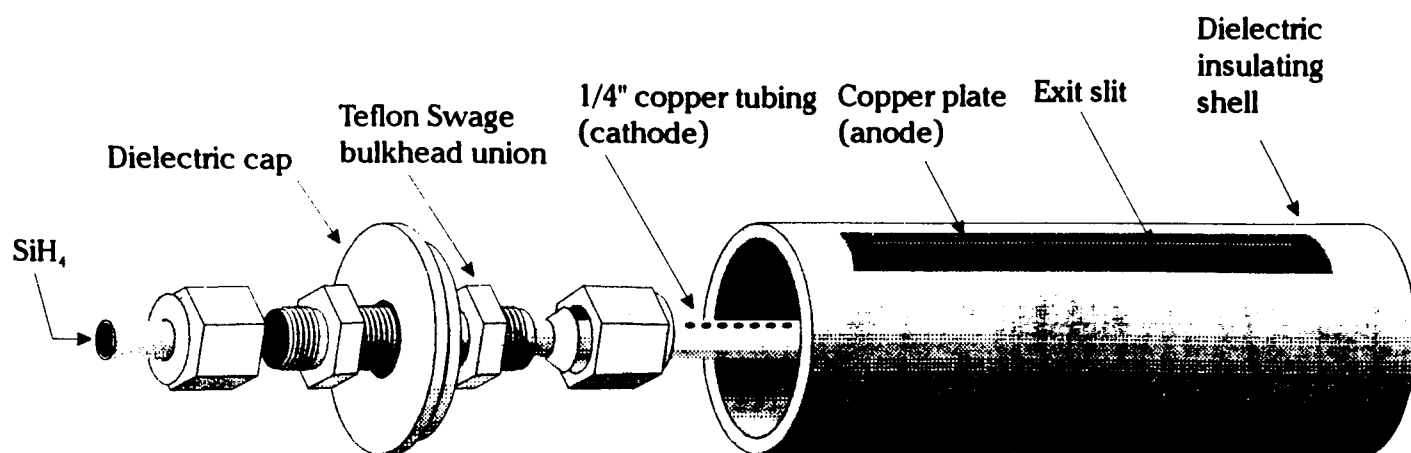
at temperatures considerably below those required to vaporize bulk silicon. Note that the process (4) is attractive because it yields two silicon atoms.

Figure 20 depicts an initial silane discharge configuration where SiH_4 passing into a nozzle arrayed copper tube (representing the cathode) then passes, inside a dielectric insulating shell, to a copper screen covered (anode) exit slit. This configuration, inserted into the previously developed SiO source configuration, replacing the high temperature Si oven (side view Figure 20(b)), has been used in preliminary experiments to pump the B-X transition of molecular bromine. The preliminary results outlined in Figure 21 suggest that well established optically pumped Br_2 (BrCl and IF) lasers with ideal excited state radiative lifetimes (B-X transition) might be accessible to an efficient SiO metastable energy transfer pump quite analogous to that observed for A state nitrogen and the halogens.

The thermal decomposition of silane is thought to be initiated through the reaction



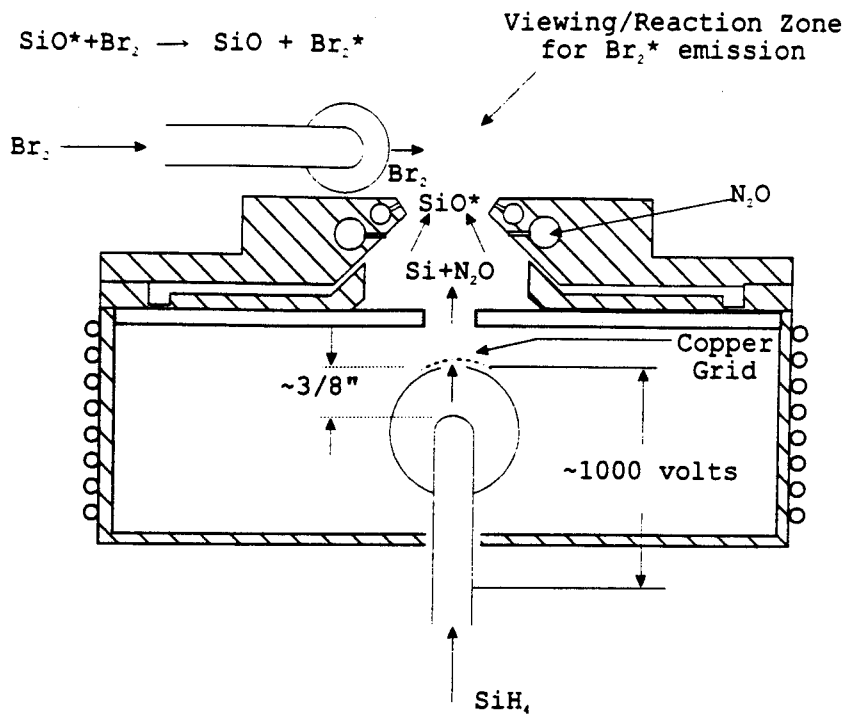
where further decomposition of the silylene (SiH_2) may progress to form atomic silicon and molecular hydrogen. This latter reaction must compete with the



DISCHARGE CONFIGURATION

Figure 20(a)

Side View



SiH₄ - N₂O - Br₂ Mixing Configuration

Figure 20(b)

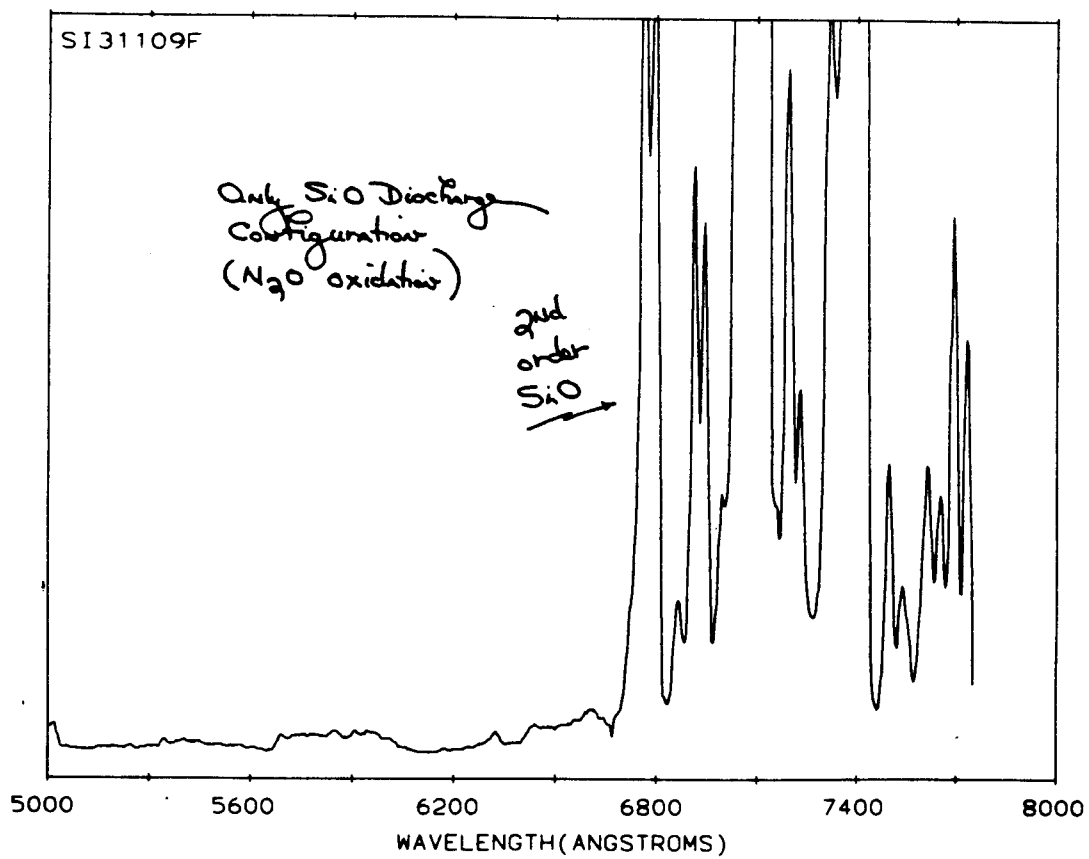


Figure 21(a)

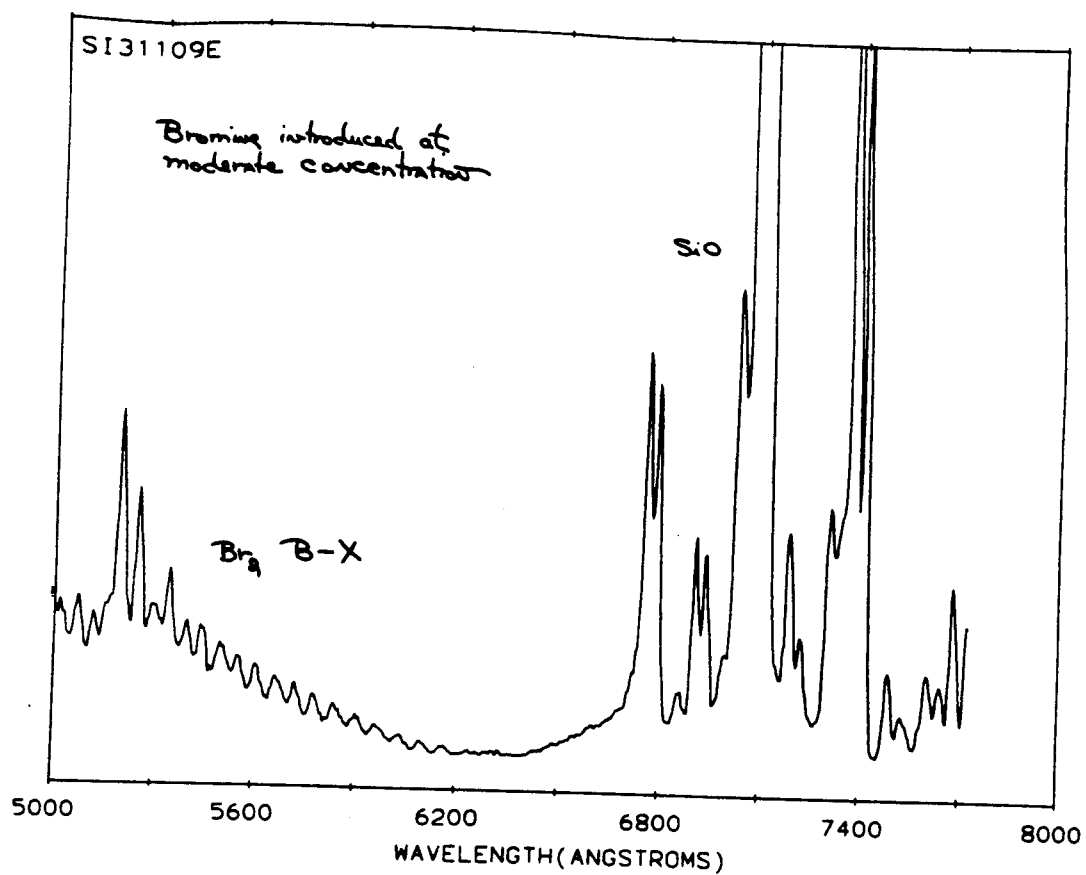


Figure 21 (b)

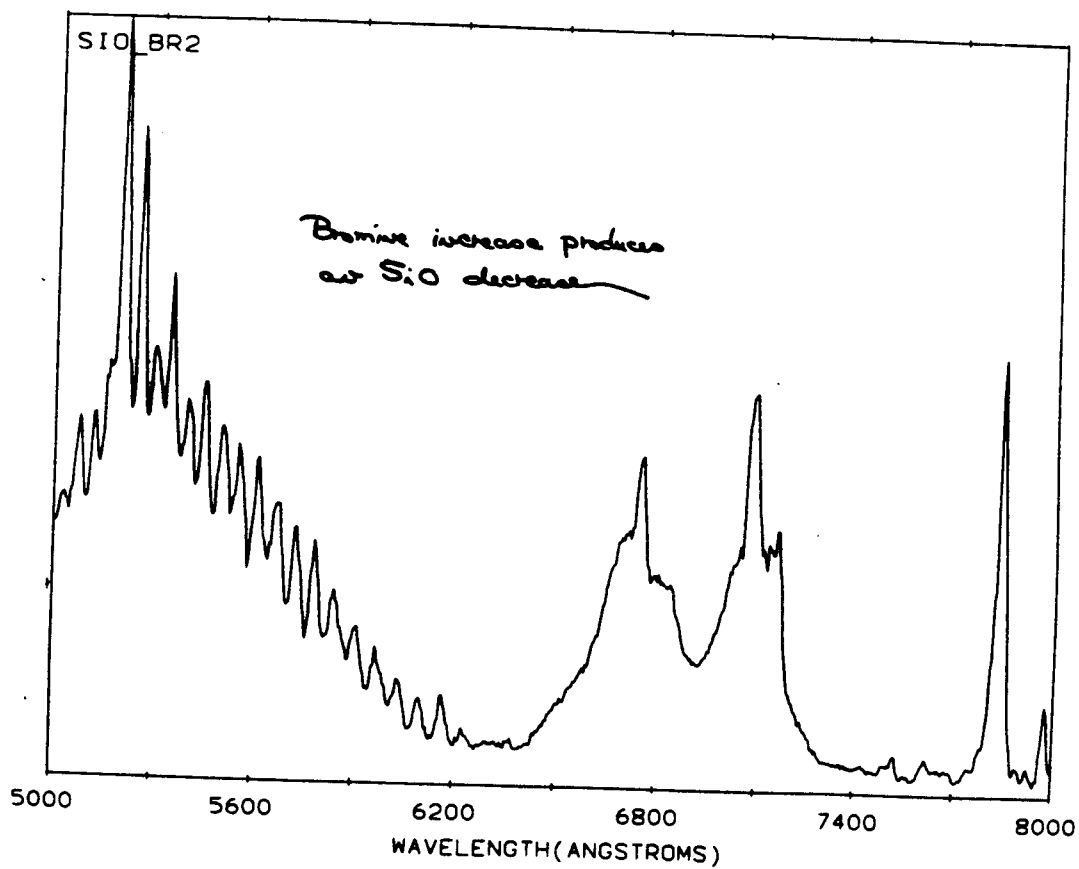


Figure 21 (c)

reaction of silylene and silane to produce higher silanes which can ultimately result in gas phase nucleation without careful control. The reactivity of silylene and silane has been suggested as an explanation for the low concentrations of SiH_2 in electric discharges through silane where it (SiH_2) is predicted to be an important intermediate of the discharged silane decomposition.⁵⁷

The considerations outlined suggest that for the pyrolysis of silane or a combination of pyrolysis and discharge through the thermolizing products to proceed completely to silicon and hydrogen, it should be accomplished in an inert diluent to prevent side reactions. In an attempt to measure the unimolecular decay rate for silylene, Votintser et al.⁵⁸ employed dilutions ranging from 0.0004 - 0.001% of silane in argon in order to study the decomposition in a shock tube environment. These considerations must also be employed when developing a thermolysis based source for the production of metastable SiO .

Figures 22, 23, and 24 indicate several early pyrolysis configurations which have been tested in the High Temperature Laboratory. Here we attempted to pyrolyze the silane directly using either a carbon (Fig. 22), nickel (Fig. 23), or tantalum wrapped ceramic (mullite) tube (Fig. 24), again placed within the modified confines of our previously developed SiO source configuration. We find significant conversion to silicon with all three designs, their limitation resulting primarily from the blockage of inlet and exit ports due to silicon condensation. This clearly signals the need for diluent gas entrainment - flow techniques as a means of limiting condensation of the silicon atoms at temperatures far below the melting point of silicon. These modifications are now under consideration in our laboratory. We are also considering further modifications in conjunction with the reconstruction of the discharge configuration outlined in Figure 20.

Figure 25 outlines a hybrid discharge-pyrolysis source which incorporates the designs of Figures 20 and 23. Here we attempted to pyrolyze the silane in a nickel tube furnace which also acted as the cathode for a discharge configuration. With some modification to include diluent flow in a more open configuration, this silicon source design appears promising.

The design depicted in Figure 26 represents a discharge device in which we attempted to better confine the gas flow by enclosing the silane inlet/electrode assembly in a teflon housing. With a proper balance of diluent gas,

clamped oven configuration for pyrolysis of silane

(Carbon oven held by a set of current carrying clamps.)

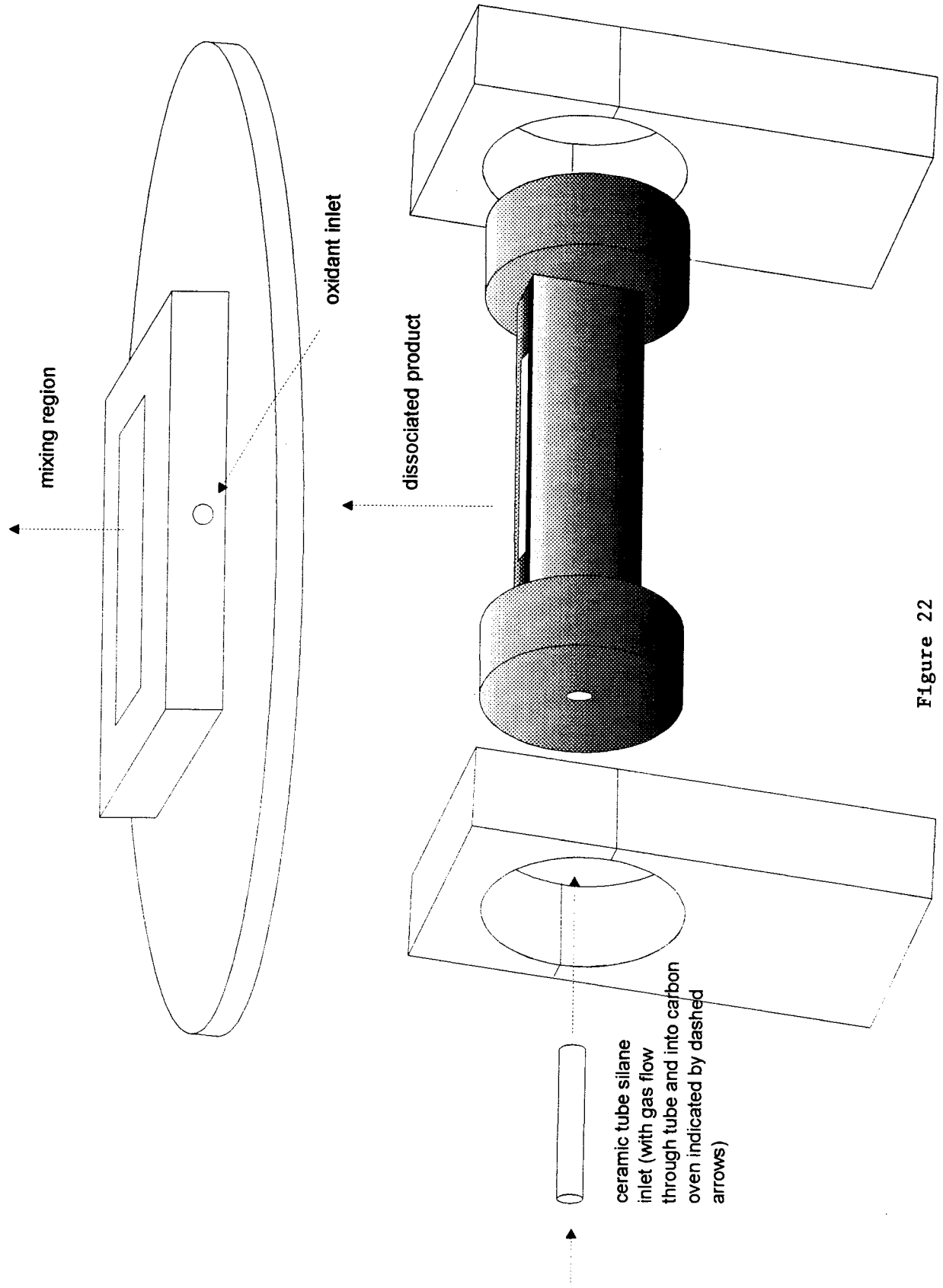


Figure 22

heated nickel tube configuration

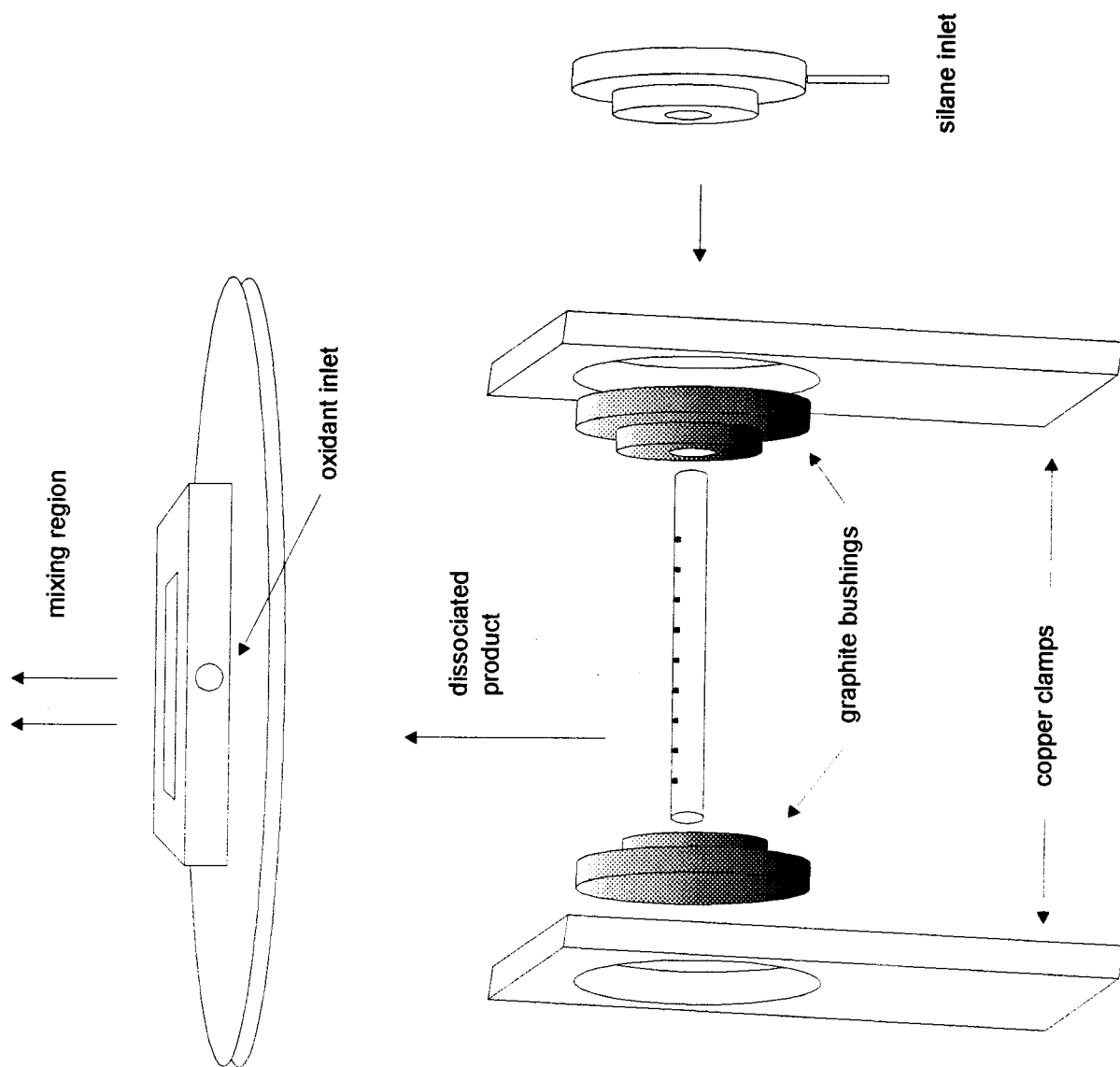


Figure 23

heated mullite tube arrangement

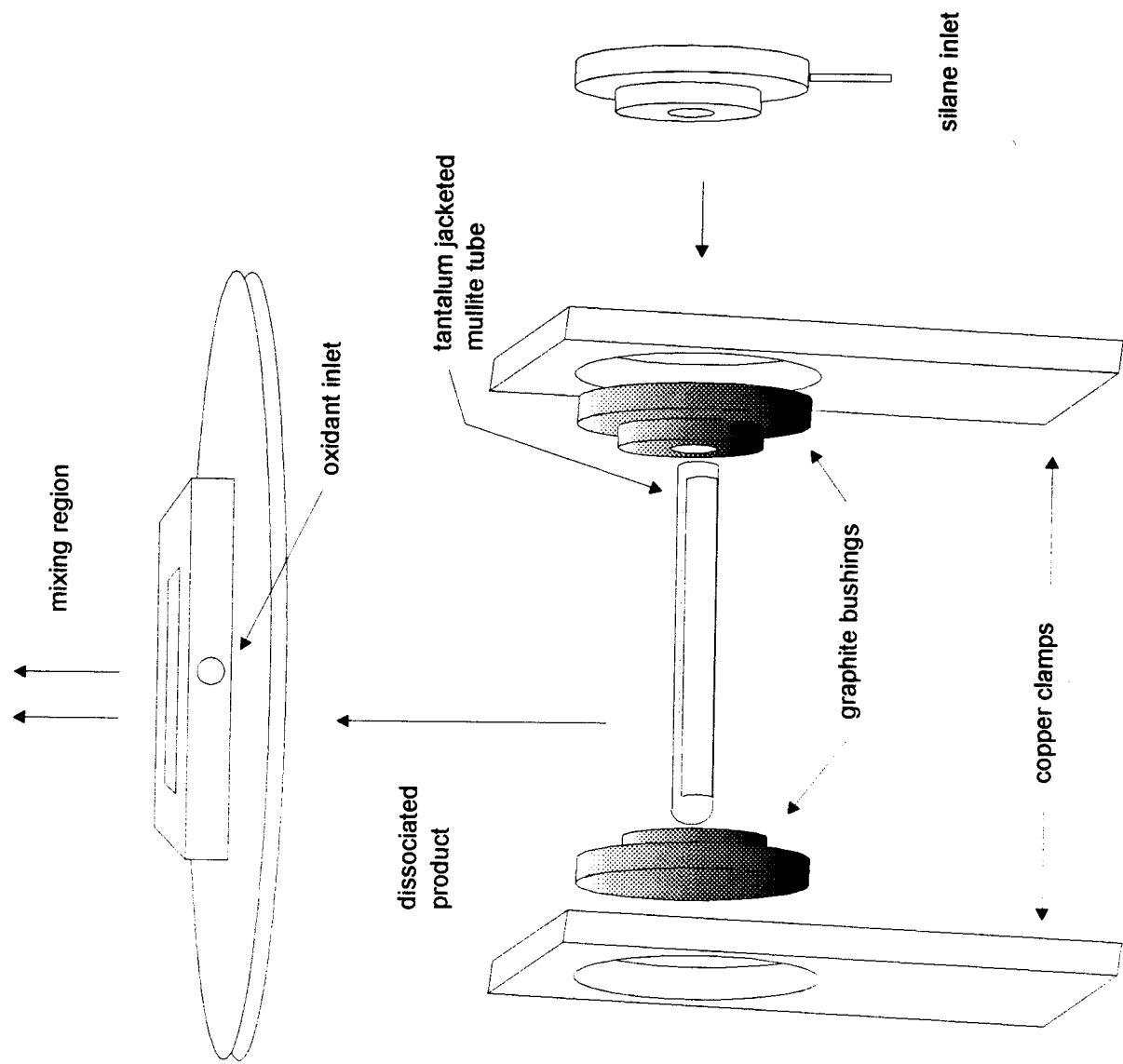


Figure 24

hybrid discharge / pyrolysis arrangement

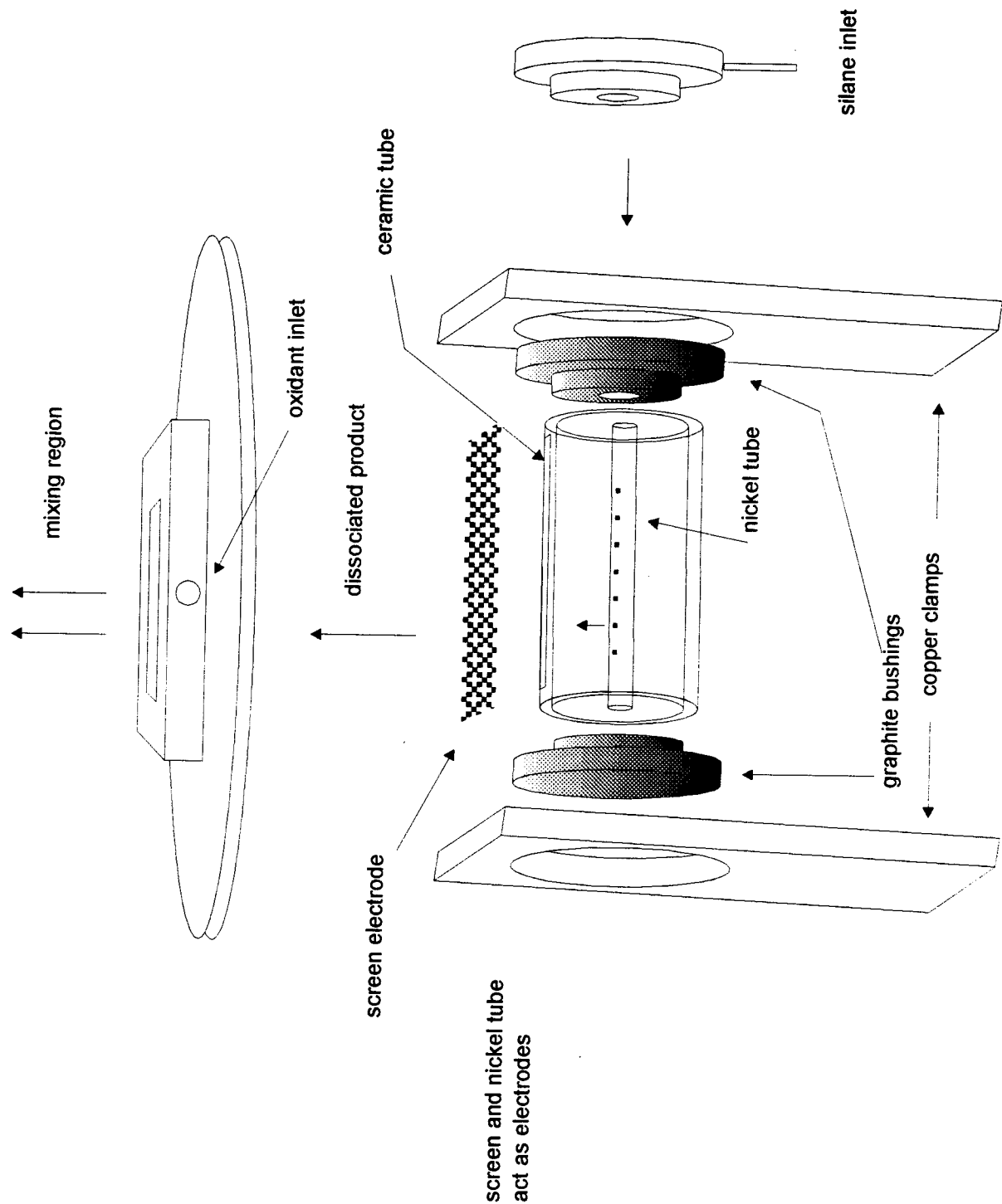
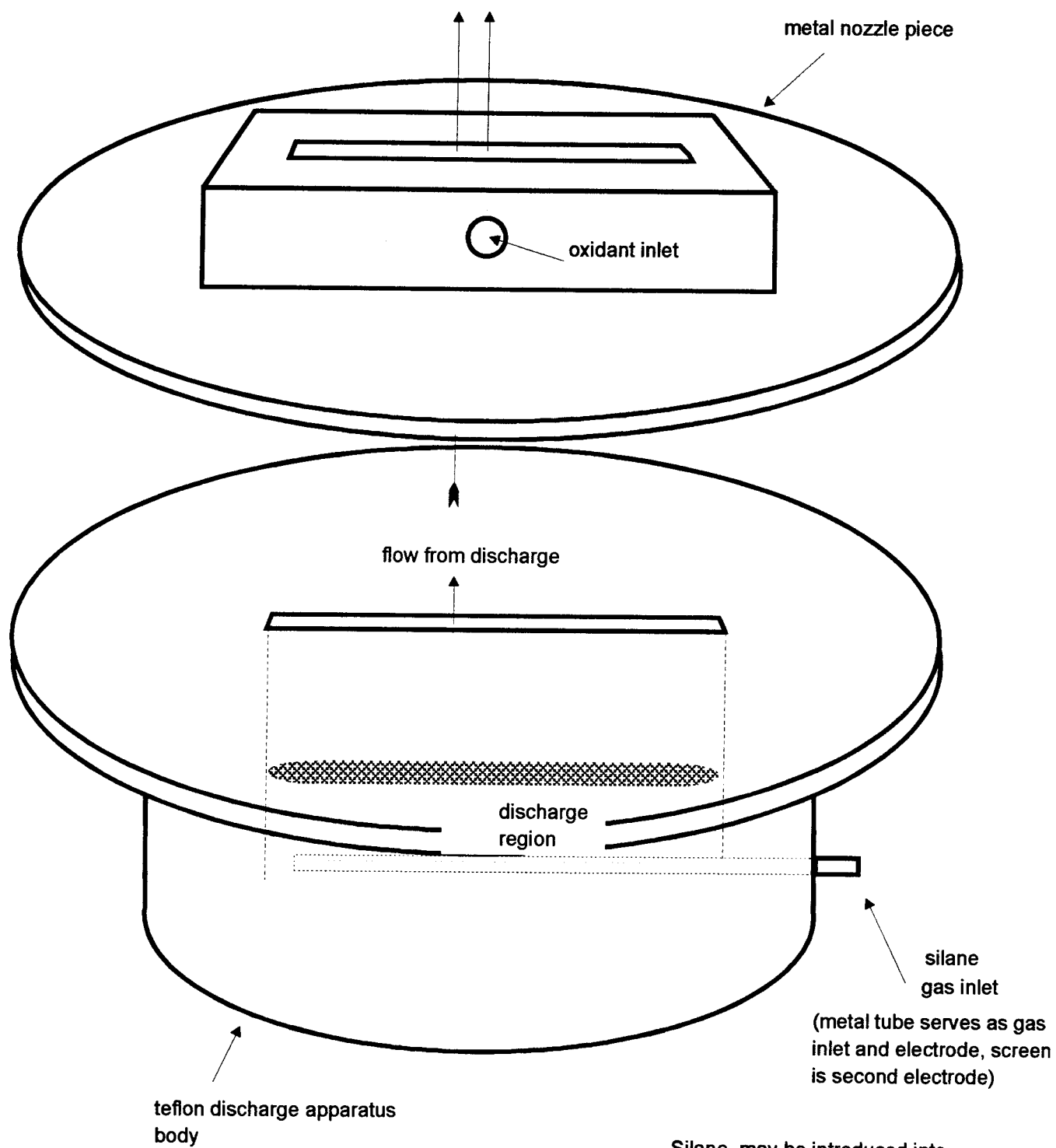


Figure 25



Silane may be introduced into discharge through the bottom inlet. Oxidant is injected through the top inlet.

Alternate: both reactants premixed and passed through the discharge.

Schematic Diagram of Discharge Apparatus

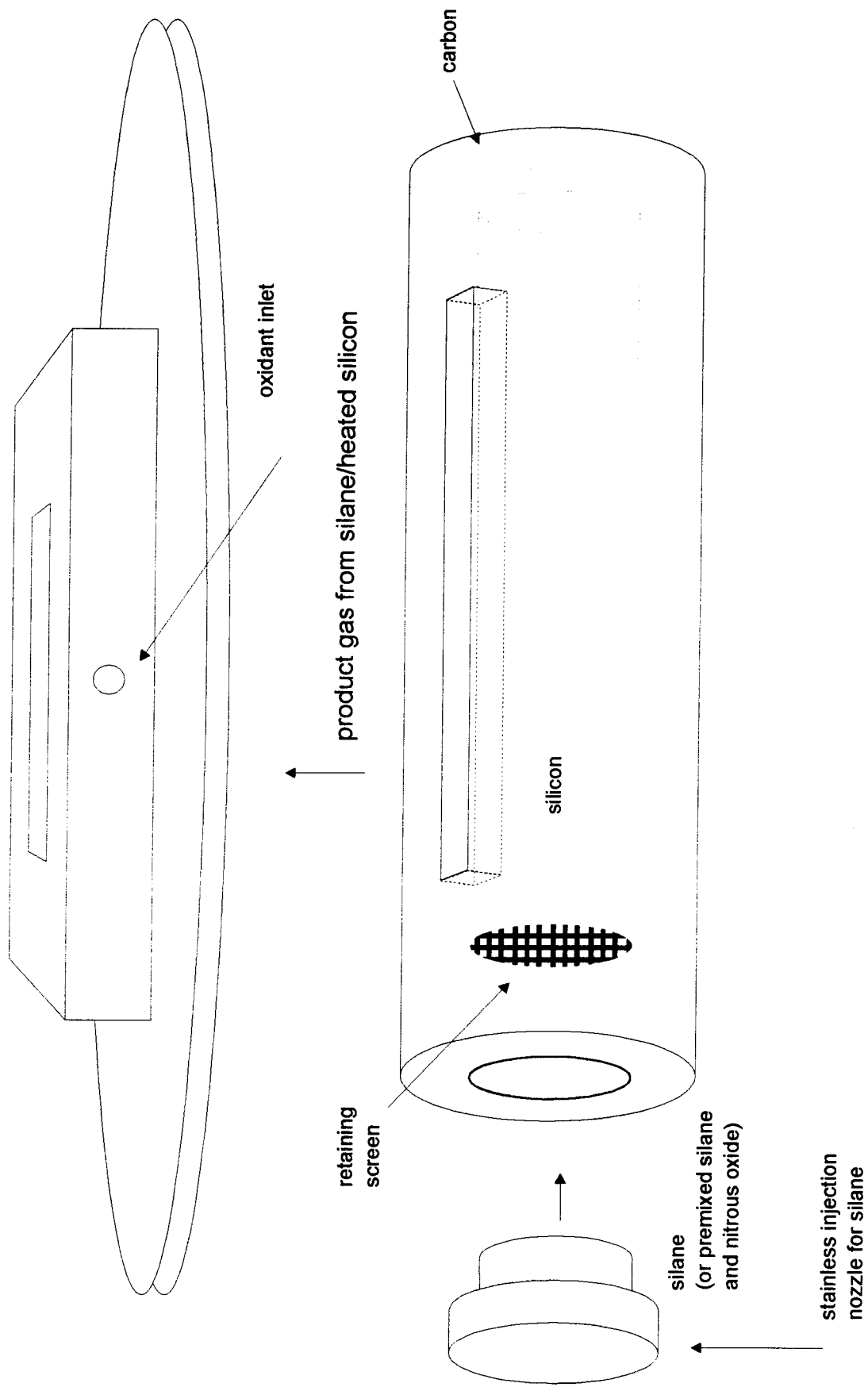
this configuration might eventually prove successful for a discharge based configuration, however, it will require modifications to avoid atomic silicon condensation in the discharge channel.

Figure 27 depicts a configuration in which we have attempted to engineer (as in Equation (4)) the conversion of a silane-silicon interaction to produce two silylene radicals and subsequently two silicon atoms. Here silane was made to flow over silicon contained and heated in a carbon tube furnace. This approach, with a proper balance of diluent also appears promising. In the absence of diluent, the efficient conversion of the silane to silicon and its subsequent condensation soon produces a blockage of oven components. If this problem can be remedied, the configuration of Fig. 27 appears to represent an excellent SiO metastable source configuration.

Figures 28 and 29 depict tubular pyrolizer configurations which we have now used in the High Temperature Laboratory to produce intense SiO metastable flames. Figure 28 depicts a single pyrolizer whereas Figure 29 depicts the tandem assembly which, mounted in a ceramic base, can be used to produce an extended path SiO metastable flame. The pyrolizers are constructed from alumina tubing ($\sim 6\text{mm}$ I.D, 10 cm in length) and employ a tantalum heating wire wrap sealed by high temperature cement and surrounded by a tantalum heat shield. Silane in an argon diluent ($\sim 1\text{-}5\%$ SiH_4) produces a significant silicon flux which, when reacted with N_2O produces the intense SiO metastable flame depicted in Figure 30.

Figures 31(a) and (b) represent an assembled and expanded view of the sintered glass reaction channel which we are using to attempt to overcome the silicon condensation problem. Here, the silane/diluent mixture passes through a sintered glass inner channel, the walls of which are permeable to an entraining argon, helium, or nitrogen gas flow (so as to prevent condensation on the inner channel walls). This device has now been used to produce a weak SiO flame and will therefore be developed further in the High Temperature Laboratory.

With improvements in the arsenal of sources we have outlined, we are confident that we will be able to obtain substantial SiO metastable concentrations in excess of $10^{14}/\text{cc}$ using a hybrid thermolysis - discharge (photolysis) source operating at a temperature considerably below the silicon metalloid melting point.



carbon piece heated directly with electric current or through a heated tantalum jacket

Figure 27

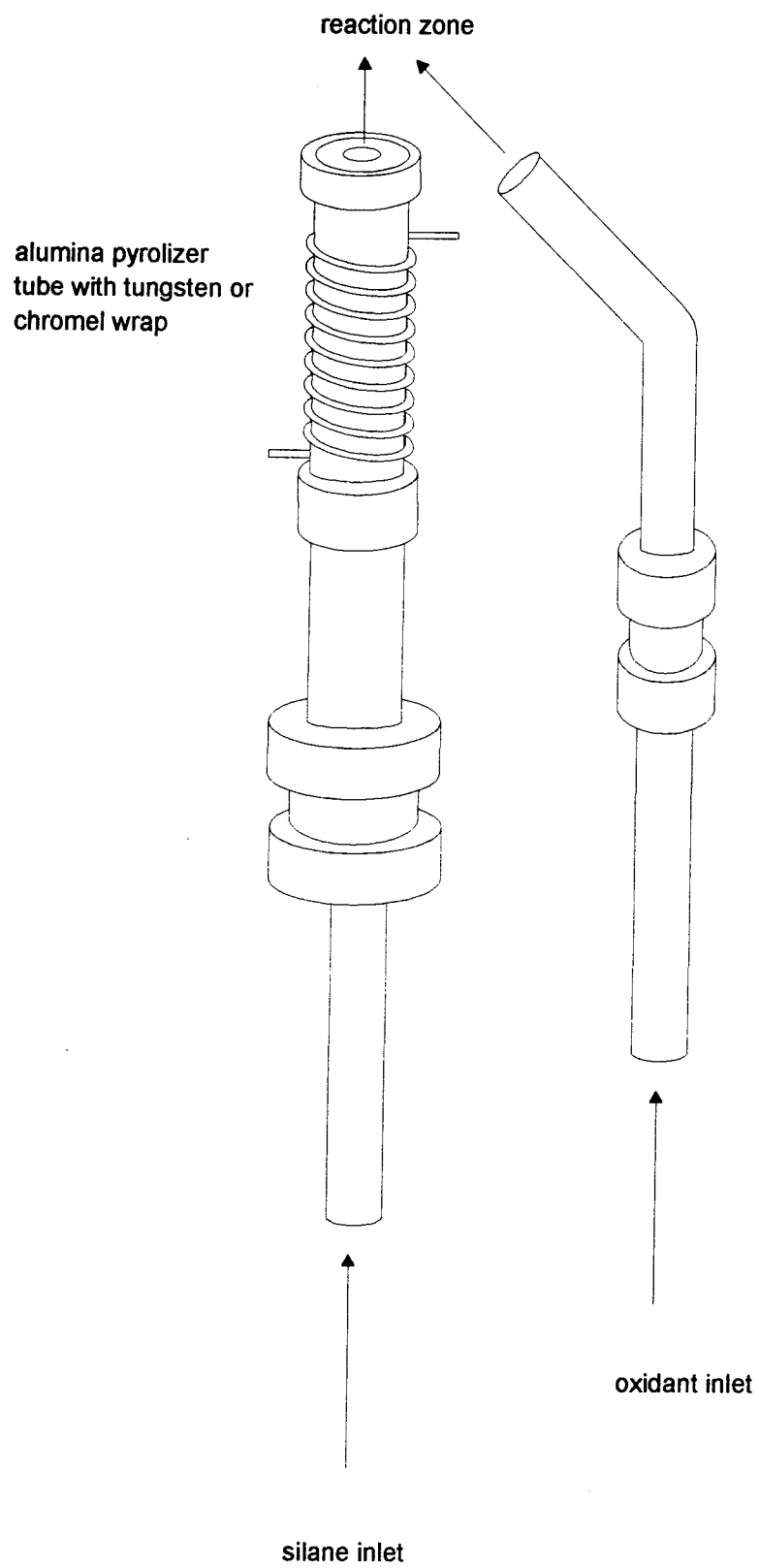


Figure 28

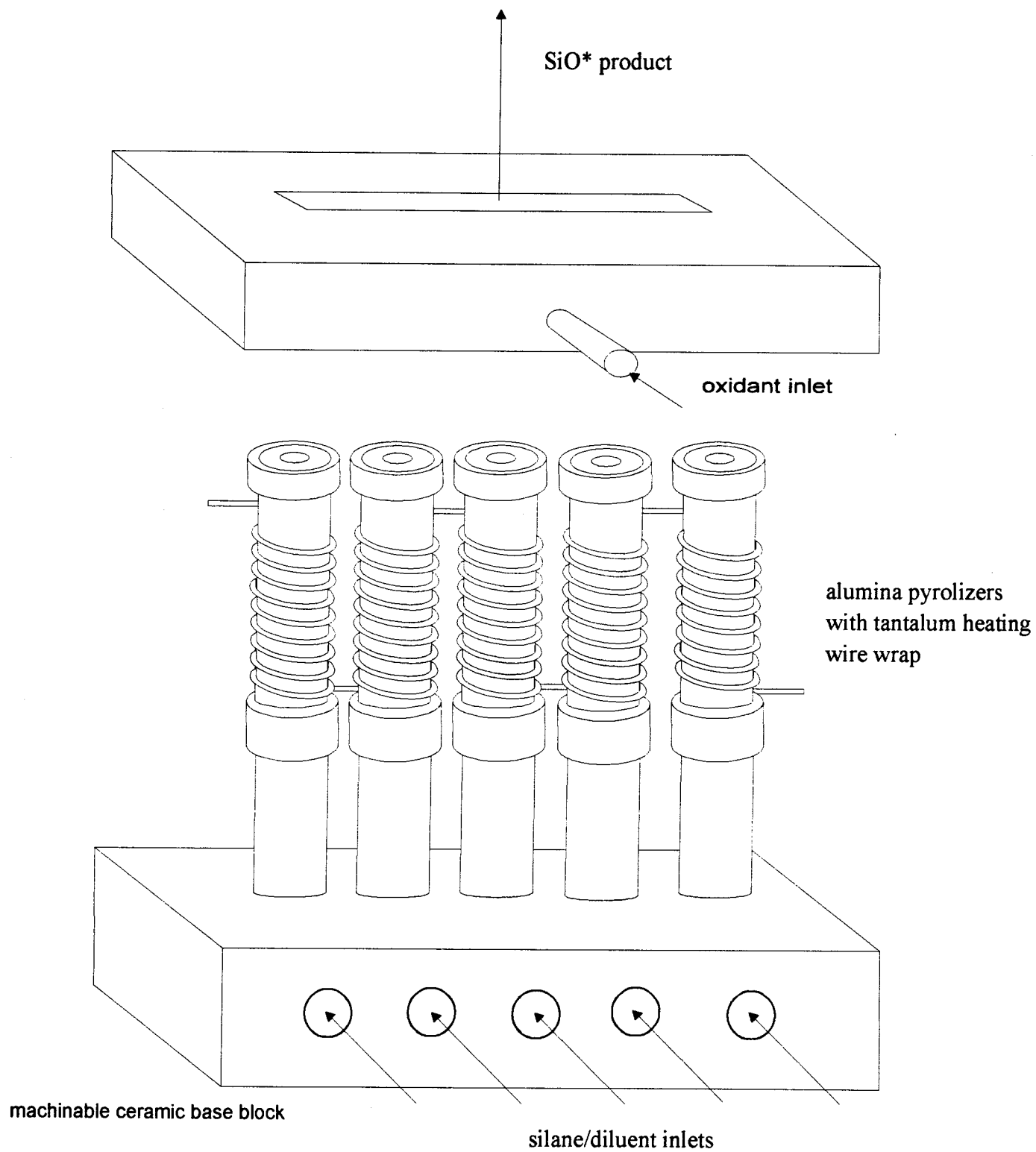
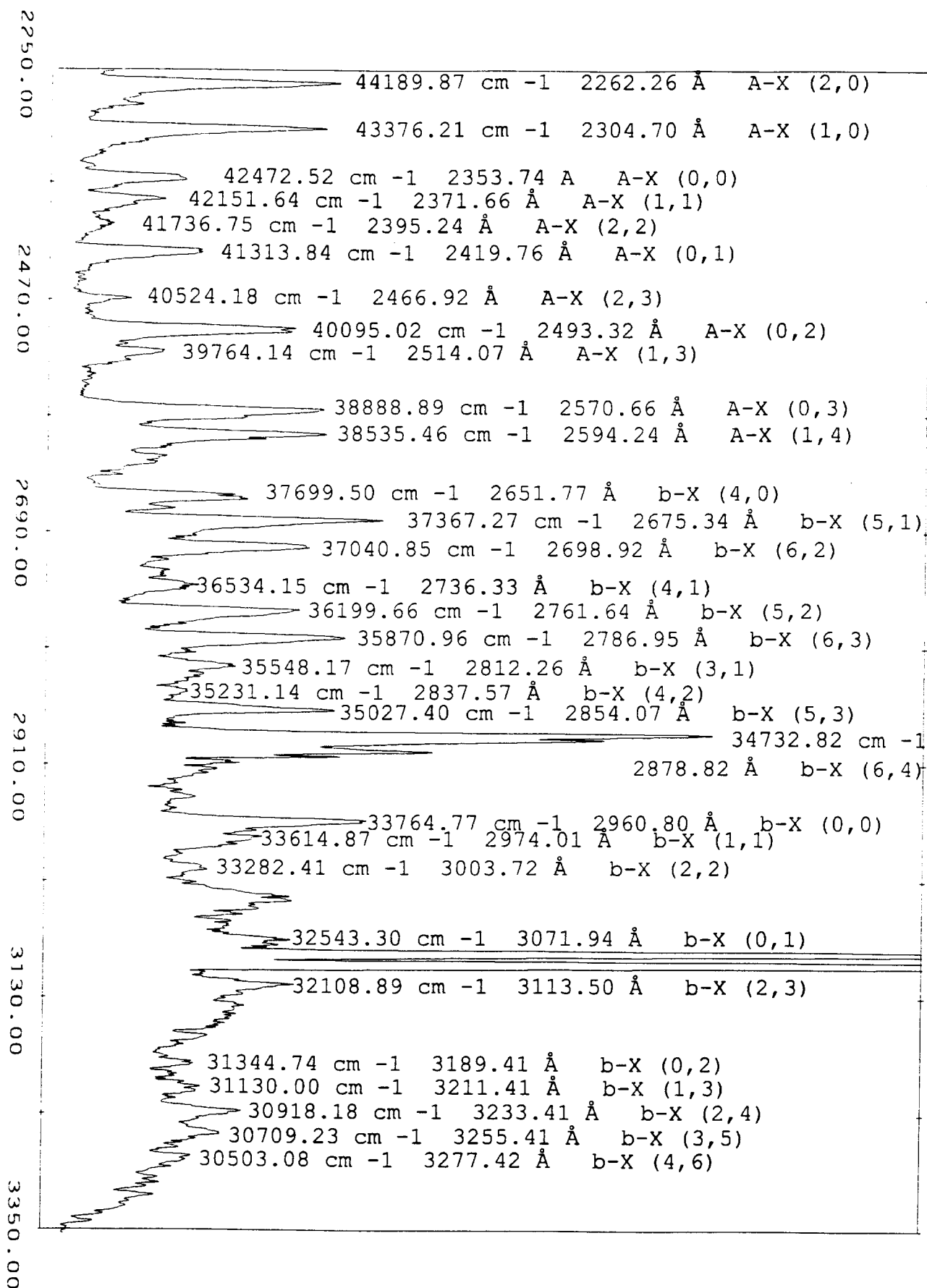
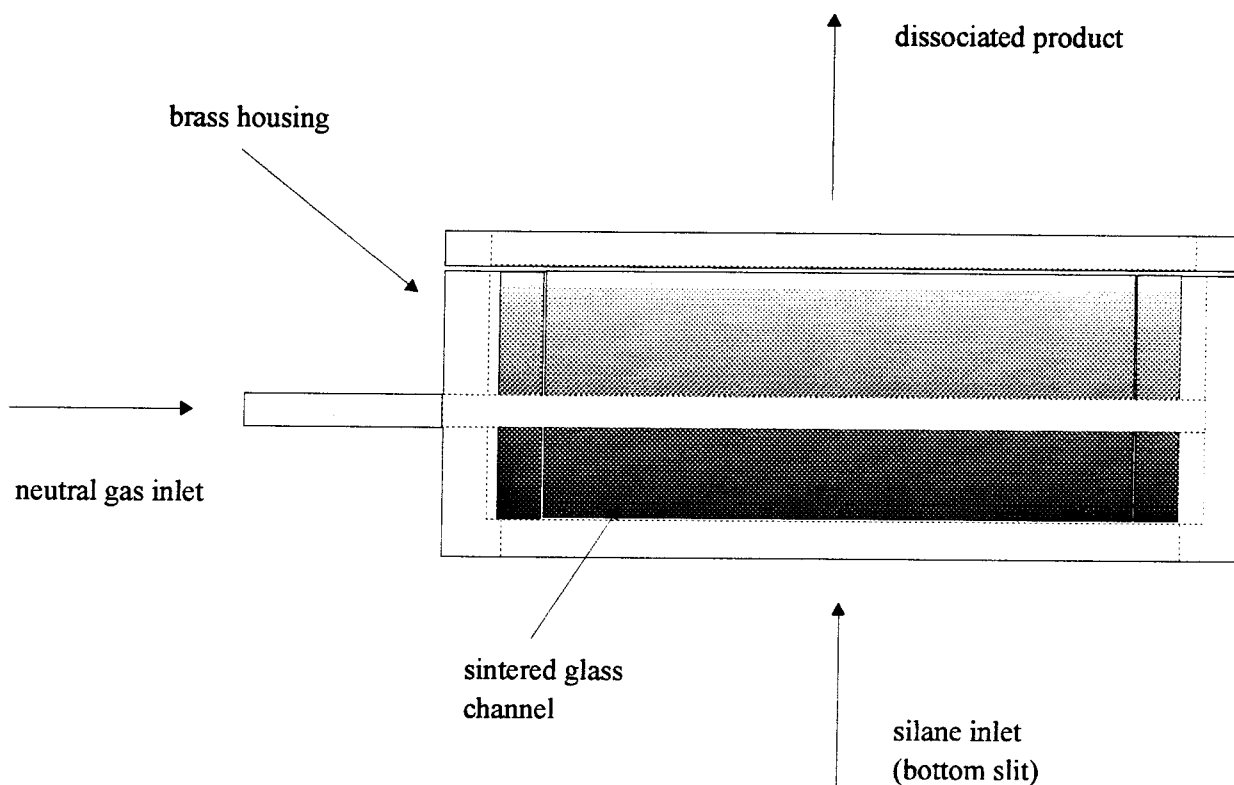


Figure 29



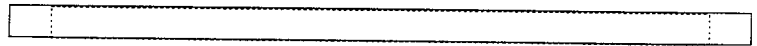


Exploded view of sintered glass channel and housing assembly. The glass assembly is sealed to a shelf in the housing and the lower face of the top plate with high temperature cement. The space between the glass channel and the housing is pressurized with a neutral gas introduced through holes in two inlet tubes (one tube is visible in this side view). The housing is heated with a Thermocoax wrap. Silane is introduced through the bottom slit in the housing, the dissociated species exit through the top slit.

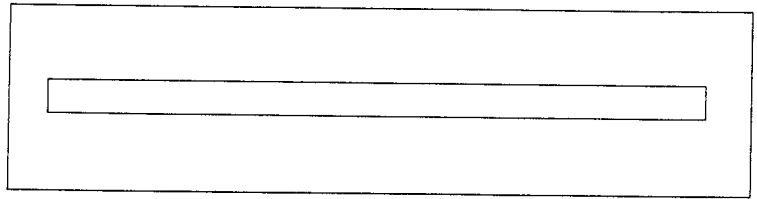
Length of brass housing is approximately 75 mm, height is 30 mm (including top plate) and width is 30 mm.

Figure 31 (a)

side view

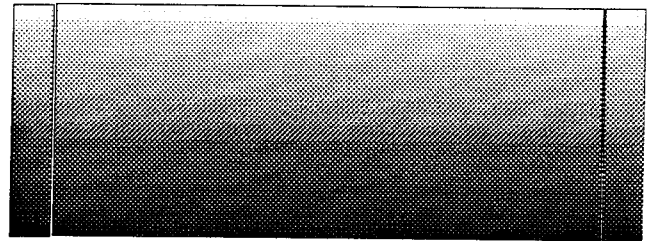


top view

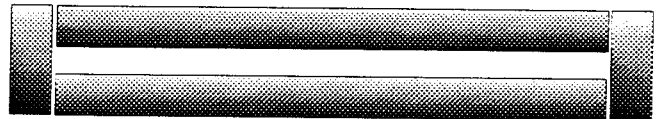


top plate (brass)

side view

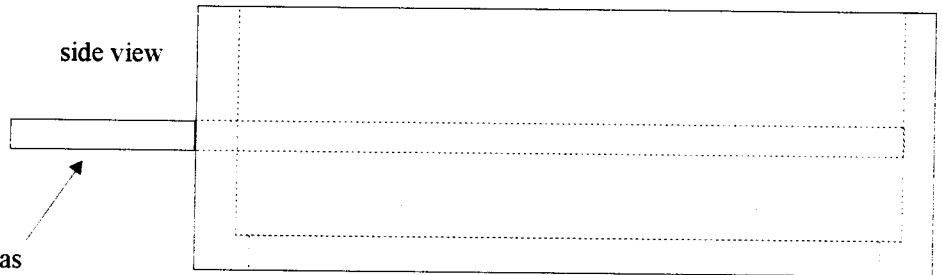


top view



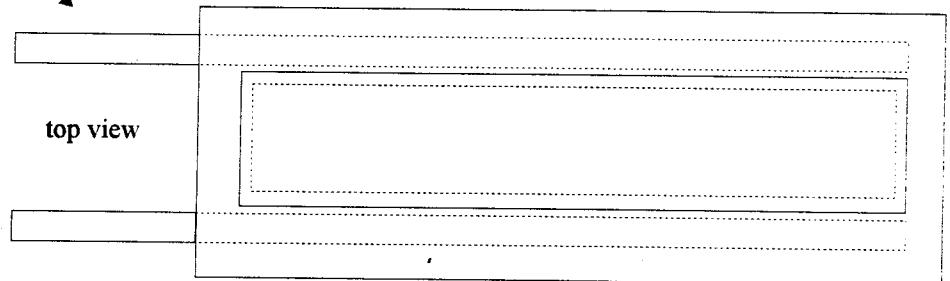
sintered glass channel

side view



neutral gas
inlets

top view



main housing (brass)

sintered glass channel and housing

Figure 31(b)

References

1. R. D. Levine and R. B. Bernstein, Molecular Reaction Dynamics, Oxford University Press, New York, 1974.
2. E. J. Mansky, W. Furr, and J. L. Gole, work in progress.
3. For example see Short Wavelength Chemical Laser Workshop, Charleston, S. C., Nov. 14-15, 1984.
4. C. R. Jones and K. D. Ware, SPIE Proceedings 380, 160 (1983). K. D. Ware and C. R. Jones, SPIE Proceedings 380, 322 (1983). S. Byron, et al. "Laser Pumping Sources", Philco Research Labs. Publication No. U-2771, July 1974. E. P. Chicklis et al., "Low-Cost Laser", Sanders Associates, Inc., Independent Research and Development Task NCG, August 1977.
5. D. M. Lindsay and J. L. Gole, J. Chem. Phys. 66, 3886 (1977).
6. M. J. Sayers and J. L. Gole, J. Chem. Phys. 67, 5442 (1977).
7. J. L. Gole and R. N. Zare, J. Chem. Phys. 57, 5331 (1972).
8. J. L. Gole and S. A. Pace, J. Chem. Phys. 73, 836 (1980).
9. W. H. Flygare, Acc. Chem. Res. 1, 121 (1968).
10. A. W. Hanner and J. L. Gole, J. Chem. Phys. 73, 5025 (1980). J. L. Gole and S. A. Pace, J. Phys. Chem. 85, 2651 (1981). J. L. Gole, B. Ohlsson, A. W. Hanner, and E. J. Greene, unpublished.
11. K. McAdam, private communication. See also A. B. F. Duncan, Rydberg Series in Atoms and Molecules, Academic Press, New York, 1971.
12. J. L. Gole, "Probing Ultrafast Energy Transfer Among the Excited States of Small High Temperature Molecules", in "Gas-Phase Chemiluminescence and Chemiionization", (Elsevier Science Publishers - A. Fontijn, editor) pg. 253.
13. We refer to processes which proceed at extremely high rates and appear to be virtually temperature independent.
14. W. H. Crumley, J. L. Gole, and D. A. Dixon, J. Chem. Phys. 76, 6439 (1982). S. H. Cobb, J. R. Woodward, and J. L. Gole, Chem. Phys. Lett. 143, 205 (1988). S. H. Cobb, J. R. Woodward, and J. L. Gole, Chem. Phys. Lett. 157, 197 (1989). S. H. Cobb, J. R. Woodward and J. L. Gole, "Continuous Chemical Laser Amplifiers in the Visible Region", Proceedings of the Fourth International Laser Science Conference, A.I.P. Conf. Proc. No. 191, Optical Science and Engineering Series 10, pg. 68.
15. J. L. Gole, J. R. Woodward, S. H. Cobb, K. K. Shen, and J. R. Doughty, SPIE Proceedings Volume 1397, Eighth International Symposium on Gas Flow and Chemical Lasers (1990), pg. 125 (and references therein).

16. "Chemically Driven Pulsed and Continuous Visible Laser Amplifiers and Oscillators", with K. K. Shen, H. Wang, and D. Grantier, Invited Talk, Proceedings of the 23rd AIAA Plasma-Dynamics and Laser Science Conference, Nashville, Tennessee, AIAA 92-2994 (1992).
17. B. Wellegehausen, in "Metal Bonding and Interactions in High Temperature Systems with Emphasis on Alkali Metals", A. C. S. Symposium Series 179, edited by J. L. Gole and W. C. Stwalley (Am. Chem. Soc., Washington, D. C.) p. 462. B. Wellegehausen, J. of Quantum Electronics 15, 1108 (1979).
18. See for example, R. S. Berry and C. W. Reimann, J. Chem. Phys. 38, 1540 (1963), R. S. Berry, J. Chem. Phys. 27, 1288 (1957), W. S. Struve, J. R. Krenos, D. L. McFadden, and D. R. Herschbach, J. Chem. Phys. 62, 404 (1975). R. C. Oldenborg, J. L. Gole, and R. N. Zare, J. Chem. Phys. 60, 4032 (1974).
19. Given Na_2 and Na_3 ionization potentials of 4.87 and 3.97 eV (A. Hermann, E. Schumacher, and L. Woste, J. Chem. Phys. 68, 2327 (1978) and an electron affinity of 3.363 eV for atomic bromine, we determine a very substantial electron jump cross section $\sigma = \pi (14.38/3.97-3.36) = 1746 \text{ \AA}^2 (1.75 \times 10^{-13} \text{ cm}^2)$ for the $\text{Na}_3 - \text{Br}$ reaction and $\sigma = \pi (14.38/(4.87-3.36)) = 285 \text{ \AA}^2 (2.85 \times 10^{-14} \text{ cm}^2)$ for the $\text{Na}_2 - \text{Br}$ reaction.
20. E. J. Mansky and J. L. Gole, work in progress.
21. J. L. Gole, G. J. Green, S. A. Pace and D. R. Preuss, J. Chem. Phys. 76, 2247 (1982), and references therein.
22. For example, M. M. Kappes, R. W. Kunz, and E. Schumacher, Chem. Phys. Lett. 91, 413 (1982).
23. We intend to facilitate the formation of Na_2 in the B, C, and C' excited states in an electronically inverted configuration. To do this, Na molecules must be present and react with halogen atoms. Here, it is important to note that the oscillator strengths for any of the larger sodium polymers (Na_n , $n > 3$) are sufficiently small verses Na_2 so that they do not interfere with the sodium dimer pump amplification cycle.
24. "Self-Flushing Optical Window to Prevent Collection of Condensates", W. H. Crumley and J. L. Gole, Rev. Sci. Instruments 57, 1692 (1986).
25. U. Gaubatz, H. Bissantz, U. Hefter, I. Colomb de Daunant, K. Bergmann, and P. L. Jones, J. Opt. Soc. Am. 6, 1386 (1989).
26. I. Littler, S. Balle, and K. Bergmann, "Molecular Beam Raman Laser with a 250 nW Threshold Pump Power", Opt. Comm. 77, 390-394, July (1990).
27. D. L. Rousseau and P. F. Williams, J. Chem. Phys. 64, 3519 (1976).
28. See, for example, J. Tang and A. C. Albrecht, "Raman Spectroscopy", edit by H. A. Szymanski (Plenum, New York, 1970), 2, pp. 33-68; A. C. Albrecht, J. Chem. Phys. 34, 1476 (1961).

29. "Chemically Enhanced Raman Scattering", with D. R. Grantier, J. Chem. Phys., to be submitted.
30. R. Balfour and A. E. Douglas, Can. Jour. Phys. 48, 901 (1970); K. Li and W. C. Stwalley, J. Chem. Phys. 59, 4423 (1973).
31. F. Reuse, S. N. Kanna, V. de Coulon, and J. Buttet, Phys. Rev. B 41, 11743 (1990).
32. "On the BiF Bond Dissociation Energy and Evaluation of the BiF Red Emission Band Systems", T. C. Devore, R. Kahlscheuer, L. Brock, and J. L. Gole, Chemical Physics 155, 423 (1991).
33. "Electronically Excited Charge Transfer Complex Formation in Magnesium Molecule - Halogen Atom Reactions Electronic Spectroscopy of Mg_xF ", T. C. Devore, R. Kahlscheuer, D. A. Dixon, H. Wang, C. B. Winstead, and J. L. Gole, in preparation.
34. D. Grantier and J. L. Gole, "The Expansion of Small Molecule Configuration Space: Highly Efficient Long Range Stabilization and Energy Transfer Involving Electronically Excited States", High Temp. Science, in press. J. L. Gole, "Highly Efficient Collisional Stabilization and the Symmetry Constrained Dynamics of High Temperature Complex Formation", J. Chem. Phys., in press. J. L. Gole, H. Wang, J. S. Joiner, and D. E. Dawson, "Confirmation of Long-Range Collision Complex Stabilization Through the Controlled Relaxation of High Internal Excitation", J. Chem. Phys., in press.
35. (a) F. Engleke, Chem. Phys. 44, 213 (1979).
 (b) W. J. Rosano and J. M. Parson, J. Chem. Phys. 84, 6250 (1986).
 (c) J. M. Parson, J. Phys. Chem. 90, 1811 (1986).
 (d) M. Menzinger, Adv. Chem. Phys. 42, 1 (1980). M. Menzinger, "The $M+X_2$ Reactions: A Case Study", in "Gas Phase Chemiluminescence and Chemiionization", A. Fontijn, editor, Elsevier Science Publishers, Amsterdam, 1985, pp. 25-66.
 (e) M. Menzinger, "Chemiluminescence and Chemi-ionization: Metal-Halogen Reactions as Paradigms of Diabatic Reaction Dynamics", Acta Physica Polonica, A73, 85 (1988).
36. D. J. Wren and Michael Menzinger, Chem. Phys. Lett. 27, 572 (1974), were the first to suggest the possibility of a collisional stabilization process in the microtorr region. However, based in some part on a misconception concerning the lifetimes of the dihalide transitions contributing to the continuum emissions (see Ref. 35(a)) and their concern with the predictions of an RRKM model, they (see (Ref. 35(b),(c),(d)) concluded that the dihalides were formed via a double harpoon mechanism involving first the formation of a highly vibrationally excited metal monohalide which subsequently reacted in a second electron jump process to form the excited state of the dihalide. It is this two step process, thought to be the correct mechanism for excited state dihalide emission³⁵ which has now been disproven in favor of collisional stabilization.

37. See for example, J. R. Woodward, S. H. Cobb, K. K. Shen, and J. L. Gole, IEEE J. Quant. Elec. 26, 1574 (1990) - invited paper. K. K. Shen, H. Wang, and J. L. Gole, IEEE J. Quant. Elec. 29, 2346 (1993) and references therein.
38. J. R. Woodward, S. H. Cobb, and J. L. Gole, "Superfluorescent Chemically Driven Visible Laser Transitions Using Fast Near Resonant Energy Transfer", Proceedings of the Fourth International Laser Science Conference, AIP Conf. Proc. No. 191, Optical Science and Engineering Series 10, pg. 63.
39. G. J. Green and J. L. Gole, Chemical Physics 100, 133 (1985).
40. R. W. Woodward, J. S. Hayden, and J. L. Gole, Chemical Physics 100, 133 (1985).
41. See reference 37 and S. H. Cobb, Ph.D. Thesis, Georgia Institute of Technology, 1988.
42. For the Na $4d^2D$ level, S. A. Kandela, Appl. Optics 23, 2151 (1984).
43. A. Gallagher and A. Lurio, Phys. Rev. 136, A87 (1964).
44. G. Roll and J. Mentel, J. Phys. D. Appl. Phys. 22, 483-487 (1989).
45. A. V. Eremin, I. M. Naboko, and S. A. Palopexhentsev, Opt. Spectrosc. (USSR) 60, 567 (1986).
46. A. S. Tribilov and A. M. Shukhtin, Opt. Spectrosc. 21, 69 (1966). See also, K. Krokell, M. Hube, W. Luhs and B. Wellegehausen, Appl. Phys. B37, 137-140 (1985).
47. (a) V. G. Mishakov and T. L. Tkachenko, Opt. Spectrosc. (USSR) 64(3), 293 (1988). (b) V. V. Kuchinskii, V. G. Mishakov, A. S. Tibilov, and A. M. Shukhtin, Opt. Spectrosc. 39, 1043 (1975) [Opt. Spectrosc. (USSR) 39, 598 (1975)]. (c) A. A. Kudryavsev, V. N. Skrevob, and T. L. Tkachenko, Opt. Spectrosc. 58, 694 (1985) [Opt. Spectrosc. (USSR) 58, 420 (1985)]. (d) V. G. Mishakov, A. S. Tibilov, and A. M. Shukhtin, Opt. Spectrosc. 31, 324 (1971) [Opt. Spectrosc. (USSR) 31, 176 (1971)]. (e) N. N. Bezuglov and A. B. Tsyganov, Opt. Spectrosc. 59, 195 (1985) [Opt. Spectrosc. (USSR) 59, 115 (1985)].
48. I. Tanarro, F. Arqueros, and J. Campos, J. Chem. Phys. 77, 1826 (1982).
49. J. W. Ager III, C. L. Talcott, and C. J. Howard, J. Chem. Phys. 85, 5584 (1986). J. R. Woodward, J. S. Hayden, and J. L. Gole, Chemical Physics 134, 395 (1989).
50. A collaborative effort is being established with Professor Lee Sentman of the Department of Aerospace Engineering at the University of Illinois. Professor Sentman is one of the world experts on the fluid dynamics and design of HF chemical lasers.

51. Chemical Laser Experiments and Analysis, Directed Energy Devices Technology Support Delivery Order No. 0015 prepared by W. Smith, S. Taylor, J. Dansereau, J. Long, and W. Warren for U. S. Army Missile Command, Directed Energy Directorate, Redstone Arsenal, Alabama 35898.
52. J. Dering, SARA Incorporated, private communication.
53. G. R. Fowles and W. T. Silvast, Appl. Phys. Lett. 6, 236 (1965).
54. A. A. Isaev and G. G. Petrash, JETP Lett. 10, 119-121 (1969).
55. Ovazio Svelto, "Principles of Lasers", 3rd Edition, pp. 302, Plenum Press, New York (1989).
56. B. S. Meyerson and J. M. Jasinski, J. Appl. Phys. 61, (2) (1987).
57. J. M. Jasinski and Jock O. Chu, J. Chem. Phys. 81, 1678 (1988).
58. V. N. Votintsev, I. S. Zaslono, V. S. Mikheev, and V. N. Smirnov, Kinetics and Catalysis 27, no. 4, pt. 2, 843 (1986).

Publications:

"A Chemically Driven Visible Laser Transition Using Fast Near-Resonant Energy Transfer to Group IIA Metals", with J. R. Woodward, S. H. Cobb, K. K. Shen, and J. L. Gole, invited paper in Special Issue of the IEEE Journal of Quantum Electronics on Electronic Transition Gas Lasers, JQE 26, 1574 (1990).

"Chemically Driven Pulsed and Continuous Visible Laser Amplifiers and Oscillators", J. L. Gole, K. K. Shen, J. R. Woodward, S. H. Cobb, and J. R. Doughty, Proceedings of the Eighth International Symposium on Gas Flow and Chemical Lasers, SPIE, Volume 1397, pg. 125 (1991).

"On the BiF bond Dissociation Energy and the Evaluation of the BiF Red Emission Band Systems", T. C. Devore, L. Brock, R. Kahlscheuer, K. Dulaney and J. L. Gole, Chemical Physics 155, 423 (1991).

"An Approach to Visible Chemical Laser Development Using Fast Near Resonant Energy Transfer", K. K. Shen, C. B. Winstead, D. Grantier, and J. L. Gole. Journal de Physique IV, Colloque C7, supplement au Journal de Physique III, Vol. 1, 609 (1991).

"Chemically Driven Pulsed and Continuous Visible Laser Amplifiers and Oscillators", J. L. Gole, K. K. Shen, H. Wang, and D. Grantier, Proceedings of the 23rd AIAA Plasma-Dynamics and Laser Science Conference, Nashville, Tennessee, AIAA 92-2994.

J. L. Gole, "Toward the Modeling of the Oxidation of Small Metal and Metalloid Molecules", in "Gas Phase Metal Reactions", edited by A. Fontijn, Elsevier, North Holland, Elsevier Science Publishers (1992), pp. 573-604.

J. L. Gole, "The Unique Complexation and Oxidation of Metal-Based Clusters", in Advances in Metal and Semiconductor Clusters, Vol. 1, Spectroscopy and Dynamics, ed. M. A. Duncan, JAI Press (1993), pg. 159-209.

J. L. Gole, "The Unique Nature of Metal Cluster Oxidation", in Proceedings of the International Symposium on the Physics and Chemistry of Finite Systems: From Clusters to Crystals, Kluwer Academic Publishers, NATO ASI Series C: Mathematical and Physical Sciences, Vol. 374 (1992), pg. 1025.

K. K. Shen, He Wang, and J. L. Gole, "Evidence for Continuous Visible Chemical Lasing from the Fast Near Resonant Energy Transfer Pumping of Atomic Sodium", JQE 29, 2346 (1993).

He Wang and J. L. Gole, "A Chemiluminescent and Laser Induced Fluorescent Probe of a New Low-Lying A' Ω 1 State of Gaseous AgF", J. Mol. Spectros. 161, 28 (1993).

He Wang and J. L. Gole, "Laser Induced Fluorescence Study and Radiative Lifetimes of the Low-Lying Electronic States of Gaseous AgF", J. Chem. Phys. 98, 9311 (1993).

T. C. Devore and J. L. Gole, "Fluorine Hot Atom Oxidation of Bismuth Vapor: A Comment on the Evaluation of the BiF Bond Energy", Chemical Physics 174, 409 (1993).

K. K. Shen, H. Wang, D. Grantier, and J. L. Gole, "Visible Chemical Lasers from Alkali Based Electronic Inversions", in Intense Laser Beams and Applications, W. E. McDermott, editor, SPIE Proceedings, Volume 1871, pg. 18 (1993).

D. Grantier, H. Wang, C. B. Winstead, and J. L. Gole, "Chemically Driven Continuous Visible Laser Amplifiers and Oscillators Based on Metal Molecule - Halogen Atom Reactions", Proceedings of the 24th AIAA Plasma-Dynamics and Laser Science Conference, Orlando, Florida, AIAA 93-3207.

J. L. Gole, K. K. Shen, H. Wang, C. B. Winstead, and J. Stephens, "Chemically Driven Visible Laser Amplifiers and Oscillators Based on Fast Electronic Energy Transfer", Proceedings of the 24th AIAA Plasmadynamics and Laser Science Conference, Orlando, Florida, AIAA 93-3209.

"Raman Pumping in the Absence of an External Light Source", with D. Grantier, J. Phys. Chem. Letters 98, 7427 (1994).

"The Expansion of Small Molecule Configuration Space: Highly Efficient Long Range Stabilization and Energy Transfer Involving Electronically Excited States", with D. R. Grantier, High Temp. Science, in press.

"Chemically Induced Processes Evidencing Raman Gain", with D. R. Grantier and P. M. Medley, Proceedings of the Tenth International Symposium on Gas Flow and Chemical Lasers, Friedrichshafen, Germany, 1994, in press.

"Highly Efficient Collisional Stabilization and the Symmetry Constrained Dynamics of High Temperature Complex Formation", J. Chem. Phys., submitted.

"Confirmation of Long-Range Collision Complex Stabilization Through the Controlled Relaxation of High Internal Excitation", with H. Wang, J. S. Joiner, and D. E. Dawson, J. Chem. Phys., submitted.

"Electronically Excited Charge Transfer Complex Formation in Magnesium Molecule - Halogen Atom Reactions-Electronic Spectroscopy of Mg_xF ", with T. C. Devore, R. Kahlscheuer, D. A. Dixon, H. Wang, and C. B. Winstead, in preparation.

"Energetics, Molecular Electronic Structure and Spectroscopy of Forming Group IIA Dihalide Complexes", in preparation.

"Chemically Enhanced Raman Scattering", with D. R. Grantier, J. Chem. Phys., to be submitted.

Invited Talks on AFOSR Sponsored Research

Eighth International Symposium on Gas Flow and Chemical Lasers, Madrid, Spain (1990) - Invited Talk "Chemically Driven Pulsed and Continuous Visible Laser Amplifiers and Oscillators".

Sixth International Laser Science Conference, Minneapolis, Minnesota (1990) "Chemically Driven Laser Amplifiers Using Fast Near Resonant Energy Transfer".

AFOSR/SDIO Contractors Meeting - Annapolis, Maryland (1990), Invited Talk - "Chemically Driven Pulsed and Continuous Visible Laser Amplifiers and Oscillators".

Southeastern Section APS Meeting - Atlanta, Georgia (1990) "Chemically Driven Laser Amplifiers Using Fast Near Resonant Energy Transfer".

East Coast Symposium on the Chemistry and Physics of Clusters and Cluster Ions, Johns Hopkins University - Invited Talk - "Formation and Unusual Oxidation of Small Clusters".

Department of Chemistry, University of Georgia, Invited Talk - Department Colloquium, "Chemically Driven Visible Laser Systems".

Department of Chemistry, Penn State University, Invited Talk - "Development of Chemically Driven Visible Laser Systems".

Phillips Laboratory, Kirkland Air Force Base - Invited Talk - "Development of Chemically Driven Visible Laser Systems".

Department of Physics, Virginia Commonwealth University, Workshop on Metal Clusters and Their Reactions, Invited Talk - "The Unique Aspects of Metal Cluster Oxidation".

Laser M2P, Second International Conference, Grenoble, France, (1991) - Invited Talk, "Chemically Driven Pulsed and Continuous Visible Laser Amplifiers and Oscillators".

202nd A.C.S. Meeting and American Chemical Congress, New York, N.Y. (1991), Symposium on Gas Phase Metal Reactions, Invited Talk, "The Unique Complexation and Oxidation of Metal Based Clusters".

Seventh Interdisciplinary Laser Science Conference, Monterey, California, (1991) - Invited Plenary Lecture; "Chemically Driven Pulsed and Continuous Visible Laser Amplifiers and Oscillators".

International Symposium on the Physics and Chemistry of Finite Systems: From Clusters to Crystals, Richmond, Virginia (1991) - Invited Talk - "The Unique Complexation and Oxidation of Metal Based Clusters".

Lasers and Electro-Optics Society, Annual Meeting, San Jose, California (1991) - Invited Talk - "Chemically Driven Pulsed and Continuous Visible Laser Amplifiers and Oscillators".

University of Central Florida, Department of Physics, Orlando, Florida (1991)
- Invited Talk - "The Unique Complexation and Oxidation of Metal Based Clusters".

23rd AIAA Plasma-Dynamics and Laser Science Conference, Nashville, Tennessee (1992) - Invited Talk - "Chemically Driven Pulsed and Continuous Visible Laser Amplifiers and Oscillators".

SPIE OE* LASE '93, Los Angeles, California (1993) - Requested Talk - "Visible Chemical Lasers from Alkali Based Electronic Inversions".

Atlanta Area Chemical Physics Seminar (1993) - Invited Talk - "Symmetry Constrained Dynamics of Group IIA Dihalide Formation".

AFOSR Conference on High Energy Density Materials (1993) - "Geometrical Isomerization and Light Metalloid Molecule Oxidation as a Means of Producing High Impulse Propellants".

24th AIAA Plasma Dynamics and Laser Science Conference, Orlando, Florida (1993) - Requested Talk - "Chemically Driven Visible Laser Amplifiers and Oscillators Based on Fast Electronic Energy Transfer".

24th AIAA Plasma Dynamics and Laser Science Conference, Orlando, Florida (1993) - Requested Talk - "Chemically Driven Visible Laser Amplifiers and Oscillators Based on Metal Molecule - Halogen Atom Reactions".

John L. Margrave Research Symposium, Rice University, Houston, Texas (1994) - "Chemically Enhanced Raman Scattering".

Gordon Research Conference on Advanced High Temperature Materials, Meridan, N. H. (1994) - "Raman Pumping in the Absence of an External Light Source".

Tenth International Symposium on Gas Flow and Chemical Lasers, Friedrichshafen, Germany (1994), "Chemically Driven Continuous Visible Laser Amplifiers and Oscillators Based on Metal Molecule-Halogen Atom Reactions".

Scientific Personnel Supported by this Project (Degrees Awarded)

James L. Gole (Principal Investigator).

K. K. Shen (Pulsed and continuous energy transfer systems, cavity construction, laser amplifier and oscillator based on energy transfer from SiO to Na). Ph.D., August 1993.

D. Grantier (Cavity construction for Na₃-X amplifier system, development of Na₃-F chemiluminescent probe studies).

He Wang, Postdoctoral (partial-assistance in cavity construction and modification, development of high resolution laser gain experiments and laser probes of chemical laser reaction products, extrapolation of Na₃-X reaction schemes, extrapolation of SiO-Na energy transfer scheme to SiO-Pb, SiO-Cu, and SiO-Sn systems).

C. B. Winstead (partial assistance in experiments and cavity construction) - Ph.D. anticipated March-May, 1995.

R. Kahlscheuer - Master of Science in Physics awarded (formulated expts. to study alkaline earth trimer - halogen atoms rxns (Mg₃-F...), assisted in cavity construction and source development).

James Stephens (SiO-Na Energy Transfer System, Development of Silane (SiH₄) Based Si and SiO Metastable Sources).

T. C. Devore (analysis of Mg_x-F, Bi_x-F, F₂, reactive systems).

D. A. Dixon (quantum chemistry on Mg_x-F reactive system).

E. J. Mansky (formulation of theories to explain selectivity in Na₃-X reactions).

John Bray (assistance in cavity construction, study of copper molecule - halogen atom extrapolations on alkali (Na) metal system - NSF REU program).

Jason Pugh (assistance in cavity construction - NSF REU program).

Alan Kauppi, J. Steven Joiner, and Douglas Dawson (undergraduate assistants to K. K. Shen and He Wang).

APPENDIX I

"A Chemically Driven Visible Laser Transition Using Fast Near-Resonant Energy Transfer to Group IIIA Metals," J. R. Woodward, S. H. Cobb, K. K. Shen, and J. L. Gole invited paper in Special Issue of the IEEE Journal of Quantum Electronics on Electronic Transition Gas Lasers, JQE 26, 1574 (1990).

A Chemically Driven Visible Laser Transition Using Fast Near-Resonant Energy Transfer

JAMES R. WOODWARD, STEPHEN H. COBB, KANGKANG SHEN, AND JAMES L. GOLE
(Invited Paper)

Abstract—Evidence is obtained which demonstrates the potential for developing purely chemical visible lasers based on rapid near-resonant energy transfer from metastable excited triplet states of germanium and silicon monoxide ($a^3\Sigma^+$, $b^3\Pi$) to select metal atoms. In this study, the Group IIIA metal atoms were chosen as the energy receptors for the energy transfer-pump sequence. Excited triplet states were generated from the Ge-O₃, Ge-N₂O, Si-N₂O, and Si-NO₂ reactions; the bulk of the experimental results was obtained with a germanium-based system. The energy stored in the long-lived triplet states is transferred to pump $X^2P_{1/2}$ thallium, indium, and gallium atoms to their lowest lying $^2S_{1/2}$ states; the process with thallium and gallium atoms appears particularly efficient. Adopting a pumping sequence in which a premixed Ge-Tl atom combination is oxidized, we observe a system temporal behavior which suggests the creation of a population inversion producing a gain condition and forming the basis for full cavity oscillation on the Tl $7^2S_{1/2}$ - $6^2P_{3/2}$ transition at 535 nm. In an extremely efficient energy transfer, GeO metastables formed in the Ge-O₃ reaction rapidly pump those Tl atoms with which they are intimately mixed to populate the $^2S_{1/2}$ excited state, creating a temporary population inversion with respect to the upper $X^2P_{3/2}$ component of the ground 2P thallium atom configuration. This sequence produces an intense short-lived photon pulse whose intensity can exceed by an order of magnitude that associated with Tl $^2S_{1/2}$ - $^2P_{3/2}$ fluorescence. Based upon the extent of the reaction-energy transfer zone, a system parameterization suggests that at minimum, we have observed a superfluorescent laser pulse (versus amplified spontaneous emission) created on the Tl $7^2S_{1/2}$ - $6^2P_{3/2}$ transition whose duration in a self-terminating sequence does not exceed 5 ns FWHM. (A similar, albeit less pronounced, effect is observed in the chemically more complex Ga-Ge-O₃ system.) Of the eight possible ways to combine the germanium-based reactants outlined above to obtain an energy transfer pump of Tl or Ga atoms, only those sequences involving the oxidation of a premixed metalloid-metal mixture display the manifestation of what appears to be a superfluorescent event; the results suggest that this sequence allows for the rapid interaction of a high concentration of the pumping metalloid oxide and Group IIIA metal on a time scale comparable to the $^2S_{1/2}$ radiative lifetime. The current observations are in excellent agreement with those results obtained previously in the study of "superradiance" from Tl discharges. The observation of a gain condition is further substantiated when the single-pass Ge-Tl-O₃ system is converted to a multipass oscillator configuration (~3% output coupling) with a corresponding increase of up to ten times the output power of the single-pass configuration, a substantial increase in the ratio of superfluorescence to fluorescence, and the display of a significant directionality. This approach, which makes use of fast intermolecular energy transfer, shows the promise of extrapolation to several additional systems whose radiative lifetimes greatly exceed those of $^2S_{1/2}$ Tl and Ga atoms.

Manuscript received December 1, 1989; revised May 2, 1990. This work was supported in part by the Georgia Tech Foundation under a Grant from Mrs. Betty Peterman Gole, the U.S. Army Research Office through the Short Term Innovative Research Program, and the U.S. Air Force Office of Scientific Research—U.S. Army Research Office.

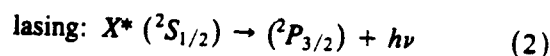
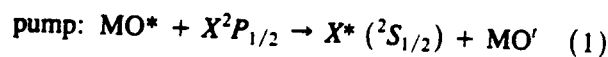
The authors are with the High Temperature Laboratory, Center for Atomic and Molecular Science and the School of Physics, Georgia Institute of Technology, Atlanta, GA 30332.

IEEE Log Number 9037369.

INTRODUCTION

THE development of chemically driven visible lasers has attracted the attention of several researchers over the past 20 years. On the basis of these studies, it has been suggested that most successful electronic transition chemical lasers will require a two-step approach in which chemical energy is released and stored in an initial step, and this energy is then rapidly transferred to an appropriate laser medium in a second step [1]. Although, in rare cases, an alternative and more direct route may be possible [2], the pursuit of a successful energy transfer mechanism has been the subject of the present study. We have chosen to implement the energy transfer sequence using metastable electronically excited states of SiO and GeO formed in highly exothermic chemical reactions as a means of energy transfer pumping visible laser transitions in the Group IIIA metals Ga, In, and Tl. In this effort, we obtain evidence which suggests the efficient pumping of thallium and gallium atoms to obtain amplification in the form of a superfluorescent laser pulse associated with the Tl $7^2S_{1/2}$ - $6^2P_{3/2}$ (0.535 μ m) and Ga $5^2S_{1/2}$ - $4^2P_{3/2}$ (0.417 μ m) transitions. Further, we have observed what appears to be the manifestation of laser oscillation associated with the thallium $7^2S_{1/2}$ - $6^2P_{3/2}$ transition pumped through energy transfer from GeO. The results obtained in the current study are in excellent agreement with those obtained by Isaev and Petrash in their study of "superradiant" emission from Tl discharges [3].

We wish to make use of the near-resonant fast intermolecular energy transfer scheme



where the metal oxide MO* corresponds to the low-lying metastable $a^3\Sigma^+$ and $b^3\Pi$ states of SiO and GeO formed in the Si-N₂O, Si-NO₂, Ge-N₂O, and Ge-O₃ reactions and MO' corresponds to the ground state vibrationally excited oxide. In the present study, the metal oxide excitation must be transferred rapidly to a Group IIIA atom pumping the ground $X^2P_{1/2}$ state to the excited $^2S_{1/2}$ level (Fig. 1). Subsequently, the Group IIIA atoms in this level emit radiation, a component of which is associated with the $^2S_{1/2}$ - $X^2P_{3/2}$ transition to the upper spin orbit component of the ground electronic state. Provided that the $^2S_{1/2}$ level can be pumped at a rate comparable to the ex-

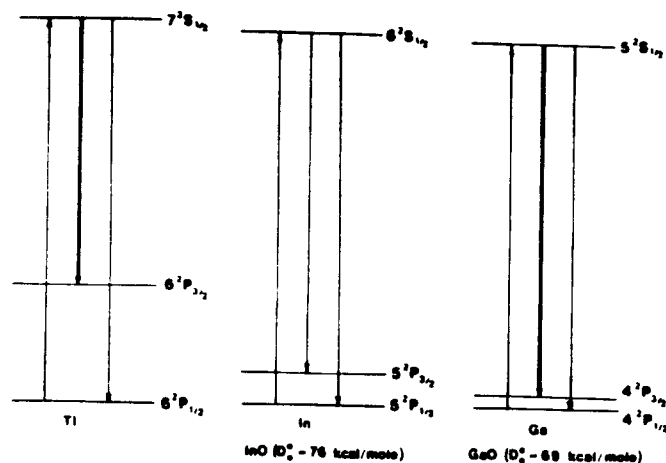


Fig. 1. Comparison of low-lying energy levels in thallium, indium, and gallium. Dark arrows indicate superfluorescent transitions.

cited state radiation lifetime or the $X^2P_{3/2}$ atoms can be removed rapidly from the reaction zone, the pulsed reaction-amplification sequence (1, 2) can be initiated. Here, we present evidence which suggests that the $^2S_{1/2}$ - $^2P_{3/2}$ transition can be made superfluorescent for thallium and gallium atoms provided that the metalloid silicon and germanium atoms are first intimately mixed with thallium or gallium atoms, followed by initiation of the reaction-amplification sequence. Because the $^2P_{3/2}$ level is metastable, this is a self-terminating system.

Gallium, indium, and thallium were chosen as promising candidates for the transfer scheme considered because these atoms have regular ground electronic 2P states with substantial spin-orbit splittings [4], 826.24 cm^{-1} (Ga), 2212.56 cm^{-1} (In), and 7792.7 cm^{-1} (Tl), and excited $^2S_{1/2}$ states which, for thallium and gallium, are in very near resonance with the SiO or GeO triplet states. Photodissociation lasers involving the upper $^2S_{1/2}$ atomic state were already known to exist [5] operating on the strongly allowed $^2S_{1/2}$ - $^2P_{3/2}$ transition; however, of most importance to this study are the results of Isaev and Petrash [3] who obtain evidence for "superradiant" emission from $^2S_{1/2}$ Tl atoms pumped in a discharge configuration. Further, the $^2S_{1/2}$ - $^2P_{3/2}$ transition bears an analogy to the level structure associated with the iodine atom chemical laser [6]-[12].

The success of our outlined approach depends on 1) the ability to produce copious quantities of the SiO and GeO metastable energy storage states in "high quantum yield" chemiluminescent reactions [1], 2) the ability to produce reasonable Group IIIA atom $X^2P_{1/2}$ concentrations and simultaneously minimized $X^2P_{3/2}$ concentrations before the processes 1) and 2) are made to occur [1], and 3) the small energy defect (near-resonant) highly efficient intermolecular energy transfers (Fig. 2) that can take place between the Group IIIA metals, especially Tl and Ga, and the SiO and GeO metastable states, leading to the pumping of those levels accessible via excitation of the lowest $^2P_{1/2}$ spin-orbit component of the Group IIIA atom ground state.

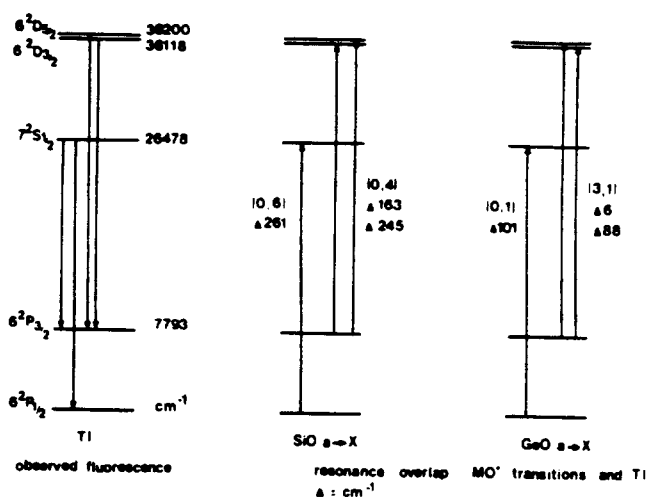


Fig. 2. Energy level diagrams for thallium, SiO $a-X$, and GeO $a-X$. Energy increments associated with $v' = 0$, SiO $a^3\Sigma^+$, and the Tl $7^2S_{1/2}$ - $6^2P_{1/2}$, $6^2D_{5/2}$ - $6^2P_{3/2}$, and $6^2D_{5/2}$ - $6^2D_{3/2}$ transitions, $v' = 0$, GeO $a^3\Sigma^+$, and the Tl $7^2S_{1/2}$ - $6^2P_{3/2}$ transition, and $v' = 3$, GeO $a^3\Sigma^+$, and the Tl $6^2D_{5/2}$ - $6^2P_{3/2}$ and $6^2D_{5/2}$ - $6^2P_{1/2}$ transitions are indicated as exemplary (Δ) in wavenumbers. See also Tables I and II.

There are six possible reactions involving silicon and germanium atoms and the oxidants N_2O , NO_2 , and O_3 . In order to produce the metastable SiO and GeO storage states, we have selected four combinations excluding the Ge- NO_2 and Si- O_3 reactions. The exothermicity of the Ge- NO_2 reaction precludes triplet state formation. The Si- O_3 reaction, while sufficiently exothermic, is strongly dominated by a reactive branching into short-lived excited singlet states [13], [14], and the Si-Tl- O_3 system displays minimal energy transfer pumping of the Tl $^2S_{1/2}$ excited state level.

Recent studies in our laboratory [1], [13] correlated with those of previous workers [13], [15] indicate the following. 1) The Si- N_2O and Ge- N_2O reactions appear to be spin conserving, favoring substantial metastable $a^3\Sigma^+$ (SiO, GeO) and $b^3\Pi$ (SiO) electronic state production. 2) When the Si- N_2O and Si- NO_2 reactions are studied across a wide pressure range from very low pressures to several torr, one monitors a combination of vibrational relaxation within the $a^3\Sigma^+$ and $b^3\Pi$ manifolds, as well as ultrafast energy transfer between the coupled $a^3\Sigma^+$ - $b^3\Pi$ states [1]. This forms a triplet state reservoir which is, at best, *weakly coupled* to the ground electronic, $X^1\Sigma^+$ state (non-radiative). 3) There have, as yet, been no accurate measures of the yield of excited triplet states; however, for the Si- N_2O reaction [1], a lower bound of 500 has been determined for the ratio (excited triplet/excited singlet). 4) Spin selection rules appear to break down for the Ge- O_3 reaction which is dominated by GeO $a^3\Sigma^+$ and $b^3\Pi$ emission features [6], [13]. These system parameters and the observed substantial triplet fluorescence for the reactions considered indicate the possibility of producing copious quantities of metastable triplet states which can be used in formulating a system analogous to the O_2 ($^1\Delta_g$)-iodine transfer laser [6]-[12].

Given that we produce the high concentration of metal

atoms and metastable metal oxides required for a sufficient energy transfer pumping of the Group IIIA metals, the upper $^2P_{3/2}$ component of the Group IIIA metal ground electronic states would correspond to the terminal level in a three-level laser sequence. We require that this level be minimally populated before the lasing-pump sequence (1, 2) is initiated or that it be rapidly depleted 1) in a reactive encounter occurring simultaneously with the formation of the metal oxide metastable states, or 2) through highly efficient collision-induced relaxation in passage through the reaction-energy transfer zone. Thallium was chosen for initial experiments because its $X^2P_{3/2}$ level is 7793 cm^{-1} above the $X^2P_{1/2}$ level, thus minimizing the thermal population of this upper level during metal vaporization, subsequent entrainment, and passage to the reaction-energy transfer zone ($N_{3/2} \leq e^{-10}(N_{1/2})$ at $T \leq 1100\text{ K}$). Thallium is also an ideal candidate because it will not compete with those reactive processes forming the metastable states of SiO and GeO. The TlO bond is weak if not unstable [16], and any oxidation processes involving its formation are highly exothermic.

We have obtained the bulk of our experimental results with the germanium-based systems primarily because of the ease with which one can generate intense germanium fluxes (versus silicon). The efficiency of the above outlined processes for $X = \text{Tl}$ ($^2P_{1/2}$) and GeO metastables formed in the Ge- O_3 reaction is such that a "superfluorescent" laser spike some ten times the normal $^2S_{1/2}$ - $^2P_{3/2}$ fluorescent intensity would appear to be generated on a time scale less than 5–8 ns in a self-terminating system. A similar, albeit less pronounced, effect is observed in the more complex gallium-based experiments where both the initial thermal population of the Ga $^2P_{3/2}$ level and the possible reaction of both the $^2P_{3/2}$ and $^2P_{1/2}$ spin-orbit components complicate the system. Therefore, the following discussion will focus primarily on the Ge-Tl- O_3 system which has now also been operated in a full oscillator configuration.

We emphasize that there are eight possible sequence combinations of the reactants Ge, Tl, Ga, N_2O , and O_3 which involve metastable metal oxide formation and allow the efficient energy transfer pumping of thallium and gallium $^2S_{1/2}$ excited states. Of these combinations, only those which involve the intimate mixing of germanium and the Group IIIA metal atoms before the initiation of the oxidation process yield results which suggest the generation of a temporary population inversion and concomitant gain condition.

EXPERIMENTAL

Experimental apparatus designs and procedures for the oxidation of Si and Ge have been explained in detail elsewhere [1], [17]. The experimental configurations which we describe were constructed both within and surrounding a large vacuum chamber.

The Group IV metal to be oxidized was held in a low-porosity carbon crucible (Micro-Mech, type T6) heated by a tungsten basket heater [Fig. 3(a), R. D. Mathis]. To

produce a metal vapor pressure in the range 10^{-1} –1 torr, Ge and Si are heated to temperatures in excess of 1800 and 2000 K, respectively. The metal vapor effusing from the crucible was further drawn out of the oven region by an entraining argon flow. A basic multiple collision entrainment-flow configuration provided Si and Ge fluxes well in excess of $10^{17}\text{ atoms/cm}^2 \cdot \text{s}$ used to form the SiO and GeO metastables in the reaction-energy transfer zone. In those experiments in which the manifestations of energy transfer from the SiO or GeO metastables to Ga, In, or Tl atoms were studied, the silicon or germanium was brought to a temperature for operation over a time frame ranging from 1 to 3 h. For those premixed Ge-Tl based experiments in which characteristics suggesting laser amplification were studied, the germanium was brought to a temperature slightly above melting, and then ramped up so as to expend between 7–10 g of the metal-oid over a time frame of 10–20 min. This corresponds to a germanium flux well in excess of $6 \times 10^{19}\text{ atoms/cm}^2 \cdot \text{s}$ (7–10 g expended in 1 h) at the orifice of the source crucible. If we estimate that under normal effusive conditions, the flux will decrease by a factor of 10 at the reaction zone, the germanium concentration will be well in excess of $10^{14}/\text{cm}^3$.

The indicated Ge concentrations correspond to stringent lower bounds for the argon, and to a lesser extent, the oxidant flows have a concentrating effect as they sheath the germanium, the oxidant reacting to form the metastable metal oxide and the product metal oxide itself. If the metastable metal oxides used in this study are produced under single-collision conditions where emission of a photon occurs before subsequent collisions, the resulting chemiluminescence is highly diffuse, filling a substantial portion of the reaction chamber. This behavior results primarily from the long radiative lifetime of the metastable metal oxide excited states in combination with a $\cos \theta$ dominated flow distribution. In contrast, the multiple collision energy transfer configuration is characterized by an intense conical flame which is focused to a pinnacle in a region in close proximity to its intersection [Fig. 3(b)] with an entrained thallium atom flow. The focusing effect of the argon sheath serves to greatly enhance the Ge atom and GeO metastable concentrations.

An entrained silicon flux under multiple collision conditions will react with NO_2 and N_2O to produce the $a^3\Sigma^-$ and $b^3\Pi$ states of SiO (Fig. 4), and with O_3 to produce both the a and b states and the SiO $A^1\Pi$ state [1] where the $A^1\Pi$ - $X^1\Sigma^+$ emission strongly dominates the chemiluminescent reactive branching. The $\text{Si} + \text{O}_3$ reaction apparently does not produce a useful metastable SiO excited state concentration as spin conservation appears to play an important role in all three Si reactions [1], [13], [15], [16]. An entrained Ge flux will react with N_2O under multiple collision conditions to produce the $a^3\Sigma^+$ state of GeO, and with O_3 to produce strong emission dominated by the $a^3\Sigma^+$ and $b^3\Pi$ states of GeO (Fig. 6), spin conservation playing a smaller role in this reaction [18]. If SiO is produced from the Si- O_3 reaction, the energy transfer

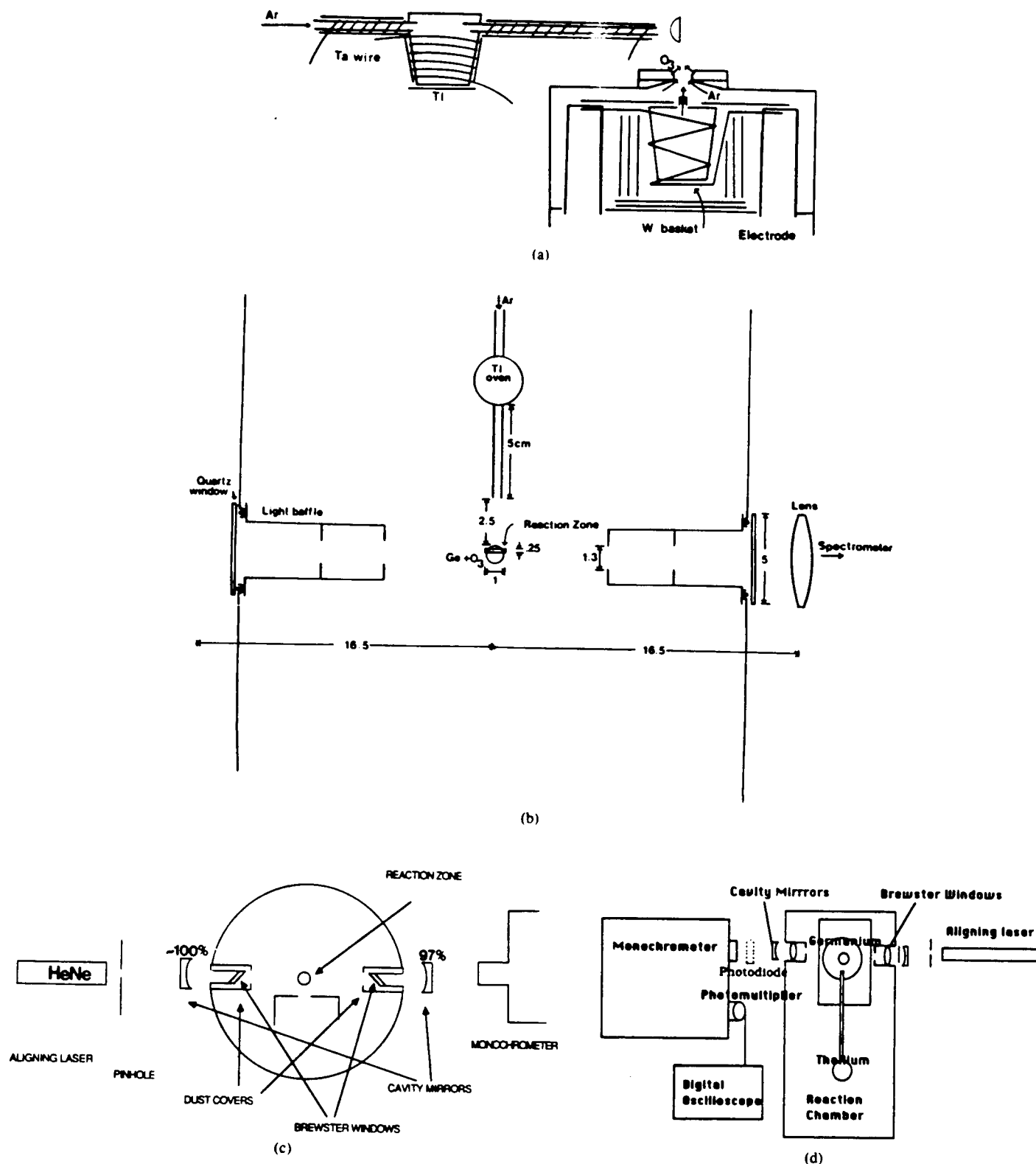


Fig. 3. (a) Oven configurations and orientations for 1) the vaporization of thallium subsequently entrained in argon in a horizontal gas flow, and 2) silicon or germanium (M) beams or flows entrained in argon and subsequently oxidized with O_2 , N_2O , or NO_2 (only Si) to yield the metastable $a^3\Sigma^+$ and $b^3\Pi$ and states of SiO and GeO (and the much shorter lived $A^1\Pi$ state). The directions of the argon flows are indicated in the figure, as is the oxidant ring inlet. The semi-circle indicates the reaction-energy transfer zone observed by eye and corresponding to thallium blue-green fluorescence. See text for discussion. (b) Overview of oven systems and photon path to the spectrometer/PMT detection system for energy transfer and single-pass amplification studies. The 1×0.25 cm reaction zone was estimated by visual observation of the Tl fluorescence. The circle indicates the Ge or Si oven system and the oxidant ring inlet. (c) Side view of full cavity configuration including HeNe alignment laser, 100% high reflecting concave (cavity) mirror, and 3% output coupler. See text for discussion. (d) Schematic overview of full laser cavity configuration showing aligning HeNe laser and positions of photodiode and spectrometer-PMT combination detectors. See text for discussion.

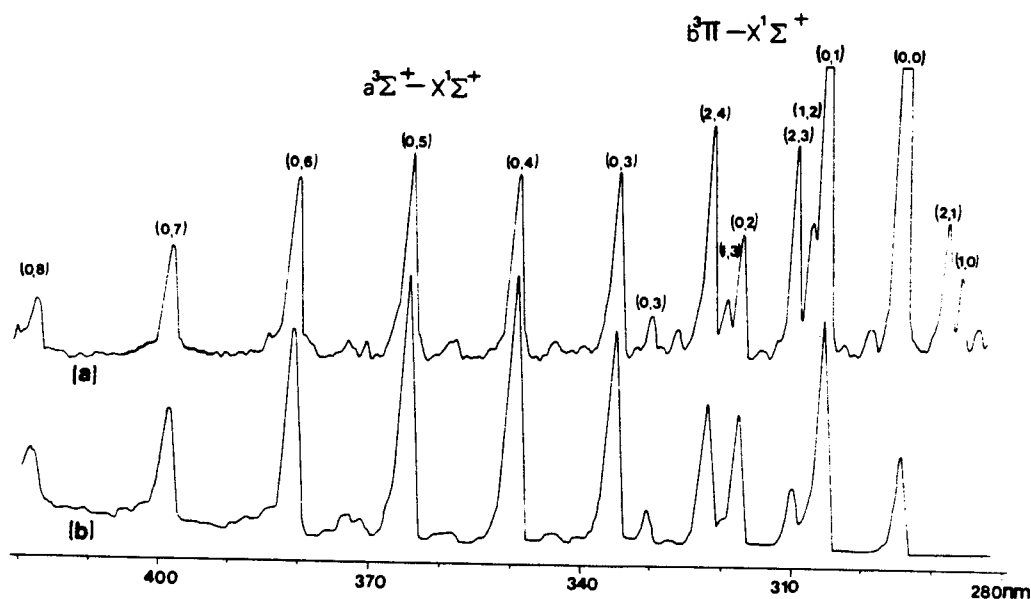


Fig. 4. Comparison of chemiluminescent spectra for the reactions (a) $\text{Si} + \text{N}_2\text{O} + \text{Ar} \rightarrow \text{SiO}^* + \text{N}_2 + \text{Ar}$, and (b) $\text{Si} + \text{NO}_2 + \text{Ar} \rightarrow \text{SiO}^* + \text{NO} + \text{Ar}$ taken under multiple collision conditions ($P_T \approx 1$ torr).

sequence (1, 2) is barely detected, and little $\text{Tl } ^2S_{1/2}$ atomic emission is observed as a result of the chemical pumping of ground state $X^2P_{1/2}$ atoms. This result indicates the importance of metastable metal oxide triplet state production to ensure a successful pumping sequence and the potential for excitation of a visible laser transition. Because the SiO and GeO $A^1\Pi$ radiative lifetimes are extremely short [13], [14], the necessary time frame for energy storage is lost.

The various oxidants were introduced into the reaction zone via a concentric ring injector system [Fig. 3(a)]. Two methods were employed in mixing the reactants. For those experiments in which the effect of thallium on the SiO or GeO triplet state fluorescence was studied, the Group IIIA metal was introduced into a clearly visible conical metal oxide flame. However, in those experiments in which the short-time temporal behavior of the thallium $^2S_{1/2} - ^2P_{3/2}$ emission feature was monitored, argon entrained Tl and Ge atoms were first intimately mixed, the reactive and energy transfer sequences being subsequently initiated through the introduction of the appropriate oxidant.

Thallium was placed in an aluminum oxide crucible (Coors Ceramics Company) and heated to temperatures ranging to 1150 K using the tantalum wire (Rembar) wound resistive heating configuration shown in Fig. 3(a). The maximum operating temperature provides a vapor pressure in excess of 1 torr. Argon carrier gas was passed into connecting alumina tubes and through the tightly press-fit high-density (T6) carbon top cap of the thallium crucible, flowing over the liquified thallium and forming a flow of Tl-Ar directed perpendicular to and intersecting the reaction zone. The Tl flux to this zone ranges from $5 \times 10^{18}/\text{cm}^2 \cdot \text{s}$ to in excess of $8 \times 10^{20}/\text{cm}^2 \cdot \text{s}$. The effects of a cooler entraining argon stream entering the crucible region were reduced considerably by heating the argon inlet tube. The entire reaction zone configuration is

placed in a considerably larger vacuum chamber whose capacity renders a sharp dropoff in reactant concentration away from the reaction zone. The considerably higher temperatures and modified configurations used to maintain comparable and requisite vapor pressures for the indium and gallium systems will be discussed in a later paper [6], [19].

In a typical experiment, the graphite crucible holding the Si or Ge and the crucible holding the Group IIIA metal were brought to temperature over a 2 h period. The graphite cap and attached alumina tubing were heated in advance of the Group IIIA metal in order to prevent condensation of the metal vapor on the cooler alumina surface. Typical operating pressures consisted of 25–100 mtorr of oxidant and 400–500 mtorr of argon, these gases being introduced via the concentric flow and ring injector systems to react with and entrain Si or Ge. The Tl vapor was typically backed by a 25–100 mtorr pressure of argon inducing a flow toward the reaction zone. The total chamber operating pressure was between 450 and 600 mtorr.

An overhead scale diagram of the oven systems, reaction zone, and photon path to the detection systems used to study energy transfer and the temporal behavior associated with the $\text{Tl } ^2S_{1/2} - ^2P_{3/2}$ emission events is depicted in Fig. 3(b). The 1×0.25 cm reaction zone was determined by overhead visual inspection of the Tl fluorescence from the Ge- O_3 -Tl system. The location of the fluorescence zone is determined primarily by the intersection of the entrained Ge and thallium flows. It varies especially with respect to vertical height above the metal oxide source, and to a much lesser extent with respect to position along the horizontal. The circle in Fig. 3(b) represents the Si and Ge oven system and ring inlet.

Spectra were taken with a 1 m scanning monochromator (Spex, model 1704) and detected with RCA 4840 and EMI 9808 photomultiplier tubes wired for fast response and

powered by a Fluke 415B high-voltage power supply. Signals were passed to a partially damped picoammeter (Keithley 417B) and recorded on a strip chart recorder (Leeds and Northrup). In order to monitor the temporal behavior of the system, the Spex 1704-PMT-spectrometer combination was combined with a digital oscilloscope. With the spectrometer set at the wavelengths corresponding to Tl atomic emission lines and several MO* emission regions, the temporal behavior of the emission signals was assessed. The photomultiplier output was sent to a LeCroy 9400 125 MHz digital oscilloscope and recorded on a Hewlett-Packard 7470A plotter.

The optical system depicted in Fig. 3(b) was modified to a full-cavity configuration as indicated in Fig. 3(c) and (d). The temporal behavior of the full-cavity configuration was monitored using both photomultiplier- and fast photodiode-based detection systems. This experiment will be outlined more fully in a following section.

RESULTS

Energy Transfer Pumping of Tl Atoms

Since thallium was deemed the most promising candidate for the energy transfer sequence considered, initial experiments focused on the creation of a substantial MO* metastable population and the observation of an MO*-Tl energy transfer. The manifestation of this energy transfer was readily observed with the thallium oven system operative at temperatures ranging from approximately 800 K, corresponding to a thallium vapor pressure of 10^{-2} torr. The UV-visible spectrum corresponding to the emitting products in the reaction-energy transfer zone was studied both with and without thallium introduction (Figs. 4-6). Figs. 5 and 6 depict a collage of emission spectra obtained for the exemplary Si-N₂O-Tl and Ge-O₃-Tl systems. For both combinations, the observed emission resulting from the excitation of thallium atoms demonstrates the apparent symbiotic relationship between the depletion of the metastable MO* $a^3\Sigma^+$ and $b^3\Pi$ emissions and the subsequent enhancement of the Tl 7^2S-6^2P and 6^2D-6^2P emission features. Systematic elimination of the reactants involved in the metal oxidations, whose optical signatures are considered in Figs. 5 and 6, demonstrated that the formation of MO* metastable species was required to observe the atomic fluorescence from thallium. *The most important facet of the data presented in Figs. 5 and 6 is that it would appear to demonstrate an extremely efficient transfer from the MO* products of the silicon and germanium oxidations to thallium atoms.* That is, the observed fluorescence from the SiO and GeO metastable states virtually disappears as the thallium concentration in the reaction-energy transfer zone increases, and thus couples away the energy made available by the metastable storage states. An indication of this efficiency is also apparent upon visual inspection of the reaction-energy transfer zone. Both the violet GeO and SiO flames were observed to turn bright green as Tl vapor was introduced.

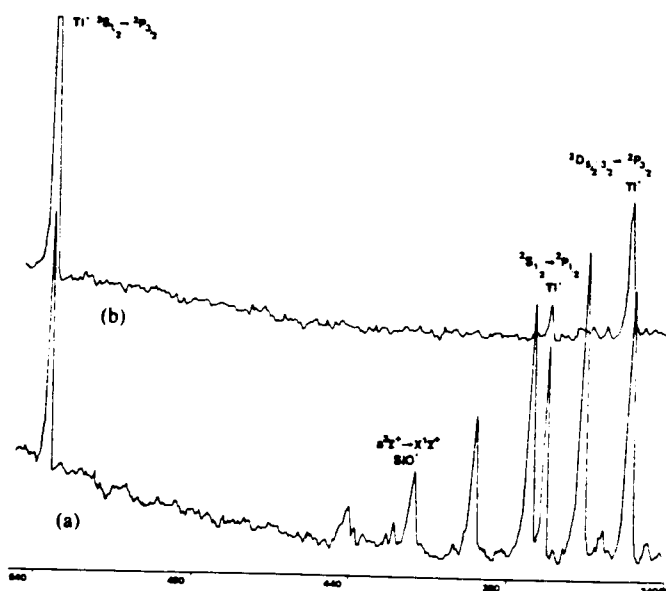


Fig. 5. Comparison of thallium-SiO energy transfer spectra. Metastable SiO molecules were created in the reaction $\text{Si} + \text{N}_2\text{O} \rightarrow \text{SiO}^* + \text{N}_2$. (a) Spectrum recorded with low Tl flux, showing substantial intensity in the $\text{SiO}^* a^3\Sigma^+ - X^1\Sigma^+$ transition features. (b) Spectrum recorded with high Tl flux (~ 1 torr Tl vapor pressure). Note the dominance of the Tl atomic emission peaks and the virtual absence of SiO* features. Spectral resolution is 8 Å.

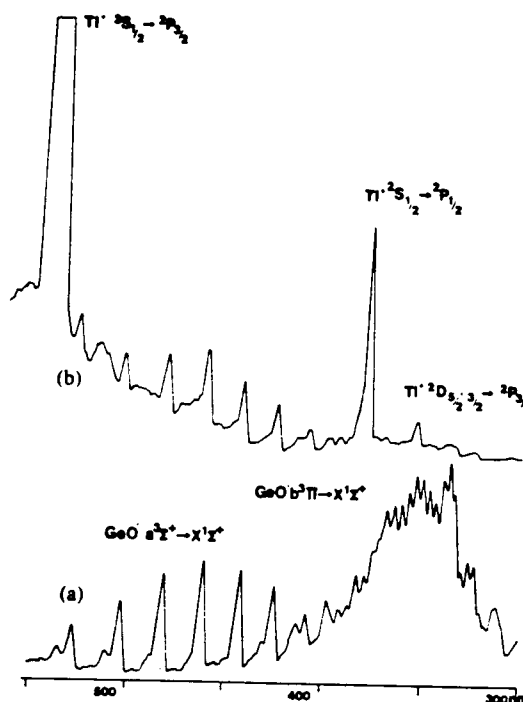


Fig. 6. Comparison of thallium-GeO transfer spectra. Metastable GeO molecules were created in the reaction $\text{Ge} + \text{O}_3 \rightarrow \text{GeO}^* + \text{O}_2$. (a) Spectrum recorded with minimal Tl flux, showing substantial intensity in the $\text{GeO}^* b^3\Pi - X^1\Sigma^+$ transition features. (b) Spectrum recorded with high Tl flux (~ 1 torr vapor pressure). Note the dominance of the Tl atomic emission peaks and the intensity reduction in the GeO* features. Spectral resolution is 12 Å.

Trends in Energy Transfer

It is unlikely that observed behavior in the thallium-based systems can be attributed to strong quenching of the

SiO or GeO fluorescence via either collision-induced intersystem crossing to high-vibrational levels of the ground electronic state or to the reaction of the oxidant with the Group IIIA metal atom. Previous studies of the silicon [1] and germanium [16] oxidation systems indicate minimal coupling of the triplet manifold with the ground electronic $X^1\Sigma^+$ state. This inhibits a ready collision-induced transfer to ground state levels, at least in the pressure range over which these data were obtained.

Further trends observed in our studies of the manifold of Group IIIA metal atom systems would also seem to eliminate both reactive and collisional quenching as a means of explaining the significant decrease in triplet state emission and the attendant increase in the intensity of thallium emission [6], [19]. For these atoms of similar molecular electronic structure, there are considerable differences in both the completeness of energy transfer and the ease with which it is accomplished. In the thallium system, the thallium oxide bond is known to be extremely weak, and ground state $^2P_{1/2}$ thallium atoms may be considered unreactive. By comparison, however, In reacts with O_3 in an exothermic process to form InO ($D_0^0 = 76 \pm 10$ kcal/mole [21]), depleting available O_3 and indium, which can conceivably result in a diminished GeO emission intensity. Yet when a vapor pressure of indium in excess of 1 torr is introduced into a GeO flame, only a weak indium fluorescence is observed, while the GeO triplet features remain strong and virtually undiminished. The behavior of the gallium system is also inconsistent with collisional quenching [6], [19].

One trend appears to correlate with the behavior of the Ga, In, and Tl systems. In order to assess the likelihood of a successful energy transfer from the metastable states of SiO and GeO to the Group IIIA metal atoms, we considered the energy match between appropriate transitions involving states of the molecule and atom. We suggest that a near-resonant condition is requisite in order to obtain the most efficient energy transfer. In Tables I and II, we consider several of the GeO and SiO $a^3\Sigma^+ - X^1\Sigma^+$ and $b^3\Pi - X^1\Sigma^+$ transition energies and their near resonance with the Group IIIA metal atomic energy level separations associated with the laser pump transitions of interest. We note that the energy resonances of the metal oxide transitions from $v' = 0$ form a pattern in the $a-X$ bands of both GeO and SiO. For these transitions, we find that the thallium system exhibits the most favorable resonances, followed closely by the gallium system. The nearest resonances in the indium system are separated by more than 275 cm^{-1} . Also, if we consider the number of SiO and GeO transitions which lie in the neighborhood of the energy necessary to pump the thallium atom, this system has the greatest number of available energy transfer paths. Thus, we expect the thallium atom to participate in near-resonant energy transfer more efficiently than does gallium, both systems being far more efficient than indium. In view of the trends observed, near-resonant energy transfer would appear to play an important role in these systems.

TABLE I
NEAR RESONANCES OF SiO* ($a^3\Sigma^+$, $b^3\Pi - X^1\Sigma^+$) AND GROUP IIIA $^2S_{1/2} - X^2P_{1/2}$ ATOMIC TRANSITIONS IN ENERGY TRANSFER LASER PUMPING PROCESS

Atom	Upper Atomic Level	SiO (v', v'')			
		$a-X$		$b-X$	
		Trans.	$\Delta E\text{ (cm}^{-1}\text{)}^a$	Trans.	$\Delta E\text{ (cm}^{-1}\text{)}^a$
Ga	$^2S_{1/2}$	(0, 7)	-267.4	—	—
In	$^2S_{1/2}$	(0, 8)	463.9	—	—
Tl	$^2S_{1/2}$	(0, 6)	261.5	(6, 11) (7, 12) (8, 13) (11, 15)	-273.5 -87.5 97.5 -361.5

^aAtomic level energy-molecular level energy.

TABLE II
NEAR RESONANCES OF GeO* ($a^3\Sigma^+$, $b^3\Pi - X^1\Sigma^+$) AND GROUP IIIA $^2S_{1/2} - X^2P_{1/2}$ ATOMIC TRANSITIONS IN ENERGY TRANSFER LASER PUMPING PROCESS

Atom	Upper Atomic Level	GeO (v', v'')			
		$a-X$		$b-X$	
		Trans.	$\Delta E\text{ (cm}^{-1}\text{)}^a$	Trans.	$\Delta E\text{ (cm}^{-1}\text{)}^a$
Ga	$^2S_{1/2}$	(0, 3) (2, 4)	140.6 -166.4	— —	— —
In	$^2S_{1/2}$	(0, 3) (1, 4)	-275.1 46.9	— —	— —
Tl	$^2S_{1/2}$	(0, 1) (1, 2) (2, 2) (4, 4)	-101.5 243.5 -382.5 307.5	(2, 7) (4, 9)	-310.5 122.5

^aAtomic level energy-molecular level energy.

Self-Absorption in the Tl System

The data in Figs. 5 and 6 also demonstrate that at the highest concentrations of thallium atoms used in these experiments, self-absorption by ground state $6^2P_{1/2}$ ($X^2P_{1/2}$) thallium atoms must be considered. The relative intensities of the $^2S_{1/2} - ^2P_{3/2}$ and $^2S_{1/2} - ^2P_{1/2}$ fluorescence features are approximately in the ratio 8:1 at the highest self-absorbed thallium concentrations (Figs. 5 and 6); however, studies of these relative intensities as a function of the thallium source temperature demonstrate that this ratio at lower thallium concentration appears to be in virtual agreement with the oscillator strength ratio $A_{535}/A_{377.7} = 1.16 \pm 0.05$ [23]. This behavior is demonstrated in Fig. 5 where the representative spectrum at lower thallium flux is obtained at a thallium vapor pressure corresponding closely to 10^{-2} torr [22] and the upper, clearly $P_{1/2}$ self-absorbed, spectrum is obtained near the upper operating temperature of the thallium oven system corresponding approximately to a 1 torr [22] vapor pressure. Based upon vapor pressure, entrainment-flow considerations, and the timed rate of depletion of Tl atoms, we estimate that the concentration of Tl atoms in the small reaction-energy transfer zone varies from $\sim 10^{14}/\text{cm}^3$ to an upper bound of $\sim 10^{16}/\text{cm}^3$ for the two spectra depicted in Fig. 5.

One might expect to observe the effects of self-absorption even at the lower thallium concentrations; however, it must be noted that the concentration gradient drops off sharply from the mixing and reaction zone, limiting the effect or at least our ability to monitor its manifestation. Thus, the corrected intensity of the $^2S_{1/2}$ - $^2P_{3/2}$ and $^2S_{1/2}$ - $^2P_{1/2}$ emission features agrees closely with the oscillator strength ratio. This experimentally measured ratio of intensities is significant for it also demonstrates that under the excitation conditions of the present experiments, self-absorption by the eventually formed metastable $P_{3/2}$ level, which is populated in largest part through the oxidation-energy transfer pump sequence, plays a minor role unless the cross section for $P_{3/2}$ self-absorption vastly exceeds that for $P_{1/2}$. The similar $^2S_{1/2}$ - $^2P_{3/2}$ and $^2S_{1/2}$ - $^2P_{1/2}$ oscillator strengths and the direct proportionality of these oscillator strengths to the cross section for self-absorption preclude this possibility.

At the highest Tl $^2P_{3/2}$ concentrations, the pumping scheme outlined previously and considered in more detail shortly will produce a maximum of 1×10^{12} $^2P_{3/2}$ Tl atoms/cm³ in the reaction zone over the period when those effects which would appear to be characteristic of lasing action are observed. This concentration is some two orders of magnitude less than that producing no detectable self-absorption due to Tl $^2P_{1/2}$. It thus implies that $P_{3/2}$ self-absorption will probably not be detected in the present configuration.

Chemical Pumping of Tl $^2D_{5/2, 3/2}$

The $^2D_{5/2, 3/2}$ - $6^2P_{3/2}$ thallium emission features have also been observed at the highest thallium beam concentrations, although it is apparent (Fig. 5) that the rate of formation of Tl $^2S_{1/2}$ vastly exceeds that for the excitation of $^2D_{5/2, 3/2}$. Both the Si-N₂O and Ge-O₃ reactions are sufficiently exothermic to pump the 2D manifold through excitation of $^2P_{1/2}$ Tl atoms; however, the 2D - $^2P_{1/2}$ energy increment is not in near resonance with the SiO or GeO level structure. We suggest that the observed features might also result from the chemical pumping of efficiently produced $6^2P_{3/2}$ atoms via the sequence of reactions 1) and 2) followed by the fast *near-resonant* transfer



Because the ratio of $P_{1/2}$ to $P_{3/2}$ Tl atoms in the reaction-energy transfer zone is $\sim 10^4/1$, it is not possible to readily assess the relative importance of near-resonant energy transfer in pumping the 2D manifold.

Evidence Suggesting Short-Lived Amplification and Superfluorescence Associated with the (Ge-Tl)-O₃ System

In order to obtain lasing action and amplification based on the $^7S_{1/2}$ - $6^2P_{3/2}$ Tl atom transition, one must successfully create a population inversion between the $^2S_{1/2}$ and $^2P_{3/2}$ levels. This requires that the system be rapidly

energy transfer pumped on a time scale of $\sim 10^{-8}$ s commensurate with the $^7S_{1/2}$ radiative lifetime [23]. The thallium $6^2P_{3/2}$ level is metastable, as the $6^2P_{3/2}$ - $6^2P_{1/2}$ ($X^2P_{3/2}$ - $X^2P_{1/2}$) radiative lifetime is between 0.1 and 1 s [24]. Thus, $^2P_{3/2}$ atoms must be removed from the mixing and reaction zone primarily through diffusion or collisional deactivation (see the following) or lasing action will cease. A laser operating on the $^7S_{1/2}$ - $6^2P_{3/2}$ transition will be self-terminating. In analogy to the nitrogen laser, the observation of amplified spontaneous emission or superfluorescence in the form of an enhanced photon emission proceeding a fluorescence component and at a much greater intensity can indicate the probability that a population inversion has been created.

In order to assess the possible observation of a short-lived stimulated emission process associated with the Tl $^2S_{1/2}$ - $^2P_{3/2}$ transition, we monitored the temporal behavior of the Ge-O₃-Tl system; with the Spex 1704 spectrometer set at 535 nm (1 nm resolution) to overlap the Tl $^2S_{1/2}$ - $^2P_{3/2}$ emission feature, the photomultiplier output signal was sent to a LeCroy 9400 125 MHz [25] digital oscilloscope. The onset of metal oxide formation and subsequent energy transfer in previously mixing Ge-Tl flows was controlled with the O₃ introduction into the reaction-energy transfer zone through a triggered pulsed valve or a manual needle valve. With the Ge and Tl flows into the reaction zone established (Tl $\sim 10^{16}$ atoms/cm³, Ge $\geq 10^{14}$ atoms/cm³), the O₃ was introduced into the reaction-energy transfer zone, initiating MO* formation and energy transfer to Tl atoms. This process was accompanied by the emission of 535 nm photons in a process which appears to display the manifestation of both stimulated emission and normal fluorescent events.

In order to assess the probability of what appears to be a superfluorescent event, the digital oscilloscope was triggered by the emission rate associated with the reaction energy transfer process at a response level set considerably higher than the system fluorescence level or the phototube dark current. Using the optical configuration depicted in Fig. 3(b), the observed fluorescence signal associated with the thallium 535 nm line generated from both a (Ge-Tl)-O₃ [Fig. 7(a)] and Ge+O₃→GeO*+Tl interaction sequence was measured at approximately 50 mV. In contrast, the much more intense and short-lived emission signal depicted in Fig. 7(b) appears to demonstrate a stimulated emission process (superfluorescence) measured at approximately 500 mV with an FWHM not exceeding 5-8 ns. It must be emphasized that the trigger indicated in Fig. 7(b) does not correspond to the introduction of O₃ into the system, but rather to the flag of an amplified emission level detected by the phototube. The system is monitored after reaction and energy transfer have been initiated and the photon emission corresponding to the $^2S_{1/2}$ - $^2P_{3/2}$ transition builds to a preset triggering level well in excess of that for fluorescence and phototube dark current.

After the observation of a stimulated emission spike, when the population inversion has been depleted, the sig-

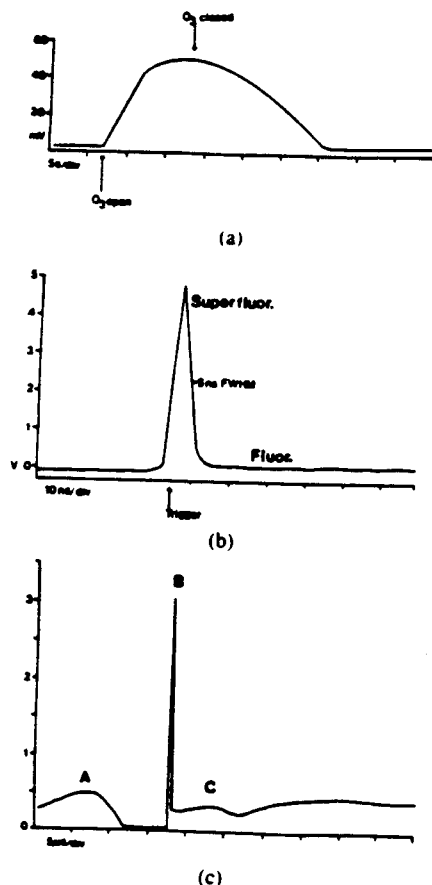


Fig. 7. (a) Tl $7^2S_{1/2}$ - $6^2P_{3/2}$ (535.1 nm) fluorescence pumped through energy transfer from GeO^* ($a^3\Sigma^+$, $b^3\Pi$) formed in the Ge-O_3 reaction. As the O_3 source valve opens, the Tl fluorescence signal reaches its maximum; with the O_3 valve closed, the Tl fluorescence slowly diminishes. Superfluorescence is not detected because of the temporal resolution of the oscilloscope associated with this long time scale. (b) Tl $7^2S_{1/2}$ - $6^2P_{3/2}$ (535.1 nm) superfluorescence observed at a signal trigger level of 0.2 V. The trigger of the superfluorescence is by signal level, and not by reactant mixing, which occurs on a much longer time scale. The measured FWHM is ~ 5 ns compared to $\tau \sim 7.5$ ns, the radiative lifetime of the $7^2S_{1/2}$ level. A return to the fluorescence level is seen subsequent to the superfluorescent pulse. (c) Tl $7^2S_{1/2}$ - $6^2P_{3/2}$ (535.1 nm) fluorescence + superfluorescence in a system suffering an interruption of the reaction-energy transfer process. In the region B we observe a thallium superfluorescence signal following an ~ 10 μs absence of the thallium fluorescence. In the region C, we return to the Tl fluorescence signal level following the self-termination of the superfluorescence due to population of the Tl $6^2P_{3/2}$ level.

nal returns to the normal fluorescent level. When the Spex monochromator was set so as to monitor the Tl fluorescence features at 377.7 nm (Tl $7^2S_{1/2}$ - $6^2P_{1/2}$) and 352.5 nm (Tl 2^1D - $6^2P_{3/2}$) or an MO^* emission feature, no signal spike [Fig. 7(b)] was observed. Further, the temporal behavior monitored in Fig. 7(b) is characteristic only of the oxidation of premixed metalloid-metal mixtures. In all cases studied, when the metastable metal oxide is first formed and subsequently interacts with a Group IIIA metal, the $7^2S_{1/2}$ emission signal intensity is at a level commensurate with fluorescence. These results would seem to indicate that the intensity spike recorded in Fig. 7(b) is attributable to a short-lived stimulated emission process which we tentatively associate with superfluorescence (see also the following).

A further intriguing aspect of the GeO^* -Tl system is depicted in Fig. 7(c) [26]. The unpredicted observation of stimulated emission while monitoring the 535 nm, $7^2S_{1/2}$ - $6^2P_{3/2}$, Tl fluorescence resulted from experimental instabilities which momentarily reduced the supply of germanium or ozone required to produce $\text{Tl}^* 7^2S_{1/2}$ and halted the Tl fluorescence for $t \approx 10$ μs . When reactant instabilities halt the thallium fluorescence for $t \approx 10$ μs , the pumping process begins the subsequent recycling of the system; the intensity spikes associated with stimulated emission are also observed to recycle with this process. We suggest that if the energy transfer event is interrupted long enough so as to produce a complete loss of the fluorescence signal for $t \approx 10$ μs , the $6^2P_{3/2}$ state of thallium is depleted from the reaction-energy transfer-amplification zone to the extent that, when the energy transfer sequence resumes, the population inversion between the $7^2S_{1/2}$ and $6^2P_{3/2}$ levels is reestablished. An absence of the fluorescence for $t \approx 10$ μs can result from the momentary loss of any of the reactants from the reaction zone.

The $6^2P_{3/2}$ level population may be depleted through two primary mechanisms: 1) diffusion out of the reaction-energy transfer zone and away from the photon path to the detector employed in the experiment, and 2) relaxation to the $6^2P_{1/2}$ level. If we assume that our thallium source corresponds to an effusive oven heated to 1100 K and that the thallium mixing with the argon entrainment gas forming a directed flow undergoes cooling collisions, the thallium atoms have a velocity of between 4 and 7×10^4 $\text{cm} \cdot \text{s}^{-1}$. This will allow the directed thallium atoms to travel across our ~ 0.25 cm fluorescence reaction diameter in 4–8 μs [Fig. 3(b)]. Collisional relaxation of thallium $6^2P_{3/2}$ atoms involving either ground state GeO or Ar atoms may also be possible since each thallium atom undergoes between 1 and 25 collisions in 10 μs (dependent on the size of the collisional diameter assumed for the thallium atom) [27]. Finally, we must note a third possibility. Because of the large $7^2P_{3/2}$ excitation energy, the Tl $7^2P_{3/2}$ - O_3 reaction is virtually thermoneutral. Therefore, the reactive removal of $7^2P_{3/2}$ Tl atoms from the amplification zone also represents a possible loss mechanism. Any of these factors can contribute to the loss of the Tl $6^2P_{3/2}$ population and to the recycling of superfluorescence resulting from a momentary loss of the germanium or oxidant supply to the reaction zone.

It must be emphasized that the region encompassed by the fluorescence zone as viewed from the top of the apparatus (Fig. 3(b) and the experimental section) represents an upper bound to that volume from which stimulated emission is observed. In fact, the diameter of the stimulated emission region may be considerably smaller. Further, the nature of the experiment is such that the zone which displays amplification upon buildup of the necessary population inversion is not precisely spatially reproduced with each ozone pulse, but may move vertically with respect to the silicon or germanium source oven. While this does not greatly affect the observation of a

stimulated emission event, it makes the observation of a consistently reproducible power output due to cavity oscillation difficult.

The temporal width of the short-lived signals recorded in Fig. 7(b) and (c) must also be considered. The LeCroy 9400 digital oscilloscope operating in single-shot mode operates at a specified time resolution of 10 ns, although it is possible that a 5 ns temporal event can be adequately recorded [25]. Therefore, the temporal width of the intensity spikes recorded in Fig. 7(b) and (c) may well be less than 5 ns (see the following discussion). Further, their measured intensity might also be taken as a lower bound to the peak intensity, again due to limitations of the scope response to short pulses. The effect of response time may be indicated if we compare the peak intensities associated with the 10 ns/div and 5 μ s/div scans [26] in Fig. 7(b) and (c).

Evidence for Laser Oscillation

In order to obtain laser oscillation associated with the $\text{TI } ^7\text{S}_{1/2}-6^2\text{P}_{3/2}$ transition, a full cavity configuration was constructed as in Fig. 3(d) with two Brewster angle windows [Mellos Griot BK-7 ($n = 1.519$)] optimized at 535 nm to minimize reflectivity losses. The optical cavity consists of two concave mirrors, one "totally reflective" mirror whose radius of curvature is 2m, and an output coupler of 3% transmissivity, also with 2m radius of curvature. The cavity length is 30 cm, and thus the two mirrors are in a stable resonator configuration. Using this configuration, we have successfully monitored output signals enhanced by a factor of four-ten times the single-pass amplification at 535 nm, which suggests oscillation in a moderate Q cavity [28].

The reaction-energy transfer-amplification region corresponds to the intersection of the germanium, thallium, and ozone flows and is estimated to be ~ 1 cm in length. It may not be surprising to find that the amplification region is associated in some part with the "shock zone" where the directed metal-metal oxide and thallium flows intersect; however, this possibility must be modeled and carefully assessed in future experiments. The nature of the present experiment is such that the reaction-amplification zone may shift randomly, primarily in the vertical direction, during a pulsing sequence unless the experimental conditions are repeated precisely. This shift of the amplification zone can create some difficulty in the alignment of the cavity configuration. The HeNe laser depicted in Fig. 3(c) and (d) is used to establish a reasonable cavity alignment as it specifies the region of the short (relative to cavity length) amplification zone that will be sampled. The experiments will be successful provided that a substantial $^2\text{S}_{1/2}$ thallium concentration can be created in the more refined zone specified by the HeNe laser on a time scale commensurate with the $^2\text{S}_{1/2}$ radiative lifetime. Alignment is more critical than that required for the single-pass configuration discussed in the previous section, and the present cavity may not be optimal [28].

The laser-cavity system was also probed temporally using the 125 MHz digital oscilloscope [25]. The cavity [Fig. 3(c) and (d)] was aligned, using the HeNe laser, with the incident slit of a Spex 1704 monochromator set at 535.1 nm, operating at ~ 1 nm resolution (entrance and exit slit dimensions 0.95 mm width, 10 mm height) and placed ~ 20 cm behind the output coupling mirror. The output from the RCA 4840 PMT used previously was again sent to the digital oscilloscope.

With the present configuration, it is possible to make a maximum of five passes through the cavity and $\text{TI } ^2\text{S}_{1/2}$ amplification zone within the time frame of the apparent stimulated emission pulse associated with the $\text{TI } ^2\text{S}_{1/2}-^2\text{P}_{3/2}$ transition. If the reflected light in the cavity passes through the entire length of the amplification zone, the cavity oscillation should produce a substantial increase in output power relative to that for the single-pass output from the optical configuration of Fig. 3(c) sans cavity mirrors. Several experiments have been conducted both with and without cavity mirrors. We find that the signal recorded (Fig. 8) in full cavity configuration is between four and ten times more intense than the superfluorescent laser pulse recorded in the absence of the full laser cavity. Further, the superfluorescence-to-fluorescence ratio increases to well over 100. This is apparent in Fig. 8 where the fluorescence signal following the superfluorescent spike is of negligible intensity. These increases in intensity exceed by at least a factor of two the signal expected for ideal reflection in the absence of a gain medium, and cannot be accounted for on the basis of geometric factors.

In a second experimental configuration, we replaced the spectrometer [Fig. 3(e)] with a fast photodiode (LeCroy Model 40D Optical Deactivator -0.5 mm² detector area, risetime < 1.0 ns) placed 20 cm from the laser cavity. The output from this photodiode was again sent directly to the digital oscilloscope. The combination of the photomultiplier and photodiode experiments indicated peak output powers exceeding several watts. This should be compared to the 600-900 W peak power levels recorded by Isaev and Petrash [3] using pulsed discharges through a 20 cm path.

The nature of the reaction-amplification zone dictates that the full cavity output power for the configuration described above can fluctuate. In fact, in those instances where the cavity is misaligned resulting in minimal reflections through the amplification zone, the output extracted through the 3% output coupler may simply be due to single-pass amplification. This will be improved through extension of the reactant interaction region and a lengthening of the amplification zone, leading to greater cavity stabilization. In the experiment described, when the laser cavity mirrors are walked from their aligned positions, the apparent manifestation of oscillation can be made to cease, and a much weaker signal due to single-pass amplification is detected. We submit that the combination of results obtained in the present study suggests the temporal and directional characteristics which are to be associated with an oscillating laser system.

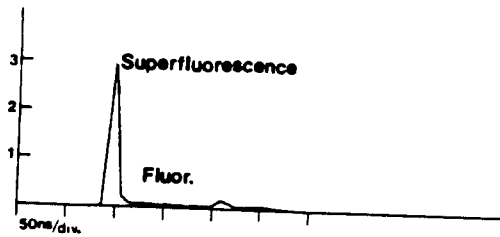


Fig. 8. (a) Tl $7^2S_{1/2}$ - $6^2P_{3/2}$ (535.1 nm) superfluorescent oscillation observed with full laser cavity configuration. The ratio of the superfluorescence to that fluorescence which follows after self-termination of lasing action and is barely visible in the figure is close to 100. See text for discussion.

DISCUSSION—FUTURE CONSIDERATIONS

The characteristics which we observe in the present study suggest to us that we have accomplished a significant energy transfer from metastable states of silicon and germanium oxide to efficiently pump thallium atoms, and that we can observe transient gain and oscillation on the Tl $7^2S_{1/2}$ - $6^2P_{3/2}$ transition. It is clear that the efficient pumping of thallium atoms to the $7^2S_{1/2}$ level requires the copious production of metastable silicon and germanium oxide in an inherently selective process versus that associated with the formation of a "Maxwell-Boltzmann-like" distribution of electrons used to pump a discharge configuration [3]. Further, the temporal behavior which appears to us to signal a stimulated emission process is greatly facilitated by the premixing of germanium and thallium flows, both of which are at high concentration, corresponding to entrained fluxes in the range of $10^{20}/\text{cm}^2 \cdot \text{s}$ [29]. In order to obtain amplification, we must create a population inversion between the Tl $7^2S_{1/2}$ and $6^2P_{3/2}$ levels on a time scale comparable to the $7^2S_{1/2}$ radiative lifetime. In analogy to a discharge-pumped configuration, we may write

$$\begin{aligned} d(N_r)/dt = & k_1(\text{trans})N_0 n_{\text{MO}}^* \\ & + k_1(\text{relax}) N_m(n_{\text{MO}} + n_{\text{O}_3} + n_{\text{Tl}}) \\ & - N_r A_r - N_r[k_2(\text{relax}) \\ & \cdot (n_{\text{MO}} + n_{\text{O}_3} + n_{\text{Tl}})] - P. \end{aligned} \quad (5)$$

$$\begin{aligned} d(N_m)/dt = & k_2(\text{trans})N_0 n_{\text{MO}} + N_r A_{rm} \\ & + k_3(\text{relax}) N_r(n_{\text{MO}} + n_{\text{O}_3} + n_{\text{Tl}}) \\ & - N_m A_m - N_m k_4(\text{relax}) \\ & \cdot (n_{\text{MO}} + n_{\text{O}_3} + n_{\text{Tl}}) + P \end{aligned} \quad (6)$$

where N_0 , N_m , and N_r correspond to the populations of the ground $^2P_{1/2}$, metastable $^2P_{3/2}$, and $^2S_{1/2}$ levels of thallium (Fig. 1) with $N_0 \gg N_r$, N_m , $k_1(\text{trans})$ and $k_2(\text{trans})$ correspond to the energy transfer pumping rate constants,

$k_1(\text{relax})$ - $k_4(\text{relax})$ correspond to rate constants for collisional relaxation (or excitation) by $\text{MO} = \text{GeO}(\text{SiO})$, O_3 , and Tl , MO^* signifies metastable $\text{GeO}(\text{SiO})$, $A_r = A_r + A_{rm}$ and A_m correspond to spontaneous emission rates for the $^2S_{1/2}$ and $^2P_{3/2}$ levels (Fig. 1) where $A_r \gg A_m$, and P is the stimulated emission power due to the $^2S_{1/2}$ - $^2P_{3/2}$ transition.

We envision the pumping process in the bulk of the current experiments as involving the formation of the metastable germanium oxide in the immediate vicinity of a thallium atom as we oxidize the thallium-germanium mixture. This near-resonant pumping process can be quite efficient, and a rate constant $k_1(\text{trans})$ in excess of $1 \times 10^{-9} \text{ cm}^3/\text{atom} \cdot \text{s}$ is by no means unrealistic [30]. In contrast, the collisional excitation of $^2P_{3/2}$ metastable thallium atoms to the $^2S_{1/2}$ level by GeO "near-resonant" pumping, O_3 , or Tl is much less probable [31]. Collisional deactivation of the $^2S_{1/2}$ level is less likely due to its short radiative lifetime.

The first term in (5) can dominate the radiative relaxation term $N_r A_r$ as the magnitude of this product is intimately tied to the N_r pumping rate. It would not be unreasonable to expect the near-resonant pumping process to produce $^2S_{1/2}$ Tl at a rate ranging between 10^{19} and $10^{22} \text{ cm}^{-3} \cdot \text{s}$, whereas the corresponding radiative relaxation rate should range between 10^{16} and $10^{19} \text{ cm}^{-3} \cdot \text{s}$ [32].

In (6), the formation of $^2P_{3/2}$ thallium via radiative decay $N_r A_{rm}$ of $^2S_{1/2}$ Tl dominates radiative loss from the metastable $^2P_{3/2}$ level and collisional relaxation from the short-lived $^2S_{1/2}$ level. It may be possible to pump ground state thallium atoms to the metastable $^2P_{3/2}$ level in a near-resonant energy transfer from ground state GeO , but such a process may be readily recycled by collisional relaxation of the $^2P_{3/2}$ level. Further, both of these processes will likely occur on a time scale much longer than the $^2S_{1/2}$ radiative lifetime.

The previous discussion emphasizes the dominance of the Tl $^2S_{1/2}$ energy transfer pumping and subsequent radiative loss terms as they influence our ability to build a transient population inversion on the Tl $^2S_{1/2}$ - $^2P_{3/2}$ transition. We suggest that the pumping rate which we can achieve through the oxidation of premixed Ge-Tl flows allows the creation of a transient amplification process. In order to achieve the necessary population inversion corresponding to a gain $e^{al} \approx 10/\text{pass}$ through the gain medium [33], we require the pumping of 6×10^{11} Tl $^2S_{1/2}$ atoms on a time scale of 10^{-8} s , corresponding to a rate of $6 \times 10^{19} \text{ cm}^3/\text{s}$. This pumping rate is feasible for the configuration we have employed in this study.

The results obtained here bear many analogies to the discharge configuration employed by Isaev and Petrash [3]. These authors have used a "Maxwell-Boltzmann-like" distribution of electrons to pump ground state thallium atoms at a comparable concentration to that employed in the present study. These authors obtain a peak output power of 900 W from a 20 cm path length dis-

charge through thallium vapor [34]. By comparison, we monitor peak powers which range from several to tens of watts in the present configuration. These relative power levels are quite reasonable.

The Suggestion of a Superfluorescent Event

A consideration of our experimental configuration and reactant concentrations leads us to believe that the apparent stimulated emission which we observe is best attributed to superfluorescence as opposed to amplified spontaneous emission. Based upon the geometry of the system and the visual observation of the thallium fluorescence, we assume a cylindrical amplification zone of length 1 cm and diameter considerably less than 1/4 cm, with a $^2S_{1/2}$ - $^2P_{3/2}$ population difference, which corresponds to a concentration $\Delta N = 2\text{--}5 \times 10^{11}/\text{cm}^3$ [35]. Our estimated reaction zone-amplification length $\mathcal{L} = 1$ cm, based upon the observation of fluorescence, is much shorter than the cooperation length $\mathcal{L}_c \approx 20\text{--}35$ cm, calculated from the relation [36]

$$\mathcal{L}_c = \phi (4\pi c \tau_{sp} / (\Delta N) \lambda^2)^{1/2}$$

where $\phi = \ln(2\pi/\theta_0) = 16$ ($\theta_0 = (\Delta N)^{-1/2} (2\pi)^{-1/4} (\alpha \mathcal{L})^{-3/4} \approx 6 \times 10^{-7}$, α = gain coefficient) is a logarithmic function of θ_0 , the initial tipping angle of the Bloch vector. The gain coefficient $\alpha = 2.3 \text{ cm}^{-1}$ is determined on the basis of $G = e^{\alpha \mathcal{L}} = 10$ for one pass through a 1 cm reaction-amplification path, τ_{sp} is the $^2S_{1/2}$ radiative lifetime $= 7.5 \times 10^{-9}$ s, and $\lambda = 535.1$ nm is the wavelength of the transition.

An \mathcal{L}_c much greater than \mathcal{L} suggests that it is reasonable to conclude that the stimulated emission corresponds to a superfluorescent process [36], [37]. Amplified spontaneous emission (molecular nitrogen laser), in contrast, requires that \mathcal{L} be much greater than \mathcal{L}_c [38]. For an initially totally inverted superfluorescent system, ϕ typically has a value between 10 and 25, in agreement with our determined value. Based upon our apparent observed gain $G = 10$ and our estimated reaction length of 1 cm, we determine a gain coefficient $\alpha = 2.3 \text{ cm}^{-1}$. This coefficient can also be calculated from the relation

$$\alpha = (T_2/\tau_{sp})(\Delta N)\lambda^2/8\pi = 3.3 \text{ cm}^{-1}$$

where $T_2 = 1.1 \times 10^{-9}$ s is the reciprocal of the inhomogeneous Doppler linewidth, we have taken $\Delta N = 2 \times 10^{11}$, and all other quantities have been defined previously. It is to be noted that the α value determined in these experiments may represent a lower bound because of the response time of the digital oscilloscope [33]. If we attempt to correct for this response time, the superfluorescent/fluorescent ratio may be as much as 2.5 times greater than detected. This would correspond to an α value of 3.2 cm^{-1} . The agreement between the determined values of α is encouraging.

Finally, the temporal width of the superfluorescence output pulse can be calculated from the relation

$$\tau_w = \phi (8\pi \tau_{sp} / (\Delta N) \lambda^2 \mathcal{L})$$

to be 5.3×10^{-9} s. This value should be compared to the measured FWHM of $\sim 5 \times 10^{-9}$ s [Fig. 7(b)].

Further Considerations—Extrapolation of the Energy Transfer Concept

The features in Figs. 7 and 8 which we attribute to a stimulated emission process appear to have an ~ 5 ns FWHM. In view of the time resolution of the digital oscilloscope used in this study, this must be viewed as an upper bound until more definitive measurements on a shorter time scale can be made with a scope whose terminal resolution exceeds 1 ns. Further, the roundtrip passage time in the cavity configuration which we have described is also 1 ns. It would, therefore, not be surprising to find that our oscillator pulse may, in fact, be two-three unresolved pulses, separated in time by approximately 1 ns.

In order to pump the thallium $^2S_{1/2}$ level so as to obtain amplification, we must achieve the necessary upper state concentration on a time scale comparable to the $^2S_{1/2}$ - $^2P_{3/2}$ lasing transition. We believe that the necessary pumping rate is attained in large part by virtue of the intimate premixing of high Ge-Tl concentrations, and that the effect is signaled by the specific mode by which we must obtain the short enhanced photon bursts depicted in Figs. 7 and 8. While we anticipate that the triggering of the reactive process takes place on a time scale no less than a microsecond, the substantial population of GeO molecules formed in the energy transfer zone will not be lost to radiative decay, and will be in intimate contact with a substantial concentration of nonreactive ground state thallium atoms. We are continuing our investigation of the nature of the process leading to the temporal behavior depicted in Figs. 7 and 8, currently redesigning our source configurations to both lengthen and closely stabilize the reaction zone-amplification region. These modifications should considerably enhance the power output that we can obtain from the thallium system. In conjunction with this effort, we are concerned with the detailed modeling of mixing-reaction-diffusion rates in these partially premixed systems [39]. It will also be appropriate to establish whether the formation of a shock zone at the intersection of the reactant flows in the reaction-amplification region is effectual.

Because of its short radiative lifetime, the Tl $^2S_{1/2}$ state is not an ideal laser candidate for high-power energy extraction. However, the concepts of which we have made use can be generalized to longer lived excited states and laser transitions which do not terminate on metastable levels. For example, we are currently using SiO metastables

to pump the near resonant Na $4d^2D$ and $5s^2S$ levels observing the $4d^2D$, $5s^2S$ - $3p^2P$ transitions of the sodium atom with radiative lifetimes of 60 and 500 ns, respectively. The $3p^2P$ - $3s^2S$ Na D -line transition rapidly depletes the terminal laser level. Gain has now been measured on the $4d^2D$ - $3p^2P$ transition.

ACKNOWLEDGMENT

It is a pleasure to acknowledge most helpful discussions with Dr. R. C. Oldenborg, Dr. S. Baughcum, and Dr. E. Dorko concerning this study.

REFERENCES

- [1] J. L. Gole and G. J. Green, *Chem. Phys.*, vol. 100, p. 133, 1985; R. Woodward, J. S. Hayden, and J. L. Gole, *Chem. Phys.*, vol. 100, p. 153, 1985 and references therein; Short Wavelength Chem. Laser Workshop, Charleston, SC, Nov. 1984.
- [2] S. H. Cobb, J. R. Woodward, and J. L. Gole, "A chemical process producing a continuous laser amplifier in the visible region," *Chem. Phys. Lett.*, vol. 143, p. 205, 1988; — "Continuous chemical amplification of single and multimode lasers in the visible region," *Chem. Phys. Lett.*, vol. 157, p. 197, 1989.
- [3] A. A. Isaev and G. G. Petrash, "Investigation of pulse gas-discharge lasers utilizing atomic transitions," in *Pulse Gas-Discharge Atomic and Molecular Lasers*, N. G. Basov, Ed., transl. by A. Tobulewicz, Ed., *Sov. J. Quantum Electron.* New York and London: Consultants Bureau.
- [4] C. E. Moore, *Atomic Energy Levels*, Vols. 1, 2, 3, Nat. Stand. Ref. Data Ser. Washington, DC: Natl. Bur. Stand., 1971, p. 35.
- [5] R. Burnham, *Appl. Phys. Lett.*, vol. 30, no. 3, p. 132, 1977; D. J. Ehrlich, J. Maya, and R. M. Osgood, *Appl. Phys. Lett.*, vol. 33, no. 11, p. 931, 1978; H. Hemmati and G. J. Collins, *Appl. Phys. Lett.*, vol. 34, no. 12, p. 844, 1979.
- [6] S. H. Cobb, Ph.D. dissertation, Georgia Inst. Technol., Atlanta, 1988.
- [7] R. G. Derwent and B. A. Thrush, *Chem. Phys. Lett.*, vol. 9, p. 591, 1971.
- [8] A. T. Pritt, Jr., R. D. Coombe, D. Pilipovich, R. I. Wagner, D. Benard, and C. Dymek, *Appl. Phys. Lett.*, vol. 31, p. 745, 1977.
- [9] W. E. McDermott, N. R. Pchelkin, D. J. Benard, and R. R. Bousek, *Appl. Phys. Lett.*, vol. 32, p. 469, 1978.
- [10] R. J. Richardson and C. E. Wiswall, *Appl. Phys. Lett.*, vol. 35, p. 138, 1979.
- [11] R. G. Dermont and B. A. Thrush, *Disc. Faraday Soc.*, vol. 53, p. 162, 1972; D. J. Benard, W. E. McDermott, N. R. Pchelkin, and R. R. Bousek, *Appl. Phys. Lett.*, vol. 34, p. 40, 1979.
- [12] For a good review, see H. Hohl and K. L. Kompa, "The photochemical iodine laser," in *Handbook of Chemical Lasers*, R. W. Gross and J. F. Bott, Ed., New York: Wiley, 1976, p. 667.
- [13] G. J. Green, Ph.D. dissertation, Georgia Inst. Technol., Atlanta, 1982.
- [14] S. B. Oblath, G. J. Green, and J. L. Gole, unpublished results.
- [15] See [1] and G. Hager, R. Harris, and S. G. Hadley, *J. Chem. Phys.*, vol. 63, p. 2810, 1975; G. Hager, L. E. Wilson, and S. G. Hadley, *Chem. Phys. Lett.*, vol. 27, p. 439, 1974.
- [16] H. G. Howell, *Proc. Phys. Soc.*, vol. 57, p. 32, 1945.
- [17] G. J. Green and J. L. Gole, *Chem. Phys.*, vol. 46, p. 67, 1980, vol. 69, p. 357, 1982.
- [18] J. L. Gole and M. McQuaid, unpublished.
- [19] J. R. Woodward, K. K. Shen, S. H. Cobb, C. Winstead, and J. L. Gole, to be published.
- [20] See [14], [18], [1], and also R. W. Field, A. Lagerqvist, and I. Renhorn, *Physica Scripta*, vol. 14, p. 298, 1976.
- [21] L. V. Gurvich, M. M. Novikov, and V. G. Ryabova, *Opt. Spectroscopy*, vol. 18, p. 68, 1965; L. V. Gurvich and I. V. Veits, *Izv. Akad. Nauk. S.S.S.R.*, vol. 22, p. 673, 1958; R. P. Burns, G. DeMaria, J. Drowart, and M. G. Inghram, *J. Chem. Phys.*, vol. 38, p. 1035, 1963. See also A. G. Gaydon, *Dissociation Energies and Spectra of Diatomic Molecules*. London: Chapman and Hall, 1968.
- [22] Based on a combination of crucible temperature measurements employing optical pyrometry to determine a temperature of 800 K for the onset of a clearly observable Tl emission and a maximum operating temperature of 1150 K, and the timed rate of loss of thallium from its source.
- [23] A. Gallagher and A. Lurio, *Phys. Rev.*, vol. 136, p. A87, 1964.
- [24] J. Wiesenfeld, private communication.
- [25] The digital oscilloscope also has an attachment to operate at ~200 MHz; however, the majority of data taken in this study was taken in the 125 MHz mode.
- [26] Note that the peak height in the 10 ns/div scan is 500 mV, whereas that in the 5 μ s/div scan is only 300 mV. We attribute this difference at least in part to the characteristic response of the digital oscilloscopes on these two time scales. That is, on the 5 μ s/div scale, the scope RC time constant is sufficiently long so as to diminish its ability to respond to the full pulse height.
- [27] See, for example, H. S. Johnston, *Gas Phase Reaction Rate Theory*. New York: Ronald, 1966.
- [28] Increases in power output from the cavity (versus the single-pass output) due to oscillation will depend on the portion of the amplification zone sampled during each pass through the cavity. If we define a high Q cavity as one with 1% or less loss and a moderate Q cavity as operative with between 1 and 3% loss, the present cavity with a 3% output coupler is at best a moderate Q device in the absence of scattering and refraction losses.
- [29] The concentration of dimeric or polymeric germanium or thallium molecules is expected to be two-three orders of magnitude lower than the atomic concentration in the subsonic flows used in this experiment. See, for example, J. E. Kingcade, Jr., U. V. Choudary, and K. A. Gingerich, *Inorg. Chem.*, vol. 18, p. 3094, 1979; J. Drowart and G. DeMaria, *J. Chem. Phys.*, vol. 30, p. 308, 1959; A. Kant and B. Strauss, *J. Chem. Phys.*, vol. 45, p. 822, 1966.
- [30] J. Herbelin, private communication at Short Wavelength Chem. Laser Workshop, SAIC Inc., Atlanta, GA, Apr. 1989.
- [31] However, at high thallium and germanium concentrations, the interaction between GeO and Tl metastables may efficiently pump the Tl $^2D_{3/2, 5/2}$ levels.
- [32] Self-absorption by ground state thallium atoms will decrease this rate where A_r is best written as $A_r = A_{ro}F + A_mF$ is a fraction decreasing with increasing self-absorption.
- [33] The temporal scan corresponding to Fig. 7(b) was obtained using a 50 Ω load for fast time response. The observed photomultiplier voltage, 0.5 V, ascribed to the stimulated emission process, therefore corresponds to a tube current of 0.1 A. This high tube current can result in changes in the dynode voltages and photomultiplier gain. However, when the light signal is attenuated, the waveform associated with the light pulse impinging on the detection system does not appear to change. Further assuming that we may not have correctly detected a change in waveform, it is certainly relevant that the transient "high-voltage" signal is associated with a particular mixing configuration; the photomultiplier must be responding to a considerably higher light level, although any modification in the tube gain may lead to an amplification of the true relative signal. This suggests the possibility of a lower overall gain G and gain coefficient α , and places a lesser requirement on the requisite pumping rate for the Tl $^2S_{1/2}$ level. However, one must also consider the opposite effect of the less than optimal response of the digital oscilloscope used in this study (see also [26]).
- [34] The thallium vapor zone in these experiments is not homogeneous.
- [35] Determined on the basis of 1) the estimated concentration of GeO* produced in the reaction zone, and 2) the assumption of a $10 \times$ gas kinetic rate for the transfer of the energy stored in GeO* to $X^2P_{1/2}$ thallium atoms to produce Tl* ($^2S_{1/2}$). The Ge concentration in the reaction zone is well in excess of 10^{14} atoms/cm³ and can approach $\sim 10^{15}$ /cm³, whereas the ozone concentration is close to $\sim 7 \times 10^{14}$ /cm³. Using the rate constant of Davis *et al.* for the Si-N₂O reaction as a guide (8.11×10^{-11} cm³/atom \cdot s, P. M. Swearingen, S. J. Davis, and R. M. Niemczyk, *Chem. Phys. Lett.*, vol. 55, p. 274, 1978), and estimating a quantum yield of 10%, we suggest that the rate of GeO* production can reach $\sim 2 \times 10^{10}$ molecules/cm³ \cdot s in the GeO-Tl intersection region. With a thallium atom concentration $\sim 10^{16}$ /cm³ and a rate constant for the energy transfer from GeO* to Tl in excess of 10^{-9} cm³ \cdot molecule⁻¹ \cdot s⁻¹, we estimate that the Tl* formation rate could reach a maximum of 1×10^{21} \cdot cm⁻³ \cdot s⁻¹ in the reaction-amplification zone, easily leading to a buildup of the

$Tl^+ 2S_{1/2}$ state to the high $10^{11}/\text{cm}^3$ range in the time scale necessary to observe a superfluorescent event.

- [36] J. C. MacGillivray and M. S. Feld, *Phys. Rev.*, vol. A23, p. 1334, 1981.
- [37] In this analysis, we are assuming that the stimulated emission process is at least superfluorescent; however, we cannot rule out a superradiant event.
- [38] O. Svelto, in *Principles of Lasers*, 2nd ed. New York: Plenum, 1982.
- [39] In this effort, we will use the Acuchem computer program for modeling complex chemical reaction systems. See W. Brown, J. T. Heron, and D. K. Kahaner, *Int. J. Chem. Kinetics*, vol. 20, pp. 51-62, 1988. We thank J. Herbelin and B. Koffend for providing us with copies of this program.



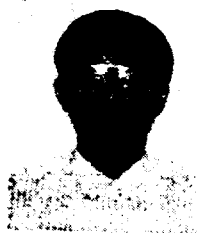
James R. Woodward was born in Kansas City, MO, on September 27, 1960. He received the B.S. and M.S. degrees in chemistry from Furman University, Greenville, SC, in 1982 and 1983, respectively.

He worked as a Research Assistant through 1984 and was a Research Scientist through 1987 with the School of Physics, Georgia Institute of Technology, Atlanta, where he was involved in several experimental efforts in the High Temperature Chemical Physics Laboratory involving the study of highly exothermic chemiluminescent reactions, laser-induced fluorescence studies of small metal clusters, and the characterization of metal cluster oxidation reactions. In 1987 he joined the Advanced Technology Department of the General Electric Company where he is concerned with the laser spectroscopy of halogen lamps and mass spectrometry and quartz crystal microbalance measurements of *E*-mix loss rate during activation and operation of fluorescent lamps.



Stephen H. Cobb was born in Big Rock, TN, on May 7, 1959. He received the B.S. and M.S. degrees in engineering physics from Murray State University, Murray, KY, in 1980 and 1981, respectively. He received the Ph.D. degree from the Georgia Institute of Technology, Atlanta, in 1988 with an emphasis on studies in chemical physics related to metal cluster oxidation and visible chemical laser development.

From May 1981 to August 1984, he was employed by McDonnell Douglas Corporation, St. Louis, MO, as an engineer in the Physics and Optics Laboratory, Flight Laboratory Development Division of McDonnell Aircraft Company. In August 1988, he joined the faculty of Murray State University as an Assistant Professor of physics. In addition to teaching, his interests include near infrared reflectance spectroscopy and high resolution alkali metal fluorescence studies.



Kangkang Shen was born in Hangzhou, China, on October 28, 1958. He received the B.S. degree in optical engineering from Zhejiang University, Hangzhou, China, in 1982. He received the M.Sc. degree in physics from San Diego State University, CA in 1987 and transferred to the Georgia Institute of Technology, Atlanta, where he is currently a graduate student in the High Temperature Laboratory pursuing laser induced fluorescence studies of metal cluster oxidation and visible chemical laser development.

From 1982 to 1985 he was employed by Zhejiang University as an engineer in the Spectroscopy Division of the Central Laboratory of Zhejiang University.



James L. Gole was born in Chicago, IL, on September 17, 1945. He received the B.S. degree in chemistry from the University of California, Santa Barbara, where he was an NSF Undergraduate Research Fellow, in 1967. He received the Ph.D. degree from Rice University, Houston, TX, in 1971 where he was a Phillips Petroleum Research Fellow. He was an NSF Postdoctoral Fellow at Columbia University, NY, from 1971 to 1973.

He joined the Department of Chemistry, Massachusetts Institute of Technology, Cambridge, in 1973 and in 1977 moved to the School of Chemistry of the Georgia Institute of Technology, Atlanta, where he became a Professor of chemistry in 1981. In 1983, he joined the School of Physics, GIT, where he is currently a Professor of physics.

He is interested in the molecular electronic structure of high temperature molecules, chemiluminescence techniques as applied to the study of molecular dynamics and the determination of molecular parameters, laser induced fluorescence, high temperature vacuum ultraviolet spectroscopy and quantum chemistry. His current fields of interest include high temperature chemical physics, laser spectroscopy of small metal clusters and metal cluster oxides, chemiluminescent phenomena as applied to the study of reaction dynamics and the nature of metal cluster oxide and halide formation, ultrafast intra and intermolecular energy transfer, chemical lasers and quantum chemistry. He has filed 6 patents and has published about 120 papers.

Dr. Gole is currently chairman of the ILS Conference, the APS Laser Science Topical Groups Conference on Laser Science, Chairman of Lasers in Chemistry and Biology of the Quantum Electronics and Laser Science Conference and a member of the editorial board of High Temperature Science. In 1989 he received the Sustained Research Award of the Sigma Xi Research Society and in 1990 was named GIT Outstanding Faculty Research Author. He is a member of Sigma Xi, Phi Lambda Upsilon, AAAS, APS, and ACS.

APPENDIX II

"Chemically Driven Pulsed and Continuous Visible Laser Amplifiers and Oscillators",
K. K. Shen, J. R. Woodward, S. H. Cobb, J. R. Doughty, and J. L. Gole, Proceedings
of the Eighth International Symposium on Gas Flow and Chemical Lasers, SPIE,
Volume 1397, pg. 125 (1990)

Reprinted from

**Eighth International Symposium on
Gas Flow
and Chemical Lasers**

**10-14 September 1990
Madrid, Spain**



SPIE Volume 1397

CHEMICALLY DRIVEN PULSED AND CONTINUOUS VISIBLE LASER AMPLIFIERS AND OSCILLATORS

J. L. Gole, J. R. Woodward, S. H. Cobb, K. K. Shen and J. R. Doughty
Georgia Institute of Technology, Atlanta, Georgia 30332, U.S.A.

ABSTRACT

Two approaches to visible chemical laser development are outlined. An extremely efficient near resonant intermolecular energy transfer from selectively formed metastable states of SiO and GeO to sodium atoms is used to form a sodium atom laser amplifier representing an extension of the outlined concept producing the first visible (535 nm) chemical laser amplifier and oscillator based on a thallium atom receptor. We outline the thallium laser concept and the development of the sodium based energy transfer system for laser amplification and oscillation in the wavelength ranges - 569 and 616 nm. In a second approach, we rely on the high cross section (pumping efficiency) highly selective and exothermic sodium trimer-halogen atom reactions to produce continuous sodium dimer laser amplifiers. Optical gain through simulated emission is demonstrated in regions close to 527 (3.8% for individual rovibronic level ($\alpha = 8 \times 10^{-3}/\text{cm}$)), 492, and 460 nm (~ 2.3% for indiv. rovibronic level). Potential extensions to the ultraviolet are noted.

INTRODUCTION

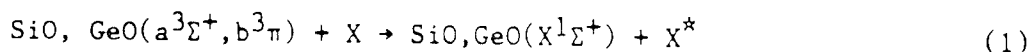
We have employed certain unique aspects of a very select group of highly exothermic simple metal oxidations in order to develop what appear to be the first chemically driven laser amplifiers (and oscillators) operative in the visible spectral region.¹ One class of these systems operates in a pulsed configuration relying on ultrafast near resonant intermolecular energy transfer² from metastable storage states formed in chemical reaction to subsequently amplifying thallium (535 nm), gallium (417 nm), and sodium (569 nm) atom transitions, the thallium system now being converted to a multipass oscillator configuration. A second system operates on the creation of a continuous population inversion based on the chemical pumping of sodium dimer (Na₂) and thusfar showing amplification at 527, 492, and 460 nm.¹

Chemically Driven Visible Laser Transitions from Ultrafast Energy Transfer

We have been concerned with the demonstration of pulsed chemically driven visible laser amplifiers and oscillators based on the near resonant fast energy transfer pumping of potentially lasing atomic transitions. Toward this goal, we have developed techniques to form copious quantities of the metastable SiO and GeO $a^3\Sigma^+$ and $b^3\Pi$ states as the products of the primarily spin conserving Si-N₂O,³ Si-NO₂,⁴ Ge-N₂O, and Ge-O₃ reactions. These long-lived triplet states act as an energy reservoir for fast near resonant intermolecular energy transfer to efficiently pump atomic transitions. With this approach we have obtained short-lived amplification and oscillation from atomic thallium at 535 nm (gain coeff. $\alpha \geq 2.5/\text{cm}$)^{2,5}. We have extended this concept to the pumping of sodium and potassium atom transitions which show the promise of producing higher duty cycle operation, and have now demonstrated gain in the Si-SiO-Na system at 569 nm.

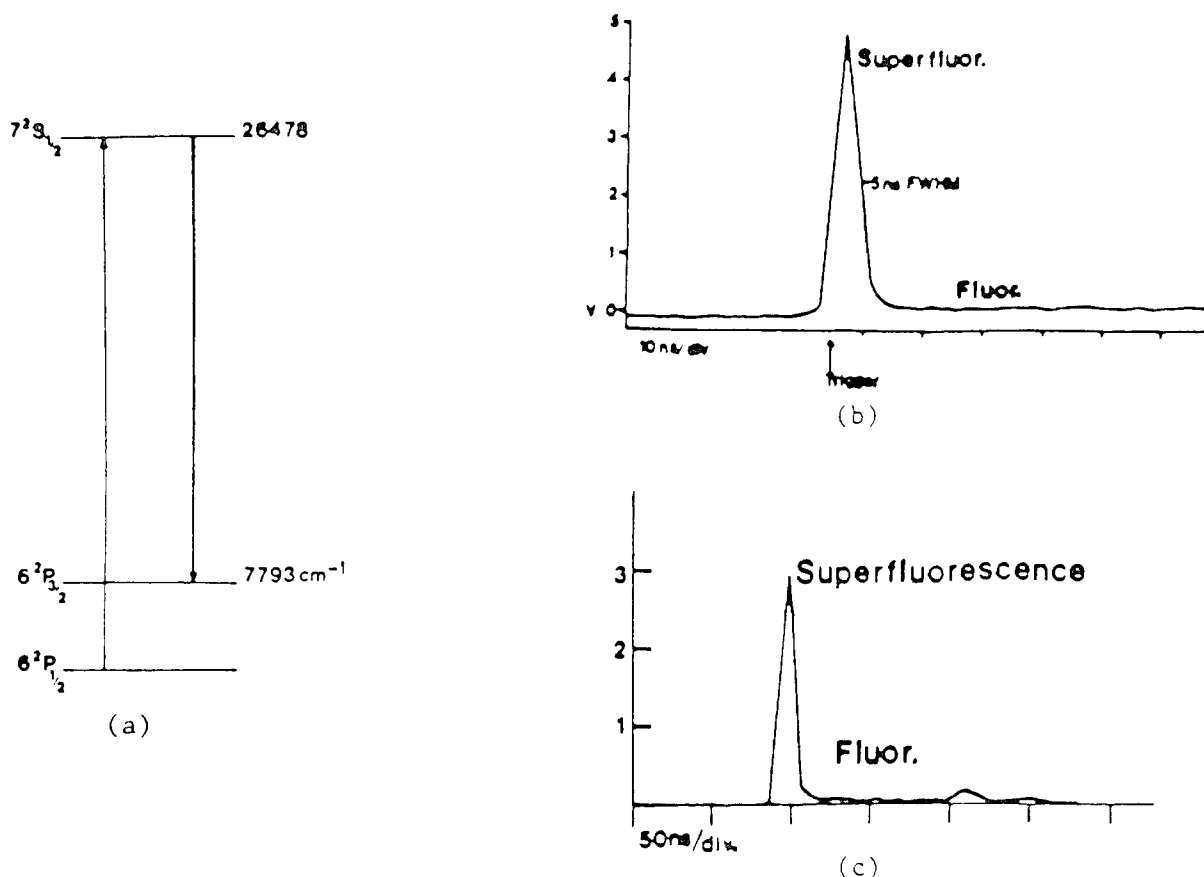
The SiO and GeO $a^3\Sigma^+$ and $b^3\Pi$ states form a combined metastable triplet state

reservoir which is, at best, weakly coupled to the ground electronic $X^1\Sigma^+$ state (minimal nonradiative transfer). This reservoir can be maintained and can be made to transfer its energy to pump an atom of interest if a near resonant energy transfer is feasible. We make use of an efficient intermolecular energy transfer process



where X^* represents the electronically excited atomic species from which we wish to obtain lasing action. The success of this outlined scheme depends on the rates for the reactions forming the SiO or GeO metastables⁶ and the rate of the MO^* ($M=\text{Si}, \text{Ge}$) - X intermolecular energy transfer strongly influenced by near resonances between the MO^* and X^* energy levels.

Initially, the Group IIIA metal thallium, was chosen as a promising candidate for the transfer scheme considered because this atom has a regular ground electronic 2P state with a substantial spin-orbit splitting (7792.7 cm^{-1})⁷ and an excited $^2S_{1/2}$ upper state in near resonance with the SiO and GeO triplet states. In addition,



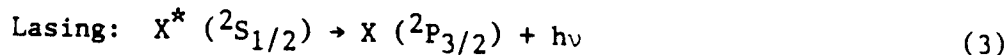
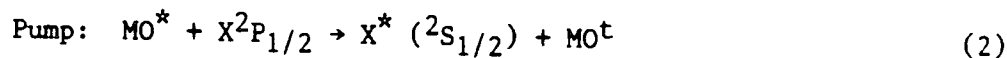
Figures 1

Figure 1(a) Tl atom energy levels.

Figure 1(b) Tl $7^2S_{1/2} - 6^2P_{3/2}$ (535.1nm) superfluorescence observed at a signal trigger level of 0.2V (fluorescent level - 0.045V). The trigger of the superfluorescence is by signal level and not by reactant mixing which occurs on a much longer time scale. The measured FWHM is < 5 nsec compared to $\tau = 7.5$ n-sec, the radiative lifetime of the $7^2S_{1/2}$ level. A return to the fluorescence level is seen subsequent to the superfluorescent pulse. No such superfluorescent pulse is associated with the Tl $7^2S_{1/2} - 6^2P_{1/2}$ (377.7nm) transition.

Figure 1(c) Tl $7^2S_{1/2} - 6^2P_{3/2}$ (535.1nm) superfluorescent oscillation observed with full laser cavity configuration. The superfluorescence/fluorescence ratio (fluorescence following self-termination of lasing action) is now in excess of 100.

photodissociation lasers involving the corresponding upper $^2S_{1/2}$ atomic state were already known for all of the Group IIIA atoms, these operating on the strongly allowed $^2S_{1/2} - X^2P_{3/2}$ transition and producing laser action⁸ at 417 (Ga), 451 (In) and 535 nm (Tl). We make use of the scheme (Figure 1(a))



Here, the metal oxide excitation is transferred to the Group IIIA atom, pumping from the $X^2P_{1/2}$ to the energetically accessible electronically excited $^2S_{1/2}$ level, this level subsequently undergoing the (potential laser) transition $^2S_{1/2} - X^2P_{3/2}$ to what corresponds to an initially sparsely populated $^2P_{3/2}$ spin orbit component ($N_{3/2} \leq e^{-10} (N_{1/2})$ at $T \leq 1100K$) in the Tl system.

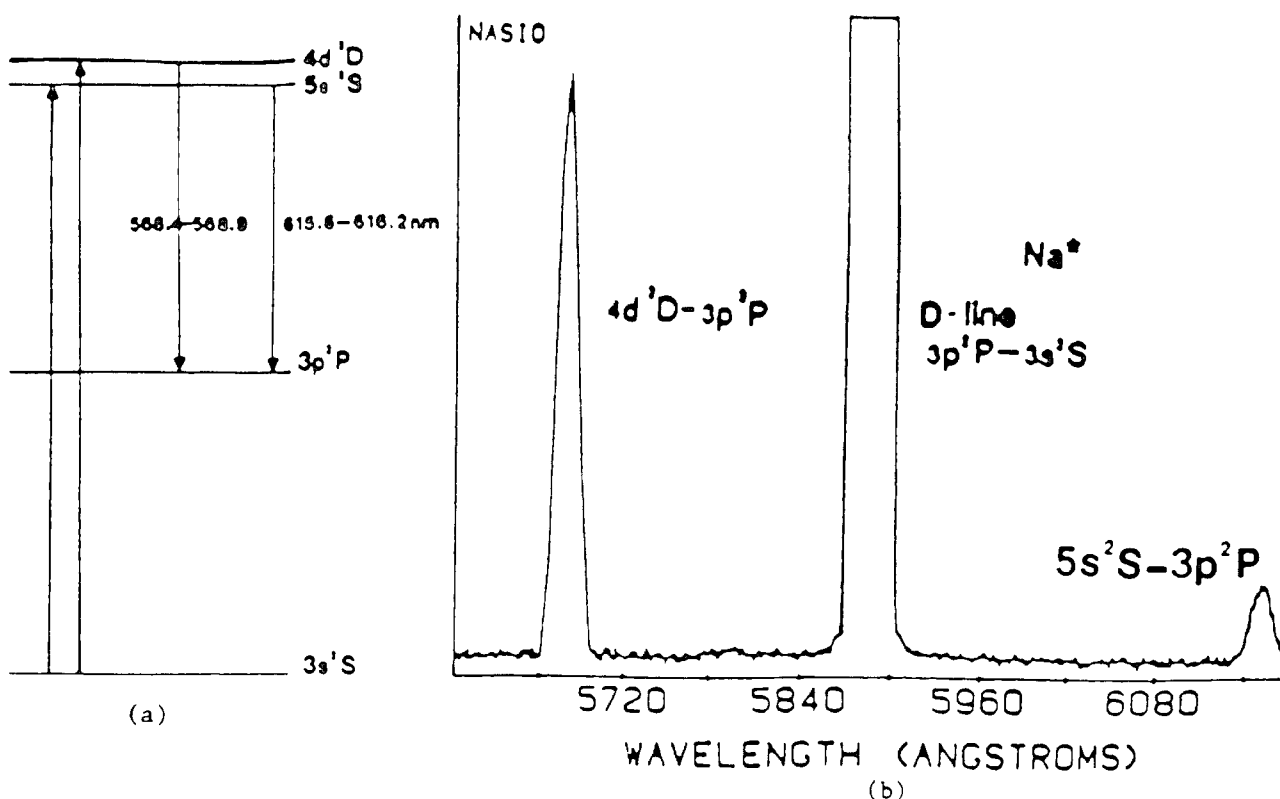
The efficiency of the outlined process for $X = Tl (^2P_{1/2})$, which does not react to form the metal monoxide, is such that a "superfluorescent" laser spike (Fig. 1(b)) some 10 times the normal $^2S_{1/2} - ^2P_{3/2}$ fluorescent intensity is generated on less than a 5ns time scale.⁹ As the population of the $P_{3/2}$ metastable level builds in this system, the $^2S_{1/2} - ^2P_{3/2}$ population inversion is lost and lasing ceases. The signal level in the remainder of the temporal scan corresponds to $^2S_{1/2} - ^2P_{3/2}$ fluorescence.

We have now extended the Tl atom laser amplifier concept to develop the corresponding laser oscillator. In a stable resonant cavity intermediate to a near planar - near confocal configuration ($g_1=g_2=17/20$) with 3% output coupling, we obtain a substantial increase in output power ($\sim 10X$) accompanied by a substantial increase in the ratio of superfluorescence to fluorescence (≥ 100) (Fig. 1(c)) verses the single pass amplifier. This output is obtained with up to three passes through the amplifying medium in the time scale over which the population inversion is maintained^{2,9,10} ($\sim 3-5$ ns). Amplification and oscillation are obtained with high reactant concentrations ($Si(Ge) \geq 2 \times 10^{14}/cm^3$, $Tl \geq 1 \times 10^{16}/cm^3$, oxidant $\geq 5 \times 10^{14}/cm^3$)² and only in those systems in which the Si or Ge and Tl are premixed before the oxidation - energy transfer - amplification cycle is initiated.² A major focus of our continuing efforts has been to extend the near resonant energy transfer concept to atomic sodium or potassium as a means of forming higher duty cycle laser amplifiers, optimizing the efficiency of these created laser amplifiers, and subsequently optimizing these systems so as to produce efficient laser oscillators.

Extension of the Near Resonant Intermolecular Energy Transfer Concept to Na and K Atom Transitions

While our initial efforts have been focused primarily on a pump of thallium atom excited states, we have now extended the near resonant energy transfer concept with an emphasis on obtaining an efficient pump for longer lived emitters (allowing a further increase in energy storage in the laser cavity). In this respect the more nearly energy transfer resonant Na system energy level scheme depicted in Fig. 2 is well suited. Here, in developing this system and its potassium analog we not only take advantage of the chemical pumping of the considerably longer lived 2S or 2D levels of the sodium atom but also we replace the metastable Tl $^2P_{3/2}$ state (Fig. 1), the terminal laser level in our amplifier-oscillator concept, with a rapidly depleted low-lying electronic state corresponding to the upper level of the Na D-line

transition.



Figures 2

Figure 2(a) Na atom energy level scheme and pumping cycles to produce $4d^2D$ and $5s^2S$ excited states.

Figure 2(b) Typical energy transfer pumping spectrum for Na $4d^2D-3p^2P$ and $5s^2S-3p^2P$ transitions and $3p^2P-3s^2S$ sodium D-line emission. The D-line emission results both from direct energy transfer pumping from ground state NaO and from fluorescence to the $3p^2P$ level.

Oscillator strengths for transitions among the Na levels depicted in Fig. 2(a) are catalogued and compared to Tl in Table 1. To an even greater degree than the Tl and Ga systems, a near resonant energy match to the receptor atoms of interest certainly pervades in the Na and K systems where both metastable SiO and GeO can be used to energy transfer pump from the $3s^2S$ Na ground state ($4s^2S$ in K) to the $4d^2D$ and $5s^2S$ levels ($5d^2D$ and $6s^2S$...in K). In the Tl system laser action is terminated through the filling of the $P_{3/2}$ level, however, in the sodium system (Fig. 2(a)) the terminal laser level is the extremely short-lived upper level of the Na D-line. The $3p^2P-3s^2S$ transition is characterized by a high oscillator strength facilitating rapid loss of the terminal laser level to create ground state sodium atoms which Figs. 2(a) and 2(b) demonstrate are again amenable to near resonant energy transfer pumping.

While the $5s^2S$ and $4d^2D$ levels are not readily assessed in an optically pumped transition, Fig. 2(b) demonstrates that, using SiO metastables formed in the Si-N₂O reaction, we have now successfully energy transfer pumped Na atoms to the $2S$ and $2D$ levels where they subsequently emit radiation at ~ 616 nm and 569 nm as they undergo transition to the $3p^2P$ levels. These transitions are characterized by moderate to

small oscillator strengths. The assessed Na cycle with its 50^{11} to 500^{11} nanosecond upper state radiative lifetimes (vs. Tl $^2S_{1/2}$ at $\sim 7^{11}$ nsec.¹¹) and short-lived terminal laser level would appear ideally suited to obtain high duty cycle laser amplifiers and oscillators. In fact, we have now measured gain in the sodium system at ~ 569 nm ($\alpha = 0.27/\text{cm}$) consistent with our previous observations in the Ge-GeO-Tl system.² Gain measurements were carried out using an optical train surrounding a short reaction-energy transfer-amplification region, the entire device closely paralleling an ingenious design used by Roll and Mentel¹² to measure new laser lines in SeII employing amplified spontaneous emission.

While our continued emphasis has been on the sodium system and the results presented in Fig. 2(b) involve a metastable SiO pump, it is also feasible to use GeO metastables for energy transfer pumping. The efficient pumping of the 2S and 2D states of sodium and potassium is significant because their increased radiative lifetimes can lead to more efficient energy storage in a laser cavity while the higher oscillator strength of the $3p^2P-3s^2S$ transition in sodium ($4p^2P-4s^2S$ in K) facilitates rapid loss of the terminal laser level to create ground state sodium atoms. Figure 2 demonstrates that the resultant atoms are again amenable to near resonant energy transfer pumping.

Table I
Transition Probabilities Among Select Low-Lying States
of Atomic Sodium^a and Thallium^b

Transition	Composite Einstein A Coeff.	Averaged Oscillator Strength, f
Na 5s 2S - 3p 2P	0.072	0.0137
Na 4d 2D - 3p 2P	0.131	0.106
Na 3p 2P - 3s 2S (Na D-line)	0.629	0.982
Tl ^b 7s $^2S_{1/2}$ - 6p $^2P_{1/2}$	0.617	
Tl ^b 7s $^2S_{1/2}$ - 6p $^2P_{3/2}$	0.716	
Tl ^c 6p $^2P_{3/2}$ - 6p $^2P_{1/2}$	< 0.01	

a. See References 11.

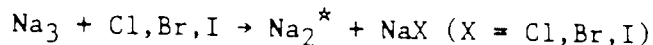
b. Estimated on the basis of data in Refs. 11.

c. Radiative lifetime on order of 1 second, J. Wiesenfeld, private communication.

In our successful efforts with the Tl system we have demonstrated a laser system with a gain coefficient $\alpha \sim 2.5/\text{cm}$. The extension to the longer-lived states of sodium and potassium shows yet more promise. Given the appropriate engineering and the ability to overcome the critical scaling parameters of cavity stability at high powers, we suggest that the select systems which we have outlined will be scalable to megawatt peak power levels as the necessary reactants can be synthesized in a highly volatile form, clearly enhancing the ability to create much higher reactant and product concentrations.

Continuous Chemical Laser Amplifiers in the Visible Region

We have been concerned with the high cross section, highly exothermic $\text{Na}_3 - \text{X}$ (Cl, Br, I) reactions which form Na_2^* in several of its excited electronic states.¹ The optical signatures for the processes



encompass emission from a limited number of Na_2 band systems. Surprisingly, the observed emission is characterized by sharp well defined emission regions¹ (Figures 3,4) superimposed on a much weaker but perceptible background. As Fig. 4 demonstrates, these sharp emission features are not readily explained by invoking a purely fluorescent process.¹

The sharp nature of several of the B-X, C-X, and C'-X Na_2 fluorescence features (Fig. 3) and their correlation in certain regions to the emission characteristic of optically pumped Na_2 laser systems¹³ (ex: $528.2\text{nm} (\nu', \nu'') = (6,14)\text{B-X}$) suggests the possibility that stimulated emission might be associated with certain of the Na_2 emission products. Laser gain measurements have been carried out to assess this possibility.

In order to carry out these studies, we have developed (Fig. 5(a)) a unique source configuration which allows the supersonic expansion of pure sodium vapor to create a Na_3 concentration not previously attained in a reaction amplification zone. Using argon ion pumped dye lasers to study the $\text{Na}_3 + \text{Br}$ reaction we have scanned (Fig. 5(b)) the entire wavelength region from 420 to 600nm (Figure 3) at 0.5 cm^{-1} resolution (FWHM)¹ and the regions around 527nm and 460nm (Fig. 4) at 0.007 cm^{-1} resolution using a ring dye laser.¹ We find that laser gain and hence amplification is characteristic of certain select regions and that several of the sharper and more pronounced emission features apparent in the spectra depicted in Figure 3 correspond to a stimulated emission process and to the establishment of a population inversion. Our ring dye laser studies demonstrate that the strong feature at $\sim 527\text{nm}$ (Fig. 4) corresponds to stimulated emission from between four and seven unresolved rotational levels.

Optical gain through stimulated emission has been measured at 0.5 cm^{-1} resolution in the regions 527nm (1% gain), 492nm (0.3% gain) and 460.5nm (0.8% gain), correlating precisely with the reactive process and the relative intensities of those features observed while monitoring the light emitted from the $\text{Na}_3\text{-Br}$ and $\text{Na}_3\text{-I}$ reactions (Figs. 3,4). High resolution ring dye laser scans in the 527nm region indicate that the gain for the system is close to 3.8% for an individual rovibronic transition with approximately four to seven transitions showing gain. At 459.8 nm we have measured 2.3% gain for an individual rotational level. These results demonstrate the continuous amplifying medium for a visible chemical laser in at least three wavelength regions.¹ At no other scanned wavelengths have we observed gain. In the region of the sodium D-line, a substantial absorption and hence loss is monitored as a function of the trimer-halogen atom reaction.

Because of the low Na_3 ionization potential and the high halogen electron affinities,¹⁴ the $\text{Na}_3\text{-halogen}$ atom reactions are expected to proceed via an electron jump mechanism with extremely high cross sections,¹⁵ producing substantial Na_2 excited state populations. The created population inversions monitored thusfar are thought to be sustained by the large number of free halogen atoms reacting with the

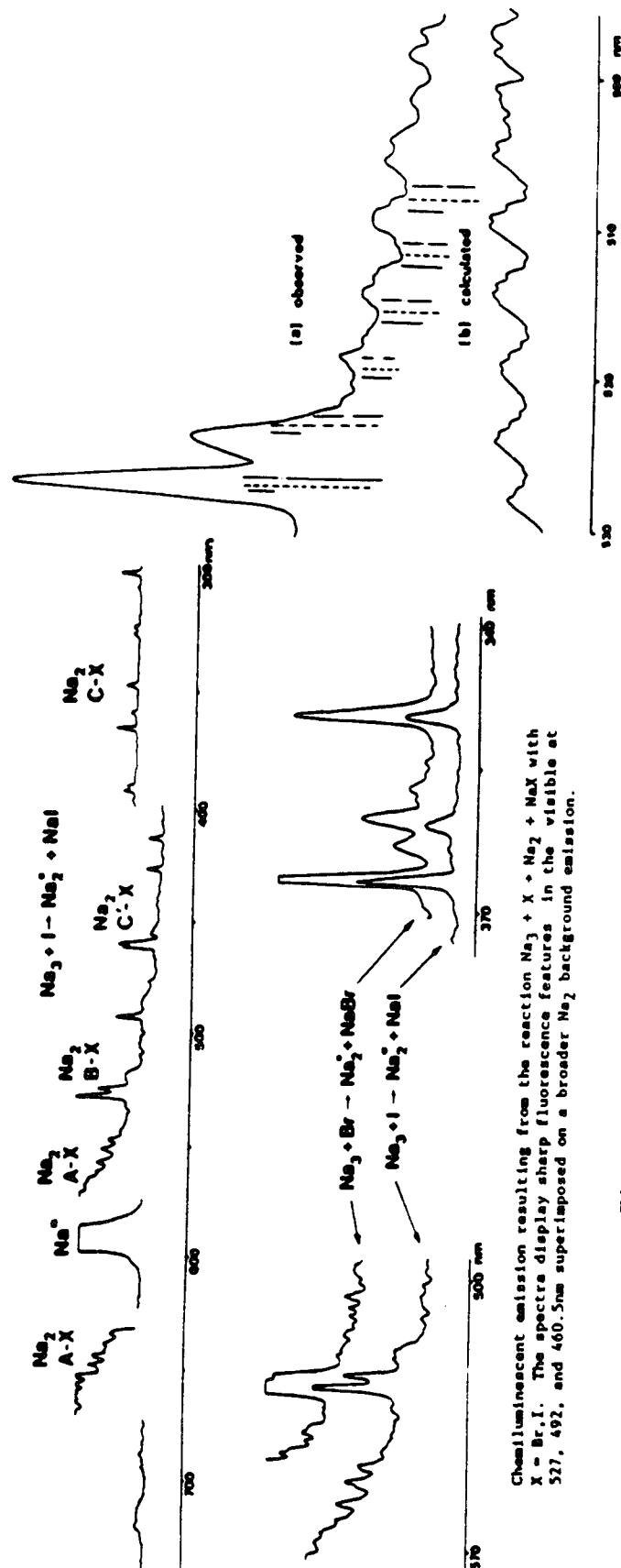


Figure 3

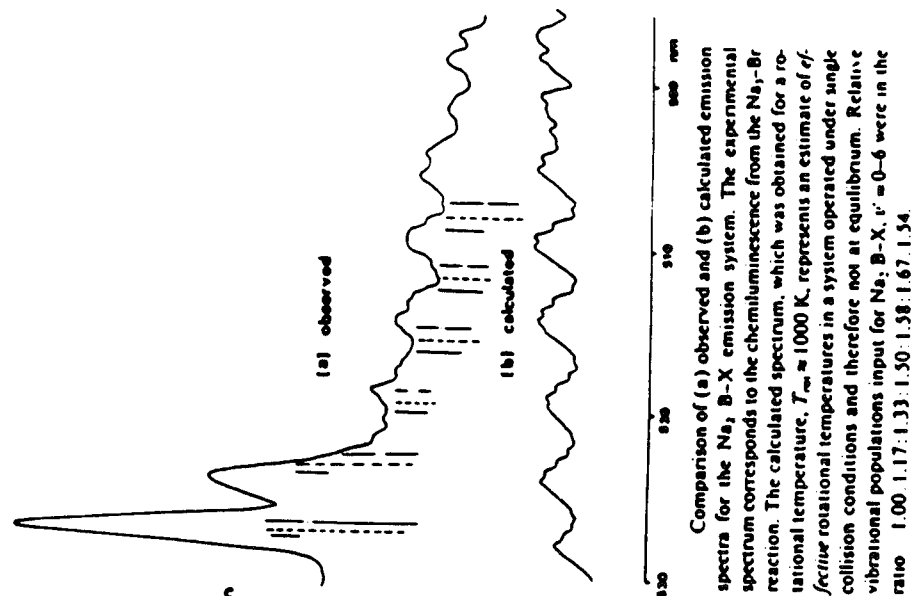
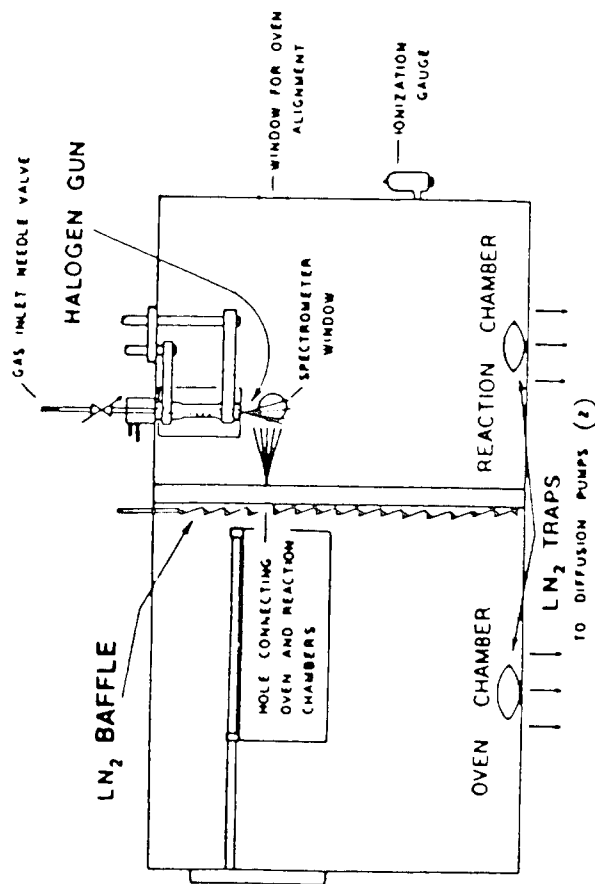
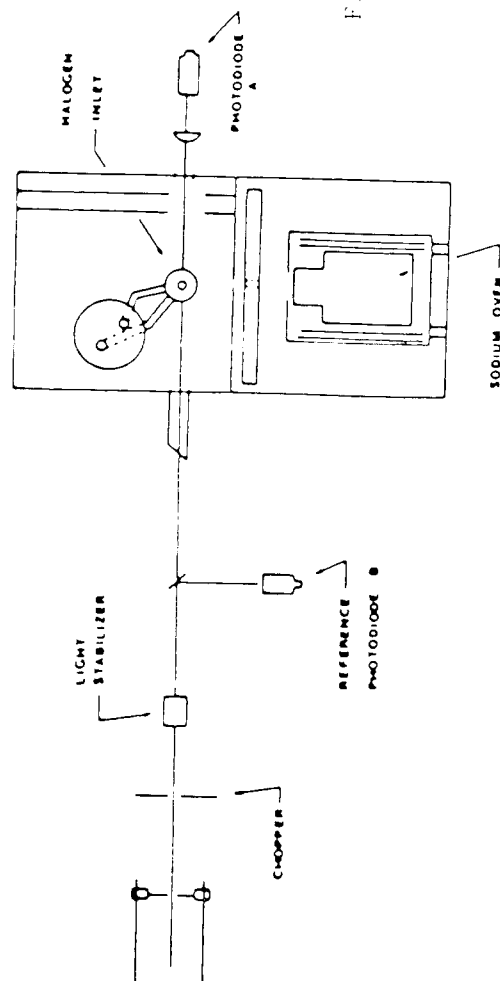


Figure 4



a



b

Figures 5

Na₂ Chemical Laser Amplifier

- Broadband Amplification (0.5cm⁻¹ FWHM)

1% at 527nm

0.3% at 492 nm

0.8 % at 461nm

All other Regions 400-600nm no gain

At Na D-line substantial loss

- Narrowband Amplification (0.007cm⁻¹ FWHM)

3.8% at 526.9nm

~ 2.3% at 459.8nm

Individual Rotational Transitions

Na_2 molecules in those ground state levels on which the transitions emanating from the Na_2 excited states terminate as well as collisional relaxation of ground state sodium molecules. The cross section for reaction of vibrationally excited ground state Na_2 is expected to be quite substantial relative to that corresponding to collision induced vibrational deactivation of the Na_2 manifold. Extremely efficient reactions rapidly deplete the lower state levels in this system allowing one to sustain a continuous population inversion.

Our major efforts thusfar have focused on the Na_2 B-X spectral region and the potential development of a laser oscillator at wavelengths in the vicinity of 527 and 460nm. We are also concerned with the extension of these studies further into the ultraviolet region primarily as they assess states of considerably longer radiative lifetime.

The Na_2 ~ 395, ~ 365, and ~ 350nm emission regions depicted in Fig. 6 represent a portion of the optical signatures for the $\text{Na}_3\text{-Br}$ reaction. They are of interest for they correspond again to sharp emission features, on a broad and weak background, whose appearance cannot be readily explained in terms of a purely fluorescent process. They are tentatively associated, at least in part with a very recently ascribed double minimum excited electronic state¹⁶ ($2^1\Sigma_u^+ - X^1\Sigma_g^+$).

The radiative lifetimes associated with this double minimum state are complex and longer (>40ns) than those associated with the Na_2 B-X region. These longer lifetimes of course enhance the potential energy storage in a laser cavity. This, in turn, suggests that the laser gain studies already performed should be extended to this spectral region in order to assess the feasibility of using these transitions as the source of laser amplifiers extending far into the ultraviolet. Further, we will want to extend these studies to the other alkali metals, taking advantage of the possibility for forming laser amplifiers extending both to considerably shorter and longer wavelength.

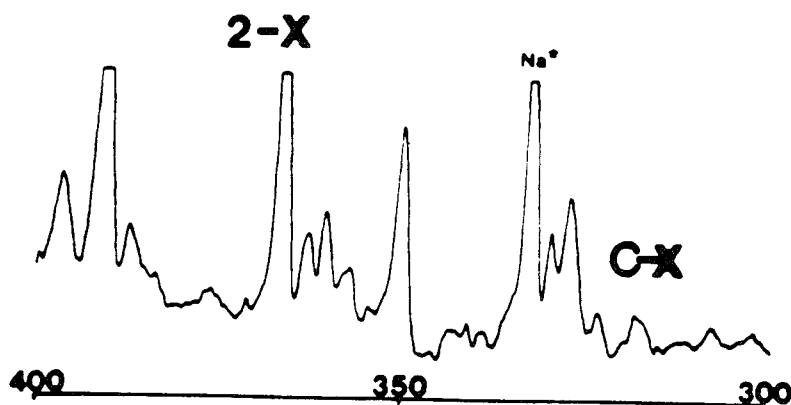


Figure 6 Chemiluminescence from the reaction $\text{Na}_3 + \text{Br} \rightarrow \text{Na}_2^* + \text{NaBr}$. The spectrum is dominated by the Na_2 $C^1\Pi_u - X^1\Sigma_g^+$ and $2^1\Sigma_u^+ - X^1\Sigma_g^+$ emission features.

ACKNOWLEDGEMENT

It is a pleasure to acknowledge most helpful discussions with Drs. R. C. Oldenborg, S. Baughcum, and E. Dorko concerning this study. The support of the Georgia Tech Foundation through a grant from Mrs. Betty Peterman Gole, the Army Research Office through the Short Term Innovative Research Program and the Air Force Office of Scientific Research - Army Research Office is greatly appreciated.

REFERENCES

1. W. H. Crumley, J. L. Gole, and D. A. Dixon, *J. Chem. Phys.* 76, 6439 (1982).
S. H. Cobb, J. R. Woodward, and J. L. Gole, *Chem. Phys. Lett.* 143, 205 (1988).
S. H. Cobb, J. R. Woodward, and J. L. Gole, *Chem. Phys. Lett.* 157, 197 (1989).
S. H. Cobb, J. R. Woodward, and J. L. Gole, "Continuous Chemical Laser Amplifiers in the Visible Region", Proceedings of the Fourth International Laser Science Conference, A.I.P. Conf. Proc. No. 191, Optical Science and Engineering Series 10, pg. 68.
2. J. R. Woodward, S. H. Cobb, K. K. Shen, and J. L. Gole, "A Chemically Driven Visible Laser Transition Using Fast Near Resonant Energy Transfer", to appear in a Special Issue of the IEEE Journal of Quantum Electronics on Electronic Transition Gas Lasers. J. R. Woodward, S. H. Cobb, and J. L. Gole, "Super-fluorescent Chemically Driven Visible Laser Transitions Using Fast Near Resonant Energy Transfer", Proceedings of the Fourth International Laser Science Conference, A.I.P. Conf. Proc. No. 191, Optical Science and Engineering Series 10, pg. 63.
3. G. J. Green and J. L. Gole, *Chemical Physics* 100, 133 (1985).
4. R. W. Woodward, J. S. Hayden, and J. L. Gole, *Chemical Physics* 100, 153 (1985).
5. "A Chemically Driven Visible Laser Operative at 535nm", K. K. Shen, S. H. Cobb, J. R. Woodward, and J. L. Gole, *Chem. Phys. Lett.*, in press.
6. P. M. Swarengen, S. J. Davis, and T. M. Niemczyk, *Chem. Phys. Lett.* 55, 274 (1978).
7. C. E. Moore, "Atomic Energy Levels", N. B. S. Circular 467, Volumes I, II, and III. See also, R. W. F. Gross and J. F. Bott, *Handbook of Chemical Lasers*, Wiley and Sons, New York, 1976.
8. S. Chilukuri, *Appl. Phys. Lett.* 34, 284 (1979). H. Hemmati and G. J. Collins, *Appl. Phys. Lett.* 34, 844 (1979). R. Burnham, *Appl. Phys. Lett.* 30, 132 (1977). D. J. Ehrlich, J. Maya, and R. M. Osgood, *Applied Physics Letters*, 33(11), 931 (1978).
9. See also, A. A. Isaev and G. G. Petrash, "Investigation of Pulse Gas-Discharge Lasers Utilizing Atomic Transitions", in *Pulse Gas-Discharge Atomic and Molecular Lasers*, edited by N. G. Basov, translated by A. Tobulewicz, editor, Soviet Jour. of Quantum Electronics, Consultants Bureau, New York and London.

10. The number of passes is dictated by the cavity length which is 30 cm in the present configuration.
11. See for example, NBS Special Publication 505, Bibliography on Atomic Transition Probabilities (1914 through October 1977) and Supplement I (November 1977 through March 1980), U. S. Department of Commerce/National Bureau of Standards. for Thallium see A. Gallagher and A. Lurio, Phys. Rev. 136, A87 (1964).
12. G. Roll and J. Mentel, J. Phys. D. Appl. Phys. 22, 483-487 (1989).
13. B. Wellegehausen, in "Metal Bonding and Interaction in High Temperature Systems with Emphasis on Alkali Metals", A. C. S. Symposium Series 179, edited by J. L. Gole and W. C. Stwalley (Am. Chem. Soc., Washington, D. C.) p. 462, B. Wellegehausen, J. of Quantum Electronics 15, 1108 (1979).
14. See for example, R. S. Berry and C. W. Reimann, J. Chem. Phys. 38, 1540 (1963), R. S. Berry, J. Chem. Phys. 27, 1288 (1957), W. S. Struve, J. R. Krenos, D. L. McFadden, and D. R. Herschbach, J. Chem. Phys. 62, 404 (1975). R. C. Oldenborg, J. L. Gole and R. N. Zare, J. Chem. Phys. 60, 4032 (1974).
15. Given Na₂ and Na₃ ionization potentials of 4.87 and 3.97 eV (A. Hermann, E. Schumacher, and L. Woste, J. Chem. Phys. 68, 2327 (1978) and an electron affinity of 3.363 eV for atomic bromine, we determine a very substantial electron jump cross section $\sigma = \pi (14.38/3.97-3.36) = 1746 \text{ \AA}^2 (1.75 \times 10^{-13} \text{ cm}^2)$ for the Na₃ - Br reaction and $\sigma = \pi (14.38/(4.87-3.36)) = 285 \text{ \AA}^2 (2.85 \times 10^{-14} \text{ cm}^2)$ for the Na₂ - Br reaction.
16. W. C. Stwalley, private communication.

APPENDIX III

"An Approach to Visible Chemical Laser Development Using Fast Near Resonant Energy Transfer", K. K. Shen, C. B. Winstead, D. Grantier, and J. L. Gole, Journal De Physique IV, Colloque C7, supplement au Journal de Physique III, Vol. 1, 609 (1991).

AN APPROACH TO VISIBLE CHEMICAL LASER DEVELOPMENT USING FAST NEAR
RESONANT ENERGY TRANSFER

J.L. GOLE, K.K. SHEN, C.B. WINSTEAD and D. GRANTIER

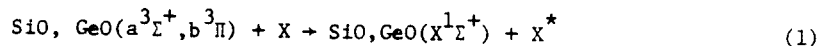
School of Physics, Georgia Institute of Technology, Atlanta, Georgia 30332, USA

Abstract - Extremely efficient near resonant intermolecular energy transfer from selectively formed metastable states of SiO and GeO is used to pump select receptor atoms with a focus on the creation of visible chemical laser amplifiers and oscillators. Visible transitions associated with thallium ($\lambda = 535\text{nm}$), gallium ($\lambda = 417\text{nm}$), sodium ($\lambda = 569, 616, 819\text{nm}$), and potassium receptor atoms have been considered. A detailed outline of the alkali based systems is presented.

1. Introduction

Certain unique aspects of a very select group of high quantum yield, highly exothermic simple metal or metalloid oxidations show the promise of creating an energy storage medium which can be used to develop what appear to be the first chemically driven laser amplifiers (and oscillators) operating in the visible spectral region.¹ Created population inversions rely on ultrafast near resonant intermolecular energy transfer from metastable oxide storage states formed in chemical reaction to pump subsequently amplifying receptor atom transitions including those associated with thallium ($\lambda = 535\text{nm}$), gallium ($\lambda = 417\text{nm}$), and sodium ($\lambda = 569, 616, 819\text{nm}$). To accommodate the desired pump sequence, we have developed techniques to form copious quantities of the metastable SiO and GeO $a^3\Sigma^+$ and $b^3\Pi$ states as the products of the primarily spin conserving Si-N₂O,² Si-NO₂,³ Ge-N₂O, and Ge-O₃ reactions. These long-lived triplet states act as an energy reservoir which can be used for fast near resonant energy transfer to efficiently pump atomic transitions.

One might envision the SiO and GeO " $a^3\Sigma^+$ " and " $b^3\Pi$ " states as forming a combined metastable triplet state reservoir which is, at best, weakly coupled to the ground electronic $X^1\Sigma^+$ state (minimal nonradiative transfer). This reservoir can be maintained and can be made to transfer its energy to pump an atom of interest if a near resonant energy transfer is feasible. Thus, we make use of an efficient intermolecular energy transfer process



where X^* represents the electronically excited atomic species from which we wish to obtain lasing action. The success of this outlined scheme depends on the rates for the reactions forming the SiO or GeO metastables⁴ and the rate of the MO^* ($\text{M}=\text{Si, Ge}$) - X intermolecular energy transfer strongly influenced by near resonances between the MO^* metastable and X^* energy levels.

The amplifiers which are of interest operate on a variety of duty cycles dictated primarily by the transition rates associated with the electronic transitions of

those receptor atoms forming the amplifying medium. While the potentially lasing atomic transitions may constrain the system to operate in a short pulsed configuration similar to the nitrogen laser,¹ the potential exists to considerably enhance this duty cycle. With the outlined approach, we have obtained short-lived amplification and oscillation from atomic thallium at 535 nm (gain coeff. $\alpha > 2.5/\text{cm}$).^{1,5} We have extended this concept to the pumping of sodium and potassium atom transitions which show the promise of producing higher duty cycle operation, and have now demonstrated amplification in the Si-SiO-Na system at $\lambda = 569, 616, \text{ and } 819\text{nm}$. Here we consider primarily the results obtained for this sodium based system and outline some further evidence for oscillation at $\lambda = 569\text{nm}$.

2. The Thallium Laser Amplifier and Oscillator as a Basis for Comparison

The nature of the thallium laser amplifier and oscillator we have developed in our laboratory is discussed in detail elsewhere.¹ The Ge-GeO-Tl system operates on the basis of rapid energy transfer from GeO metastables to Tl atoms triggered by the oxidation of premixed Ge/Tl at concentrations exceeding $10^{15}/\text{cc}$.^{1,5} This system was chosen for study because (among other attributes¹) of the low threshold for lasing⁶ on the Tl $7^2S_{1/2} - 6^2P_{3/2}$ transition and because of the potential for a highly efficient near resonant ($\Delta E \leq 250 \text{ cm}^{-1}$) pump of ground state Tl $6^2P_{1/2}$ atoms to the $7^2S_{1/2}$ excited state. These advantages are, however, balanced by the short radiative lifetime associated with the $7^2S_{1/2}$ level and the metastability of the $P_{3/2}$ terminal laser level. The self-emitting, $\lambda = 535 \text{ nm}$, Tl laser amplifier is superfluorescent. Thus, the conversion of the Tl system to a laser oscillator, strongly influenced by the cooperation length⁷ of the stable cavity configurations employed in this effort, produces an output, obtained with up to three passes through the amplifying medium, on the short time scale over which the population inversion is maintained^{1,8,9} ($\sim 3\text{-}5\text{ns}$). The Tl system is difficult to oscillate because of this short pulse mode. Further, because it is superfluorescent,⁷ the output power, obtained on full cavity oscillation with a 30cm stable configuration does not greatly exceed ($\times 10$) the output for single pass amplification.

3. Fast Intermolecular Energy Transfer Pumping of Na and K Transitions

In order to compensate the disadvantages inherent to a Tl based laser system and to demonstrate the generic nature of the outlined approach, we have extended the near resonant energy transfer concept to atomic sodium or potassium as a means of forming higher duty cycle laser amplifiers, optimizing the efficiency of these created laser amplifiers, and subsequently optimizing these systems so as to produce efficient laser oscillators. By choosing the Na and K based systems, we focus on longer-lived emitters⁵ as a means of enhancing energy storage in the laser cavity. In this respect, the more nearly energy transfer resonant Na system energy levels, partially outlined in Fig. 1, are well suited. To an even greater degree than the Tl and Ga systems, a near resonant energy matchup to the receptor atoms of interest certainly prevails in the Na and K systems where both metastable SiO and GeO can be used to energy transfer pump from the $3s^2S$ Na ground state ($4s^2S$ in K) to the $4d^2D$ and $5s^2S$ levels ($5d^2D$ and $6s^2S$...in K). In the Tl system laser action is terminated through the filling of the $P_{3/2}$ level, however, in the sodium system (Fig. 1(a)) the terminal laser level is the extremely short-lived upper level of the Na D-line. The $3p^2P - 3s^2S$ transition is characterized by a high oscillator strength facilitating rapid loss of the terminal laser level to create ground state sodium atoms which Figs. 1(a) and 1(b) demonstrate are again amenable to near resonant energy transfer pumping given sufficient silicon monoxide metastable formation.

While the $5s^2S$ and $4d^2D$ levels are not readily assessed in an optically pumped transition, Fig. 1(b) demonstrates that, using SiO metastables formed in the Si-N₂O reaction, we have now successfully energy transfer pumped Na atoms to the $2S$ and $2D$ levels where they subsequently emit radiation at $\sim 616 \text{ nm}$ and 569 nm as they undergo

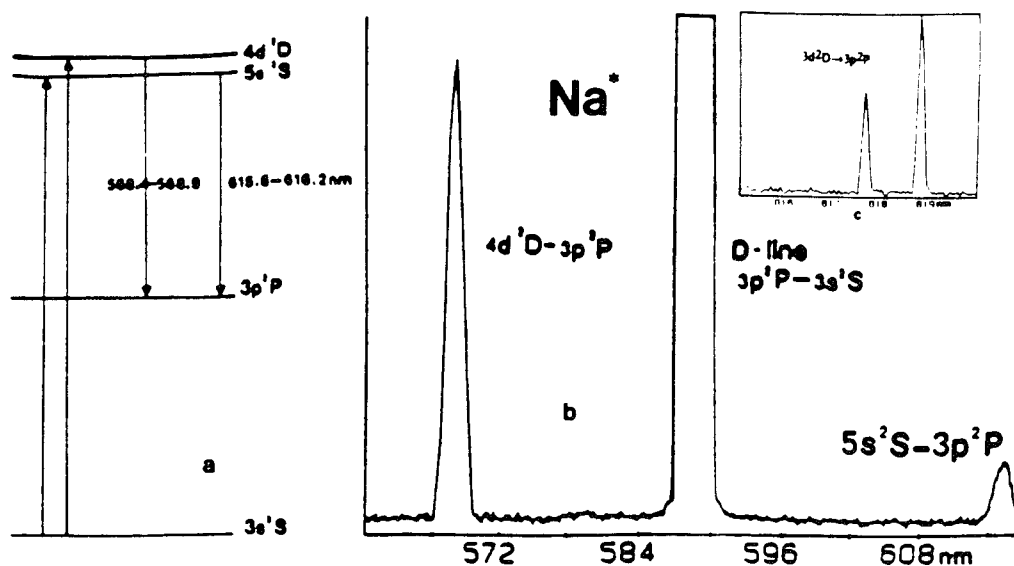


Figure 1. (a) Na atom energy level scheme and pumping cycles to produce $4d^2D$ and $5s^2S$ excited states.

(b) Typical energy transfer pumping spectrum from Na $4d^2D - 3p^2P$ and $5s^2S - 3p^2P$ transitions and $3p^2P - 3s^2S$ sodium D-line emission. The D-line emission results both from direct energy transfer pumping from ground state NaO and from fluorescence to the $3p^2P$ level.

(c) Energy transfer pumping spectrum corresponding to Na $3d^2D - 3p^2P$ transition.

transition to the $3p^2P$ levels. These transitions are characterized by moderate to small oscillator strengths. The assessed Na cycle with its 50^{10} to 100^{10} nano-second upper state radiative lifetimes (vs. $Tl\ 2S_{1/2}$ at $\sim 7nsec.$ ¹⁰) and short-lived terminal laser level would appear ideally suited to obtain high duty cycle laser amplifiers and oscillators. Also, as indicated in Figure 1(c), we have obtained evidence for the energy transfer pump of the Na $3d^2D$ level with which is associated an atomic emission at $\lambda \sim 819nm$ ascribed to the Na $3d^2D - 3p^2P$ transition. Both the transitions at $\lambda \sim 569\ nm$ ($\alpha_{max} \sim 0.27/cm$) and $\lambda \sim 819\ nm$ ($\alpha_{max} \sim 0.04/cm$) have been repeatedly shown to demonstrate gain.

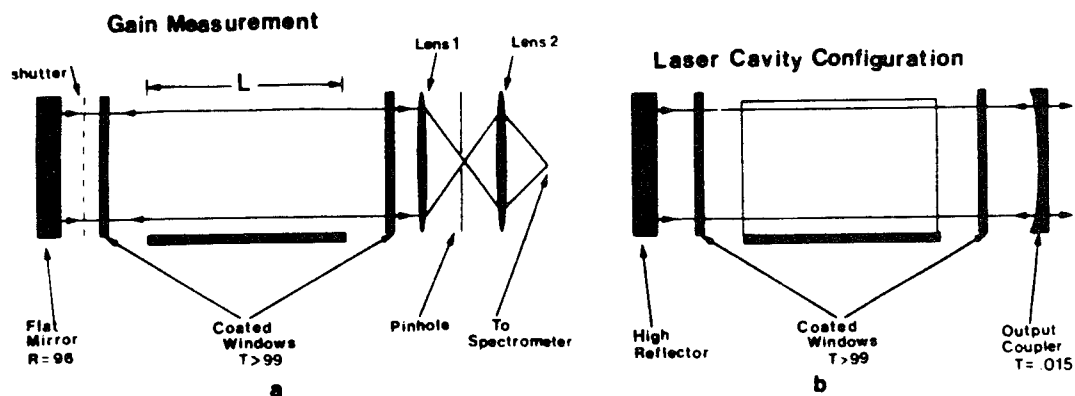


Figure 2. Gain measurement and laser cavity configurations.

In approaching the outlined laser schemes, self absorption associated with the Na D-line must be a concern. Evidence is obtained for moderate self-absorption in the present experiments, however concern with the possible deleterious effect which such a pumping of the Na D-line might have on transitions terminating in the $3p^2P$

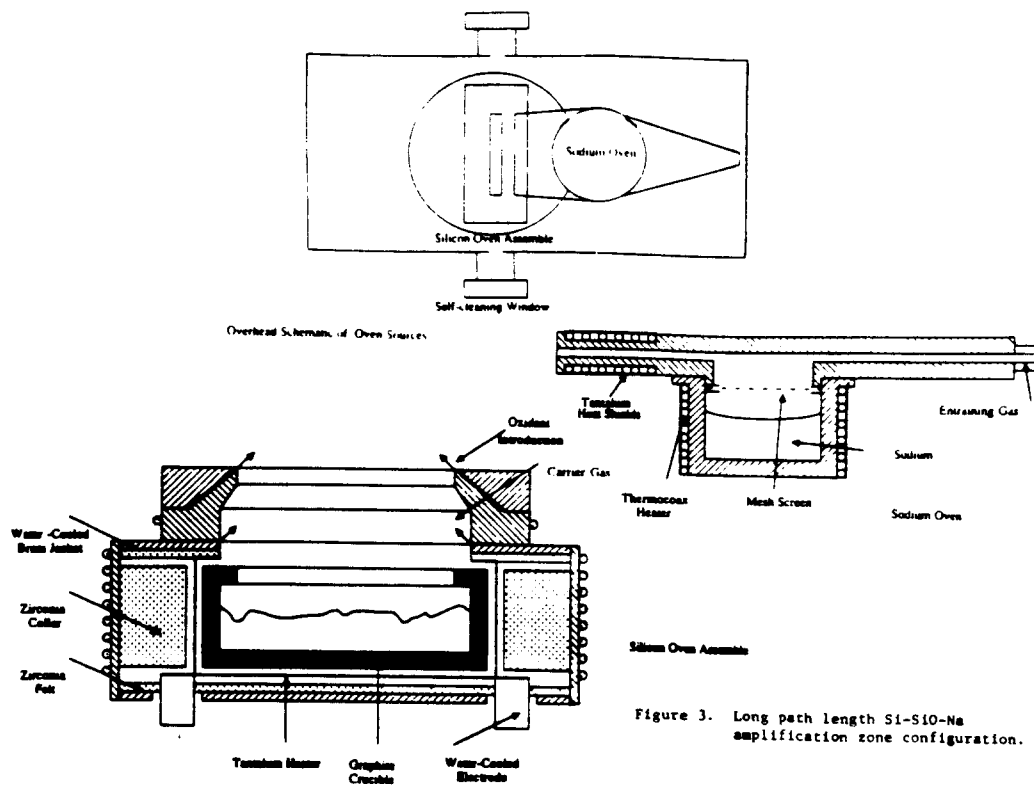


Figure 3. Long path length Si-SiO-Na amplification zone configuration.

level is greatly alleviated by the Na discharge experiments of Tribilov and Shukhtin which demonstrate a surprising¹¹ lasing action on the Na $4s^2S - 3p^2P$ transitions in the infrared region.

Gain measurements were carried out using the optical train depicted in Fig. 2(a)¹² surrounding either a short (~ 1 -2cm) reaction - energy transfer - amplification region^{1,5} or the recently constructed ~ 5 cm amplification zone associated with the larger scale cavity configuration depicted in Fig. 3. This optical train parallels the ingenious design of Roll and Mentel¹² to measure new laser lines in Se II employing amplified spontaneous emission (ASE). The gain coefficient α , can be calculated from

$$\alpha = \frac{1}{L} \ln (I_2 - I_1 / I_1 R T^2)$$

where L is the effective gain medium length, I_1 is the single pass ASE intensity and I_2 is the double pass ASE intensity, R is the mirror reflectivity, and T is the transmission of the "cavity" vacuum chamber window in front of the mirror.

The cavity configuration depicted in Fig. 3 has been constructed to facilitate conversion of an original (~ 1 cm) reaction - energy transfer - amplification zone cavity configuration^{1,5} to a considerably more versatile and longer path length device. Using this device, our amplification path length is increased to 5 cm. The newly constructed device can take advantage of three entrainment flow configurations for silicon or germanium in the cycle producing SiO and GeO metastables, one of which is depicted in Fig. 3. These flow configurations produce the longest path length SiO (GeO) metastable flames (~ 5 + cm) ever obtained. The long path length silicon entrainment flame can be intersected at angles close to 90° by an entrained flow of sodium atoms (Fig. 3). The entrained silicon and sodium flows can be moved relative to each other and hence with respect to the reaction - energy transfer -

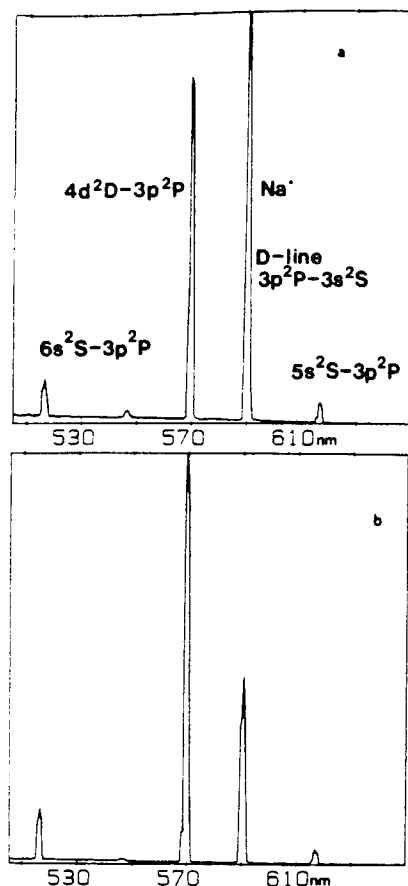


Fig. 4. Single pass (a) ASE intensity versus double pass (b) ASE intensity for the Si-SiO-Na amplification.

output intensity which rapidly decays to a steady state cavity amplification. This behavior occurs over an extremely narrow angle tuning range. The ratio of the output for the full cavity to that obtained for single pass amplification is at least a factor of five in the apparently steady-state mode. This enhancement was observed for a period in excess of one hour. The enhancement was determined by blocking the rear high reflector which must curtail oscillation in the system. Walking the cavity mirrors quickly destroyed this amplification. Upon realignment, sharp increases in intensity, followed by a decay to the steady state amplification, were again observed. In subsequent experiments, when only a fluorescent medium associated with the $4d^2D - 3p^2P$ Na transition is formed due to improper cavity operation as evidenced by gain measurements (low Na atom concentration) at 569 nm, the maximum steady state enhancement obtained varies between 1.6 and 1.8, a factor of three lower than that obtained with $\alpha = 0.05$. Further the sharp increase in intensity following mirror (cavity) alignment was not observed.

We suggest that these initial results are quite encouraging. We believe that the optimization of both the optical train and reactant mixing, considering the rate limiting effect of the silicon concentration and the importance of sodium atomization,

amplification zone to optimize conditions for formation of the gain medium.

The long path combined silicon and germanium oxidation and alkali entrainment source configuration is now being tested in order to optimize its use to create a chemical laser oscillator. We have carried out the first experiments to obtain full cavity oscillation with this system. Because the cavity conditions can vary precipitously from run to run, a gain measurement must accompany each attempt to obtain evidence for oscillation. The stark results obtained for the cavity of Fig. 3 operating in a moderate gain condition are indicated in Fig. 4 where the scan (a) corresponds to single pass ASE and the scan (b) depicts the double pass ASE intensity (measured with the optical train depicted in Fig. 2(a)) and associated with the Na atom transitions depicted in the figure. Here, the gain coefficient associated with the Na $4d^2D - 3p^2P$ transition, $\alpha \approx 0.11$.

Our efforts to obtain oscillation in a pulsed mode have focused on the Si-SiO-Na system and, in particular, on the Na $4d^2D - 3p^2P$ transition. Under less than optimal conditions, we measured a gain for the Na $4d^2D - 3p^2P$ transition which corresponded to $\alpha < 0.05/\text{cm}$, clearly notably less than the α_{max} ($\approx 0.27/\text{cm}$) which has been obtained. However for a 5cm long gain medium this corresponds to 0.25 per pass through the entire zone. The gain measurement system was replaced by the full cavity configuration depicted in Fig. 2(b) with a 1% output coupler and an $\sim 99.9\%$ high reflector (1 cm diameter). The gain medium was ~ 5 cm in length and the cavity, operating in a stable configuration ($g_1 g_2 \sim 0.89$), was 44cm in length. Using this configuration and tuning the output coupler and high reflector after adjusting the mixing Si, N_2O , and Na flows, we find a sharp increase in

will allow us to improve and optimize the output from this system. While we attempted to improve the output in the experiment described above by adjusting the output coupler, we observed evidence for much higher output levels for a narrow range of angle tuning but were unable to hold these power levels for more than a short time period. This may be due to the stability of the gain medium as determined by the efficiency of mixing and pumping, however, the characteristics we observe might also be attributed to spiking and the onset of gain saturation. Clearly much more experimentation will be needed to pin down cavity parameters and optimal operation.

While our continued emphasis has been on the sodium system and the results presented in Fig. 1(b) involve a metastable SiO pump, it is also feasible to use GeO metastables for energy transfer pumping. In fact, the formulation of potassium based amplifiers associated with the $5d^2D - 4p^2P$ ($\lambda \approx 581, 583\text{nm}$), $4d^2D - 4p^2P$ ($\lambda \approx 694, 697\text{nm}$) and $6s^2S - 4p^2P$ ($\lambda \approx 691, 694\text{nm}$) potassium atom transitions might best be accomplished with pumping by GeO metastables. We will continue to pursue these experiments.

ACKNOWLEDGEMENT

It is a pleasure to acknowledge most helpful discussions with Drs. R. Jones, Bill Watt, T. Cool, and E. Dorko concerning this study. The support of the Georgia Tech Foundation through a grant from Mrs. Betty Peterman Gole, the Army Research Office through the Short Term Innovative Research Program and the Air Force Office of Scientific Research - Army Research Office is greatly appreciated.

References

1. J. R. Woodward, S. H. Cobb, K. K. Shen and J. L. Gole, IEEE, J. Quant. Electronics 26, 1574 (1990).
2. G. J. Green and J. L. Gole, Chemical Physics 100, 133 (1985).
3. R. W. Woodward, J. S. Hayden and J. L. Gole, Chemical Physics 100, 153 (1985).
4. P. M. Swearingen, S. J. Davis and T. M. Niemczyk, Chem. Phys. Lett. 55, 274 (1978).
5. J. L. Gole, J. R. Woodward, S. H. Cobb, K. K. Shen and J. R. Doughty, SPIE Proceedings Volume 1397, Eighth International Symposium on Gas Flow and Chemical Lasers (1990), pg. 125 (and references therein).
6. S. Chilukuri, Appl. Phys. Lett. 34, 284 (1979). H. Hemmati and G. J. Collins, Appl. Phys. Lett. 34, 844 (1979). R. Burnham, Appl. Phys. Lett. 30, 132 (1977). D. J. Ehrlich, J. Maya and R. M. Osgood, Appl. Phys. Lett. 33(11), 931 (1978).
7. J. C. MacGillivray and M. S. Feld, Phys. Rev. A 23, 1334 (1981).
8. See also, A. A. Isaev and G. G. Petrash, "Investigation of Pulse Gas-Discharge Lasers Utilizing Atomic Transitions", in Pulse Gas-Discharge Atomic and Molecular Lasers, edited by N. G. Basov, translated by A. Tobulewicz, editor, Soviet Jour. of Quantum Electronics, Consultants Bureau, New York and London.
9. The number of passes was dictated by a 30 cm cavity length.
10. See for example, NBS Special Publication 505, Bibliography on Atomic Transition Probabilities (1914 through October 1977) and Supplement I (November 1977 through March 1980), U. S. Department of Commerce/National Bureau of Standards. For Thallium see A. Gallagher and A. Lurio, Phys. Rev. 136, A87 (1964).
11. A. S. Tibilov and A. M. Shukhtin, Opt. Spectrosc. 21, 69 (1966). See also, D. Krokkel, M. Hube, W. Luhs and B. Wellegehausen, Appl. Phys. B37, 137-140 (1985).
12. G. Roll and J. Mentel, J. Phys. D. Appl. Phys. 22, 483-487 (1989).

APPENDIX IVA

"On the BiF Bond Dissociation Energy and the Evaluation of the BiF Red Emission Band Systems", T. C. Devore, L. Brock, R. Kalscheuer, K. Dulaney, and J. L. Gole, Chemical Physics 155, 423 (1991).

On the BiF bond dissociation energy and an evaluation of the BiF red emission band systems

T.C. Devore¹, L. Brock¹, R. Kahlscheuer, K. Dulaney² and J.L. Gole

*High Temperature Laboratory Center for Atomic and Molecular Science and School of Physics,
Georgia Institute of Technology, Atlanta, GA 30332, USA*

Received 8 May 1991

The chemiluminescent emission from the $\text{Bi} + \text{F}_2$ and $\text{Bi}_2 + \text{F}$ reactions has been characterized. A study of the chemiluminescent reaction of argon entrained bismuth vapor and molecular fluorine over a substantial pressure range (60–333 Pa) provides evidence for two distinct electronic transitions of BiF in the region 565–740 nm, at least one of which is thought to terminate in the BiF “1” ($X_2\ 1$) state arising from the $^3\Sigma^-(\sigma^2\pi^4\pi^{*2})$ configuration of BiF. The observed transitions with $\nu_{00} \approx 17631\text{ cm}^{-1}$ and $\nu_{00} \approx 15244$ or 15784 cm^{-1} exhibit pronounced upper state vibrational relaxation and are characterized, especially at the highest pressures, by a dominance of progressions emanating in $v' = 0$ and terminating in several v'' lower state levels. The higher energy transition with $\nu_{00} \approx 17631\text{ cm}^{-1}$ is believed to terminate in the recently observed BiF “1” state with $\nu_{00} \approx 6768\text{ cm}^{-1}$ ($X_2\ 1 - X_1O^+$). The upper state, denoted A' , with $T_0 \approx 24400\text{ cm}^{-1}$ is believed also to be a “1” state based on limited high resolution data for at least two bands of the system. The correlation made here is in close accord with recent quantum chemical calculations which suggest that the “1” state lies $\approx 7200\text{ cm}^{-1}$ above $v'' = 0$, XO^+ . The levels of the A' upper state appear to correlate precisely with several BO^+ perturber state levels. This perturber state, thought to lie less than 2000 cm^{-1} above the $AO^+(II)$ state may play an important role with respect to energy disposal among the excited states of the BiF molecule. The second transition with $\nu_{00} \approx 15244$ or 15784 cm^{-1} also appears to terminate in the “1” state suggesting a second upper state, denoted A'' , lying at $22552 \pm 545\text{ cm}^{-1}$ virtually isoergic with $AO^+(II)$. Alternatively, the second transition might emanate from the $v' = 0$ upper state level at $T_0 \approx 24400\text{ cm}^{-1}$ terminating in a lower state with $T_0 \approx 8615\text{ cm}^{-1}$. In order to establish the dissociation energy of the BiF molecule and to determine whether this controversial bond is closer to 3 or 5 eV, both the $(\text{Bi}, \text{Bi}_2) + \text{F}_2$ and $(\text{Bi}, \text{Bi}_2) + \text{F}$ reactive systems have been studied. Combined results based on the observation of the chemiluminescent $\text{Bi} + \text{F}_2$ and $\text{Bi}_2 + \text{F}$ reactive encounters producing BiF $AO^+(II) - XO^+$ and $BO^+ - XO^+$ emission features suggest that the BiF bond energy is closer to 5 eV.

1. Introduction

The suggestion of an energy pooling-energy transfer pumping of BiF excited states, employing metastable NF, to develop a visible chemical laser system has lead to renewed interest in the low-lying electronic states of BiF [1]. Balasubramanian [2] has carried out relativistic CI calculations for the four lowest electronic states of the BiF molecule. These calculations show that the ground state corresponds to the XO^+ component of the $^3\Sigma^-(\sigma^2\pi^4\pi^{*2})$ configuration and the “1” state arising from this configuration is $\approx 7200\text{ cm}^{-1}$ higher in energy. This result is in close agreement with the very recent elegant study

of Fink et al. [3] which establishes the location of the “1” state for all of the bismuth halides: a T_e value of $6752.7944(12)\text{ cm}^{-1}$ is determined for the $X_2\ 1 - X_1O^+$ transition of BiF. Balasubramanian has also suggested that the “2” state ($^2\Delta$) and the $AO^+(II)$ state have T_e values of 14595 cm^{-1} and 25931 cm^{-1} , respectively.

The BiF XO^+ and $AO^+(II)$ states have been well characterized experimentally. Jones and McClean [4] have assigned 65 bands in the region 422–542 nm to the $AO^+(II) - XO^+$ transition of BiF. Thirty three of these transitions have been rotationally analyzed and the ground state molecular constants determined agree well with those obtained from the analysis of the microwave spectrum [5]. Ross et al. [6] have extended the vibrational analysis, observing electronic transitions involving all vibrational levels up

¹ Department of Chemistry, James Madison University.

² Department of Physics, Furman University.

to $v' = 25$ and $v'' = 36$ for the AO^+ (II) and the XO^+ states, respectively. The radiative lifetimes for levels $v' \leq 6$ were also determined [7].

It is possible that electronic transitions terminating in the "1" system may have also been observed. Several investigators [8–11] have reported a band system in the red region which Balasubramanian [2] has suggested might correspond to the AO^+ (II) \rightarrow 1 transition. However, each of the previous analyses of this red system offer a different interpretation, and Ross et al. [6] have recently used Fourier transform spectroscopy to observe a large number of bands in the region all of which are assignable to transitions involving high vibrational levels of the AO^+ (II) and O^+ states. Thus, any information which might provide some further clarification of the transitions associated with this region would seem to be warranted. In the course of the present study, we have observed strongly pressure dependent (entraining argon) emission which, in concert with the recent studies of Fink et al. and Ross et al., suggests an alternate interpretation for the observed features in the red region.

At least two additional BiF electronic states are thought to have T_e values near 26000 cm^{-1} . A band system first reported by Patel and Narayanan [8] in the 380 nm region has been rotationally analyzed by Jones and McClean [12] who have assigned this system to the $\text{BO}^+ \rightarrow \text{XO}^+$ transition. These authors also found that the BO^+ state is highly perturbed by the AO^+ state and one (perhaps two) additional unknown states. Good rotational and vibrational constants were established for the BO^+ state; T_e values were estimated and approximate B values were determined for several of the additional perturber state levels.

The major impetus for the present study of the bismuth–fluorine system was initially a significant discrepancy in the suggested values for the dissociation energy of BiF. Specifically, the much larger bond energy recently determined by Ross et al. [6] suggested, counter to previous studies [2,4,13,14], the possible population of BiF excited states emitting in the visible and ultraviolet in a single collision chemiluminescent Bi-F_2 reactive process; a study of this process would allow the evaluation of the BiF bond strength [15]. Gaydon [13] estimated the BiF dissociation energy to be $2.65 \pm 0.2 \text{ eV}$. Rai and Singh

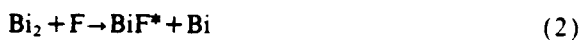
[14] have used an empirical ionic model based upon the assessed ground state molecular constants to estimate a BiF dissociation energy close to 3 eV. From the indication of excited state level separations signaling a possible predissociation of the AO^+ state, Jones and McClean [4] have suggested that the BiF dissociation energy is less than 3.14 eV. Balasubramanian [2] calculates a dissociation energy of 2.63 eV. Although not in total agreement, these values are consistent with Gaydon's initial estimate.

However, Ross et al. [6] have employed a long extrapolation based on a LeRoy–Bernstein plot using their improved ground state molecular constants to estimate the dissociation energy. Because the vibrational spacings for the highest ground state levels observed in their study were still $\approx 350 \text{ cm}^{-1}$ some two eV's above the lowest ground state levels, they concluded that previous estimates of the dissociation energy were low and suggested that the dissociation energy was $\approx 5 \text{ eV}$. This value considerably exceeds that predicted by a linear Birge–Sponer extrapolation which usually yields an upper bound to the dissociation energies [13] for polar and ionic molecules.

The reaction between bismuth vapor and fluorine has proven to be an effective means for producing the excited states of BiF [6,7]. In addition, investigations of similar systems [15] have shown that a careful analysis of the reaction energetics can provide an accurate determination of the product molecule dissociation energy. Because several questions remain about the dissociation energy and low-lying states of BiF, the reactions between bismuth vapor and molecular and atomic fluorine have been investigated to determine if more could be learned about the molecular electronic structure of the BiF molecule. These efforts are designed to combine data obtained in the study of the two chemiluminescent reactive encounters



and



2. Experimental

As a means of studying several processes involving

the formation of metal oxides and halides and metal atom based complexes, we have developed a number of continuous flow entrainment sources. These sources are discussed in detail elsewhere [16].

In this study, carried out primarily in the multiple collision pressure regime [17], bismuth was evaporated from a specially machined graphite crucible (Micromechanisms, Billerica, MA). The crucible was placed in a resistively heated tungsten basket heater (R.D. Mathis, Long Beach, CA) which was insulated with Zirconia cloth (Zircar, Florida, NY). The bismuth was heated to temperatures ranging approximately between 900 and 1100 K, producing a crucible vapor pressure ranging to ≈ 250 Pa. The metal flux issuing from the crucible was entrained in argon (HoloX, 99.999%) and brought to the viewed reaction zone.

Two oxidation configurations were employed. In one set of experiments, F_2 (Air products, 98%) entering from a concentric ring injector inlet, intersected the entrained metallic flux. In a second set of experiments, fluorine atoms were formed through electric discharge through SF_6 , producing primarily SF_5 and atomic fluorine. The voltage applied to two electrodes separated by $1/4"$ on a $1/4"$ i.d. insulated glass tube, through which SF_6 flows, was increased to achieve maximum chemiluminescent intensity. This was achieved at 1300 V. The effluents from the discharge were made to intersect the entrained metallic flux. In the absence of either a bismuth vapor flow or a discharge through SF_6 , no chemiluminescent emission is observed. A discharge through SF_6 in the absence of the bismuth vapor flow produces no BiF emission. In addition, no emission associated with the bismuth vapor flow is monitored at wavelengths extending to 1000 nm. This is certainly not surprising for the bismuth atom constituency is such that even the lowest-lying metastable $Bi\ ^2D$ state at 11419 cm^{-1} represents a mole fraction between 10^{-8} and 10^{-6} that of ground state $^4S\ (3/2)$ atoms over the 900–1100 K temperature range of the experiment.

As the vacuum chamber was evacuated by a mechanical pump (Kinney KT-150), the effluent from those experiments involving molecular fluorine could be passed over 8-14 mesh activated alumina to scrub F_2 and prevent fouling of the pump oil. Alternatively, the effluents from the discharged SF_6 configuration were trapped at liquid nitrogen temperature in a glass

trap preceding the mechanical pump. In the multiple collision configurations, the oxidant pressure ranged from 1.3 to 5.3 Pa and the total pressure in the system, corresponding primarily to argon entrainment gas, was between 60 and 333 Pa as measured by a Veeco thermocouple gauge attached to the wall of the reaction chamber. These measured pressures may be as much as 50% lower than the actual values [16].

The chemiluminescent emission was focused onto the entrance slit of a 1-m Spex 1704 scanning monochromator operated in first order with a Bausch and Lomb 1200 groove/mm grating blazed at 500 nm. A dry ice cooled EMI 9808 red sensitive photomultiplier tube was used to detect the dispersed fluorescence. The signal from this phototube was fed to a Keithley 417 fast picoammeter; the output from the picoammeter was sent to an Apple computer for data acquisition. The analog signal from the picoammeter was digitized to a value read by the Apple over a time period, t , subsequently calculating an averaged value in that time interval. The computer also simultaneously drove the monochromator as the data was fully displayed during a given scan of the spectrum. Data was recorded on floppy diskettes to permit further analysis.

3. Results and discussion

3.1. Observed electronic transitions

The spectrum observed when a moderate flux of argon entrained Bi vapor reacts with F_2 under multiple collision conditions is depicted in fig. 1. Three distinct band systems are readily identified. The strong features near 450 nm correspond to the $AO^+(II) \rightarrow XO^+$ transition of BiF [3,5]. All features near 450 nm can be assigned to transitions from $v' \leq 4$, $AO^+(II)$. The relative intensities indicate that these AO^+ levels might be characterized reasonably by a nearly Boltzmann population distribution with an effective vibrational temperature approximating 700 K, however weak emission from several higher lying levels of the $AO^+(II)$ state ($v'' > 15$) extends to considerably longer wavelength. The emission from these higher vibrational levels, which may result from a second reactive process distinct from that producing the dominant A-X emission (see following), is the

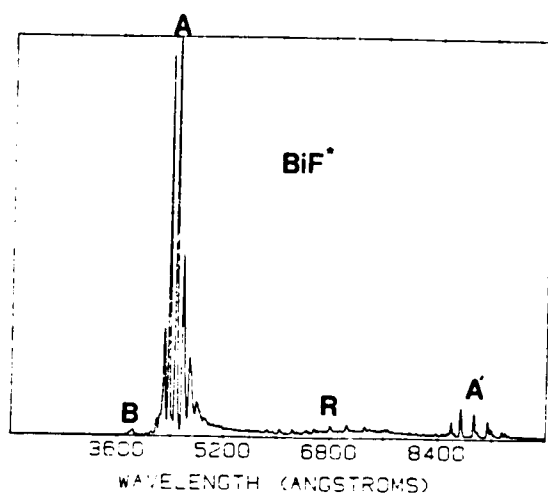


Fig. 1. Chemiluminescent emission spectra resulting from the reaction between argon entrained bismuth vapor and F_2 under multiple collision conditions. The bands labeled A (first order) and A' (second order) identify the $AO^+ \rightarrow XO^+$ transition, the bands labeled B correspond to the $BO^+ \rightarrow XO^+$ transition and the bands labeled R correspond to the "red system" bands considered in the text. Spectral resolution is 1 nm.

subject of further study in other laboratories [6].

The band near 380 nm corresponds to the origin sequence for the $BO^+ \rightarrow XO^+$ transition [8,12]. This system is weak and poorly resolved so that little new information could be obtained from its study.

The "red" systems observed from 565 to 740 nm in the present study contain each band which has been assigned by a number of investigators [8–11]. However, several additional bands are also observed which have not been reported by any previous investigators. Certain of these features are quite dominant, especially at higher pressure, where the A–X emission features present in the spectrum are quenched. Since bands assigned to high vibrational levels of the $AO^+(II) \rightarrow XO^+$ transition by Ross et al. [6] are also found to be present in this region, the A–X system and its potential further extrapolation has also been considered.

The bands observed in the red region were found to change markedly as the pressure (primarily argon) in the reaction zone changed (fig. 2). At 70 Pa all of the observed features have similar intensities. No clear patterns are observed and no obvious progressions can be identified. Although the signal to noise ratio is marginal and an analysis was not at-

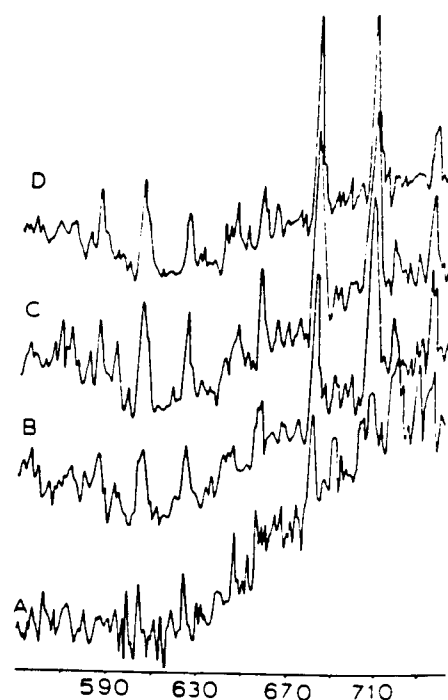


Fig. 2. Chemiluminescent emission spectra resulting from the reaction between argon entrained bismuth vapor and molecular fluorine under multiple collision conditions. The spectra correspond to a study of the BiF "red system" bands as a function of reaction zone pressure. The pressures shown are 65 Pa (trace A), 93 Pa (trace B), 130 Pa (trace C) and 160 Pa (trace D). Spectral resolution is 1 nm. See text for discussion.

tempted, the features reported by Ross et al. [6] appear to be present. As the (argon) pressure in the reaction zone is increased, several bands increase in intensity relative to others in this region. These bands are sharp and red degraded. They form two distinct vibrational progressions with similar relative intensities and vibrational spacings. The measured band head frequencies of these dominating features agree well with several of the frequencies previously reported for the "red system" bands [8–11], but not with the frequencies associated with the the $AO^+(II) \rightarrow XO^+$ systems reported by Ross et al. [6]. These differences, and their markedly different pressure dependent behavior indicate that the dominant bands do not arise from high vibrational levels associated with the $AO^+ \rightarrow XO^+$ transition.

The spectrum of the red region at higher resolution and 250 Pa pressure is shown in fig. 3a. At this pressure, the two band groupings which grow with pres-

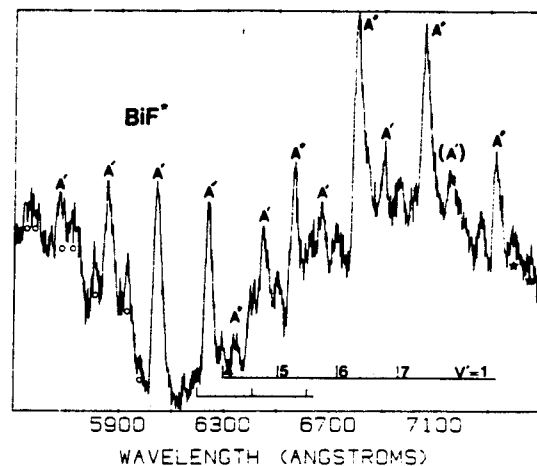
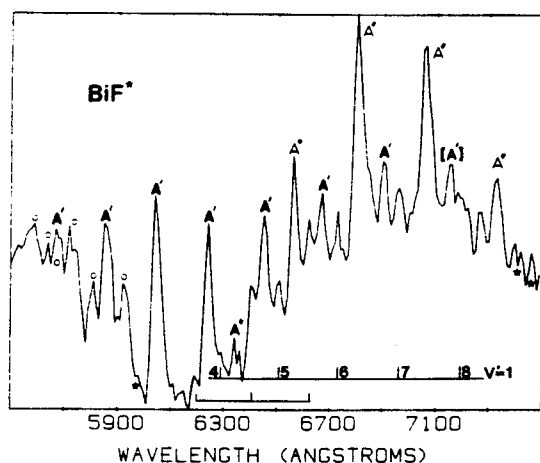
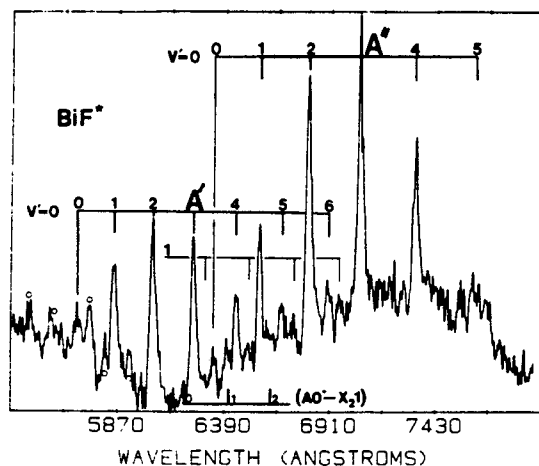


Fig. 3. Chemiluminescent emission spectra resulting from the reaction between argon entrained bismuth vapor and F_2 under multiple collision conditions. (a) The spectrum of the BiF "red system" bands is readily observed at 250 Pa pressure. The two progressions which increase relative to other features are marked A' and A'' in the figure. Also noted in (a) and more apparent in (b) and (c), which correspond to spectra observed at 110 and 130 Pa exhibiting less quenching, are features marked with open circles (\circ) to indicate bands which have been determined to arise from the $AO^+ \rightarrow XO^+$ transition and features associated with A' , $v' = 1$ levels. The stars indicate features which probably correspond to $v' \geq 1$ extrapolations of the $A'-X_2 1$ and $A''-X_2 1$ systems. In the lower portion of the figures are indicated the locations of three weak features which appear to correlate with the expected location of "weak" $AO^+(II)-X_2 1$ transitions from the $v' = 0$ level of $AO^+(II)$ to $v'' = 0, 1, 2$ for $X_2 1$. These features may also correlate with $A'-X_2 1, v'' = 3$ transitions. See text for discussion. Spectral resolution is 0.2 nm.

sure are readily identified. In addition several weak features are still present which are more readily identified, and far less quenched, in the 110 and 130 Pa spectra depicted in figs. 3b,c. Many clearly correspond to the high vibrational level A-X transitions reported by Ross et al. [6]. Several of the additional weaker and seemingly pressure quenched features have not been reported previously and would appear to represent vibrationally excited levels associated with a portion of the red systems or extensions of the $AO^+ \rightarrow XO^+$ band system.

The two distinct stronger systems in the quenched spectrum (fig. 3a) appear to display the same vibrational spacings (table 1), suggesting that they both terminate in the same lower state. Since the phototube/spectrometer response is dropping with in-

creasing wavelength, the longer wavelength features dominate the observed spectrum. Further, consistent with the pressure dependent behavior of the observed systems is their assignment to emission associated with the lowest $v' = 0$ upper state level, terminating in several lower state levels. The dominant features in the spectrum of fig. 3a are still considerably weaker than the low v' $AO^+(II)-XO^+$ features in fig. 1. This implies that the radiative lifetimes of the red system electronic transitions exceed substantially those of the A-X transition. The data in figs. 4a,b demonstrates that the A-X band system displays significant vibrational relaxation as the entrainment gas pressure is changed from 67 to 333 Pa. At the higher pressure, the $v' = 0$ transitions are clearly dominant. It would not be surprising to find that the

Table I
Observed band heads and assignments for the "red system" bands of BiF at pressures in excess of 250 Pa

Bandhead location (cm ⁻¹)	Intensity	Assignment	J (cm ⁻¹)
A¹"-X₂1^a			
17631 ± 10	(0.07)	(0,0)	
17089 ± 10	(0.20)	(0,1)	542
16556 ± 10	(0.33)	(0,2)	533
16030 ± 10	(0.25)	(0,3)	526
15511 ± 10	(0.13)	(0,4)	519
15000 ± 10	(0.09)	(0,5)	511
14500 ± 10	[(0.08)]	(0,6)	(500)
A¹"-X₂1^b			
15784 ± 10	(0.06)	(0,0)	540
15244 ± 10	(0.19)	(0,1)	534
14710 ± 10	(0.35)	(0,2)	526
14184 ± 10	(0.27)	(0,3)	518
13666 ± 10	(0.19)	(0,4)	

^a For an origin band at 17631 cm⁻¹, $\nu = 17902 - 543(\nu'' + 1/2) + 2.5(\nu'' + 1/2)^2$.

^b For an origin band at 15784 cm⁻¹ (see text for discussion), $\nu = 16055 - 543(\nu'' + 1/2) + 2.5(\nu'' + 1/2)^2$.

longer-lived upper states associated with the red band system display a similar vibrational relaxation. Relaxation to $\nu' = 0$ may correspond to a major source of the dominance of the features identified in fig. 3.

The frequency separations indicated in table I demonstrate that the observed features are not associated with the XO⁺ state. However, these frequency separations (table I) are certainly consistent with the vibrational parameters ($\omega_e \approx 543.0558(24)$, $\omega_e x_e \approx 2.3996(15)$) most recently determined by Fink et al. [3] for the X₂1 ("1") state of BiF ($\nu_0 = 6768.808$ cm⁻¹). This "1" state is calculated to be ≈ 7280 cm⁻¹ above the XO⁺ state [2]. The observed vibrational frequency separation (table I) while larger than that estimated by Balasubramanian is consistent with this calculation [2].

The assignment of the upper state is less certain although an overall energy level pattern which appears consistent with all previous studies can be found. Chakoo and Patel [11] observed part of the bands identified here and assigned them as arising from different vibrational levels of the same excited state. While this was a reasonable conclusion, their analysis included some of the high vibrational levels associated with the AO⁺(II)-XO⁺ transition. If we exclude these A-X bands, the spacings and relative in-

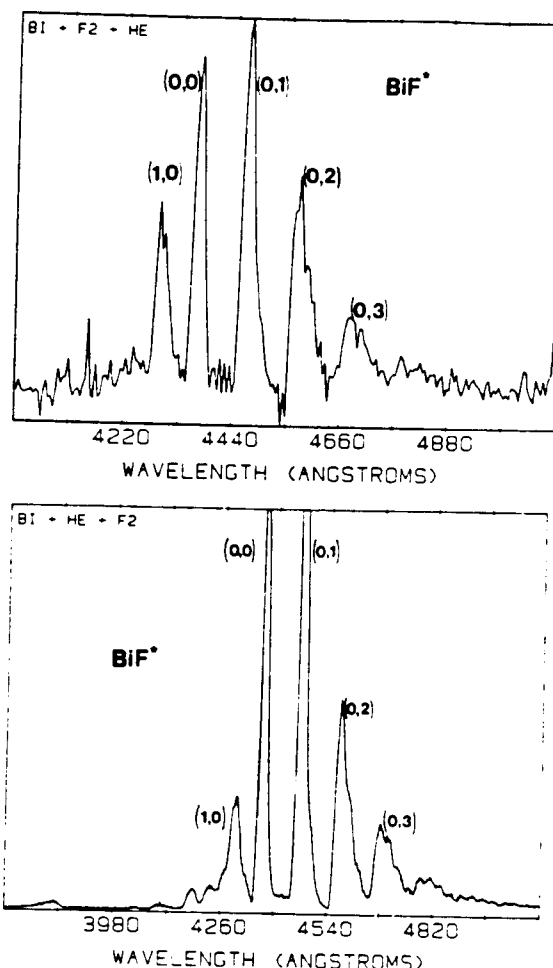


Fig. 4. Comparison of chemiluminescent emission spectra resulting from the reaction between argon entrained bismuth vapor and F₂ under multiple collision conditions. Spectrum (a) depicts the BiF AO⁺(II)-X₂O⁺ emission spectrum obtained at a total pressure close to 67 Pa whereas spectrum (b) depicts the A-X emission observed at a total pressure of 333 Pa (primarily argon). These spectra reveal a strong vibrational relaxation to $\nu' = 0$, AO⁺(II). Spectral resolution is 0.8 nm for both spectra. See text for discussion.

tensities observed here are not consistent with their assignments. Further, recent calculations [18] which attempt to determine Franck-Condon factors using the Chakoo and Patel [11] data suggest that either their determined B values or vibrational assignments are incorrect. Based on the data which Chakoo and Patel [11] present, and our current observations we favor a significant reevaluation of their vibrational analysis. Their B values appear consistent with their

catalogued rotational structure, although their J numbering may require some revision. We suggest that the dominant features in fig. 3 should be assigned to two transitions both of which incorporate bands from the Chakoo and Patel analysis and are not associated with the $\text{AO}^+(\text{II})$ upper state.

The relative intensities of the groupings (table 1) observed in the present study do not change with pressure. While it is possible that an energy transfer process selectively populates certain vibrational levels of the upper state and that these levels radiate before they can be relaxed, it is more likely that the observed emission emanates from the $v'=0$ level of two different long-lived excited states whose transition moments are greatly exceeded by the A-X system. This can facilitate vibrational relaxation, with increasing pressure, in the excited state manifold on the time scale for emission. The limited upper state vibrational frequency information obtained in the present study (table 2 and fig. 3), compared also with that of prior workers [8-11] and with the A-X relaxation discussed previously, suggests that this is a reasonable assumption. The energy level pattern determined from the following considerations appears consistent with the results of a perturbation analysis on the $\text{AO}^+(\text{II})-\text{XO}^+$ and BO^+-XO^+ band systems by Jones and McLean [4,12].

Balasubramanian [2] has suggested that the $\text{AO}^+(\text{II}) \rightarrow "1"$ transition might be observed in the "red" energy region. While it is tempting to associate one of the two transitions catalogued in table 1 with

this system, the data of Fink et al. [3] provide evidence to indicate that this is an unlikely possibility. From the location of the $\text{AO}^+(\text{II})$ [4], $\text{X}_2 1$ [3], and XO^+ states, it is possible to infer the location of the $\text{AO}^+(\text{II})-\text{X}_2 1$ band features. The spectra in figs. 3a-c show three weak features which might be assigned to the (0,0), (0,1), and (0,2) transitions of this system.

The upper state of the grouping with band origin tentatively assigned at 17631 cm^{-1} (table 1) may correlate with several of the perturber levels identified by Jones and McLean [4]. These authors analyzed and catalogued several perturbations of the BO^+ state. Interactions with BO^+ , $v'=0$, centered at $J=48$ and 78 were correlated with $T_p=26129.2 \text{ cm}^{-1}$, $B_p=0.201 \text{ cm}^{-1}$, and $T_x=26292 \text{ cm}^{-1}$, $B_x=0.210 \text{ cm}^{-1}$, respectively. A further interaction with the $v'=2$ level centered at $J=51$ was correlated with $T_z=27350 \text{ cm}^{-1}$, $B_z=0.195 \text{ cm}^{-1}$. In addition, a level y , located close to the $v'=11$ level of the AO^+ state and associated with a perturbation of BO^+ , $v'=1$ (centered at $J=82$) was noted but no rotational parameters were determined from extra lines in the vicinity of the observed perturbation. We will suggest that the upper state of the "17631 cm^{-1} " band grouping correlates with certain of these perturber levels.

Chakoo and Patel [11] have rotationally analyzed two bands of the "17631 cm^{-1} " system corresponding to the (0,2) and (0,3) features assigned in table 1. The upper state rotational constant which these authors have determined, $0.2107(5) \text{ cm}^{-1}$, is only slightly larger than the rotational constant for the $\text{AO}^+(\text{II})$ state, $0.20913(3) \text{ cm}^{-1}$, [4], suggesting that the upper state associated with these bands lies at similar internuclear distance to the A state. This also suggests that the overlap of the vibrational levels of this state with those of the BO^+ state will be similar to that between the AO^+ and BO^+ states, facilitating similar interactions. Concomitantly, the interaction of this perturber state with the $\text{AO}^+(\text{II})$ state is expected to be minimal.

Based on the assumption that the feature at 17631 cm^{-1} catalogued in table 1 corresponds to the origin band for a transition which may emanate from at least one of the perturber states identified by Jones and McLean [4] and terminating in the $v=0$ level of the BiF "1" ($\text{X}_2 1$) state, we determine that T_0 for this

Table 2
Observed states and molecule constants for BiF

State	$T_e(\text{cm}^{-1})$	$\omega_e(\text{cm}^{-1})$	$\omega_e x_e(\text{cm}^{-1})$	$B_e(\text{cm}^{-1})$
$\text{XO}^+ \text{ a)}$	0	512.81	2.35	0.22998
$\text{X}_2 1 \text{ b)}$	6753	543.0	2.40	0.23512
$\text{AO}^+(\text{II}) \text{ a)}$	22957	383.8	3.5	0.20913
$\text{A}'' \text{ c)}$	22552	—	—	—
$\text{A}' \text{ c,d)}$	22400	"397"	"3.1"	0.210
$\text{BO}^+ \text{ a)}$	26001	626.8	6.6	0.2309

a) Literature data from ref. [4].

b) Rounded values from ref. [3]. Data obtained in the present study is consistent with $\nu_{00}=6768 \text{ cm}^{-1}$, $\omega_e \approx 543 \text{ cm}^{-1}$, $\omega_e x_e \approx 2.5 \text{ cm}^{-1}$.

c) T_0 , this work

d) $T_e \approx 24399 - (397/2) + (3.1/4) - (512.8/2) + (2.35/4) \approx 24341 \text{ cm}^{-1}$.

A' state lies at $\approx 24399 \text{ cm}^{-1}$. From the features identified in figs. 3b,c, we determine the upper state constants given in table 2 for the 17631 cm^{-1} band system and, on this basis, estimate that the $v'=5$ level of this state lies at 26292 cm^{-1} , whereas the $v'=8$ level lies at 27352 cm^{-1} . These energies are in very good agreement with the "x" and "z" perturber state levels identified by Jones and McLean [4]. The determined T_0 values in table 2 are based on the reasonable identification of the origin bands for the $\text{AO}^+(\text{II})\text{--}''1''$ and $\text{A}''\text{--}''1''$ transitions in BiF. If the observed highest frequency bands for these transitions do not terminate in the $v=0$ level of the $''1''$ state, the determined T_0 values will be at a higher energy than the true value. However, the correlation which these assignments in concert with those of Fink et al. [3] dictate with respect to the perturber levels identified by Jones and McLean [4] and the $\text{AO}^+(\text{II})\text{--}\text{X}_1\text{O}^+$ transition energies suggests that the origin bands have been identified.

A suggested assignment for the long wavelength red emission system is considerably more difficult. The temptation to assign these bands to a transition also terminating in the $\text{X}_2 1$ sublevel is fostered by the close agreement between the vibrational level separations observed in this region (table 2) and those of the $''17631 \text{ cm}^{-1}$ features ($\text{A}'' 1\text{--}\text{X}_2 1$). However, an assessment of trends among the group V fluorides PF, AsF, and SbF [19] also suggests that the low lying states of the BiF molecule, in which the transitions monitored in this study terminate, have very similar vibrational frequencies. Therefore it is not clear whether the observed features emanate from the same upper state as do the $\text{A}'' 1\text{--}\text{X}_2 1$ features or terminate in the same lower state. If the lower energy red system with $\nu_{00} \approx 15244$ or 15784 cm^{-1} terminates in the $''1''$ state, this suggests an upper state lying at $22552 \pm 545 \text{ cm}^{-1}$, virtually within one vibrational quantum of the $\text{AO}^+(\text{II})$ state. Alternatively, this transition may emanate from the same $v'=0$ upper state level at $T_0 = 24400 \text{ cm}^{-1}$, terminating in a lower state with $T_0 \approx 8615 \text{ cm}^{-1}$.

Of the two assignments outlined above, we favor the $\text{X}_2 1$ state as the terminal level of the long wavelength red system. In the absence of firm experimental data and considering the trends in the group V halides [19], it would not be difficult to surmise that the $^1\Delta$ state of BiF lies close to 8600 cm^{-1} . How-

ever, the quantum chemical calculations of Balasubramanian [2] predict the $^1\Delta$ state to lie at 14595 cm^{-1} and Fink et al. find some evidence for this state at 11255 cm^{-1} . This question will best be resolved in a high resolution study, as the definitive identification of the $^1\Delta$ state remains to be accomplished. We also note that several weak unassigned features are observed throughout the $565\text{--}740 \text{ nm}$ region. These features can be fit to the vibrational frequency separations for the $\text{AO}^+(\text{II})\text{--}\text{XO}^+$ transition and will be the subject of further study [6] in other laboratories.

If we accept the T_0 for the A'' perturber state as 24399 cm^{-1} with $B_0 = 0.2107(5) \text{ cm}^{-1}$, and associate the T_x perturber level identified by Jones and McLean with $v'=5$ and the T_z level ($B_z = 0.195 \text{ cm}^{-1}$) with $v'=8$, we can make several additional determinations. The assignment for the $v=0$ and 8 levels suggests an α_c value of 0.00197 cm^{-1} , comparing consistently with the known states of the BiF molecule [4,12] and yielding $B_c = 0.211(7) \text{ cm}^{-1}$. This value of α_c should be compared to that determined using the Pekeris formula

$$\alpha_c = 6(\omega_c \chi_c B_c^3)^{1/2} / \omega_c - 6B_c^2 / \omega_c = 0.00192 \text{ cm}^{-1}, \quad (3)$$

with $\omega_c \approx 397$ and $\omega_c \chi_c \approx 3.1 \text{ cm}^{-1}$. Thus suggests that the A'' perturber state has a somewhat stronger bond than the $\text{AO}^+(\text{II})$ state, consistent with the calculated B_c value. The approximate level structure for the low-lying states of BiF is indicated in fig. 5.

3.2. Energetics of the bismuth-fluorine system

The vapor in equilibrium with molten bismuth is known to contain nearly equal concentrations of bismuth atoms and dimers with lesser concentrations of trimer and tetramer [20]. We find that the reaction of the constituents of the bismuth vapor flux and F_2 under near single collision conditions clearly produces intense emission from the BiF $\text{AO}^+(\text{II})$ state. The population of the A state through the reaction of Bi atoms,



with

$$\Delta E \approx D_0^0(\text{BiF}) - D_0^0(\text{F}_2), \quad (4)$$

requires that the BiF dissociation energy be of order-

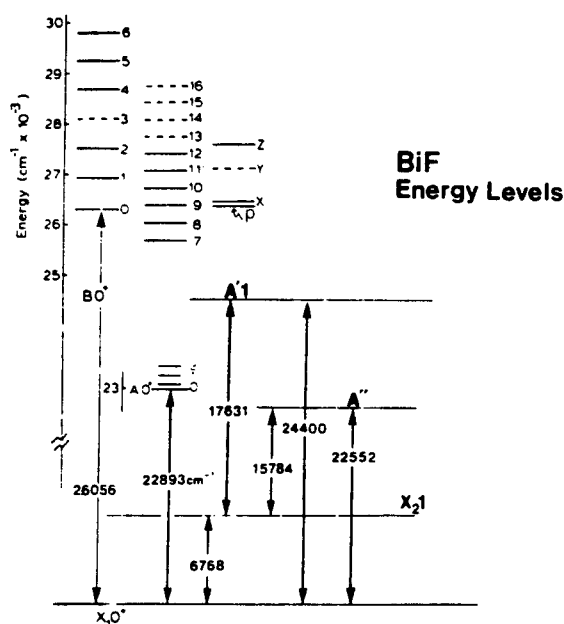


Fig. 5. Approximate energy level diagram for the electronic states of the BiF molecule.

4.45 eV to populate the observed AO^+ (II) levels.

The previously suggested values of the BiF dissociation energy do not exceed 3.14 eV which implies that, in sharp contrast to the recent suggestion of Ross et al. [6], the reaction (1) is only 1.55 eV exothermic and will not produce visible and ultraviolet radiation. However, initial estimates of the bond energy were based on very limited Birge-Sponer extrapolations [13] and fits to ionic models [14]^{#1}. The value of 3.14 eV suggested by Jones and McLean [4] is based on the observation of features associated with the AO^+ (II) state that might signal the onset of predissociation. Yet, no direct evidence for a predissociation has been obtained. A value of the BiF dissociation energy in excess of 4.45 eV would be consistent with the recent value reported by Ross et al. [6]. This, at first glance, suggests that the much higher value of the BiF dissociation energy may be appropriate; however, we must also consider that $\approx 50\%$ of the bismuth beam constituency is bismuth dimer and

focus on the possible four center reaction of bismuth dimer and molecular fluorine, viz.



which liberates considerably more energy with

$$\Delta E \sim 2D_0^0(\text{BiF}) - D_0^0(\text{Bi}_2) - D_0^0(\text{F}_2). \quad (6)$$

The reaction (5) has the potential to distribute ≈ 3.05 eV of excess energy to the reaction products provided that the BiF bond energy is 3.25 eV. If all of this energy is partitioned into electronic excitation of one of the BiF products, the AO^+ (II) state may be populated. The Bi_2 molecule vaporizing from its source (crucible) may possess a significant vibrational excitation, as even more energy can be made available to the reaction (5). Thus this reaction might lead to the observed chemiluminescence. If the BiF dissociation energy is substantially above 3.25 eV, the reaction (5) can pool sufficient energy to populate the BO^+ state and high vibrational levels of the AO^+ (II) state. Thus, it is difficult to readily ascribe the source of the observed chemiluminescent emission and to establish the dissociation energy of BiF using only the bismuth vapor-fluorine molecule combination.

In order to provide some clarification of the BiF bond energy, it is appropriate to consider the bismuth dimer-fluorine atom reaction



This reaction liberates from ≈ 1.05 to 3.05 eV for a BiF bond energy ranging from 3.0 to 5.0 eV. If the reaction (2) produces a substantial A-X emission signal, this provides a strong indication that the recent suggestion of Ross et al. [6] ascribing the higher BiF bond energy is correct.

Fluorine atoms were produced using an electric discharge through SF_6 . This is a particularly attractive system for, if we consider reaction with the entire bismuth vapor constituency, the reaction of bismuth atoms with either SF_3 molecules produced in the discharge or the parent SF_6 is not sufficiently exothermic to yield visible chemiluminescence^{#2}. The

^{#1} It is somewhat disconcerting that a simple ionic model calculation based on the known ground state bond distance of $\text{BiF}(4)$ gives $D_e \approx 3.05$ eV.

^{#2} The SF_3 -F and SF_4 -F bond energies are both in excess of 3.25 eV. Therefore the reaction of bismuth atoms or dimers with SF_3 or SF_4 is not sufficiently exothermic to populate the BiF AO^+ (II) state. In the absence of a discharge to produce atomic fluorine no chemiluminescence is observed.

collisionally stabilized bismuth atom-fluorine atom three body radiative association can produce visible chemiluminescence if the BiF bond energy exceeds 2.85 eV. However the emission is expected to be comparatively weak [21]. The reaction (2) can produce strong A-X emission provided that the BiF bond energy exceeds 4.9 eV.

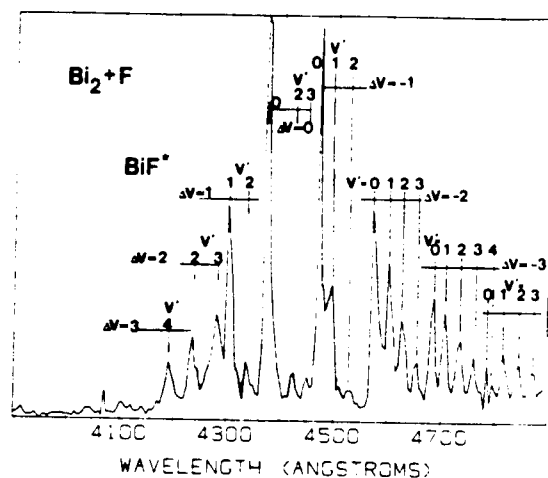
We have successfully employed the reaction (2) to produce the intense BiF AO⁺(II)-XO⁺ emission spectrum depicted in fig. 6a. This spectrum demonstrates that the Bi₂+F reaction (2) is sufficiently exothermic to produce the BiF AO⁺(II) state with $v' = 1-4$. The observed spectrum for the A-X transition taken at a resolution of 1 nm should be compared with the spectrum depicted in fig. 6b taken for the Bi₂(Bi, Bi₂)+F₂ system at a resolution of 0.8 nm. The A-X spectrum associated with the "Bi₂+F" reactive process appears to display a lower rotational excitation for the A-X features. Further, the "red system" bands of table 1 appear considerably weaker if not completely absent and the emission from the B-X band system is considerably sharpened³³.

These observations and our inability to observe emission from high vibrational levels of the AO⁺(II) state would also seem to support the minor role played by a collisionally stabilized bismuth atom-fluorine atom radiative association.

The observation of a strong BiF AO⁺(II)-X chemiluminescence associated with the Bi₂+F reaction implies that the BiF bond energy exceeds 4.9 eV³⁴. Of course, this value does not consider the internal energy associated with the reacting Bi₂ molecule and the relative translational energy of reactant interaction. Nor does it consider the final relative translational energy of separation of the products. We suggest that the results obtained in this study imply a BiF bond energy in excess of 4.5 eV. Further studies are in progress to refine this value.

³³ The sharper nature of the BiF BO⁺-XO⁺ band system suggests the population of fewer vibrational levels in the BO⁺ state.

³⁴ Based on a Bi₂ bond energy of 2.04 eV [22] calculated on the basis of thermochemical data assuming a Σ ground state and disregarding other low-lying states and an AO⁺(II), $v' = 0$ energy ≈ 2.85 eV. The population of vibrational levels $v' = 1-4$ at a minimum adds 0.18 eV to this total, however, one must also consider the contribution of the internal excitation of those bismuth dimer molecules which react and the relative translational energy of the reactants Bi₂ and F.



red band systems characterizing the $\text{Bi}_2 + \text{F}$ system. This will be the subject of further study.

4. Conclusions

The chemiluminescent spectrum resulting from the reaction of bismuth vapor and molecular fluorine at a variety of pressures provides evidence of two electronic transitions which terminate in the BiF^+1 state arising from the $^3\Sigma^- (\sigma^2\pi^4\pi'^2)$ configuration of BiF .

A combined study of the BiF chemiluminescence from the $\text{Bi} + \text{F}_2$ and $\text{Bi}_2 + \text{F}$ reactions has been used to establish a value of the BiF bond energy close to 4.5 eV. This is in agreement with the recent study of Ross et al. [6].

Acknowledgement

We thank Dawn Jordan for providing helpful assistance with these experiments. TCD and LB would like to thank the NSF-RUI program (CHE8900938) for support during the period over which this work was undertaken. KD would like to thank the NSF for an REU summer fellowship. JLG acknowledges helpful communications with R. Bacis, B. Koffend, Michael Heaven, E. Dorko, T. Cool and E.H. Fink, who provided his results prior to publication. JLG also acknowledges the Air Force Office of Scientific Research-Army Research Office and the Strategic Defense Initiative for partial support of this research.

References

- [1] J.M. Herbelin and R.A. Klingberg, *Intern. J. Chem. Kinetics* 16 (1984) 849.
- [2] K. Balasubramanian, *Chem. Phys. Letters* 127 (1986) 324.
- [3] E.H. Fink, K.D. Setzer, D.A. Ramsay and M. Vervloet, *Chem. Phys. Letters*, to be published.
- [4] W.E. Jones and T.D. McLean, *J. Mol. Spectry* 90 (1981) 481.
- [5] P. Kuijpers and A. Dymanus, *Chem. Phys.* 24 (1977) 97.
- [6] A.J. Ross, R. Bacis, J. D'Incan, C. Effutin, B. Koffend, A. Topouzkhanian and J. Verges, *Chem. Phys. Letters* 166 (1990) 539.
- [7] R.F. Heidner III, H. Helvajian, J.S. Holloway and J.B. Koffend, *J. Chem. Phys.* 84 (1986) 2137.
- [8] M.M. Patel and P.S. Narayanan, *Indian J. Pure & Appl. Phys.* 5 (1967) 223.
- [9] M.N. Avasthi, *Spectrosc. Letters* 3 (1970) 157.
- [10] P.S. Murty, D.V.K. Rao, Y.P. Reddy and P.T. Rao, *Spectrosc. Letters* 8 (1975) 217.
- [11] K.J. Chakoo and M.M. Patel, *Indian J. Pure & Appl. Phys.* 17 (1979) 189.
- [12] W.E. Jones and T.D. McLean, *J. Mol. Spectry* 83 (1980) 317.
- [13] A.G. Gaydon, *Dissociation Energy and Spectra of Diatomic Molecules*, 3rd Ed. (Chapman and Hall, London, 1968).
- [14] B. Rai and J. Singh, *Spectrosc. Letters* 4 (1971) 129.
- [15] R.N. Zare, Ber. Bunsenges. *Phys. Chem.* 78 (1974) 153; D.R. Preuss and J.L. Gole, *J. Chem. Phys.* 66 (1977) 2994; J.L. Gole and D.R. Preuss, *J. Chem. Phys.* 66 (1977) 3000; L.H. Dubois and J.L. Gole, *J. Chem. Phys.* 66 (1977) 779.
- [16] M.J. McQuaid, K. Morris and J.L. Gole, *J. Am. Chem. Soc.* 110 (1988) 5280; R. Woodward, P.N. Le, M. Temmen and J.L. Gole, *J. Phys. Chem.* 91 (1987) 2637.
- [17] D.M. Lindsay and J.L. Gole, *J. Chem. Phys.* 66 (1977) 3886; J.L. Gole and S.A. Pace, *J. Chem. Phys.* 73 (1980) 836; C.L. Chalek and J.L. Gole, *J. Chem. Phys.* 65 (1976) 2845; J.L. Gole and S.A. Pace, *J. Phys. Chem.* 65 (1981) 2651; J.L. Gole, *Ann. Rev. Phys. Chem.* 27 (1976) 525; W.J. Sayers and J.L. Gole, *J. Chem. Phys.* 67 (1977) 5442; G.J. Green and J.L. Gole, *Chem. Phys.* 46 (1980) 67, and references therein; G.J. Green and J.L. Gole, *Chem. Phys. Letters* 69 (1980) 45; A.W. Hanner and J.L. Gole, *J. Chem. Phys.* 73 (1980) 5025; J.L. Gole, *Probing Ultrafast Energy Transfer Among the Excited States of Small High Temperature Molecules*, in: *Gas Phase Chemiluminescence and Chemiionization*, ed. A. Fontijn (Elsevier, Amsterdam, 1985) p. 253.
- [18] R. Bacis, private communication.
- [19] K.P. Huber and G. Herzberg, *Constants of Diatomic Molecules*, (Van Nostrand, Princeton, 1979).
- [20] F. Kohl, O.M. Uy and K.D. Carlson, *J. Chem. Phys.* 47 (1967) 2667; L. Rovner, A. Drowart and J. Drowart, *Trans. Faraday Soc.* 63 (1967) 2906.
- [21] G. Herzberg, *Spectra of Diatomic Molecules* (Van Nostrand, Princeton, 1950) and references therein.
- [22] F. Kohl, O.M. Uy and K.D. Carlson, *J. Chem. Phys.* 47 (1967) 2667; D. Rovner, A. Drowart and J. Drowart, *Trans. Faraday Soc.* 63 (1967) 2906.

APPENDIX IVB

"Flourine Hot Atom Oxidation of Bismuth Vapor: A Comment on the Evaluation of the BiF bond Energy", T. C. Devore, and J. L. Gole, *Chemical Physics* 174, 409 (1993).

Fluorine hot atom oxidation of bismuth vapor. A comment on the evaluation of the BiF bond energy

T.C. Devore

Department of Chemistry, James Madison University, Harrisonburg, VA 22807, USA

and

J.L. Gole

School of Physics and High Temperature Laboratory, Georgia Institute of Technology, Atlanta, GA 30332, USA

Received 25 February 1993

The energetics of the chemiluminescent reaction between bismuth dimers and fluorine atoms (T.C. Devore et al., Chem. Phys. 155 (1991) 423; 156 (1991) 156) has been evaluated to better refine a determination of the bismuth fluoride dissociation energy. By directly examining the spectrum of the SF_6 discharge used to generate the F atoms to establish the significant energy imparted to these dissociation products and by exploring F atom chemiluminescent reactions with known energetics, the F atom beam is established to have contributed a maximum of 0.8–0.9 eV to the chemiluminescent process. Based upon the observed population of the $v' = 4$ level of the $\text{BiF A}0^+$ state resulting from the $\text{Bi}_2 + \text{F}$ reaction, a BiF bond energy of 3.9 ± 0.2 eV is established. This value is slightly higher than a very recent evaluation of the BiF bond energy (Yoo et al., Chem. Phys. 166 (1992) 215) but disagrees with previous determinations in the literature. Many of the previous evaluations of the group 15 halide dissociation energies have been based on Birge–Sponer extrapolations. The data now available for BiF permits an evaluation of the nature of these extrapolations for this molecule. The limitations of these extrapolations and possible corrections for these shortcomings are presented.

1. Introduction

Although the stabilities and molecular electronic structure of the group 15 halides, PX-BiX have been rather sparsely characterized (table 1) [1–18], considerable recent interest has been focused on the BiF molecule [19]. This interest has been based, in part, on the desire to energy transfer pump the $\text{BiF A}0^+$ (II) state in order to form a visible chemical laser operating on the $\text{A-X } (0^+)$ transition at wavelengths close to 450 nm. We have recently [16,17] been concerned with an evaluation of the BiF red emission systems which emanate from two excited electronic states located at energies and internuclear distances in close proximity ($< 2000 \text{ cm}^{-1}$) to the $\text{BiF A}0^+$ (II) state. This density of states, specific to the BiF molecule and representing some considerable deviation from the trends characterizing the lighter group

15 halides (fluorides), strongly influences the apparent level structure of the BiF A state.

In response to the intriguing suggestion by Ross et al. [15] that the BiF bond energy was close to 5 eV, exceeding by 2 eV previous estimates in the literature, we obtained an estimate of the BiF bond dissociation energy through a comparative evaluation of the chemiluminescent Bi_x (Bi , Bi_2) + F_2 and $\text{Bi}_2 + \text{F}$ reactive encounters. Based on an evaluation of the reaction energetics for the $\text{Bi}_2 + \text{F}$ reaction *uncorrected* for (1) vibrational excitation in Bi_2 and (2) the translational energy of those F atoms reacting with the bismuth dimer, we estimated that the upper limit for the bond energy of BiF could exceed 4.5 eV but indicated that the energetics needed to be refined before an accurate upper limit could be determined [16]. In this communication, we summarize the results of our studies to refine [17] this initially estimated value, taking into account the significant

Table I
Evaluated dissociation energies for group 15 halides PX-BiX

Element	Dissociation energy for MX (X = F, Cl, Br, I) in electron volts ^{a)}			
	F	Cl	Br	I
F	4.5 ± 1 ^{b)} [1], 4.55 ± 0.4 [2]	-	-	-
As	4.2 ^{c)} [3]	-	-	-
Sb	4.5 ± 1 ^{d)} [6]	3.7 ± 0.5 ^{b)} [5]	3.2 ± 0.6 ^{b,e)} [4]	2.5 ± 1 ^{b,e)} [7]
Bi	2.65 ± 0.3 ^{e)} [11-13] ^{b)} , > 4 ^{f)} 3.14 [21], 3.76 ± 0.13 [18]	3.13 ± 0.1 ^{b)} [9,10]	2.74 ± 0.01 ^{b,e)} [7,8]	

^{a)} References in parentheses.

^{b)} Linear Birge-Sponer extrapolation.

^{c)} Theoretical calculation.

^{d)} Linear Birge-Sponer extrapolations give values ranging from 4.2 to 5.7 - suggested by ref. [14].

^{e)} Suggested by ref. [14].

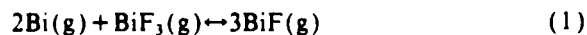
^{f)} Refs. [15-17].

^{g)} Mass spectrometry.

translational energy associated with fluorine atoms produced from an SF₆ discharge, discuss the implications of this refinement correlated with other recent studies of the BiF bond energy [15,18] and consider the recently proposed parameterizations of Yoo et al. [18], to evaluate the BiF bond dissociation energy.

2. The BiF bond dissociation energy

Recently Yoo et al. [18] have used photoion yield curves and a second and third law treatment based on the ion intensities for the reaction



to establish the dissociation energy of BiF as 3.76 ± 0.13 eV. This value is nearly 1 eV larger than the previously accepted values for the dissociation energy, 2.65 eV estimated from spectroscopic data by Gaydon [14], 3.0 eV determined using an empirical ionic model by Rai and Singh [20], and less than 3.14 eV determined by Jones and Mclean [21] from a possible predissociation of the A0⁺ state; however, it is over 1 eV lower than the value of nearly 5 eV determined by Ross et al. [15] from a long extrapolation of vibrational level separations based on a Leroy-Bernstein [22] plot using the ground state molecular constants.

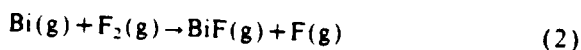
In investigating the spectroscopy and dynamics of the chemiluminescent reactions between bismuth va-

por (Bi, Bi₂) and fluorine atoms and molecules, we [16,17] have focused some considerable attention on the intense chemiluminescent emission from the Bi₂+F reaction. In our initial study [16] we suggested, in agreement with Ross et al. [15], that the upper limit for the BiF dissociation energy could be greater than 4.5 eV [16]. However, it was also stated that a more careful assessment of the internal energy of the reactants, particularly the translational energy of the F atom beam in the Bi₂+F atom reaction, would be needed before a more precise value for the upper limit of the dissociation energy could be determined.

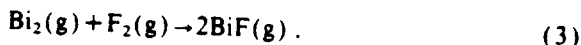
We have now further refined these experiments through an assessment of the F atom beam produced in the SF₆ discharge employed to study the Bi₂+F reaction. It is clear that the F atoms are produced with a significant translational energy and that the translational energy is involved in the reaction since the F atom based chemiluminescent signature in the vicinity of the oxidant source displays a substantial directionality relative to that characterizing the bismuth vapor/F₂ interaction. Based upon a comparison of the reaction energetics for several known systems, we suggested an upper bound value of 4.2 ± 0.2 eV for the BiF bond energy based on an F atom translational energy in excess of 0.5 eV [17]. This F atom energy has now been more stringently parameterized to energies of order 0.8-0.9 eV. With this correction, assuming differences in the translational energy of the other reactants and products are negligible, the ther-

mochemical cycle [16,17]²¹ involving Bi₂ and hot F atoms suggests a BiF bond energy of order 3.9 ± 0.2 eV, slightly higher than that given by Yoo et al. [18]. The uncertainty is based upon estimates of the uncertainty in the F atom energy and will allow for possible vibrational excitation in the Bi₂.

The determination of Yoo et al. [18] and our refinement of the dissociation energy provide insight into the chemiluminescent signature observed for the interaction of bismuth vapor and F₂ [16,17]. This reactive system produces strong emission from the low-lying vibrational levels of the A0⁺ state and weak emission from the B0⁺ state and high vibrational levels of the A0⁺ state [16]. If the reaction



contributed to the observed strong chemiluminescence, this would require that the BiF bond energy exceed 4.45 eV [16,17]. Since the dissociation energy of BiF is close to 4 eV, the reaction (2) can produce only vibrationally excited ground state BiF. The Bi₂ present as a substantial constituent of the bismuth flux must react to produce BiF excited electronic states via the four center reaction [16,24]

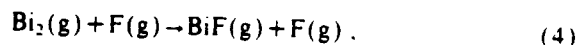


Since the $\nu=6$ level of the B0⁺ state and high vibrational levels of the A0⁺ (II) state ($\nu' > 20$ was identified with certainty in ref. [16] and Ross et al. [15] reported $\nu' = 26$ under similar experimental conditions) are populated, at least 3.7 eV of excess energy can be deposited into the product molecules formed via reaction (3). If we ignore the possible internal energy in the reactants and use 3.76 eV as the dissociation energy of BiF, reaction (3) can generate approximately 3.9 eV in one of the BiF products. Thus, up to ≈95% of the available reaction exothermicity can be deposited into one of the two product BiF molecules during the reaction! This large percentage of the reaction energy, pooled into only one of the product species, suggests that it may be possible to use chemiluminescent dimer reactions to provide reasonable estimates for bond energies. Further investigation will be needed to (1) determine if this conclusion will hold in general and (2) assess the

conditions under which this limit is reached. If this is a general result, the energetics of chemiluminescent cluster reactions could provide insight into cluster binding energies as well as product dissociation energies.

3. The Bi₂-F reaction

The chemiluminescence from the reaction



where the F atoms are produced via a discharge through SF₆ has now been more thoroughly investigated [16,17]. The $\nu' = 4$ level of the BiF A0⁺ state is populated by the reaction but emission from the B0⁺ state and high vibrational levels of the A0⁺ state are not readily observed. Approximately 3 eV of excess energy is required to produce the observed emission. Since reaction (3) is exothermic by less than 2 eV, Yoo et al. [18] questioned whether the Bi₂ + F reaction was studied [16] by Devore et al. and suggested that F₂ production in the discharge provided the necessary reactant to produce the observed emission in the bismuth vapor/SF₆ discharge system. This possibility was carefully considered [16]. There is no evidence to support the assumption that F₂ is present in the discharge system. The spectrum of the SF₆ discharge was examined [17] to determine if F₂ molecules were produced. A dispersed spectrum of the directly viewed discharge through pure SF₆ reveals (fig. 1) considerable F atom emission, some HF emission, and an as yet unidentified sulfur-based emitter (possibly SF₅); however, the orange F₂ recombination emission bands [25], which are readily detected, were not observed. Further, if we examine the discharge tube configuration in a direction perpendicular to the reactant exit port, we monitor no emission. The generated potential reactants are relaxed to their ground states (or very low-lying excited states) before exiting the discharge source [17]. While it is possible that the SF₆ cylinder may have contained some F₂, this does not seem likely. Finally, we observe [16] that there are several significant differences in the BiF spectra observed for the F₂ based reactive system and the F atom-Bi₂ reaction (3) which have been detailed previously [16,17]. Consequently, clear evidence against an F₂ contaminant

²¹ Using $D_0^0(\text{BiF}) \geq D_0^0(\text{Bi}_2) + E_{\text{internal}}(\text{BiF}) - E_{\text{internal}}(\text{Bi}_2) - E_{\text{trans}}(\text{F})$. For $D_0^0(\text{Bi}_2)$, see ref. [23].

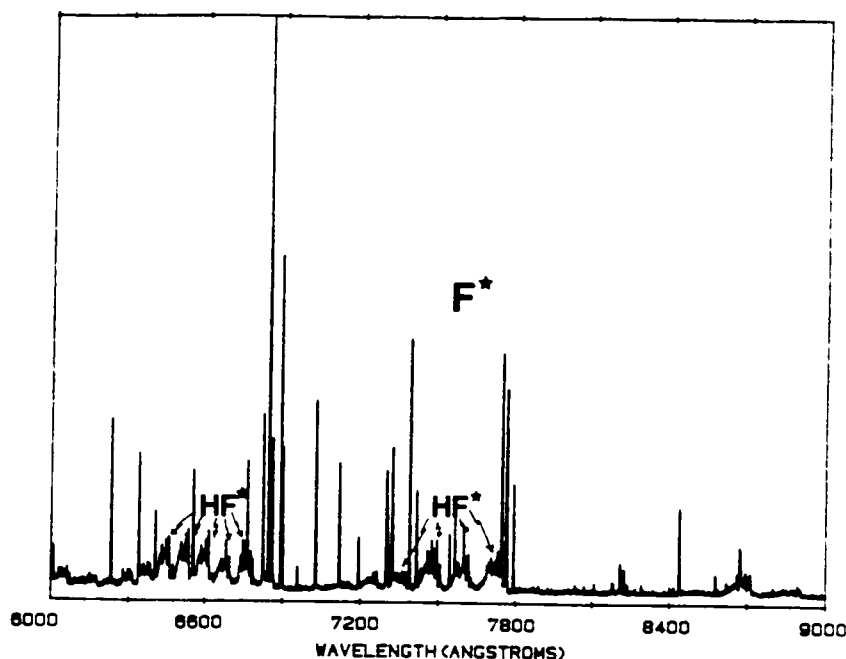


Fig. 1. Emission spectrum observed in the region $\lambda > 600$ nm after passing a high voltage discharge through SF_6 . The spectrum was obtained by aligning the discharge with a spectrometer monitoring the emission. The sharp line-like features correspond to fluorine atom transitions. The open structure band-like features correspond to HF overtone transitions. Spectral resolution is 0.1 nm.

is obtained. Further, it is clear from the F atom emission associated with the SF_6 discharge, that considerable energy has been provided to the F atoms. We observe the reaction of hot F atoms with bismuth vapor.

4. The Birge-Sponer extrapolation – bonding parameterization

Yoo et al. [18] have attempted to evaluate the accuracy of the Birge-Sponer extrapolation in determining the dissociation energy of BiF. Contrary to the image left by their discussion, we [16] did not explore this concept previously. The statement made in the introduction of ref. [16] is based on the discussion given by Gaydon [14] and later reiterated by Atkins [26], meant to note that the Birge-Sponer extrapolation can yield an upper bound to the bond energy. Nevertheless, the evaluation of the Birge-Sponer extrapolation for the group 15 halides is a noble undertaking since the dissociation energies for these molecules are not well established and are derived, at

least in part, from these extrapolations [17]. Yoo et al. [18] performed a linear least-squares extrapolation of the last 10 ground state vibrational levels ($v'' = 26.5$ to 36.5) reported by Ross et al. [15] to estimate a value for $D_0(\text{BiF})$ of 4.17 eV. This determined bond energy is notably larger than the experimental value of 3.76 eV which they found for the dissociation energy. The extrapolation, using only the last 10 observed levels is, of course, arbitrary and their motivation for choosing these levels for the extrapolation is not clear. As shown in table 2, a different value for the dissociation energy is obtained depending upon the number and location of the levels used in the extrapolation. Interestingly, if all 36 ground state energy levels reported by Ross et al. [15] are used for a linear least-squares treatment, D_0 is estimated to be 3.83 eV, a value which is within experimental error of the experimentally determined dissociation energy. However, as demonstrated in the Birge-Sponer plot of fig. 2, the vibrational energies are clearly non-linear. Both the lower and the higher vibrational levels lie above the least-square line suggesting that a linear extrapolation will underestimate

Table 2

Apparent values determined for the dissociation energy of BiF by linear Birge–Sponer extrapolation using a subset of the ground state energy levels determined by Ross et al. [15]

Levels used	D_0 (eV)
0–5	3.38
0–10	3.45
0–15	3.55
0–20	3.62
0–25	3.69
0–30	3.75
0–36	3.83
5–36	3.85
10–36	3.89
16–36	3.99
21–36	4.06
26–36	4.17
31–36	4.30

the dissociation energy determined on the basis of evaluating the area under the $\Delta G_{v+1/2}$ versus v curve. If only the first five energy levels are used, a typical experimental limitation, the value determined on the basis of linear extrapolation, 3.38 eV, is roughly 10% low. At least for BiF, extrapolations for the first few levels underestimate the dissociation energy while

extrapolations from the upper levels, for which the second-order anharmonicity correction term is beginning to become important, overestimate the dissociation energy. If this trend would hold in general, it may be possible to establish upper and lower limits for the dissociation energy using this approach.

Yoo et al. [18] suggest that the dissociation energies obtained from linear Birge–Sponer plots can be modified to give excellent estimates for the dissociation energy by using the corrections for ionicity suggested by Hildenbrand [27,28]. In this case, they predict dissociation energies for the group 15 halides in excellent agreement with the experimental values using a linear Birge–Sponer extrapolated dissociation energy based upon only the first few observed ground state energy levels. While this might be a very encouraging result, it is *discomforting to note that as more levels are added, the agreement between the experimental value and the predicted value becomes worse*. A better strategy here might be to use the well known relationship between the harmonic vibrational frequency and the first anharmonicity constant [29,30] for the Morse potential

$$D_e \approx \omega_e^2 / 4\omega_e x_e$$

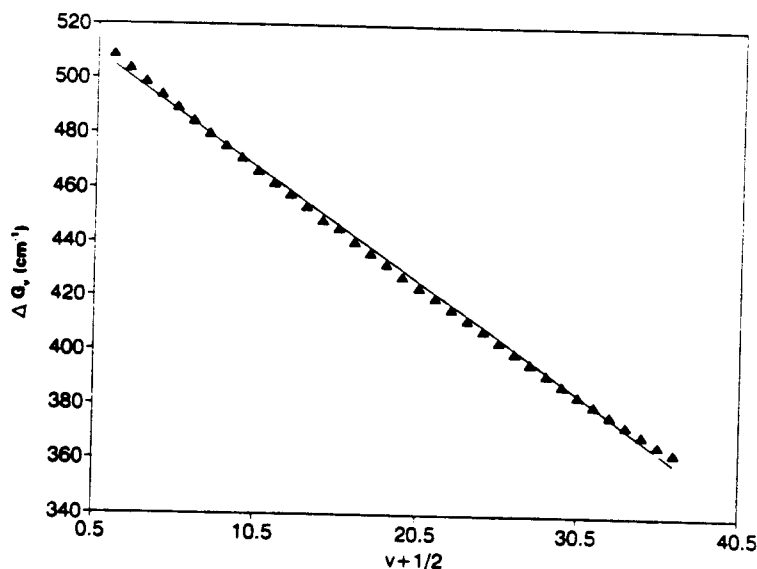


Fig. 2. Comparison of observed vibrational spacings for the $v'' = 0.5$ –36.5 levels of the ground $X0^+$ state of BiF with a linear least-squares Birge–Sponer extrapolation using the entire manifold of known ground state energy levels. The deviation of the observed data from linearity can readily be seen. See text for discussion.

to estimate the uncorrected dissociation energy in the Hildenbrand equations. These corrections would then be independent of the number of levels used and the corrections could be related to modifications in the potential well due to ionicity. Investigations into the reliability of this approach are in progress.

It should be possible to accurately determine the dissociation energy from extended spectroscopic data such as that available for BiF. The data of Ross et al. [15] can be fit to a power series to evaluate the spectroscopic constants. These constants can then be used to calculate all of the vibrational spacings below the dissociation limit. The dissociation energy was evaluated by summing over all vibrational spacings [30].

$$D_0 = \sum_v \Delta G_{v+1/2}.$$

with

$$\Delta G_{v+1/2} = \omega_e - 2\omega_e x_e(v+1) + \omega_e y_e(3v^2 + 6v + \frac{13}{4}).$$

Although very good data exist for ground state levels up to $v=36$, the constants derived from non-linear analysis do not give $\Delta G_{v+1/2}$ values that converge to zero for fits up to sixth order. Since higher-order fits are not experimentally justified, further evaluation has been limited to a second-order analysis. The constants derived for a second-order fit are given in table 3. Vibrational spacings calculated using these constants reach a minimum near $v=120$. If a small third-order correction term is added to make $\Delta G_{v+1/2}=0$ at $v=120$, the dissociation energy calculated for BiF by summing over the vibrational energies is 3.8 eV; a value agreement to within experimental error of the measured value. Although there is some uncertainty in the parameterization, it is likely that this procedure will provide good estimates for the vibrational energy if enough vibrational levels are known so as to

Table 3

Molecular constants determined by fitting the energy levels of Ross et al. [15] to the equation $v=a+bv+cv^2+dv^3$, where $a=\omega_e-2\omega_e x_e+\frac{13}{4}\omega_e y_e$, ..., $b=-2\omega_e x_e+6\omega_e y_e$, ..., $c=3\omega_e y_e$, ...

Constant	Value determined	Lit. Value
ω_e	513.33	512.81 cm ⁻¹
$\omega_e x_e$	2.424	2.35 cm ⁻¹
$\omega_e y_e$	6.248×10^{-1}	- cm ⁻¹
d	1×10^{-4}	- cm ⁻¹
D_0	3.8	3.76 eV

provide a reasonable estimate for the anharmonicity constants.

Acknowledgement

We thank David Grantier and Jeffrey Kispert for helpful assistance with the additional experiments outlined here and acknowledge data taken from the work of John Bray on the Cu₂+F system, Lauri Brock, Dawn Jordan, and Kenneth Dulaney on the Mn₂+F system, C.B. Winstead and H. Wang on the Mg₂+F system, and He Wang on the Ag₂+F system. TCD would like to thank the NSF-RUI program (CHE8900938) for partial support of this research. JLG acknowledges helpful communications with R. Bacis, B. Koffend, Michael Heaven, E. Dorko, T. Cool and E.H. Fink, who provided his results prior to publication. JLG also acknowledges the Air Force Office of Scientific Research-Army Research Office and the Strategic Defence Initiative for partial support of this research.

References

- [1] A.E. Douglas and M. Frackowiak, Can. J. Phys. 40 (1962) 832.
- [2] L.V. Gurvich et al., Thermodynamic properties of individual substances, Vols. 1, 2 (USSR Academy of Sciences, Moscow, 1962) [in Russian].
- [3] P.A. O'Hare, R. Batana and A.C. Wahl, J. Chem. Phys. 59 (1973) 6495.
- [4] N.L. Singh and M.N. Avasthi, Indian J. Pure Appl. Phys. 1 (1963) 197.
- [5] W. Jevons, Proc. Phys. Soc. 48 (1936) 563.
- [6] H.G. Howell and G.D. Rochester, Proc. Phys. Soc. 51 (1939) 329.
- [7] T.A.P. Rao and P.T. Rao, Indian J. Phys. 36 (1962) 85.
- [8] F. Morgan, Proc. Soc. 49 (1936) 41.
- [9] S. Sankaranarayanan, M.M. Patel and P.S. Narayan, Proc. Indian Acad. Sci. 56 (1962) 171.
- [10] D. Cubicciotti, J. Phys. Chem. 64 (1960) 791.
- [11] P. Venkateswarlu and B.N. Khanna, Proc. Indian Acad. Sci. A51 (1960) 14.
- [12] K.C. Joshi, Proc. Phys. Soc. 78 (1961) 610.
- [13] S. Sankaranarayanan, P.S. Narayanan and M.P. ... , Proc. Indian Acad. Sci. 59 (1964) 378.
- [14] R.B. Singh and D.K. Rai, Can. J. Phys. 43 (1965) 829.
- [15] A.G. Gaydon, Dissociation energies and spectra of diatomic molecules, 3rd Ed. (Chapman and Hall, London, 1968).

- [15] A.J. Ross, R. Bacis, J. D'Incan, C. Effutin, B. Koffend, A. Topouzkhanian and J. Verges, *Chem. Phys. Letters* 166 (1990) 539.
- [16] T.C. Devore, L. Brock, R. Kahlscheuer, K. Dulaney and J.L. Gole, *Chem. Phys.* 155 (1991) 432.
- [17] J.L. Gole, in: *Gas phase metal reactions*, ed. A. Fontijn (North-Holland, Amsterdam, 1992) pp. 578-604.
- [18] R.K. Yoo, B. Ruscic and J. Berkowitz, *Chem. Phys.* 166 (1992) 215.
- [19] J.M. Herbelin and R.A. Klingberg, *Intern. J. Chem. Kinetics* 16 (1984) 849;
R.F. Heidner III, H. Helvajian, J.S. Holloway and J.B. Koffend, *J. Chem. Phys.* 84 (1986) 2137;
D.J. Benard and B.K. Winker, *J. Appl. Phys.* 69 (1991) 2805.
- [20] B. Rai and J. Singh, *Spectry. Letters* 4 (1971) 129.
- [21] W.E. Jones and T.D. McLean, *J. Mol. Spectry.* 83 (1980) 317.
- [22] R.J. Leroy, in: *Molecular spectroscopy*, Vol. 1, eds. R.F. Barrow, D.A. Long and D.J. Millen (Chemical Society, London, 1973) p. 113; *J. Chem. Phys.* 73 (1980) 6003.
- [23] F. Kohl, O.M. Uy and K.D. Carlson, *J. Chem. Phys.* 47 (1967) 2667;
D. Rouner, A. Drowart and J. Drowart, *Trans. Faraday Soc.* 63 (1967) 2906.
- [24] J.M. Parson, B.S. Cheong, R.P. Kampf and M.D. Oberlander, Effects of electronic excitation and dimerization of metals on product state distributions, in: *Gas phase metal reactions*, ed. A. Fontijn (North-Holland, Amsterdam, 1992).
- [25] H.G. Gale and G.S. Monk, *Astrophys. J.* 69 (1929) 77;
T.L. Porter, *J. Chem. Phys.* 48 (1968) 2071.
- [26] P.W. Atkins, *Physical chemistry*, 4th Ed. (Freeman, San Francisco, 1990) p. 487.
- [27] D.L. Hildenbrand, *Advances in high temperature chemistry*, Vol. 1 (Academic Press, New York, 1967) p. 193.
- [28] D.L. Hildenbrand and E. Murad, *J. Chem. Phys.* 51 (1969) 807.
- [29] G. Herzberg, *Molecular spectra and molecular structure*, Vol. 1, *Spectra of diatomic molecules* (Van Nostrand, Princeton, 1950) p. 439.
- [30] J.M. Hollas, *Modern spectroscopy* (Wiley, New York, 1987) p. 119.

APPENDIX V

"Toward the Modeling of the Oxidation of Small Metal and Metalloid Molecules", in "Gas Phase Metal Reactions", edited by A. Fontijn, Elsevier, North Holland, Elsevier Science Publishers, (1992) pp. 573-604.

Toward the Modeling of the Oxidation of Small Metal and Metalloid Molecules

James L. Gole

High Temperature Laboratory, Center for Optical Science and Engineering
and School of Physics, Georgia Institute of Technology, Atlanta, Georgia
30332

ABSTRACT

Oven based entrainment flow and supersonic expansion techniques are used to form small metal and metalloid molecules and to study their unusual oxidation behavior. These metal and metalloid molecules oxidize to form not only a distinct class of metal atom grouped cluster oxides and halides under kinetically as opposed to thermodynamically controlled conditions but also unusual (unexpected) excited electronic state product distributions. We exemplify this behavior by considering the optical signatures associated with the formation of the asymmetric silver and copper clustered oxides from the silver and copper cluster oxidation reactions. We also contrast the emission spectra generated for the asymmetric and symmetric isomers of Cu_2O , comparing these with theory. A subset of the oxidation studies touches on the sodium trimer - halogen atom reactions, $(\text{Na}_3 - \text{X}(\text{Cl}, \text{Br}, \text{I}))$, which create a continuous electronic population inversion based on the chemical pumping of Na_2 with laser amplification throughout the visible and into the ultraviolet. The study of highly exothermic oxidation processes also yields interesting surprises concerning even the diatomic metal halides. This is exemplified by comparing the $\text{Bi}_x + \text{F}_2$ and $\text{Bi}_x + \text{F}$ chemiluminescent reactions, extracting parameters for several new low-lying excited electronic states and obtaining an estimate of the BiF bond dissociation energy notably higher than that previously recommended in the literature.

INTRODUCTION

As the papers in this symposium volume clearly indicate, gas phase metal reactions have long played an important role in a wide diversity of processes.¹ However, despite their importance and the creative effort which has been expended in their study,^{2,3} much remains to be learned about even the simplest highly exothermic oxidation processes involving metal or metalloid species, the factors which control product branching in the reactive process, and the molecular electronic structure of the sometimes unique products of reaction. In this chapter, we outline recent progress in our laboratory to characterize the oxidation of small metal and metalloid molecules, a research effort which is beginning to yield several interesting surprises related to reactive branching and product molecular electronic structure. These studies also bear

correlation with the ongoing research in the laboratories of John Parson, Nadir Sadeghi, John Dyke, Scott Anderson, Nancy Garland and Peter Armentrout considered in other chapters of this volume.

Our emphasis will be on oxidation phenomena associated with metal and metalloid clusters which correspond primarily to small polyatomic molecules. However, in approaching this regime, we also find interesting surprises associated with metal atom and dimer reactions and the bonding in diatomic molecules which are the products of the oxidation process. In particular, the halides of the Group 15 elements are intriguing and rather sparsely studied. As we extend the study of the reactivity of metal atoms and dimers to small clusters, we are afforded an opportunity to graphically demonstrate a dramatic and sometimes unexpected oxidation behavior whose study may provide new insights on the nature of chemical reactivity as well as influencing models of molecular electronic structure.

It is well recognized that most heterogeneous conversion processes require intimate interaction with the surface of a condensed phase. The widespread applicability of these processes in a variety of practical applications encompassing metal combustion, chemical vapor deposition, plasma etching, and general industrial catalysis has fueled a significant theoretical and experimental research effort to understand the intimate interactions associated with surface participation and reactivity. An increasingly popular and potentially enlightening component of this effort now involves the modeling of a small group of interacting atoms (cluster) on the surface. Within this framework the detailed study of small clusters and their oxidation to produce metal clustered oxides can provide needed insights relevant to the incorporation of local interactions into modeling at much larger scales.

In effect, studies of gas phase metal cluster oxidation afford the opportunity to characterize the intermediate region bordered on the one side by the gas phase oxidation of metallic atoms and dimers and on the other by the surface oxidation of the bulk metallic phase. It has been suggested that these studies may provide information useful for the assessment of short and long range factors affecting surface oxidation.⁴ With an emphasis on their unique nature as well as the potential which their study offers for both theoretical and experimental extrapolation to much larger scales appropriate to describing bulk properties, several elegant technologies are emerging to study clusters and their compounds. However, despite many impressive approaches, the internal mode structure and dynamics associated not only with the metal clusters themselves⁵ but also with the products of their kinetically controlled oxidation has been largely neglected.

The limited information which is available⁶⁻⁸ demonstrates that metal clusters undergo a unique and, in many instances, totally unexpected reactive branching.⁹ The study of this reactive branching is fundamental to the development of rules required to extrapolate from simple $A + BC$ reactions. Further, the analysis of the quantum level structure of product metal cluster oxides and halides formed in highly exothermic oxidation processes provides detailed and fundamental information on molecular structure and bonding.⁶⁻⁹ In correlation with molecular dynamics simulations and quantum chemistry this data can serve as a touchstone for the development of a reasonable framework to describe (1) highly exothermic combustion processes or (2) local cooperative atomic phenomena and mobilities, the fingerprint of which can be useful

in modeling the interface at metal cluster oxide surfaces where, for example, catalytic behavior is most likely influenced.

We have been concerned with the study of the oxidation dynamics which a number of metal (and metalloid) clusters undergo as they form a distinct class of metal atom grouped cluster oxides⁶ and halides⁷ under kinetically as opposed to thermodynamically controlled conditions. An effort has also begun to characterize the internal mode structure of the product metal clustered oxides and halides. In developing these studies, we have analyzed the first vibrationally resolved optical signatures for several "asymmetric" metal cluster oxides.⁶ We have also demonstrated the first visible chemical laser amplifier from a metal cluster oxidation process.⁸ The information already obtained graphically demonstrates the dramatic and unexpected oxidation behavior characteristic of small metal cluster reactions.

In the first part of our discussion, we consider recent results obtained in the study of the interaction of bismuth vapor with molecular and atomic fluorine¹⁰ and the need for further extensive studies of the bond energies and molecular electronic structure of the halides of the Group 15 elements. We will then emphasize the unique nature of metal cluster oxidations as we outline the development of continuous visible chemical laser amplifiers from a metal cluster oxidation reaction. We then outline a portion of the information garnered thusfar on the quantum levels of metal cluster oxide and fluoride compounds, M_xO_y and M_xF_y . These studies not only outline the potential use of chemiluminescence as a means of characterizing metal cluster oxide quantum levels, but also they suggest future laser induced fluorescent probes of the metal cluster oxides.

NATURE OF METAL AND METALLOID MOLECULE SOURCES

In the present discussion, we will not summarize the experimental techniques for generating large concentrations of small metal clusters in a highly exothermic oxidizing environment. The devices we have used and are continuing to develop are well outlined elsewhere.¹¹

Briefly, the products of metal cluster oxidation may be studied using a combination of chemiluminescent (product formation in excited electronic states for highly exothermic oxidation) and laser fluorescent techniques. In these applications one must be cognizant that observations of the internal mode structure, associated especially with the polyatomic products of metal cluster oxidation, may be plagued by the rapid depletion of excited state populations due to non-radiative processes. These processes can dominate and deplete the product constituency either before the emission of a monitoring photon (chemiluminescence)¹² can occur or before an appropriate laser spectroscopic probe can be made operative.¹³ In order to overcome this difficulty, we require the development of intense metal cluster sources which offer a viable means to compensate for the dominant quenching of the optical signatures associated with the polyatomic emitters of interest.

Quantum level probes of the products of metal cluster oxidation are being developed with a current emphasis on two distinct source configurations. In one configuration a stream of metal clusters formed through the "supersonic expansion" of the metallic element of interest is made to intersect a selected oxidant (modified beam-gas configuration), the products of reaction being studied using a combination of chemiluminescent

and laser fluorescent techniques. This configuration has been used to study the sodium trimer-halogen atom reactions.⁸ Of possibly more significance is the development of a second more versatile source configuration which lies intermediate to a low pressure molecular beam and high pressure flow device.¹⁴ Clusters are formed from a high metal flux source and further agglomerated by an entraining argon or helium flow maintained at room to liquid nitrogen temperature. Using this source, we have successfully obtained the first quantal information on the energy levels and optical signatures of several metal cluster oxides and select halides (M_nO , M_nX). Our focus in these studies is to be distinguished from recent very exciting investigations in which small to intermediate size clusters have been generated in flow systems,¹⁵ reacting with reagents in another merging continuous or pulsed flow stream under high pressure (~ 300 -500 torr) conditions. The products of reactivity in these merged flows have been measured mass spectrometrically extracting important kinetic information; however, the technique is not yet oriented to a direct measure of structural or dynamic properties.

AN EVALUATION OF THE BOND ENERGY AND LOW-LYING STATES OF THE BiF MOLECULE-EXTENSION TO ADDITIONAL GROUP 15 HALIDES

There has been interest in the energy transfer pumping of BiF excited states, employing metastable NF in order to develop a visible chemical laser system. These efforts, among others, have focused attention on the low-lying electronic states and molecular electronic structure of the BiF molecule.¹⁶ Recently, we have carried out a detailed study of the pressure dependent chemiluminescent emission from the $Bi_x + F_2$ and $Bi_2 + F$ reactions.¹⁰ The main impetus for this study stemmed from our interest in the substantial discrepancy between reported values for the dissociation energy of the BiF molecule and the significance of the correct value to bonding trends in the Group 15 halides.

Ross et al.¹⁷ have recently given a value of ~ 5 eV for the BiF dissociation energy. This value substantially exceeds the ~ 3 eV values previously reported.¹⁸⁻²¹ Gaydon²⁰ has estimated the BiF dissociation energy to be 2.65 ± 0.2 eV. This value seems surprising in view of the clear, albeit limited, data reflecting trends in the bismuth and antimony halides, outlined in Table I, and the expectation that the fluoride bond energies generally considerably exceed those of the heavier halides.²² However, Rai and Singh have used an empirical ionic model based upon the determined ground state molecular constants to estimate a BiF dissociation energy close to 3 eV. From the indication of excited state level separations signaling a possible predissociation of the AO^+ state, Jones and McClean¹⁹ have suggested that the BiF dissociation energy is less than 3.14 eV. Finally, Balasubramanian¹⁸ calculates a dissociation energy of 2.63 eV. Although not in total agreement, these values are consistent with Gaydon's initial estimate and a bond energy of 3 eV.

Ross et al.¹⁷ employed a long extrapolation based on a LeRoy-Bernstein²³ plot using improved ground state molecular constants¹⁷ to estimate the dissociation energy. Because the vibrational spacings for the highest ground state levels observed in their study were still ~ 350 cm^{-1} some two eV's above the lowest ground state levels, they concluded that previous estimates of the dissociation energy were low and suggested that the dissociation energy was ~ 5 eV. This value considerably exceeds that predicted by a Linear Birge-Sponer extrapolation which usually

yields an upper bound to the dissociation energies²⁰ for polar and ionic molecules, however, the arguments presented by these authors bear consideration.

Clearly, a substantial discrepancy and considerable controversy exists over the BiF bond energy. The value reported by Ross et al.¹⁷ suggests, counter to earlier studies, the possible population of BiF excited states emitting in the visible and ultraviolet regions in a single collision chemiluminescent Bi-F₂ reactive encounter.²⁴ The reaction between bismuth vapor and fluorine has proven to be an effective means for producing the excited states of BiF.^{17,25} In addition, investigations of similar systems²⁴ have shown that a careful analysis of reaction energetics can provide an accurate determination of the product molecule dissociation energy. However, in the bismuth-fluorine system, the problem is more complex. In order to assess several aspects of those questions associated with the dissociation energy and low-lying states of BiF, the reactions between bismuth vapor and both molecular and atomic fluorine were investigated to determine if more could be learned about the molecular electronic structure of the BiF molecule. These efforts were designed to combine data obtained in the study of the two potentially chemiluminescent reactive encounters



and



"The Chemiluminescent Emission from the Bismuth Vapor - F₂ Reaction - Low-Lying States of BiF"

We have studied the chemiluminescent reaction of helium entrained bismuth vapor and molecular fluorine at pressures approaching 10⁻² Pa and over the substantially higher pressure range between 66 and 333 Pa.¹⁰ The spectrum observed when a moderate flux of helium entrained bismuth vapor reacts with F₂ under multiple collision conditions is depicted in Figure 1. At least three distinct band systems are readily identified. The strong feature near 450 nm corresponds to the AO⁺(II) - XO⁺ transition of BiF.^{26,27} The band near 380 nm corresponds to the origin sequence for the BO⁺ → XO⁺ transition.^{28,29} The "red" systems observed from 565 to 740 nm contain numerous bands, some of which have been assigned by previous investigators^{28,30-32} and a number which had not previously been reported nor analyzed before a recent study in our laboratory.¹⁰

A closeup of the red region reveals (Fig. 2) certain emission features, dominant especially at higher pressures, where the A - X emission features associated with higher vibrational levels of the BiF A state are quenched. The features near 450 nm can be readily assigned to transitions from v' ≤ 4, AO⁺(II)¹⁰. Their relative intensities suggest that these AO⁺ levels might be characterized reasonably by a nearly Boltzmann population distribution with an effective vibrational temperature approximating 700 K;¹⁰ however, weak emission from several higher lying levels of the AO⁺(II) state (v'' > 15) extends to considerably longer wavelength. The emission from these higher vibrational levels is the subject of further study in other laboratories.¹⁷

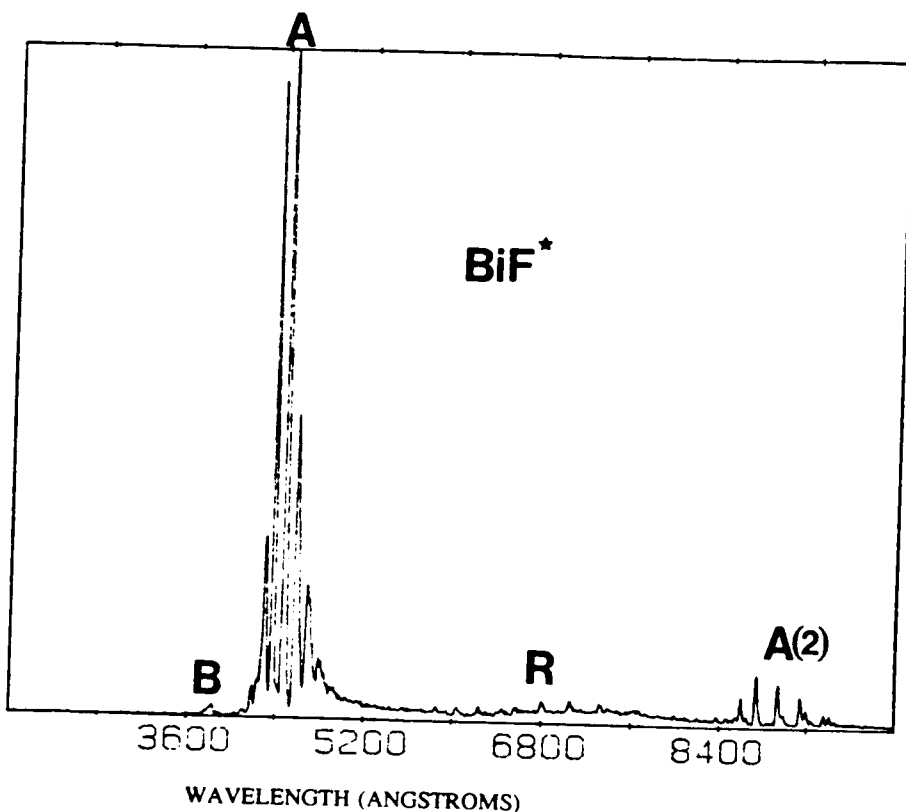


Figure 1: Chemiluminescent emission spectra resulting from the reaction between helium entrained bismuth vapor and F_2 under multiple collision conditions. The bands labeled A (first order) and A(2) (second order) identify the $\text{AO}^+ \rightarrow \text{XO}^+$ transition, the bands labeled B correspond to the $\text{BO}^+ \rightarrow \text{XO}^+$ transition and the bands labeled R correspond to the "red system" bands considered in the text. Spectral Resolution is 1 nm.

The bands observed in the red region between 565 and 740 nm were found to change markedly with pressure (primarily helium) in the reaction zone.¹⁰ The analysis of this pressure dependence over a substantial range provides evidence for two distinct electronic transitions of BiF , at least one of which is thought to terminate in the BiF "1" (X_{21}) state arising from the $3\Sigma^-(\sigma^2 \pi^4 \pi^{*2})$ configuration of BiF . Here the BiF ground state corresponds to the XO^+ component of the $3\Sigma^-$ configuration and the "1" state arising from this configuration lies $\sim 6800 \text{ cm}^{-1}$ higher in energy.²⁶

The observed transitions in the red region with $\nu_{00} \sim 17631 \text{ cm}^{-1}$ and $\nu_{00} \sim 15244 \text{ cm}^{-1}$ exhibit pronounced upper state vibrational relaxation and are characterized, especially at the highest pressures, by a dominance of progressions emanating in $\nu' = 0$ and terminating in several ν'' lower state levels (Table I). The higher energy transition with

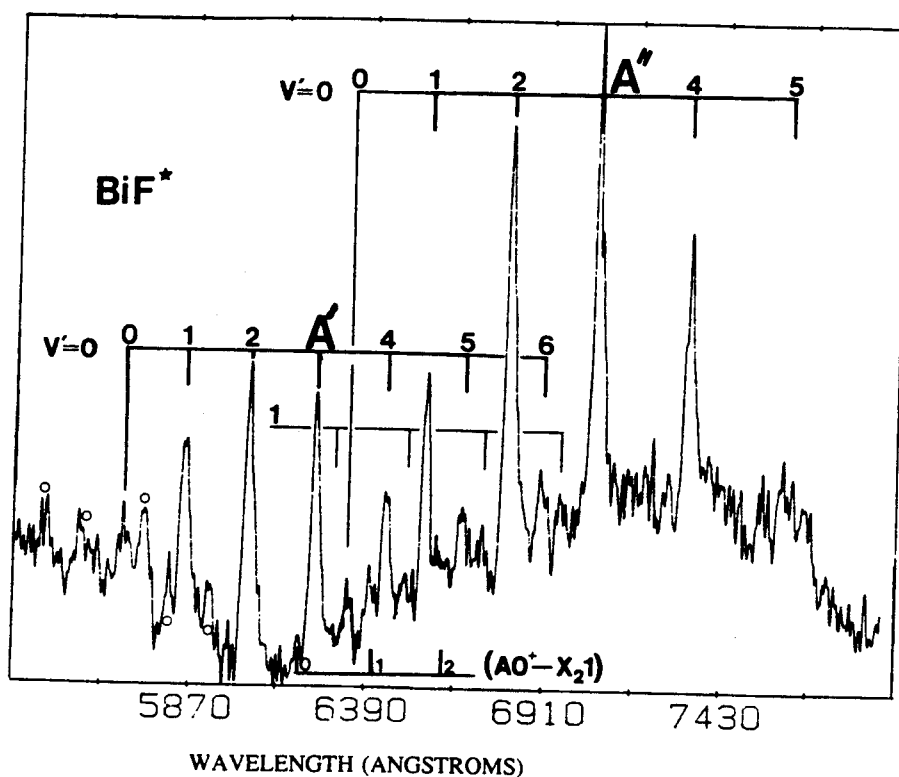


Figure 2: Chemiluminescent emission spectrum resulting from the reaction between helium entrained Bi vapor and F_2 under multiple collision conditions. The spectrum of the BiF "red system" bands is readily observed at 250 Pa pressure. The two progressions which increase relative to other features are marked A' and A'' in the figure. Also noted are features marked with open circles (o) to indicate bands which have been determined to arise from the $\text{AO}^+ \rightarrow \text{XO}^+$ transition and features associated with A' , $v' = 1$ levels. The stars indicate features which probably correspond to $v' \geq 1$ extrapolations of the $A' - \text{X}_2^+$ and $A'' - \text{X}_2^+$ systems. In the lower portion of the figure we indicate the locations of three weak features which appear to correlate with the expected location of "weak" AO^+ (II) - X_2^+ transitions from the $v' = 0$ level of AO^+ (II) to $v'' = 0, 1, 2$ for X_2^+ . These features may also correlate with $A' - \text{X}_2^+$, $v' = 3$ transitions. Spectral resolution is 0.2 nm.

$\nu_{00} \sim 17631 \text{ cm}^{-1}$ is believed to terminate in the recently observed BiF "1" state with $\nu_{00} \sim 6768 \text{ cm}^{-1}$ ($\text{X}_2^+ - \text{X}_1^+ \text{O}^+$).²⁶ The upper state, denoted A' (Fig. 2) with $T_0 \sim 24400 \text{ cm}^{-1}$, is believed also to be a "1" state based on limited high resolution data for at least two bands of the system. The correlation made here is in close accord with recent quantum chemical calculations¹⁸ which suggest that the "1" state lies $\sim 7200 \text{ cm}^{-1}$ above $v'' = 0$, XO^+ . The levels of the A' upper state appear to correlate precisely with several BO^+ perturber state levels. This A' perturber state,

Table I

Observed Band Heads and Assignments for the "red system" Bands of BiF
At Pressures in Excess of 250 Pa

A'' ¹ - X ₂ 1			
Bandhead location (cm ⁻¹) ^a	Intensity	Assignment	(cm ⁻¹)
17631 ± 10	(0.07)	(0,0)	542
17089 ± 10	(0.20)	(0,1)	533
16556 ± 10	(0.33)	(0,2)	526
16030 ± 10	(0.25)	(0,3)	519
15511 ± 10	(0.13)	(0,4)	511
15000 ± 10	(0.09)	(0,5)	(500)
14500 ± 10	[(0.08)]	(0,6)	

a. For an origin band at 17631 cm⁻¹ = 17902 - 543 (v''+1/2) + 2.5(v''+1/2).²

A'' - X ₂ 1			
Bandhead location (cm ⁻¹) ^b	Intensity	Assignment	(cm ⁻¹)
15784 ± 10	(0.06)	(0,0)	540
15244 ± 10	(0.19)	(0,1)	534
14710 ± 10	(0.35)	(0,2)	526
14184 ± 10	(0.27)	(0,3)	518
13666 ± 10	(0.19)	(0,4)	

b. For an origin band at 15784 cm⁻¹ = 16055 - 543(v''+1/2) + 2.5(v''+1/2).²

thought to lie less than 2000 cm⁻¹ above the AO⁺(II) state (Table II, Fig. 3), may play an important role with respect to energy disposal among the excited states of the BiF molecule. A second set of transitions with v₀₀ ~ 15244 or 15784 cm⁻¹ also appears to terminate in the "1" state¹⁰ suggesting a second upper state, denoted A'' with T₀ ~ 22012 or 22552 cm⁻¹, virtually isoergic with AO⁺(II). Alternatively, if the second transition emanates from the v' = 0 upper state level at T₀ ~ 24400 cm⁻¹ it might terminate in a lower state with T₀ ~ 8615 cm⁻¹.¹⁰ While this latter possibility cannot be eliminated without a high resolution analysis, as discussed elsewhere,¹⁰ we favor the former assignment. Searches were

Table II

Observed states and molecular constants for BiF.

State	$T_e(\text{cm}^{-1})$	$\omega_e(\text{cm}^{-1})$	$\omega_e x_e(\text{cm}^{-1})$	$B_e(\text{cm}^{-1})$
$XO^+{}^a$	0	512.81	2.35	0.22998
X_21^b	6753	543.0	2.40	0.23512
$AO^+(II)^a$	22957	383.8	3.5	0.20913
A''^c	22552	--	--	---
$A'^{c,d}$	24400	"397"	"3.1"	0.210
$BO^+{}^a$	26001	626.8	6.6	0.2309

^aLiterature data from Ref. 19.^bRounded values from Ref. 26. Data obtained in present study is consistent with $\nu_{00} \approx 6768 \text{ cm}^{-1}$, $\omega_e \approx 543 \text{ cm}^{-1}$, $\omega_e x_e \approx 2.5 \text{ cm}^{-1}$.^c T_0 this work.

$$d T_e = 24399 + (397/2) - (3.1/4) - (512.8/2) + (2.35/4) \approx 24341 \text{ cm}^{-1}.$$

also made for the allowed $AO^+ - X_21$ and $A' - X_1O^+$ transitions as well as features associated with the $A'' - X_1O^+$ band system. The $AO^+ - X_1O^+$ transition, from which some emission features involving $v' = 0$, AO^+ , may have been observed (Fig. 2) appears to be weak (small transition moment). Features associated with an $A'' - X_1O^+$ transition could not be clearly identified as they encompass the wavelength region dominated by intense $AO^+ - X_1O^+$ emission. These features might be observed by a lifetime separated technique. A definitive search for the $v' = 0$, $v'' = 0, 1, 2$, $A' - X_1O^+$ transitions, which again are weak, is still ongoing in our laboratory. As with the $A'' - X_1O^+$ system, transitions to the $v'' = 3$ or higher levels of the X_1O^+ state will underlie the intense $AO^+ - X_1O^+$ system. A summary of the BiF states and energy level patterns is given in Table II and Figure 3.

"Energetics of the Bismuth-Fluorine System"

The vapor in equilibrium with molten bismuth contains nearly equal concentrations of bismuth atoms and dimers.³³ The constituents of the bismuth vapor flux and F_2 react under near single collision conditions and at higher pressures in dilute helium to produce intense emission from the $AO^+(II)$ state. The population of the A state through the reaction of Bi atoms



with

$$\Delta E \sim D_0^0(\text{BiF}) - D_0^0(\text{F}_2) \quad (3)$$

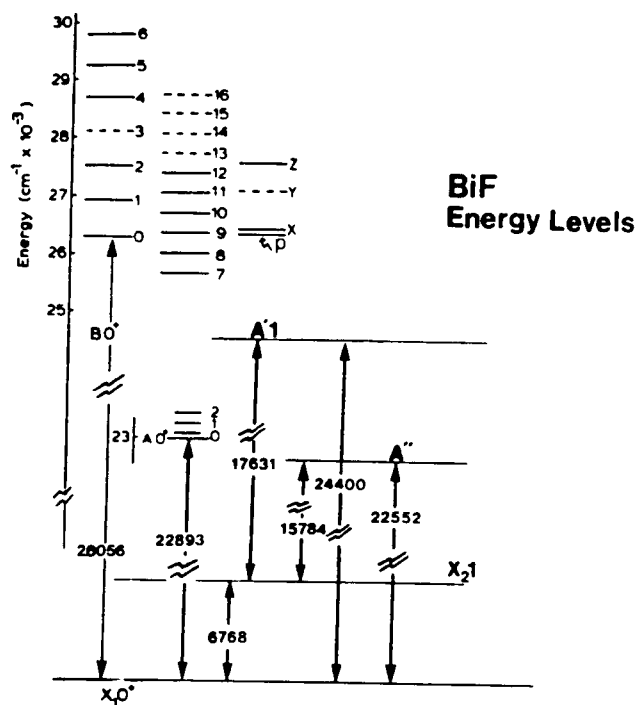


Figure 3: Approximate energy level diagram for the electronic states of the BiF molecule. The notation x,y,z,p is that for perturber levels identified in reference 19 and discussed in more detail in reference 10.

requires that the BiF dissociation energy be of order 4.45 eV to populate the observed $AO^+(II)$ levels. However, we must also consider that $\sim 50\%$ of the bismuth beam constituency is bismuth dimer and focus on the possible four center reaction of bismuth dimer and molecular fluorine viz.



which liberates considerably more energy with¹⁰

$$\Delta E \sim 2 D_0^0(BiF) - D_0^0(Bi_2) - D_0^0(F_2) . \quad (5)$$

The reaction (4) has the potential to distribute ~ 2.95 eV of excess energy to the reaction products provided that the BiF bond energy is 3.20 eV. If all of this energy is partitioned into electronic excitation of one of the BiF products, the $AO^+(II)$ state may be populated. The Bi_2 molecule vaporizing from its source (crucible) may possess a significant

vibrational excitation, as even more energy can be made available to the reaction (4). Thus, this reaction might lead to the observed chemiluminescence. If the BiF dissociation energy is substantially above 3.25 eV., the reaction (4) can pool sufficient energy to populate the BO^+ state and high vibrational levels of the $AO^+(II)$ state. Thus, it is difficult to readily ascribe the source of the observed chemiluminescent emission and to establish the dissociation energy of BiF using only the bismuth vapor - fluorine molecule combination.

In order to provide some clarification of the BiF bond energy, we therefore considered means to characterize the bismuth dimer-fluorine atom reaction



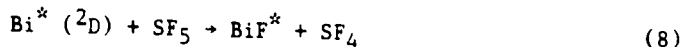
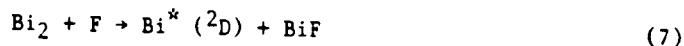
This reaction liberates from ~ 1.05 to 3.05 eV for a BiF bond energy ranging from 3.0 to 5.0 eV. If the reaction (2) produces a substantial A-X emission signal, this provides a strong indication that the BiF bond energy considerably exceeds 3 eV.

An electric discharge through SF_6 was used to generate fluorine atoms in order to study the Bi_2 -F reaction. In addition, we are currently using this source to study the product excited state metal fluoride emitters, formed in the reaction of copper, silver, and magnesium atoms and molecules. For the range of studies considered, we have deduced that the chemiluminescent emission products of the SF_6 based discharge emanate primarily from F atom reactions where the F atoms may possess significant translational energy. CuF chemiluminescence from both copper dimer (Cu_2)-F atom and metastable copper atom (2D) - SF_6 reactions has been observed. However, little or no evidence is obtained for the similarly exothermic reaction of ground state Cu 2S or the considerably more energetic metastable Cu 2D reaction with the weaker SF_4 -F bond to produce CuF excited state emitters. If we consider the bismuth vapor constituency, the reaction of ground state bismuth atoms with either SF_5 molecules produced in the discharge or the parent SF_6 is not sufficiently exothermic to yield chemiluminescence.¹⁰ The collisionally stabilized bismuth atom - fluorine atom three body radiative association can produce visible chemiluminescence if the BiF bond energy exceeds 2.85 eV. However the emission is expected to be comparatively weak.³⁴ The reaction (2) should produce strong A-X emission if the BiF bond energy exceeds 4.9 eV or if additional energy contributions from vibrationally excited bismuth dimers or translationally hot F atoms are available.

To produce the relaxed BiF spectra depicted in Figs. 1-4, the majority of the experiments considered herein have been carried out under multiple collision conditions (compare to Fig. 3 of Parson et al. in this volume). This is, however, a dilute gas environment as the total pressure is due primarily to an entraining (metal or metalloid) helium gas. This environment will facilitate relaxation but; in general, does not promote energy pooling reactions^{6,11} which lead to a significant increase in product excitation over that which would be observed under single collision conditions. Nevertheless, the reactant concentrations used in this experiment are considerably in excess of those characterizing a beam-gas environment, and we should consider two energy pooling processes.

A sequential mechanism that might yield chemiluminescence under

multiple collision conditions is



which, based on an $\text{SF}_4 - \text{F}$ bond strength of 2.3 eV,³⁵ could be sufficiently exothermic to populate the $\text{BiF } \text{BO}^+$ state. In considering this possibility, we have searched for the "heavy atom" $\text{Bi}^* ({}^2\text{D})$ emission, and can find no evidence for the presence of the $J = 3/2$ component of the

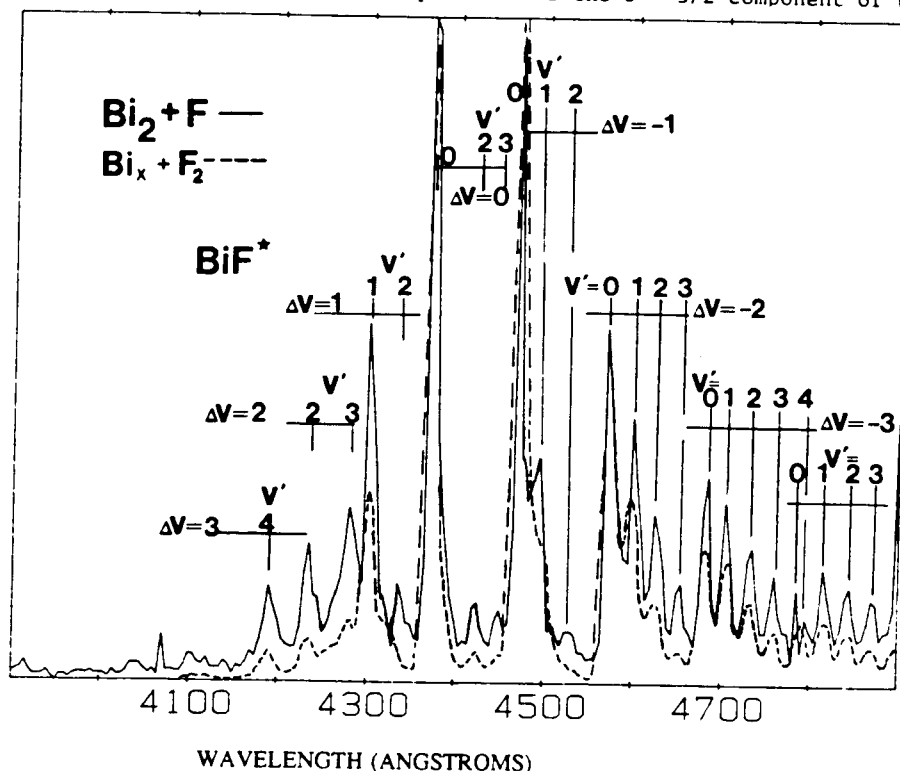


Figure 4: Comparison of chemiluminescent emission spectra resulting from the reactions between helium entrained bismuth vapor and atomic and molecular fluorine under multiple collision conditions. (a) The $\text{BiF } \text{AO}^+(\text{II}) - \text{X}_1\text{O}^+$ spectrum resulting from the $\text{Bi}_2 - \text{F}$ (generated via electric discharge through SF_6) reaction taken at a background pressure of 200 Pa (primarily helium). (b) The $\text{BiF } \text{AO}^+(\text{II}) - \text{X}_1\text{O}^+$ spectrum resulting from the interaction of bismuth vapor and molecular fluorine obtained at a background pressure of 200 Pa (primarily helium). Only sequence groupings are indicated in the figure. Band heads are denoted (v', v'') where v' denotes the vibrational quantum number of the upper state and v'' denotes the lower state vibrational quantum number. Resolution for spectrum (a) is 1 nm and that for spectrum (b) is 0.8 nm.

2D state. It has been possible to observe this $J = 3/2$ emission when discharging through the bismuth vapor constituency used in these experiments. Further, as we have noted, we find little or no evidence for SF_5 based chemiluminescent reactions in the other systems we have studied. While the bismuth dimer concentrations are certainly higher than those obtained in our copper based oxidation studies, the copper metastable concentrations parallel those expected from a combination of reactions (7) and (8). Therefore a dominant contribution from reactions (7) and (8) is difficult to rationalize.

One might also consider the energy pooling reactions of highly vibrationally excited ground state BiF products. While further studies will be needed to unequivocally rule out this possibility, the bulk of information obtained using the discharge configuration and comparisons with results obtained for the $Bi_x + F_2$ reactions would suggest little evidence for this process as the source of the BiF $AO^+(II) - XO^+$ emission depicted in Figure 4.

We attribute the BiF $AO^+(II) - XO^+$ emission spectrum in Fig. 4 to the $Bi_2 + F$ reaction (2). This spectrum demonstrates that the $Bi_2 + F$ reaction (2) is sufficiently exothermic to produce the BiF $AO^+(II)$ state with $v' = 1-4$. The observed spectrum for the A-X transition taken at a resolution of 1 nm can be compared to that for the $Bi_x + F_2$ system taken at a resolution of 0.8 nm. The A-X spectrum associated with the " $Bi_2 + F$ " reactive process displays a lower rotational excitation for the A-X features. Further, the "red system" bands of Table II appear considerably weaker if not completely absent.

While the observation of a strong BiF $AO^+(II) - X$ chemiluminescence associated with the $Bi_2 + F$ reaction can imply that the BiF bond energy exceeds 4.9 eV,¹⁰ we must also consider the internal energy associated with the reacting Bi_2 molecule and the relative translational energy of reactant interaction. We suggest that the F atoms produced in the discharge may have energies in excess of 0.5 eV. Therefore, the results obtained imply a bond energy close to 4.2 ± 0.2 eV. Further studies are in progress to refine this value.

The lower values of the BiF dissociation energy considered previously do not exceed 3.14 eV. However, these initial estimates of the bond energy were based on very limited Birge-Sponer extrapolations²⁰ and fits to ionic models.²¹ It is somewhat disconcerting that a simple ionic model calculation based on the known ground state bond distance of BiF¹⁹ gives $D_e \approx 3.05$ eV. The value of 3.14 eV suggested by Jones and McLean¹⁹ is based on the observation of features associated with the $AO^+(II)$ state that might signal the onset of predissociation. Yet, no direct evidence for a predissociation has been obtained. The value of the BiF dissociation energy which we determine, even with further refinements, suggests that a bond energy in the 3 eV range is highly unlikely. We thus conclude that the BiF bond energy should be revised to a value exceeding 4 eV.

"Group 15 Halide Bond Energies"

The results we have obtained for the BiF molecule certainly indicate, as suggested by Ross et al.¹⁷ that the bond energy of this fluoride is significantly greater than previously envisioned. However, this study also focuses attention on the paucity of information con-

cerning the dissociation energies of the Group 15 halides, PX - BiX.^{20,36-49} The situation is outlined in Table III.

It is striking that virtually no information on bond strength is available on the arsenic halides. The value quoted for the AsF bond strength is based on a theoretical calculation³⁸ supported by limited experimental data. The situation for the phosphorous halides is not much improved, the data for PF being based in large part on a linear Birge-Sponer extrapolation³⁶ showing slight positive curvature. The antimony halides SbBr,³⁹ SbCl,⁴⁰ and SbF,^{41,52} especially the fluoride, are particularly intriguing. They demonstrate a clear trend, albeit with large energy spread, which would suggest that the fluoride bond strength exceeds 4 eV. The SbF ground state may be complex²⁰ as the dissociation energies obtained from several Birge Sponer extrapolations range from 4.2 to 5.7 eV. In view of the overall trends indicated in Table III, it seems difficult to rationalize the suggested value of 2.65 ± 0.2 eV²⁰ for the BiF dissociation energy. It would also appear that the bond strengths of the fluorides are all in excess of 4 eV.

Table III

Evaluated Dissociation Energies for Group 15 Halides

PX - BiX

Element	Dissociation Energy for MX (X = F, Cl, Br, I) in Electron Volts (References in Parenthesis)			
	F	Cl	Br	I
P	$4.5 \pm 1^a(35), 4.55 \pm 0.4$	---	---	---
As	$4.2^b(37)$	---	---	---
Sb	$4.5 \pm 1^c(40, 41)$	$3.7 \pm 0.5^a(39)$	$3.2 \pm 0.6^a, d(38)$	---
Bi	$2.65 \pm 0.3^d(46-48)^a, > 4^e$ $3.14(19)$	$3.13 \pm 0.1^f(44, 45)$	$2.74 \pm 0.01^a, d(42, 43)$	$2.5 \pm 1^a, d(42)$

a. Linear Birge Sponer Extrapolation.

b. Theoretical calculation.

c. L. B. S. X.'s give values ranging from 4.2 to 5.7 - suggested by 20.

d. Suggested by 20.

e. References 10, 17.

f. Mass spectrometry.

The situation might be remedied for the heavier halides (AsX, SbX, BiX) using chemiluminescent techniques. If the bond strengths of the heavier Group 15 fluorides range to the higher values suggested by the literature and the current results on BiF are indicative, it should be possible to study these species. We are currently beginning a study of antimony fluoride.

A CONTINUOUS VISIBLE CHEMICAL LASER AMPLIFIER FROM A METAL CLUSTER OXIDATION REACTION

We have previously used the supersonic expansion of pure sodium vapor to study the photodissociation of the sodium trimer.⁵⁰ This study was facilitated because alkali metal based species have comparatively

high transition probabilities, those for the alkali metal atom or dimer electronic states being among the largest recorded.⁵¹ In part, because of the ready detectability of the alkali atom and dimer electronic transitions, we initiated studies of what were felt to be the simplest metal cluster oxidation reactions, the alkali trimer-halogen atom reactions, producing reaction products with well defined and characterized electronic transitions. In retrospect, the study of alkali dimer and trimer - halogen atom reactive encounters has demonstrated several surprises.

The high cross section, highly exothermic $\text{Na}_3 - \text{X}$ (Cl, Br, I) reactions form Na_2^* in several of the sodium dimer excited electronic states⁵² indicated schematically in Figure 5. The energetics of the reactive processes of interest are indicated in the figure. The $\text{Na}_3\text{-Cl}$ and $\text{Na}_3\text{-Br}$ reactions are sufficiently exothermic to readily populate the $\text{A } ^1\Sigma_u^+$, $\text{B } ^1\Pi_u$, $\text{C } ^1\Sigma_u^+$ and $\text{C } ^1\Pi_u$ states of sodium dimer. The available energy results from the formation of a moderately strong sodium halide bond and the rupture of a weak sodium trimer bond. The $\text{Na}_3\text{-I}$ reaction is

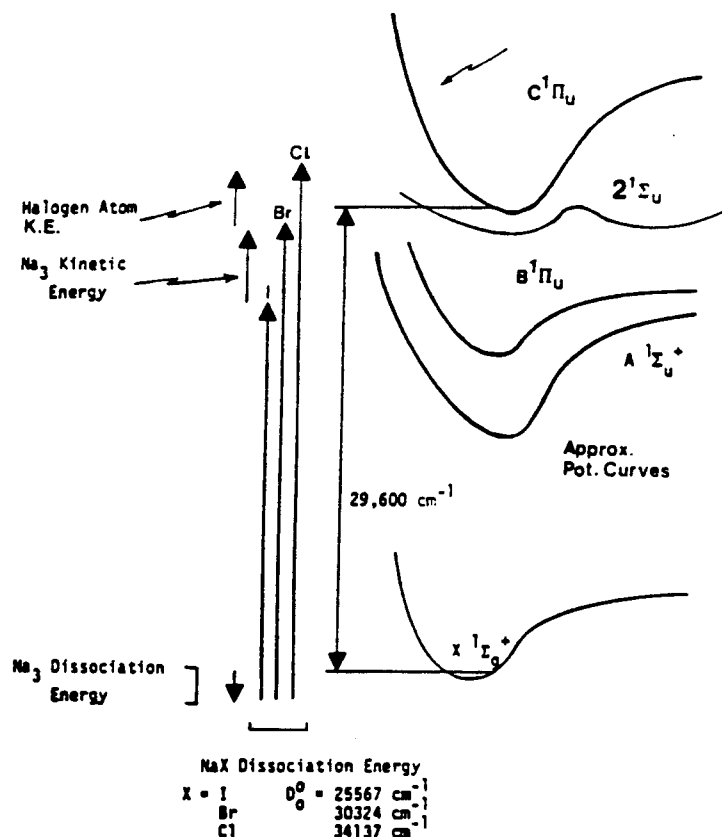
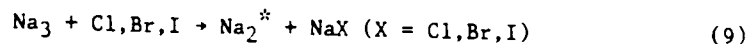


Figure 5: Energetics associated with the formation of Na_2 produced by the $\text{Na}_3 - \text{X}$ (Cl, Br, I) chemiluminescent reaction. Potential curves are drawn approximately.

much less exothermic. However, the contribution of the Na_3 kinetic energy and the reaction of halogen atoms, generated from a 1500 K source, in the high energy tail of their kinetic energy distribution allows the population of a few vibrational levels in the Na_2 $C^1\Pi_u$ state and several levels of the double minimum C' state. The optical signatures for the processes



encompass emission from a limited number of Na_2 band systems including the A, B, C, and C' states. Surprisingly, the observed emission is characterized by sharp, well defined, emission regions⁵² (Figures 6,7) superimposed on a much weaker but perceptible Na_2^* dominated background. As Fig. 7 demonstrates, through comparison with the best fit calculated sodium dimer spectrum, these sharp emission features are not readily explained by invoking a purely fluorescent process involving sodium dimer.⁵²

The sharp nature of several of the B-X, C-X, and C' -X Na_2 emission features (Fig. 6), their near exponential growth with Na_3 concentration relative to the background Na_2 fluorescence, and their correlation in certain regions to the emission characteristic of optically pumped Na_2 laser systems (ex: 528.2 nm (v', v'') = (6,14)B-X) suggested that stimulated emission, associated with certain of the Na_2 emission products might have been observed. Laser gain measurements were subsequently carried out to assess this possibility.

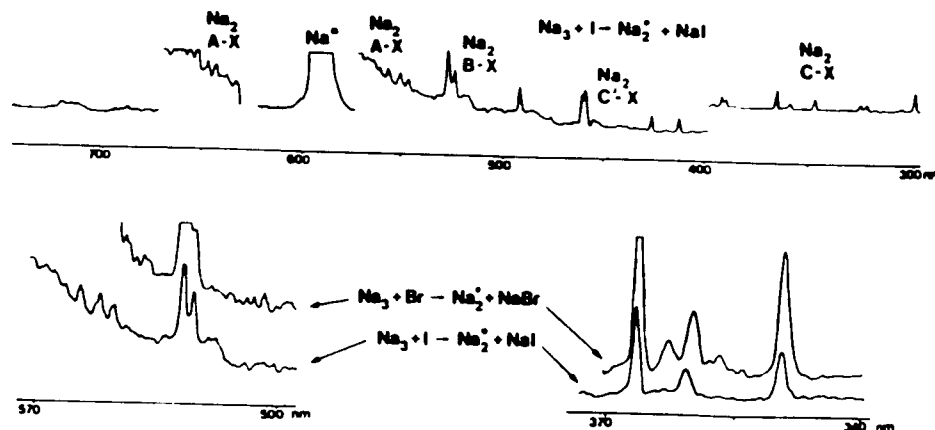


Figure 6: Chemiluminescent emission from the $\text{Na}_3 + \text{Br}$ and $\text{Na}_3 + \text{I}$ reactions forming excited states of Na_2 , whose optical signature dominates the observed emission, and the sodium halide. Sharp emission features superimposed on a broad background are apparent including those at ~ 527 , ~ 492 , ~ 460.5 , ~ 436 , and ~ 426 nm. Spectral resolution is ~ 0.6 nm. See text for discussion.

In order to perform these studies, a unique source configuration discussed in detail elsewhere^{11,52} was developed which allowed the supersonic expansion of pure sodium vapor to create a Na_3 concentration not previously attained in a reaction-amplification zone. In these

studies, pure sodium was expanded to produce a supersonic flow which passed into an LN_2 baffled reaction chamber. Here the supersonically expanding Na_x beam was met by an intersecting flow of halogen atoms. In order to operate above threshold, the expenditure of sodium was carried out in a very short time frame (~ 1200 vs. $3600 - 10,000$ seconds for a typical chemiluminescent experiment - Fig. 6) to produce well in excess of $10^{13}/\text{cc}$ trimer molecules in the reaction zone.⁵⁴ The concentration produced is between 10 and 500 times the maximum concentration for the fluorescence experiments ($[\text{Na}_3] \sim 3 \times 10^{12}/\text{cc}$) depicted in Figures 6 and

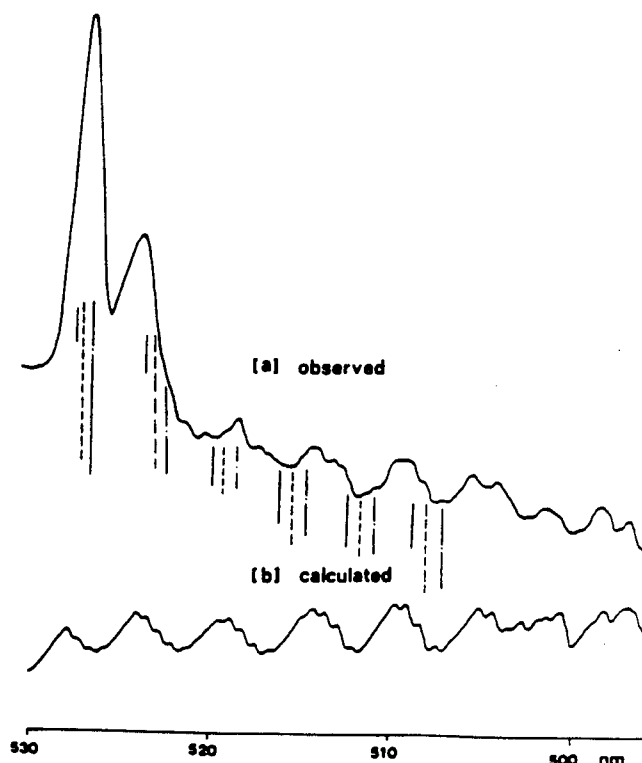


Figure 7: Comparison of (a) observed and (b) calculated emission spectra for the Na_2 B-X emission system. The experimental spectrum corresponds to chemiluminescence from the Na_3 -Br reaction. The calculated spectrum, which was obtained for a rotational temperature, $T_{\text{Rot}} \sim 1000\text{K}$, represents an estimate of effective rotational temperatures for Na_2 product formation under near single collision conditions and therefore not at equilibrium. Relative vibrational populations input for Na_2 B-X, $v' = 0-6$ were in the ratio 1.00:1.17:1.33:1.50:1.58:1.67:1.54. The location of contributions from vibrational levels $v' = 6$ (—), 5(---), and 4(-.-) of the Na_2 B state in transition to vibrational levels $v'' = 14-9$, $v'' = 13-8$, and $v'' = 12-7$ of the Na_2 ground state are indicated.

7. These figures are based on (1) an increased flux from the oven, (2) an increased beam directionality, and (3) an increased percentage of trimer in the beam.⁵² In all of the experiments, halogen atoms were produced by transiting halogen molecules through a needle valve assembly into a high temperature carbon furnace.⁵⁴ This device produces halogen atoms, with > 95% efficiency, which exit the furnace into the reaction zone initiating the trimer-halogen atom chemical reaction. The halogen flow is adjusted to optimize gain.^{52(b)}

Using argon ion pumped dye lasers to study the $\text{Na}_3 + \text{Br}$ reaction, we have scanned the entire wavelength region from 420 to 600 nm (Figure 6) at 0.5 cm^{-1} resolution (FWHM).^{11,52} The regions around 527 nm (Fig. 7) have been scanned at 0.007 cm^{-1} resolution using a passively locked ring dye laser.⁵² Laser gain and hence amplification is found to be characteristic of several of the sharper emission features apparent in the spectra depicted in Figure 7 suggesting that these features correspond to a stimulated emission process and to the establishment of a population inversion.^{11,52} The ring dye laser studies suggest that the strong feature at 527 nm (Fig. 7) is associated with stimulated emission from a maximum of four to five unresolved rotational levels. With an improved scanning capability, it should be possible to assign the monitored features to rotational levels associated with specific P, Q, and R branch transitions involving rotational levels $J' \approx 35 \pm 5$ in the B^1_u state.

Optical gain through stimulated emission measured at 0.5 cm^{-1} resolution in the regions 527 nm (1% gain), 492 nm (0.3% gain) and 460.5 nm (0.8% gain), correlates precisely with the reactive process and the relative intensities of those sharp features observed while monitoring the light emitted from the $\text{Na}_3\text{-Br}$ and $\text{Na}_3\text{-I}$ reactions (Figs. 6,7). The high resolution ring dye laser scans in the 527 nm region indicate that the gain for the system is close to 3.8% for an individual rovibronic transition. At 459.8 nm, a gain of 2.3% has been measured for an individual rovibronic transition. These results demonstrate the continuous amplifying medium for a visible chemical laser in at least three wavelength regions.⁵² A loss of the gain condition is readily detected as the trimer concentration decreases.^{11,52} The gain observed in these systems is strongly dependent on both the Na_3 and halogen atom concentration. As the probe laser power was changed, the amplification signal was found to vary linearly with laser power, indicating that the measurements were taken in the small signal gain regime.

In order to further verify that these gain observations were not artifacts which could be observed at any wavelength including those corresponding to an intense spectral feature, the gain experiments were repeated at several wavelengths including that for the sodium D-line at 588.9 nm. No gain was observed at any other wavelength in the 420-600 nm region. At the Na D-line wavelength the signal was seen to decrease significantly, indicating considerable scattering or absorption of the probe laser photons.^{11,52} Thus the observation of gain is localized to select wavelength regions.

Because of the low Na_3 ionization potential and the high halogen electron affinities,⁵⁵ the Na_3 -halogen atom reactions are expected to proceed via an electron jump mechanism with extremely high cross sections,⁵⁶ producing substantial Na_2 excited state populations. The created population inversions monitored thusfar are thought to be sustained by (1) the large number of free halogen atoms reacting with

Na_2 molecules in those ground state levels on which the transitions emanating from the Na_2 excited states terminate, removing these levels, and (2) collisional relaxation of ground state sodium molecules.⁵² The cross section for reaction of vibrationally excited ground state Na_2 is expected to be substantial relative to that corresponding to collision induced vibrational deactivation of the Na_2 manifold. Extremely efficient reactions thus greatly aid the rapid depletion of the lower state levels in this system allowing one to sustain a continuous population inversion.

A major effort in our laboratory now focuses on the conversion of these Na_2 laser amplifiers and the development of laser oscillators at wavelengths in the vicinity of 527 and 460 nm. We also are concerned with the extension of these Na_3 based studies further into the ultraviolet, with the study of additional alkali trimer halogenation reactions,⁵² and with the modeling of these reactive encounters. The current results certainly indicate an unusual and unexpected oxidation behavior which may be manifest in a number of metal cluster reactions. This suggests that the study of these processes will aid the development of new insights in chemical reactivity.

OXIDATION IN MORE COMPLEX METAL AND METALLOID CLUSTER SYSTEMS

We have developed entrainment flow devices^{11,14} which facilitate the generation of a substantial and usable continuous flux of small metal clusters. Using these devices, it has been possible to record the optical signatures of the reaction products associated with the oxidation of small boron ($\text{B}_x + \text{NO}_2, \text{N}_2\text{O}$)^{6(a)-(c)}, copper ($\text{Cu}_x + \text{O}_3, \text{Cl}_2, \text{Cl}, \text{F}_2$)^{6(a),57,58}, silver ($\text{Ag}_x + \text{O}_3, \text{Cl}_2$)^{6(a),(d),58}, manganese ($\text{Mn}_x + \text{O}_3$)^{6(b),(e)}, chromium ($\text{Cr}_x + \text{O}_3, \text{F}_2$)^{7,59} and magnesium ($\text{Mg}_x + \text{F}, \text{Cl}$)⁶⁰ clusters. With the development of a sufficient metal cluster flow, we have obtained the first quantal information on the energy levels of several asymmetric metal clustered oxides, M_nO_y ($n \geq 2$) and preliminary data on the copper, chromium, and magnesium clustered chlorides and fluorides. Thusfar, this work has led to three general observations concerning cluster reactions.

(1) Cluster oxidations, through a multicentered reaction capability (excluding fluorine and chlorine atom rxns.), often yield product molecules in higher energy states than have been accessible to the corresponding atomic reactions.

(2) The products of metal cluster reactions encompass metal rich molecules. In many cases, metal-metal bonds are present and behave with an unusual fluxionality in these product molecules.

(3) Kinetics rather than thermodynamics most often controls the nature of the initially formed products of metal cluster oxidation.

We exemplify these trends with a focus on the oxidation of small silver and copper clusters.

"Silver Cluster Oxidation"

The oxidation of a moderately agglomerated silver flow with ozone under multiple collision conditions produces emission from the $A^2\Pi$ (400-420 nm) and $B^2\Pi$ (320-370 nm) states of AgO .^{6,7} Neither the reaction of silver atoms nor the reaction of silver dimers are sufficiently energetic to populate these AgO product states; the emission must result from

the oxidation of Ag_3 or larger silver clusters.¹¹ At higher silver fluxes, one finds that the AgO emission is quenched and the observed spectrum is characterized by a combination of Ag_xO ($x \geq 2$) and Ag_2 band systems. The reactions or energy transfer producing the Ag_2 emission have not been clearly established. However, multi-centered processes represent the most likely source of this product emission.^{6,7,11}

The characterization of the silver clustered oxides can provide insights into molecular structure, bonding, and atomic mobility in the Ag_xO species as an aid to the modeling of their behavior in the bulk metal clustered-oxidized surface. This may contribute to our understanding of the manner in which an oxidized silver surface acts to catalyze⁶¹ the epoxidation of ethene or the dehydrogenation of methanol or influences the photographic process.⁶² A contribution to the modeling effort can be gained from the study of Ag_2O and from the extension of these Ag_2O studies to the higher metal clustered oxides Ag_xO ($x \geq 3$).

In order to study the oxidation of small silver clusters using an entrainment flow device^{5(a),11,14} silver metal is heated in a specially designed graphite crucible to temperatures between 1400 and 1700K. The high silver flux emanating from the crucible ($\geq 10^{18}/\text{cm}^2\text{-sec}$) is entrained in a flow of rare gas (He, Ar) at room temperature. Agglomeration in the system occurs both as a result of (1) the high metal flux and (2) the cooling of the silver vapor by the room temperature entrainment gas. At a suitable point above the furnace assembly, ozone is introduced into the flow to produce the chemiluminescent flame corresponding in large part to an optical signature for the silver clustered oxides. The reactants and products are subsequently fed into a small quadrupole mass spectrometer.^{11,14} Thus, in these studies it is possible to combine the energetic constraints of the chemiluminescent process and distinct optical signatures, with limited mass spectrometry, for product identification.

The $\text{Ag}_x + \text{O}_3$ reaction produces a product molecule emitter whose spectrum extends from 506 to 680 nm (Fig. 8) and which has tentatively been assigned to Ag_2O . The chemiluminescent spectrum, which is also constrained by the energetics of multicentered processes,^{5(a),11,14} between 500 and 700 nm contains two distinct emission band regions which have been assigned as the "A-X" and "B-X" band systems of Ag_2O . The A-X transition which onsets at ~ 630 nm is well fit by the expression

$$\nu(\text{cm}^{-1}) = 15670 - 165 \nu_2'' + 0.4 (\nu_2'')^2$$

The B-X transition which onsets at 506 nm is well fit by the expression

$$\nu_{\nu_1'', \nu_2'', \nu_3''}(\text{cm}^{-1})$$

$$\nu_{\nu_1'', \nu_2'', \nu_3''}(\text{cm}^{-1}) =$$

$$19766 - 442\nu_1'' - 165\nu_2'' - 256\nu_3'' + 6(\nu_1'')^2 + 6\nu_1''\nu_3'' + 25\nu_1''\nu_2''.$$

Three vibrational frequencies (442 cm^{-1} , 165 cm^{-1} , and 256 cm^{-1}) established for the molecular emitter suggest that it contains a Ag-Ag bond. The 440 cm^{-1} frequency is readily assigned to the Ag-O stretch. Since the geometry of the molecular emitter has not been established experimentally, there is uncertainty in the assignment of the two low frequency modes. Either the 165 cm^{-1} or the 256 cm^{-1} frequency might reasonably be assigned as a silver-silver stretch. The spectral features

which onset at ~ 630 nm display only a single vibrational frequency separation whereas the shorter wavelength band system displays all three frequencies. This behavior would suggest that both a substantial bond angle and bond length change accompany the transition associated with the higher energy band system. In contrast, the lone ~ 165 cm^{-1} separation associated with the 630 nm system is indicative of a change in bond angle

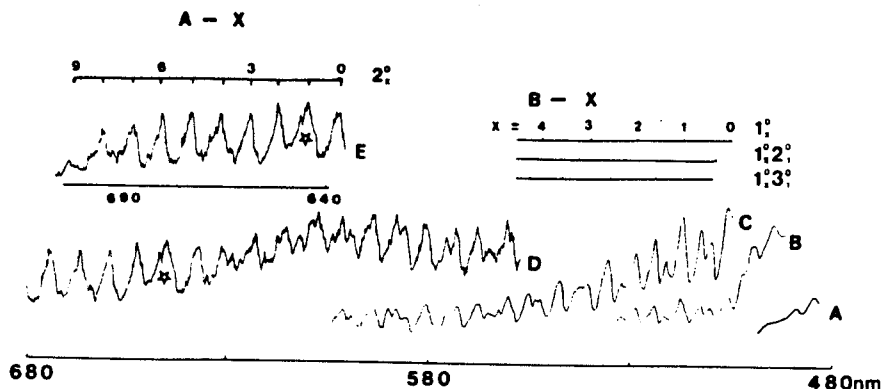


Figure 8: Chemiluminescent spectrum for the reaction of small silver clusters entrained in argon at a total pressure of 400 mTorr. The spectrum was taken with an EMI 9808 phototube at a resolution of 0.8nm. Reaction is with ozone. Scan A depicts the long-wavelength end of the ~ 440 nm system. Scan B depicts the relative intensities of the tail of the 440-nm system and the 500-nm system correlated with Ag_2O . Scan C depicts the 500-nm band system transition region. The assignments for the first 12 bands are noted. This system displays the Ag-O stretching, Ag-Ag stretching, and AgAgO bending frequencies ($\nu_1 \approx 442$ (denoted 1 in the figure), $\nu_2 = 165$ cm^{-1} (denoted 2 in the figure), and $\nu_3 \approx 256$ ($\nu_{\text{Ag-Ag}}$ - denoted 3 in the figure)). Scan D depicts the continuation of the 500-nm system which becomes more complex with emission to higher vibrational quantum levels. This system blends into the 630-nm system (E) correlated also with Ag_2O . Scan E depicts the 630-nm band system (correlated with Ag_2O) which may extend to shorter wavelength blending with the 500-nm system. This system is associated with a long progression in the Ag_2O bending mode (~ 165 cm^{-1} - denoted 2 in the figure).

or bond length but not both, the later being unlikely because it should signal the observation of two stretch frequencies. For this reason the 165 cm^{-1} frequency is assigned to the bending mode of the Ag_2O molecule.

The assignment of the A-X and B-X band systems is consistent with the emission characteristics of a number of similar polyatomic systems.⁶³ The frequency expression for the B-X system displays large anharmonicity terms ($25\nu_1^2/\nu_2^2$). This is consistent with the rather floppy nature of metal clusters⁶⁴ and their compounds. The observed frequencies are consistent with a nonlinear Ag-Ag-O structure, with emission from the asymmetric cluster oxides characterizing these kinetically controlled oxidation experiments in contrast to the thermodynamically more stable

symmetric species.

The assignment of the spectral features in Figure 8 to the asymmetric Ag_2O molecule is further substantiated by local density functional calculations carried out on the symmetrical Cu_2O , Cu_2S , Ag_2O , and Ag_2S molecules.⁶⁵ These calculations suggest the vibrational frequencies catalogued in Table IV. The symmetric stretch frequencies

Table IV

Calculated Vibrational Frequencies^a (cm^{-1}) for Cu_2O , Ag_2O , Cu_2S , Ag_2S

Mode	Cu_2O	Ag_2O	Cu_2S	Ag_2S
stretch s	679	514	465	364
stretch a	583	458	353	278
bend	163	89	143	70

a. At the Local Density Functional level of approximation.

should be ~ 10% higher than those observed experimentally⁶⁶ (see also discussion of CuOCu following) and thus we predict that the spectrum for symmetric Ag_2O should be characterized by a symmetric stretch frequency approaching 450 cm^{-1} and a bending mode which does not exceed 85 cm^{-1} . If anharmonic coupling plays an important role in the symmetric isomer, it may be possible to observe features associated with an ~ 400 cm^{-1} asymmetric stretch. Clearly, these characteristics do not correlate well with the spectrum considered in the present discussion.

In some preliminary experiments the mass spectrometric sampling capability alluded to previously has been employed to aid spectral assignment. The improvement of this capability will be an important aspect of future experiments especially at higher silver agglomeration. At these higher silver fluxes or under conditions in which the entraining helium and argon are cooled so as to approach dry ice (196 K) or liquid nitrogen (77 K) temperature, further spectral features emerge at 680 nm (Fig. 9). We have now tentatively observed at least two further systems possibly associated with the higher silver clustered oxides Ag_xO ($x > 2$). These are the subject of further study in our laboratory.

"Copper Cluster Oxidation"

The reaction exothermicity for the process



is $1.76 \pm 0.05 \text{ eV}$. This process is energetic enough to populate the $v' = 2$ level of the $\text{CuO } \delta^2\Sigma^+$ state. The chemiluminescent spectrum observed for reaction (9) under near single collision conditions is in excellent agreement with the available energy for the atomic oxidation process.

If the energy liberated in a multicentered copper cluster reaction is largely collected in one of the reaction product molecules, a considerable enhancement of the available energy to populate product

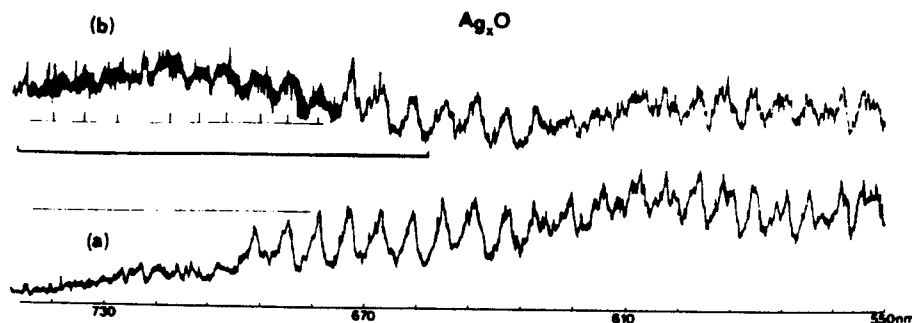
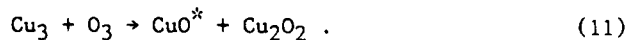


Figure 9: Chemiluminescent spectra for the reaction of small silver clusters entrained in dry ice cooled argon at a total pressure of 400 m Torr. The spectrum was taken with an EMI 9808 phototube at a resolution of 0.7nm. Reaction is with ozone. Observed spectral emission in the region 550-730 nm believed to correlate with the metal cluster oxides Ag_xO_y ($x \geq 2$). The upper spectrum is obtained at considerably higher silver flux and appears to demonstrate the onset of a new band system (boldfaced) at $\lambda \geq 660\text{nm}$.

molecule excited electronic states can be obtained. The oxidation of copper clusters produced in an entrained copper flow (copper flux $\geq 10^{18} \text{ cm}^{-2}\text{-sec}$) with ozone under multiple collision conditions produces emission (Figure 10) which originates from the $\delta^2\Sigma^+$, $D^2\Delta$, $C^2\Pi$, $B^2\Delta$, $A'^2\Sigma^+$, and $A''^2\Sigma^+$ states of CuO . The population of these states requires up to 1 eV more energy than is available from the copper atom reaction. This increased exothermicity could be provided by the reaction of vibrationally hot copper dimer or, equally likely with moderate to high metal agglomeration, by the reaction of ground state copper trimer via the process



Under a variety of experimental conditions, the first emission spectra for both the asymmetric copper clustered oxides and the symmetric CuOCu molecule have now been successfully generated.⁵⁷ A selection of the data obtained for these copper oxides is indicated in Figures 10 and 11 where emission spectra for both symmetric and asymmetric Cu_2O as well as the higher order copper clustered Cu_xO ($x \geq 2$) complexes¹¹ are displayed.

Significant differences between the electronic spectra and energy levels for the CuCuO and CuOCu molecules are evidenced not only by the distinctly different location of emission features but also by the appearance, extent, and intensity of these features. The spectral features for the CuCuO molecule (Fig. 10) at $\sim 600 \text{ nm}$ appear to result from a short progression in a 132 cm^{-1} bending mode whereas the observed structured emission spectra for the $\text{CuOCu } ^1B_2 - ^1A_1$ transition appear to be dominated by a moderate progressions in the ground ($\sim 640 \text{ cm}^{-1}$) and excited ($\sim 409 \text{ cm}^{-1}$) state symmetric stretching modes. The spectral features recorded for CuOCu bear a strong correlation with recent quantum chemical calculations by Bauschlicher, Langhoff, and Siegbahn⁶⁷ (Table V). These authors have estimated bond lengths, bond angles, transition

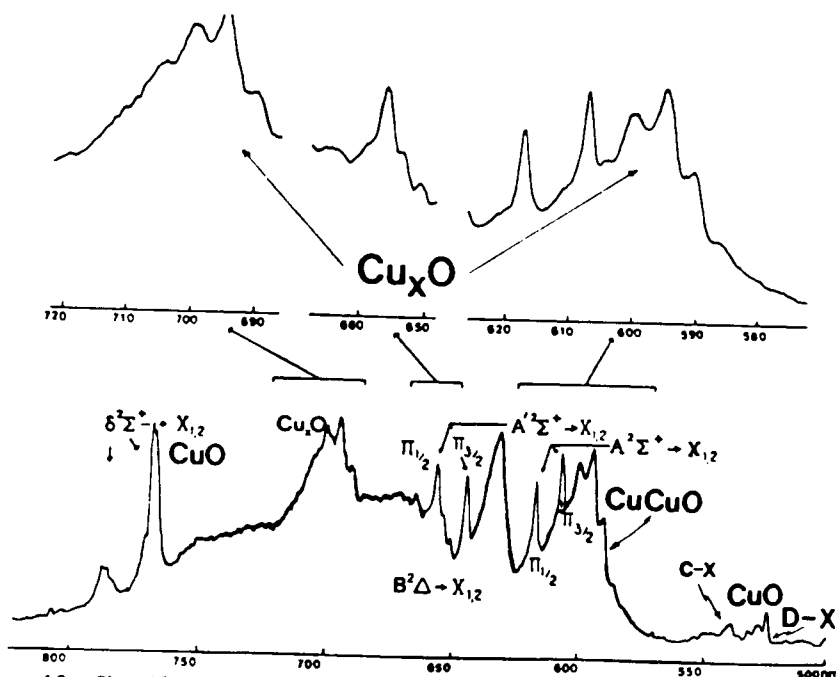


Figure 10: Chemiluminescent spectrum resulting from the multiple collision ($P_{\text{Tot}} \sim 600$ mTorr) oxidation of small copper molecules and clusters. Clusters are formed in a moderate copper agglomeration mode and oxidized with ozone. The emission spectrum, taken with an EMI 9808 phototube at a resolution of 0.8 nm is dominated by CuO, and Cu_xO ($x \geq 2$) emission features where the polyatomic emitters correspond to the copper clustered oxides.

Table V

Calculated Properties of Ground and Excited States of Symmetrical Cu_2O

STATE	$r(\text{Cu-O})$ (Angstroms)	BOND ANGLE (Degrees)	T_e (APPROX.) (cm^{-1})
$1A_1$ (Ground)	1.793	105.7	0
$1B_1$ (0.3) ^a	1.964	81.4	14221
$1A_1$ (1.6) ^a	1.921	180.0	17181
$1B_2$ (1.0) ^a	1.956	77.3	20336
$1A_2$ (0.1) ^a	1.942	123.3	22133

^aTransition Moment in Atomic Units.

moments, and electronic state locations for the ground and several excited electronic states of the CuOCu molecule. The calculations are currently undergoing further refinement, especially in correlation with the data derived from the emission spectra depicted in Figure 11. However, the relative intensities of the CuOCu 1A_1 and 1B_2 transitions depicted in Figure 11 are in very good agreement with the calculated relative transition moments. Further, the change in bond angle and bond length predicted for the ${}^1A_1 - {}^1A_1$ transition ($\Delta\theta$ - a substantial 75°) is commensurate with a long virtually unresolved progression dominated by

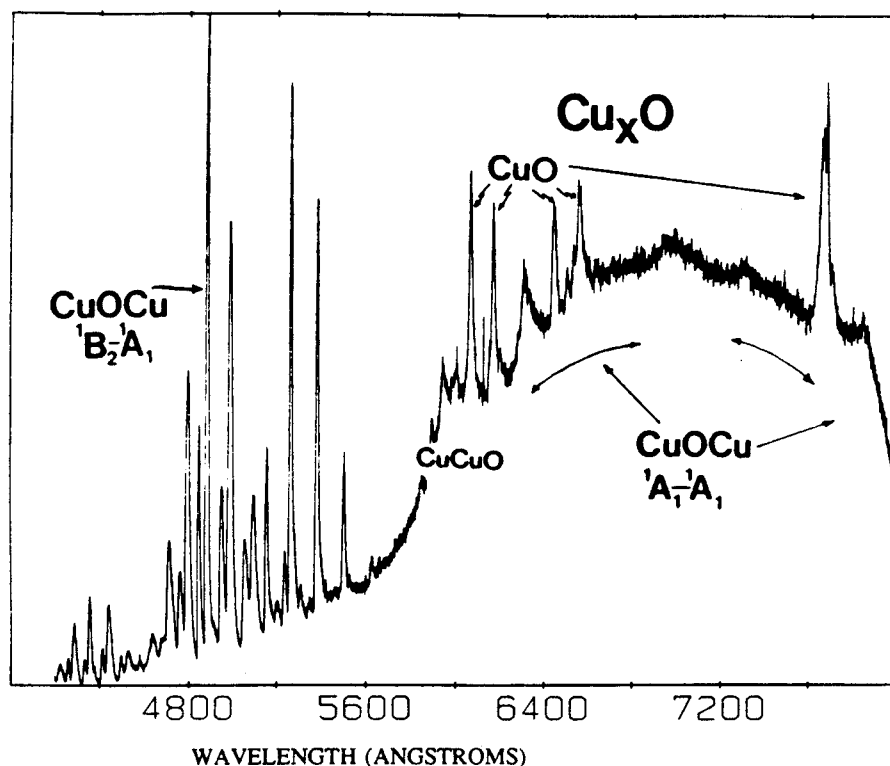


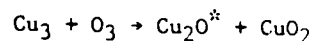
Figure 11: Chemiluminescent spectrum taken under multiple collision conditions in a non-effusive agglomeration mode dominated by emission from the symmetric CuOCu molecule but also showing emission corresponding to CuO and to the asymmetric CuCuO molecule. The spectrum was taken with an EMI 9808 phototube at a resolution of 0.5 nm.

the CuOCu bending mode, much like that characterizing a similar transition in the water molecule at the fringes of the vacuum ultraviolet region.⁶³ For the ${}^1B_2 - {}^1A_1$ transition, the experimental data indicate a ground state symmetric stretch frequency of $\sim 640 \text{ cm}^{-1}$ ($\nu'' = 640 \pm 10 \text{ cm}^{-1}$) and an excited state symmetric stretch frequency of $409 \pm 10 \text{ cm}^{-1}$.

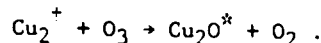
The spectroscopy of the copper cluster oxides is now the focus of considerable further study. This effort includes laser induced fluorescence at moderate and higher resolution to facilitate the

evaluation of further vibrational mode structure and the determination of both the CuCuO and CuOCu ground state geometries.

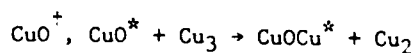
Using the constraints on the minimum reaction exothermicity necessary to facilitate a chemiluminescent reactive process and limited mass spectrometric data,¹¹ one can suggest the following most likely mechanisms for formation of the copper oxide emitters which give rise to the spectra depicted in Figs. 10 and 11. In the moderate to high agglomeration mode,¹¹ the CuCuO* isomer whose emission is located near 600 nm is most likely formed via the reaction



while lower-lying states may be formed through reaction of copper dimer

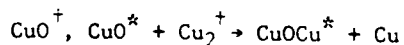


Here, the asterisks indicate electronic and the dagger indicates vibrational excitation. The higher-lying states of CuOCu, may be formed via the reactions of vibrationally excited or possibly electronically excited CuO



(¹B₂, (¹A₂) Table V)

In the moderate agglomeration mode the CuOCu states may be formed through the process



(¹A₁, ¹B₁)

The experimental evidence which supports these tentative mechanisms will await further confirmation.

These studies of the copper cluster oxides are now providing the impetus for the quantum chemical generation of potential functions for the ground and excited states of the isomers of these molecules. Potential functions now generated for CuOCu and CuCuO indicate that while these molecules are quite bent they are also characterized by very flat bending mode potentials. It appears that there is a high probability for interconversion of these two isomers. The generated potential functions can be gauged by their fit of experimental vibrational frequencies generated in our initial experimental studies. This study may also bear some relevance to the assessment of the role which the copper oxide lattice plays in high T_c superconductors.⁶⁸ Here the movement of the copper and oxygen atoms as dictated by the Cu_xO potential function, especially the out-of-plane bending of these species, may play a role in the high T_c mechanism.

"Extensions of the Metal Cluster Oxidation Concept"

Our studies of the copper and silver cluster oxides as they pertain to the modeling of bulk systems are being extended to additional metal and metalloid species. The source which we have developed to study the Bi₂ + F reactions is now being used to investigate the fluorine atom

oxidation of copper⁵⁸ and magnesium⁶⁰ clusters. The fluorine and chlorine atom oxidations of small copper molecules are of particular interest as we consider the analogy between the single valence *s* electron copper and sodium oxidation reactions. These studies correlate strongly with the elegant work of Parson,⁶⁹ Sadeghi,⁷⁰ and coworkers. In the copper-fluorine system, we have observed not only CuF chemiluminescence from the copper dimer - fluorine atom reaction⁵⁸ but also the formation of CuF excited states from the reaction of metastable $^2D_{3/2,5/2}$ copper atoms with SF₆. This effort complements the recent study of metastable copper - Cl₂,⁹¹ F₂⁶⁹⁻⁷⁰ reactive encounters considered also in other chapters of this volume. These efforts are being extended to form the electronically excited copper cluster fluorides Cu_{x-1}F and the corresponding chlorides from Cu_x (*x* ≥ 3) + F(Cl) reactive encounters. In an attempt to generate the Mg₂ excimer analogs of the Na₂ laser amplifiers discussed previously, we are attempting to form magnesium clusters and observe the excited state products of their oxidation with F and Cl atoms. Surprisingly, preliminary results on this system signal the formation of an excited state Mg_xF and Mg_xCl complexes whose chemiluminescent spectra are now the subject of intense study in our laboratory.

Our initial observations^{11,14} suggest that larger cluster oxide species with significant metal-metal bonding can be made and explored using combined chemiluminescent and LIF techniques. It may be possible to generate species, the fingerprints of which are relevant to the detailed microscopic description of those properties which can contribute to the catalytic behavior of an oxidized metal surface or, in a future study of silicon cluster halogenation, to the nature and quality of a surface etch (Si_n + X (X=Cl, Cl₂, F, F₂)). As an ultimate goal, we wish to develop a detailed description of the intimate environment associated with the metal cluster-oxygen or metal cluster-halogen interaction, (1) determining how small clusters of metal atoms interact with the oxygen or halogen atom and (2) considering the dynamic behavior which these clustered atoms may exhibit as they move about the oxygen or halogen atom. Using a combination of chemiluminescent and laser fluorescent probes of the asymmetric metal clustered oxides, it should be possible to establish structures and determine, through bond angle and vibrational frequency determination, the manner in which these small metal clusters interact with an oxygen atom when they are formed in a unique kinetically controlled environment. It is precisely this information which can provide the productive tension between experiment and theory required for the development of systematically constructed and meaningful model systems describing the nature of ligand-metal surface interactions.

ACKNOWLEDGEMENT

We thank the National Science Foundation, the ACS-PRF, the Eastman Kodak Company, the Georgia Tech Foundation through a grant from Mrs. Betty Peterman Gole, and the Army Research Office and the Air Force Office of Scientific Research. This work would not have been possible without the capable assistance of J. R. Woodward, S. H. Cobb, K. X. He, M. McQuaid, K. K. Shen, C. B. Winstead, T. R. Burkholder, D. Grantier, R. Kahlscheuer and J. Bray, and collaboration with T. C. Devore, D. A. Dixon, S. Langhoff, and C. W. Bauschlicher.

REFERENCES

1. "Gas Phase Chemiluminescence and Chemiionization", A. Fontijn, editor, Elsevier Science Publishers, 1985.
2. M. Menzinger, *Adv. Chem. Phys.* 42 (1980) 1.
3. (a) "The Physics and Chemistry of Small Clusters", (editors: P. Jena, B. K. Rao, and S. N. Khanna) NATO ASI Series, Series B: Physics, Volume 158, Plenum Press, New York and London, 1986. (b) "Metal Clusters", edited by M. Moskovits, Wiley-Interscience, John Wiley and Sons, New York, 1986. (c) "Metal Bonding and Interactions in High Temperature Systems", J. L. Gole and W. C. Stwalley, Eds., ACS Symp. Ser. 179 (1982). (d) "Diatomic Metals and Metallic Clusters", Symp. Faraday Soc. 14 (1980). (e) M. Morse, *Chem. Reviews* 86 (1986) 1049.
4. T. N. Taylor, C. T. Campbell, J. W. Rogers, Jr., W. P. Ellis, and J. M. White, *Surface Science* 134 (1983) 529.
5. Na₃: (a) A. Herrmann, M. Hofmann, S. Leutwyler, E. Schumacher, and L. Woste, *Chem. Phys. Lett.* 62 (1979) 216; (b) J. L. Gole, G. J. Green, S. A. Pace, and D. R. Preuss, *J. Chem. Phys.* 76 (1982) 2247; (c) G. Delacretaz, E. R. Grant, R. L. Whetten, L. Woste, and J. W. Zwanziger, *Phys. Rev. Lett.* 56 (1986) 2598.
 Cu₃: (d) M. D. Morse, J. B. Hopkins, P. R. R. Langridge-Smith, and R. E. Smalley, *J. Chem. Phys.* 79 (1983) 5316; (e) W. H. Crumley, J. S. Hayden, and J. L. Gole, *J. Chem. Phys.* 84 (1986) 5250; (f) E. A. Rohlfing and J. J. Valentini, *Chem. Phys. Lett.* 126 (1986) 113.
 Ag₃: (g) P. Y. Cheng and M. A. Duncan, *Chem. Phys. Lett.* 152 (1988) 341.
 Al₃: (h) Z. Fu, G. W. Lemire, Y. M. Hamrick, S. Taylor, J.-C. Shui, and M. D. Morse, *J. Chem. Phys.* 88 (1988) 3524.
 Ni₃: (i) K. M. Ervin, J. Ho, and W. C. Lineberger, *J. Chem. Phys.* 89 (1988) 4514. (j) R. W. Woodward, S. H. Cobb, and J. L. Gole, *J. Phys. Chem.* 92 (1988) 1404.
 Cu₄⁺: (k) M. F. Jarrold and K. M. Creegan, *Chem. Phys. Lett.* 166 (1990) 116.
 C_x: (l) P. F. Bernath, K. H. Kinkle, and J. J. Keady, *Science* 244 (1989) 562; (m) J. Heath, A. L. Cooksy, M. H. W. Gruebele, C. A. Schumuttermaer, and R. J. Saykally, *Science* 244 (1989) 564; (n) N. Mozzen-Ahmadi, A. R. W. McKellar, and T. Amano, *J. Chem. Phys.* 91 (1989) 2140.
 Si_x: (o) T. N. Kitsopoulos, C. J. Chick, A. Weaver, and D. M. Neumark, "Vibrationally Resolved Photoelectron Spectra of Si₃⁻ and Si₄⁻", *J. Chem. Phys.* 93 (1990) 6108. (p) C. B. Winstead, K. X. He, T. Hammond, and J. L. Gole, "Electric Field Enhanced Laser Induced Plasma Spectroscopy of Jet Cooled Silicon Trimer", *Chem. Phys. Letts.* 181 (1991) 222.
6. (a) R. W. Woodward, P. N. Le, M. Temmen, and J. L. Gole, *J. Phys. Chem.* 91 (1987) 2637; (b) J. L. Gole, "Quantum Level Probes of Small Metal Clusters and Their Oxidations", American Institute of Physics Conference Proceedings, No. 160, *Advances in Laser Science II - Optical Science and Engineering Series 8*, pg. 439; (c) T. C. Devore, R. W. Woodward and J. L. Gole, *J. Phys. Chem.* 92 (1988) 6919; (d) R. W. Woodward, P. N. Le, T. C. Devore, D. A. Dixon, and J. L. Gole, *J. Phys. Chem.* 94 (1990) 756; (e) T. C. Devore, J. R. Woodward, and

- J. L. Gole, *J. Phys. Chem.* 93 (1989) 4920; (f) M. J. McQuaid and J. L. Gole, "Stability and Oxidation of Metal Based CO and CO₂ Complexes", Proceedings of the Fourth International Laser Science Conference, A.I.P. Conf. Proc. No. 191, Optical Science and Engineering Series 10, pg. 687.
7. T. C. Devore, M. McQuaid, and J. L. Gole, *High Temp. Science* 29 (1990) 1.
 8. S. H. Cobb, J. R. Woodward, and J. L. Gole, *Chem. Phys. Lett.* 143 (1988) 205; 156 (1989) 197.
 9. T. C. Devore and J. L. Gole, "Oxidation of Small Metal Clusters", Proceedings of the Sixth International Conference on High Temperature Materials, *High Temperature Science* 27 (1989) 49.
 10. "On the BiF Bond Dissociation Energy and Evaluation of the BiF Red Emission Band Systems", T. C. Devore, L. Brock, R. Kahlscheuer, K. Dulaney, and J. L. Gole, *Chemical Physics* 155 (1991) 423.
 11. James L. Gole, "The Unique Dynamics of Metal Cluster Oxidation and Complexation", to appear in Advances in Metal and Semiconductor Clusters, Vol. I, Spectroscopy and Dynamics, ed. M. A. Duncan, JAI Press, in press.
 12. See for example, (a) D. R. Preuss and J. L. Gole, *J. Chem. Phys.* 66 (1977) 2994; (b) J. L. Gole and D. R. Preuss, *J. Chem. Phys.* 66 (1977) 3000; (c) L. H. Dubois and J. L. Gole, *J. Chem. Phys.* 66 (1977) 779. (d) D. M. Lindsay and J. L. Gole, *J. Chem. Phys.* 66 (1977) 3886; (e) J. L. Gole and S. A. Pace, *J. Chem. Phys.* 73 (1980) 836; (f) C. L. Chalek and J. L. Gole, *J. Chem. Phys.* 65 (1976) 2845; (g) J. L. Gole and S. A. Pace, *J. Phys. Chem.* 65 (1981) 2651; (h) J. L. Gole, *Ann. Rev. Phys. Chem.* 27 (1976) 525.
 13. See for example references and discussion in (a) J. L. Gole, "The Gas Phase Characterization of the Molecular Electronic Structure of Small Metal Clusters and Cluster Oxidation", in "Metal Clusters", edited by M. Moskovits, (John Wiley and Sons); (b) M. D. Morse, J. B. Hopkins, P. R. Langridge Smith and R. E. Smalley, *J. Chem. Phys.* 79 (1983) 5216.
 14. Note that this present approach bears some resemblance to the liquid nitrogen entrainment - induced agglomeration of metal clusters used by Stein and coworkers and Solliard. These authors formed much larger aggregates which they studied using electron diffraction techniques. See for example, (a) B. G. de Boer and G. D. Stein, *Surf. Sci.* 106 (1981) 84. (b) C. Solliard, Ph.D. Thesis, Ecole Polytechnique Federal de Lausanne, Switzerland, 1983. (c) See also *Surf. Sci.* 106 (1981) 58. *J. de Phys. C2* (1977) 167.
 15. (a) S. J. Riley, E. K. Parks, L. G. Pobo, and S. Wexler, *Ber. Bunsenges. Phys. Chem.* 88 (1984) 287. (b) S. C. Richtsmeier, E. K. Parks, K. Liu, L. G. Pobo, and S. J. Riley, *J. Chem. Phys.* 82 (1985) 3659. (c) E. K. Parks, K. Liu, S. C. Richtsmeier, L. G. Pobo, and S. J. Riley, *J. Chem. Phys.* 82 (1985) 5470. (d) K. Liu, E. K. Parks, S. C. Richtsmeier, L. G. Pobo, and S. J. Riley, *J. Chem. Phys.* 83 (1985) 2882. (e) R. L. Whetten, D. M. Cox, D. J. Trevor, and A. Kaldor, *Phys. Rev. Lett.* 54 (1985) 1494. (f) R. L. Whetten, D. M. Cox, D. J. Trevor, and A. Kaldor, *J. Phys. Chem.* 89 (1985) 566. (g) D. J. Trevor, R. L. Whetten, D. M. Cox, and A. Kaldor, *J. Am. Chem. Soc.* 107 (1985) 528. (h) D. M. Cox, D. J. Trevor, R. L. Whetten, E. A. Rohlfing and A. Kaldor, *Phys. Rev. B1*, in press. (i) M. E. Geusic, M. D. Morse, and R. E. Smalley, J.

- Chem. Phys. 82 (1985) 590. (j) M. E. Geusic, M. D. Morse, S. C. O'Brien, and R. E. Smalley, Rev. Sci. Instr. 56 (1985) 2123.
 (k) M. D. Morse, M. R. Geusic, J. R. Heath, and R. E. Smalley, J. Chem. Phys. 83 (1985) 2293.
16. J. M. Herbelin, and R. A. Klingberg, Intern. J. Chem. Kinetics 16 (1984) 849.
 17. A. J. Ross, R. Bacis, J. D'Incan, C. Effantin, B. Koffend, A. Topouzkhanian, and J. Verges, Chem. Phys. Letts 166 (1990) 539.
 18. K. Balasubramanian, Chem. Phys. Letts. 127 (1986) 324.
 19. W. E. Jones, and T. D. McLean, J. Molec. Spectrosc. 90 (1981) 481.
 20. A. G. Gaydon, "Dissociation Energy and Spectra of Diatomic Molecules", 3rd ed., Chapman and Hall, London, 1968.
 21. B. Rai, and J. Singh, Spectrosc. Lett. 4 (1971) 129.
 22. See reference 20 and helpful discussions with D. L. Hildenbrand. See also K. H. Lau and D. L. Hildenbrand, J. Chem. Phys. 76 (1982) 2646, P. K. Kleinschmidt, K. H. Lau, and D. L. Hildenbrand, J. Chem. Phys. 74 (1981) 653, K. H. Lau and D. L. Hildenbrand, J. Chem. Phys. 71 (1979) 1572, D. L. Hildenbrand, J. Electrochem. Soc. 126 (1979) 1396, D. L. Hildenbrand, J. Chem. Phys. 48 (1968) 3657, E. Murad, R. P. Main, and D. L. Hildenbrand, J. Chem. Phys. 45 (1966) 263. C. L. Chalek and J. L. Gole in Proceedings of the Electrochemical Society, Electrothermics and Metallurgy, Atlanta, GA, 1977, Proceedings on "High Temperature Metal Halide Chemistry", Vol. 78-1, p. 278, The Electrochemical Society and references therein.
 23. R. J. LeRoy, in "Molecular Spectroscopy", Vol. I, eds. R. F. Barrow, D. A. Long and D. J. Millen (Chem. Soc. London, 1973), p. 113; J. Chem. Phys. 73 (1980) 6003.
 24. R. N. Zare, Ber. Bunsenges. Phys. Chem. 78 (1974) 153. D. R. Preuss and J. L. Gole, J. Chem. Phys. 66 (1977) 2994; J. L. Gole and D. R. Preuss, J. Chem. Phys. 66 (1977) 3000; L. H. Dubois and J. L. Gole, J. Chem. Phys. 66 (1977) 779.
 25. R. F. Heidner III, H. Helvajian, J. S. Holloway, and J. B. Koffend, J. Chem. Phys. 84 (1986) 2137.
 26. E. H. Fink, K. D. Setzer, D. A. Ramsay, and M. Vervloet, Chem. Phys. Lett. 179 (1991) 95.
 27. P. Kuijpers, and A. Dymanus, Chem. Phys. 24 (1977) 97.
 28. M. M. Patel, and P. S. Narayanan, Indian J. Pure Appl. Sci. 5 (1967) 223.
 29. W. E. Jones, and T. D. McLean, J. Molec. Spectrosc. 83 (1980) 317.
 30. M. N. Avasthi, Spectrosc. Letters 3 (1970) 157.
 31. P. S. Murty, D. V. K. Rao, Y. P. Reddy, and P. T. Rao, Spectrosc. Letters 8 (1975) 217.
 32. K. J. Chakoo, and M. M. Patel, Indian J. Pure Appl. Phys. 17 (1979) 189.
 33. F. Kohl, O. M. Uy, and K. D. Carlson, J. Chem. Phys. 47 (1967) 2667. L. Rovener, A. Drowart, and J. Drowart, Trans. Faraday Society 63 (1967) 2906.
 34. G. Herzberg, Spectra of Diatomic Molecules, Van Nostrand and Company, 1950 and references therein.
 35. T. Kiang and R. N. Zare, J. Am. Chem. Soc. 102 (1980) 4024.
 36. A. E. Douglas and M. Frackowiak, Can. J. Phys. 40 (1962) 832.
 37. L. V. Gurvich et al., Thermodynamic Properties of Individual Substances, Vols. 1 and 2 (in Russian) U. S. S. R. Academy of

- Science (1962).
38. P. A. O'Hare, R. Batana, and A. C. Wahl, *J. Chem. Phys.* 59 (1973) 6495.
 39. N. L. Singh and M. N. Avasthi, *Indian Jour. of Pure and Appl. Phys.* 1 (1963) 197.
 40. W. Jevons, *Proc. Phys. Soc.* 48 (1936) 563.
 41. H. G. Howell and G. D. Rochester, *Proc. Phys. Soc.* 51 (1939) 329.
 42. T. A. P. Rao and P. T. Rao, *Indian Jour. Phys.* 36 (1962) 85.
 43. F. Morgan, *Proc. Roy. Soc.* 49 (1936) 41.
 44. S. Sankaranarayanan, M. M. Patel, and P. S. Narayan, *Proc. Ind. Acad. Sci.* 56 (1962) 171.
 45. D. Cubicciotti, *J. Phys. Chem.* 64 (1960) 791.
 46. P. Venkateswarlu and B. N. Khanna, *Proc. Indian Acad. Sci.* A51 (1960) 14.
 47. K. C. Joshi, *Proc. Phys. Soc.* 78 (1961) 610.
 48. S. Sankaranarayanan, P. S. Narayanan, and M. M. Patel, *Proc. Indian Acad. Sci.* 59 (1964) 378.
 49. R. B. Singh and D. K. Rai, *Canad. J. Phys.* 43 (1965) 829.
 50. (a) G. J. Green, S. A. Pace, D. R. Preuss and J. L. Gole, *J. Chem. Phys.* 76 (1982) 2247.
(b) J. S. Hayden, J. R. Woodward, and J. L. Gole, *J. Chem. Phys.* 90 (1986) 1799.
 51. W. C. Stwalley, private communication.
 52. (a) W. H. Crumley, J. L. Gole and D. A. Dixon, *J. Chem. Phys.* 76 (1982) 6439. (b) S. H. Cobb, J. R. Woodward, and J. L. Gole, *Chem. Phys. Lett.* 143 (1988) 205. (c) S. H. Cobb, J. R. Woodward, and J. L. Gole, *Chem. Phys. Lett.* 157 (1989) 197. (d) S. H. Cobb, J. R. Woodward and J. L. Gole, "Continuous Chemical Laser Amplifiers in the Visible Region", *Proceedings of the Fourth International Laser Science Conference, A.I.P. Conf. Proc. No. 191, Optical Science and Engineering Series 10*, pg. 68.
 53. (a) B. Wellegehausen, *I.E.E.E. of Quant. Elect.* 15 (1979) 1108.
(b) P. L. Jones, U. Gaubatz, U. Hefter, and K. Bergmann, *Appl. Phys. Lett.* 42 (1983) 222. (c) B. Wellegehausen, in "Metal Bonding and Interactions in High Temperature Systems with Emphasis on Alkali Metals", A. C. S. Symposium Series 179, edited by J. L. Gole and W. C. Stwalley (Am. Chem. Soc., Washington, D. C.), p. 462.
 54. (a) W. H. Crumley, Ph.D. Thesis, Georgia Institute of Technology, 1985. (b) S. H. Cobb. Ph.D. Thesis, Georgia Institute of Technology, 1988.
 55. See for example, (a) R. S. Berry and C. W. Reimann, *J. Chem. Phys.* 38 (1963) 1540, (b) R. S. Berry, *J. Chem. Phys.* 27 (1957) 1288, (c) W. S. Struve, J. R. Krenos, D. L. McFadden and D. R. Herschbach, *J. Chem. Phys.* 62 (1975) 404. (d) R. C. Oldenborg, J. L. Gole and R. N. Zare, *J. Chem. Phys.* 60 (1974) 4032.
 56. Given Na_2 and Na_3 ionization potentials of 4.87 and 3.97 eV (A. Hermann, E. Schumacher, and L. Woste, *J. Chem. Phys.* 68 (1978) 2327, and an electron affinity of 3.3363 eV for atomic bromine, we determine a very substantial electron jump cross section $\sigma = \pi (14.38/3.97-3.36) = 1746 \text{ \AA}^2 (1.75 \times 10^{-13} \text{ cm}^2)$ for the $\text{Na}_3 - \text{Br}$ reaction and $\sigma = \pi (14.38/4.87-3.36) = 285 \text{ \AA}^2 (2.85 \times 10^{-14} \text{ cm}^2)$ for the $\text{Na}_2 - \text{Br}$ reaction.
 57. (a) T. C. Devore, C. W. Bauschlicher, Jr., S. R. Langhoff, Per E. M. Siegbahn, M. Sulkes and J. L. Gole, *Formation, Electronic Spectra,*

- and Electronic Structure of the Low-Lying Singlet States of Symmetrical Cu_2O , to be submitted for publication. (b) T. C. Devore, C. W. Bauschlicher, Jr., T. Burkeholder and J. L. Gole, A Comparative Study of the Oxidation of Atomic Copper and Higher Copper Clusters Under a Single and Multiple Collision Conditions; Electronic Structure of the Asymmetric Copper Clustered Oxides, Cu_xO , to be submitted for publication.
58. K. K. Shen, C. Winstead, L. Brock, K. Dulaney, T. Devore and J. L. Gole, work in progress.
 59. T. C. Devore and J. L. Gole, *Chemical Physics* 133 (1989) 95.
 60. R. Kahlscheuer, T. C. Devore, J. Bray and C. B. Winstead, work in progress.
 61. (a) "The Physics of Latent Image Formation in the Silver Halides", A. Baldereschi, W. Czaja, E. Tosatti and M. Tosi, eds., World Scientific, Singapore, 1984. (b) "The Theory of the Photographic Process", T. H. James, ed., MacMillan, New York, 1977.
 62. "Ethylene and Industrial Derivatives", S. A. Miller and Ernest Benn, eds., MacMillan, New York, 1977.
 63. See G. Herzberg, Spectra of Polyatomic Molecules, Van Nostrand Reinhold, 1977.
 64. M. Morse, *Chem. Phys. Lett.* 133 (1987) 8.
 65. "Description of the Ground State Electronic Structures of Cu_2O , Cu_2S , Ag_2O , and Ag_2S ", D. A. Dixon and J. L. Gole, *Chemical Physics Letters*, in press.
 66. D. A. Dixon, *J. Phys. Chem.* 92 (1988) 86.
 67. To be published - see reference 56 - used by permission.
 68. D. A. Dixon, private communication.
 69. R. W. Schwenz and J. M. Parson, *J. Chem. Phys.* 73 (1980) 259.
 70. P. Baltayan, F. Hartmann, J. C. Pebay-Peyroula, and N. Sadeghi, *Chem. Phys. Lett.* 120 (1988) 123. N. Sadeghi - private communication of unpublished results.
 71. R. W. Schwenz and J. M. Parson, *Chem. Phys. Lett.* 71 (1980) 524.

APPENDIX VI

"The Unique Nature of Metal Cluster Oxidation", J. L. Gole, in Proceedings of the International Symposium on the Physics and Chemistry of Finite Systems: From Clusters to Crystals, Kluwer Academic Publishers, NATO ASI Series C: Mathematical and Physical Sciences, Vol. 374 (1992) pg. 1025.

THE UNIQUE NATURE OF METAL CLUSTER OXIDATION

JAMES L. GOLE
High Temperature Laboratory
Center for Optical Science and Engineering
and School of Physics
Georgia Institute of Technology
Atlanta, Georgia 30332

ABSTRACT. Oven based entrainment flow and supersonic expansion techniques are used to form small metal and metalloid molecules and to study their unusual oxidation behavior. These metal and metalloid molecules oxidize to form not only a distinct class of metal atom grouped cluster oxides and halides under kinetically as opposed to thermodynamically controlled conditions but also unusual (unexpected) excited electronic state product distributions. We exemplify this behavior with a focus on copper cluster oxidation, contrasting the emission spectra generated for the asymmetric and symmetric isomers of Cu_2O and comparing these with theory. A subset of the oxidation studies touches on the sodium trimer - halogen atom reactions, $(\text{Na}_3 - \text{X}(\text{Cl}, \text{Br}, \text{I}))$, which create a continuous electronic population inversion based on the chemical pumping of Na_2 with laser amplifiers throughout the visible and the extension of these studies to copper and magnesium trimer halogenation.

INTRODUCTION

The cluster oxidation process, the unique products of metal cluster oxidative transformation, and the optical signatures of the products of oxidation may have important implications for the extension of concepts in molecular reaction dynamics and the fingerprinting of local surface reactive environments. The study of cluster oxidation provides a unique opportunity to address an unusual and multicentered reaction chemistry and can furnish information on grouped metal atom-oxidant interactions which can serve as an important component in the modeling of chemically significant systems on a much larger macroscopic scale.

At present, the internal mode structure and dynamics associated not only with bare metal and metalloid clusters¹ but also with their kinetically controlled oxidation²⁻⁵ is still largely neglected. The limited information which is available demonstrates a unique oxidation behavior and virtually unexpected reactive branching.³ In approaching the study of the oxidation dynamics which a number of metal (and metalloid) clusters undergo as they form a distinct class of metal atom grouped cluster oxides² and halides³ under kinetically as opposed to thermodynamically

cally controlled conditions. We have been concerned with the characterization of the internal mode structure of the product metal clustered oxides and halides. In developing these studies, we have analyzed the first vibrationally resolved optical signatures² for several "asymmetric" metal cluster oxides, and demonstrated the first visible chemical laser amplifier from a metal cluster oxidation process.⁴ These studies graphically illustrate the dramatic and unexpected oxidation behavior characteristic of small metal cluster reactions and point to the potential for developing new insights on the nature of chemical reactivity. We consider several examples.

"Oxidation of Metal and Metalloid Cluster Systems"

We have developed entrainment flow devices^{5,7} which facilitate the generation of a substantial and usable continuous flux of small metal clusters. Using these devices, it has been possible to record the optical signatures of the reaction products associated with the oxidation of small boron ($B_n + O_2, n=2,3$),^{2(a)-(c)} copper ($Cu_n + O_2, n=1,2,3$),^{2(a),2(b),2(c)} silver ($Ag_n + O_2, n=1,2$),^{2(a),(d)} manganese ($Mn_n + O_2, n=1,2$),^{2(a)} chromium ($Cr_n + O_2, n=1,2$),^{2(a)} and magnesium ($Mg_n + O_2, n=1,2$) clusters. With the generation of a sufficient metal cluster flow, subsequently oxidized, we obtain quantal information on the energy levels of several asymmetric metal clustered oxides, M_nO_x ($n \geq 2$) and preliminary data on the copper, chromium, and magnesium clustered chlorides and fluorides. Thusfar, this work has led to three general observations concerning cluster reactions.

(1) Cluster oxidations, through a multicentered reaction capability (excluding fluorine and chlorine atom rxns.), often yield product molecules in higher energy states than have been accessible to the corresponding atomic reactions.

(2) The products of metal cluster reactions encompass metal rich molecules. In many cases, metal-metal bonds are present and behave with an unusual fluxionality in these product molecules.

(3) Kinetics rather than thermodynamics most often controls the nature of the initially formed products of metal cluster oxidation. Quantum level probes of the products of metal cluster oxidation are being developed with a current emphasis on two distinct source configurations. In one configuration a stream of metal clusters formed through the "supersonic expansion" of the metallic element of interest is made to intersect a selected oxidant (modified beam-gas configuration), the products of reaction being studied using a combination of chemiluminescent and laser fluorescent techniques. This configuration is being used to study the sodium trimer-halogen atom reactions.⁸ The second, more versatile source configuration to which we have alluded to above lies intermediate to a low pressure molecular beam and high pressure flow device.^{6,7} Clusters are formed from a high metal flux source and further agglomerated by an entraining argon or helium flow maintained at room to liquid nitrogen temperature. These clusters are subsequently oxidized by a concentric oxidant flow, the resulting products being passed to a small mass spectrometer system. Using this agglomeration flow source, we have successfully obtained the first quantal information

on the energy levels and optical signatures of several metal cluster oxides and select halides (M_nO_x, M_nX). In these studies, it is possible to combine the energetic constraints of the chemiluminescent process, distinct optical signatures, and mass spectrometry for product identification.

"Copper Cluster Oxidation"

The reaction exothermicity for the process



is 1.76 ± 0.05 eV. This process is energetic enough to populate the $v' = 2$ level of the $CuO \delta_{1/2}^+$ state. The chemiluminescent spectrum observed for reaction (1) under single collision conditions with atomic copper dominant is in excellent agreement with the available energy for the atomic oxidation process.

If the energy liberated in a multicentered copper cluster reaction is largely collected in one of the reaction product molecules, a considerable enhancement of the available energy to populate product molecule excited electronic states can be obtained. The oxidation of copper clusters produced in an entrained copper flow (copper flux $\geq 10^{18}$ /cm²-sec) with ozone under multiple collision conditions produces emission (Figure 1) which originates from the $D^2\delta$, $C^2\Pi$, $A^2\Sigma$, $B^2\Delta$ and $A'^2\Sigma$

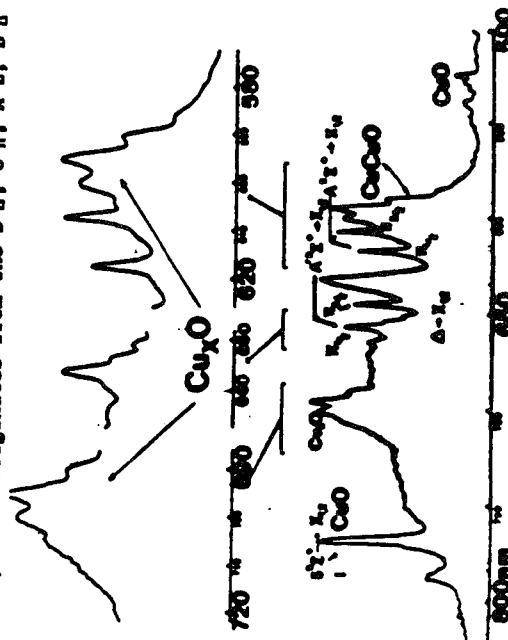


Figure 1: Chemiluminescent spectrum resulting from the multiple collision (10^{18} to 600 after) oxidation of small copper molecules and clusters. Clusters are formed in a moderate copper agglomeration mode and oxidized with ozone. The emission spectrum, taken with an EMI 9608 phototube at a resolution of 0.5 nm is dominated by CuO , and Cu_2O ($n \geq 2$) emission features where the polyatomic emitters correspond to the copper clustered oxides.

states of CuO. These emission features are not observed under conditions in which one simply increases the copper atom flux promoting a substantial increase in the CuO $\delta^2\pi^+$ emission. The population of the higher-lying states in CuO requires more energy than is available from the copper atom reaction. This increased exothermicity could be provided by the reaction of vibrationally hot copper dimer or, equally likely with moderate to high metal agglomeration, by the reaction of ground state copper trimer via the process



Under a variety of experimental conditions, the first emission spectra for both the asymmetric copper clustered oxides and the symmetric CuO molecule have now been successfully generated. A selection of the data obtained for these copper oxides is indicated in Figures 1 and 2 where emission spectra for both symmetric and asymmetric CuO, as well as the higher order copper clustered, Cu₂O (x ≥ 2) complexes are displayed.

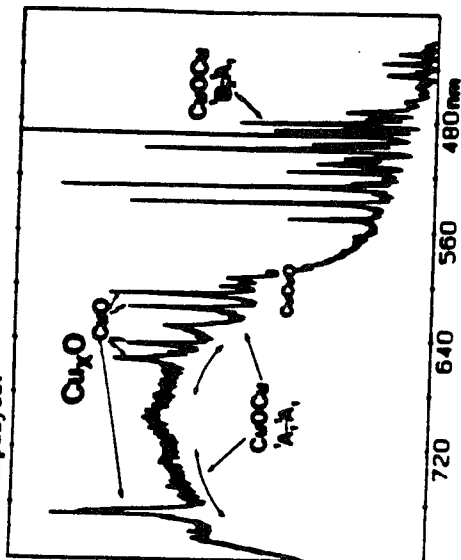


Figure 2: Chemiluminescent spectrum taken under multiple collision conditions in a non-effusive agglomeration mode dominated by emission from the symmetric CuO molecule but also showing emission corresponding to CuO and to the asymmetric CuO molecule. The spectrum was taken with an BFI 9600 phototube at a resolution of 0.3 nm.

Significant differences between the electronic spectra and energy levels for the CuO and CuO₂ molecules are evidenced not only by the distinctly different location of emission features but also by the appearance, extent, and intensity of these features. The spectral features for the CuO molecule (Fig. 1) at ~ 600 nm appear to correspond to a short progression in a 132 cm⁻¹ bending mode whereas the observed structured emission spectrum for the CuO₂ B₂ - A₁ transition appears to be dominated by moderate progressions in the ground and

excited state symmetric stretching modes of the symmetric isomer. The spectral features recorded for CuO₂ bear a strong correlation with recent quantum chemical calculations by Baushlicher, Langhoff, and Siegbahn¹¹ (Table I). These authors have estimated bond lengths, bond angles, transition moments, and electronic state locations for the ground and several excited states of the CuO₂ molecule. The calculations are

Table I

Calculated Properties of Ground and Excited States of Symmetrical Cu₂O

STATE	r(Cu-O) (Angstroms)	BOND ANGLE (Degrees)	T ₀ (APPROX.) (cm ⁻¹)
¹ A ₁ (Ground)	1.793	105.7	0
¹ B ₁ (0.3) ^a	1.964	81.4	14221
¹ A ₁ (1.6) ^a	1.921	180.0	17181
¹ B ₂ (1.0) ^a	1.956	77.3	20336
¹ A ₂ (0.1) ^a	1.942	123.3	22133

^aTransition Moment in Atomic Units.

currently undergoing further refinement, especially in correlation with the data derived from the emission spectra depicted in Figure 2. However, the relative intensities of the CuO₂ A₁ and B₂ transitions depicted in Figure 2 are in very good agreement with the calculated relative transition moments. Further, the change in bond angle and bond length predicted for the A₁ - A₁ transition (θ - a substantial 75°) is commensurate with a long virtually unresolved progression dominated by the CuO₂ bending mode, much like that characterizing a similar transition in the water molecule at the fringes of the vacuum ultraviolet region.¹² For the B₂ - A₁ transition, the experimental data indicates a ground state symmetric stretch frequency of 640 cm⁻¹ (ν = 640 ± 10 cm⁻¹) and an excited state symmetric stretch normal mode frequency of 409 ± 10 cm⁻¹.

The spectroscopy of the copper cluster oxides is now the focus of considerable further study. This effort includes laser induced fluorescence at moderate and higher resolution to facilitate the evaluation of further vibrational mode structures and the determination of both the CuO and CuO₂ ground state geometries. Potential functions now generated for CuO and CuO₂¹³ indicate that these molecules are quite bent although they are also characterized by very flat bending mode potentials. It appears that CuO can undergo a facile isomerization to CuO₂ with a high probability for interconversion of the two isomers.

A study of the isomer interconversion may bear some relevance to the assessment of the role which copper oxide plays in high T_c superconductors.¹³ Here the movement of the copper and oxygen atoms as dictated by the Cu_2O potential function, especially the vibrational modes associated with out-of-plane bending, may play a role in the high T_c mechanism.

A Continuous Visible Chemical Laser Amplifier from a Metal Cluster

The alkali metals are particularly amenable to detection with transition probabilities among alkali metal atom or dimer electronic states being among the largest recorded.¹⁴ Therefore, with a desire to initiate efforts focused on the study of metal cluster oxidation, it seemed appropriate to study what were felt to be the simplest metal cluster oxidation reactions, the alkali trimer-halogen atom reactions, producing reaction products with well defined and characterized electronic transitions. In retrospect, the study of alkali trimer-halogen atom reactive encounters was a natural choice.

The high cross section, highly exothermic $\text{Na}_2 - \text{X}$ ($\text{Cl}, \text{Br}, \text{I}$) reactions form Na_2 in several of the sodium dimer excited electronic states [5] indicated schematically in Figure 3. The energetics of the

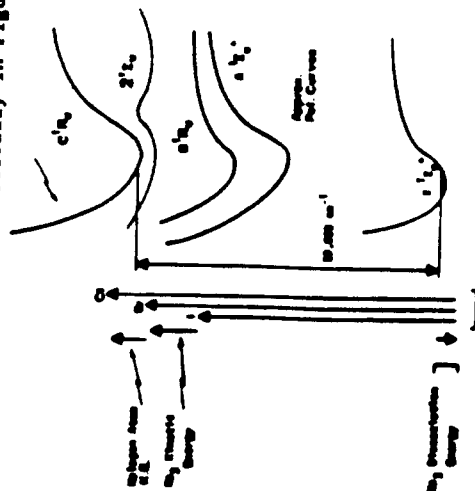
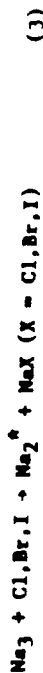


Figure 3: Energetics associated with the formation of Na_2 produced by the $\text{Na}_3 - \text{X}$ (Cl, Br, I) chemiluminescent reaction. Potential curves are drawn approximately.

reactive processes of interest are indicated in the figure. The $\text{Mg}_2\text{-Cl}$ and $\text{Mg}_2\text{-Br}$ reactions are sufficiently exothermic to readily populate the $\text{A } {}^1\Sigma_u^+$, $\text{B } {}^1\Pi_u$, $\text{C}' (2 {}^1\Sigma_u^+ - X {}^1\Sigma_u^+)$ and $\text{C } {}^1\Pi_u$ states of sodium dimer. The available energy results from the formation of a moderately strong sodium halide bond and the rupture of a weak sodium trimer bond. The $\text{Mg}_2\text{-I}$ reaction is much less exothermic. However, the contribution of the Mg_2 kinetic energy and the reaction of halogen atoms, generated from a 1500 K source, in the high energy tail of their kinetic energy distribution allows the population of a few vibrational levels in the $\text{Mg}_2 \text{C } {}^1\Pi_u$ state and several levels of the double minimum C' state. The

Optical signatures for the processes



encompass emission from a limited number of Na_2 band systems including the A, B, C, and C' states. Surprisingly, the observed emission is characterised by sharp, well defined, emission regions¹⁵ (Figures 4.5)

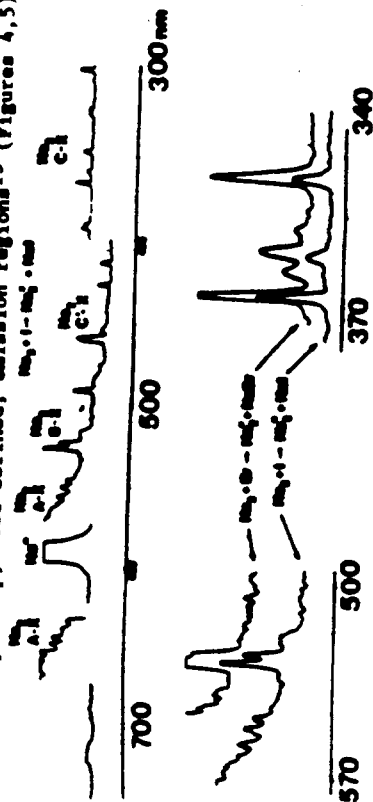


Figure 4: Chemiluminescent emission from the $\text{Mg}_2 + \text{Br}$ and $\text{Mg}_2 + \text{I}$ reactions forming excited states of Mg^* , whose optical signatures dominated the observed emission, and the sodium halides. Sharp emission features superimposed on a broad background are apparent including those at 317, 492, 449.5, 436, and 496 nm. Spectral resolution is 0.6 nm. See text for discussion.

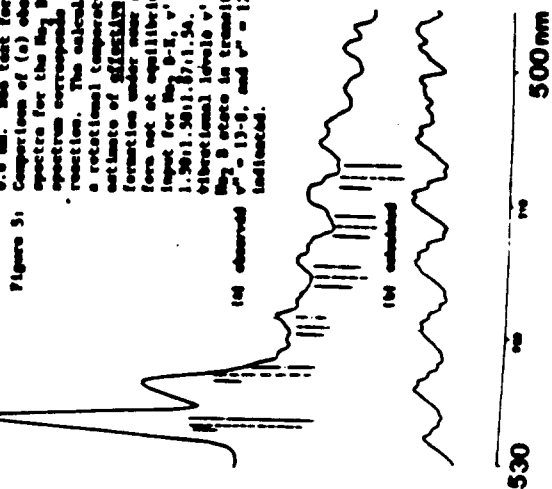


Figure 5: Comparison of (a) observed and (b) calculated emission spectra for the Hg B-X emission system. The experimental spectrum corresponds to chemiluminescence from the $\text{Hg}-\text{Br}_2$ reaction. The calculated spectrum, which was obtained for a rotational temperature, $T_{\text{rot}} = 1000^\circ\text{K}$, represents an estimate of **efficiency** rotational temperatures for Hg_2 product formation under near single collision conditions and therefore not at equilibrium. Relative vibrational populations input for the B-X, $v' = 0-6$ were in the ratio 1.00:1.17:1.33:1.50:1.50:1.71:1.50. The location of contributions from vibrational levels $v' = 6$ (—), 5(---), and 4(---) of the Hg_2 B state in transition to vibrational levels $v'' = 14-9$, $v'' = 13-0$, and $v'' = 12-7$ of the Hg_2 ground state are indicated.

superimposed on a much weaker but perceptible Na_2 dominated background. As Fig. 5 demonstrates, through comparison with the best fit calculated sodium dimer spectrum, these sharp emission features are not readily explained by invoking a purely fluorescent process involving sodium dimer.

The sharp nature of several of the B-X, C-X, and C'-X Na_2 emission features (Fig. 4), their near exponential growth with Mg_2 concentration relative to the background Na_2 fluorescence, and their correlation in certain regions to the emission characteristic of optically pumped Na_2 laser systems (ex: 528.2 nm (v', v'') = $6, 14$ (B-X)) suggested that stimulated emission, associated with certain of the Na_2 emission products might have been observed. Laser gain measurements were subsequently carried out to assess this possibility.

In order to perform these studies, a unique source configuration, discussed in detail elsewhere^{6,15}, was developed which allowed the supersonic expansion of pure sodium vapor to create a Mg_2 concentration not previously attained in a reaction-amplification zone. In order to operate above threshold (gain) we produce in excess of $10^{13}/\text{cc}$ trimer molecules in this reaction zone. The concentration produced is between 10 and 500 times the maximum concentration for the fluorescence experiments ($[\text{Mg}_2] \sim 3 \times 10^{12}/\text{cc}$) depicted in Figures 4 and 5. In all of the experiments, halogen atoms were produced from halogen molecules in a high temperature carbon furnace¹⁶ with $\sim 95\%$ efficiency. These halogen atoms exit the furnace into the reaction zone initiating the trimer-halogen atom chemical reaction. The halogen flow is adjusted to optimize gain.^{15(b)}

Laser gain and hence amplification is found to be characteristic of several of the sharper and more pronounced emission features apparent in the spectra depicted in Figure 4 (Mg_2 - Br) corresponding to a stimulated emission process and to the establishment of a population inversion. Optical gain through stimulated emission, measured at 0.5 cm^{-1} resolution in the regions 527 nm (1X gain), 492 nm (0.3X gain), and 460.5 nm (0.8X gain), correlates precisely with the reactive process and the relative intensities of those sharp features observed while monitoring the light emitted from the Mg_2 -Br and Mg_2 -I reactions (Figs. 4, 5). High resolution ring dye laser scans (0.007 cm^{-1}) in the 527 nm region indicate that the gain for the system is close to 3.8% for an individual rovibronic transition with approximately four to five transitions near 527 nm showing gain. At 459.8 nm , a gain of 2.3% has been measured for an individual rovibronic transition. These results demonstrate the continuous amplifying medium for a visible chemical laser in at least three wavelength regions.¹⁵

The gain observed in these systems is strongly dependent on both the Mg_2 and halogen atom concentration. As the probe laser power was changed, the amplification signal was found to vary linearly indicating that the measurements were taken in the small signal gain regime. In order to further verify that these gain observations were not artifacts which could be observed at any wavelength including those corresponding to an intense spectral feature, the gain experiment was repeated at several wavelengths including the sodium D-line wavelength at 588.9 nm . No gain was observed at any other wavelength in the 420 - 600 nm region.

At the Na D-line wavelength the signal was seen to decrease significantly, indicating considerable scattering or absorption of the probe laser photons.

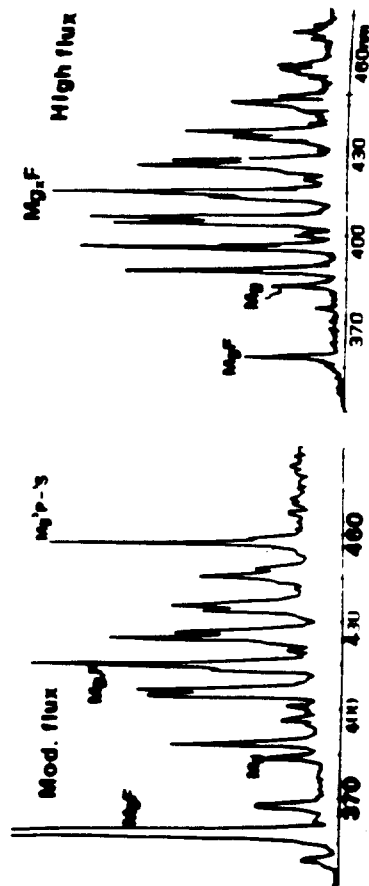
Because of the low Mg_2 ionization potential and the high halogen electron affinities,¹⁷ the Mg_2 -halogen atom reactions are expected to proceed via an electron jump mechanism with extremely high cross sections,¹⁸ producing substantial Mg_2 excited state populations. The created population inversions monitored thus far are thought to be sustained by (1) the large number of free halogen atoms reacting with Mg_2 molecules in those ground state levels on which the transitions emanating from the Mg_2 excited states terminate and (2) collisional relaxation of vibrationally excited ground state Mg_2 is expected to be substantial relative to that corresponding to collision induced vibrational deactivation of the Mg_2 manifold. Extremely efficient reactions thus greatly aid the rapid depletion of the lower state levels in this system allowing one to sustain a continuous population inversion. The current results certainly indicate an unusual and unexpected oxidation behavior which may be manifest in a number of metal cluster reactions. This suggests that the study of these processes will aid the development of new insights on chemical reactivity.

"Extensions of Metal Cluster Oxidation Studies"

The oxidation studies which we have exemplified for the copper and sodium systems and briefly outlined for other reactive combinations are now being extended to additional metal and metalloid based constituents.¹⁹ A source which we have developed to study the $\text{Bi}_2 + \text{F}$ reaction¹⁹ is now being used to investigate the fluorine atom oxidation of copper¹¹ and magnesium¹¹ clusters. The fluorine atom oxidations of small copper molecules are of particular interest as we consider the analogy between the single valence electron copper and sodium oxidation reactions. These copper studies also correlate strongly with the elegant work of Parson,²⁰ Sedeghi,²¹ and coworkers.

We are completing studies of the CaF chemiluminescence from the copper dimer - fluorine atom reaction. The effort is being extended to form the electronically excited copper cluster fluorides $\text{Cu}_x\text{-F}$ from Cu_x ($x \geq 3$) + F reactive encounters. Also, in an attempt to generate the Mg_2 excimer analogs of the Mg_2 laser amplifiers discussed previously, we are attempting to form magnesium clusters and observe the excited state products of their oxidation with F and Cl atoms. Surprisingly, preliminary results on this system signal the formation of excited state Mg_2F (Fig. 6) and Mg_2Cl charge transfer complexes where x is most likely two. The chemiluminescent spectra depicted in Fig. 6 are thought to result in part from the magnesium trimer reaction which, under the experimental conditions surveyed thus far, appears to produce minimal Mg_2 fluorescence. These systems are now the subject of continued study in our laboratory.

Our initial observations^{6,7} suggest that larger cluster oxide species with significant metal-metal bonding can be made and explored using combined chemiluminescent and LIF techniques. It may be possible

[illegible]

to generate species, the fingerprints of which are relevant to the detailed microscopic description of those properties which can contribute to the catalytic behavior of an oxidized metal surface or, in a future study of silicon cluster halogenation, to the nature and quality of a surface etch ($\text{Si}_n + \text{X} (\text{X}=\text{Cl}, \text{Cl}_2, \text{F}, \text{F}_2)$). As an ultimate goal, we wish to develop a detailed description of the intimate environment associated with the metal cluster-oxygen or metal cluster-halogen interaction. (1) determining how small clusters of metal atoms interact with the oxygen or halogen atoms and (2) considering the dynamic behavior which these clustered atoms may exhibit as they move about the oxygen or halogen atom. Using a combination of chemiluminescent and laser fluorescence probes of the metal clustered oxides, it should be possible to establish structures and determine, through bond angle and vibrational frequency evaluation, the manner in which these small metal cluster groupings interact with an oxygen atom when they are formed in a kinetically controlled environment. It is precisely this information which can provide the productive tension between experiment and theory required for the development of systematically constructed and meaningful model systems describing the nature of ligand-metal surface interactions.

ACKNOWLEDGEMENT

We thank the National Science Foundation, the ACS-PRF, the Eastman Kodak Company, the Georgia Tech Foundation through a grant from Mrs. Betty Peterman Cole, and the Army Research Office and the Air Force Office of Scientific Research. This work would not have been possible without the capable assistance of J. R. Woodward, S. H. Cobb, K. X. He, M. McQuaid, K. K. Shen, C. B. Winstead, T. R. Burkholder, D. Grantier, R. M. Kahlscheuer and J. Bray, and collaboration with T. C. Devore, D. A. Dixon, S. Langhoff, and C. W. Bauschlicher.

REFERENCES

1. Na₃: (a) A. Herrmann, M. Hofmann, S. Lautaylor, E. Schumacher, and L. Woste, *Chem. Phys. Lett.* **62** (1979) 216; (b) J. L. Gole, G. J. Green, S. A. Pace, and D. R. Preuss, *J. Chem. Phys.* **76** (1982) 2247; (c) G. Delacretas, E. R. Grant, R. L. Whetten, L. Woste, and J. W. Zwanziger, *Phys. Rev. Lett.* **56** (1986) 2598.
- Cu₃: (d) M. D. Morse, J. B. Hopkins, P. R. R. Langridge-Smith, and R. E. Sealley, *J. Chem. Phys.* **79** (1983) 5316; (e) W. H. Crumley, J. S. Hayden, and J. L. Gole, *J. Chem. Phys.* **84** (1986) 5250; (f) E. A. Rohlfing and J. J. Valentini, *Chem. Phys. Lett.* **126** (1986) 113.
- Ag₃: (g) P. Y. Cheng and M. A. Duncan, *Chem. Phys. Lett.* **152** (1988) 341.
- Al₃: (h) Z. Fu, G. W. Lemire, Y. M. Harick, S. Taylor, J.-C. Shui, and M. D. Morse, *J. Chem. Phys.* **88** (1988) 3524.
- Ni₃: (i) K. M. Ervin, J. Ho, and W. C. Lineberger, *J. Chem. Phys.* **89** (1988) 4514. (j) E. W. Woodward, S. H. Cobb, and J. L. Gole, *J. Phys. Chem.* **92** (1988) 1404.
- Cu₄⁺: (k) M. F. Jarrold and K. M. Green, *Chem. Phys. Lett.* **166** (1990) 116.
- Cu₂⁺: (l) P. F. Bernath, K. H. Kinkle, and J. J. Keady, *Science* **244** (1989) 562; (m) J. Heath, A. L. Cooky, M. H. W. Groebels, C. A. Schmuttmeyer, and R. J. Saykally, *Science* **244** (1989) 564; (n) M. Morzen-Ahmadi, A. R. W. McKellar, and T. Amano, *J. Chem. Phys.* **91** (1989) 2140.
- Si₄⁺: (o) T. N. Kitsopoulos, C. J. Chick, A. Weaver, and D. M. Neumark, "Vibrationally Resolved Photoelectron Spectra of Si₃⁺ and Si₄⁺", *J. Chem. Phys.* **93** (1990) 6108. (p) C. B. Winstead, K. X. He, T. Hammond, and J. L. Gole, "Electric Field Enhanced Laser Induced Plasma Spectroscopy of Jet Cooled Silicon Trimer", *Chem. Phys. Lett.* **181** (1991) 222.
2. (a) E. W. Woodward, P. M. Le, M. Tannen, and J. L. Gole, *J. Phys. Chem.* **91** (1987) 2637; (b) J. L. Gole, "Quantum Level Probes of Small Metal Clusters and Their Oxidations", *American Institute of Physics Conference Proceedings*, No. 160, *Advances in Laser Science II - Optical Science and Engineering Series 6*, pp. 439; (c) T. C. Devore, E. W. Woodward and J. L. Gole, *J. Phys. Chem.* **92** (1988) 6919; (d) E. W. Woodward, P. M. Le, T. C. Devore, D. A. Dixon, and J. L. Gole, *J. Phys. Chem.* **94** (1990) 756; (e) T. C. Devore, J. R. Woodward, and J. L. Gole, *J. Phys. Chem.* **93** (1989) 4920; (f) M. J. McQuaid and J. L. Gole, "Stability and Oxidation of Metal Based CO and CO₂ Complexes", *Proceedings of the Fourth International Laser Science Conference*, A.I.P. Conf. Proc. No. 191, *Optical Science and Engineering Series 10*, pp. 687.
3. T. C. Devore, M. McQuaid, and J. L. Gole, *High Temp. Science* **29** (1990) 1.
4. S. H. Cobb, J. R. Woodward, and J. L. Gole, *Chem. Phys. Lett.* **143** (1988) 205; **156** (1989) 197.
5. T. C. Devore and J. L. Gole, "Oxidation of Small Metal Clusters", *Proceedings of the Sixth International Conference on High*

6. "The Unique Dynamics of Metal Cluster Oxidation and Complexation", to appear in *Advances in Metal and Semiconductor Clusters*, Vol. I, Spectroscopy and Dynamics, ed. M. A. Duncan, JAI Press, in press.
7. Note that this present approach bears some resemblance to the liquid nitrogen entrapment - induced agglomeration of metal clusters used by Stein and coworkers and Solliard. These authors formed much larger aggregates which they studied using electron diffraction techniques. See for example, (a) B. G. de Boer and G. D. Stein, *Surf. Sci.* 106 (1981) 84. (b) C. Solliard, Ph.D. Thesis, Ecole Polytechnique Federal de Lausanne, Switzerland, 1983. (c) See also *Surf. Sci.* 106 (1981) 58. J. de Phys. C2 (1977) 167.
8. (a) T. C. Devore, C. W. Bauschlicher, Jr., S. R. Langhoff, Per E. M. Siegbahn, M. Sulkes and J. L. Gole, Formation, Electronic Spectra, and Electronic Structure of the Low-Lying Singlet States of Symmetrical Cu_2O , to be submitted for publication. (b) T. C. Devore, C. W. Bauschlicher, Jr., T. Burkeholder and J. L. Gole, A Comparative Study of the Oxidation of Atomic Copper and Higher Copper Clusters Under a Single and Multiple Collision Conditions; Electronic Structure of the Asymmetric Copper Clustered Oxides, Cu_3O , to be submitted for publication.
9. K. E. Shen, C. Winstead, L. Brock, K. Dulaney, T. Devore and J. L. Gole, work in progress.
10. T. C. Devore and J. L. Gole, *Chemical Physics* 133 (1989) 95.
11. To be published - see reference 8.
12. See G. Herzberg, *Spectra of Polyatomic Molecules*, Van Nostrand Reinhold, 1977.
13. D. A. Dixon, private communication.
14. W. C. Stwalley, private communication.
15. (a) W. H. Crumley, J. L. Gole and D. A. Dixon, *J. Chem. Phys.* 76 (1982) 6439. (b) S. H. Cobb, J. R. Woodward, and J. L. Gole, *Chem. Phys. Lett.* 143 (1988) 205. (c) S. H. Cobb, J. R. Woodward, and J. L. Gole, *Chem. Phys. Lett.* 157 (1989) 197. (d) S. H. Cobb, J. R. Woodward and J. L. Gole, "Continuous Chemical Laser Amplifiers in the Visible Region", Proceedings of the Fourth International Laser Science Conference, A.I.P. Conf. Proc. No. 191, Optical Science and Engineering Series 10, pg. 68.
16. (a) W. H. Crumley, Ph.D. Thesis, Georgia Institute of Technology, 1985. (b) S. H. Cobb, Ph.D. Thesis, Georgia Institute of Technology, 1988.
17. See for example, (a) R. S. Berry and C. W. Reimann, *J. Chem. Phys.* 38 (1963) 1540, (b) R. S. Berry, *J. Chem. Phys.* 27 (1957) 1288, (c) W. S. Struve, J. R. Krenos, D. L. McFadden and D. R. Herschbach, *J. Chem. Phys.* 62 (1975) 404. (d) R. C. Oldenborg, J. L. Gole and R. N. Zare, *J. Chem. Phys.* 60 (1974) 4032.
18. Given Na_2 and Na_3 ionization potentials of 4.87 and 3.97 eV (A. Hermann, E. Schumacher, and L. Woste, *J. Chem. Phys.* 68 (1978) 2327, and an electron affinity of 3.363 eV for atomic bromine, we determine a very substantial electron jump cross section $\sigma = \pi$

$(14.38/3.97-3.36) = 1746 \text{ \AA}^2 (1.75 \times 10^{-13} \text{ cm}^2)$ for the $\text{Na}_3 - \text{Br}$ reaction and $\sigma = \pi (14.38/4.87-3.36) = 285 \text{ \AA}^2 (2.85 \times 10^{-14} \text{ cm}^2)$ for the $\text{Na}_2 - \text{Br}$ reaction.

"On the BiF Bond Dissociation Energy and Evaluation of the BiF Red Emission Band Systems", with T. C. Devore, L. Brock, and K. Dulaney, *Chemical Physics*, in press.

- 19.
20. R. W. Schwenz and J. M. Pearson, *J. Chem. Phys.* 73 (1980) 259.
21. P. Baltayan, F. Hartmann, J. C. Pebay-Peyroula, and M. Sadeghi, *Chem. Phys. Lett.* 120 (1988) 123. M. Sadeghi - private communication of unpublished results.

APPENDIX VII

"Chemically Driven Pulsed and Continuous Visible Laser Amplifiers and Oscillators", K. K. Shen, H. Wang, D. Grantier and J. L. Gole, Invited Talk, Proceedings of the 23rd AIAA Plasma-Dynamics and Laser Science Conference, Nashville, Tennessee, AIAA 92-2994 (1992).



AIAA 92-2994

**Chemically Driven Pulsed and Continuous
Visible Laser Amplifiers and Oscillators**

J. L. Gole, K. K. Shen, H. Wang, and D. Grantier
School of Physics, Georgia Institute of Technology
Atlanta, GA 30332

**AIAA 23rd
Plasmadynamics & Lasers Conference
July 6-8, 1992 / Nashville, TN**

CHEMICALLY DRIVEN PULSED AND CONTINUOUS VISIBLE LASER AMPLIFIERS AND OSCILLATORS

J. L. Cole, K. K. Shen, H. Wang, and D. Grantier
School of Physics
Georgia Institute of Technology
Atlanta, Georgia 30332

ABSTRACT

We outline procedures to develop the first visible chemical laser amplifiers and oscillators. Correlated with a brief outline of the principles of laser action, we discuss two approaches to the formation of electronically inverted atomic and diatomic configurations based on (1) highly efficient near resonant intermolecular energy transfer and (2) highly efficient and selective fast direct chemical reaction. Using a very near resonant energy transfer from selectively formed metastable states of SiO and GeO ($a^3\Sigma^+$, $b^3\Pi$) to select metal atoms, we form thallium, gallium, sodium, and potassium atom laser amplifiers at $\lambda = 535, 417, 569, 818, \text{ and } 581 \text{ nm}$. The metastable triplet states are generated in high yield from the Ge-O₃, Si-N₂O, and Si-NO₂ reactions. The energy stored in the triplet states is transferred in a near resonant process to pump $X^2P_{1/2}$ Tl or Ga atoms to their lowest lying $2S_{1/2}$ states, and $X^2S_{1/2}$ Na(K) atoms to their lowest excited $3d^2D$, $4d^2D$ ($5d^2D$ in potassium), and $5s^2S$ ($6s^2S$) states. Adopting a pumping sequence in which a premixed Group IV A metalloid-receptor atom combination is oxidized, we observe a system temporal behavior which suggests the creation of a population inversion producing a gain condition in the Tl, Ga, Na, and K systems and forming the basis for full cavity oscillation on the Tl $7^2S_{1/2} - 6^2P_{3/2}$ transition at 535 nm and the Na $4d^2D - 3p^2P$ transition at 569 nm. Concepts employed to create amplification and oscillation in these systems are also applicable to the efficient energy transfer pumping of potential amplifying transitions in the lead (Pb), copper (Cu - analog of Cu vapor laser), and tin (Sn) receptor atoms. Based on the successful production of visible chemical laser amplifiers from direct selective chemical reaction we seek to develop and scale chemically driven visible and ultraviolet lasers. Amplifiers are to be produced using the highly efficient and selective formation of alkali dimer, $M_2 = Na_2, (Li_2)$, excited states from the alkali trimer-halogen atom ($M_3 - X(Cl, Br, I)$) reactions. These chemical laser amplifiers have already employed the extremely high cross section $Na_n (n=2,3) - X(Cl, Br, I)$ reactions to create a continuous electronic population inversion based on the chemical pumping of sodium dimer (Na_2). Optical gains through stimulated emission has been demonstrated in select regions close to 527, 492, and 460 nm with potential extension to the $\sim 412.5, \sim 365, \text{ and } \sim 350 \text{ nm}$ regions. Results obtained are in close analog to optically pumped alkali dimer lasers. A model which invokes the vibrational and rotational selectivity inherent to a dissociative ionic recombination process ($Na_3^+ + X^- \rightarrow Na_2 + NaX$), in correlation with the coupling between select sodium dimer excited states, may provide a semiquantitative explanation of the observed behavior. The observed gain (max. of 4% at $\sim 527 \text{ nm}$ corres. to $8 \times 10^{-3}/\text{cm}$ for individual

rotational levels) can be enhanced considerably with a more versatile source configuration. The considered amplifiers are being optimized and modeled with a focus to increasing amplifier gain length and amplifying medium concentration so as to facilitate their conversion to visible chemical laser oscillators. The study of additional analog systems suggests that the two concepts considered will be generic.

INTRODUCTION

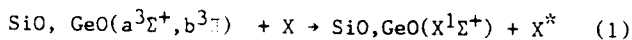
While there are a plethora of highly exothermic chemiluminescent reactions, only a small fraction of these show the promise of producing electronically inverted population distributions. We have employed certain unique aspects of a very select group of high excited state quantum yield, highly exothermic, metal and metalloid oxidations in order to develop what appear to be the first chemically driven laser amplifiers (and oscillators) operative in the visible spectral region.¹ One class of these systems operates in a pulsed configuration relying on ultrafast near resonant intermolecular energy transfer² from metastable storage states formed in chemical reaction as a pump for subsequently amplifying atomic receptors. A second system operates on the direct chemical pumping of sodium dimer (Na_2) in close analogy to optically pumped alkali dimer lasers.

High quantum yield, highly exothermic, simple metal or metalloid oxidation reactions, which involve a branching to long-lived metastable states, show the promise of creating an energy storage medium to pump atomic transitions with an established high propensity for lasing action. This hybrid approach attempts to circumvent the problems associated with short-lived electronic transitions taking place on a time-scale much faster than the typical reactive mixing in a chemical laser cavity (in contrast to infrared transitions) and the weak coupling of the photon flux associated with long-lived metastable electronic transitions to a laser cavity (low Q). To accommodate the desired pump sequence, we have developed techniques to form copious quantities of the metastable SiO and GeO $a^3\Sigma^+$ and $b^3\Pi$ states as the products of the primarily spin conserving Si-N₂O,³ Si-NO₂,⁴ Ge-N₂O, and Ge-O₃ reactions. These long-lived triplet states act as an energy reservoir for fast near resonant intermolecular energy transfer to efficiently pump atomic transitions. Using this approach we have obtained short-lived pulsed amplification and oscillation from atomic thallium at 535 nm (gain coeff. $\alpha \geq 2.5/\text{cm}$)^{2,5}. We have extended this concept to the pumping of sodium and potassium atom transitions which show the promise of producing higher duty cycle operation, and have now demonstrated continuous gain and potential low-level oscillation in the Si-SiO-Na system at 569 nm.

We have also been concerned with the development of the high cross section, highly exothermic $\text{Na}_2\text{X}(\text{Cl}, \text{Br}, \text{I})$ reactions as they selectively form Na_2^* in several of its excited electronic states. The demonstrated chemical laser amplifiers must rely on the extremely high cross section Na_n ($n=2,3$) + $\text{X}(\text{Cl}, \text{Br}, \text{I})$ reactions to create a continuous electronic population inversion based on the chemical pumping of sodium dimer (Na_2). Optical gain through stimulated emission has been demonstrated in the regions close to 527, 492, and 460.5 nm. Results in close analog to optically pumped alkali dimer lasers are noted, the pumping now being demonstrated for the first time in a purely chemical environment.

CHEMICALLY DRIVEN VISIBLE LASER TRANSITIONS FROM ULTRAFAST ENERGY TRANSFER

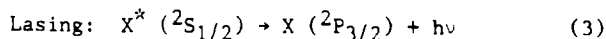
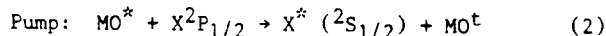
One might envision those SiO and GeO " $a^3\Sigma^+$ " and " $b^3\Sigma^-$ " metastable states (lifetimes between 10^{-1} and 10^{-2} seconds) formed in the $\text{Si-N}_2\text{O}$,³ Si-NO_2 ,⁴ and Ge-O_3 ^{1,2} reactions as a combined metastable triplet state reservoir which is, at best, weakly coupled to the ground electronic $X^1\Sigma^+$ state of the metal oxide (minimal nonradiative transfer). This reservoir can be maintained and can be made to transfer its energy to pump an atom of interest if a near resonant energy transfer is feasible. We make use of an efficient intermolecular energy transfer process



where X^* represents the electronically excited atomic species from which we wish to obtain lasing action. The success of this outlined scheme depends on the rates for the reactions forming the SiO or GeO metastables⁶ and the rate of the $\text{MO}^* (\text{M}=\text{Si}, \text{Ge}) - \text{X}$ intermolecular energy transfer, strongly influenced by near resonances between the MO^* and X^* energy levels. The amplifiers which are of interest operate on a variety of duty cycles dictated primarily by the radiative and collisional quenching associated with the electronic transitions of those receptor atoms forming the amplifying medium. While the potentially lasing atomic transitions may constrain the system to operate in a short pulsed configuration similar to the nitrogen laser, this duty cycle might be considerably enhanced in favorable situations.

The Thallium System

Initially, the Group IIIA metal thallium, was chosen as a promising candidate for the transfer scheme considered because this atom has a regular ground electronic 2P state with a substantial spin-orbit splitting (7792.7 cm^{-1})⁷ and an excited $^2S_{1/2}$ upper state in near resonance with the SiO and GeO triplet states. In addition, photodissociation lasers involving the corresponding upper $^2S_{1/2}$ atomic state were already known for all of the Group IIIA atoms, these operating on the strongly allowed $^2S_{1/2} - X^2P_{3/2}$ transition and producing laser action⁸ at 417 (Ga), 451 (In) and 535 nm (Tl). We make use of the scheme (Figure 1(a))



Here, the metal oxide excitation is transferred to the Group IIIA atom, pumping from the $X^2P_{1/2}$ to the energetically accessible electronically excited $^2S_{1/2}$ level, this level subsequently undergoing the (potential laser) transition $^2S_{1/2} - X^2P_{3/2}$ to what corresponds to an initially sparsely populated $^2P_{3/2}$ spin orbit component ($N_{3/2} \leq e^{-10} (N_{1/2})$ at $T \leq 1100\text{K}$) in the Tl system.

The efficiency of the outlined process for $\text{X} = \text{Tl} (^2P_{1/2})$, which does not react to form the metal monoxide, is such that a "superfluorescent" laser spike (Fig. 1(b)) some 10 times the normal $^2S_{1/2} - ^2P_{3/2}$ fluorescent intensity is generated on less than a 5ns time scale.⁹ As the population of the $P_{3/2}$ metastable level builds in this system, the $^2S_{1/2} - ^2P_{3/2}$ population inversion is lost and lasing ceases. The signal level in the remainder of the temporal scan corresponds to $^2S_{1/2} - ^2P_{3/2}$ fluorescence. This system is similar to the self-terminating nitrogen laser, however, in contrast, we observe superfluorescence as opposed to amplified spontaneous emission (ASE). A similar albeit much less pronounced effect is observed when gallium replaces thallium,² however, the energy transfer pumping of indium atoms by SiO and GeO metastables is found to be considerably less efficient. In contrast to the Tl or Ga systems where, to first order, the energy gap is less than 250 cm^{-1} , the closest indium levels are separated by more than 500 cm^{-1} from the potential SiO or GeO energy storage levels. No evidence for amplification is found in the indium system. The potential for near resonant transfer is clearly quite important in these systems.

We have also extended the Tl atom laser amplifier concept to develop the corresponding laser oscillator. In a stable resonant cavity intermediate to a near planar - near confocal configuration ($g_1=g_2=17/20$) with 3% output coupling, we obtain a substantial increase in output power ($\sim 10\times$) accompanied by a substantial increase in the ratio of superfluorescence to fluorescence (≥ 100 (Fig. 1(c)) versus the single pass amplifier. This output is obtained with up to three passes through the amplifying medium in the time scale over which the population inversion is maintained^{2,9,10} ($\sim 3-5 \text{ ns}$). Amplification and oscillation are obtained with high reactant concentrations ($\text{Si}(\text{Ge}) \geq 2 \times 10^{14}/\text{cm}^3$, $\text{Tl} \geq 1 \times 10^{16}/\text{cm}^3$, oxidant $\geq 5 \times 10^{14}/\text{cm}^3$)² and only in those systems in which the Si or Ge and Tl are premixed before the oxidation - energy transfer - amplification cycle is initiated.² The results obtained are in excellent agreement with the study of "superradiance" in Tl discharges by Isaev and Petrash.⁹

The Thallium Laser Amplifier and Oscillator as a Basis for Comparison

The nature of the thallium laser amplifier and oscillator we have developed in our laboratory is discussed in detail elsewhere,² however, it is important that we summarize the attributes, characteristics, and disadvantages of this system for the comparative assessment of additional candidate systems. The Ge-GeO-Tl system must be triggered by the oxidation of premixed $\text{Ge}(\text{Si})/\text{Tl}$ at concentrations exceeding $10^{15}/\text{cc}$.^{2,11} The threshold for lasing⁸ on the $\text{Tl } ^2S_{1/2} - ^6P_{3/2}$ transition is

low, the potential for a highly efficient near resonant ($\Delta E \leq 250 \text{ cm}^{-1}$) pump of ground state Tl $6^2P_{1/2}$ atoms to the $7^2S_{1/2}$ excited state is manifest, and the formation of TlO is precluded (unlike the gallium system) so as to considerably minimize interference with the formation of SiO and GeO metastables. These advantages are, however, balanced by the short radiative lifetime associated with the $2^2S_{1/2}$ level and the metastability of the $P_{3/2}$ terminal laser level. The self-terminating, $\lambda = 535 \text{ nm}$, Tl laser amplifier is superfluorescent. Thus, the conversion of the Tl system to a laser oscillator, strongly influenced by the cooperation length¹² of the stable cavity configurations employed in this effort, produces an output obtained with up to three passes through the amplifying medium on the time scale over which the population inversion is maintained^{2,9,10} ($\sim 3\text{-}5 \text{ ns}$). The Tl system is difficult to oscillate because of its short pulse mode. Further, because it is superfluorescent,¹² the output power obtained on full cavity oscillation does not greatly exceed ($\times 10$) the output for single pass amplification.

In response to the shortcomings inherent to the Tl atom system, a major focus of our continuing efforts has been to extend the near resonant energy transfer concept to atomic sodium or potassium as a means of forming higher duty cycle laser amplifiers, maximizing the efficiency of these created laser amplifiers, and subsequently optimizing these systems so as to produce efficient laser oscillators.

Extension of the Near Resonant Intermolecular Energy Transfer Concept to Fast Pumping of Na and K Atom Transitions

In order to compensate the disadvantages inherent to a Tl based laser system and to demonstrate the generic nature of the outlined approach, we have extended the near resonant energy transfer concept to atomic sodium and potassium as a means of forming higher duty cycle laser amplifiers and oscillators. By choosing the Na and K based systems, we focus on longer-lived emitters¹¹ as a means of enhancing energy storage in the laser cavity. In this respect, the more nearly energy transfer resonant (SiO or GeO metastables) Na system energy levels, partially outlined in Fig. 2, are well suited. Here, in developing this system and its potassium analog, we not only take advantage of the chemical pumping of the considerably longer lived 2^2S or 4^2D levels of the sodium atom but also we replace the metastable Tl $2^2P_{3/2}$ state (Fig. 1), the terminal laser level in our amplifier-oscillator concept, with a rapidly depleted low-lying electronic state corresponding to the upper level of the Na D-line transition.

Oscillator strengths for transitions among the Na levels depicted in Fig. 2(a) are catalogued and compared to Tl in Table 1.¹³ To an even greater degree than the Tl and Ga systems, a near resonant energy match up to the receptor atoms of interest certainly prevails in the Na and K systems where both metastable SiO and GeO can be used to energy transfer pump from the $3s^2S$ Na ground state ($4s^2S$ in K) to the $4d^4D$ and $5s^2S$ levels ($5d^4D$ and $6s^2S$...in K). In the Tl system laser action is terminated through the filling of the $P_{3/2}$ level, however, in the sodium system (Fig. 2(a)) the

terminal laser level is the extremely short-lived upper level of the Na D-line. The $3p^2P - 3s^2S$ transition is characterized by a high oscillator strength facilitating rapid loss of the terminal laser level to create ground state sodium atoms which Figs. 2(a) and 2(b) demonstrate are again amenable to near resonant energy transfer pumping. While the $5s^2S$ and $4d^4D$ levels are not readily accessed in an optically pumped transition, Fig. 2(b) demonstrates that, using SiO metastables formed in the Si-N₂O reaction, we have now successfully energy transfer pumped Na atoms to the 2^2S and 4^2D levels where they subsequently emit radiation at $\lambda \sim 616 \text{ nm}$ and 569 nm as they undergo transition to the $3p^2P$ levels. These transitions are characterized by moderate to small oscillator strengths. The assessed Na cycle with its 50^{13} to 100^{13} nanosecond upper state radiative lifetimes (vs. Tl $2^2S_{1/2}$ at $\sim 7 \text{ nsec}$.¹³) and short-lived terminal laser level would appear ideally suited to obtain high duty cycle laser amplifiers and oscillators. Also, as indicated in Figure 2(a), we have obtained evidence for the energy transfer pump of the Na $3d^2D$ level with which is associated an atomic emission at $\lambda \sim 819 \text{ nm}$ ascribed to the Na $3d^2D - 3p^2P$ transition. Both the transitions at $\lambda \sim 569 \text{ nm}$ ($\alpha_{\text{max}} \approx 0.27/\text{cm}$)¹⁴ and $\lambda \sim 819 \text{ nm}$ ($\alpha_{\text{max}} \approx 0.04/\text{cm}$) demonstrate gain.

In approaching the outlined laser schemes, self absorption associated with the Na D-line must be considered. Evidence is obtained for moderate self-absorption in the present experiments, however concern with the possible deleterious effect which such a pumping of the Na D-line might have on transitions terminating in the $3p^2P$ level is greatly alleviated by the Na discharge experiments of Tibilov and Shukhtin¹⁵ which demonstrate a surprising¹⁵ lasing action on the Na $4s^2S - 3p^2P$ transitions in the infrared region.

Configuration for Gain Measurement

Gain measurements have been carried out on the sodium system using three different experimental configurations. The simplest of these measurements uses the optical train depicted in Fig. 3(a)¹⁶ surrounding either a short ($\sim 1\text{-}2 \text{ cm}$) reaction - energy transfer - amplification region^{2,11} or a recently constructed $\sim 5 \text{ cm}$ amplification zone associated with the larger scale cavity configuration depicted in Fig. 4. The optical train parallels the ingenuous design of Roll and Mentel¹⁶ to measure new laser lines in Se II employing amplified spontaneous emission (ASE). The gain coefficient α , can be calculated from

$$\alpha = \ln((I_2 - I_1)/I_1 R T^2) \quad (4)$$

where L is the effective gain medium length, I_1 is the single pass ASE intensity and I_2 is the double pass ASE intensity, R is the mirror reflectivity, and T is the transmission of the "cavity" vacuum chamber window in front of the mirror (this can also be a Brewster angle window).

A second series of more complex gain measurements have also been carried out employing the configuration depicted in Figure 5 and the long path length configuration depicted in Figure 4. Here, we have employed the output from a sodium discharge lamp at $\lambda = 569 \text{ nm}$ to measure gain on the

Na $4d^2D - 3p^2P$ transition. The enhancement of the Na $4d^2D - 3p^2P$ emission line (or other sodium transitions) can be evaluated by singling out the transition of interest with a 10 nm bandpass filter. This output is then beam-split into two paths, one of which passes through the amplification zone. We then evaluate the A-B signal channel in a standard AC lock-in detection mode. Using this configuration we predict gains which are believed to represent lower bounds to the true values due to the significant radial extent (cross sectional area) of the lamp output intersecting the mixing zone and gain medium. Finally, the sodium lamp can be replaced by the output from a high resolution (0.007cm^{-1}) ring dye laser to carry out laser gain measurements in a frequency scanning (laser with calibration vs. iodine) mode.

Amplification Zone Extension

The cavity configuration depicted in Fig. 4 has been constructed to facilitate conversion of an original ($\sim 1\text{cm}$) reaction - energy transfer - amplification zone cavity configuration to a considerably more versatile and longer path length device. This construction can take advantage of three entrainment flow configurations for silicon or germanium in the cycle producing SiO and GeO metastables, one of which is depicted in Fig. 4. These flow configurations produce the longest path length SiO metastable flame ($\sim 5 + \text{cm}$) ever obtained. The entrainment flow configuration must be designed to create large concentrations of SiO (GeO) metastables which are intersected at $\sim 90^\circ$, in subsonic flow, by a high concentration of sodium or potassium atoms. The entrained silicon and sodium flows can also be moved in-situ relative to each other and hence with respect to the reaction - energy transfer - amplification zone to optimize conditions for formation of the gain medium.

Our focus in continually improving the system must be, in large part, on the optimization of reactant mixing considering the rate limiting effect of the silicon concentration, the importance of virtually complete sodium atomization, and the confinement of the reactants and receptors to the cavity axis region. Further, we must insure that the reactant and entrainment flows (reaction zones) are controlled so as to protect the cavity windows from the condensation of metastable silicon or germanium oxide and/or sodium or potassium. This latter requirement is met (Fig. 4), in part, using "self cleaning" optical windows¹⁷ with a protective helium (not argon) flow. The "rate limiting" silicon concentration signals a focus on the modification of the oven source configuration depicted in Figure 4 so as to continually improve the silicon atom flux as well as the flow conditions whereby this reactant is transferred to the reaction-energy transfer-amplification zone. As such, we must be concerned with the evaluation and improvement of reactant flow patterns in the cavity as well as with the simultaneous improvement of the optical train surrounding the reaction zone.

The mixing zone of Fig. 4 is greatly stabilized by the moderate sized (15 cubic feet) ballast separating the 150cm pump and reaction chamber. The current 90° intersection of the SiO (GeO) and Na atom flows, once stabilized, can be used to clearly establish a continuous lasing

action, however, this is by no means the ideal mixing configuration. We are currently constructing a concentric as opposed to 90° SiO-Na intersection region. Once in place, this configuration should further improve the results which we outline in the following paragraphs.

Gain Measurements

A readily reproducible result obtained using the optical train depicted in Fig. 3(a) for gain measurement (Roll-Mentel configuration) is presented in Figure 6. Here, the scan (a) corresponds to single pass ASE (I_1 in Eq. 4) obtained with a shutter placed in front of the high reflector in Figure 3(a) whereas the scan (b) depicts the double pass ASE intensity (I_2 in Eq. 4) measured with the high reflector open to and aligned with the gain medium (see below). The coarse alignment of both the gain and cavity configurations depicted in Fig. 3 is accomplished with a HeNe laser positioned ~ 15 feet from the cavity.

The stark change in the relative intensities of the 569 nm Na $4d^2D - 3p^2P$ and Na D-line emissions for the single and double pass ASE output is quite evident in Figure 6. The ratio of the double to single pass intensity for the 569 nm feature depicted in Figure 6 is 2.6/1, however, this is by no means the optimal value that has been achieved. Under optimal operating conditions, using a 1" diameter 99.9% high reflector,¹⁸ we have achieved conditions such that the ratio of light output when the rear high reflector is accessed to that when the rear high reflector is blocked ranges consistently from 3.4 to 3.8. This is a ratio which demonstrates clear gain and should be compared with (1) the ratio for pure fluorescence (Na D-line and higher lying Na transitions) which is usually between 1.1 and 1.2 for the Na D-line and has never exceeded 1.6 for any other Na fluorescence features, and (2) the theoretical maximum value for the ratio expected for pure fluorescence in a high Q cavity which is 2. The results, obtained under conditions when the cavity has not reached the gain threshold demonstrate that there are significant cavity losses over the 44 cm path of the optical configuration.

We are currently working to further minimize cavity losses. The Na atom transitions at $\lambda \approx 569$ nm ($\alpha_{\text{cavity}} \sim 0.1-0.15/\text{cm}$), $\lambda \approx 616$ nm ($\alpha_{\text{cavity}} \sim 0.03-0.05/\text{cm}$), and $\lambda \approx 819$ nm ($\alpha_{\text{cavity}} \sim 0.02-0.03/\text{cm}$) have all been shown to demonstrate gain. The value of α at 569 nm should be compared to that obtained using the Na lamp based gain measurement technique and experimental configuration depicted in Fig. 5. Here a bandpass filter is used to select the 569 nm output from the lamp. In this mode we determine a lower bound to the gain per pass at 569 nm as the cross sectional area of the Na lamp input to the reaction zone considerably exceeds that of the optical train. When the 569 nm light exciting the gain medium is focused onto the entrance slit of the spectrometer, the measured gain is diluted by the mismatch in cross-sectional area. We measure a calibrated gain in excess of 5%/pass through the amplification zone.

Full Cavity Measurements

We replace the gain measurement system with a full mirror laser cavity configuration in which the output coupling (1" diameter mirror) exceeds 4.5% and we employ the same 1" diameter 99.9% high reflector as used in the gain evaluation studies. With the same gain medium, up to 5 cm in length, and a cavity, 44 cm in length, operating in a stable configuration ($g_1 g_2 \sim 0.56$), we achieve results which, to first order, demonstrate the potential for cavity oscillation. Upon tuning the output coupler and high reflector after adjusting the mixing Si, N_2O , and Na flows, we achieve conditions, at low to moderate sodium flux, such that the ratio of the full cavity output to single pass amplification is between 20 and 25/1 in an apparently steady state mode. These experiments were carried out using the particular reactive flow configuration depicted in Fig. 4. The ratio for full cavity enhancement was determined by blocking the rear high reflector and measuring the output relative to that for the full cavity. Walking the cavity mirrors (angle tuning) destroyed the amplification. Upon realignment, similar increases in intensity at the steady state value were again observed. It must be emphasized that these results are sharply dependent on the angle tuning of the cavity. By comparison, when using the reaction - amplification zone configuration of Fig. 4 when only a fluorescent medium associated with the $4d^2D - 3p^2P$ Na transition is formed, as evidenced by gain measurements at 569 nm and at the Na D-line, we find a typical steady state enhancement between 1.2 and 1.4.

The 4.5% output coupler presents a substantial loss in the present mode of operation. If we replace this output coupler with a 0.2% output coupler and operate the system under near optimum reactive flow conditions in a stable cavity configuration with $g_1 g_2 \sim 0.82$, we find that the ratio of the output for full cavity operation to that obtained with a blocked high reflector (Figure 7) easily exceeds $10^3/1$. Further, the ratio of output power for the 4.5% output coupled configuration to that for the 0.2% output coupled configuration is only 1.9/1. The corresponding ratios obtained for pure fluorescence using the 0.2% output coupled cavity were close to 2 for a number of Na atom transition features and greater than 1.8 for the Na D-line. These latter ratios are typical of the measured behavior when conditions in the reaction-amplification zone are such that the cavity reactive flow environment does not produce a gain condition. We have also observed intermediate behavior associated with the establishment of moderate but not optimal gain conditions. For these intermediate ranges the ratio of outputs is found to vary from 50 to 200/1. These results taken collectively would suggest the observation of low-level continuous oscillation.

While the results we have obtained are quite promising, there is room for considerable improvement. It remains to increase both the Si and Na atom concentration in the reaction zone while maintaining atomization. This increase may lead to a leveling off and eventual loss of the gain condition if self-absorption on the Na D-line transitions becomes a dominant factor or SiO triplet self quenching begins to play a deleterious role.

Evidence is obtained for some self-absorption at high sodium concentration when the atom production dominates the concomitant SiO metastable production; however, concern with the possible deleterious effect which such a pumping of the Na D-line might have on transitions terminating in the $3p^2P$ level is somewhat alleviated by the Na discharge experiments of Tribilov and Shukhtin.¹⁵

Extensions to Additional Energy Transfer Pumped Atomic Receptors

While our continued emphasis has been on the sodium system and the results presented involve a metastable SiO pump, it is also feasible to use GeO metastables for energy transfer pumping. In fact, we have obtained evidence that the energy transfer pumping of the sodium analog potassium based amplifiers associated with the $5d^2D - 4p^2P$ ($\lambda = 581, 583$ nm), $4d^2D - 4p^2P$ ($\lambda = 694, 697$ nm), and $6s^2S - 4p^2P$ ($\lambda = 691, 694$ nm) potassium atom transitions might best be accomplished with pumping by GeO metastables. We hope to pursue these experiments.

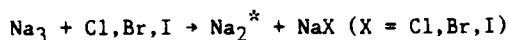
We have also successfully energy transfer pumped potential amplifying transitions in lead (Pb), copper (Cu), and tin (Sn) receptor atoms. Two of these systems are particularly intriguing. Figure 8 demonstrates the results we have obtained when using SiO metastables ($Si-N_2O$) to pump lead receptor atoms. Observed Pb transitions are indicated to the right of the figure. First, we notice that self absorption involving ground state Pb atoms is so dominant that no emission to the X^3P_0 ground state is observed. Second, we find significant pumping of both the $1S_0$ and $1D_2$ levels. The corresponding transitions from the $1S_0$ level terminate in the lowest X^3P_2 (531.2 nm) and X^3P_1 (462 nm) levels. It is thought that collisional quenching and relaxation of the $1S_0$ level will be minimal relative to that of the X^3P manifold.¹⁹ This may lead to potential inversions and amplification at $\lambda = 462, 531$ nm.¹⁹ The well known lead laser transition at $\lambda = 723$ nm²⁰ with an A value $\sim 10^6$ sec⁻¹ terminates on the $1D_2$ level. Surprisingly, we find no evidence for this transition which emanates from the upper $3P_1^o$ level (Fig. 8). We do find evidence for the $3P_1^o - X^3P_1$ and $3P_1^o - X^3P_2$ transitions and for the $1D_2 - 3P_1$ transition at 733 nm.²¹ This suggests that the $3P_1 - 1D_2$ transition may be self-absorbed due to a significant $1D_2$ population. If we have observed the manifestation of a substantial $1D_2$ population does this result from direct energy transfer pumping or is the $1D_2$ state populated by the 723 nm transition at times considerably shorter than the time scale for the present observations? This must be assessed in future experiments. The results obtained for the energy transfer pumping of lead atoms certainly suggest the possibility of additional amplifier systems. It is particularly encouraging that some of these may represent four level systems which obviate the self absorption bottleneck that may plague the Si-SiO-Na system at high Na concentration.

The near resonant energy transfer pumping of copper vapor is of interest not only because of the close analogy which it bears to the sodium and potassium systems but also, as Figure 9 indicates, because it is possible to energy transfer pump the

copper vapor laser transitions²² using metastable SiO (Si-SiO-Cu system). However, it is also of interest that the results demonstrated in Figure 9 were obtained using an approach which represents a significant extrapolation from the configuration² in which the "premixed" Tl/Ge mixture has been used to obtain pulsed amplification on the Tl $^2S_{1/2} - ^2P_{3/2}$ transition. Here, Si and Cu were premixed and co-vaporized from a single crucible. The resulting mixture was then oxidized to yield the observed energy transfer pumping spectrum depicted in Figure 9. It is worth noting that N₂O, used as the oxidant, produces a dark reaction with copper vapor. We thus find many intriguing variations on the thallium, gallium, and sodium based systems which we intend to pursue in the near future.

CONTINUOUS CHEMICAL LASER AMPLIFIERS IN THE VISIBLE REGION BASED ON HIGHLY EFFICIENT AND SELECTIVE CHEMICAL REACTION

The optical signatures for the processes



encompass emission from a limited number of Na₂ band systems. Surprisingly, the observed emission is characterized by sharp well defined emission regions¹ (Figures 10,11) superimposed on a much weaker perceptible and analyzable Na₂ background fluorescence. As Fig. 11 demonstrates, these sharp emission features are not readily explained by invoking a purely fluorescent process.¹

The sharp nature of several of the B-X, C-X, and C'-X Na₂ fluorescence features (Fig. 10), their correlation in certain regions to the emission characteristic of optically pumped Na₂ laser systems²³ (ex: 528.2 nm (ν', ν'') = (6,14) B-X), and the near exponential growth of these features relative to the background Na₂ fluorescence spectrum with increasing Na₃ concentration, suggested the possibility that stimulated emission might be associated with certain of the emitting Na₂ reaction products. Laser gain measurements have been carried out to assess this possibility.

In order to carry out the gain studies, we further developed (Fig. 12(a)) a unique source configuration which allows the supersonic expansion of pure sodium vapor to create a Na₃ concentration not previously attained in a reaction-amplification zone. Using argon ion pumped dye lasers to study the Na₃ + Br reaction we have scanned (Fig. 12(b)) the entire wavelength region from 420 to 600 nm (Figure 10) in ~3 nm intervals at 0.5 cm⁻¹ resolution (FWHM)¹ and the regions around 527 nm and 460 nm (Fig. 11) at 0.007 cm⁻¹ resolution using a ring dye laser.¹ We find that laser gain and hence amplification is associated with very limited regions of the spectrum, the observations suggesting that several of the sharp emission features apparent in Figure 10 correspond to a stimulated emission process and to the establishment of a population inversion. Our ring dye laser studies demonstrate that the strong feature at ~527 nm (Fig. 11) appears to result from a stimulated emission process involving between four and seven unresolved rotational levels.

Optical gain through stimulated emission has

been measured at 0.5 cm⁻¹ resolution in the regions 527 nm (1% gain), 492 nm (0.3% gain) and 460.5 nm (0.8% gain), correlating precisely with the reactive process and the relative intensities of those features observed while monitoring the light emitted from the Na₃-Br and Na₃-I reactions (Figs. 10,11). High resolution ring dye laser scans in the 527 nm region indicate that the gain for the system is a minimum of 3.8% for an individual rovibronic transition with approximately four to seven individual rotational transitions showing gain. At 459.8 nm we have measured a 2.3% gain for an individual rotational transition. These results demonstrate the continuous amplifying medium for a visible chemical laser in at least three wavelength regions.¹ At no other scanned wavelengths have we observed gain. In fact, in scanning the 420-600 nm region, we generally observe slight losses of the laser photon flux due primarily to scattering (to only a negligible extent, absorption) on transit through the Na₃-Br reaction zone. In the region of the sodium D-line, a substantial absorption and hence loss is monitored as a function of the trimer-halogen atom reaction.¹

Because of the low Na₃ ionization potential and the high halogen electron affinities,²⁴ the Na₃-halogen atom reactions are expected to proceed via an electron jump mechanism with extremely high cross sections,²⁵ producing substantial Na₂ excited state populations. The question of why the Na₃-X reactions appear to demonstrate vibrational and rotational selectivity associated with certain wavelength regions may be dealt with by invoking a model for the dissociative ionic recombination, Na₃⁺ + X⁻ → Na₂⁺ + NaX, and the curve crossings which influence the distribution of product molecules for this process.²⁶ This model, coupled with an analysis of the electronic coupling between select sodium dimer excited states²⁶, may provide a semiquantitative explanation of the observed population inversions.

The created population inversions monitored thusfar are thought to be sustained by the large number of free halogen atoms reacting with the Na₂ molecules in those ground state levels on which the transitions emanating from the Na₂ excited states terminate and collisional relaxation of the ground state sodium dimer molecules. The cross section for reaction of vibrationally excited ground state Na₂ is expected to be quite substantial relative to the cross section for collision induced vibrational deactivation of the Na₂ manifold. Extremely efficient reactions greatly assist the depletion of the lower state levels in this system allowing one to sustain a continuous population inversion.

Our major efforts thusfar have focused on the Na₂ B-X spectral region and the potential development of laser oscillators at wavelengths in the vicinity of 527 and 460 nm. In order to approach these studies we are developing the means to create a considerably longer path length amplification region. This effort is outlined in the following section. We are also concerned with the extension of these studies further into the ultraviolet region primarily as they access states of considerably longer radiative lifetime.

The Na₂ ~395, ~365, and ~350 nm emission regions depicted in Fig. 13 represent a portion of

the optical signature for the $\text{Na}_3\text{-Br}$ reaction. They are of interest for they correspond again to sharp emission features superimposed on a broader weak background. Their appearance cannot be readily explained in terms of an easily understood fluorescent process. The features are tentatively associated, at least in part with a very recently ascribed double minimum excited electronic state²⁷ ($2^1\Sigma_u^+ - X^1\Sigma_g^+$) of the sodium dimer molecule. The radiative lifetimes associated with this double minimum state are complex and longer ($\sim 40\text{ns}$) than those associated with the $\text{Na}_2\text{ B-X}$ region. These longer lifetimes might be used advantageously to enhance the potential energy storage in a laser cavity. This, in turn, suggests that the laser gain studies already performed in the visible region should be extended in order to assess the feasibility of using $2^1\Sigma_u^+ - X^1\Sigma_g^+$ transitions as the source of laser amplifiers extending far into the ultraviolet.

Development of an Extended Path Length $\text{Na}_3 - \text{X}$ (Cl, Br, I) Reaction - Amplification Zone

We desire to considerably improve the magnitude of the amplification demonstrated previously for sodium dimer amplifiers at ~ 527 , ~ 492 , and $\sim 460\text{ nm}$. The apparatus depicted in Figure 12 now produces a substantial Na_3 concentration ($\geq 10^{13}/\text{cc}$) albeit in a limited reaction-amplification zone. In order to demonstrate continuous chemical laser oscillation, however, it is desirable to create an enhanced sodium trimer-halogen atom reaction zone not only in terms of reactant concentration but also with respect to the amplification zone path length. The overall apparatus design depicted in Figure 14 is meant to accommodate high intersecting reactant flows from both sodium trimer and (dual rotatable) halogen atom sources in order to produce a considerably enhanced concentration of Na_2 amplifiers over a significantly extended path length relative to that previously obtained. With this ultimate goal, we are constructing a system which attempts to increase the Na_3 reaction - amplification zone concentration by repositioning the trimer and halogen atom sources relative to each other and facilitating the halogenation process much closer to the alkali nozzle itself, in a gas dynamic configuration. We also incorporate the facility for the in-situ adjustment of the alkali and halogen source positions. This includes the ability to rotate dual alkali-trimer-flow-encompassing halogen atom slit sources (Figs. 14(b), 14(d)) so as to optimize flow mixing. Further, as a means of increasing the reaction zone and gain length we have developed and are testing a continuous flow slit source technology to create at least a 5cm long amplification zone.

Figure 14(a) exemplifies in schematic one of the moderate temperature slit source configurations which we will use to supersonically expand either pure or seeded sodium vapor. These slit sources have a capacity between four and eight times that of the design diagrammed in Figure 12.¹ The small circular "pinhole" nozzle used in the design of Figure 12 is now replaced by a slit approximately 100μ in width by $2\frac{1}{2}"$ in length. The overall design pictured in Fig. 14(a) in side and partial frontal view corresponds to a full seeded configuration. Here helium or argon can be passed

through the diverging gas source assembly, flowing over molten sodium, the mixture then being expanded through the frontal nozzle slit configuration. In a pure sodium supersonic expansion, the Na_3 constituency is dominated by a much larger atom and cold dimer concentration.²⁹ These constituents do not interfere at the Na_2 amplifier wavelengths characteristic of the Na_3 -halogen atom reaction systems, however, it is desirable to minimize the atom and dimer while increasing the trimer concentration. The trimer concentration can be altered and improved through an appropriate adjustment of the supersonic expansion conditions shifting the distribution to higher sodium polymers. By seeding the expansion with helium, argon, or other noble gas atoms several researchers³⁰ have demonstrated that the atom and dimer concentrations can be made quite small relative to the much larger sodium polymers.³⁰ We do not wish to operate at these extreme expansion conditions but, rather, seek a middle ground which will allow us to produce primarily the trimer and a few larger clusters.³¹ This condition can be accomplished through the appropriate adjustment of parameters which can be manipulated in the expansion including (1) the rear oven stagnation pressure (argon + sodium), (2) the frontal nozzle temperature, and (3) the ratio of the supersonic expansion source pressure to the overall expansion chamber pressure.

The oven stagnation chamber capacity of the slit source depicted in Figure 14 considerably exceeds that of the design indicated in Fig. 12. The rear stagnation oven and frontal nozzle unit operate independently and are heated using separate wrappings of thermocoax. The slit attachment depicted in the figure is a single unit. Although we anticipate that this slit configuration and its replacements will operate for several experimental runs, we have also constructed recyclable slit designs which employ replaceable razor blades to create the desired expansion orifices. The slits, which will be described elsewhere,²⁸ use a double pressure fit construction connected to the nozzle channel.

In the overall experimental design depicted in Figure 14, the sodium slit source, connected to a liquid nitrogen cooled bulkhead apparent in the figure, is positioned relative to the dual halogen slit sources located above and below what we envision as the position of an alkali sheath created upon expansion from the alkali slit source. The halogen atom slit sources constructed from T6 graphite can be heated to temperatures in excess of 1500K to insure the efficient dissociation of halogen molecules. They are designed to optimize the interaction of the alkali trimer and halogen atoms over the entire width of the intersecting reactant sheaths created as the dual halogen flow intersects the alkali constituency. The optical train defining the laser cavity, encompassed on each end by self cleaning optical windows as indicated in Fig. 14(b), is parallel to the intersection of the alkali and halogen flows. This reaction zone cavity configuration is designed to allow for 1) short transit of the reactants Na_3 and $\text{X} = \text{Cl, Br, I}$ to the reaction - amplification zone, 2) flexible movement of these sources with respect to each other and with respect to the flow patterns created in the system and 3) minimal interaction of these reactants with laser cavity windows. To

insure this minimal interaction, the self-cleaning optical windows noted previously⁷ are used.

The reaction zone is to be evacuated through a 35 cubic foot ballast tank followed by a 1250 CFM Stokes - Roots-Blower combination. The reaction zone and cavity chamber can be isolated from the ballast + pump combination using a gate valve assembly. This assures the capability for ready separation of the cavity after a run and facilitates leak testing and repair of the isolated cavity using a considerably smaller pumping system. The cavity, itself, is mobile and can be removed, after experimentation, for cleaning.

Through a repositioning of the alkali and halogen reactant sources to close proximity, one can create a significant improvement in the Na_3 concentration in the reaction zone over that which already produces a concentration of Na_2 necessary to obtain amplification. This is further improved with the large capacity sodium slit source configuration. While it will be possible to operate the new cavity with a pure metal supersonic expansion for periods at least comparable to those used previously, a notable additional improvement is obtained by converting the system to high metal mole fraction seeded supersonic mixed sodium-helium (argon) expansion so as to substantially increase the sodium trimer concentration relative to that obtained in pure sodium expansion.

Extension of the Na_3 - $\text{X}(\text{Cl}, \text{Br}, \text{I})$ Amplifier Concept

The Na_2 amplifiers which we have characterized in the visible region operate on bound-bound transitions. It is not difficult to envision an extrapolation on the Na_3 - X reaction concept which involves the alkaline earth metal trimers and the formation of excited state dimers which can undergo bound-free excimer transitions. With this focus, we are attempting to generate the M_2 excimer analogs of the Na_2 laser amplifiers discussed previously. The ground electronic state of Mg_2 is very weakly bound,³² however, detailed calculations suggest the Mg_2 - Mg bond strength may be on the order of 0.6 eV,³³ quite comparable to that of Na_3 . We are now forming magnesium molecules, specifically Mg_2 and Mg_3 , and observing the excited state products of their oxidation with F and Cl atoms. A halogen atom discharge source which we have developed to study the $\text{Bi}_2 + \text{F}$ reaction³⁴ is being used to investigate the $\text{Mg}_2\text{-F}$, $\text{Mg}_3\text{-F}$, $\text{Mg}_2\text{-Cl}$, and $\text{Mg}_3\text{-Cl}$ reactions. These studies will soon be extrapolated to the heavier alkaline earths, Ca_x - Ba_x . To date, we have not observed strong Mg_2 emission from the Mg_3 - F, Cl reactions, however, surprisingly, preliminary results on this system signal the formation of excited state Mg_xF and Mg_xCl charge transfer complexes where x is most likely two. Although we have not yet demonstrated the potential for forming an Mg_2^* based excimer amplifier laser system, the creation of a long-lived Mg_xF complex suggests that, with some modification, this may be feasible.

The Na_2 amplifiers which we have demonstrated have been studied using the unique but not optimal source configuration depicted in Figure 12 which allows the supersonic expansion of pure sodium vapor to create a Na_3 concentration not previously attained in a reaction - amplification zone. In

excess of 100 grams of sodium are expended through a small nozzle orifice ($\leq 0.020''$) on a time frame of ~ 20 minutes to create a trimer reaction zone concentration well in excess of $10^{13}/\text{cc}$. These concentrations have been generated from a source positioned ~ 13.5 cm from the reaction - amplification zone which is within one centimeter of the halogen atom source. While this device may not be optimal for producing a chemical laser oscillator, it can be used to assess the potential for chemical laser amplifiers from the reactions of the lighter alkali metal trimer, lithium, or to evaluate the extension of the oxidant range to fluorine atoms. We have modified the apparatus for operation with molecular and atomic fluorine by installing a multistage alumina trap backed by a 150 CFM Kinney pump. Further, in order to operate with fluorine, we find that the carbon-based oven dissociation sources used with the heavier halogens must be modified using nickel tubing inserts. Finally, we have constructed molybdenum based double oven lithium supersonic expansion sources in order to test the viability of lithium trimer-halogen atom reactions as a means of producing lithium dimer chemical laser amplifiers.

ACKNOWLEDGEMENT

It is a pleasure to acknowledge most helpful discussions with Drs. R. Jones, Bill Watt, T. Cool, Stan Patterson, Rolf Gross, Sherwin Amamoto, John Dering, and E. Dorko concerning this study. The support of the Georgia Tech Foundation through a grant from Mrs. Betty Peterman Gole, the Army Research Office through the Short Term Innovative Research Program and the Air Force Office of Scientific Research - Army Research Office is greatly appreciated.

REFERENCES

1. W. H. Crumley, J. L. Gole, and D. A. Dixon, J. Chem. Phys. **76**, 6439 (1982). S. H. Cobb, J. R. Woodward, and J. L. Gole, Chem. Phys. Lett. **143**, 205 (1988). S. H. Cobb, J. R. Woodward, and J. L. Gole, Chem. Phys. Lett. **157**, 197 (1989). S. H. Cobb, J. R. Woodward, and J. L. Gole, "Continuous Chemical Laser Amplifiers in the Visible Region", Proceedings of the Fourth International Laser Science Conference, A.I.P. Conf. Proc. No. 191, Optical Science and Engineering Series 10, pg. 68.
2. J. R. Woodward, S. H. Cobb, K. K. Shen, and J. L. Gole, "A Chemically Driven Visible Laser Transition Using Fast Near Resonant Energy Transfer", in IEEE Journal of Quantum Electronics (Electronic Transition Gas Lasers, JOE **26**, 1574 (1990). J. R. Woodward, S. H. Cobb, and J. L. Gole, "Superfluorescent Chemically Driven Visible Laser Transitions Using Fast Near Resonant Energy Transfer", Proceedings of the Fourth International Laser Science Conference, A.I.P. Conf. Proc. No. 191, Optical Science and Engineering Series 10, pg. 63.
3. G. J. Green and J. L. Gole, Chemical Physics **100**, 133 (1985).
4. R. W. Woodward, J. S. Hayden, and J. L. Gole, Chemical Physics **100**, 153 (1985).
5. "A Chemically Driven Visible Laser Operative at

- 535 nm", K. K. Shen, S. H. Cobb, J. R. Woodward, and J. L. Gole, Chem. Phys. Lett., submitted.
6. P. M. Swearingen, S. J. Davis, and T. M. Niemczyk, Chem. Phys. Lett. 55, 274 (1978).
 7. C. E. Moore, "Atomic Energy Levels", N. B. S. Circular 467, Volumes I, II, and III. See also, R. W. F. Gross and J. F. Bott, Handbook of Chemical Lasers, Wiley and Sons, New York, 1976.
 8. S. Chilukuri, Appl. Phys. Lett. 34, 284 (1979). H. Hemmati and G. J. Collins, Appl. Phys. Lett. 34, 844 (1979). R. Burnham, Appl. Phys. Lett. 30, 132 (1977). D. J. Ehrlich, J. Maya, and R. M. Osgood, Appl. Phys. Lett. 33(11), 931 (1978).
 9. See also, A. A. Isaev and G. G. Petrash, "Investigation of Pulse Gas-Discharge Lasers Utilizing Atomic Transitions", in Pulse Gas-Discharge Atomic and Molecular Lasers, edited by N. G. Basov, translated by A. Tobulewicz, editor, Soviet Jour. of Quantum Electronics, Consultants Bureau, New York and London.
 10. The number of passes is dictated by the cavity length which was ~ 30 cm.
 11. J. L. Gole, J. R. Woodward, S. H. Cobb, K. K. Shen, and J. R. Doughty, SPIE Proceedings Volume 1397, Eighth International Symposium on Gas Flow and Chemical Lasers (1990), pg. 125 (and references therein).
 12. J. C. MacGillivray and M. S. Feld, Phys. Rev. A 23, 1334 (1981).
 13. See for example, NBS Special Publication 505, Bibliography on Atomic Transition Probabilities (1914 through October 1977) and Supplement I (November 1977 through March 1980), U. S. Department of Commerce/National Bureau of Standards. For Thallium see A. Gallagher and A. Lurio, Phys. Rev. 136, A87 (1964).
 14. This result was obtained in a short ~ 1 cm path length configuration. A more typical value is $\alpha \sim 0.10/\text{cm}$ in the longer path length zone indicated in Figure 4. See also, "An Approach to Visible Chemical Laser Development Using Fast Near Resonant Energy Transfer", by J. L. Gole, K. K. Shen, C. B. Winstead, and D. Grantier, Journal de Physique IV, Colloque C7, supplement au Journal de Physique III, Vol. 1, December 1991, pg. 609.
 15. A. S. Tibilov and A. M. Shukhtin, Opt. Spectrosc. 21, 69 (1966). See also, K. Krokell, M. Hube, W. Luhs and B. Wellegehausen, Appl. Phys. B37, 137-140 (1985).
 16. G. Roll and J. Mentel, J. Phys. D. Appl. Phys. 22, 483-487 (1989).
 17. "Self-Flushing Optical Window to Prevent Collection of Condensates", W. H. Crumley, and J. L. Gole, Rev. Sci. Instruments 57, 1692 (1986).
 18. To insure that the measurements were not an artifact tied to the nature of the high reflector, several mirrors ranging from 96 to 99.9% reflective, were tested.
 19. J. Derina, private communication.
 20. G. R. Fowles and W. T. Silvest, Appl. Phys. Lett. 6, 1 (1965).
 21. A. A. Isaev and G. G. Petrash, JETP Lett. 10, 119 (1969).
 22. Orazio Svelto, "Principles of Lasers", 3rd Edition, pp. 302, Plenum Press, New York (1989).
 23. B. Wellegehausen, in "Metal Bonding and Interaction in High Temperature Systems with Emphasis on Alkali Metals", A. C. S. Symposium Series 179, edited by J. L. Gole and W. C. Stwalley (Am. Chem. Soc., Washington, D. C.) p. 462, B. Wellegehausen, J. of Quantum Electronics 15, 1108 (1979).
 24. See for example, R. S. Berry and C. W. Reimann, J. Chem. Phys. 38, 1540 (1963), R. S. Berry, J. Chem. Phys. 27, 1288 (1957), W. S. Struve, J. R. Krenos, D. L. McFadden, and D. R. Herschbach, J. Chem. Phys. 62, 404 (1975). R. C. Oldenberg, J. L. Gole and R. N. Zare, J. Chem. Phys. 60, 4032 (1974).
 25. Given Na_2 and Na_3 ionization potentials of 4.87 and 3.97 eV (A. Hermann, E. Schumacher, and L. Woste, J. Chem. Phys. 68, 2327 (1978) and an electron affinity of 3.363 eV for atomic bromine, we determine a very substantial electron jump cross section $\sigma = \pi (14.38/3.97 - 3.36)^2 = 1746 \text{ \AA}^2 (1.75 \times 10^{-13} \text{ cm}^2)$ for the $\text{Na}_3 - \text{Br}$ reaction and $\sigma = \pi (14.38/(4.87 - 3.36))^2 = 285 \text{ \AA}^2 (2.85 \times 10^{-14} \text{ cm}^2)$ for the $\text{Na}_2 - \text{Br}$ reaction.
 26. E. J. Mansky and J. L. Gole, work in progress.
 27. W. C. Stwalley, private communication.
 28. J. L. Gole, D. Grantier, C. B. Winstead, and K. K. Shen, to be published.
 29. J. L. Gole, G. J. Green, S. A. Pace and D. R. Preuss, J. Chem. Phys. 76, 2247 (1982), and references therein.
 30. For example, M. M. Kappes, R. W. Kunz, and E. Schumacher, Chem. Phys. Lett. 91, 413 (1982).
 31. We wish to facilitate the formation of Na_2 in the B, C, and C' excited states in an electronically inverted configuration. To do this, Na_3 molecules must be present and react with halogen atoms. Here, it is important to note that the oscillator strengths for any of the larger sodium polymers (Na_n , $n \geq 3$) are sufficiently small versus Na_2 so that they do not interfere with the sodium dimer pump amplification cycle.
 32. R. Balfour and A. E. Douglas, Can. Jour. Phys. 48, 901 (1970); K. Li and W. C. Stwalley, J. Chem. Phys. 59, 4423 (1973).
 33. F. Reuse, S. N. Kanna, V. de Coulon, and J. Buttet, Phys. Rev. B 41, 11743 (1990).
 34. "On the BiF Bond Dissociation Energy and Evaluation of the BiF Red Emission Band Systems", T. C. Devore, R. Kahlscheuer, L. Brock, and J. L. Gole, Chemical Physics 155, 423 (1991).

Table I
Transition Probabilities Among Select Low-Lying States
of Atomic Sodium^a and Thallium^b

Transition	Composite Einstein A. Coeff.	Averaged Oscillator Strength, f
Na 5s ² S - 3p ² P	0.072	0.0137
Na 4d ² D - 3p ² P	0.131	0.106
Na 3p ² P - 3s ² S (Na D-line)	0.629	0.982
Tl ^b 7s ² S _{1/2} - 6p ² P _{1/2}	0.617	
Tl ^b 7s ² S _{1/2} - 6p ² P _{3/2}	0.716	
Tl ^c 6p ² P _{3/2} - 6p ² P _{1/2}	≤0.01	

a. See References 13.

b. Estimated on the basis of data in Refs. 13.

c. Radiative lifetime on order of 1 second, J. Wiesenfeld, private communication.

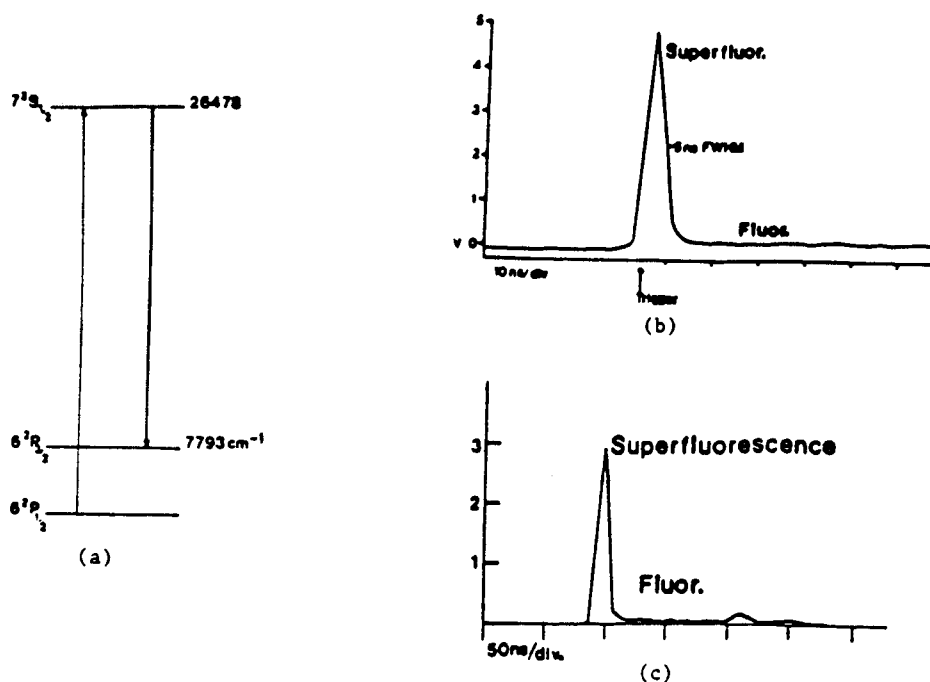


Figure 1(a): Tl atom energy levels.

Figure 1(b): Tl 7 ²S_{1/2} - 6 ²P_{3/2} (535.1nm) superfluorescence observed at a signal trigger level of 0.2V (fluorescent level ~ 0.045V). The trigger of the superfluorescence is by signal level and not by reactant mixing which occurs on a much longer time scale. The measured FWHM is 5.5 nsec compared to T = 7.5 n-sec, the radiative lifetime of the 7 ²S_{1/2} level. A return to the fluorescence level is seen subsequent to the superfluorescent pulse. No such superfluorescent pulse is associated with the T 7 ²S_{1/2} - 6 ²P_{3/2} (377.7nm) transition.

Figure 1(c): Tl 7 ²S_{1/2} - 6 ²P_{3/2} (535.1nm) superfluorescent oscillation observed with full laser cavity configuration. The superfluorescence/fluorescence ratio (fluorescence following self-termination of lasing action) is now in excess of 100.

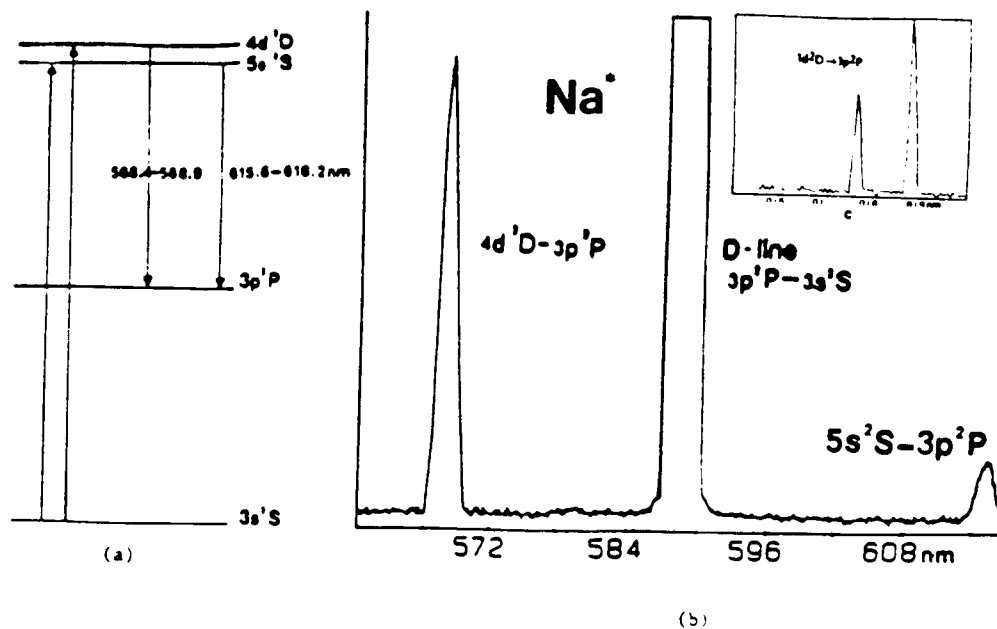


Figure 2(a): Na atom energy level scheme and pumping cycles to produce $4d^2D$ and $5s^2S$ excited states.

Figure 2(b): Typical energy transfer pumping spectrum for Na $4d^2D - 3p^2P$ and $5s^2S - 3p^2P$ transitions and $3p^2P - 3s^2S$ sodium D-line emission. The D-line emission results both from direct energy transfer pumping from ground state N_2O and from fluorescence to the $3p^2P$ level.

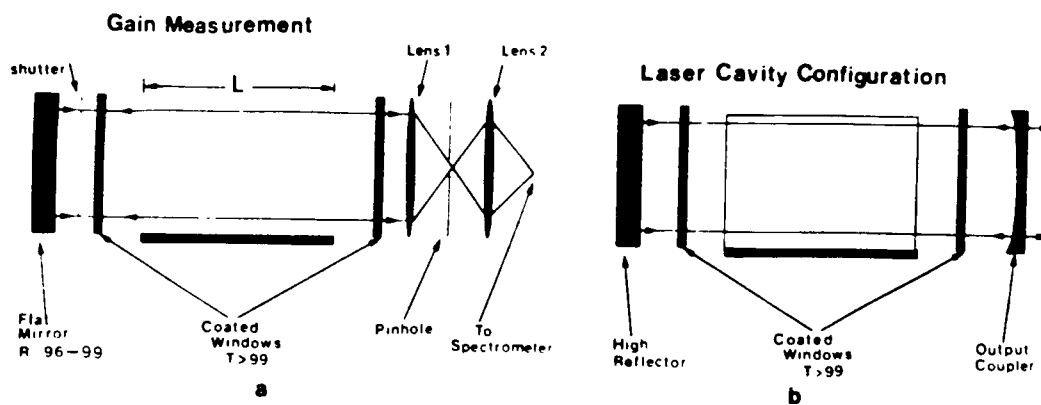


Figure 3(a): Gain measurement configuration after Roll and Mentel (ref. 16). The region marked L in the figure corresponds to the reaction - amplification zone.

Figure 3(b): Laser cavity configuration to characterize potential oscillation in the Si-SiO-Na system at 569 and 616 nm.

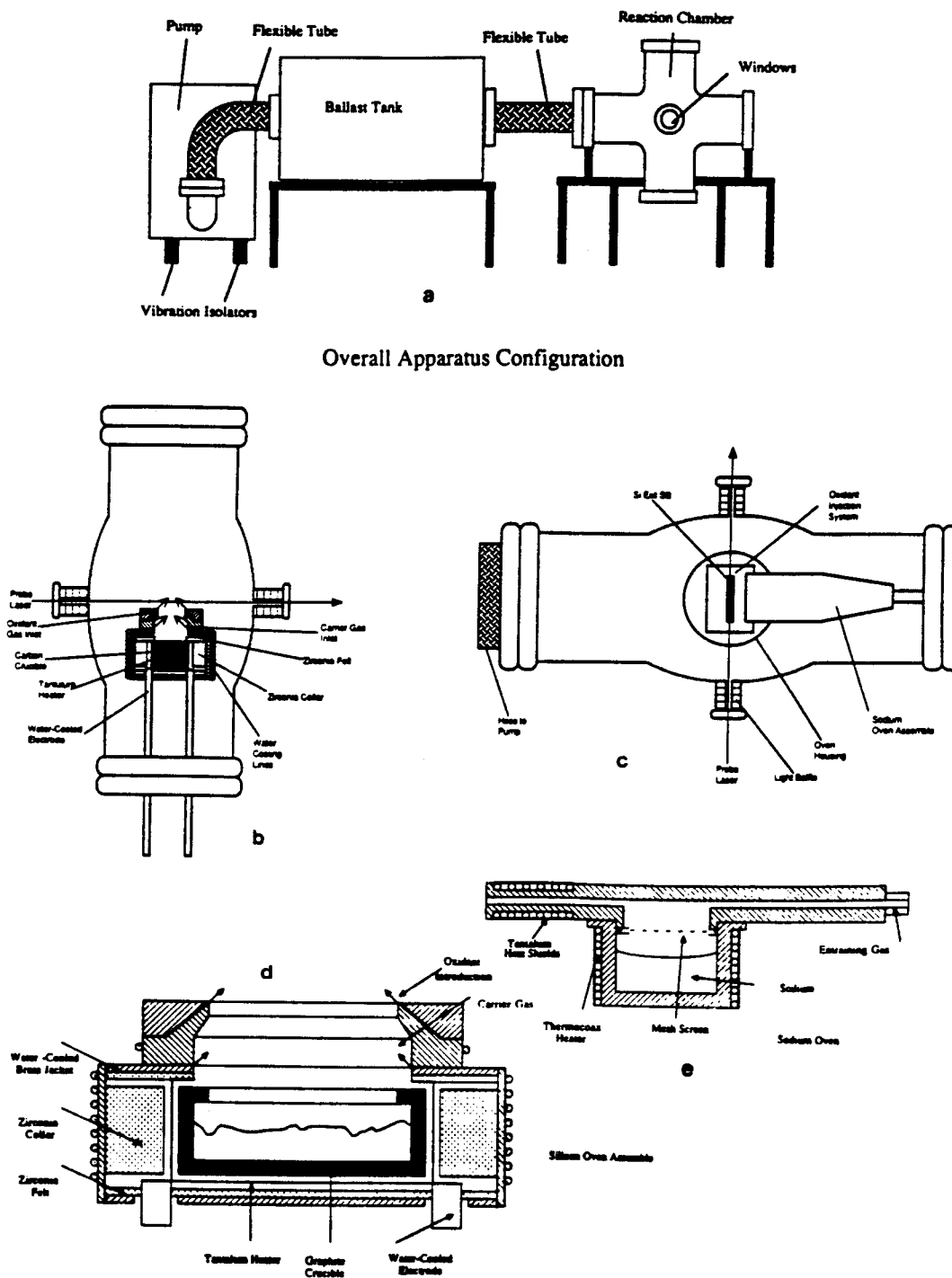


Figure 4: (a) Schematic of reaction chamber and windows defining optical train, ballast tank to moderate pumping fluctuations, and pumping configuration for extended path length Si-SiO (Si-N₂O)-Na reaction amplification zone. (b),(c) Side and overhead views of reaction chamber showing positioning of Si oven source, relative locations of Si and Na oven sources, oxidant injection system, and relative positions of these devices with respect to the optical train. (d),(e) Closeup view of silicon and sodium oven assemblies.

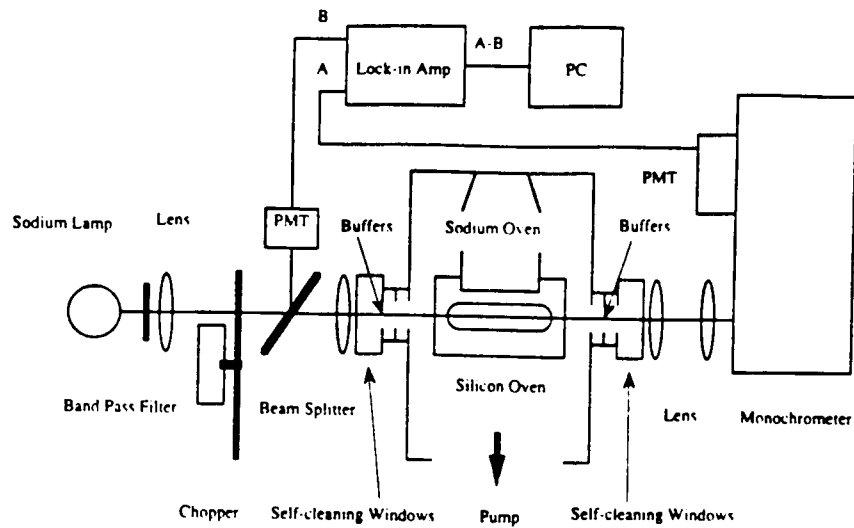


Figure 5: Schematic of Na lamp based gain measurement configuration. Single mode high resolution dye laser gain studies can also be accomplished with this configuration by substituting the output from a ring dye laser for the sodium lamp and bandpass filter. The cross sectional area of the sodium lamp output, input to the reaction - amplification zone, greatly exceeds that of the ring dye laser.

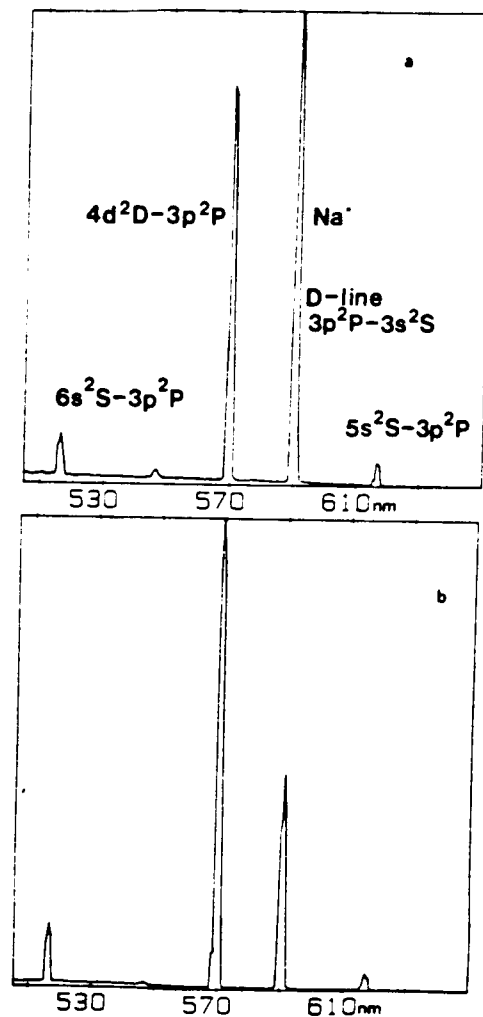


Figure 6(a): Single pass continuous amplified spontaneous emission (ASE) intensity (I_1) measured using the gain configuration depicted in Figure 3(a) for the Si-SiO-Na system.

Figure 6(b): Double pass continuous amplified spontaneous emission (ASE) intensity (I_2) measured also using the gain configuration depicted in Fig. 3(a) for the Si-SiO-Na system. The ratio of the I_2/I_1 intensity for the 569nm Na emission feature is 2.6/1 for this individual study and can approach 3.8/1 under optimal conditions for the system.

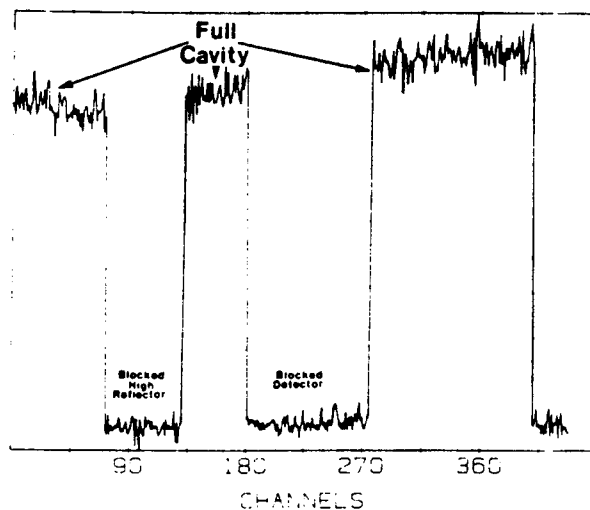
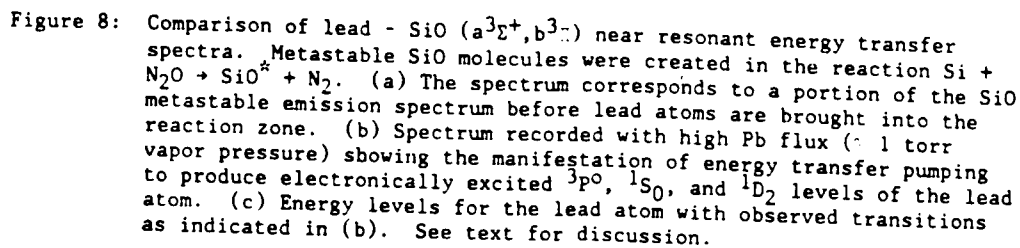
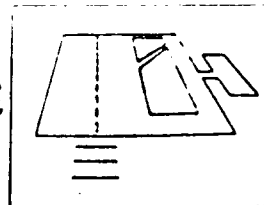


Figure 7: Full cavity output created with $\sim 0.2\%$ output coupling for the continuous Si-SiO(Si-N₂O)-Na amplifier at $\sim 569\text{nm}$. These measurements were taken in continuous flow with the cavity configuration depicted in Fig. 3(b). The full cavity output is compared to that obtained with both a blocked high reflector and with the entire cavity isolated from the signal detection system. The ratio of the output obtained for the full cavity to that obtained with a blocked high reflector exceeds $10^3/1$.



APPENDIX B
STOP BAR CONTROL SYSTEM
MANUFACTURER'S DESCRIPTIVE MATERIAL

STOP BAR CONTROL SURFACE MOVEMENT GUIDANCE BRITE*



ADB
A Siemens Company

1227M

COMPLIANCE WITH STANDARDS

ICAO : In compliance with recommendations for A-SMGCS.

FAA : Approved for use as Stop Bar control and monitoring system according to AC 150/5340-XX dated May 12, 1992 ; manufactured to current version of Advisory Circular 120-57. In full compliance with the A-SMGCS ASTA concept.

USES

Today there is a growing need for a ground movement guidance and control system to prevent incursions onto an active runway and collisions between aircraft, especially during conditions of low visibility.

The ADB BRITE System, an addressable electronic module, is an essential component in surface movement and guidance control systems (SMGCS).

It provides a basis for selective control and monitoring of a single light or group of lights plus a variety of aircraft sensors. The location of individual lamp failures can also be monitored.

Since there is no requirement to install separate communication cables, the Bidirectional Series Transceiver system (BRITE) provides true bi-directional communication on new and existing airfield lighting series circuits.

SALIENT FEATURES

- True bi-directional communication on series circuit is provided without requiring separate cables.
- May be retrofitted into any existing series circuit system.
- High communications rate between the Master and any Remote BRITE (4800 Baud).
- High degree of communications reliability through the use of CRC16 (Cyclic Redundancy Check) error checking on communications signal between Master and Remote BRITE.
- Extremely rugged surge protection provided on all external wiring connections of Master and Remote units.
- One Master can communicate with up to 255 Remotes.
- Remote BRITE designed to meet the 15000 V DC primary dielectric strength requirement given in the FAA L-830/L-831 isolation transformer specification.
- Strong, waterproof (NEMA 6P rated) construction allows the Remote BRITE to be placed at any L-867/L-868 base location on the airfield.
- Test port is available to test Remote BRITE in the field.
- Re-enterable construction of Remote BRITE allows reduced maintenance costs in comparison with resin-filled units.
- 50 Hz or 60 Hz operation.

SYSTEM DESCRIPTION

A typical BRITE system may have the following components (Fig. 4):

- Master BRITE (Fig. 1)
- Remote BRITE(s) (Fig. 2)
- Presence sensors/detectors (Fig. 3)
- Bypass Unit(s) (Fig. 7)

*Patents pending.

Copyright ©1993 by ADB-ALNACO, INC. All rights reserved.

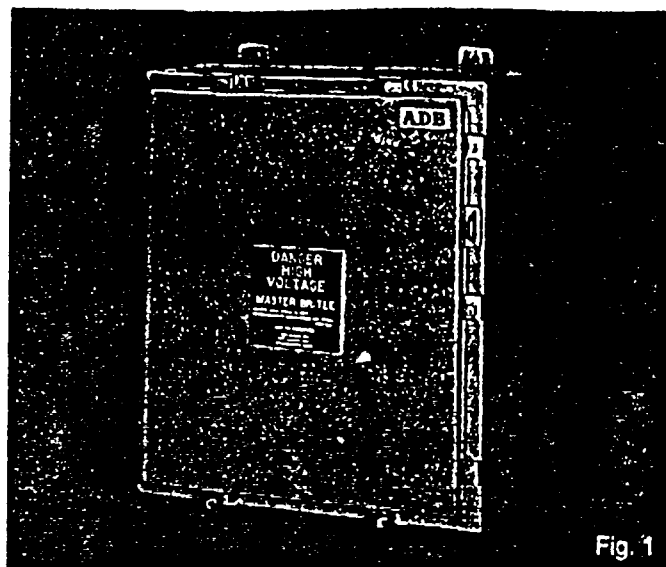


Fig. 1

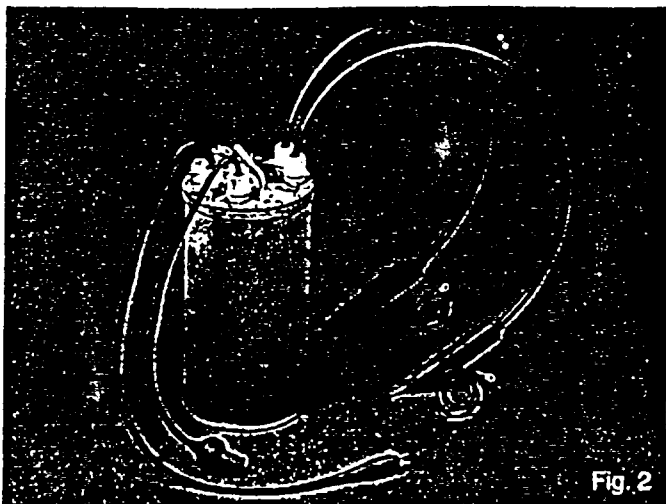


Fig. 2

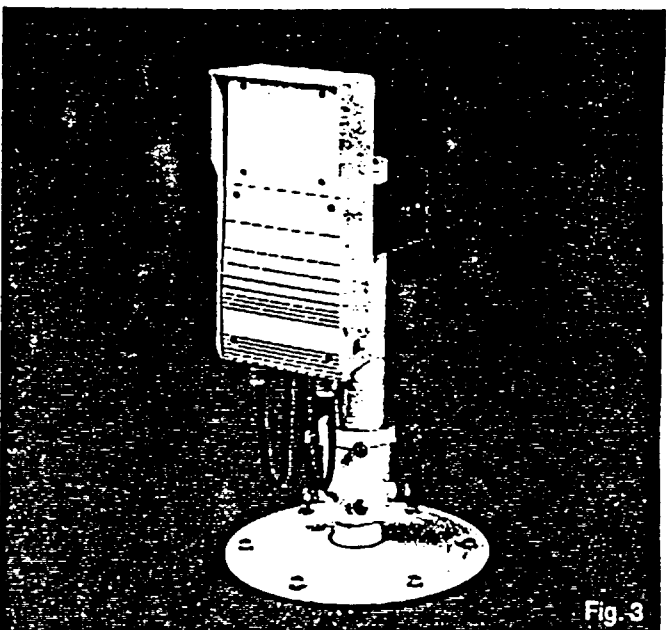
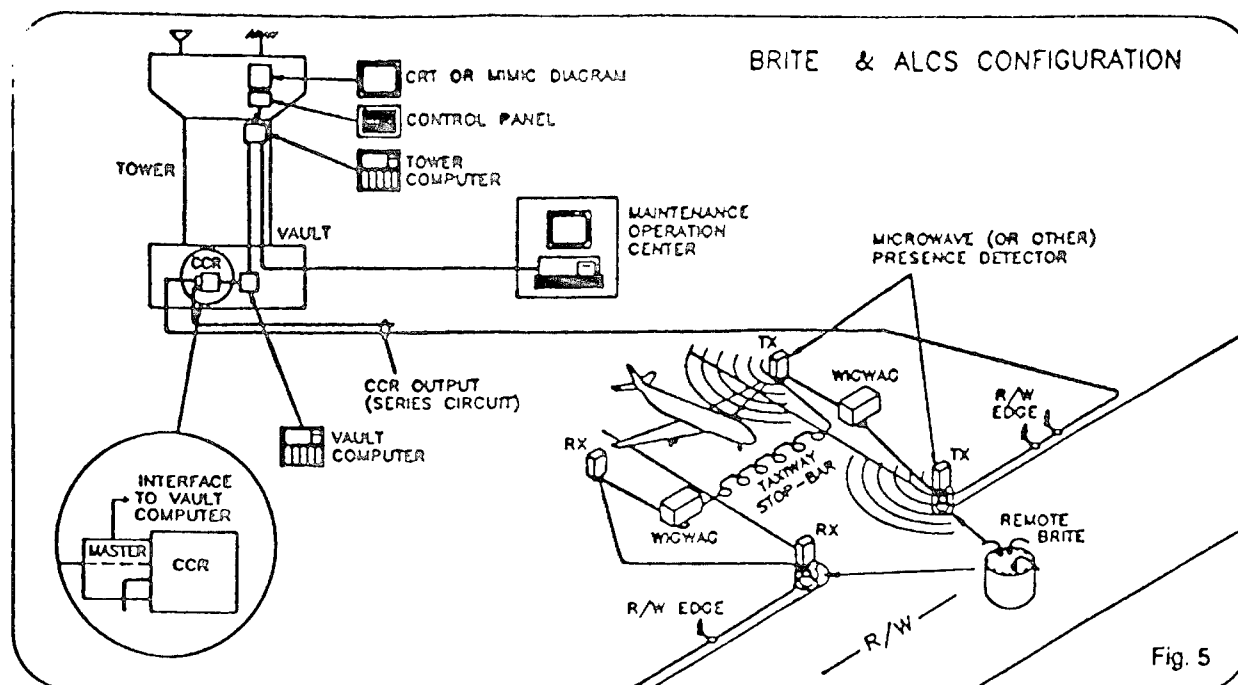


Fig. 3



Normally the BRITE system is used in conjunction with an Airport Lighting Computer System (ALCS), also shown on fig. 5, with the following components:

Tower Control Panel

Serves as the primary operator interface with the BRITE system. It can be a conventional FAA L-821 control panel, a pushbutton panel or a touch-sensitive screen. The conventional mimic diagram using lamps or LED's as indicators or optical fiber may be replaced by a CRT monitor.

Tower Computer

- Translates operator inputs into airfield lighting commands. It continuously scans the control panel settings and decides which lights should be controlled and to what circuit they belong. It then transmits the commands to the AFL Substation Controller (Vault Computer).
- The Tower Computer also collects fault and other data from the AFL Substation and, after processing, sends a status report to the Tower Control Panel and to the Maintenance Center Computer if provided.

AFL Substation Controller (Vault Computer)

- Its main task is to transmit the commands received from the Tower Computer to the Master BRITE and to the CCR's. It will also transfer to the Tower Computer the back indication signals received from the Remote BRITE's via the Master BRITE.
- In case of communication failure between the Tower and AFL Substation Computers (Vault Computers), the latter will set all CCR's to a pre-defined "fail-safe" setting. Each Remote BRITE will also revert to a pre-defined "fail-safe" setting.

Presence Sensors and Detectors

Various types of presence sensors:

- Microwave
- Piezoelectric
- Inductive loop
- etc...

may be controlled and monitored by a Remote BRITE. Automatic control and monitoring of taxiway stop bars and taxiway centerline lights is thus possible and can be incorporated into the ALCS. The system can then be incorporated as a subsystem into a Surface Movement and Guidance Control System (SMGCS).

Optionally

A computer and a CRT monitor are installed at the Maintenance Center. The main purpose of the Maintenance Center Computer is to collect information for statistics and maintenance planning.

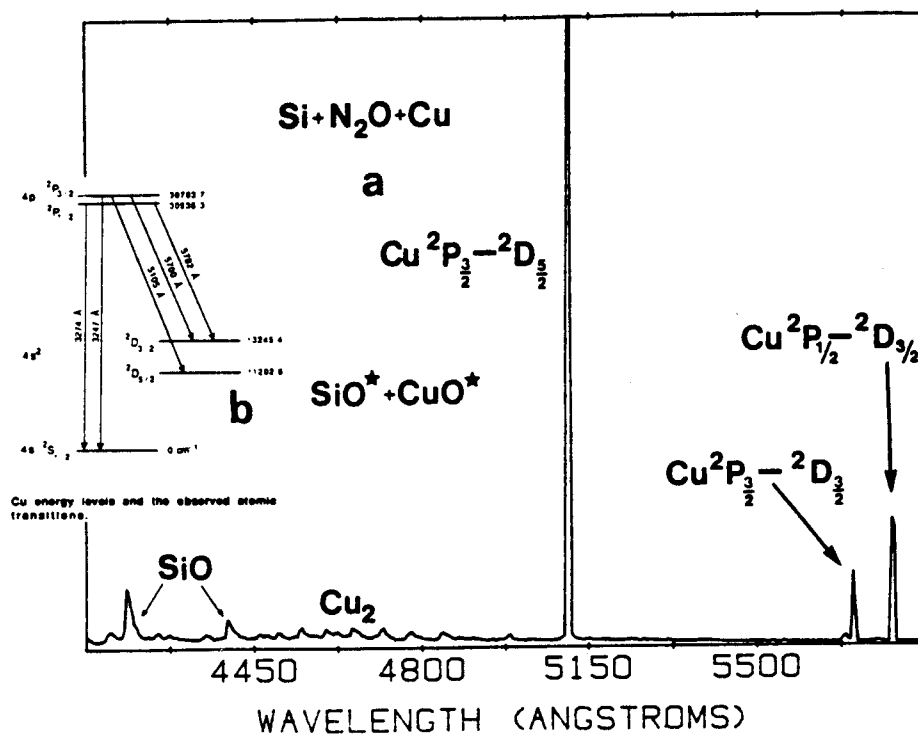


Figure 9: Copper - SiO ($a^3\Sigma^+$, $b^3\Pi$) near resonant energy transfer spectra generated from a "premixed" Si-Cu mixture subsequently oxidized with N₂O. (a) Spectrum showing a portion of the SiO metastable emission, the $\text{Cu}^2\text{P}_{3/2} - ^2\text{D}_{5/2}$ blue green emission line (copper vapor laser) and the $\text{Cu}^2\text{P}_{3/2,1/2} - ^2\text{D}_{3/2}$ yellow-orange emission features. (b) Energy levels for the copper atom with observed transitions as indicated in (a). See text for discussion.

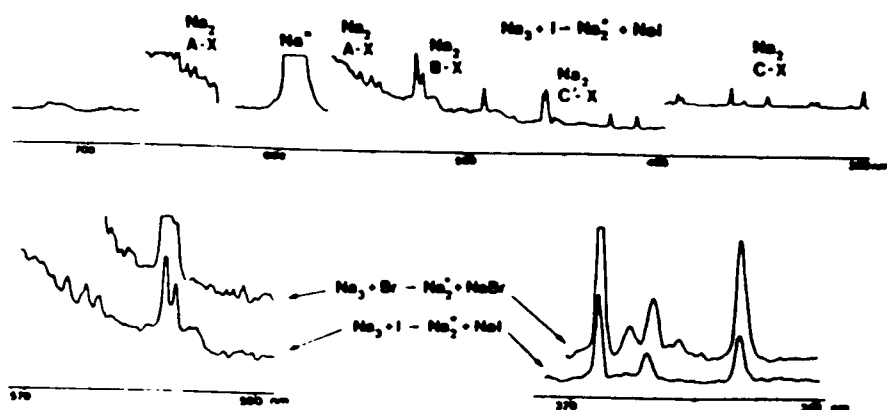


Figure 10: Chemiluminescent emission resulting from the reaction $\text{Na}_3 + \text{X} \rightarrow \text{Na}_2 + \text{NaX}$ with $\text{X} = \text{Br}, \text{I}$. The spectra display sharp fluorescence features in the visible at 527, 492, and 460.5nm superimposed on a broader Na_2 background emission.

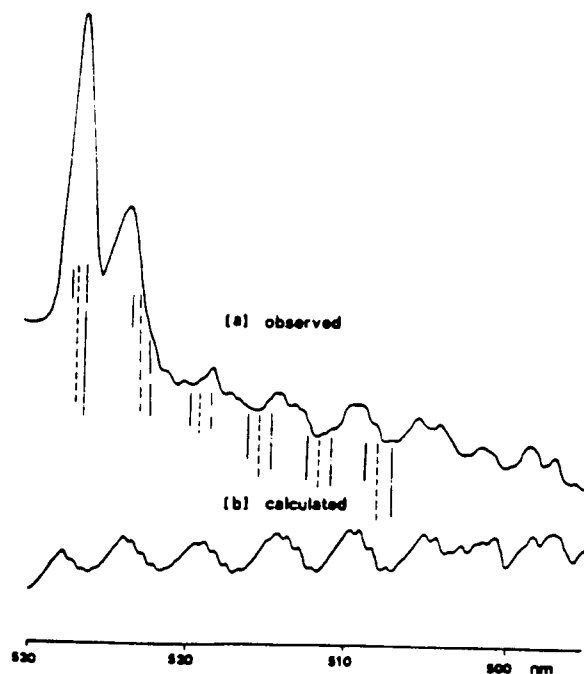


Figure 11: Comparison of (a) observed and (b) calculated emission spectra for the $\text{Na}_2 \text{ B-X}$ emission system. The experimental spectrum corresponds to the chemiluminescence from the $\text{Na}_2\text{-Br}$ reaction. The calculated spectrum, which was obtained for a rotational temperature, $T_{\text{rot}} \approx 1000\text{K}$, represents an estimate of effective rotational temperatures in a system operated under single collision conditions and therefore not at equilibrium. Relative vibrational populations input for $\text{Na}_2 \text{ B-X}$, $v' = 0-6$ were in the ratio 1.00:1.17:1.33:1.50:1.67:1.54.

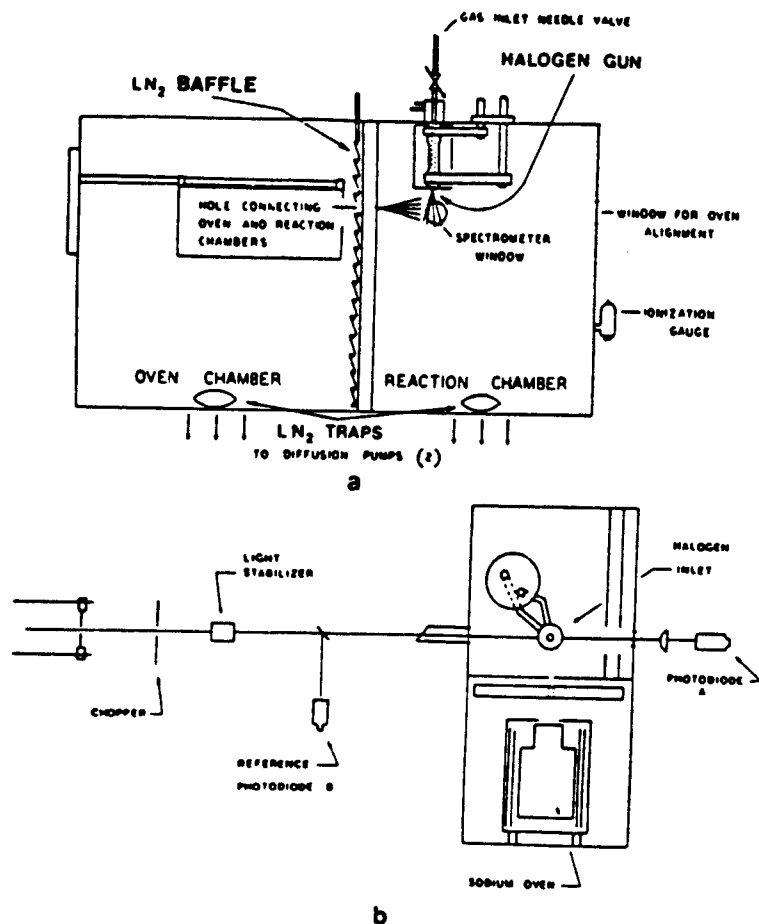


Figure 12: Schematic of (a) apparatus for the study of the chemiluminescent Na_3 - X reactions and (b) the arrangement of the experimental configuration for measuring gain from the Na_3 - X metathesis.

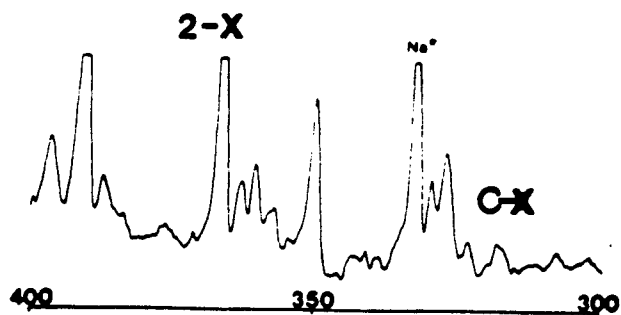


Figure 13: Chemiluminescence from the reaction $\text{Na}_3 + \text{Br} \rightarrow \text{Na}_2^* + \text{NaBr}$. The spectrum is dominated by the Na_2 $C^1\Pi_u - X^1\Sigma_g^+$ and $2^1\Sigma_u - X^1\Sigma_g^+$ emission features.

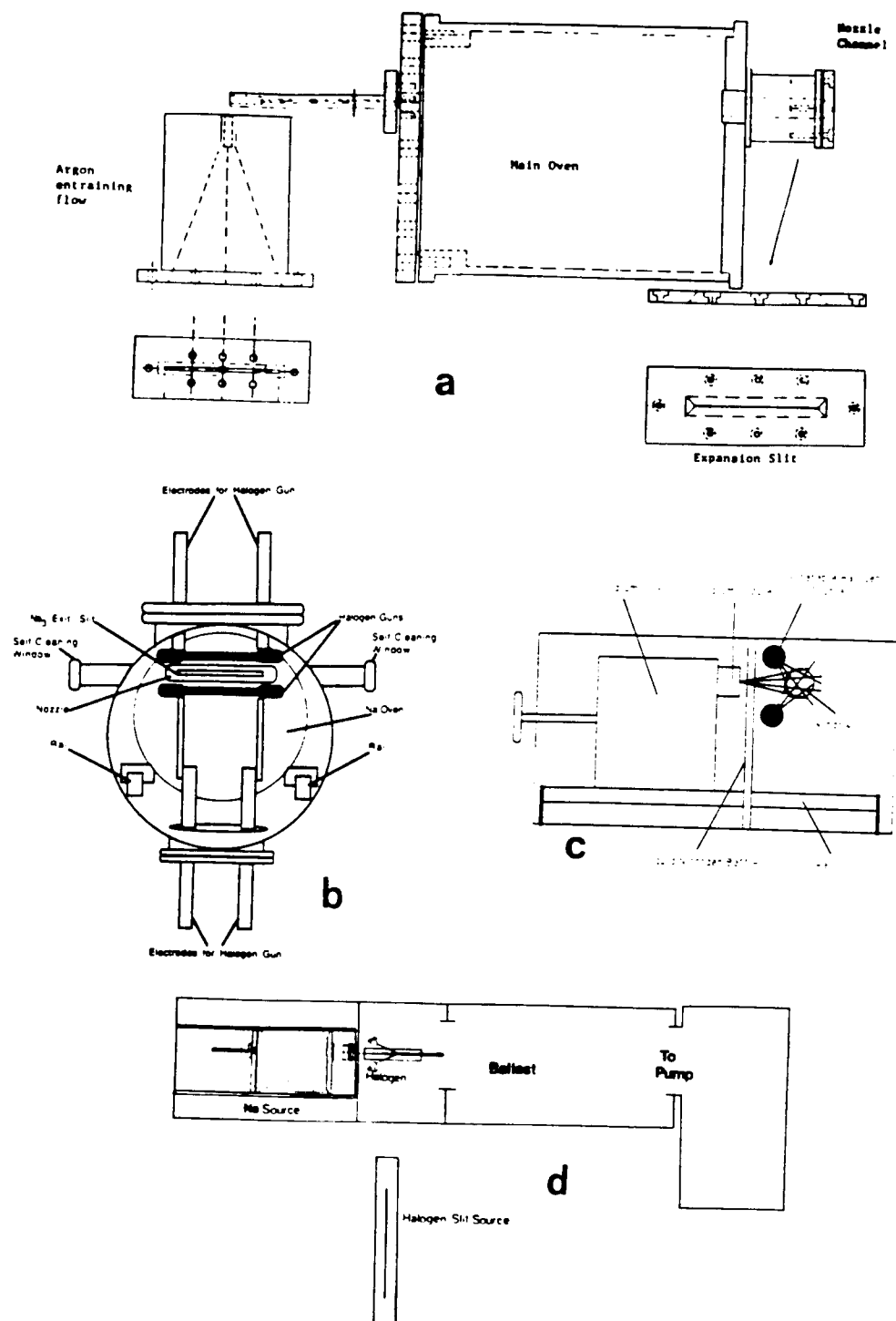


Figure 14: Schematics of upscaled Na_3 -halogen atom reactive flow configurations. (a) Schematic of sodium slit source configuration with argon entrainment flow device for seeded expansion, (b),(c) Front and side views of upscaled reaction-vacuum chamber configuration showing positions of halogen and sodium sources, (d) Schematic of upscaled vacuum chamber and pumping configurations. See text for discussion.

APPENDIX VIII

"Evidence for Continuous Visible Chemical Lasing from the Fast Near Resonant Energy Transfer Pumping of Atomic Sodium", K. K. Shen, H. Wang, and J. L. Gole, JQE 29 , 2346 (1993).

Evidence for Continuous Visible Chemical Lasing from the Fast Near Resonant Energy Transfer Pumping of Atomic Sodium

K. K. Shen, H. Wang, and J. L. Gole

Abstract—Energy transfer from selectively formed metastable states of SiO is used to pump sodium atom laser amplifiers at $\lambda \approx 569$ nm ($4d^2D-3p^2P$), $\lambda \approx 616$ nm ($5s^2S-3p^2P$), and $\lambda \approx 819$ nm ($3d^2D-3p^2P$). The $a^3\Sigma^+$ and $b^3\Pi$ states of SiO are generated in high yield from the $\text{Si} + \text{N}_2\text{O} \rightarrow \text{SiO} + \text{N}_2$ reaction. The energy stored in the triplet states is transferred in a highly efficient collisional process to pump sodium atoms to their lowest excited $3d^2D$, $4d^2D$, and $5s^2S$ states. Adopting a sequence in which high concentrations of silicon and sodium atoms are mixed and oxidized, we monitor a *continuous* amplification (gain condition) which suggests the creation of a population inversion among the receptor sodium atom energy levels and forms the basis for full cavity oscillation on the Na $4d^2D-3p^2P$ transition at 569 nm. The generic concept employed to create amplification and oscillation in this system should also be applicable to the efficient energy transfer pumping of potential amplifying transitions in potassium (K), lead (Pb), copper (Cu—analogue of Cu vapor laser), and tin (Sn) receptor atoms.

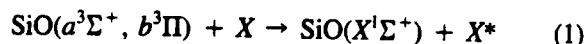
I. INTRODUCTION

THE development of visible chemical lasers has continued to represent an elusive and challenging scientific problem for the past quarter century [1]. In addressing this challenge, [2]–[6] we have recently been concerned with the development of two generic approaches, utilizing the inherently large cross sections which characterize certain electronic energy transfer processes [7] to create population inversions on electronic transitions. We rely on a limited group of selective, fast, and direct “electron jump” chemical reactions [2] or on highly efficient intramolecular or intermolecular energy transfer processes [3]–[6] involving electronically excited states. Here, we address the creation of an electronically inverted atomic configuration through highly efficient intermolecular energy transfer from electronically excited metastable storage states to atomic receptors with a high propensity for lasing action. We present evidence for the electronic-to-electronic (E–E) energy transfer pumping of

sodium atom based amplifiers corresponding to the Na $4d^2D-3p^2P$, $5s^2S-3p^2P$, and $3d^2D-3p^2P$ transitions at ~ 569 , ~ 616 , and ~ 819 nm and the concomitant full cavity oscillation on the $4d^2D-3p^2P$ transition at $\lambda \approx 569$ nm.

In order to pump the Na atom levels ($3d^2D$, $4d^2D$, $5s^2S$) of interest in this study, we first must form sufficient quantities of the metastable SiO $a^3\Sigma^+$ and $b^3\Pi$ states as the products of the primary spin conserving $\text{Si}-\text{N}_2\text{O}^8$ and $\text{Si}-\text{NO}_2^9$ reactions. One might envision the SiO “ $a^3\Sigma^+$ ” and “ $b^3\Pi$ ” metastable states (lifetimes estimated to be between 10^{-1} and 10^{-3} s) as a combined metastable triplet state reservoir which is, at best, weakly coupled to the ground electronic $X^1\Sigma^+$ state of the metal oxide. As a result of their long radiative lifetime, these reservoir states can be maintained and subsequently made to transfer their energy to pump selected atomic transitions. To first order, such a pumping process for the atomic receptor will be most efficient if a near resonant energy exchange from the metastable metal oxide reservoir is feasible.

We make use of the efficient intermolecular energy transfer process



where X^* represents the electronically excited atomic species from which we wish to obtain lasing action and the SiO $a^3\Sigma^+$ and $b^3\Pi$ states are formed under multiple collision conditions in a focused argon or helium entrainment flow such that the nascent product distribution of the $\text{Si}-\text{N}_2\text{O}^8$ or $\text{Si}-\text{NO}_2^9$ reactions is rotationally thermalized and vibrationally relaxed [3, Fig. 4] to the lowest levels of the triplet state manifold. The success of this outlined scheme depends on the rates for the reactions forming the SiO or GeO metastables [10], [11] and the rate of the MO^* ($M = \text{Si}, \text{Ge}$)– X intermolecular energy transfer, which, we anticipate, will be influenced by the nature of near resonances between the MO^* and X^* energy levels.

The outlined energy transfer process is found experimentally to be quite efficient for sodium (as well as potassium) atoms. To an even greater degree than that inherent to the previously studied chemically pumped Tl-based [3]–[6] amplifier–oscillator system [3, Tables I and II] at $\lambda \approx 535$ nm, there exist near resonant matchups ($\Delta E \approx 100 \text{ cm}^{-1}$) to receptor atom levels of interest in

Manuscript received January 4, 1993. This work was supported by the Georgia Tech Foundation through a grant from Mrs. Betty Peterman Gole, the Army Research Office through the Short Term Innovative Research Program, the Air Force Office of Scientific Research, and the Army Research Office and AFOSR/SDIO.

This paper is dedicated to the memory of Dr. Les Karlovitz, whose enthusiasm for life and the pursuit of academic excellence as the Dean of the College of Science and Liberal Studies will always be revered.

The authors are with the School of Physics, Georgia Institute of Technology, Atlanta, GA 30332.

IEEE Log Number 9210255.

TABLE I
NEAR RESONANCES OF SiO^* ($a^3\Sigma^+$, $b^3\Pi-X^1\Sigma^+$) AND SELECT Na AND K
ATOMIC TRANSITIONS IN ENERGY TRANSFER LASER PUMPING^a

TRANSITIONS IN ENERGY TRANSFER LASER PUMPING					
Atom	Upper Atomic Level	SiO(v' , v'')			
		$a - X$		$b - X$	
		Trans.	$\Delta E(\text{cm}^{-1})^b$	Trans.	$\Delta E(\text{cm}^{-1})^b$
Na	$4d^2D_{5/2, 3/2}$	—	—	(1,0) (2,1)	294 45
Na	$5s^2S_{1/2}$	(0,0)	200	(3,2) (2,2)	-209 177
Na	$3d^2D_{5/2, 3/2}$	(1,4)	180	(3,3)	67
Na	$6s^2S_{1/2}$	(4,0)	155	(0,4)	-184
Na	$4s^2S_{1/2}$			(4,1)	137
K	$4d^2D_{5/2, 3/2}$	(0,5)	-25	No near resonances	
K	$5d^2D_{5/2, 3/2}$	(0,3)	-420	(2,7)	60
K	$6s^2S_{1/2}$	(0,5)	-70	(0,3)	20
K	$6d^2D_{5/2, 3/2}$	—	—	—	—
				(0,2) (4,5)	-286 40
K	$7s^2S_{1/2}$	—	—	(3,4) (0,3)	264 -69

^aListed potential resonances for potassium are meant to be indicative but not exhaustive.

^b—Molecular level energy—Atom level energy. Positive quantities denote exothermic energy transfer.

atomic sodium (and potassium) for both SiO and GeO metastables. We are concerned with the energy transfer pumping of levels which are not accessed through strong electric dipole transitions from the ground state of the alkali atom. Applying these criteria, we summarize the nature of relevant near resonances for the lowest vibrational levels of the $a^3\Sigma^+$ and $b^3\Pi$ states in Tables I and II. For the SiO-Na system, Table I suggests that the sodium $4d^2D$ level might be the most easily pumped followed closely by the $5s^2S$ level. The $3d^2D$ and $6s^2S$ levels appear somewhat less promising, with the potential resonances involving the $3d^2D$ level and the lowest $b^3\Pi$ vibrational levels being more favorable.

Collisions with SiO or GeO metastables [3] are used to energy transfer pump from the $3s^2S$ Na ground state ($4s^2S$ in K) to the $4d^2D$ and $5s^2S$ levels ($5d^2D$ and $6s^2S$ in K), forming the basis for amplification on the $4d^2D-3p^2P$ ($\lambda \approx 569$ nm) and $5s^2S-3p^2P$ ($\lambda \approx 616$ nm) transitions. In the sodium system (Fig. 1(a)), the $3p^2P$ terminal laser level is the short-lived upper level of the Na D-line. The $3p^2P-3s^2S$ transition is characterized by a high oscillator strength. This facilitates rapid loss of the terminal laser level to create ground state sodium atoms which, as Figs. 1(a) and (b) demonstrate, are again amenable to near resonant energy transfer pumping.

While the $5s^2S$ and $4d^2D$ levels are not readily accessed in an optically pumped transition, Fig. 1(b) demonstrates that, using SiO metastables formed in the Si-N₂O reaction, we have successfully energy transfer pumped Na atoms to the 2S and 2D levels where they subsequently emit radiation at $\lambda \approx 616$ nm and 569 nm as they undergo transition to the $3p^2P$ levels. The energy transfer process which pumps these sodium atom levels appears at least as efficient as that observed for the Tl system [3—Figs. 4,

TABLE II
NEAR RESONANCES OF GeO^* ($a^3\Sigma^+$, $b^3\Pi-X^1\Sigma^+$) AND SELECT Na AND K
ATOMIC TRANSITIONS IN ENERGY TRANSFER LASER PUMPING^a

Atom	Upper Atomic Level	$\text{GeO}(v', v'')$			
		$a - X$		$b - X$	
		Trans.	$\Delta E(\text{cm}^{-1})^b$	Trans.	$\Delta E(\text{cm}^{-1})^b$
Na	$3d^2D_{5/2,3/2}$	(2,0) (3,0) (0,2)	-367 250 130	(0,3)	-73
Na	$4s^2S_{1/2}$	(0,2)	130	—	—
Na	$6s^2S_{1/2}$	—	—	(6,0)	-180
Na	$5s^2S_{1/2}$	—	—	(2,0)	245
Na	$4d^2D_{5/2,3/2}$	—	—	(3,0) (4,0)	-401 293
K	$4d^2D_{5/2,3/2}$	(0,0) (1,1) (4,0)	160 -195 -149	—	—
K	$5d^2D_{5/2,3/2}$	(4,0)	-149	(0,2)	-123
K	$6s^2S_{1/2}$	(0,0)	110	—	—
K	$6d^2D_{5/2,3/2}$	—	—	(2,2)	-185
K	$7s^2S_{1/2}$	(4,0)	-240	(0,2)	-110

^aListed potential resonances are meant to be indicative but not exhaustive.

^b—Molecular level energy—Atom level energy. Positive quantities denote exothermic energy transfer.

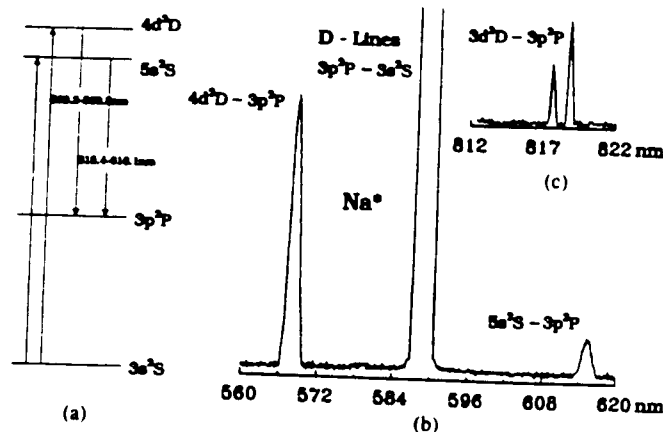


Fig. 1. (a) Na atom energy level scheme and pumping cycles to produce $4d^2D$ and $5s^2S$ excited states. (b) Typical energy transfer pumping spectrum for Na $4d^2D-3p^2P$ and $5s^2S-3p^2P$ transitions and $3p^2P-3s^2S$ sodium D-line emission. The D-line emission results both from direct energy transfer pumping from ground state NaO and from subsequent fluorescence following emission to the $3p^2P$ level. (c) Energy transfer pumping spectrum corresponding to Na $3d^2D-3p^2P$ transition.

5]. The observed Na atom transitions, originating at the $4d^2D$ and $5s^2S$ levels, are characterized by moderate oscillator strengths. The accessed Na cycle, with its 50 ($4d^2D-3p^2P$) [13] to ~ 100 ($5s^2S-3p^2P$) [14] nanosecond upper state radiative lifetimes (vs. $T_1^2S_{1/2}$ at ~ 7 ns [15]), and short-lived terminal laser level, would appear ideally suited to obtain high duty cycle laser amplifiers and oscillators. In fact, we find that these transitions demonstrate continuous gain. Further, as indicated in Fig. 1(c), we have obtained evidence for the energy transfer pump of the Na $3d^2D$ level with which is associated an atomic emission at $\lambda \approx 819$ nm ascribed to the Na $3d^2D-3p^2P$ transition. We consider a range of measurements on the Si-SiO-Na system used to demonstrate continuous gain on the $4d^2D-3p^2P$, $5s^2S-3p^2P$, and $3d^2D-3p^2P$ transi-

tions at $\lambda \approx 569$, $\lambda \approx 616$, and $\lambda \approx 819$ nm, respectively, and present evidence for continuous oscillation at $\lambda \approx 569$ nm. Appropriate spontaneous emission rates, degeneracy factors, and energy increments for the transitions of interest are summarized in Table III.

II. EXPERIMENTAL

A. "Creation of Reaction—Energy Transfer—Amplification Zone"

The reaction-energy transfer-amplification zone depicted in several views in Fig. 2 has been constructed to provide a versatile, moderate path length, amplification device. The apparatus is configured such that the Si(Ge)—SiO(GeO) source moves vertically and the Na(K) source moves horizontally relative to the amplification zone. The silicon source construction which provides an enveloping, focusing, and oxidizing sheath about the vaporizing silicon metalloid flux, is designed to concentrate the SiO metastable concentration in the vicinity of the amplification zone [3], [6]. With the silicon source temperature monitored by optical pyrometry, we estimate the Si atom concentration in the amplification zone as a minimum of 10^{14} /cc for all studies involving gain measurement. The N_2O oxidant concentration exceeds 5×10^{14} /cc and the SiO metastable concentration exceeds 10^{13} /cc based on a quantum yield exceeding 10% [16] for the spin conserving $Si(^3P) + N_2O(^1\Sigma^+) \rightarrow SiO(a^3\Sigma^+, b^3\Pi) + N_2(^1\Sigma_g^+)$ reaction [3], [6], [8]. The Si—SiO flow configuration was operated with the silicon source temperature ranging between 1600 and 1800°C with the majority of the gain measurements conducted at the highest temperatures. The helium or argon entraining flow rate ranged between 300 and 450 mL/min, and the N_2O flow rate ranged between 1 and 5 mL/min. The conditions which we outline are adjusted to produce maximum gain in a given experiment and provide the longest path length SiO metastable flame yet realized.

The entrained Si—SiO flow is intersected at 90°, in subsonic flow, by a flux of sodium atoms which, based upon the Na source temperature and the measured rate of expenditure of sodium from the source, exceeds 10^{18} /cm²-s in the reaction zone, corresponding to a density of order 10^{13} /cc. The concentration of Na atoms is controlled experimentally, through the appropriate choice of oven source temperature and entrainment flow, to provide maximum gain under the conditions of a given experiment. To provide the necessary flux, the temperatures of the Na source oven range between 400 and 500°C for the reservoir and 480–550°C for the entrainment flow channel (Fig. 2); typical helium or argon entrainment flow through the sodium source ranges between 30 and 90 mL/min. The entrained Si and Na flows can also be moved *in situ* relative to each other and with respect to the reaction-energy transfer-amplification zone to optimize conditions for formation of the gain medium. Typically, the silicon source is maintained in a preset stationary position while the sodium slit source is moved to a

position elevated so as to provide maximal interaction of the intersecting flows at the focus of the enveloped SiO metastable flame. The separation of the two sources is usually of the order 2 cm. It should be emphasized that the chemiluminescent emission from the Si/ N_2O "flame" is negligible in the 510–630 nm region where gain measurements (see also Fig. 5 following) on the Na $4d^2D-3p^2P$ ($\lambda \approx 569$ nm) and $5s^2S-3p^2P$ ($\lambda \approx 616$ nm) emission features are performed.

The mixing zone of Fig. 2 is greatly stabilized by the moderate sized (15 cubic feet) ballast separating the 150 cfm pump from the reaction chamber which it evacuates. Typical measured background pressures range between 10 and 30 mtorr whereas operating pressures, as measured by a thermocouple gauge well separated from the reaction zone, range between 500 and 1200 mtorr. Because there is a substantial pressure gradient between the reaction zone and the position of the monitoring thermocouple, the recorded pressures are at least 50% lower than the true pressure in the amplification region. In order to protect the cavity windows from the condensation of silicon oxide or sodium, "self-flushing" optical windows [17] were operated with a protective helium flow.

Using the described configuration, we have created an amplification zone from which we can monitor gain, as a function of slightly varying experimental conditions, on the Na $4d^2D-3p^2P$ ($\lambda \approx 569$ nm), $5s^2S-3p^2P$ ($\lambda \approx 616$ nm) and $3d^2D-3p^2P$ ($\lambda \approx 819$ nm) transitions.

B. Measurement of Optical Gain (Amplification)

1) *Roll-Mentel Configuration*: Gain measurements have been carried out on the Si—SiO—Na system using three different experimental configurations. The simplest of these measurements was performed using the optical train depicted in Fig. 3(a). This device parallels the ingenious design of Roll and Mentel [18] to study amplified spontaneous emission in HeSe lasers. L denotes the length of the gain medium created upon interaction of the SiO and the Na flows. The amplification zone, under vacuum, is surrounded (Fig. 3(a)) by two AR-coated windows (CVI PW2037C) or two Brewster angle windows (CVI W-B25SS) connected outside the self-flushing optical window denoted in the previous section.

Several flat mirror high reflectors were employed with the Roll-Mentel optical train, ranging in reflectivity from 96 to 99.9% and varying in surface coating and substrate. All of these high reflectors yielded closely comparable results, similar to those in Fig. 5, when employed for gain measurements. The output from the surrounding gain medium was sent through a Fourier aperture (pinhole) and into a monochromator using lenses 1 and 2. The monochromator allowed separation of individual emission features. Coarse alignment for both the gain configuration depicted in Fig. 3(a) and the full cavity (oscillator) configuration depicted in Fig. 3(b) was accomplished with a HeNe laser positioned as in Fig. 3(c) ~ 15 feet from the gain and full cavity configurations. After alignment, the

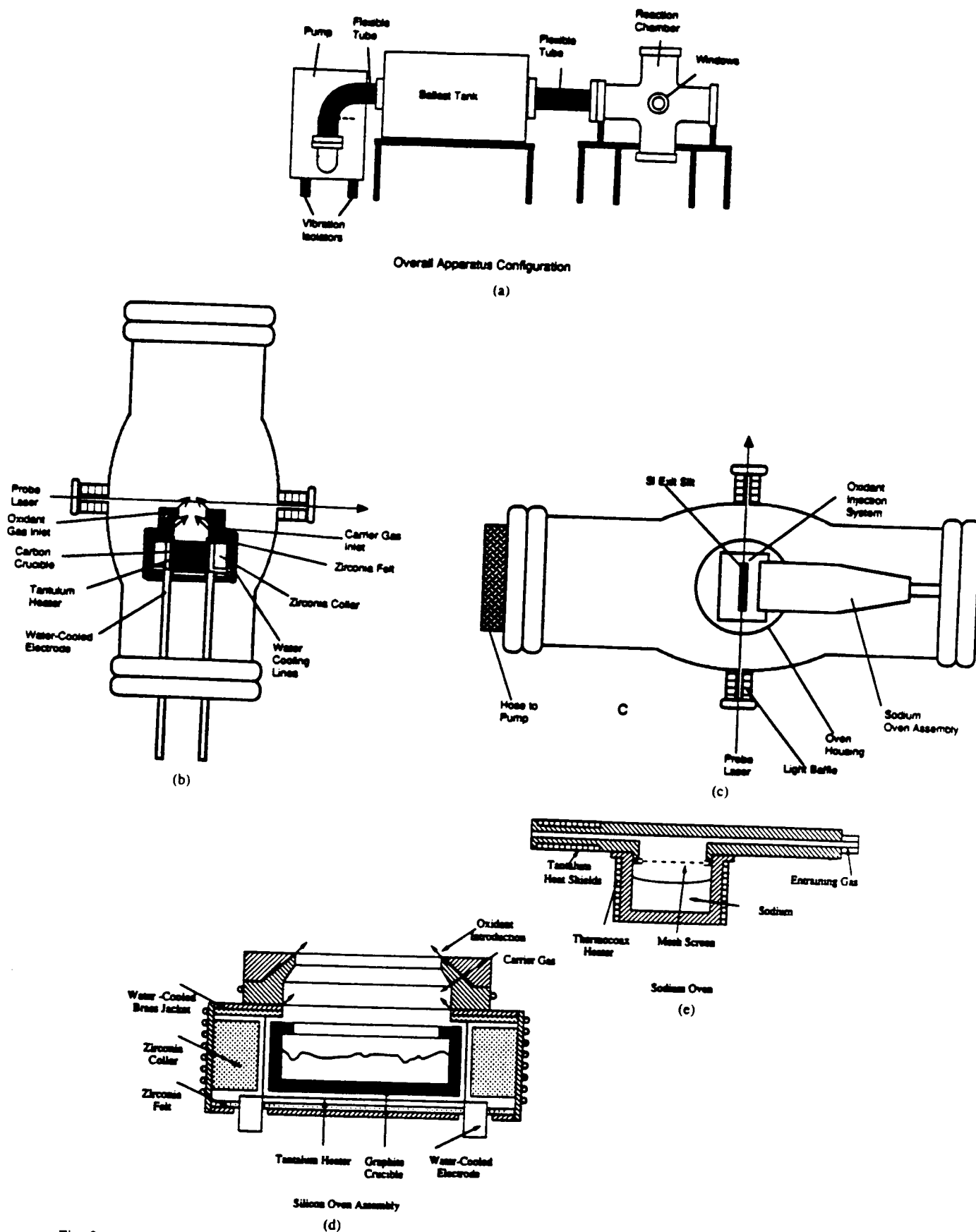


Fig. 2. (a) Schematic of reaction chamber and windows defining optical train, ballast tank to moderate pumping fluctuations, and pumping configuration, for extended path length Si-SiO (Si-N₂O)-Na reaction amplification zone. (b). (c) Side and overhead views of reaction chamber showing positioning of Si oven source, relative locations of Si and Na oven sources, oxidant injection system, and relative positions of these devices with respect to the optical train. (d), (e) Closeup view of silicon and sodium oven assemblies.

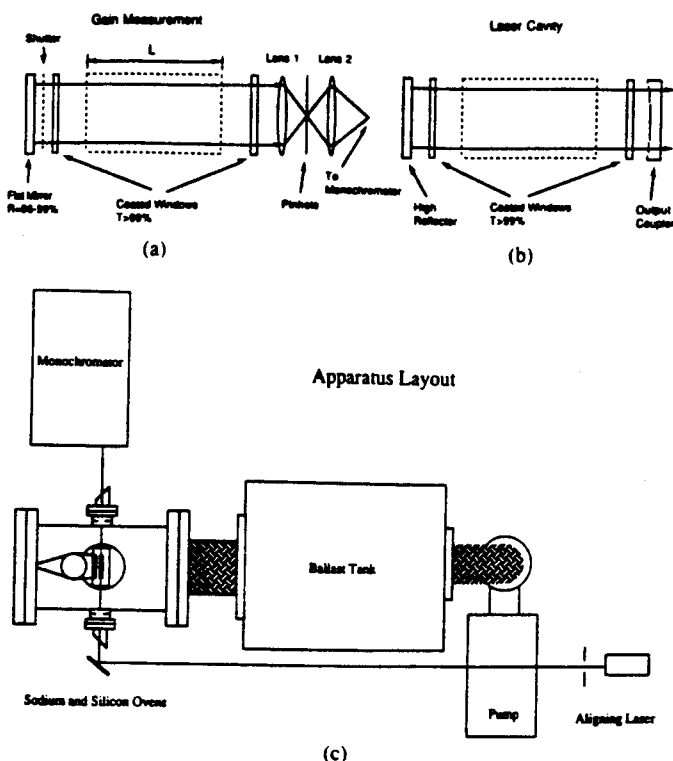


Fig. 3. (a) Gain measurement configuration after Roll and Mentel [18]. The region marked L in the figure corresponds to the reaction-amplification zone. (b) Laser cavity configuration to characterize potential oscillation in the Si-SiO-Na system at 569 nm. (c) Schematic overview of reaction chamber-amplification zone, ballast, and pump for extended path length Si-SiO(Si-N₂O)-Na gain medium. The figure indicates the coarse alignment path (~ 15 ft) for the HeNe laser and its correlation with the optical train surrounding the reaction zone and terminating at the monochromator. See also Fig. 2.

HeNe laser is no longer an integral part of the system. In other words, the configurations (Fig. 3) operate without light sources external to the reaction-amplification zone. Thus these configurations are to be distinguished from the sodium lamp and ring dye laser based gain measurements depicted in Fig. 4.

2) Sodium Discharge Lamp: Using a sodium discharge lamp and the configuration depicted in Fig. 4(a), we have measured gain on the Na $4d^2D-3p^2P$ transition at 569 nm. The enhancement of the Na $4d^2D-3p^2P$ emission line (or other sodium transitions) is evaluated by isolating the transition of interest with a 10-nm bandpass filter. The lamp light output brought into the amplification zone is evaluated, and, if necessary, made comparable to the chemiluminescent intensity using neutral density filters positioned between the bandpass filter and lens at the beginning of the optical train.

A phase sensitive detection mode was used. The output intensity of the sodium discharge lamp was modulated at a frequency of 700 Hz. A beam splitter directs a portion of the lamp output signal to a photomultiplier providing the reference signal B. The remaining light is collimated, sent through the gain medium (amplification zone), and detected, after being dispersed by the monochromator. The output photomultiplier attached to the exit slit of the monochromator provides the signal for channel A. This

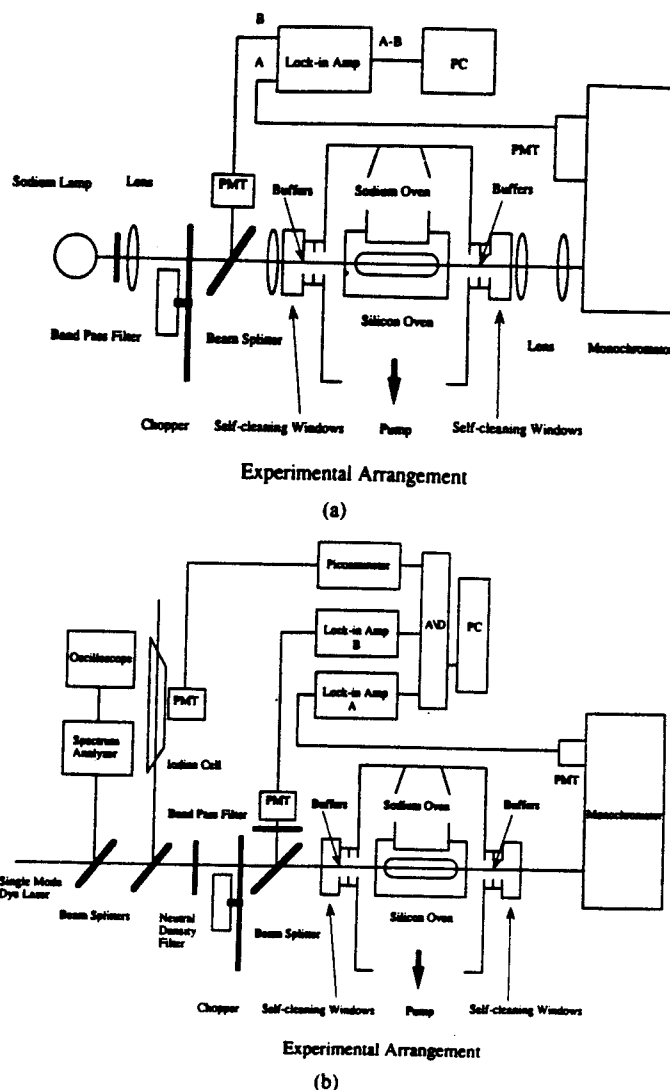


Fig. 4. (a) Schematic of Na-lamp based gain measurement configuration. The cross sectional area of the sodium lamp output, input to the reaction-amplification zone, greatly exceeds that of the gain medium. See text for discussion. (b) Schematic of ring dye laser based gain measurement configuration. The dye laser is operated single mode and scans the frequency range of the $\lambda = 569$ nm Na $4d^2D-3p^2P$ transition with calibration versus I_2 . See text for discussion.

form of detection serves two purposes in this experiment. First, it allows selective monitoring of the chemiluminescent intensity during the period of the experiment, and second, it acts as a band pass filter peaked at the laser transition of interest, when the gain measurement is made. The A-B signal difference is sent to the lockin amplifier as the gain.

Before the detection of gain in the amplification zone, it is necessary to calibrate the A-B channel by evaluating the chemiluminescent signal. After optimizing the amplification zone conditions so as to maximize a continuous chemiluminescent signal, the oxidant (N₂O) flow is cut off and the A-B lockin signal is balanced to a null value, corresponding to the complete absence of a chemiluminescent flame. For a typical run, as the N₂O flow is turned on and off producing chemiluminescence, we record the train of peaks depicted in Fig. 6, corresponding to a con-

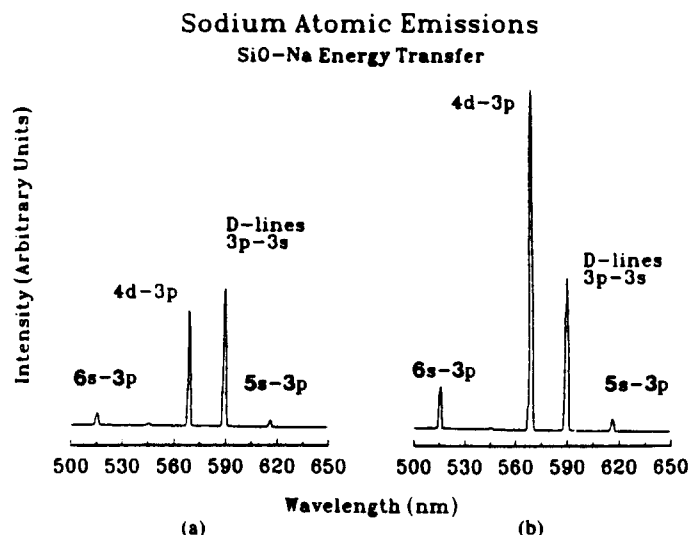


Fig. 5. (a) Single-pass continuous amplified spontaneous emission (ASE) intensity (I_1) measured using a Spex 1 meter spectrometer and RCA 4840 phototube and the gain configuration depicted in Fig. 3(a) for the Si-SiO-Na system. Spectral resolution is 1 nm. Because the figure is uncorrected for photo-tube response, decreasing from 510 to 630 nm, or grating blaze (500 nm), the emission associated with the $6s^2S-3p^2P$ transition appears more intense than that associated with the $5s^2S-3p^2P$ transition. (b) Double pass continuous amplified spontaneous emission (ASE) intensity (I_2) measured using the gain configuration depicted in Fig. 3(a) for the Si-SiO-Na system. The Na D-line intensity is comparable to that in Fig. 5(a). The ratio of the I_2/I_1 intensity for the 569-nm Na emission feature is 2.6/1 for this individual study and can approach 3.8/1 under optimal conditions for the system. Spectral resolution is ~ 1 nm (see (a)).

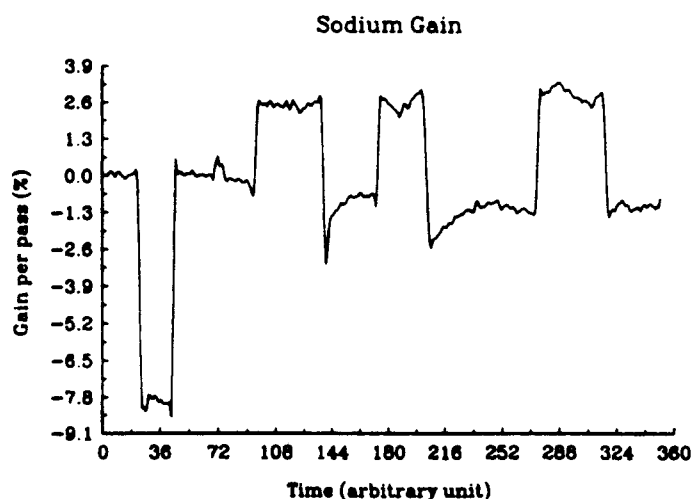
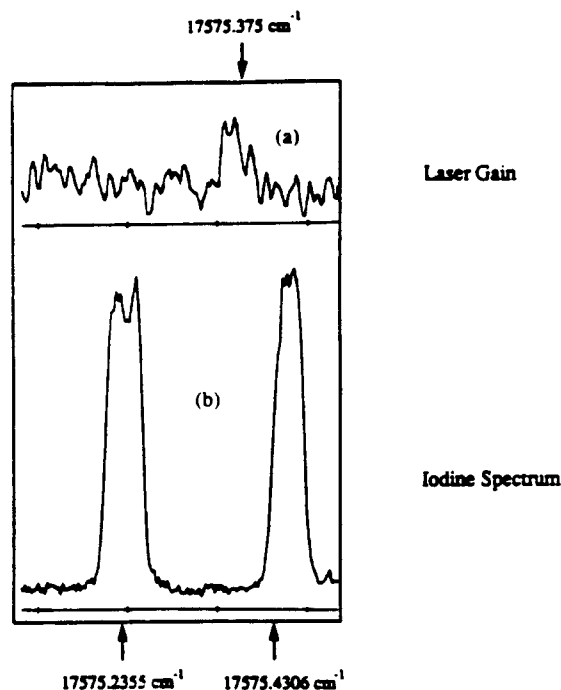


Fig. 6. Plot of gain per pass at $\lambda = 569$ nm corresponding to the Na $4d^2D-3p^2P$ transition. The negative peak corresponds to an 8% loss in the signal channel due to the insertion of a glass filter. The positive peaks (gain) correspond to the introduction of the oxidant N_2O into the reaction-energy transfer-amplification zone outlined in Figs. 2 and 4(a). See text for discussion.

tinuous gain condition during the period in which oxidant is supplied to the amplification zone.¹

3) *Scanning High Resolution Ring Dye Laser:* We have also used a cw single mode ring dye laser (Spectra Physics 380A) to perform laser gain measurements in a

¹We have also verified that the channel A signal will not increase as strong unchopped light is sent through the amplification zone-reaction chamber.



Gain Profile of Chemically Pumped Sodium Vapour

Fig. 7. (a) Continuous single-mode ring dye laser scan in the region of the $\lambda = 569$ nm Na $4d^2D-3p^2P$ transitions indicating a $\sim 1.5\%$ gain at the frequency corresponding to the $4d^2D_{5/2}-3p^2P_{3/2}$ transition (Table III). This represents a lower bound to the gain. (b) I_2 calibration spectrum. See text for discussion.

frequency scanning (laser with calibration vs. iodine) mode (Fig. 4(b)). The dye laser pumped by a Spectra Physics Model 171 Ar⁺ laser, was made to lase continuously without mode hopping over the time scale of a frequency scan in the region about 569 nm (using a mixture of R590 and R560 Rhodamine dyes). The behavior of the single mode ring dye laser output was continuously monitored using a Spectra Physics Model 450-03 spectrum analyzer. The absolute frequency was first crudely calibrated using a monochromator at 0.1 Å resolution and then monitored by comparison to a simultaneously generated high resolution I_2 spectrum. In order to insure stable ring dye laser operation, the argon laser was operated at a power of 6–7 W. The dye laser output was maintained at ~ 200 mW to prevent mode hopping.

Experiments were again carried out in an AC mode. After splitting a portion of the dye laser output to the spectrum analyzer and an I_2 cell, the remaining portion was brought over a 30-ft path to the cavity configuration where, before passing through the amplification zone to the monochromator, the power level was further reduced, using neutral density filters, to a level comparable to the chemiluminescent intensity (still maintaining a reasonable S/N). To further reduce the noise level, the chopper (Fig. 4(b)) used in these experiments was operated at 700 Hz. In addition, two lockin amplifiers (Stanford Research, SR-510) were used to insure a proper phase lock for both the reference and signal channels. Using this experimental configuration, we generate and calibrate the laser gain spectrum depicted in Fig. 7. Here, the high res-

TABLE III
SPONTANEOUS EMISSION RATES, DEGENERACY FACTORS, AND ENERGY INCREMENTS FOR Na $4d^2D-3p^2P$, $5s^2S-3p^2P$, AND $3d^2D-3p^2P$ TRANSITIONS^a

Transition	Energy (cm ⁻¹)	A Value (10 ⁷ sec ⁻¹)	g_u	g_l
$4d^2D_{5/2}-3p^2P_{3/2}$	17575.375	1.2	6	4
$4d^2D_{3/2}-3p^2P_{3/2}$	17575.41	0.21	4	4
$4d^2D_{3/2}-3p^2P_{1/2}$	17592.606	1.03	4	2
$5s^2S_{1/2}-3p^2P_{3/2}$	16227.317	0.52	2	4
$5s^2S_{1/2}-3p^2P_{1/2}$	16244.513	0.26	2	2
$3d^2D_{5/2}-3p^2P_{3/2}$	12199.476	5.4	6	4
$3d^2D_{3/2}-3p^2P_{3/2}$	12199.525	0.90	4	4
$3d^2D_{3/2}-3p^2P_{1/2}$	12216.721	4.53	4	2

^aData from *Handbook of Chemistry and Physics*, 64th Ed.

^bDegeneracy of upper level.

^cDegeneracy of lower level.

olution laser gain scan indicates gain at 17575.375 cm⁻¹ corresponding to the $4d^2D_{5/2}-3p^2P_{3/2}$ transition (Table III).²

4) *Full Cavity Measurements*: Full cavity measurements were carried out using the optical train depicted in Fig. 3(b). In effect, we replace the Roll-Mentel gain configuration with a full laser cavity operated with either AR coated or Brewster angle windows surrounding the amplification zone. No external light sources are used in these experiments. We have, thus far, adopted two stable cavity configurations, both employing a 99.9% high reflector, one with 4.5% output coupling and a second with 0.2% output coupling. In the first configuration, we surround the ~5 cm medium with a cavity, 44 cm in length and operated with $g_{l2} \sim 0.56$. With this cavity, we achieve results which, to first order, demonstrate the potential for cavity oscillation. If we replace the 4.5% output coupler, which represents a substantial cavity loss element, with a 0.2% output coupler and operate under near optimum reactive flow conditions with $g_{l2} \sim 0.82$, we obtain the results depicted in Fig. 8.

III. RESULTS AND DISCUSSION

A. Gain Measurements

A readily reproducible result obtained using the Roll-Mentel configuration (Fig. 3(a)) for continuous gain measurements is depicted in Fig. 5. The gain coefficient can be calculated from the data in Fig. 5 and the relationship

$$\alpha = \ln((I_2 - I_1)/I_1RT^2)/L. \quad (2)$$

Here, L is the effective gain medium length (medium is not necessarily uniform), R is the mirror reflectivity, and T is the transmission of the amplification zone vacuum chamber window in front of the mirror (Fig. 3(a)). I_1 is the measured (spectrometer) light intensity from the gain medium with the shutter placed in front of the high reflector in Fig. 3(a). Light of intensity, I_1 , which impinges

²Based upon the data given in Table III, the Na $4d^2D_{5/2}-3p^2P_{3/2}$ transition should represent the most favorable to achieve gain and oscillation. The $4d^2D_{5/2}$ level emits dominantly to $3p^2P_{3/2}$ whereas the $4d^2D_{3/2}$ level depletes its population to both the $3p^2P_{1/2}$ and $3p^2P_{3/2}$ levels. Consideration of collisional relaxation among the $3p^2P$ levels would also suggest that the collisionally depleted $3p^2P_{3/2}$ level is favored as the lower laser level.

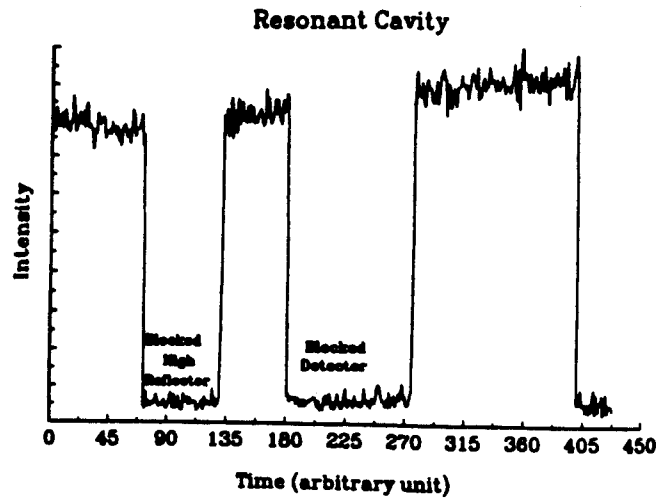


Fig. 8. Full cavity output created with ~0.2% output coupling for the continuous Si-SiO(Si-N₂O)-Na amplifier at $\lambda \approx 569$ nm. These measurements were taken in continuous flow with the cavity configuration depicted in Fig. 4(b). The full cavity output is compared to that obtained with both a blocked high reflector and with the entire cavity isolated from the signal detection system. The ratio of the output obtained for the full cavity to that obtained with a blocked high reflector exceeds $10^3/1$.

on the detector after passing through some portion of the gain medium is associated with a single pass ASE intensity. With the high reflector open to and aligned with the gain medium, we measure light of intensity, I_2 , which is contributed to by (1) light passing directly through the gain medium to the detector (I_1) and (2) light reflected back through the amplification zone from the high reflector. We refer to I_2 as the double pass ASE intensity. Thus, in Eq. (2), we compare the intensity difference ($I_2 - I_1$) to I_1 correcting for the reflectivity and transmissivity.

The stark change in the relative intensities of the 569 nm Na $4d^2D-3p^2P$ and Na D-line emissions for the single and double pass ASE output is quite evident in Fig. 5. The two spectra shown in Fig. 5 are taken under conditions optimized to the pumping of the $4d^2D$ level such that the 569 nm transition shows noticeable positive gain. The ratio of the double to single pass intensity for the 569 nm feature depicted is 2.6/1. This corresponds to a gain coefficient, $\alpha \sim 0.11$ /cm (Eq. (2)). Because of the relatively long time interval needed to scan a spectrum, the gain determined on the basis of successive scans, as depicted in Fig. 5, is by no means an optimal value. More reliable gains are determined when only one transition is monitored and the shutter in front of the total reflector is quickly closed. Under optimal operating conditions, using a 1" diameter 99.9% high reflector, we have achieved amplification such that the ratio of light output when the rear high reflector is accessed to that when the rear high reflector is blocked ranges from 3.4 to 3.8 ($\alpha \sim 0.16$ – 0.23 /cm). This is a ratio which demonstrates clear gain. It should be compared with the measured ratio for a purely fluorescent feature (Na D-line and higher lying excited state Na transitions) which is usually between 1.1 and 1.2 for the Na D-line, and corresponds to 1.6 for the $5s^2S-3p^2P$ transition whose emission is depicted in Fig. 5. The theoretical maximum value for the ratio associated with

pure fluorescence, based on a lossless single reflection, is 2. When the experimental conditions are not favorable for formation of the gain medium, we find significant losses for the reflected light (α negative in (2)) employing the same methods we have used to demonstrate the gain in Fig. 5.

The Na atom transitions at $\lambda \approx 569$ nm ($\alpha \sim 0.1-0.15$), $\lambda \approx 616$ nm ($\alpha \sim 0.03-0.05/\text{cm}$), and $\lambda \approx 819$ nm ($\alpha \sim 0.02-0.03/\text{cm}$) have all been shown to demonstrate gain. The α values given in parentheses are meant to represent typical values determined from (2) using $L = 5$ cm.

Using the Na discharge lamp based optical configuration (Fig. 4(a)), we record the train of peaks depicted in Fig. 6. These peaks correlate precisely with the introduction of the oxidant N_2O into the reaction-energy transfer-amplification zone to produce a continuous gain condition. The percent gain indicated by these peak signals is calibrated using a glass filter inserted into the signal channel so as to produce a known loss peak ($\sim 8\%$ in Fig. 6). Under the experimental conditions associated with Fig. 6, the typical gain is close to 3.6%. Calibrated gains through the amplification zone in excess of 5% can be achieved. Preliminary measurements at 616 nm indicate gains on the order of $1.2 \rightarrow 1.5\%$.

Our measured gains using the lamp based optical configuration are believed to represent lower bounds to the true values due to the significant radial extent (cross sectional area) of the lamp output which intersects a much smaller mixing zone and gain medium. When the 569-nm light exiting the gain medium is focused onto the entrance slit of the monochromator, the measured gain is diluted by the mismatch in cross sectional area as not only the gain zone but also regions of negligible gain and even absorption (pumping of $3p^2P$ level) are monitored.

The signal we record upon scanning a ring dye laser through the region encompassing 569 nm is depicted in Fig. 7. The signal corresponds to a gain in excess of 1.5% for the $4d^2D_{5/2}-3p^2P_{3/2}$ transition. This percent laser gain again represents a lower bound determination of the single pass amplification for (1) the bandwidth of the ring dye laser (effective linewidth ~ 40 MHz) is considerably smaller than the width of the 569 nm Na $4d^2D-3p^2P$ stimulated emission gain profile (~ 2 GHz) [19] and (2) the precise overlap of the sharply defined laser output beam and the amplification zone is certainly unlikely. Because of the inherently narrow bandwidth of the ring dye laser, we select a narrow velocity group within the gain profile velocity distribution. This excludes the remainder of atoms throughout the profile. In order to compare the gain levels measured in this experiment with those for the Roll-Mentel and lamp configurations, we must integrate over the gain profile taking into account the bandwidth of the probe laser. This correction will, of course, lead to the evaluation of a higher single-pass gain.

Taken as a whole, the importance of the three distinct gain measurements, is that they clearly demonstrate the formation of an energy transfer pumped sodium atom laser

amplifier. The magnitude of the gain is probably best represented by the results obtained with the Roll-Mentel configuration. However, these determined gain value correspond to that of a single pass configuration. The effective threshold gain in an oscillating full cavity, influenced both by the increased rate of loss of the population inversion due to the stimulated emission process and by the nature of reactant mixing and energy transfer in the amplification zone, will be notably smaller.

B. Full Cavity Measurements—The Indication of Oscillation

We have obtained results with 4.5% and 0.2% output coupled cavities which suggest the onset of full cavity amplification and oscillation.

In the first set of experiments, using a 4.5% output coupler and 99.9% high reflector we compare the output for the full cavity versus that with the high reflector blocked. Upon tuning the output coupler and high reflector, after adjusting the mixing Si, N_2O , and Na flows, we achieve conditions, at low to moderate sodium flux (conc. estimated to be $\sim 10^{12}/\text{cc}$ in the reaction zone), such that the ratio of the full cavity output to single pass amplification is between 20 and 25/1 in a steady state mode. Walking the cavity mirrors (angle tuning) destroys the amplification. Upon realignment, similar increases in intensity at the steady state value are again observed. We emphasize that these results are sharply dependent on the angle tuning of the cavity. By comparison, if we monitor the reaction-amplification zone configuration of Fig. 2 when only a fluorescent medium associated with the $4d^2D-3p^2P$ Na transition is formed, as evidenced by gain measurements at 569 nm and at the Na D -line, or when we are below threshold despite some stimulated emission in the cavity, we find a typical steady state enhancement between 1.2 and 1.4.

The 4.5% output coupler provides a substantial loss element in the cavity. If we replace this output coupler with a 0.2% output coupler and operate the system under near optimum reactive flow conditions in a stable cavity configuration with $g_1g_2 \sim 0.82$, we find that the ratio of the output for full cavity operation to that obtained with a blocked high reflector (Fig. 8) exceeds 10^3 . Compare also the signal level observed with the blocked high reflector and that monitored with a completely blocked detector. *This result clearly indicates continuous full cavity laser oscillation in the SiO-sodium system.*

If we operate the 0.2% output coupled cavity below threshold, monitoring a purely fluorescent process, the ratio of full cavity to single pass output (blocked high reflector) is found to be slightly greater than 1.8 for the Na D -line ($3p^2P-3s^2S$). This value should be compared to a maximum of 1.2 for the much more lossy 4.5% output coupled device. In fact, a maximum (full cavity/blocked reflector) ratio of order 1.9–1.95 is typical for all those wavelengths considered ($\lambda = 569, 616, \text{Na } D\text{-line}$) when conditions in the reaction-amplification zone are such that

no gain is monitored. We have also observed intermediate behavior associated with the establishment of moderate but not optimal gain conditions.³ Finally, we find that the ratio of the output power for the 4.5% output coupled configuration to that for the 0.2% output coupled configuration is only 1.9/1. When compared to the output coupling ratio of 22.5, this result clearly supports the presence of a stimulated emission process. *These findings in concert with the observed 10^3 enhancement monitored under near optimum reactive flow conditions signal the characteristic operation of a full oscillating cavity.*

The current results are exciting not only because they demonstrate lasing action in the visible region but also because they can be substantially enhanced with several improvements in the manner in which the lasing medium is created and the laser output is extracted from the cavity. It remains to increase both the rate limiting silicon and sodium atom concentrations in the reaction zone while maintaining atomization. This increase may lead to a leveling off and eventual loss of the gain condition if self-absorption on the Na *D*-line transitions becomes a dominant factor or SiO triplet self-quenching begins to play a deleterious role. Evidence is obtained for some self-absorption at high sodium concentration when the alkali atom production dominates the concomitant SiO metastable production.

With our sodium atom source operated, in the absence of interacting silicon or N₂O, at the temperatures which we have employed to produce the highest flux densities in the amplification zone, we have measured the attenuation of the Na *D*-line emission from the sodium discharge lamp. We find an attenuation which is less than 50%. In combination with the cross section for self-absorption, 4×10^{-14} cm², as measured by Ermin *et al.*, [20] this suggests a sodium atom concentration close to that estimated previously. Of course, in the presence of N₂O and silicon reactants, the attenuation due to self absorption, while evidenced, is considerably diminished (~5–10%). Although concern with the possible deleterious effect which a pumping of the Na *D*-line might have on transitions terminating in the $3p^2P$ level is somewhat alleviated, in the present system, by the sodium discharge experiment of Tribilov and Shukhtin [21], and the 0.01-s duration laser pulse for the Na $4s^2S-3p^2P$ infrared transition observed by Mishakov and Tkachenko [22] as quasicontinuous lasing, it must eventually limit the size of the laser system.

The 90° intersection of the SiO metastable and Na atom flows can be used to clearly establish a continuous lasing action; however this is by no means the ideal mixing configuration. With the installation of a concentrically based SiO–Na interaction–energy transfer mixing configuration, we can anticipate a further improvement in the cavity output.

The experiments conducted thus far have made use of only two distinct output coupling configurations. As well as improving reactant concentrations, the optimum output

coupling for the current cavity remains to be evaluated [23]. Finally, we are constructing a modification which will allow removal of the cavity windows that represent significant loss elements. With these improvements, the output from our full cavity configuration should be substantially enhanced.

IV. CONCLUSION AND EXTENSION

We have demonstrated continuous lasing action in the visible region using the near resonant energy transfer pumping of an atomic receptor with a high propensity to lasing action. Not only can the present cavity configuration be enhanced but also the generic nature of the concept is demonstrable.

While our emphasis has been on the sodium system and the results presented involve a metastable SiO pump, it is also feasible to use GeO metastables for energy transfer pumping (Table II). In fact, we have obtained evidence that the energy transfer pumping of the sodium analog potassium based amplifiers associated with the $5d^2D-4p^2P$ ($\lambda \approx 581, 583$ nm), $4d^2D-4p^2P$ ($\lambda \approx 694, 697$ nm), and $6s^2S-4p^2P$ ($\lambda \approx 691, 694$ nm) potassium atom transitions might best be accomplished by GeO metastables. Finally, we have also extended the concept to the successful energy transfer pumping of potential amplifying transitions in lead (Pb), copper (Cu), and tin (Sn) receptor atoms. These systems will be the subject of future study in our laboratory.

ACKNOWLEDGMENT

It is a pleasure to acknowledge most helpful discussions with Drs. R. Jones, Bill Watt, T. Cool, Stan Patterson, Rolf Gross, Sherwin Amimoto, John Dering, Glen Peram, and E. Dorko concerning this study.

REFERENCES

- [1] J. I. Steinfeld, Ed., *Electronic Transition Lasers I*. Cambridge, MA: MIT Press, 1976; L. E. Wilson, S. N. Suchard, and J. I. Steinfeld, Eds., *Electronic Transition Lasers II*. Cambridge, Massachusetts: MIT Press, 1977; Short Wavelength Chemical Laser Workshop, Charleston, SC, November 1984 and SAIC Inc., Atlanta, GA, 1989; H. Hohla and K. L. Kompa, "The photo-chemical iodine laser," in *Handbook of Chemical Lasers*, R. W. Gross and J. F. Bott, Eds. New York: Wiley, 1976, p. 667.
- [2] W. H. Crumley, J. L. Gole, and D. A. Dixon, *J. Chem. Phys.*, vol. 76, p. 6439, 1982; S. H. Cobb, J. R. Woodward, and J. L. Gole, *Chem. Phys. Lett.*, vol. 143, p. 205, 1988; S. H. Cobb, J. R. Woodward, and J. L. Gole, *Chem. Phys. Lett.*, vol. 157, p. 197, 1989; S. H. Cobb, J. R. Woodward, and J. L. Gole, "Continuous chemical laser amplifiers in the visible region," *Proceedings of the Fourth International Laser Science Conference*, A.I.P. Conf. Proc. No. 191, Optical Science and Engineering Series 10, p. 68.
- [3] J. R. Woodward, S. H. Cobb, K. K. Shen, and J. L. Gole, "A chemically driven visible laser transition using fast near resonant energy transfer," in *IEEE J. Quantum Electron.*, vol. 26, 1574, 1990; J. R. Woodward, S. H. Cobb, and J. L. Gole, "Superfluorescent chemically driven visible laser transitions using fast near resonant energy transfer," *Proceedings of the Fourth International Laser Science Conference*, A.I.P. Conf. Proc. No. 191, Optical Science and Engineering Series 10, p. 63.
- [4] J. L. Gole, J. R. Woodward, S. H. Cobb, K. K. Shen, and J. R. Doughty, *SPIE Proceedings Volume 1397, Eighth International Symposium on Gas Flow and Chemical Lasers*, 1990, p. 125.

³Ratios ranging from 40/1 to 100/1 have been routinely measured.

- [5] J. L. Gole, K. K. Shen, C. B. Winstead, and D. Grantier, "An approach to visible chemical laser development using fast near resonant energy transfer," *Journal de Physique IV, Colloque C7, supplement au Journal de Physique III*, vol. 1, Dec. 1991, p. 609.
- [6] "Chemically driven pulsed and continuous visible laser amplifiers and oscillators," by J. L. Gole, K. K. Shen, H. Wang, and D. Grantier, Invited Talk, *Proceedings of the 23rd AIAA Plasma-Dynamics and Laser Science Conference*, Nashville, TN, AIAA 92-2994.
- [7] R. D. Levine and R. B. Bernstein, *Molecular Reaction Dynamics*. New York: Oxford University Press, 1974.
- [8] G. J. Green and J. L. Gole, *Chemical Physics*, vol. 100, p. 133, 1985.
- [9] R. W. Woodward, J. S. Hayden, and J. L. Gole, *Chemical Physics*, vol. 100, p. 153, 1985.
- [10] P. M. Swearingen, S. J. Davis, and T. M. Niemczyk, *Chem. Phys. Lett.*, vol. 55, p. 274, 1978.
- [11] S. H. Cobb, M. McQuaid, and J. L. Gole, unpublished, see also refs. 3-6. D. Husain and P. E. Norris, *J. C. S. Faraday, II*, 93, 106, 335 (1978) and D. Husain and P. E. Norris, *Chemical Physics Letters*, vol. 51, p. 206, 1977.
- [12] A. Gaupp, P. Kuske, and H. J. Andra, "Accurate lifetime measurements of the lowest $^2P_{1/2}$ states in neutral lithium and sodium," *Phys. Rev. A*, vol. 26, pp. 3351-3359, 1982.
- [13] S. A. Kandela, *Appl. Optics*, vol. 23, p. 2151, 1984.
- [14] X. He, B. Li, A. Chen, and C. Zhang, *J. Phys. B., At. Molec. and Opt. Phys.*, vol. 23, p. 661, 1990.
- [15] For thallium see A. Gallagher and A. Lurio, *Phys. Rev.*, vol. 136, p. A87, 1964.
- [16] S. H. Cobb, R. Woodward, K. K. Shen, C. B. Winstead, J. M. Stephens, and J. L. Gole, work in progress.
- [17] W. H. Crumley, and J. L. Gole, "Self-flushing optical window to prevent collection of condensates," *Rev. Sci. Instruments*, vol. 57, p. 1692, 1986.
- [18] G. Roll and J. Mentel, *J. Phys. D. Appl. Phys.*, vol. 22, pp. 483-487, 1989.
- [19] J. L. Gole and K. K. Shen, unpublished calculation.
- [20] A. V. Eremin, I. M. Naboko, and S. A. Palopezhentsev, *Opt. Spectrosc. (USSR)*, vol. 60, p. 567, 1986.
- [21] A. S. Tibilov and A. M. Shukhtin, *Opt. Spectrosc.*, vol. 21, p. 69, 1966. See also, K. Krokkel, M. Hube, W. Luhs and B. Wellegehausen, *Appl. Phys. B37*, pp. 137-140, 1985.
- [22] (a) V. G. Mishakov and T. L. Tkachenko, *Opt. Spectrosc. (USSR)*, vol. 64(3), p. 293, 1988. (b) V. V. Kuchinskii, V. G. Mishakov, A. S. Tibilov, and A. M. Shukhtin, *Opt. Spektrosk.*, vol. 39, p. 1043, 1975 [*Opt. Spectrosc. (USSR)*, vol. 39, p. 598, 1975]. (c) A. A. Kudryavsev, V. N. Skrebov, and T. L. Tkachenko, *Opt. Spektrosk.*, vol. 58, p. 694, 1985 [*Opt. Spectrosc. (USSR)*, vol. 58, p. 420, 1985]. (d) V. G. Mishakov, A. S. Tibilov, and A. M. Shukhtin, *Opt. Spektrosk.*, vol. 31, p. 324, 1971 [*Opt. Spectrosc. (USSR)*, vol. 31, p. 176, 1971]. (e) N. N. Bezuglov and A. B. Tsyganov, *Opt. Spektrosk.*, vol. 59, p. 195, 1985 [*Opt. Spectrosc. (USSR)*, vol. 59, p. 115, 1985].
- [23] A. E. Siegman, *Lasers*. Mill Valley, CA: University Science Books, 1987.

Kangkang Shen was born in Hangzhou, China, on October 28, 1958. He received the B.S. degree in optical engineering from Zhejiang University, Hangzhou, China, in 1982. He received the M.Sc. degree in physics from San Diego State University, CA, in 1987 and transferred to the Georgia Institute of Technology, Atlanta, where he was a graduate student in the High Temperature Laboratory pursuing laser-induced fluorescence studies of metal cluster oxidation and visible chemical laser development. He received his Ph.D. degree in physics in July 1993, and is currently employed by GCH Systems Inc., CA.

From 1982 to 1985 he was employed as an engineer in the Spectroscopy Division of the Central Laboratory of Zhejiang University.

He Wang was born in Beijing, China, on December 17, 1955. He received the B.S. degree in optical engineering from Zhejiang University, Hangzhou, China, in 1982. He received the M.S. degree in optics (laser physics) from the Shanghai Institute of Optics and Fine Mechanics, Shanghai, China, in 1984. He received his Ph.D. degree in physics from the University of Iowa, Ames, in 1991. He was a postdoctoral fellow in the High Temperature Laboratory of the Georgia Institute of Technology, where he pursued laser-induced fluorescence studies of metal cluster oxidation and visible chemical laser development. He is currently a research scientist in the Department of Physics of the University of Connecticut, Storrs.

James L. Gole was born in Chicago, IL, on September 17, 1945. He received the B.S. degree in chemistry from the University of California, Santa Barbara, where he was an NSF undergraduate research fellow, in 1967. He received the Ph.D. degree from Rice University, Houston, TX, in 1971, where he was a Phillips Petroleum Research Fellow. He was an NSF postdoctoral fellow at Columbia University, NY, from 1971 to 1973.

He joined the Department of Chemistry, Massachusetts Institute of Technology, Cambridge, in 1973, and in 1977 moved to the School of Chemistry of the Georgia Institute of Technology, Atlanta, where he became a professor of Chemistry in 1981. In 1983, he joined the School of Physics, GIT, where he is currently a professor of Physics.

He is interested in the molecular electronic structure of high-temperature molecules, chemiluminescence techniques as applied to the study of molecular dynamics and to the determination of molecular parameters, laser-induced fluorescence, high-temperature vacuum ultraviolet spectroscopy, and quantum chemistry. His current fields of interest include high-temperature chemical physics, laser spectroscopy of small metal clusters and metal cluster oxides, chemiluminescence phenomena as applied to the study of reaction dynamics and the nature of metal cluster oxide and halide formation, ultrafast intra- and intermolecular energy transfer, chemical lasers, and quantum chemistry. He has filed 6 patents and has published about 140 papers.

Dr. Gole has been chairman of the ILS Conference, the APS Laser Science Topical Groups Conference on Laser Science, Chairman of Lasers in Chemistry and Biology of the Quantum Electronics and Laser Science Conference, and a member of the editorial board of High Temperature Science. In 1989 he received the Sustained Research Award of the Sigma Xi Research Society and in 1990 was named GIT Outstanding Faculty Research Author. He is a member of Sigma Xi, Phi Lambda Upsilon, AAAS, APS, and ACS.

APPENDIX IX

"Visible Chemical Lasers from Alkali Based Electronic Inversions", in Intense Laser Beams and Applications, K. K. Shen, H. Wang, D. Grantier, W. E. McDermott, and J. L. Gole, editor, SPIE Proceedings, Volume 1871, pg. 18 (1993).

Visible Chemical Lasers from Alkali Based Electronic Inversions

K. K. Shen, H. Wang, D. Grantier, and J. L. Gole
School of Physics
Georgia Institute of Technology
Atlanta, Georgia 30332

ABSTRACT

We discuss two approaches to create electronically inverted Na based atomic and diatomic configurations: (1) highly efficient near resonant intermolecular energy transfer and (2) highly efficient and selective fast direct chemical reaction. Using near resonant energy transfer from selectively formed metastable states of SiO and GeO ($a^3\Sigma^+$, $b^3\Pi$) to sodium atoms, we form laser amplifiers at $\lambda = 569, 616,$ and 819 nm. The metastable triplet states are generated in high yield from the Ge-O₃, Si-N₂O, and Si-NO₂ reactions. The energy stored in the triplet states is transferred in a near resonant process to pump $X^2S_{1/2}$ Na atoms to their lowest excited $3d^2D$, $4d^2D$ and $5s^2S$ states. Adopting a pumping sequence in which argon entrained, premixed, Group IV A metalloid-receptor atom combinations are oxidized, we obtain evidence for the creation of a population inversion producing a gain condition and forming the basis for full continuous cavity oscillation on Na $4d^2D - 3p^2P$ transition at 569 nm. The gain condition is further improved using a nitrogen entrainment gas which efficiently quenches Na $3p^2P$. These results are consistent with recent modeling studies of the Si-SiO-Na laser chemistry. Concepts employed to create amplification and oscillation in these systems are also applicable to the efficient energy transfer pumping of potential amplifying transitions in potassium (K), lead (Pb), copper (Cu - analog of Cu vapor laser), and tin (Sn) receptor atoms. Na₂ amplifiers have also been produced using the highly efficient and selective formation of the dimer excited states from trimer-halogen atom ($M_3 - X(Cl, Br, I)$) reactions. Optical gain through stimulated emission has been demonstrated in select regions close to $527, 492,$ and 460 nm. Results obtained are in close analog to optically pumped alkali dimer lasers. A model which invokes the vibrational and rotational selectivity inherent to a dissociative ionic recombination process ($Na_3^+ + X^- \rightarrow Na_2 + NaX$), in correlation with the coupling between select sodium dimer excited states, may provide a semiquantitative explanation of the observed behavior. The observed gain (max. of 4% at ~ 527 nm corres. to $8 \times 10^{-3}/cm$ for individual rotational levels) can be enhanced considerably with a more versatile source configuration. The considered amplifiers are being optimized and modeled with a focus to increasing amplifier gain length and amplifying medium concentration so as to facilitate their conversion to visible chemical laser oscillators.

INTRODUCTION

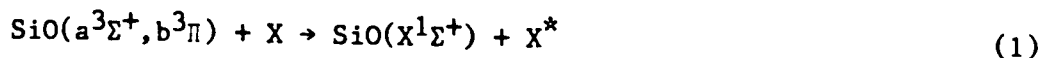
Using a select group of high excited state quantum yield, highly exothermic, metal and metalloid oxidations, we are developing chemically driven laser amplifiers (and oscillators) operative in the visible spectral region.^{1,2}

Relatively simple metal or metalloid oxidation reactions, which involve a branching to long-lived metastable states, show the promise of creating an energy storage medium to pump atomic transitions with an established high propensity for lasing action.² To accommodate this desired pump sequence, we have developed techniques to form copious quantities of the metastable SiO and GeO $a^3\Sigma^+$ and $b^3\Pi$ states as the products of the primarily spin conserving Si-N₂O,³ Si-NO₂,⁴ Ge-N₂O, and Ge-O₃ reactions. These long-lived triplet states act as an energy reservoir for fast near resonant intermolecular energy transfer to efficiently pump atomic transitions including select transitions in thallium and sodium. While the thallium system corresponds to a short pulsed superfluorescent system,² we have now demonstrated continuous gain on several Na atom transitions and obtained evidence for continuous oscillation in the Si-SiO(N₂O)-Na system at 569 nm.^{5,6}

We have also been concerned with the development of the high cross section, highly exothermic Na₃-X(Cl,Br,I) reactions as they selectively form Na₂ amplifiers. The demonstrated chemical laser amplifiers¹ rely on the extremely high cross section Na_n (n=2,3) + X(Cl,Br,I) reactions to create a continuous electronic population inversion based on the chemical pumping of sodium dimer (Na₂). Optical gain through stimulated emission has been demonstrated in the regions close to 527, 492, and 460.5 nm. Results in close analog to optically pumped alkali dimer lasers are noted, the pumping now being demonstrated for the first time in a purely chemical environment.

VISIBLE CHEMICAL LASER TRANSITIONS FROM FAST ENERGY TRANSFER TO ATOMIC SODIUM

In order to pump the 3d²D, 4d²D, and 5s²S levels of atomic sodium,⁵⁻⁷ we make use of the efficient intermolecular energy transfer process



where X* represents the electronically excited atomic species from which we wish to obtain lasing action and the SiO $a^3\Sigma^+$ and $b^3\Pi$ states are formed under multiple collision conditions in a focused argon or helium entrainment flow such that the nascent product distribution of the Si-N₂O³ or Si-NO₂⁴ reactions is rotationally thermalized and vibrationally relaxed (Ref. 2, Figure 4) to the lowest levels of the triplet state manifold. The success of this outlined scheme depends on the rates for the reactions forming the SiO or GeO metastables^{8,9} and the rate of the MO* (M=Si,Ge) - X intermolecular energy transfer, which, we anticipate, will be influenced by the nature of near resonances between the MO* and X* energy levels.

The outlined energy transfer process is found experimentally to be efficient for several sodium atom transitions. To an even greater degree than that inherent to the previously studied chemically pumped Tl based^{2,5} amplifier-oscillator system (Tables I and II of Ref. 2) at $\lambda \approx 535$ nm, there exist near resonant matchups ($\Delta E \approx 100$ cm⁻¹) to receptor atom levels of interest in atomic sodium (Table I of Ref. 7) for both SiO and GeO metastables. We are concerned with the energy transfer pumping of levels which are not accessed through strong electric dipole transitions from the ground state of the alkali atom.^{6,7} Collisions with SiO or GeO metastables are used to energy transfer pump from the 3s²S Na ground state to the Na 4d²D and 5s²S levels, forming the basis for amplification on the 4d²D - 3p²P ($\lambda \approx 569$ nm) and 5s²S - 3p²P ($\lambda \approx 616$ nm) transitions. In the sodium system (Fig. 1(a)), the 3p²P terminal laser level is the short-lived upper level of the Na D-line.¹⁰ The 3p²P - 3s²S transition is characterized by a high oscillator strength facilitating rapid loss of the terminal laser level to create ground state sodium atoms which Figs. 1(a) and 1(b)

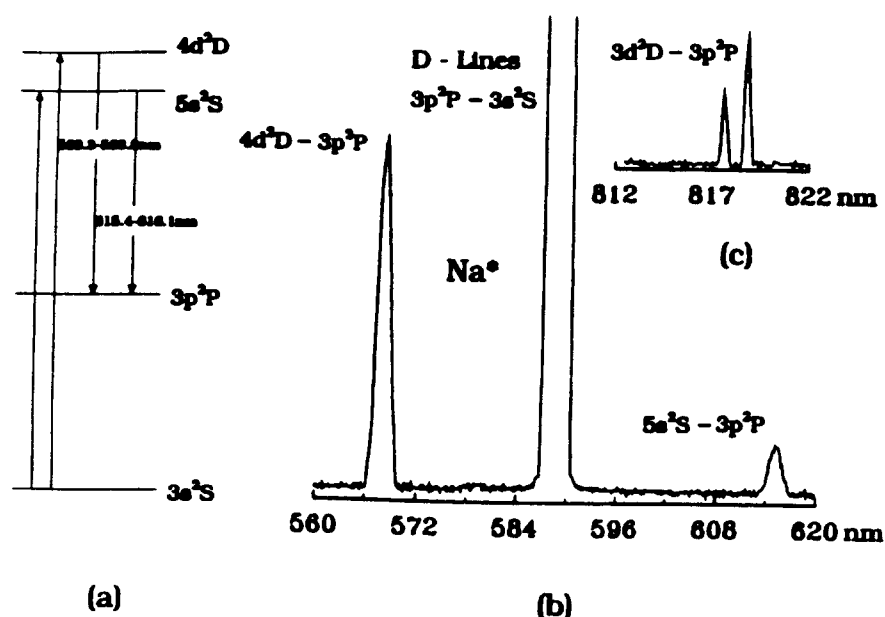


Figure 1(a): Na atom energy level schemes and pumping cycles to produce $4d^2D$ and $5s^2S$ excited states.

Figure 1(b): Typical energy transfer pumping spectrum for Na $4d^2D - 3p^2P$ and $5s^2S - 3p^2P$ transitions and $3p^2P - 3s^2S$ sodium D-line emission. The D-line emission results both from direct energy transfer pumping from ground state NaO and from subsequent fluorescence following emission to the $3p^2P$ level.

Figure 1(c): Energy transfer pumping spectrum corresponding to Na $3d^2D - 3p^2P$ transition.

demonstrate are again amenable to near resonant energy transfer pumping.

While the $5s^2S$ and $4d^2D$ levels are not readily accessed in an optically pumped transition, Fig. 1(b) demonstrates that, using SiO metastables formed in the Si-N₂O reaction, we have successfully energy transfer pumped Na atoms to the 2S and $^2D_{1/2}$ levels where they subsequently emit radiation at $\lambda \approx 616$ nm and 569 nm as they undergo transition to the $3p^2P$ levels. The energy transfer process which pumps these sodium atom levels appears at least as efficient as that observed for the Tl system (Ref. 2, Figs. 4,5). The observed Na atom transitions, originating at the $4d^2D$ and $5s^2S$ levels, are characterized by moderate oscillator strengths. The accessed Na cycle, with its 50 ($4d^2D - 3p^2P$)¹³ to ~ 100 ($5s^2S - 3p^2P$)¹⁴ nanosecond upper state radiative lifetimes (vs. Tl $^2S_{1/2}$ at ~ 7 nsec.¹⁵) and short-lived terminal laser level, would appear ideally suited to obtain high duty cycle laser amplifiers and oscillators. In fact, we find that these transitions demonstrate continuous gain. Further, as indicated in Fig. 1(c), we have obtained evidence for the energy transfer pump of the Na $3d^2D$ level with which is associated an atomic emission at $\lambda \approx 819$ nm ascribed to the Na $3d^2D - 3p^2P$ transition. We outline a range of measurements on the Si-SiO-Na system which have been used to demonstrate continuous gain on the $4d^2D - 4p^2P$, $5s^2S - 3p^2P$, and $3d^2D - 3p^2P$ transitions at $\lambda \approx 569$, $\lambda \approx 616$, and $\lambda \approx 819$ nm respectively, and summarize evidence for continuous oscillation at $\lambda \approx 569$ nm.

In approaching the outlined energy transfer laser scheme, self absorption associated with the Na D-line must be considered. Evidence is obtained for moderate self-absorption at the highest concentrations used in the present experiments, however concern with the possible deleterious effect which such a pumping of the Na D-line might have on transitions terminating in the $3p^2P$ level is greatly alleviated by the Na discharge experiments of Tibilov and Shukhtin¹⁶ which demonstrate a surprising lasing action on the Na $4s^2S - 3p^2P$ transitions in the infrared region. Further experiments in our laboratory (see following) and laser chemistry modeling¹⁷ also suggest that, despite self absorption, lasing action is still readily attainable.

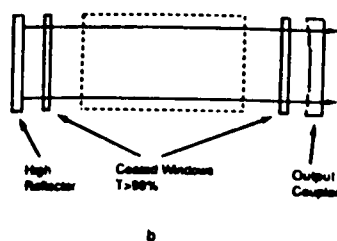
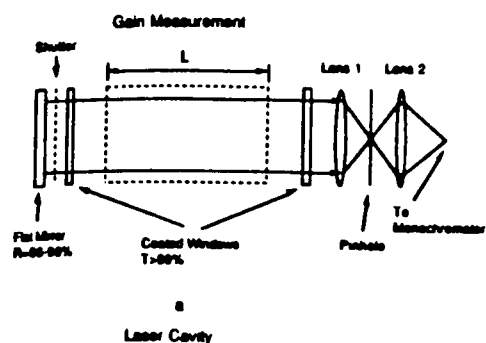
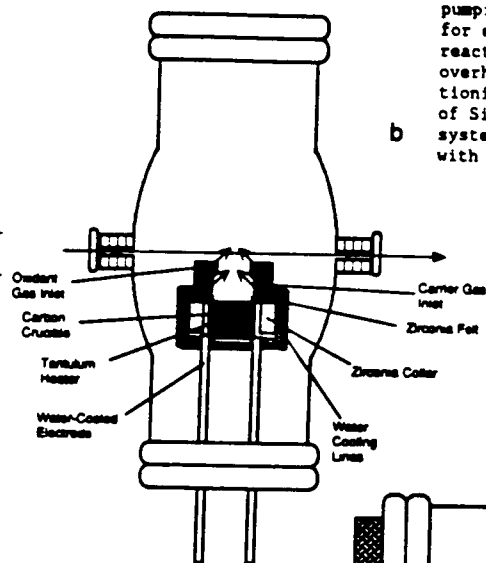


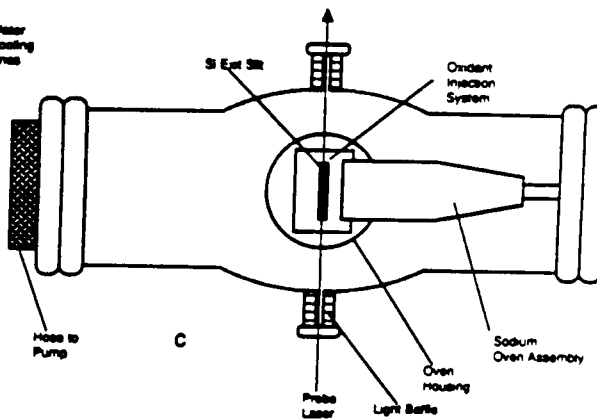
Figure 2(a): Gain measurement configuration after Roll and Mentel (ref. 18). The region marked L in the figure corresponds to the reaction-amplification zone.

Figure 2(b): Laser cavity configuration to characterize potential oscillation in the Si-SiO-Na system at 569 nm.



Overall Apparatus Configuration

Figure 3: (a) Schematic of reaction chamber and windows defining optical train, ballast tank to moderate pumping fluctuations, and pumping configuration, for extended path length Si-SiO (Si-N₂O)-Na reaction amplification zone. (b),(c) Side and overhead views of reaction chamber showing positioning of Si oven source, relative locations of Si and Na oven sources, oxidant injection system, and relative positions of these devices with respect to the optical train.



GAIN MEASUREMENTS FOR SiO-Na - NATURE OF THE REACTION-ENERGY TRANSFER-AMPLIFICATION ZONE

Gain Measurement

Gain measurements have been carried out on the sodium system using three different experimental configurations. The simplest of these measurements uses the optical train depicted in Fig. 2(a) most recently surrounding an ~ 5 cm energy transfer - amplification zone⁵⁻⁷ created using the mixing configuration depicted in Fig. 3. The optical train parallels the ingenious design of Roll and Mentel,^{7,18} used to measure amplified spontaneous emission (ASE).^{5-7,18} The gain coefficient α , can be calculated from

$$\alpha = \ln ((I_2 - I_1)/I_1 RT^2)/L \quad (2)$$

Here, L is the effective gain medium length (medium is not necessarily uniform), R is the mirror reflectivity, and T is the transmission of the amplification zone vacuum chamber window in front of the mirror (Fig. 2(a)). I_1 is the measured "single pass" (spectrometer) light intensity from the gain medium with the shutter placed in front of the high reflector. With the high reflector open to and aligned with the gain medium, we measure light of intensity, I_2 , which is contributed to by (1) light passing directly through the gain medium to the detector (I_1) and (2) light reflected back through the amplification zone from the high reflector. We refer to I_2 as the double pass ASE intensity. Thus, in Equation (2), we compare the intensity difference ($I_2 - I_1$) to I_1 correcting for the reflectivity and transmissivity.

Sodium Atomic Emissions

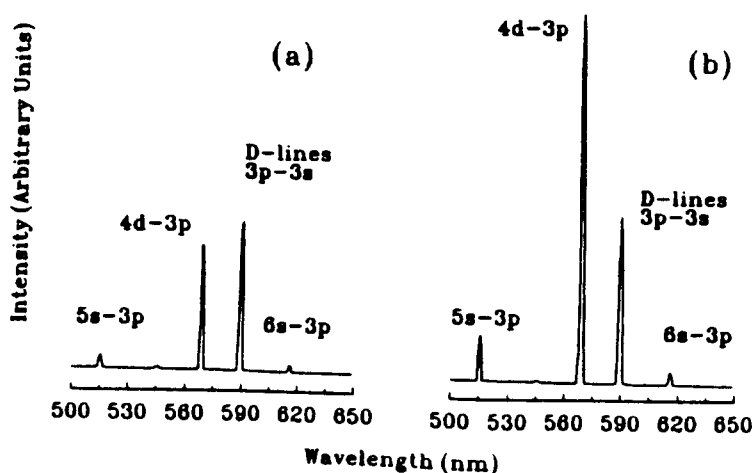


Figure 4(a): Single pass continuous amplified spontaneous emission (ASE) intensity (I_1) measured using a Spex 1 meter spectrometer and RCA 4840 phototube and the gain configuration depicted in Figure 3(a) for the Si-SiO-Na system. Spectral resolution is 1 nm. Because the figure is uncorrected for photo-tube response, decreasing from 510 to 630 nm, or grating blaze (500 nm), the emission associated with the $6s^2S - 3p^2P$ transition appears more intense than that associated with the $5s^2S - 3p^2P$ transition.

Figure 4(b): Double pass continuous amplified spontaneous emission (ASE) intensity (I_2) measured using the gain configuration depicted in Fig. 3(a) for the Si-SiO-Na system. The Na D-line intensity is comparable to that in Fig. 4(a). The ratio of the I_2/I_1 intensity for the 569 nm Na emission feature is 2.6/1 for this individual study and can approach 3.8/1 under optimal conditions for the system. Spectral resolution is ~ 1 nm (see (a)).

The stark change in the relative intensities of the 569 nm Na $4d^2D - 3p^2P$ and Na D-line emissions for the single and double pass ASE output is quite evident in Figure 4. The ratio of the double to single pass intensity for the 569 nm feature depicted is 2.6/1. This corresponds to a gain coefficient, $\alpha \sim 0.11/\text{cm}$ (Eq. 2), which is by no means the optimal value that has been achieved with the current configuration. Under optimal operating conditions, using a 1" diameter 99.9% high reflector, we have achieved amplification such that the ratio of light output when the rear high reflector is accessed to that when the rear high reflector is blocked ranges from 3.4 to 3.8 ($\alpha \sim 0.16\text{-}0.23/\text{cm}$). This is a ratio which demonstrates clear gain. It should be compared with the measured ratio for a purely fluorescent feature (Na D-line and higher lying excited state Na transitions) which is usually between 1.1 and 1.2 for the Na D-line, and corresponds to 1.6 for the $5s^2S - 5p^2P$ transition whose emission is also depicted in Figure 4. The theoretical maximum value for the ratio associated with pure fluorescence based on a lossless single reflection is 2. When the experimental conditions are not favorable for formation of the gain medium, we find significant losses for the reflected light (α negative in Eq. (2)) employing the same methods we have used to demonstrate the gain in Figure 4. The Na atom transitions at $\lambda \approx 569$ nm ($\alpha \sim 0.1\text{-}0.15$), $\lambda \approx 616$ nm ($\alpha \sim 0.03\text{-}0.05/\text{cm}$), and $\lambda \approx 819$ nm ($\alpha \sim 0.02\text{-}0.03/\text{cm}$) have all been shown to demonstrate gain. The α values given in parentheses are meant to represent typical values determined from Eq. 2 using $L \approx 5$ cm.

A second series of more complex gain measurements have involved the measurement of gain on the emission lines from a sodium discharge lamp. Here, using a configuration described in more detail elsewhere,^{6,7} we have measured the enhancement of the $\text{Na } 4d^2D - 3p^2P$ emission line (or other sodium transitions) which can be evaluated by singling out the transition of interest with a 10 nm bandpass filter. Under typical experimental conditions when selecting the 569 nm output from the lamp, we measure a calibrated gain^{6,7} close to 3.6%. Calibrated gains associated with the amplification zone which are in excess of 5% can be achieved. Preliminary measurements at 616 nm indicate gains on the order of $1.2 \rightarrow 1.5\%$. Our measured gains using the lamp based optical configuration are believed to represent lower bounds to the true values due to the significant radial extent (cross sectional area) of the lamp output which intersects a much smaller mixing zone and gain medium. When the 569 nm light exiting the gain medium is focused onto the entrance slit of the monochromator, the measured gain is diluted by the mismatch in cross sectional area as not only the gain zone but also regions of negligible gain and even absorption (pumping of $3p^2P$ level) are monitored.

We have also used the output from a high resolution ring dye laser to carry out laser gain measurements in a frequency scanning (laser with calibration vs. iodine) mode.^{6,7} Upon scanning the ring dye laser through the region encompassing the 569 nm feature, we record a gain in excess of 1.5% for the $\text{Na } 4d^2D_{5/2} - 3p^2P_{3/2}$ transition.^{7,19} This percent laser gain again represents a lower bound determination^{6,7} of the single pass amplification for (1) the bandwidth of the ring dye laser (effective linewidth ~ 40 MHz) is considerably smaller than the width of the 569 nm $\text{Na } 4d^2D - 3p^2P$ stimulated emission gain profile (~ 2 GHz) and (2) the precise overlap of the sharply defined laser output beam and the amplification zone is tenuous.^{6,7}

The three distinct gain measurements clearly demonstrate the formation of an energy transfer pumped sodium atom laser amplifier. The magnitude of the gain is probably best represented by the results obtained with the Roll-Mentel configuration. However, these determined gain values correspond to a single-pass through the amplification zone. The effective threshold gain in an oscillating full cavity, influenced both by the increased rate of loss of the population inversion due to the stimulated emission process and by the nature of reactant mixing and energy transfer in the amplification zone, will be notably smaller.

Amplification Zone

The flow configuration depicted in Fig. 3 produces the longest path length SiO metastable flame ($\sim 5 + \text{cm}$) ever obtained. The entrainment flow configuration (argon or helium) must be designed to create large concentrations of SiO (GeO) metastables which are intersected at $\sim 90^\circ$, in subsonic flow, by a high concentration of sodium (in argon or helium) atoms. The entrained silicon and sodium flows can also be moved in-situ relative to each other and hence with respect to the reaction - energy transfer - amplification zone to optimize conditions for formation of the gain medium. We are concerned with the optimization of reactant mixing considering the rate limiting effect of the silicon concentration, the importance of virtually complete sodium atomization, and the confinement of the reactants and receptors to the cavity axis region. With the silicon source temperature monitored by optical pyrometry, we estimate the Si atom concentration in the amplification zone as a minimum of $10^{14}/\text{cc}$ for all studies involving gain measurement. The N_2O oxidant concentration exceeds $5 \times 10^{14}/\text{cc}$ and the SiO metastable concentration exceeds $10^{13}/\text{cc}$.⁷ Based upon the Na source temperature and the measured rate of expenditure

of sodium from the source, exceeds $10^{18}/\text{cm}^2\text{-sec}$ in the reaction zone, which corresponds to a density of order $10^{13}/\text{cc}$.⁷ The reactant and entrainment flows must also be controlled so as to protect the cavity windows from the condensation of metastable silicon or germanium oxide and/or sodium. This latter requirement is met (Fig. 3), in part, using "self cleaning" optical windows²⁰ with a protective helium (not argon) flow. The "rate limiting" silicon concentration signals a focus on the modification of the oven source configuration depicted in Figure 3 so as to continually improve the silicon atom flux as well as the flow conditions whereby this reactant is transferred to the reaction-energy transfer-amplification zone.

The mixing zone of Fig. 3 is greatly stabilized by the moderate sized (~ 15 cubic feet) ballast separating the 150 cfm pump and reaction chamber. The current 90° intersection of the SiO (GeO) and Na atom flows, once stabilized, can be used to clearly establish a continuous lasing action, however, this is, by no means, the ideal mixing configuration. We have now constructed a device which allows the concentric mixing of Si, Na, and N_2O flows so as to replace the 90° intersection of the entrained SiO and Na flows. Once in full operation, this configuration should further improve the outlined results.

Full Cavity Measurements - The Indication of Oscillation

If we replace the gain measurement system with a full mirror laser cavity configuration in which the output coupling (1" diameter mirror) corresponds to 0.2%, employ the same 1" diameter, 99.99% reflector as used in the gain evaluation studies, and operate the system under near optimum reactive flow conditions in a stable cavity configuration with $g_1 g_2 \sim 0.82$, we find that the ratio of the output for full cavity operation to that obtained with a blocked high reflector (Figure 5) exceeds 10^3 . Compare also the signal level observed with the blocked high reflector and that monitored with a completely blocked detector. This result clearly indicates continuous full cavity laser oscillation in the SiO-sodium system.

If we operate the 0.2% output coupled cavity below threshold, monitoring a purely fluorescent process, the ratio of full cavity to single pass output (blocked high reflector) is found to be slightly greater than 1.8 for the Na D-line ($3p^2P -$

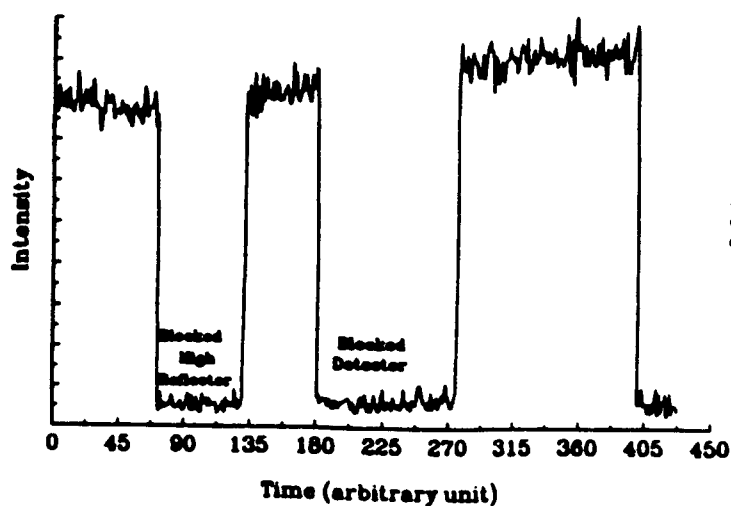


Figure 5: Full cavity output created with $\sim 0.2\%$ output coupling for the continuous Si-SiO(Si-N₂O)-Na amplifier at $\lambda = 569$ nm. These measurements were taken in continuous flow with the cavity configuration depicted in Fig. 3(b). The full cavity output is compared to that obtained with both a blocked high reflector and with the entire cavity isolated from the signal detection system. The ratio of the output obtained for the full cavity to that obtained with a blocked high reflector exceeds $10^3/1$.

$3s^2S$). This value should be compared to a maximum of 1.2 for a much more lossy 4.5% output coupled device ($g_1 g_2 \sim 0.56$). In fact, a maximum (full cavity/blocked reflector) ratio of order 1.9-1.95 is typical for all those wavelengths considered ($\lambda \approx 569, 616, \text{Na D-line}$) when conditions in the reaction-amplification zone are such that no gain is monitored. We have also observed intermediate behavior associated with the establishment of moderate but not optimal gain conditions.

Improvement of the Energy Transfer Based Configuration - Ultimate Goals

The current results are exciting not only because they demonstrate lasing action in the visible region but also because they can be substantially enhanced with

Sodium Atomic Emissions
SiO-Na Energy Transfer

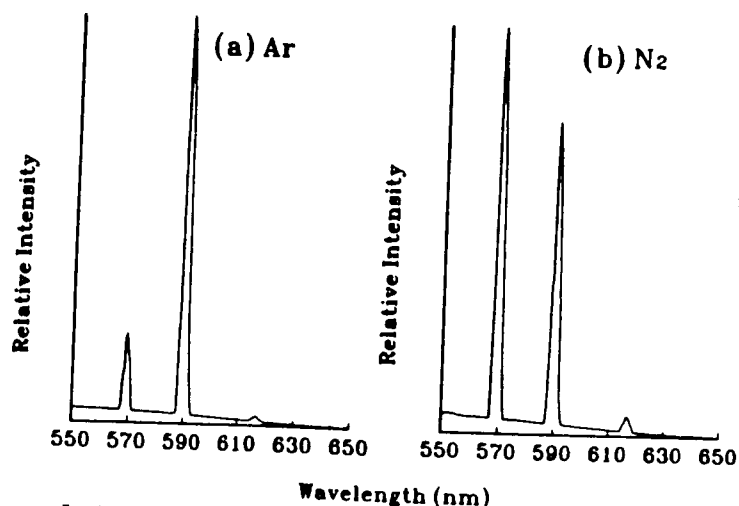


Figure 6: Energy transfer pumping spectra obtained for (a) Ar and (b) N_2 entrainment. The observed Na $4d^2D - 3p^2P$ emission feature ($\sim 569 \text{ nm}$) is seen to increase precipitously in intensity relative to the Na $3p^2P - 3s^2S$ D-line ($\sim 590 \text{ nm}$) with change of entrainment gas from argon to N_2 . See also Fig. 1.

several improvements in the manner in which the lasing medium is created and the laser output is extracted from the cavity. It remains to increase both the rate limiting silicon and sodium atom concentrations in the reaction zone while maintaining atomization. This increase may lead to a leveling off and eventual loss of the gain condition if self-absorption on the Na D-line transitions becomes a dominant factor or SiO triplet self-quenching begins to play a deleterious role. Evidence is obtained for some self-absorption at the highest sodium concentrations when the alkali atom production dominates the concomitant SiO metastable production. With our sodium atom source operated, in the absence of interacting silicon or N_2O , at the temperatures which we have employed to produce the highest flux densities in the amplification zone, we have measured the attenuation of the Na D-line emission from a sodium discharge lamp. We find an attenuation which is less than 50%. In combination with the cross section for self absorption, $4 \times 10^{-14} \text{ cm}^2$, as measured by Ermin et al.,²¹ this suggests a sodium atom concentration close to that estimated previously. Of course, in the presence of N_2O and silicon reactants, the attenuation due to self absorption, while evidenced, is considerably diminished ($\sim 5 - 10\%$).

Although concern with the possible deleterious effect which a pumping of the Na D-line might have on transitions terminating in the $3p^2P$ level is somewhat alleviated in the present system by the sodium discharge experiment of Tribilov and Shukhtin,¹⁶ and the 0.01 second duration laser pulse for the Na $4s^2S - 3p^2P$ infrared transition observed by Mishakov and Tkachenko²² as quasicontinuous lasing, it must eventually limit the size of the laser system. However, this might be forestalled to great degree if we take advantage of the efficient quenching of Na $3p^2P$ atoms which Tanarro

et al.²³ have demonstrated for N_2 and CO. In fact, if we replace the Si-SiO and Na entraining argon or helium gases^{6,7} with N_2 , we observe a pronounced effect on the energy transfer spectrum (Fig. 6) taken for an intermediate sodium flux. While the 569 nm feature is dominated by the Na D-line emission when argon is used as an entrainment gas, its intensity can be made to exceed that of the D-line when N_2 is used. This result, obtained and repeated for successive scans taken during the same experimental run, suggests the possibility for a considerable enhancement of the 569 nm output. This improvement might well result from the quenching of $Na\ 3p^2P$, however, it might also result from an increased inhibition of the $Na + N_2O \rightarrow NaO + N_2$ reaction²⁴ as the equilibrium is forced toward reactants. The specific cause will need to be assessed in future experiments.

The experiments conducted thusfar have made use of only two distinct output coupling configurations. As well as improving reactant concentrations, the optimum output coupling for the current cavity remains to be evaluated. Finally, we have constructed a modification which will allow removal of the cavity windows that represent significant loss elements. With these improvements, the output from our full cavity configuration should be substantially enhanced.

Recently, Smith et al.¹⁷ have begun a laser chemistry modeling effort on the SiO-Na system. Starting with initial concentrations of the reactants Na, Si, and N_2O which are achievable in the present system these authors have used a model which includes the 10 possible processes

1. $Si + N_2O \rightarrow SiO^* + N_2$ - metastable excited state formation
2. $Si + N_2O \rightarrow SiO + N_2$ - ground state formations - power depleting
3. $SiO^* + Na \rightarrow SiO + Na^* (4d^2D)$ - upper state amplifying transition
4. $SiO^* + Na \rightarrow SiO + Na^* (3p^2P)$ - terminal level amplifying transition
5. $SiO^* + SiO^* \rightarrow SiO + SiO$ - self quenching of SiO metastables
6. $Na^* (4d^2D) \rightarrow Na^* (3p^2P) + h\nu (569\text{ nm})$ - spontaneous emission
7. $Na^* (4d^2D) + h\nu (569\text{ nm}) \rightarrow Na^* (3p^2P) + 2h\nu (569\text{ nm})$ stimulated emission
8. $Na^* (3p^2P) + h\nu (569\text{ nm}) \rightarrow Na^* (4d^2D)$ - optical pumping
9. $Na^* (3p^2P) \rightarrow Na (3s^2S) + h\nu (589\text{ nm})$ - spontaneous emission
10. $h\nu (569) \rightarrow h\nu (569)$ outcoupling fraction for 569 nm photons (laser cavity 5 cm in length - mirror reflectivities 99.99 and 99.80%).

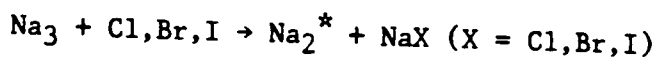
Using known kinetic rates, variable initial concentrations, reasonable and variable rates for those processes which have not been directly measured, and assuming a closed reaction in which the reactants are not replenished, Smith et al.¹⁷ have deduced temporal profiles for the Na concentration, 569 nm photon concentration, energy density, and power density. They conclude that order of magnitude increases in the initial concentration of Si or N_2O have a profound effect on the system (power density increase) whereas significant changes in the Na concentration have relatively little effect. This signals the rate limiting nature of the silicon concentration and the importance of the branching into the metastable triplet states. It is also to be noted that a significant increase in power density may be muted by SiO^* self quenching, the rate of which certainly must be established for these systems. For the diversity of initial reactant concentrations and rates used in their model, Smith et al.¹⁷ predict output power densities peaking between 100 (strong SiO^* self quenching) and 7000 mW/cc. These results, which will soon be supplemented by a more detailed modeling effort, are quite encouraging.

While our emphasis has been on the sodium system and the results presented

involve a metastable SiO pump, it is also feasible to use GeO metastables for energy transfer pumping. In fact, we have obtained evidence that the energy transfer pumping of the sodium analog potassium based amplifiers associated with the $5d^2D - 4p^2P$ ($\lambda \approx 581, 583$ nm), $4d^2D - 4p^2P$ ($\lambda \approx 694, 697$ nm), and $6s^2S - 4p^2P$ ($\lambda \approx 691, 694$ nm) potassium atom transitions might best be accomplished by GeO metastables. Finally, we have also extended the concept to the successful energy transfer pumping of potential amplifying transitions in lead (Pb), copper (Cu), and tin (Sn) receptor atoms. These systems will also be the subject of future study in our laboratory.

CONTINUOUS CHEMICAL LASER AMPLIFIERS IN THE VISIBLE REGION BASED ON HIGHLY EFFICIENT AND SELECTIVE CHEMICAL REACTION

The $Na_3 - X$ reactions form an unusual class of reactive encounters. The optical signatures for the processes



encompass emission from a limited number of Na_2 band systems. The observed dimer emission is characterized by sharp well defined emission regions¹ (Fig. 7) superimposed on a much weaker Na_2 background fluorescence. The sharp emission features are not readily explained by invoking a purely fluorescent process, and demonstrate characteristics similar to those of optically pumped Na_2 laser systems.^{1,6,25} In the visible spectral region, these features grow at a near exponential rate with increasing Na_3 concentration, relative to the Na_2 background spectrum. This suggests the possibility that stimulated emission might be associated with certain of the emitting Na_2 reaction products. Laser gain measurements carried out to assess this possibility throughout the visible region reveal optical gain through stimulated emission and the creation of population inversions on select Na_2 electronic transitions.

Measurements at 0.5 cm^{-1} resolution reveal amplification in the regions close to

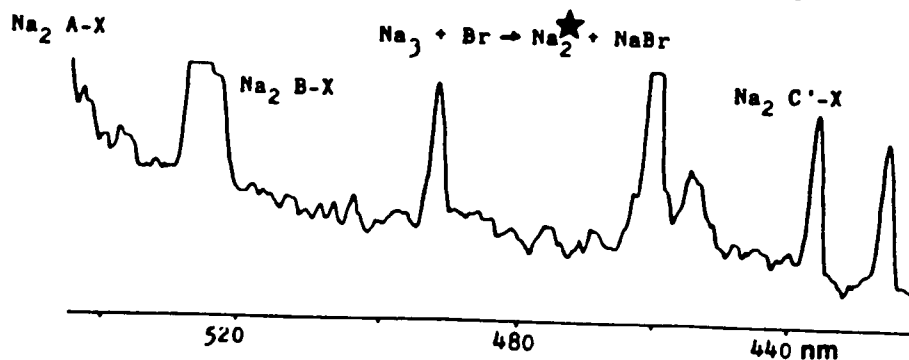


Figure 7: Chemiluminescent emission from the reaction $Na_3 + Br \rightarrow Na_2^* + NaBr$.

527 nm (1% gain), 492 nm (0.3% gain) and 460.5 nm (0.8% gain), correlating precisely with the reactive process and the relative intensities of those features observed while monitoring the light emitted from the Na_3 -Br reaction (Fig. 7). High resolution ring dye laser scans in the 527 nm region indicate that the gain for the system is a minimum of 3.8% for an individual rovibronic transition with approximately four to seven individual rotational transitions showing gain. At 459.8 nm, we have measured a 2.3% gain for an individual rotational transition. These results demonstrate the continuous amplifying medium for a visible chemical laser in at least three wavelength regions.^{1,6} At no other scanned wavelengths have we

observed gain. In fact, in scanning the entire 420-600 nm region, we generally observe slight losses of the laser photon flux due primarily to scattering (to only a negligible extent, absorption) on transit through the $\text{Na}_3\text{-Br}$ reaction zone. In the region of the sodium D-line, we monitor a substantial absorption and loss as a function of the trimer-halogen atom reaction.^{1,6} The Na_3 -halogen atom reactions are expected to proceed via an electron jump mechanism with extremely high cross sections,²⁶ producing substantial Na_2 excited state populations. The question of why the $\text{Na}_3\text{-X}$ reactions appear to demonstrate vibrational and rotational selectivity in certain wavelength regions may be explained by invoking a model for the dissociative ionic recombination, $\text{Na}_3^+ + \text{X}^- \rightarrow \text{Na}_2 + \text{NaX}$, and the curve crossings which influence the distribution of product molecules for this process.²⁷ Such a model, coupled with an analysis of the electronic coupling between select sodium dimer excited states,²⁷ appears to provide a semiquantitative explanation of the observed population inversions.

Created population inversions are thought to be sustained by the large number of free halogen atoms reacting with the Na_2 molecules in those ground state levels on which the transitions emanating from the Na_2 excited states terminate and collisional relaxation of the ground state sodium dimer molecules. The cross section for reaction of vibrationally excited ground state Na_2 is expected to be quite substantial relative to the cross section for collision induced vibrational deactivation of the Na_2 manifold. Extremely efficient reactions are thought to greatly assist the depletion of the lower state levels in this system allowing one to sustain a continuous population inversion. Our major efforts thusfar have focused on the Na_2 B-X spectral region and the potential development of laser oscillators at wavelengths in the vicinity of 527 and 460 nm. In order to approach these studies, we are developing the means to create a considerably longer path length amplification region.

Development of an Extended Path Length $\text{Na}_3 - \text{X}$ (Cl,Br,I) Reaction - Amplification Zone

We desire to considerably improve the magnitude of the amplification demonstrated previously for the sodium dimer amplifiers at ~ 527 , ~ 492 , and ~ 460 nm. In previous experiments we have produced a substantial Na_3 concentration ($\geq 10^{13}/\text{cc}$) albeit in a limited reaction-amplification zone. In order to demonstrate continuous chemical laser oscillation, however, it is desirable to create an enhanced sodium trimer - halogen atom reaction zone not only in terms of reactant concentration but also with respect to the amplification zone path length. The overall apparatus design depicted in Figure 8 is meant to accommodate high intersecting reactant flows from both sodium trimer and (dual rotatable) halogen atom sources in order to produce a considerably enhanced concentration of Na_2 amplifiers over an extended path length. This system attempts to increase the Na_3 reaction - amplification zone concentration by repositioning the trimer and halogen atom sources relative to each other and facilitating the halogenation process much closer to the alkali source nozzle itself, in a gas dynamic configuration. We incorporate the facility for the in-situ adjustment of the alkali and halogen source positions, including the ability to rotate dual alkali-trimer-flow-encompassing halogen atom slit sources (Figs. 8(b), 8(d)) so as to optimize flow mixing. Further, as a means of increasing the reaction zone and gain length, we are testing a continuous flow slit source technology to create at least an ~ 5 cm long amplification zone. Here a small circular "pinhole" nozzle used in previous experiments^{1,6} is now replaced by a slit approximately 100μ in width by $2\frac{1}{2}$ " in length.

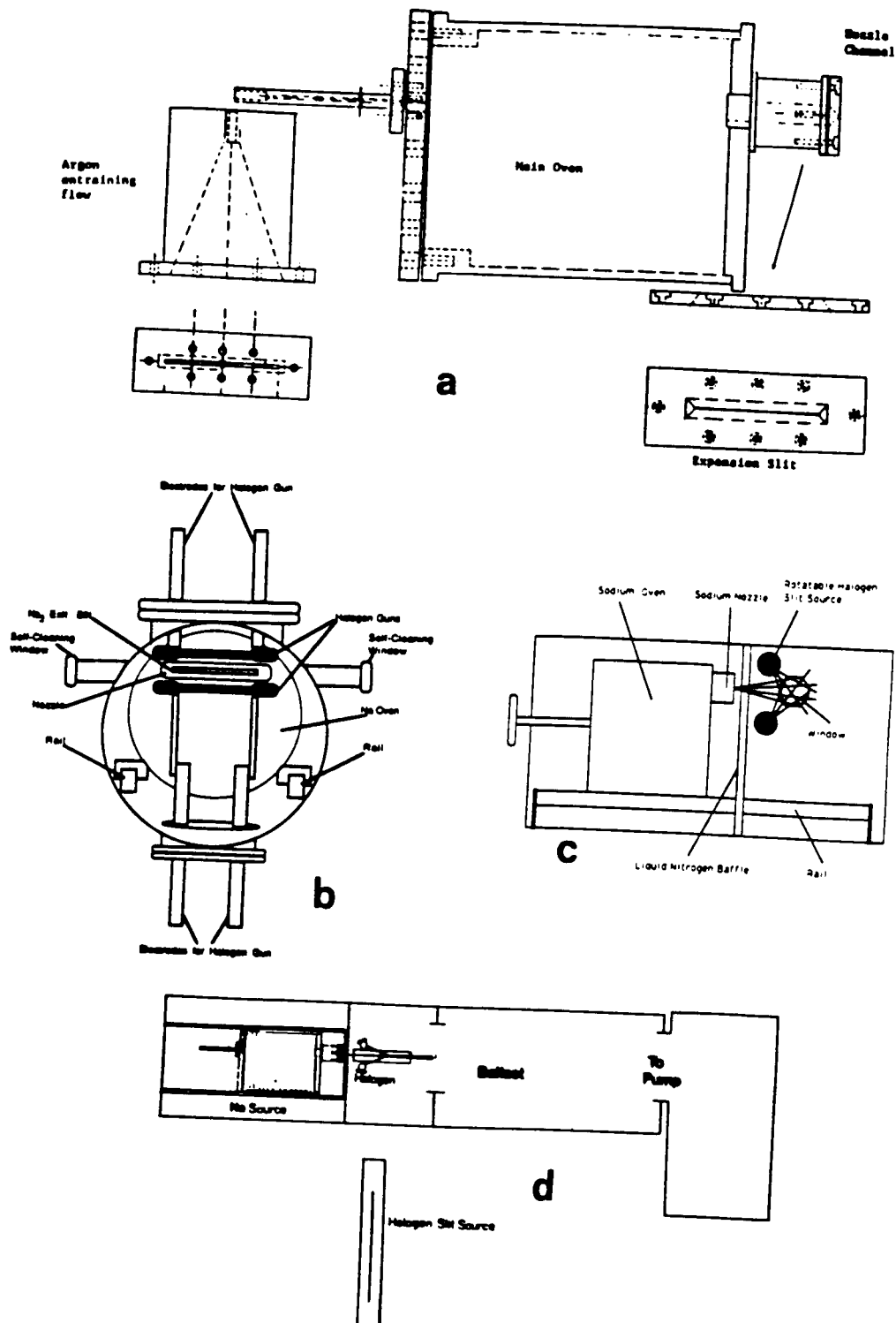


Figure 8: Schematics of upscaled Na_3 -halogen atom reactive flow configurations. (a) Schematic of sodium slit source configuration with argon entrainment flow device for seeded expansion, (b), (c) Front and side views of upscaled reaction-vacuum chamber configuration showing positions of halogen and sodium sources, (d) Schematic of upscaled vacuum chamber and pumping configurations. See text for discussion.

The overall alkali source design pictured in Fig. 8(a) in side and partial frontal view corresponds to a full seeded configuration where helium or argon can be passed through the rear diverging gas source assembly, flowing over molten sodium, the mixture then being expanded through the frontal nozzle slit configuration. In a pure sodium supersonic expansion, the Na_3 constituency is dominated by a much larger atom and cold dimer concentration.²⁸ While this constituency will not interfere at the Na_2 amplifier wavelengths characteristic of the Na_3 -halogen atom reaction systems, it is desirable to minimize the atom and dimer while increasing the trimer concentration. The trimer concentration can be altered and improved by seeding the expansion with helium, argon, or other noble gas atoms. In fact several researchers²⁹ have demonstrated that the atom and dimer concentrations can be made quite small relative to the much larger sodium polymers. We do not wish to operate at these extreme expansion conditions but, rather, seek a middle ground which will allow formation of the trimer and a few larger clusters.³⁰ This condition can be accomplished through the appropriate adjustment of parameters which can be manipulated in the expansion including (1) the rear oven stagnation pressure (argon - sodium), (2) the frontal nozzle temperature, and (3) the ratio of the supersonic expansion source pressure to the overall expansion chamber pressure.

In the overall experimental design depicted in Figure 8 the sodium slit source, connected to a liquid nitrogen cooled bulkhead apparent in the figure, is positioned relative to the dual halogen slit sources located above and below the position of an alkali sheath created upon expansion from this alkali slit source. The halogen slit sources are designed to optimize the interaction of the alkali trimer and halogen atoms over the entire width of the intersecting reactant sheaths, created as the dual halogen flow intersects the alkali constituency. The optical train defining the laser cavity, encompassed on each end by self cleaning optical windows as indicated in Fig. 8(b), is parallel to the intersection of the alkali and halogen flows. This reaction zone cavity configuration is designed to allow for 1) short transit of the reactants Na_3 and $\text{X} = \text{Cl}, \text{Br}, \text{I}$ to the reaction - amplification zone, 2) flexible movement of these sources with respect to each other and with respect to the flow patterns created in the system and 3) minimal interaction of these reactants with laser cavity windows. To insure this minimal interaction, the self-cleaning optical windows noted previously²⁰ are used. The reaction zone is evacuated through a 35 cubic foot ballast tank followed by a 1250 CFM Stokes - Roots-Blower combination.

Initial Experimental Results

In our initial successful operation of the upscaled $\text{Na}_x - \text{X}$ system, we have been concerned with the evaluation of pure sodium supersonic expansions and the optimization of expansion conditions so as to demonstrate the formation of a cooled and hence supersonically expanded sodium dimer constituency. In conjunction, we are attempting to build up the trimer concentration to the level desired to form an extended path length amplification zone. We find, not surprisingly, that the nature of the created excited state concentrations in the extended path reaction zone depend both on the positioning and orientation of the alkali and halogen sources.

With the alkali source nozzle and halogen sources positioned within 3.8 cm of each other, the alkali system operated under conditions which produce significant concentrations of cooled Na_2 , and the halogen slit sources oriented at 75° relative to the sodium flow in a direction away from the alkali nozzle, we observe the emission associated with $\text{Na}_x\text{-Br}$ reactions depicted in Fig. 9. This signature observed along the path of the optical train in Fig. 8 consists of a dominant Na_2 A-X and Na D-line and considerably weaker B-X emission feature. Further analysis

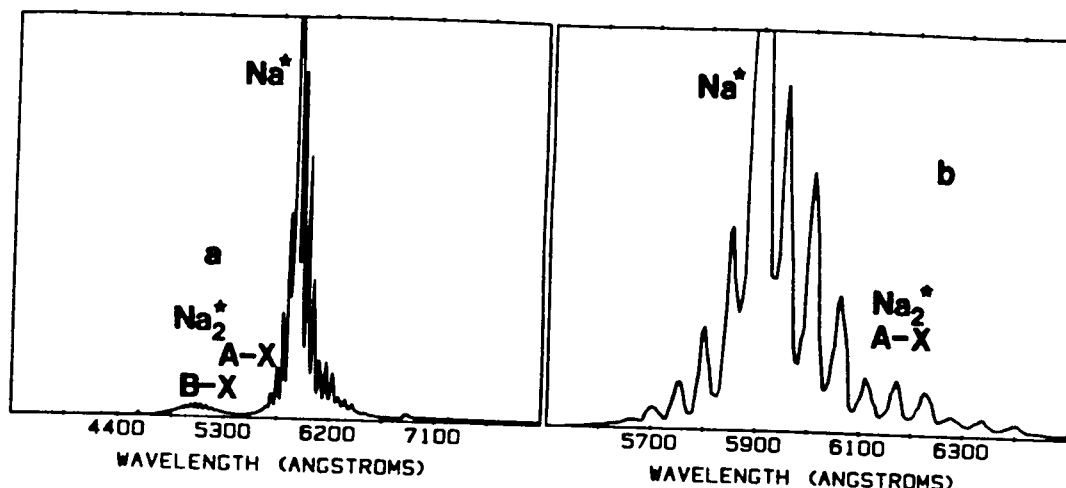


Figure 9: Na_2^* chemiluminescent emission from $\text{Na}_x\text{-Br}$ reactive encounters. See text for discussion.

suggests that the spectrum corresponds, in large part, to the selective excitation of A state vibrational levels. The observed vibrational structure, correlating with the A state in the region close to 590 nm, is associated with the lowest vibrational levels of the $\text{Na}_2 \text{X } ^1\Sigma_g^+$ ground state. The emission does not correlate with the strongest A-X transitions (Frank-Condon factors) which can be readily excited through laser induced pumping from the ground electronic state.²⁸ In fact, it corresponds to what may be a superposition of several vibrational progressions involving the $v' \geq 21$ levels of the A state (ex: $\text{Na}_2 \text{A } ^1\Sigma_u^+, v' = 21 \rightarrow \text{Na}_2, ^1\Sigma_g^+, v'' = 1-6$) or to a very selective emission from one of the $v' = 21, 24, 27, 30$, levels of the A state. Further, the sharp nature of the observed emission features suggests (and simulations confirm) that the emission is to be associated with the energy transfer pumping of cold Na_2 . The experimental conditions are such that a significant alkali dimer concentration which can react quite efficiently with Br atoms to produce ground state NaBr is present in the expansion ($T_{\text{oven}} = 875 \text{ K}$, $T_{\text{nozzle}} = 935 \text{ K}$, $P_{\text{rxn.zone}} \approx 10^{-1}$ Torr) but a substantial alkali trimer concentration may not yet be generated. We then suggest that the signature results from the energy transfer pumping of cold Na_2 by vibrationally excited NaBr , to produce an A-X emission spectrum much sharper than that characterizing the $\text{Na}_3 - \text{Br}$ reaction.¹ The precise mechanism for the energy transfer pumping of the $\text{Na}_2 \text{A}$ state is currently under study. Further, it now remains for us to continually improve the expansion conditions so as to increase the sodium trimer concentration. This will be accomplished both in a pure Na vapor expansion and with the mixed sodium-argon expansion described above and in detail elsewhere.⁶

Acknowledgement

It is a pleasure to acknowledge most helpful discussions with Drs. R. Jones, Bill Watt, T. Cool, Stan Patterson, Rolf Gross, Sherwin Amimoto, John Dering, Glen Perram, and E. Dorko concerning this study. The support of the Georgia Tech Foundation through a grant from Mrs. Betty Peterman Gole, the Army Research Office through the Short Term Innovative Research Program, the Air Force Office of Scientific Research and Army Research Office and AFOSR/SDIO is greatly appreciated.

REFERENCES

1. W. H. Crumley, J. L. Gole, and D. A. Dixon, *J. Chem. Phys.* **76**, 6439 (1982).
S. H. Cobb, J. R. Woodward, and J. L. Gole, *Chem. Phys. Lett.* **143**, 205 (1988).
S. H. Cobb, J. R. Woodward, and J. L. Gole, *Chem. Phys. Lett.* **157**, 197 (1989).
S. H. Cobb, J. R. Woodward, and J. L. Gole, *Proceedings of the Fourth International Laser Science Conference, A.I.P. Conf. Proc. No. 191, Optical Science and Engineering Series 10*, pg. 68.
2. J. R. Woodward, S. H. Cobb, K. K. Shen, and J. L. Gole, *IEEE Jour. of Quant. Elect. JQE* **26**, 1574 (1990). J. R. Woodward, S. H. Cobb, and J. L. Gole, *Proceedings of the Fourth International Laser Science Conference, A.I.P. Conf. Proc. No. 191, Optical Science and Engineering Series 10*, pg. 63.
3. G. J. Green and J. L. Gole, *Chemical Physics* **100**, 133 (1985).
4. R. W. Woodward, J. S. Hayden, and J. L. Gole, *Chemical Physics* **100**, 153 (1985).
5. J. L. Gole, J. R. Woodward, S. H. Cobb, K. K. Shen, and J. R. Doughty, *SPIE Proceedings Volume 1397, Eighth International Symposium on Gas Flow and Chemical Lasers* (1990), pg. 125 (and references therein). J. L. Gole, K. K. Shen, C. B. Winstead, and D. Grantier, *Journal de Physique IV, Colloque C7, supplement au Journal de Physique III, Vol. 1, December 1991*, pg. 609.
6. J. L. Gole, K. K. Shen, H. Wang, and D. Grantier, "Chemically Driven Pulsed and Continuous Visible Laser Amplifiers and Oscillators", *Proceedings of the 23rd AIAA Plasma-Dynamics and Laser Science Conference, Nashville, Tennessee, AIAA 92-2994* (1992).
7. K. K. Shen, H. Wang, and J. L. Gole, "Evidence for Continuous Visible Chemical Lasing from the Fast Near Resonant Pumping of Atomic Sodium", *IEEE Journal of Quantum Electronics*, in press.
8. P. M. Swearengen, S. J. Davis, and T. M. Niemczyk, *Chem. Phys. Lett.* **55**, 274 (1978).
9. S. H. Cobb, M. McQuaid, and J. L. Gole, unpublished, see also references 3-6.
D. Husain and P. E. Norris, *J. C. S. Faraday, II*, **93**, 106, 335 (1978) and
D. Husain and P. E. Norris, *Chemical Physics Letters* **51**, 206 (1977).
10. A. Gaupp, P. Kuske, and H. J. Andra, "Accurate Lifetime Measurements of the Lowest $^2P_{1/2}$ States in Neutral Lithium and Sodium", *Physical Review A*, Vol. 26, pp. 3351-3359 (1982).
11. *Elementary Atomic Structure*, by G. K. Woodgate, Clarendon Press, Oxford, 1980.
12. C. E. Moore, "Atomic Energy Levels", N. B. S. Circular 467, Volumes I, II, and III. See also, R. W. F. Gross and J. F. Bott, *Handbook of Chemical Lasers*, Wiley and Sons, New York, 1976.
13. For the Na $4d^2D$ level, S. A. Kandela, *Appl. Optics* **23**, 2151 (1984).
14. For the Na $5s^2S$ level, X. He, B. Li, A. Chen, and C. Zhang, *J. Phys. B., At. Molec. and Opt. Phys.* **23**, 661 (1990).
15. A. Gallagher and A. Lurio, *Phys. Rev.* **136**, A87 (1964).
16. A. S. Tibilov and A. M. Shukhtin, *Opt. Spectrosc.* **21**, 69 (1966). See also, K. Krokkel, M. Hube, W. Luhs and B. Wellegehausen, *Appl. Phys.* **B37**, 137-140 (1985).
17. *Chemical Laser Experiments and Analysis, Directed Energy Devices Technology Support Delivery Order No. 0015 prepared by W. Smith, S. Taylor, J. Dansereau, J. Long, and W. Warren for U. S. Army Missile Command, Directed Energy Directorate, Redstone Arsenal, Alabama 35898.*
18. G. Roll and J. Mentel, *J. Phys. D. Appl. Phys.* **22**, 483-487 (1989).
19. The Na $4d^2D_{5/2} - 3p^2P_{3/2}$ transition should represent the most favorable to achieve gain and oscillation. The $4d^2D_{5/2}$ level emits dominantly to $3p^2P_{3/2}$ whereas the $4d^2D_{3/2}$ level depletes its population to both the $3p^2P_{1/2}$ and $3p^2P_{3/2}$ levels. Consideration of collisional relaxation among the $3p^2P$ levels

would also suggest that the collisionally depleted $3p^2P_{3/2}$ level is favored as the lower laser level.

20. "Self-Flushing Optical Window to Prevent Collection of Condensates", W. H. Crumley, and J. L. Gole, *Rev. Sci. Instruments* **57**, 1692 (1986).
21. A. V. Eremin, I. M. Naboko, and S. A. Palopezhentsev, *Opt. Spectrosc. (USSR)* **60**, 567 (1986).
22. (a) V. G. Mishakov and T. L. Tkachenko, *Opt. Spectrosc. (USSR)* **64**(3), 293 (1988). (b) V. V. Kuchinskii, V. G. Mishakov, A. S. Tibilov, and A. M. Shukhtin, *Opt. Spektrosk.* **39**, 1043 (1975) [*Opt. Spectrosc. (USSR)* **39**, 598 (1975)]. (c) A. A. Kudryavsev, V. N. Skrebov, and T. L. Tkachenko, *Opt. Spektrosk.* **58**, 694 (1985) [*Opt. Spectrosc. (USSR)* **58**, 420 (1985)]. (d) V. G. Mishakov, A. S. Tibilov, and A. M. Shukhtin, *Opt. Spektrosk.* **31**, 324 (1971) [*Opt. Spectrosc. (USSR)* **31**, 176 (1971)]. (e) N. N. Bezuglov and A. B. Tsyganov, *Opt. Spektrosk.* **59**, 195 (1985) [*Opt. Spectrosc. (USSR)* **59**, 115 (1985)].
23. I. Tanarro, F. Arqueros, and J. Campos, *J. Chem. Phys.* **77**, 1826 (1982).
24. J. W. Ager III, C. L. Talcott, and C. J. Howard, *J. Chem. Phys.* **85**, 5584 (1986). J. R. Woodward, J. S. Hayden, and J. L. Gole, *Chemical Physics* **134**, 395 (1989).
25. B. Wellegehausen, in "Metal Bonding and Interaction in High Temperature Systems with Emphasis on Alkali Metals", A. C. S. Symposium Series 179, edited by J. L. Gole and W. C. Stwalley (Am. Chem. Soc., Washington, D. C.) p. 462, B. Wellegehausen, *J. of Quantum Electronics* **15**, 1108 (1979).
26. See for example, R. S. Berry and C. W. Reimann, *J. Chem. Phys.* **38**, 1540 (1963), R. S. Berry, *J. Chem. Phys.* **27**, 1288 (1957), W. S. Struve, J. R. Krenos, D. L. McFadden, and D. R. Herschbach, *J. Chem. Phys.* **62**, 404 (1975). R. C. Oldenborg, J. L. Gole and R. N. Zare, *J. Chem. Phys.* **60**, 4032 (1974). Given Na_2 and Na_3 ionization potentials of 4.87 and 3.97 eV (A. Hermann, E. Schumacher, and L. Woste, *J. Chem. Phys.* **68**, 2327 (1978) and an electron affinity of 3.363 eV for atomic bromine, we determine a very substantial electron jump cross section $\sigma = \pi (14.38/3.97-3.36) = 1746 \text{ \AA}^2 (1.75 \times 10^{-13} \text{ cm}^2)$ for the $\text{Na}_3 - \text{Br}$ reaction and $\sigma = \pi (14.38/(4.87-3.36)) = 285 \text{ \AA}^2 (2.85 \times 10^{-14} \text{ cm}^2)$ for the $\text{Na}_2 - \text{Br}$ reaction.
27. E. J. Mansky and J. L. Gole, work in progress.
28. J. L. Gole, G. J. Green, S. A. Pace and D. R. Preuss, *J. Chem. Phys.* **76**, 2247 (1982), and references therein.
29. For example, M. M. Kappes, R. W. Kunz, and E. Schumacher, *Chem. Phys. Lett.* **91**, 413 (1982).
30. We wish to facilitate the formation of Na_2 in the B, C, and C' excited states in an electronically inverted configuration. to do this, Na_3 molecules must be present and react with halogen atoms. Here, it is important to note that the oscillator strengths for any of the larger sodium polymers (Na_n , $n \geq 3$) are sufficiently small verses Na_2 so that they do not interfere with the sodium dimer pump amplification cycle.

APPENDIX X

"Chemically Driven Continuous Visible Laser Amplifiers and Oscillators Based on Metal Molecule - Halogen Atom Reactions", D. Grantier, H. Wang, C. B. Winstead, and J. L. Gole, Proceedings of the 24th AIAA Plasma-dynamics and Laser Science Conference, Orlando, Florida, AIAA 93-3207 (1993).



AIAA 93-3207

**Chemically Driven Continuous
Visible Laser Amplifiers and
Oscillators Based on Metal
Molecule - Halogen Atom
Reactions**

D. Grantier, H. Wang, C. B. Winstead, and J. Gole
School of Physics, Georgia Institute of Technology
Atlanta, GA 30332

**AIAA 24th
Plasmadynamics & Lasers Conference
July 6-9, 1993 / Orlando, FL**

For permission to copy or republish, contact the American Institute of Aeronautics and Astronautics
370 L'Enfant Promenade, S.W., Washington, D.C. 20024

CHEMICALLY DRIVEN CONTINUOUS VISIBLE LASER AMPLIFIERS AND OSCILLATORS
BASED ON METAL MOLECULE - HALOGEN ATOM REACTIONS

D. Grantier, H. Wang, C. B. Winstead and J. Gole
School of Physics
Georgia Institute of Technology
Atlanta, GA 30332

ABSTRACT

Using the highly efficient and selective formation of sodium dimer excited states from the sodium trimer-halogen atom $\text{Na}_3\text{-X}(\text{F}, \text{Cl}, \text{Br}, \text{I})$ reactions and extrapolated analog systems, we seek to develop visible and ultraviolet lasers based on the successful production of visible chemical laser amplifiers. The $\text{Na}_3\text{-X}(\text{Cl}, \text{Br}, \text{I})$ reactions have been shown to create a continuous electronic population inversion based on the chemical pumping of sodium dimer (Na_2). Optical gain through stimulated emission has been demonstrated in the regions close to 527, 492, and 460 nm. These observations are in close analog to optically pumped alkali dimer lasers. A model which invokes the vibrational and rotational selectivity inherent to a dissociative ionic recombination process ($\text{Na}_3^+ + \text{X}^- \rightarrow \text{Na}_2 + \text{NaX}$), correlated with the coupling between select sodium dimer excited states, provides a semiquantitative explanation of the observed trends. An analysis of the system suggests that the monitored gain (max of 3.8% at ≈ 527 nm corres. to $\alpha \approx 8 \times 10^{-3}/\text{cm}$ for an individual rovibronic level) can be enhanced considerably with a more versatile source configuration. The considered amplifiers are therefore being optimized with a focus to increasing amplifier gain length and amplifying medium concentration. A device has been constructed to allow the ready movement of extended length alkali trimer and halogen atom slit sources relative to each other so as to create interacting alkali and halogen atom sheaths. The controlled intersection of these sheaths can form an extended reaction - amplification zone. This extended gain zone is required to facilitate the conversion of the created amplifiers to visible chemical laser oscillators. We report results obtained with this up-scaled device, where the alkali metal is expanded in both pure and seeded supersonic expansion. We report progress in extending the $\text{Na}_3\text{-X}$ amplifier concept to the study of the $\text{Na}_3\text{-F}$ and $\text{Li}_3\text{-X}$ alkali trimer-halogen atom based reactions, the potential excimer forming M_3 ($\text{M}=\text{Mg}, \text{Ca}, \text{Sr}, \text{Ba}, \text{ and Mn}$) - $\text{X}(\text{F}, \text{Cl}) \rightarrow \text{M}_2^* + \text{MX}$ reactions, and the correlated formation of Group IIA dihalide excited states from $\text{M} + \text{X}_2$ reactive encounters.

INTRODUCTION

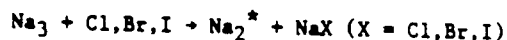
"A Highly Efficient and Selective Electron-Jump-Harpoon Process"

The collision dynamics of processes proceeding on electronically excited surfaces is fundamental to the attainment of population inversions based on electronic transitions in the visible spectral region.¹⁻³ A particular subgroup of these electronic energy transfer processes involves metal atoms or molecules of low ionization potential.

These species react very efficiently with atoms or molecules of significant electron affinity via what is termed the electron jump-harpoon process. It is this process, specifically involving the reaction of metal trimers and forming the product metal dimer and metal halide, that may represent one of the few direct chemical routes to produce electronically inverted products. The alkali trimer molecule, Na_3 , readily provides an electron to harpoon a hungry halogen atom, X, producing a switch from the interaction of two neutral species to that of two ions ($\text{Na}_3^+ + \text{X}^-$). The convergence, crossing, and interaction of the two potentials describing the neutral (covalent) and ionic (coulombic) constituencies allows an effective switch of the reactants (curve crossing). For Na_3 , with its low ionization potential, the curve crossing occurs at very long range ($> 10\text{\AA}$) leading to a high cross section for product Na_2 formation. Based upon the experimental results obtained thus far in our laboratory, the sodium trimer reactions show not only vibrational but also rotational selectivity as they create electronic population inversions in the product Na_2 . Theoretical considerations would suggest that these trimer reactions and their analogs represent key processes to yield electronically inverted products in direct chemical reaction.^{1,2}

Continuous Chemical Laser Amplifiers in the Visible Region Based on Highly Efficient and Selective Chemical Reaction

The $\text{Na}_3\text{-X}$ reactions form an unusual class of reactive encounters. The optical signatures for the processes



encompass emission from a limited group of low-lying Na_2 excited states.⁴ The observed dimer emission is characterized by sharply defined emission regions⁴ (Fig. 1) superimposed on a much weaker Na_2 background fluorescence. The sharp emission features cannot be explained by invoking a purely fluorescent process, and resemble in their behavior characteristics similar to those of optically pumped Na_2 laser systems.^{4,5,6} In the visible spectral region, these features grow at a near exponential rate with increasing Na_3 concentration, relative to the Na_2 background spectrum, suggesting the possibility that stimulated emission might be associated with certain of the emitting Na_2 reaction products. Laser gain measurements carried out to assess this possibility throughout the visible region reveal optical gain through stimulated emission and the creation of population inversions on these select Na_2 electronic transitions.

Measurements at 0.5 cm^{-1} resolution suggest amplification in regions close to 527 nm (1% gain),

492 nm (0.3% gain) and 460.5 nm (0.8% gain), correlating precisely with the reactive process and the relative intensities of those features observed while monitoring the light emitted from the $\text{Na}_3\text{-Br}$ reaction (Fig. 1). High resolution ring dye laser scans in the 527 nm region indicate that the gain for the system is a minimum of 3.8% for the dominant rovibronic transition in this region with approximately four to seven individual rotational transitions showing gain. At 459.8 nm, we also have measured a 2.3% gain for an individual rotational transition. These results demonstrate the continuous amplifying medium for a visible chemical laser in at least three wavelength regions.^{4,5} At no other scanned wavelengths do we find any indication of gain as we monitor the entire wavelength region from 420 to 600 nm. We have generally observed slight losses of the laser photon flux resulting primarily from scattering, and, to a much smaller extent, absorption upon transmission through the $\text{Na}_3\text{-Br}$ reaction zone. In the region of the sodium D-line, we monitor a substantial absorption and loss as a function of the trimer-halogen atom reaction.^{4,5}

As we have suggested in our initial comments, the $\text{Na}_3\text{-halogen}$ atom reactions are thought to proceed via an electron jump mechanism with extremely high cross sections,⁷ producing substantial Na_2 excited state populations. The question of why the $\text{Na}_3\text{-X}$ reactions appear to demonstrate vibrational and rotational selectivity in certain wavelength regions may be explained by invoking a model for the dissociative ionic recombination, $\text{Na}_3^+ + \text{X}^- \rightarrow \text{Na}_2 + \text{NaX}$, and the curve crossings which influence the distribution of product molecules for this process.² Such a model, coupled with an analysis of the electronic coupling between select sodium dimer excited states,² appears to provide a semiquantitative explanation of the observed population inversions.

Once created, the monitored population inversions are thought to be maintained in a continuously amplifying system (1) by the large number of free halogen atoms reacting with the Na_2 molecules in those ground state levels on which the transitions emanating from the Na_2 excited states terminate and (2) by collisional relaxation of the ground state sodium dimer molecules. The cross section for reaction of vibrationally excited ground state Na_2 is expected to be quite substantial relative to the cross section for collision induced vibrational deactivation of the Na_2 manifold. Extremely efficient reactions are thought to greatly assist the depletion of the lower state levels in this system allowing one to sustain a continuous population inversion. Our major efforts thusfar have focused on the $\text{Na}_2\text{-B-X}$ spectral region and the potential development of laser oscillators at wavelengths in the vicinity of 527 and 460 nm. In order to approach these studies, we have been developing the means to create a considerably longer path length amplification region.

Development of an Extended Path Length $\text{Na}_3\text{-X}$ (Cl, Br, I) Reaction - Amplification Zone

It is necessary to improve the magnitude of the amplification determined previously for the sodium dimer amplifiers at ~ 527 , ~ 492 , and

~ 460 nm. In these previous experiments we have obtained a substantial Na_3 concentration ($\geq 10^{13}/\text{cc}$) in a limited reaction-amplification zone.^{4,5} In order to demonstrate continuous chemical laser oscillation, however, it is desirable to create this enhanced sodium trimer-halogen atom reaction zone over an extended amplification zone path length. The overall apparatus design depicted in Figures 2 and 3 is meant to accommodate high intersecting reactant flows from both sodium trimer and (dual rotatable) halogen atom sources in order to produce a considerably enhanced concentration of Na_2 amplifiers over an extended path length. This system attempts to increase the Na_3 reaction-amplification zone concentration by repositioning the trimer and halogen atom sources relative to each other^{4,5} and facilitating the halogenation process much closer to the alkali source nozzle itself, in a gas dynamic configuration. We incorporate the facility for the in-situ adjustment of the alkali and halogen source positions.

In order to increase the reaction zone and gain length, we are testing a continuous flow slit source technology to create at least a 5 cm long amplification zone. Here, a small circular "pinhole" nozzle used in previous experiments^{4,5} is now replaced by a slit approximately 100 μ in width by 2 1/2" in length. Two slit configurations have been employed to accomplish this goal. The design used initially, depicted in Figure 3(a), of 0.003" width, was fabricated from 316 stainless steel using an EDM (electric discharge machining) process. These slits were not sufficiently resistive to the corrosive effects of the system reactants (primarily sodium) and quickly widened to 0.020" (~ 2 runs). An improved slit nozzle constructed from molybdenum (Fig. 3(b)) has proven considerably more resistant, widening from 0.003 to 0.006" after six experimental runs.

In order to produce a more efficient cooling in the alkali expansion it is desirable to operate with narrower slits which exhibit a minimal interaction with the expanding alkali vapor. Figures 3(c)-(e), in combination, outline a more successful design. As depicted in Figs. 3(c) and 3(d), the nozzle consists of two pieces. Two sheets of 0.005" tantalum are prepared and mounted on the back portion of the nozzle (Fig. 3(d)) as they are positioned to form the slit. The front of the nozzle, with a mildly diverging section, fits over the back portion of the device, tightly sandwiching the tantalum sheets and thus forming the actual slit (Fig. 3(e)). These tantalum sheets can be positioned under a Vickers microscope to produce a slit less than 0.003" in width. These widths are precisely adjusted and determined using single slit diffraction techniques.

The overall alkali source design pictured in Fig. 2(a) in side and partial frontal view corresponds to a full seeded configuration where helium or argon can be passed through the rear gas source assembly, flowing over molten sodium. The mixture is subsequently expanded through the frontal nozzle slit configuration. In a pure sodium supersonic expansion, the Na_3 constituency is dominated by a much larger atom and cold dimer concentration.⁸ The expanded dimer will not interfere at the Na_2 amplifier wavelengths

characteristic of the Na_3 -halogen atom reaction systems, however, it is desirable to minimize the atom and dimer while increasing the trimer concentration. The trimer concentration can be altered and improved by seeding the expansion with helium, argon, or other noble gas atoms. In fact several researchers⁹ have demonstrated that the atom and dimer concentrations can be decreased considerably relative to the much larger sodium polymers. We do not wish to operate at these extreme expansion conditions but, rather, seek a middle ground which will allow enhanced formation of the trimer over that of the pure expansion concentration.¹⁰ This condition can be realized through the appropriate adjustment of parameters which can be manipulated in the expansion including (1) the rear oven stagnation pressure (argon + sodium), (2) the frontal nozzle temperature, and (3) the ratio of the supersonic expansion source pressure to the overall expansion chamber pressure.

In the overall experimental design depicted in Figure 2(b), the sodium slit source is positioned relative to the dual halogen slit sources located above and below the reaction zone. The halogen slit sources are designed to optimize the interaction of the alkali expansion products with the created halogen atoms. The optical cavity is colinear with the geometric intersection of the planar halogen and alkali flows as indicated in Figure 2 and is terminated on each end by self-cleaning optical windows (as indicated in Figure 2(c)). The entire sodium oven and cooling jacket assembly can be translated in the forward and backward directions relative to the halogen slit sources for optimal control of the positioning of the reaction zone relative to the laser cavity. In summary, the reaction zone cavity configuration is designed to allow for (1) short transit of the reactants Na_3 and $\text{X} = \text{Cl}, \text{Br}, \text{I}$ to the reaction - amplification zone, (2) flexible movement of these sources with respect to each other and with respect to the flow patterns created in the system and (3) minimal interaction of these reactants with laser cavity windows. To insure this minimal interaction, the self-cleaning optical windows noted previously¹¹ are used. The reaction zone is evacuated through a 35 cubic foot ballast tank followed by a 1250 CFM Stokes - Roots-Blower combination.

The oven and nozzle chambers are currently heated differentially and resistively using Thermocoax wire (Amperax, inconel sheath, 0.079" diameter). The wrapped heating elements are powered by two independent Variac transformer power supplies capable of delivering 25 amps at 180 volts (a.c.). For the halogen dissociation furnaces (Fig. 2(d)), desired temperatures are achieved through the resistive heating (250+ amps, ~ 50 volts (a.c.)) of a hollowed high density carbon cylinder. The central channel of each cylinder is accessed to the reaction zone region through a single slit ~ 0.006" wide by two inches in length running midway down the cylinder. Typically, these halogen dissociation furnaces are operated at temperatures between 1700K and 1900K as determined by optical pyrometry. At these temperatures, those halogen molecules entering the radiator should be greater than 95% dissociated. The halogen, if it is liquid bromine (or iodine) is held in a glass bulk separated from the inlet to the reaction zone

by a teflon stopcock. In the case of iodine, this bulb is heated to attain the necessary flow rates which are finely controlled using a Whitey SS-22RS4 needle valve.

In a typical "seeded" argon experiment, both the rear stagnation oven and frontal nozzle are brought slowly to a temperature of ~ 450K during which time hydrogen is evolved from the sample. A small positive pressure argon purge is maintained during the entire heating cycle to prevent backstreaming of the sodium vapor into the seed gas line. With the hydrogen evolution complete, the oven can be brought rapidly to the operating temperature of a given experiment. A major aspect of our efforts has involved the continued improvement of this cycle in order to generate the initial experimental studies described in the following section. Simultaneously, the halogen furnaces are heated at a moderate rate. Since the electrodes supplying current to the halogen furnaces are water cooled (Fig. 2(b)), their temperature is increased slowly to prevent them from cracking.

Overview of Initial Experimental Results

As the operating temperature of the sodium supersonic expansion source is reached, bromine molecules are passed into and dissociated in the halogen furnaces and subsequently fed to the reaction zone. This process produces a bright yellow-green cylindrical region formed between the two halogen outlets. By varying the flow of bromine through the needle valve, we induce a change in the relative intensity and spatial extent of the emission. If the system is operated at a relatively low bromine flux, the observed chemiluminescence loses much of the characteristic yellow brightness associated with the sodium D-line emission and bears a dominantly green appearance. This is apparent for both pure and seeded expansions. As the spectrum of Figure 4 demonstrates for a pure expansion, the monitored spectral features are dominated by Na_2 B-X and A-X emission features accompanied by a weak Na D-line emission. As the bromine flux is increased, the observed emission takes on a strong yellow green appearance, due most likely to a significant increase in Na D-line emission. This is exemplified in Figure 5.¹²

In the configuration outlined in Figure 2, the halogen sources are separated by approximately 6.4 cm. The expanding sodium vapor is introduced from its source configuration at a distance from the reaction-viewing-zone which can be varied in-situ from ~ 12.7 to 3.8 cm. Thusfar, we have found that a variation over these distances has little effect on the content of the observed spectral chemiluminescence and only serves to increase or decrease the intensity of the light emission as the halogen source/alkali source distance is varied. Currently, we have chosen to operate with the alkali expansion source positioned between 5 and 3.8 cm from the halogen sources.

The halogen atom sources, while not yet rotatable in-situ can be configured to intersect the plane of the alkali expansion slit source at varying angles by adjusting their orientation prior to a given experiment. These adjustments in the

orientation of the reactant flows ($\sim \pm 15^\circ$ relative to the vertical for the halogen source - while maintaining the reaction - viewing zone orientation) do produce a change in the spectral content of the observed emission features. For example, when the horizontal component of the velocity vector of the halogen atom flow is directed parallel to the alkali flow, we observe a very weak broad spectral emission at 436.5 nm (Fig. 6(a)) correlating closely with what has been identified as a triplet-triplet bound-free transition in Na_2 .¹³ When the halogen sources are configured perpendicular to the alkali flow or are even slightly rotated from the parallel to an angle 10° antiparallel (Fig. 6(b)) to the alkali flow, a notable enhancement of the 436.5 nm feature is observed. As the halogen flow rate is increased, the 436.5 nm feature is further enhanced^{14,15} (Fig. 6(c)).

In our initial successful operation of the Na_x - X system, we were concerned with the evaluation of pure sodium supersonic expansions and the optimization of expansion conditions so as to demonstrate the formation of a cooled sodium dimer (Na_2) constituency. This process, of course, represents the first step in our attempt to build up the trimer (Na_3) concentration to the level desired to create an extended path length sodium dimer amplification zone.

With the alkali source nozzle and halogen sources positioned within 3.8 cm of each other, the alkali system operated under conditions which should produce significant concentrations of cooled Na_2 , the halogen slit sources oriented at 75° relative to the sodium flow in a direction away from the alkali nozzle a moderate bromine flux, we observe the emission associated with Na_x -Br reactions depicted in Fig. 5. This signature, observed along the path of the optical train in Fig. 2, consists of a dominant Na D-line and considerably weaker Na_2 B-X emission feature. Also associated with the D-line are several features which initially were thought to result from the selective excitation of Na_2 $A^1\Sigma_u^+$ vibrational levels. This observed structure if it corresponds to A-X emission must be associated with the lowest vibrational levels of the Na_2 X $1\Sigma_g^+$ ground state. The emission does not correlate with the strongest A-X transitions (Frank-Condon factors) which can be readily excited through laser induced pumping from the ground electronic state.⁸ In order to account for selectively produced Na_2 fluorescence features in the region of the D-line, we attempted to fit the spectrum to a linear combination of several vibrational progressions involving the $v' \geq 21$ levels of the A state (ex: Na_2 $A^1\Sigma_u^+$, $v' = 21 \rightarrow \text{Na}_2$, $1\Sigma_g^+$, $v'' = 1-6$) or to a very selective emission from one of the $v' = 21, 24, 27, 30$ levels of the A state. Further, the sharp nature of the observed emission features suggests that they might be associated with the energy transfer pumping of cooled Na_2 . The experimental conditions are such that a significant alkali dimer concentration which can react quite efficiently with Br atoms to produce ground state NaBr is present in the expansion ($T_{\text{oven}} = 875$ K, $T_{\text{nozzle}} = 935$ K, $P_{\text{rxn. zone}} = 10^{-1}$ Torr) but a substantial alkali trimer concentration may not yet be generated. This suggests that the signature might result from the energy transfer pumping of cold Na_2 by vibrationally excited NaBr ,

to produce an A-X emission spectrum much sharper than that characterizing the Na_3 - Br reaction.^{4,5} All attempts to fit the spectrum to Na_2 A-X fluorescence, consistent with the constraints we have outlined, have not been successful.

We must conclude that the features depicted in Fig. 5 do not correspond to emission from the Na_2 A state. An alternate assignment for these surprising features can be garnered from a comparison with the optical signatures associated with "seeded" sodium expansions and with the emission spectra generated in a pure sodium expansion at low bromine flux (Fig. 4) where the Na D-line is (1) considerably weaker than the Na_2 A-X and B-X fluorescence features and (2) devoid of any satellite structure. This result, obtained in pure expansion, signals the correlation of an associated intense D-line emission with the manifestation of satellite structure. Further, we note that the spectrum in Fig. 5 appears to demonstrate a synergism between the features appearing to the red and those appearing to the blue of the D-line.

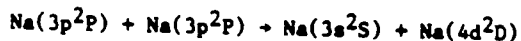
Equally revealing information is obtained from "seeded" expansion studies at moderate bromine concentrations. Figures 7(a) and 7(b) depict higher resolution scans of the region around the D-line. The dual spectra in Figure 7(b) demonstrate that each of the satellite features has associated with it a doublet character. The doublet structure might be attributed to P and R branches in a resonance fluorescence series¹⁶ resulting from the absorption of Na D-line photons. Indeed such a doublet structure induced by a Cd resonance lamp was reported by Brown in a classic resonance fluorescence study.¹⁷ Yet it appears difficult to find previous reports of such a resonance fluorescence excitation due to Na D-line optical pumping. Indeed, the Frank-Condon factors for such resonance excitations at the wavelengths of the Na D-line are not conducive to this process. We also note that the relative intensities of the doublet structures associated with the satellite features follow the relative intensities of the two D-line components (16973.4 cm^{-1} ($^2P_{3/2} - ^2S_{1/2}$ @ 589 nm), 16956.2 cm^{-1} ($^2P_{1/2} - ^2S_{1/2}$ @ 589.6 nm). This may be fortuitous,¹⁶ however, it also suggests an alternate explanation.

The satellite features in the vicinity of the Na D-line might correspond to Raman scattering. If the observed features result from Raman scattering due to the Na D-line and we assign the long and short wavelength features as corresponding to Stokes and anti-Stokes scattering components, their relative intensities should consistently predict a reasonable temperature for the Na_2 molecules experiencing the Raman effect. The relative intensities of these Stokes and anti-Stokes features and thus the ratios I_{s2}/I_{a2} , I_{s3}/I_{a3} , and I_{s4}/I_{a4} (the s-1 and a-1 bands are significantly overlapped by the D-line) should be directly proportional to $e^{\Delta E/kT}$ where ΔE is the appropriate energy increment in vibrational energy. These ratios are in excellent agreement (Table I) and suggest a sodium dimer temperature close to 200K. This temperature is quite consistent with the expected heating of the cold Na_2 produced from our slit expansion source.

Thus the evidence obtained in our overall

analysis of the data presented in Figures 5 and 7 would suggest that the features in the region of the Na D-line are best attributed to Raman scattering from an intense Na atomic emission source. This result, the attainment of a Raman spectrum on the time scale inherent to these experiments suggests an excited state Na atom concentration sufficient to produce effects normally associated with (1) resonant Raman or (2) non-resonant laser Raman experiments. These excited state concentrations portend of the unique chemical physics which will be associated with these systems.

Our previous discussion has emphasized the surprising optical effects which we have already found to characterize the Na_3 - Br reactive system at high concentration. The data in Figure 8 were obtained with $T_{\text{oven}} = 825$ K, $T_{\text{nozzle}} = 875$ K, $P_{\text{rxn. zone}} = 1.5 \times 10^{-1}$ Torr. If, in a fast ramping of the "seeded" sodium system after hydrogen evolution, we establish operating conditions close to $T_{\text{oven}} = 880$ K, $T_{\text{nozzle}} = 925$ K, $P_{\text{rxn. zone}} = 1.5 \times 10^{-1}$ Torr, a further stage in the attainment of the Na_3 - X reaction amplification configuration is obtained. The spectra in Figs. 8(a) and 8(b) obtained at this higher temperature correspond also to the introduction of a moderate bromine flux. Not only do we maintain the Na D-line excited Raman signal but we also obtain evidence for the significant excitation of the higher lying excited states of the sodium atom. These spectra bear a phenomenal similarity to the sodium fluorescence spectra, induced by Allegrini et al.¹⁸, and depicted in Figure 9. However, Allegrini et al.¹⁸ produced their spectrum with a cw dye laser tuned to the $3s^2S_{1/2} - 3p^2P_{3/2}$ D-line transition. Their spectrum (a) is obtained at a temperature of 653 K ($P_{\text{Na}} = 0.195 \text{ mm/Hg}$) and a laser pump energy of 1 W/cm^2 whereas the amplified blue green Na_2 B-X emission (b) is obtained at a temperature of 673 K (0.344 mm/Hg) and a laser pump power of 2 W/cm^2 . The atomic emissions from higher lying Na atomic states in both studies are believed to result from energy pooling processes involving the Na D-line viz.



The similarity of the spectra which we generate from a purely chemical process (with the exception of the Raman scattering) and the fluorescent data generated by Allegrini et al. with their significant laser pump powers is quite astounding and consistent with our suggestion of a Raman signal generated from the production of high Na $3p^2P$ excited atomic concentrations and the subsequent light scattering of an intense D-line photon flux by sodium dimers. These correlations further suggest that we are well on the way to generating the necessary concentrations to produce substantial emission from Na_3 - X reactive encounters. It now remains for us to continually improve the expansion conditions so as to increase the sodium trimer concentration. This will be accomplished both in a pure Na vapor expansion and with the mixed sodium-argon or sodium-helium expansion described above.

Extension of the Na_3 - X(Cl, Br, I) Amplifier Concept

Although the experimental configuration which

we have used to demonstrate amplification from the Na_3 -Br reaction is not optimal for producing a chemical laser oscillator, it can readily be used to assess the possibility of forming chemical laser amplifiers from the reactions of lithium trimer with halogen atoms and to evaluate the extension of the oxidation process to fluorine atoms. The later experiments, specifically studies of the Na_3 -F reactive encounters are now underway. We have also constructed a molybdenum based double oven lithium supersonic expansion source which can be used to test the viability of lithium trimer-halogen atom reactions as a means of producing lithium dimer chemical laser amplifiers.

The Na_2 amplifiers which we have characterized in the visible region operate on bound-bound transitions. It is not difficult to envision an extrapolation on the Na_3 -X reaction concept which involves the readily ionizable alkaline earth metal trimers and the formation of excited state dimers which can undergo bound-free excimer transitions. With this focus, we are attempting to generate the M_2 excimer analogs of the Na_2 laser amplifiers discussed previously. The ground electronic state of Mg_2 is very weakly bound.¹⁹ However, detailed calculations suggest the Mg_2 - Mg bond strength may be on the order of 0.6 eV,²⁰ quite comparable to that of Na_3 . We are now forming magnesium molecules, specifically Mg_2 and Mg_3 , and observing the excited state products of their oxidation with F and Cl atoms. A halogen atom discharge source which we have developed to study the $\text{Bi}_2 + \text{F}$ reaction^{21,22} is being used to investigate the Mg_2 -F, Mg_3 -F, Mg_2 -Cl, and Mg_3 -Cl reactions. To date, we have not observed strong Mg_2 emission from the Mg_3 - F, Cl reactions, however, surprisingly, preliminary results on this system signal the formation of excited state Mg_xF (Figure 10) and Mg_xCl charge transfer complexes where x is most likely two. Although we have not yet demonstrated the potential for forming an Mg_2^* based excimer amplifier laser system, the creation of a long-lived Mg_xF complex suggests that, with some modification, this may be feasible. Further it should also be possible to extend these studies to the reactions of the heavier alkaline earths Ca_x - Ba_x . A similar situation must also prevade if we consider the reaction of readily ionized manganese trimer molecules with fluorine or chlorine atoms. Again the manganese dimer molecule is very weakly bound in its ground electronic state. The dissociation energy (D_0) of dimanganese has been estimated by a variety of methods to be between 0.02 and 0.15 eV.²³ The force constant calculated for the manganese trimer bond, $0.38 \text{ m-dyne/\AA}^{24}$ is four times larger than that of diatomic manganese suggesting that Mn_3 is also much more tightly bound than Mn_2 , but more weakly bound than Na_3 . These characteristics, in conjunction with a respectable MnF bond energy (4.35 eV.²⁵) suggest that the $\text{Mn}_3 + \text{F} \rightarrow \text{Mn}_2^* + \text{MnF}$ reactive encounter may represent a feasible source of excimer emission.

Finally, we should note the correlation which these suggested extrapolations have with the complementary study of the Group IIA metal-halogen molecule reactions as they lead to the formation of the Group IIA dihalide. As a complement to the study of the alkaline earth molecule reactions which we outline, we have used a combination of single and multiple collision chemiluminescent

studies and laser induced fluorescence spectroscopy²⁶ to (1) demonstrate the highly efficient collisional stabilization of electronically excited Group IIA dihalide collision complexes formed in direct $M + X_2 \rightarrow MX_2$ reactive encounters, (2) delineate the first direct evidence for symmetry constraints associated with dihalide formation in the $M + X_2$ insertion process, (3) obtain the first discrete emission spectra for these dihalide complexes, and (4) demonstrate that the dihalide formation via the collisionally stabilized $M + X_2$ reactive association may well involve a dominant branching into electronically excited states of the dihalide complex suggesting the possibility of an electronic population inversion.

The demonstrated collisional stabilization is not readily explained within the RRKM framework suggesting that new models will be necessary to explain the efficient interaction of electronically excited states as well as highly vibrationally excited ground states. The data from this study now begins to provide important information on the efficient stabilization of excited state intermediate complexes, defining a much broader range of interaction than has typically been associated with collisional stabilization phenomena. The demonstrated interaction range of these dihalides and the enhanced interaction of high temperature molecules in general has direct implication for the understanding of molecular formation and energy transfer in the high stress environments which include not only those created in a chemical laser system or combustor but also in a high impulse propulsion system.

Acknowledgement

It is a pleasure to acknowledge most helpful discussions with Drs. R. Jones, Bill Watt, T. Cool, Stan Patterson, Rolf Gross, Sherwin Amimoto, John Dering, Glen Perram, and E. Dorko concerning this study. The support of the Georgia Tech Foundation through a grant from Mrs. Betty Peterman Gole, the Army Research Office through the Short Term Innovative Research Program, the Air Force Office of Scientific Research and Army Research Office and AFOSR/SDIO is greatly appreciated.

References

1. R. D. Levine and R. B. Bernstein, *Molecular Reaction Dynamics and Chemical Reactivity*, Oxford University Press, New York, 1987.
2. E. J. Mansky and J. L. Gole, work in progress.
3. Short Wavelength Chemical Laser Workshop, Charleston, S.C., Nov. 14-15, 1984.
4. W. H. Crumley, J. L. Gole, and D. A. Dixon, *J. Chem. Phys.* **76**, 6439 (1982). S. H. Cobb, J. R. Woodward, and J. L. Gole, *Chem. Phys. Lett.* **143**, 205 (1988). S. H. Cobb, J. R. Woodward, and J. L. Gole, *Chem. Phys. Lett.* **157**, 197 (1989). S. H. Cobb, J. R. Woodward, and J. L. Gole, *Proceedings of the Fourth International Laser Science Conference, A.I.P. Conf. Proc. No. 191, Optical Science and Engineering Series 10*, pg. 68.
5. J. L. Gole, K. K. Shen, H. Wang, and D. Grantier, "Chemically Driven Pulsed and Continuous Visible Laser Amplifiers and Oscillators", *Proceedings of the 23rd AIAA Plasma-Dynamics and Laser Science Conference*, Nashville, Tennessee, AIAA 92-2994 (1992).
6. B. Wellegehausen, in "Metal Bonding and Interaction in High Temperature Systems with Emphasis on Alkali Metals", A. C. S. Symposium Series 179, edited by J. L. Gole and W. C. Stwalley (Am. Chem. Soc., Washington, D. C.) p. 462, B. Wellegehausen, *J. of Quantum Electronics* **15**, 1108 (1979).
7. See for example, R. S. Berry and C. W. Reimann, *J. Chem. Phys.* **38**, 1540 (1963), R. S. Berry, *J. Chem. Phys.* **27**, 1288 (1957), W. S. Struve, J. R. Krenos, D. L. McFadden, and D. R. Herschbach, *J. Chem. Phys.* **62**, 404 (1975). R. C. Oldenberg, J. L. Gole and R. N. Zare, *J. Chem. Phys.* **60**, 4032 (1974). Given Na_2 and Na_3 ionization potentials of 4.87 and 3.97 eV (A. Hermann, E. Schumacher, and L. Woste, *J. Chem. Phys.* **68**, 2327 (1978) and an electron affinity of 3.363 eV for atomic bromine, we determine a very substantial electron jump cross section $\sigma = \pi (14.38 / (4.87 - 3.36))^2 = 285 \text{ \AA}^2 (2.85 \times 10^{-14} \text{ cm}^2)$ for the $Na_2 - Br$ reaction.
8. J. L. Gole, G. J. Green, S. A. Pace and D. R. Preuss, *J. Chem. Phys.* **76**, 2247 (1982), and references therein.
9. For example, M. M. Kappes, R. W. Kunz, and E. Schumacher, *Chem. Phys. Lett.* **91**, 413 (1982).
10. We wish to facilitate the formation of Na_2 in the B, C, and C' excited states in an electronically inverted configuration. To do this, Na_3 molecules must be present and react with halogen atoms. Here, it is important to note that the oscillator strengths for any of the larger sodium polymers ($Na_n, n \geq 3$) are sufficiently small versus Na_2 so that they do not interfere with the sodium dimer pump amplification cycle.
11. "Self-Flushing Optical Window to Prevent Collection of Condensates", W. H. Crumley, and J. L. Gole, *Rev. Sci. Instruments* **57**, 1692 (1986).
12. K. K. Shen, H. Wang, D. Grantier, and J. L. Gole, "Visible Chemical Lasers from Alkali Based Electronic Inversions", *Proceedings of SPIE OE'93 Conference*, January 16-23, 1993, Los Angeles, CA, in press.
13. J. T. Bahns and W. C. Stwalley, *Applied Physics Letters* **44**, 826 (1984).
14. G. Pichler, J. T. Bahns, K. M. Sando, W. C. Stwalley, D. D. Konowalow, L. Li, R. W. Field, and W. Muller, *Chem. Phys. Letters* **129**, 425 (1986).
15. A. Kopystynska and L. Moi, *Physics Reports* **92**, 135 (1982).
16. With a P-R branch separation given by $4B_v'' (J+1/2) = R(J-1) - P(J+1)$ and Na_2 ground state constants $B_0 = 0.154707$, $\alpha_0 = 0.000874 \text{ cm}^{-1}$ we find $B_v''=0 = 0.15427$ and for a frequency separation of order $15-20 \text{ cm}^{-1}$ and $4B_v''=0 = 0.61708 \text{ cm}^{-1}$ the implied ground state J value lies between 24 and 32. For v'' increasing, these J values increase. From the relationship $J_{\text{max}} = 0.59 [T(^{\circ}\text{K})/B_v'']^{1/2}$ Na_2 $J_{\text{max}}=0$ at room temperature (300K) has a J_{max} of 26. At 200 $^{\circ}\text{K}$, $J_{\text{max}} = 21$. Thus it is not possible at this time to unequivocally rule out the possible assignment of the doublet

structure to the peaking of P and R branches in a $1\Sigma_u^+ - 1\Sigma_g^+$ transition. See G. Herzberg, Spectra of Diatomic Molecules, Van Nostrand and Company, 1966.

17. W. G. Brown, Z. Physik 82, 768 (1933).
18. M. Allegrini, G. Alzetta, A. Kopystynska, L. Moi, and G. Orriolis, Opt. Commun. 22, 329 (1977).
19. R. Balfour and A. E. Douglas, Can. Jour. Phys. 48, 901 (1970); K. Li and W. C. Stwalley, J. Chem. Phys. 59, 4423 (1973).
20. F. Reuse, S. N. Khanna, V. de Coulon, and J. Buttet, Phys. Rev. B 41, 11743 (1990).
21. T. C. Devore, R. Kahlscheuer, L. Brock, and J. L. Gole, "On the BiF Bond Dissociation Energy and Evaluation of the BiF Red Emission Band Systems", Chemical Physics 155, 423 (1991).
22. T. C. Devore and J. L. Gole, "Fluorine Hot Atom Oxidation of Bismuth Vapor: A Comment on the Evaluation of the BiF Bond Energy", submitted to Chemical Physics, in press.
23. A. T. L. Haslett, M. Moskovits, and A. L. Weitzmann, J. Molec. Spectrosc. 135, 259 (1989).
24. K. D. Bier, T. L. Haslett, A. D. Kirkwood, and M. Moskovits, J. Chem. Phys. 89, 6 (1989).
25. M. Kent, T. Ehlert, and J. L. Margrave, JACS 86, 5090 (1964).
26. H. Wang, J. Towson, and J. L. Gole, "The Chemistry of Group IIA Dihalide Formation from Alkaline Earth Atom-Halogen Interactions", in preparation.

Table 1

i	$\frac{I_{s_i}}{I_{a_i}}$	T (K)
1	2.1	390
2	4.1	205
3	4.6	188
4	4.4	195

Table 1: Ratio of relative intensities of stokes (I_{s_i}) vs. antistokes (I_{a_i}) features shown with corresponding calculated vibrational temperatures corresponding to those features seen in figures 5 and 7. I_{s_i} denotes the i^{th} stokes feature from the Na D line. I_{a_i} denotes the antistokes feature. The ratio, I_{s_i}/I_{a_i} may not accurately represent the actual vibrational temperature of the Raman (dimer) scatterer due to partial overlap of the feature with the Na D line. See text for discussion.

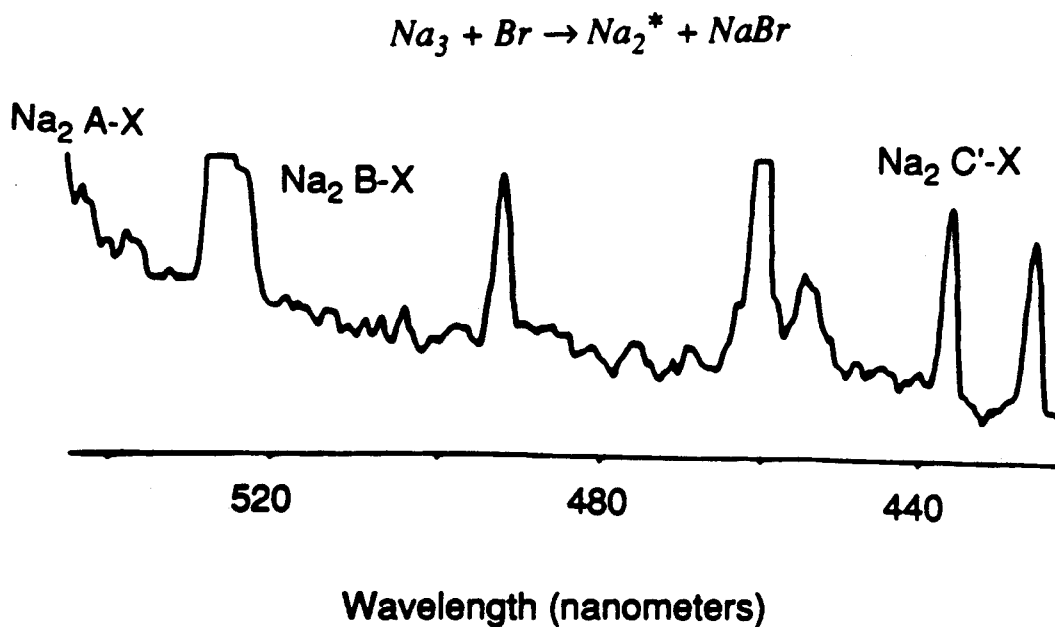


Figure 1: Chemiluminescent emission resulting from the reaction $\text{Na}_3 + \text{Br} \rightarrow \text{Na}_2 + \text{NaBr}$. The spectra display sharp fluorescence features in the visible at ~527, ~492, ~460.5 nm superimposed on a broader Na₂ background emission.

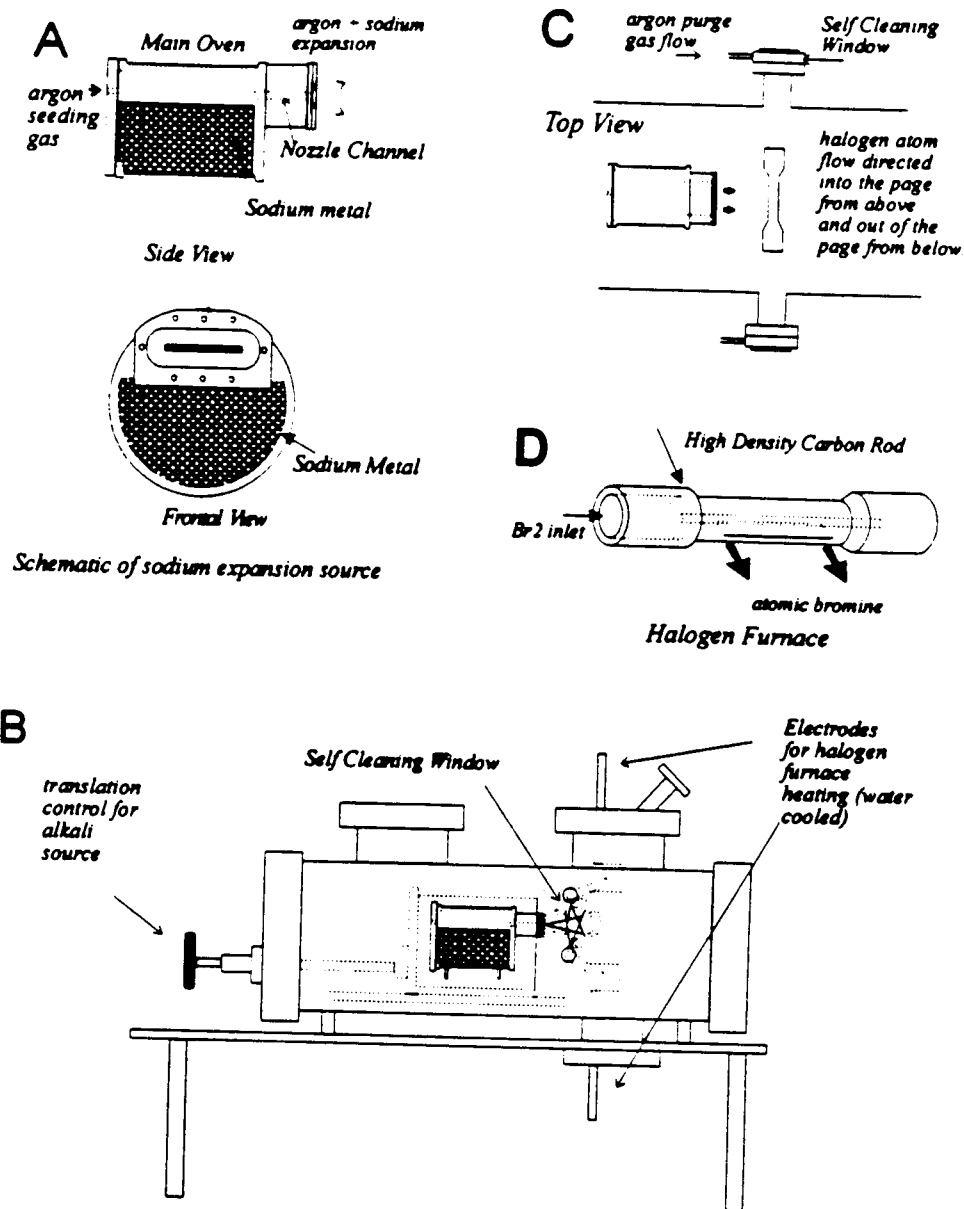
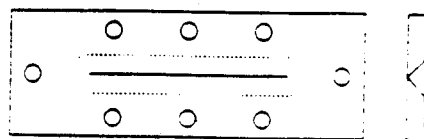


Figure 2(a): Schematic of the alkali metal planar supersonic expansion source. This device allows for the sodium vapor to be cooled in a "pure" expansion (without carrier gas) or in a "seeded" flow, in which argon or helium is used to maintain a high backing pressure and hence produce a colder expansion.

Figure 2(b): Experimental overview of reaction chamber. The orientation of the alkali expansion source depicted in Fig. 2(a) is shown relative to the positions of the halogen atom sources. The alkali oven system is constructed so as to allow for its in-situ translation during the experiment.

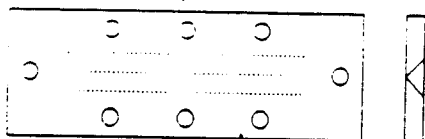
Figure 2(c): Overview of experimental reaction chamber configuration from above. The spatial coincidence of the reaction zone and the optical train is demonstrated.

Figure 2(d): Schematic of halogen atom planar flow source. See text for discussion.



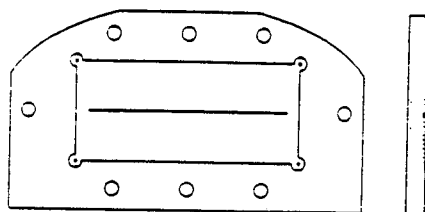
A

Stainless steel expansion slit



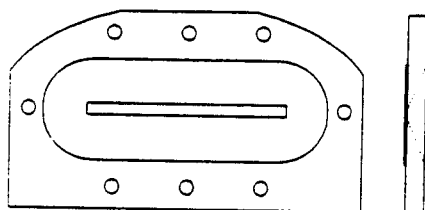
B

Molybdenum expansion slit



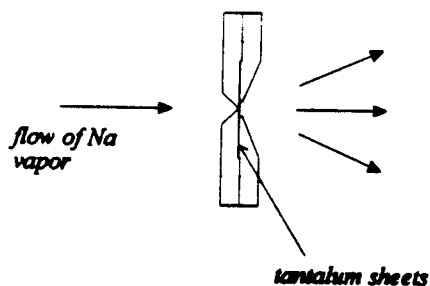
C

Rear plate of a dual-plate nozzle configuration.



D

Front plate of a dual-plate nozzle configuration



E

Schematic showing fit of front and rear plates forming the tantalum slit

- Figure 3(a):** Stainless steel nozzle of 0.003" width constructed using an EDM technique and tested in preliminary stages of the experiment.
- Figure 3(b):** Molybdenum slit nozzle following an identical design to the slit depicted in Fig. 3(a). This slit proved considerably more resistive to alkali erosion.
- Figure 3(c):** Rear plate of a dual-plate nozzle configuration (stainless steel).
- Figure 3(d):** Front plate of a dual-plate nozzle configuration (stainless steel).
- Figure 3(e):** Schematic depiction of the nozzle assembly from the front and back plates depicted in Figures 3(c) and 3(d). The two plates sandwich two parallel sheets of 0.005" tantalum which comprise a 0.003" expansion slit. See text for discussion.

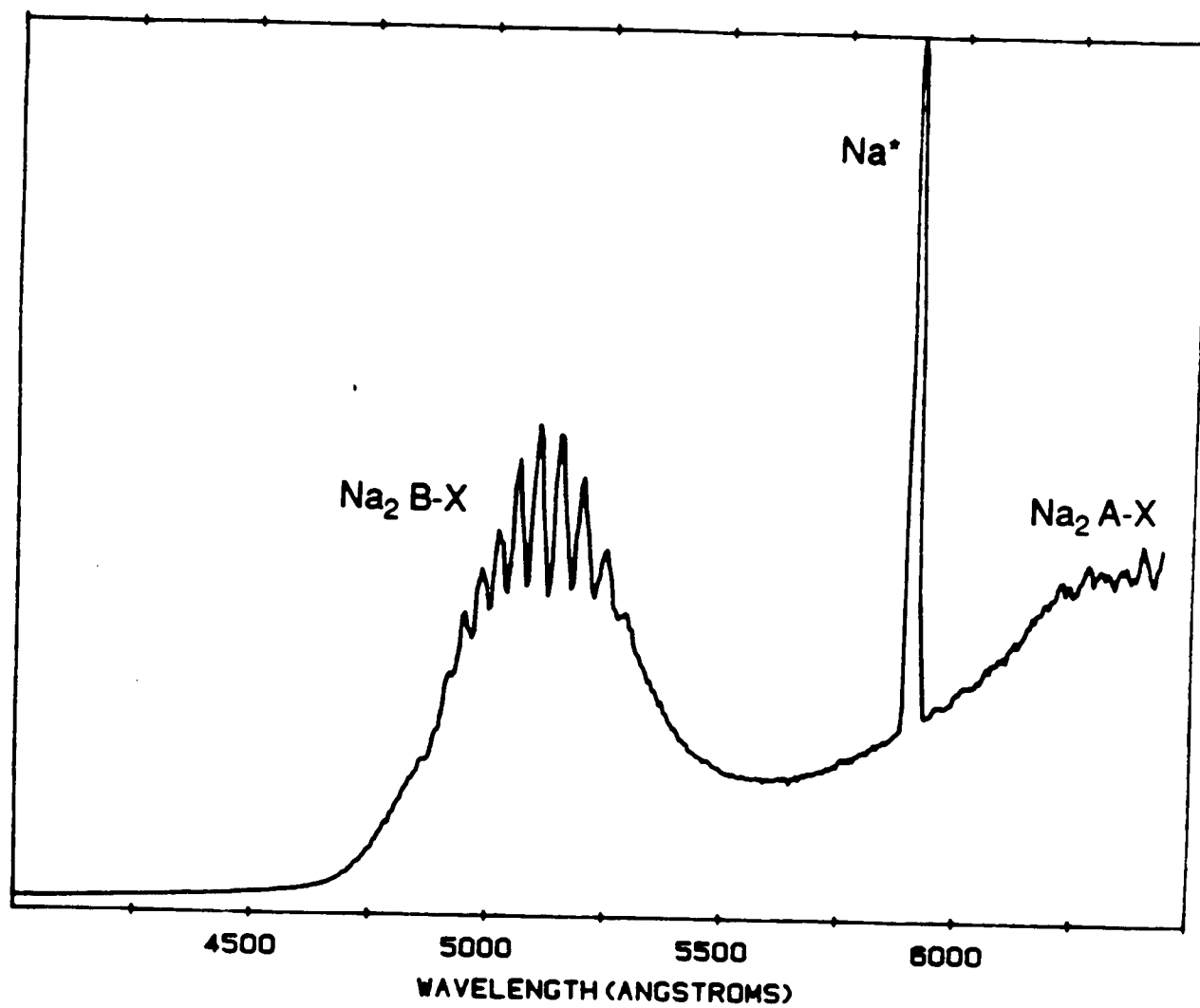


Figure 4: Na₂ B-X and A-X chemiluminescent emission spectrum recorded at low bromine flux under pure sodium expansion conditions.

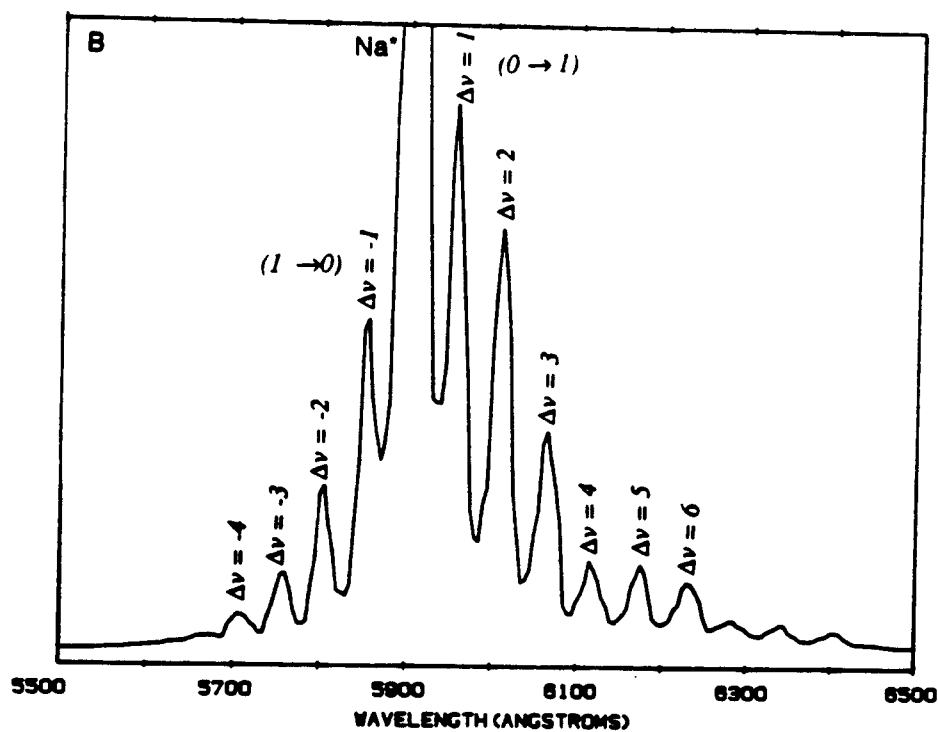
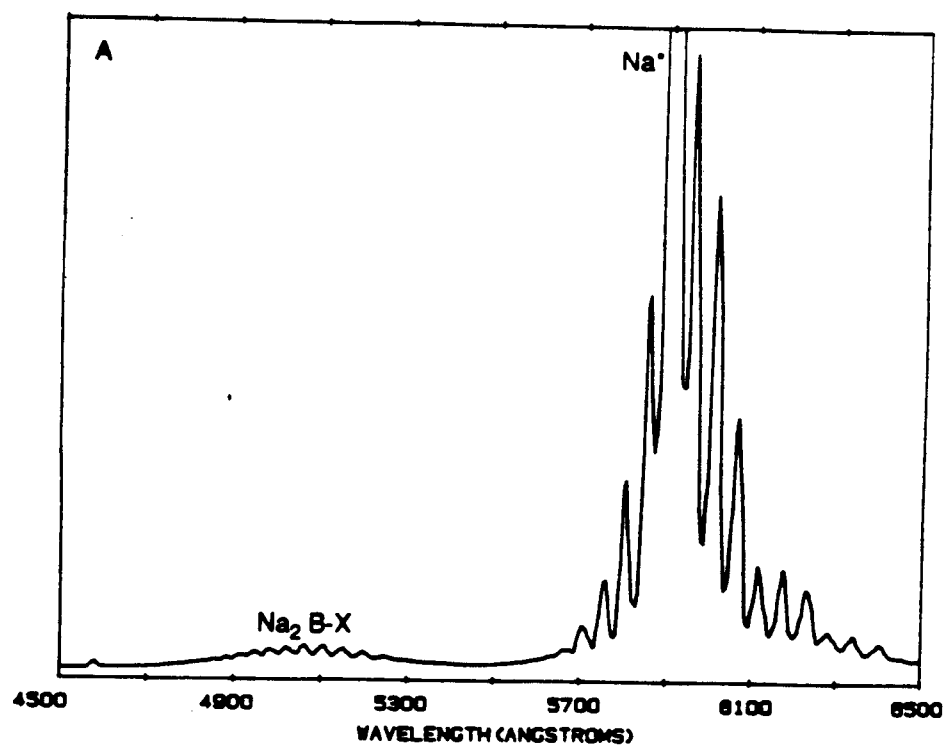


Figure 5: Na_2^* chemiluminescent emission from $\text{Na}_x\text{-Br}$ reactive encounters. The system was operated at moderate bromine flux using a pure sodium expansion. See text for discussion.

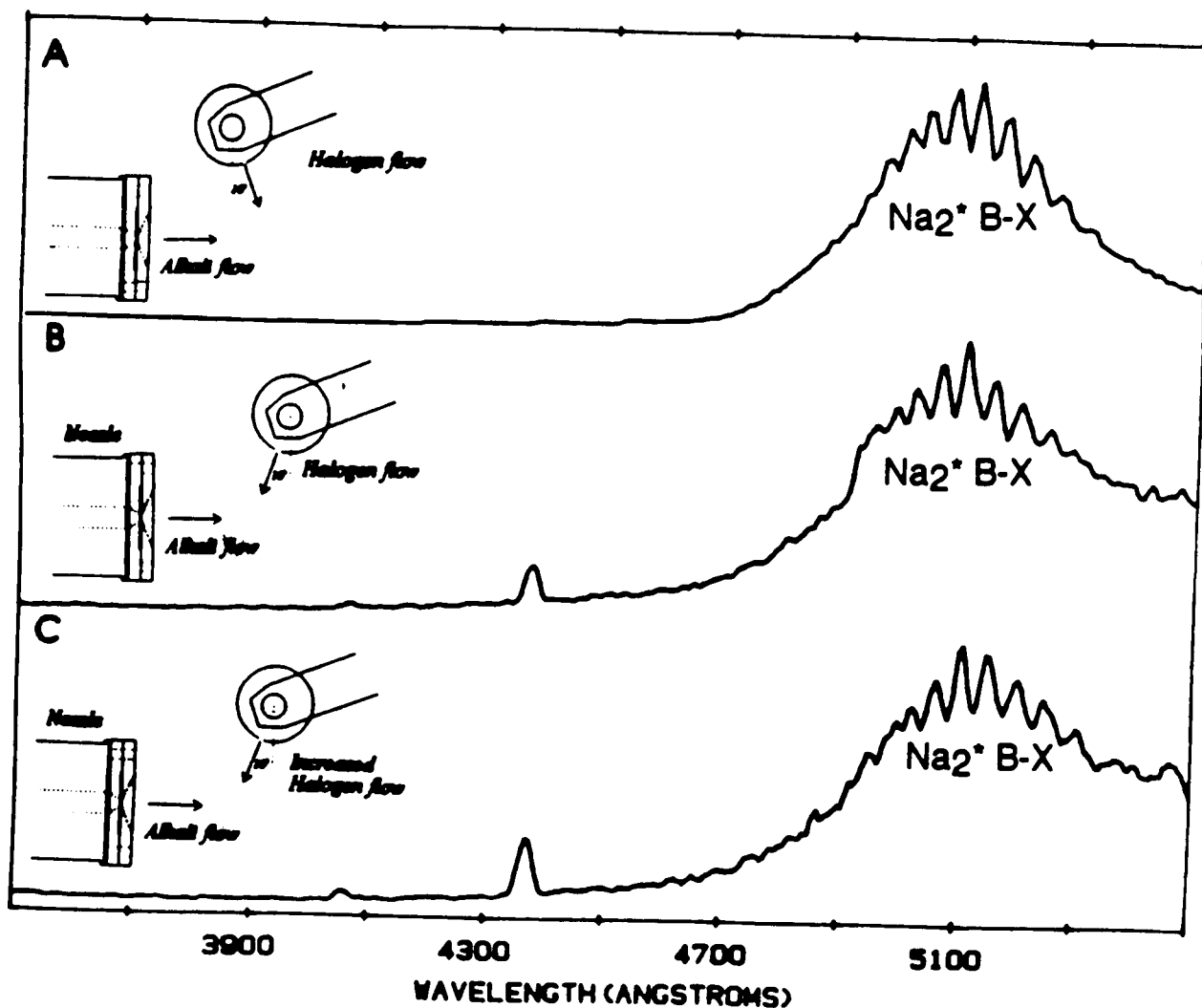


Figure 6: Demonstration of the effect of halogen flow relative to the alkali flow. (a) The halogen flow is oriented to flow with a vector flow component parallel to the alkali expansion. (b) The halogen flow is oriented so as to oppose the supersonic expansion. (c) Same as (b) with increased flow. See text for discussion.

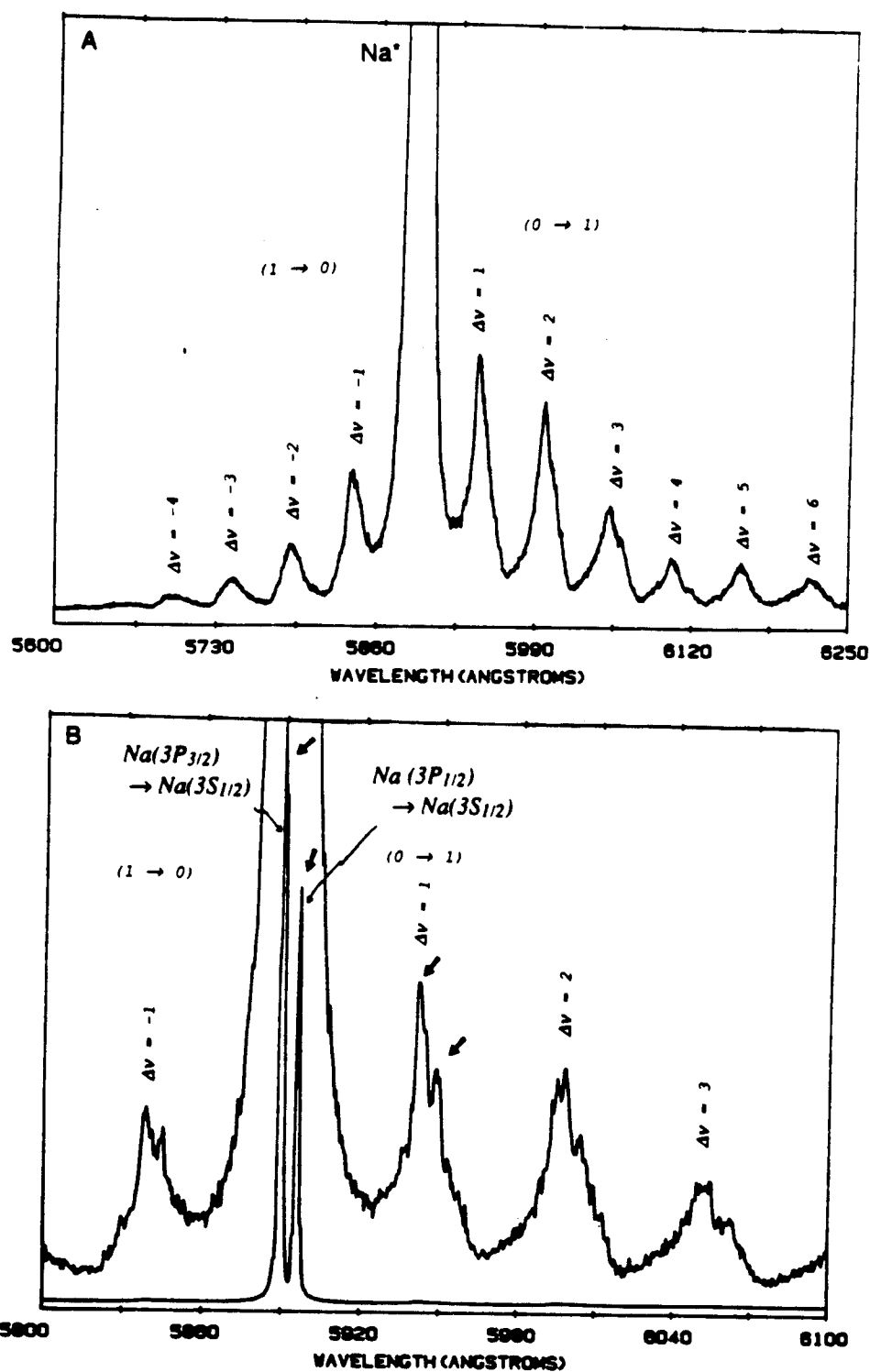


Figure 7: High resolution scans of Na⁺ induced Raman spectra showing transitions associated with the labeled lower state levels. (a) 0.1 nm resolution scan. (b) 0.05 nm resolution scan. Note the correlation of the relative intensities of the peaks corresponding to the doublets of each side band with the relative intensities of the Na(3P_{3/2}) → Na(3S_{1/2}) and the Na(3P_{1/2}) → Na(3S_{1/2}) emission features (indicated by arrows).

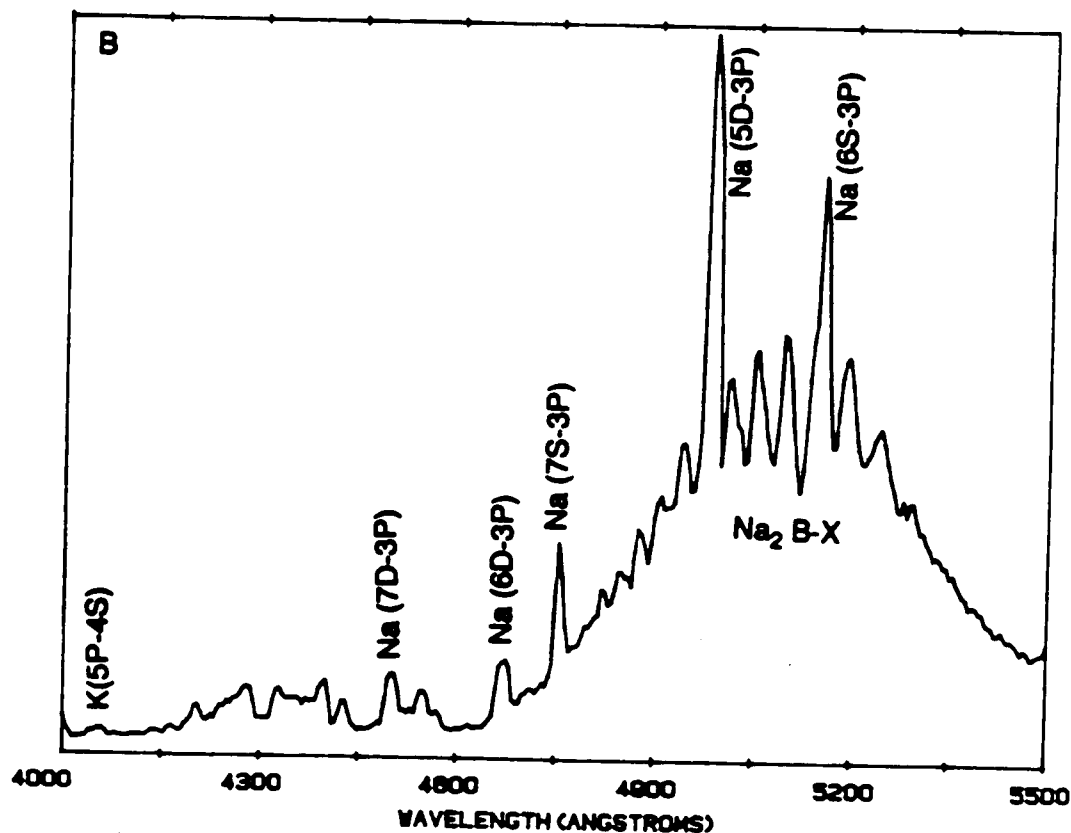
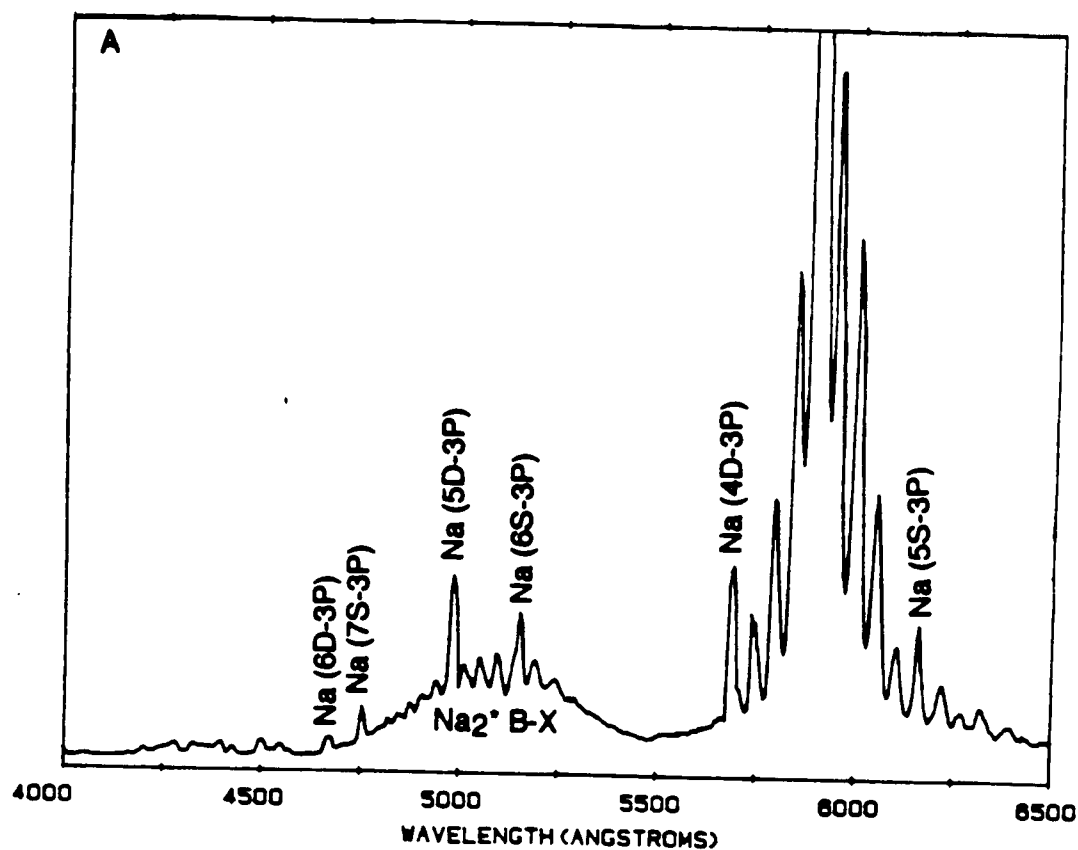


Figure 8: Chemiluminescence spectrum obtained at high bromine and sodium flux demonstrating the pumping of higher excited states of the sodium atom, most likely through energy pooling, (a) in the wavelength region 400-650 nm, and (b) 400-550 nm. Note that figure (b) represents a magnification of figure (a). $T_{\text{oven}} = 880\text{K}$. $T_{\text{nozzle}} = 925\text{K}$.

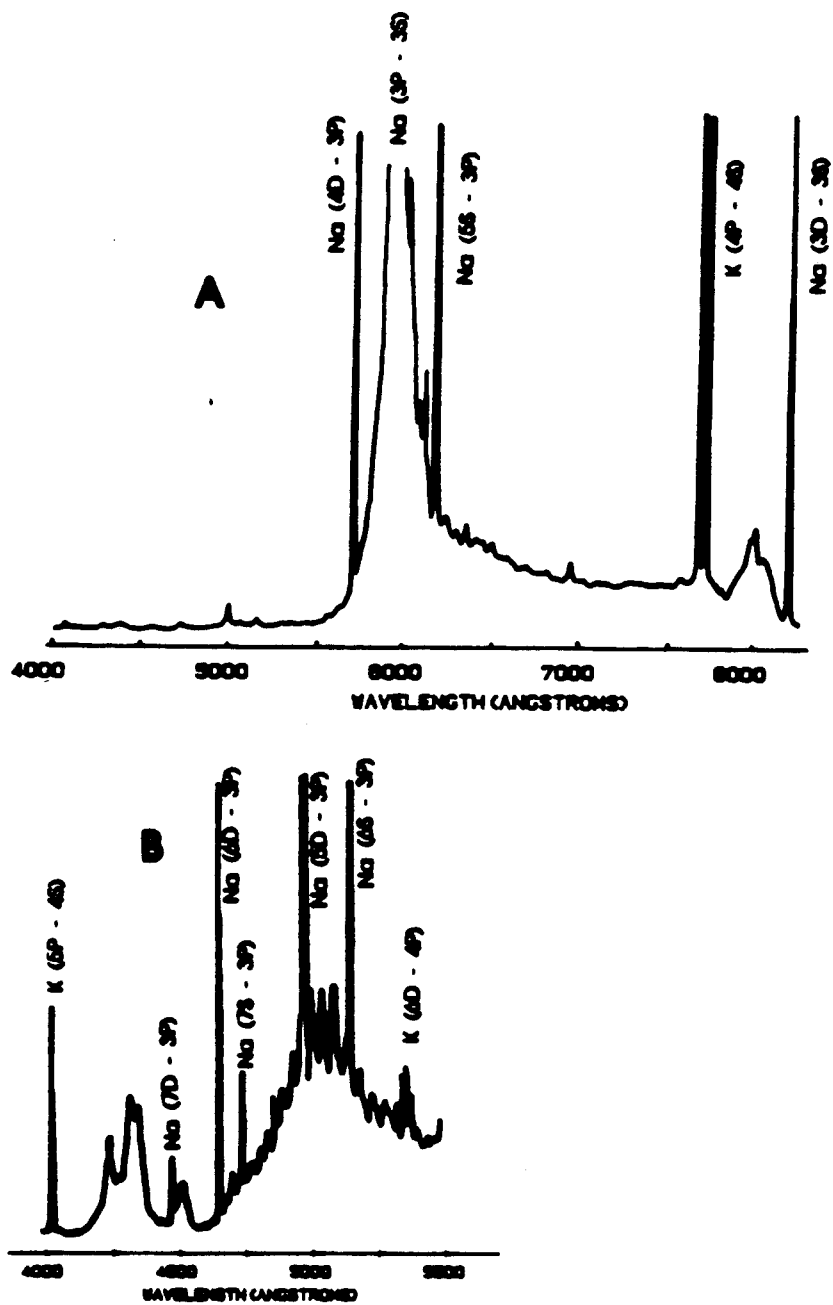


Figure 9: Laser induced sodium fluorescence spectra obtained by Allegrini et al.¹⁸ See text for discussion.

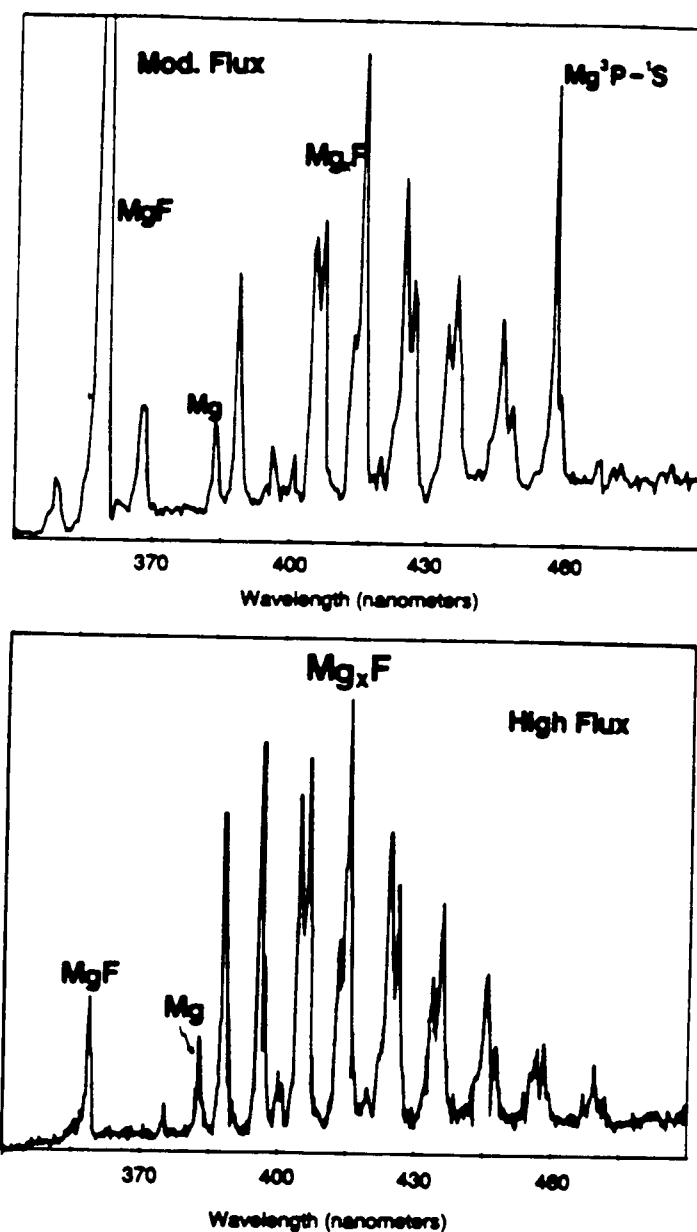


Figure 10: Chemiluminescent spectra resulting from the reaction of small magnesium molecules (Mg_2 , Mg_3), formed in a high metal mole fraction agglomeration flow of dry ice cooled helium, with fluorine atoms. The observed spectra correspond to MgF ($A^2\Pi - X^2\Sigma^+$), $Mg\ 3p - 1s$, $3s - 3p$, and $3d - 3p$ atomic, and Mg_xF emission features, which vary in intensity with increasing mole fraction of magnesium. The progression of bands associated with the Mg_xF emitter (charge transfer complex), where x is likely 2, appears to correspond to a progression in the MgF stretch on which is superimposed features associated with an Mg_2^+ moiety. Preliminary studies indicate that $MgF\ A^2\Pi$ and $Mg\ 3p$ are formed from the $Mg_2 + F$ reaction, $Mg\ 3d$ and $Mg\ 3s$ are formed from an energy pooling process involving $Mg\ 3p$ and $MgF\ A^2\Pi$ and the Mg_xF charge transfer emission results from the Mg_3-F reaction. The spectra are taken with an RCA 1P28 phototube at 1 nm resolution.

APPENDIX XI

"Chemically Driven Visible Laser Amplifiers and Oscillators Based on Fast Electronic Energy Transfer", K. K. Shen, H. Wang, C. B. Winstead, and J. L. Gole, Proceedings of the 24th AIAA Plasmadynamics and Laser Science Conference, Orlando, Florida, AIAA 93-3209 (1993).



AIAA 93-3209

**Chemically Driven Visible Laser
Amplifiers and Oscillators Based
on Fast Electronic Energy Transfer**

**J.L. Gole, K. K. Shen, H. Wang, C. B. Winstead and J.
Stephens**

**School of Physics, Georgia Institute of Technology
Atlanta, GA. 30332**

**AIAA 24th
Plasmadynamics & Lasers Conference
July 6-9, 1993 / Orlando, FL**

**For permission to copy or republish, contact the American Institute of Aeronautics and Astronautics
370 L'Enfant Promenade, S.W., Washington, D.C. 20024**

CHEMICALLY DRIVEN VISIBLE LASER AMPLIFIERS AND OSCILLATORS
BASED ON FAST INTERMOLECULAR ELECTRONIC ENERGY TRANSFER

J. L. Gole, K. K. Shen, H. Wang, C. B. Winstead and J. Stephens
School of Physics
Georgia Institute of Technology
Atlanta, GA 30332

ABSTRACT

Efficient near-resonant intermolecular energy transfer from selectively formed metastable states of SiO and GeO ($a^3\Sigma^+, b^3\Pi$) has been used to form continuous sodium and potassium atom based laser amplifiers at 569 nm (Na), 616 nm (Na), 819 nm (Na), and 581 nm (K). Adopting a variety of pumping sequences in which substantial concentrations of the energy storing metastables are brought into intimate contact with the appropriate atomic receptor, either as a premixed metalloid (Si, Ge)-receptor atom (Na, K) combination is oxidized or through intersection of the metastable pump-receptor atom flows, we have energy transfer pumped $X^2S_{1/2}$ Na atoms (SiO) to their excited $4d^2D$ and $5s^2S$ states and $2S_{1/2}$ K atoms (GeO) to their $5d^2D$ state. We observe a system temporal behavior, signaling the creation of a population inversion, and corresponding to a gain condition on the Na $4d^2D - 3p^2P$ (α (gain coeff.) $\geq 0.1/\text{cm}$) transition at 569 nm, the Na $5s^2S - 3p^2P$ ($\alpha > 0.03/\text{cm}$) transition at 616 nm, and the K $5d^2D - 4p^2P$ ($\alpha > 0.08/\text{cm}$) transition at 581 nm. The gain condition, established for the sodium system using three independent (Roll-Mentel ratio method, sodium lamp line-selected gain measurement, high resolution ring dye laser gain measurement) monitoring techniques, forms the basis for full cavity oscillation on the Na $4d^2D - 3p^2P$ and $5s^2S - 3p^2P$ transitions at 569 and 616 nm. At 569 nm, with 0.2% output coupling from a full cavity configuration surrounding a 5 cm reaction - energy transfer - amplification zone formed by the 90° intersection of entrained metastable SiO and Na atom flows, we have achieved an optimum continuous light output exceeding 10^3 times that observed with a blocked (single pass) high reflector. This observation of the manifestation of oscillation is consistent with recent modeling studies. Improvements in reactant mixing and active medium concentration through implementation of a concentric flow configuration, the optimization of output coupling, and the operation of the full cavity optical train in windowless configuration, all of which promise a considerable improvement in cavity output, are summarized. Within a generic framework, the first order approach to the creation of amplifiers and oscillators in the alkali based systems might also be extrapolated to exploit the efficient near resonant energy transfer pumping of potential amplifying transitions in lead (Pb), copper (Cu-analog of Cu vapor laser), and tin (Sn) receptor atoms.

Approach to Energy Transfer Pumping

The approach which we outline to develop the first visible chemical laser amplifiers and oscillators¹⁻⁵ has relied on a two step procedure wherein chemical energy is produced and stored in a

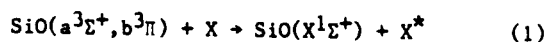
first step and then transferred in a collision induced process to an appropriate lasing medium in a second step. Following this scheme, we can attempt to produce inversions using (1) "ultrafast" intramolecular energy transfer among the excited electronic states of small diatomic molecules⁶⁻⁹ or (2) intermolecular transfer from electronically excited metastable storage states to readily lasing atomic receptors. The nature of the amplifying medium dictates the required temporal separation of the two steps of interest.

In developing visible chemical lasers from energy transfer related processes, it is important to note that electronically and highly vibrationally excited molecules, with their inherently diffuse electron density and large amplitude vibrational motions simply interact more efficiently than do ground state molecules in their lowest vibrational-rotational levels. We have determined that several diatomic metal monoxides display collision induced electronic-to-electronic (E-E)⁷⁻¹⁰ and vibrational-to-electronic (V-E)¹¹ intramolecular energy transfers which proceed at rates comparable to or far in excess of gas kinetic. Transfers from metastable to shorter lived excited states may proceed at rates which approach 500 times gas kinetic (cross sections well in excess of 4000 \AA^2). It appears that even the low-lying electronic states of several simple high temperature molecules (the products of metal oxidation) interact with a collision partner which induces energy transfer with a much larger impact parameter than previously anticipated. In a sense we are dealing with "pseudo-macromolecules" which display many of the characteristics inherent to Rydberg states¹² with their large transfer and relaxation cross sections. In several cases the rates for the observed transfers may be comparable to the radiative lifetimes associated with the usually shorter lived and potentially useful upper levels in which the intramolecular transfer terminates.¹³ Rates of this magnitude, properly employed, can be competitive with optical pumping!

At some point, there is little distinction between fast intramolecular energy transfer processes, correlating with electronic state couplings and the periods of molecular vibrations (rotations), and intermolecular energy transfer, governed by the duration of collisions with electronically excited states.¹⁴ It is therefore reasonable to expect certain near resonant intermolecular energy transfers to proceed with extremely high cross sections. We consider that an electronically excited molecule, with its diffuse electron density, has a much larger interaction range as it influences reaction and collision partners. The increased interaction rates which several experiments now suggest are certainly encouraging for the development of visible chemical lasers from energy transfer processes.

Relatively simple metal or metalloid oxidation reactions, which involve a branching to long-lived metastable states in a high quantum yield process, while rare, show the promise of creating an energy storage medium to pump atomic transitions with an established high propensity for lasing action.¹ To accommodate this desired pump sequence, we have developed techniques to form copious quantities of the metastable SiO and GeO $a^3\Sigma^+$ and $b^3\Pi$ states as the products of the primarily spin conserving Si-N₂O,¹⁵ Si-NO₂,¹⁶ Ge-N₂O, and Ge-O₃ reactions. These long-lived triplet states act as an energy reservoir for fast near resonant intermolecular energy transfer to efficiently pump atomic transitions including select transitions in sodium,²⁻⁵ potassium,²⁻⁵ thallium,^{1,2} gallium,^{1,2} lead,^{3,4} copper,^{3,4} and tin.^{3,4} Here, we focus primarily on the electronic-to-electronic (E-E) energy transfer pumping of sodium atom based amplifiers corresponding to the Na $4d^2D - 3p^2P$, $5s^2S - 3p^2P$, and $3d^2D - 3p^2P$ transitions at ~ 569 , ~ 616 , and ~ 819 nm and the concomitant full cavity oscillation on the $4d^2D - 3p^2P$ transition at $\lambda \approx 569$ nm. We also consider the implications of the results obtained with sodium as they apply to the future development of potassium, lead, copper, and tin atom based systems.

In order to pump the $3d^2D$, $4d^2D$, and $5s^2S$ levels of atomic sodium,²⁻⁴ we make use of the efficient intermolecular energy transfer process



where X^* represents the electronically excited atomic species from which we wish to obtain lasing action and the SiO $a^3\Sigma^+$ and $b^3\Pi$ states are formed under multiple collision conditions in a focused argon or helium entrainment flow such that the nascent product distribution of the Si-N₂O¹⁵ or Si-NO₂¹⁶ reactions is rotationally thermalized and vibrationally relaxed (Ref. 1, Figure 4) to the lowest levels of the triplet state manifold. The success of this outlined scheme depends on the rates for the reactions forming the SiO or GeO metastables^{17,18} and the rate of the $\text{MO}^* (\text{M}=\text{Si}, \text{Ge}) - X$ intermolecular energy transfer, which, we anticipate, will be influenced by the nature of near resonances between the MO^* and X^* energy levels.

The outlined energy transfer process is found experimentally to be quite efficient for sodium (as well as potassium) atoms. To an even greater degree than that inherent to the previously studied chemically pumped Tl based^{1,2} amplifier-oscillator system (Tables I and II of Ref. 1) at $\lambda \approx 535$ nm, there exist near resonant matchups ($\Delta E \approx 100 \text{ cm}^{-1}$) to receptor atom levels of interest in atomic sodium (and potassium) for both SiO and GeO metastables. We are concerned with the energy transfer pumping of levels which are not accessed through strong electric dipole transitions from the ground state of the alkali atom. Applying these criteria, we summarize the nature of relevant near resonances for the lowest vibrational levels of the $a^3\Sigma^+$ and $b^3\Pi$ states of SiO and GeO and the Na and K atomic transitions in Tables I and II. For the SiO - Na system, Table I suggests that the sodium $4d^2D$ level might be most easily pumped followed closely by the $5s^2S$ level. The $3d^2D$ and $6s^2S$ levels appear somewhat less promising, with the potential reson-

ances involving the $3d^2D$ level and the lower $b^3\Pi$ vibrational levels being more favorable. A similar analysis for the potassium (Tables I and II) and lead (Tables III and IV) atom transitions suggests that, at least to first order, both systems are comparable if not more favorable than sodium. In fact, Table V suggests the possibility for an efficient energy transfer pumping of the upper $4p^2P$ levels of the copper vapor laser and Table VI enumerates a select group of tin atom receptors. All of these systems show promise for the development of energy transfer based amplifiers and while the primary focus of our discussion will be the SiO-Na system, the devices which we are developing to create, enhance, and characterize this amplifying medium are designed for ready conversion to similar studies of potassium, lead, copper, and tin energy transfer pumping.

Evidence for Efficient Energy Transfer Pumping

Collisions with SiO or GeO metastables have been used to energy transfer pump from the $3s^2S$ Na ground state to the Na $3d^2D$, $4d^2D$ and $5s^2S$ levels forming the basis for amplification on transitions from these levels to the $3p^2P$ terminal laser level (Fig. 1(a)), the short-lived upper level of the Na D-line.¹⁹ Because the $3p^2P - 3s^2S$ transition is characterized by a high oscillator strength, it facilitates rapid loss²⁻⁵ of the terminal laser level, especially in a D-line quenching environment, creating ground state Na atoms which are again amenable to near resonant energy transfer pumping.

The $3d^2D$, $4d^2D$, and $5s^2S$ levels are not readily accessed via optical pumping²⁰ from the ground $3s^2S$ state of the sodium atom, however, as Figs. 1(b) and 1(c) demonstrate, using SiO metastables formed in the Si-N₂O reaction, we have successfully energy transfer pumped Na atoms to the $2S$ and $2D$ levels where, for the $3d^2D$, $5s^2S$, and $4d^2D$ levels, they subsequently emit radiation at ≈ 819 , 616 , and 569 nm ²¹ as they undergo transition to the $3p^2P$ levels. The observed Na atom transitions, originating at the $4d^2D$ and $5s^2S$ levels, are characterized by moderate oscillator strengths. The accessed Na cycle, with its 50 ($4d^2D - 3p^2P$)²² to ~ 100 ($5s^2S - 3p^2P$)²³ nanosecond upper state radiative lifetimes (vs. Tl $2S_{1/2}$ at 7nsec.^{1,24}) and short-lived terminal laser level, would appear ideally suited to obtain high duty cycle laser amplifiers and oscillators. In fact, we find that these transitions demonstrate continuous gain. In following sections, we outline a range of measurements on the Si-SiO-Na system which can be readily extrapolated to the potassium, lead, copper, and tin systems and which have been used to demonstrate continuous gain on the $4d^2D - 4p^2P$, $5s^2S - 3p^2P$, and $3d^2D - 3p^2P$ transitions at $\lambda \approx 569$, $\lambda \approx 616$, and $\lambda \approx 819 \text{ nm}$ respectively, and obtain evidence for continuous oscillation at $\lambda \approx 569 \text{ nm}$.

As figures 2, 3, and 4 suggest the efficient energy transfer pumping manifest in the SiO-sodium system is also clearly apparent for potassium (Fig. 2), lead (Fig. 3), and copper (Fig. 4) receptors. As in the sodium based spectrum of Fig. 1,²⁻⁴ the K D-line transitions (K $4p^2P - 4s^2S$) at $\lambda \approx 767-770 \text{ nm}$ dominates emission from the $6s^2S$, $7s^2S$, $4d^2D$, $5d^2D$, and $6d^2D$ levels, all of which feed the short-lived

4p²P upper level of the K D-line. Preliminary experiments using an SiO pump suggest gain on the 6s²S - 4p²P, 7s²S - 4p²P, 5d²D - 4p²P, and 6d²D - 4p²P transitions with an estimated gain coefficient $\alpha \sim 0.08$ for the 5d²D - 4p²P amplifier at $\lambda \sim 581$ nm. While we have emphasized the use of an SiO pump for the sodium system, Table II demonstrates that several potential potassium based amplifiers might best be created using GeO metastables.³⁻⁵

Figure 3 demonstrates the results we have obtained when using SiO metastables (Si-N₂O) to pump lead receptor atoms. Observed Pb transitions are indicated to the right of the figure. We notice that self-absorption involving ground state X ³P₀ lead atoms is so dominant that no emission to the ground state is observed. This self absorption is even more pronounced than that observed for the Tl system. We find significant pumping of both the ¹S₀ and ¹D₂ levels, as Table III suggests and Table IV indicates, might be considerably improved with a GeO metastable pump. The transitions from the ¹S₀ level terminate in the lowest X ³P₂ (531.2 nm) and X ³P₁ (462 nm) levels. If collisional quenching and relaxation of the ¹S₀ level are minimal relative to that of the X ³P manifold (³P₂, ³P₁) it may be possible to create population inversions on the ¹S₀ - ³P₂ and ¹S₀ - ³P₁ transitions and produce amplification at 531.2 and 462 nm. The well known lead laser transition at $\lambda = 723$ nm²⁵ corresponding to a ³P₀ - ¹D₂ transition (Fig. 3) has an A value close to 10⁶ sec⁻¹ yet we find no evidence for this transition. We do, however, find evidence for both the ³P₀ - X ³P₁ and ³P₀ - X ³P₂ transitions and for the ¹D₂ - ³P₁ transition at 733 nm.²⁶ These results suggest that the ³P₀ - ¹D₂ transition may be self absorbed due to a significant ¹D₂ population which also facilitates the observation of the 733 nm transition. It will be important to assess whether the manifestation of a significant ¹D₂ population results from direct energy transfer pumping or whether the ¹D₂ state is populated by the 723 nm laser transition on a time scale considerably shorter than that for the observation of energy transfer.¹ The results obtained for the energy transfer pumping of lead atoms certainly suggest the possibility of creating additional amplifiers. It is particularly encouraging that some of the associated transitions may operate within four level systems thus obviating the self-absorption bottleneck that may plague the Si-SiO-Na system at high sodium concentration.

Figure 4 demonstrates results obtained for the Si-SiO-Cu system obtained using an approach representing a significant extrapolation from the mixing configuration which we have outlined previously and consider in following sections. Here Si and Cu were premixed at room temperature and co-vaporized from a single crucible. The mixture was then oxidized to yield the energy transfer pumping spectrum in Figure 4.

With the examples given in Figures 1-4 (Tables I - VI), it should be apparent that a variety of energy transfer pumping configurations might be invoked to produce amplification across the visible region.

GAIN MEASUREMENTS FOR SiO-Na - NATURE OF THE REACTION-ENERGY TRANSFER-AMPLIFICATION ZONE FOR SODIUM BASED EXPERIMENTS

Gain Measurement

Gain measurements have been carried out on the amplification region created in the sodium system using three different experimental configurations. The simplest of these measurements employs the optical train depicted in Fig. 5(a) most recently surrounding a ~ 5 cm energy transfer - amplification zone²⁻⁴ created using the mixing configuration depicted in Fig. 6. The optical train parallels the ingenuous design of Roll and Mentel,^{4,27} used to measure amplified spontaneous emission (ASE).^{2-4,27} The gain coefficient α , can be calculated from

$$\alpha = \ln((I_2 - I_1)/I_1 RT^2)/L \quad (2)$$

Here, L is the effective gain medium length (the medium is not necessarily uniform), R is the mirror reflectivity, and T is the transmission of the amplification zone vacuum chamber window in front of the mirror (Fig. 5(a)). I_1 is the measured "single pass" (spectrometer) light intensity from the gain medium with the shutter placed in front of the high reflector. With the high reflector open to and aligned with the gain medium, we measure light of intensity, I_2 , which is contributed to by (1) light passing directly through the gain medium to the detector (I_1) and (2) light reflected back through the amplification zone from the high reflector. We refer to I_2 as the double pass ASE intensity. Thus, in Equation (2), we compare the intensity difference ($I_2 - I_1$) to I_1 correcting for the reflectivity and transmissivity.

A considerable change in the relative intensities of the 569 nm Na 4d²D - 3p²P and Na D-line emissions for the single and double pass ASE output is quite evident in Figure 7. The ratio of the double to single pass intensity for the 569 nm feature depicted in the Figure is 2.6/1, corresponding to a gain coefficient, $\alpha \sim 0.11/\text{cm}$ (Eq. 2), which is by no means the optimal value that has been achieved with the current configuration. Under optimal operating conditions, using a 1" diameter 99.9% high reflector, we have achieved amplification such that the ratio of light output when the rear high reflector is accessed to that when the rear high reflector is blocked ranges from 3.4 to 3.8 ($\alpha \sim 0.16$ - $0.23/\text{cm}$). This is a ratio which demonstrates clear gain. It should be compared with the measured ratio for a purely fluorescent feature (Na D-line and higher lying excited state Na transitions) which is usually between 1.1 and 1.2 for the Na D-line, and corresponds to 1.6 for the 5s²S - 5p²P transition whose emission is also depicted in Figure 7. The theoretical maximum value for the ratio associated with pure fluorescence based on a lossless single reflection is 2. When the experimental conditions are not favorable for formation of the gain medium, we measure significant losses for the reflected light (α negative in Eq. (2)) employing the same methods we have used to demonstrate the gain in Figure 7. The Na atom transitions at $\lambda \approx 569$ nm ($\alpha \sim 0.1$ - 0.15), $\lambda \approx 616$ nm ($\alpha \sim 0.03$ - $0.05/\text{cm}$), and $\lambda \approx 819$ nm ($\alpha \sim 0.02$ - $0.03/\text{cm}$) have all been shown to demonstrate gain. The α values given in

parentheses are meant to represent typical values determined from Eq. 2 using $L = 5$ cm.

In a second series of more complex gain measurements we have determined gain on the emission lines from a sodium discharge lamp. Using a configuration described in more detail elsewhere,^{3,4} we have measured the enhancement of the $\text{Na } 4d^2D - 3p^2P$ emission line (or other sodium transitions) which can be evaluated by singling out the transition of interest with a 10 nm bandpass filter. Under working experimental conditions, using the selected 569 nm output from the lamp, we have measured a calibrated gain close to 3.6%. Calibrated gains associated with the amplification zone which are in excess of 5% have been achieved in a few cases. Preliminary measurements at 616 nm indicate a lower gain, on the order of $1.2 \rightarrow 1.5\%$. These measured gains using the lamp based optical configuration are believed to represent lower bounds to the true values due to the significant radial extent (cross sectional area) of the lamp output which intersects a much smaller mixing zone and gain medium. When the 569 nm light exiting the gain medium is focused onto the entrance slit of the monochromator, the measured gain is diluted by the mismatch in cross sectional area as not only the gain zone but also regions of negligible gain and even absorption (pumping of $3p^2P$ level) are monitored.

We have also used the output from a high resolution ring dye laser to carry out laser gain measurements in a frequency scanning mode (laser calibrated with iodine).^{2,4} Upon scanning the ring dye laser through the region encompassing the 569 nm feature, we record a gain in excess of 1.5% for the $\text{Na } 4d^2D_{5/2} - 3p^2P_{3/2}$ transition.^{5,28} This percent laser gain also represents a lower bound determination^{3,4} of the single pass amplification. This results because (1) the bandwidth of the ring dye laser (effective linewidth ~ 40 MHz) is considerably smaller than the width of the 569 nm $\text{Na } 4d^2D - 3p^2P$ stimulated emission gain profile (~ 2 GHz) and (2) the precise overlap of the sharply defined laser output beam and the amplification zone is tenuous.^{3,4}

These three distinct gain measurements clearly demonstrate the formation of an energy transfer pumped sodium atom laser amplifier. The magnitude of the gain is probably best represented by the results obtained with the Roll-Mentel configuration. However, it is important to note that these determined gain values correspond to a single-pass through the amplification zone. The effective gain in an oscillating full cavity, influenced both by the increased rate of loss of the population inversion due to the stimulated emission process and by the nature of reactant mixing and energy transfer in the amplification zone, will be notably smaller.

Amplification Zone

The flow configuration depicted in Fig. 6 produces the longest path length SiO metastable flame (~ 5 + cm) thus far obtained. This entrainment flow configuration was designed to create large concentrations of SiO (GeO) metastables intersected at $\sim 90^\circ$, in subsonic flow, by a high concentration of sodium atoms. The choice of

entrainment gas for the vast majority of the initial experiments has been helium or argon for both the silicon and sodium flows, however, these gases have been replaced by N_2 and soon will be at least partially converted to a mixture of N_2 and CO in an attempt to carefully modify the chemistry of the amplification zone. The configuration of Fig. 6 has also been designed so that the entrained silicon and sodium flows can be moved in-situ relative to each other and hence with respect to the reaction - energy transfer - amplification zone to optimize conditions for formation of the gain medium. In developing the crossed interaction zone to its full extent, we have been concerned with the optimization of reactant mixing considering the rate limiting effect of the silicon concentration, the importance of virtually complete sodium atomization, and the confinement of the reactants and receptors to the cavity axis region. With the silicon source temperature monitored by optical pyrometry, we estimate the Si atom concentration in the amplification zone as a minimum of $10^{14}/\text{cc}$ for all studies involving gain measurement. The N_2O oxidant concentration exceeds $5 \times 10^{14}/\text{cc}$ and the SiO metastable concentration exceeds $10^{13}/\text{cc}$.⁴ Based upon the Na source temperature, the measured rate of expenditure of sodium from the source exceeds $10^{18}/\text{cm}^2\text{-sec}$ in the reaction zone, which corresponds to a density of order $10^{13}/\text{cc}$.⁴ The reactant and entrainment flows must also be controlled so as to protect the cavity windows from the condensation of metastable silicon or germanium oxide and/or sodium. This latter requirement is met (Fig. 6), in part, using "self cleaning" optical windows²⁹ with a protective helium (not argon) flow. The "rate limiting" silicon concentration signals a focus on the modification of the oven source configuration depicted in Figure 6 so as to continually improve the silicon atom flux as well as the flow conditions whereby this reactant is transferred to the reaction-energy transfer-amplification zone.

The mixing zone of Fig. 6 is greatly stabilized by the moderate sized (~ 15 cubic feet) ballast separating the 150 cfm pump and reaction chamber. The 90° intersection of the SiO (GeO) and Na atom flows, once stabilized, can be used to clearly establish a continuous lasing action, however, this is, by no means, the ideal mixing configuration. We have now constructed and are attempting to test and optimize devices which allow the concentric mixing of Si, Na, and N_2O flows so as to replace the 90° intersection of the entrained SiO and Na flows.

Full Cavity Measurements - The Indication of Oscillation

Using the 90° intersecting flow configuration we replace the gain measurement system with a full mirror laser cavity in which the output coupling (1" diameter mirror) corresponds to 0.2%. We employ the same 1" diameter, 99.9% reflector as used in the gain evaluation studies, and operate the system under near optimum reactive flow conditions in a stable cavity configuration with $g_1g_2 \sim 0.82$. We find that the ratio of the output for full cavity operation to that obtained with a blocked high reflector (Figure 8) exceeds 10^3 . Compare this also to the signal level observed (Fig. 8) with the blocked high reflector and that

monitored with a completely blocked detector. This result clearly indicates continuous full cavity laser oscillation in the SiO-sodium system.

If we operate the 0.2% output coupled cavity below threshold, monitoring a dominantly fluorescent process, the ratio of full cavity to single pass output (blocked high reflector) is found to be slightly greater than 1.8 for the Na D-line ($3p^2P - 3s^2S$). This value should be compared to a maximum of 1.2 for a much more lossy 4.5% output coupled device ($g_{182} \approx 0.56$). In fact, a maximum (full cavity/blocked reflector) ratio of order 1.9-1.95 is typical for all those wavelengths considered ($\lambda = 569, 616, \text{Na D-line}$) when conditions in the reaction-amplification zone are such that no gain is monitored. We have also observed intermediate behavior associated with the establishment of moderate but not optimal gain conditions.

Improvement of the Energy Transfer Based Configuration - Ultimate Goals

The current results are exciting not only because they demonstrate lasing action in the visible region but also because they should be substantially enhanced with several improvements in the manner in which the lasing medium is created and the laser output is extracted from the cavity. It remains to increase both the rate limiting silicon and sodium atom concentrations in the reaction zone while maintaining atomization. A logical way to approach this problem involves the conversion of the intersecting flow configuration of Figure 6 to a concentric interaction configuration. We are currently testing and modifying the two designs depicted in Figs. 9(a) and (b) as a means of attaining higher reactant - amplifying medium concentrations. These two designs attempt to create a more efficient mixing of those constituents forming the amplifying medium. In both designs, the sodium source is now placed directly above the silicon source, however, the designs differ in the sequence in which they introduce the reactants. The design of Figure 9(a) first creates the SiO metastables through the Si-N₂O reaction and subsequently interacts the entrained metastables with an entrained Na flow. In the slightly modified design of Fig. 9(b) we attempt to premix concentric entrained flows of silicon and sodium, oxidizing the mixture with N₂O. The two designs depicted in Figure 9 both result in a substantial enhancement of reactant concentration and mixing as evidenced especially for the configuration of Fig. 9(b) by the significant 100 fold increase in light emission from the reaction zone as monitored through a side-angle viewing port (Fig. 6). However, they also produce a significant increase in particulate matter and gas phase condensibles for which the current pumping system does not appear to be well suited. These condensibles have the attendant affect of degrading cavity windows, substantially increasing loss elements in the optical train. With some modification of the pumping system, the realignment of entrainment flows, the modification of entrainment gases to best suit the chemistry of the system, and the adjustment of window protecting flows, these problems should be greatly alleviated.

The increase of reactant concentrations may lead to a leveling off and eventual loss of the gain condition if self-absorption on the Na D-line transitions becomes a dominant factor or SiO triplet self-quenching begins to play a deleterious role. Evidence is obtained for some self-absorption at the highest sodium concentrations when the alkali atom production dominates the concomitant SiO metastable production. With our sodium atom source operated, in the absence of interacting silicon or N₂O, at the temperatures which we have employed to produce the highest flux densities in the amplification zone, we have measured the attenuation of the Na D-line emission from a sodium discharge lamp. We find an attenuation which is much less than 50%. In combination with the cross section for self absorption, $4 \times 10^{-14} \text{ cm}^2$, as measured by Ermin et al.,³⁰ this suggests a sodium atom concentration close to that estimated previously. Of course, in the presence of N₂O and silicon reactants, the attenuation due to self absorption, while evidenced, is considerably diminished ($\sim 5 - 10\%$).

Although concern with the possible deleterious effect which a pumping of the Na D-line might have on transitions terminating in the $3p^2P$ level is somewhat alleviated in the present system by the sodium discharge experiments of Tribilov and Shukhtin,³¹ and the 0.01 second duration laser pulse for the Na $4s^2S - 3p^2P$ infrared transition observed by Mishakov and Tkachenko³² as quasicontinuous lasing, it must eventually limit the size of the laser systems. However, this might be forestalled to great degree if we take advantage of the efficient quenching of Na $3p^2P$ atoms which Tanarro et al.³³ have demonstrated for N₂ and CO. In fact, if we replace the Si-SiO and Na entraining argon or helium gases^{3,4} with N₂, we observe a pronounced effect on the energy transfer spectrum (Fig. 10) taken for an intermediate sodium flux. While the 569 nm feature is dominated by the Na D-line emission when argon is used as an entrainment gas, its intensity can be made to exceed that of the D-line when N₂ is used. This result, obtained and repeated for successive scans taken during the same experimental run, suggests the possibility for a considerable enhancement of the 569 nm output. This improvement might well result from the quenching of Na $3p^2P$, however, it might also result from an increased inhibition of the $\text{Na} + \text{N}_2\text{O} \rightarrow \text{NaO} + \text{N}_2$ reaction as the equilibrium is forced toward reactants.³⁴

There is reason to believe that the extension of this chemistry will provide further improvements in the system. It is desirable that we insure the efficient oxidation of silicon atoms by N₂O, however the subsequent reaction of N₂O, whether in excess or scattered by the flow, with those Na atoms to which we wish to transfer energy is clearly undesirable. This can be prevented in large part if these N₂O molecules are allowed to react with CO. To enhance this possibility, and with an eye to improving the quenching results depicted in Figure 10, we will soon operate our system with the simultaneous CO entrainment of sodium and the N₂ entrainment of silicon.

The experiments conducted thusfar have made use of only two distinct output coupling configurations. As well as improving reactant

concentrations, the optimum output coupling for the current cavity remains to be evaluated. Finally, we have constructed a modification which will allow removal of the cavity windows that represent significant loss elements. With these improvements, the output from our full cavity configuration should be substantially enhanced.

System Modeling

Recently, Smith et al.³⁵ have begun a laser chemistry modeling effort on the SiO-Na system. Starting with the initial concentrations of the reactants Na, Si, and N₂O which are achievable in the present system these authors have used a model which includes the 10 possible processes

1. $\text{Si} + \text{N}_2\text{O} \rightarrow \text{SiO}^* + \text{N}_2$ - metastable excited state formation.
2. $\text{Si} + \text{N}_2\text{O} \rightarrow \text{SiO} + \text{N}_2$ - ground state formation - power depleting.
3. $\text{SiO}^* + \text{Na} \rightarrow \text{SiO} + \text{Na}^* (4d^2D)$ - upper state amplifying transition.
4. $\text{SiO}^* + \text{Na} \rightarrow \text{SiO} + \text{Na}^* (3p^2P)$ - terminal level amplifying transition.
5. $\text{SiO}^* + \text{SiO}^* \rightarrow \text{SiO} + \text{SiO}$ - self quenching of SiO metastables.
6. $\text{Na}^* (4d^2D) \rightarrow \text{Na}^* (3p^2P) + h\nu (569 \text{ nm})$ - spontaneous emission.
7. $\text{Na}^* (4d^2D) + h\nu (569 \text{ nm}) \rightarrow \text{Na}^* (3p^2P) + 2h\nu (569 \text{ nm})$ stimulated emission.
8. $\text{Na}^* (3p^2P) + h\nu (569 \text{ nm}) \rightarrow \text{Na}^* (4d^2D)$ - optical pumping.
9. $\text{Na}^* (3p^2P) \rightarrow \text{Na} (3s^2S) + h\nu (589 \text{ nm})$ - spontaneous emission.
10. $h\nu (569 \text{ nm}) \rightarrow h\nu (569 \text{ nm})$ outcoupling fraction for 569 nm photons (laser cavity 5 cm in length - mirror reflectivities 99.99 and 99.80%.

Using known kinetic rates, variable initial concentrations, reasonable and variable rates for those processes which have not been directly measured, and assuming a closed reaction in which the reactants are not replenished, Smith et al.³⁵ have deduced temporal profiles for the Na concentration, 569 nm photon concentration, energy density, and power density. They conclude that order of magnitude increases in the initial concentration of Si or N₂O have a profound effect on the system (power density increase) whereas significant changes in the Na concentration have relatively little effect. This signals the rate limiting nature of the silicon concentration and the importance of the branching into the metastable triplet states. It is also to be noted that a significant increase in power density may be muted by SiO^{*} self quenching, the rate of which certainly must be established for these systems. For the diversity of initial reactant concentrations and rates used in their model, Smith et al.³⁵ predict output power densities peaking between 100 (strong SiO^{*} self quenching) and 7000 mW/cc. These results, which will soon be supplemented by a more detailed modeling effort, are quite encouraging.

Acknowledgement

It is a pleasure to acknowledge most helpful discussions with Drs. R. Jones, Bill Watt, T. Cool, Stan Patterson, Rolf Gross, Sherwin Amimoto, John

Dering, Glen Perram, and E. Dorko concerning this study. The support of the Georgia Tech Foundation through a grant from Mrs. Betty Peterman Gole, the Army Research Office through the Short Term Innovative Research Program, the Air Force Office of Scientific Research and Army Research Office and AFOSR/SDIO is greatly appreciated.

REFERENCES

1. J. R. Woodward, S. H. Cobb, K. K. Shen, and J. L. Gole, IEEE Jour. of Quant. Elect. JQE **26**, 1574 (1990). J. R. Woodward, S. H. Cobb, and J. L. Gole, Proceedings of the Fourth International Laser Science Conference, A.I.P. Conf. Proc. No. 191, Optical Science and Engineering Series 10, pg. 63.
2. J. L. Gole, J. R. Woodward, S. H. Cobb, K. K. Shen, and J. R. Doughty, SPIE Proceedings Volume 1397, Eighth International Symposium on Gas Flow and Chemical Lasers (1990), pg. 125 (and references therein). J. L. Gole, K. K. Shen, C. B. Winstead, and D. Grantier, Journal de Physique IV, Colloque C7, supplement au Journal de Physique III, Vol. 1, December 1991, pg. 609.
3. J. L. Gole, K. K. Shen, H. Wang, and D. Grantier, "Chemically Driven Pulsed and Continuous Visible Laser Amplifiers and Oscillators", Proceedings of the 23 AIAA Plasma-Dynamics and Laser Science Conference, Nashville, Tennessee, AIAA 92-2994 (1992).
4. K. K. Shen, H. Wang, and J. L. Gole, "Evidence for Continuous Visible Chemical Lasing from the Fast Near Resonant Pumping of Atomic Sodium", IEEE Journal of Quantum Electronics, in press.
5. K. K. Shen, H. Wang, D. Grantier, and J. L. Gole, "Visible Chemical Lasers From Alkali Based Electronic Inversions" Proceedings of SPIE OE^{*} LASE '93 Conference, January 16-23, 1993, Los Angeles, California, in press.
6. D. M. Lindsay and J. L. Gole, J. Chem. Phys. **66**, 3886 (1977).
7. M. J. Sayers and J. L. Gole, J. Chem. Phys. **67**, 5442 (1977).
8. J. L. Gole and R. N. Zare, J. Chem. Phys. **57**, 5331 (1972).
9. J. L. Gole and S. A. Pace, J. Chem. Phys. **73**, 836 (1980).
10. W. H. Flygare, Acc. Chem. Res. **1**, 121 (1968).
11. A. W. Hanner and J. L. Gole, J. Chem. Phys. **73**, 5025 (1980). J. L. Gole and S. A. Pace, J. Phys. Chem. **85**, 2651 (1981). J. L. Gole, B. Ohlsson, A. W. Hanner, and E. J. Greene, unpublished.
12. K. McAdam, private communication. See also A. B. F. Duncan, Rydberg Series in Atoms and Molecules, Academic Press, New York, 1971.
13. J. L. Gole, "Probing Ultrafast Energy Transfer Among the Excited States of Small High Temperature Molecules", in "Gas-Phase Chemiluminescence and Chemionization", (Elsevier Science Publishers - A. Fontijn, editor) pg. 253.
14. R. D. Levine and R. B. Bernstein, Molecular Reaction Dynamics, Oxford University Press, New York, 1974. E. J. Mansky, W. Furr, and J. L. Gole, work in progress.
15. G. J. Green and J. L. Gole, Chemical Physics **100**, 133 (1985).
16. R. W. Woodward, J. S. Hayden, and J. L. Gole,

- Chemical Physics 100, 153 (1985).
17. P. M. Swearingen, S. J. Davis, and T. M. Niemczyk, Chem. Phys. Lett. 55, 274 (1978).
 18. S. H. Cobb, M. McQuaid, and J. L. Gole, unpublished, see also references 3-6.
 19. D. Husain and P. E. Norris, J. C. S. Faraday, II, 93, 106, 335 (1978) and D. Husain and P. E. Norris, Chemical Physics Letters 51, 206 (1977).
 19. A. Gaupp, P. Kuske, and H. J. Andra, "Accurate Lifetime Measurements of the Lowest $2p_{1/2}$ States in Neutral Lithium and Sodium", Physical Review A, Vol. 26, pp. 3351-3359 (1982).
 20. Elementary Atomic Structure, by G. K. Woodgate, Clarendon Press, Oxford, 1980.
 21. C. E. Moore, "Atomic Energy Levels", N. B. S. Circular 467, Volumes I, II, and III. See also, R. W. F. Gross and J. P. Bott, Handbook of Chemical Lasers, Wiley and Sons, New York, 1976.
 22. For the Na $4d^2D$ level, S. A. Kandela, Appl. Optics 23, 2151 (1984).
 23. For the Na $5s^2S$ level, X. He, B. Li, A. Chen, and C. Zhang, J. Phys. B., At. Molec. and Opt. Phys. 23, 661 (1990).
 24. A. Gallagher and A. Lurio, Phys. Rev. 136, A87 (1964).
 25. G. R. Fowles and W. T. Silvest, Appl. Phys. Lett. 6, 236 (1965).
 26. A. A. Isaev and G. G. Petrash, JETP Lett. 10, 119-21 (1969).
 27. G. Roll and J. Mentel, J. Phys. D. Appl. Phys. 22, 483-487 (1989).
 28. The Na $4d^2D_{5/2} - 3p^2P_{3/2}$ transition should represent the most favorable to achieve gain and oscillation. The $4d^2D_{5/2}$ level emits dominantly to $3p^2P_{3/2}$ whereas the $4d^2D_{3/2}$ level depletes its population to both the $3p^2P_{1/2}$ and $3p^2P_{3/2}$ levels. Consideration of collisional relaxation among the $3p^2P$ levels would also suggest that the collisionally depleted $3p^2P_{3/2}$ level is favored as the lower laser level.
 29. "Self-Flushing Optical Window to Prevent Collection of Condensates", W. H. Crumley, and J. L. Gole, Rev. Sci. Instruments 57, 1692 (1986).
 30. A. V. Eremin, I. M. Naboko, and S. A. Palopezhentsev, Opt. Spectrosc. (USSR) 60, 567 (1986).
 31. A. S. Tribilov and A. M. Shukhtin, Opt. Spectrosc. 21, 69 (1966). See also, K. Krokkel, M. Hube, W. Luhs and B. Wellegehausen, Appl. Phys. B37, 137-140 (1985).
 32. (a) V. G. Mishakov and T. L. Tkachenko, Opt. Spectrosc. (USSR) 64(3), 293 (1988). (b) V. V. Kuchinskii, V. G. Mishakov, A. S. Tibilov, and A. M. Shukhtin, Opt. Spektrosk. 39, 1043 (1975) [Opt. Spectrosc. (USSR) 39, 598 (1975)]. (c) A. A. Kudryavsev, V. N. Skrebov, and T. L. Tkachenko, Opt. Spectrosc. 58, 694 (1985) [Opt. Spectrosc. (USSR) 58, 420 (1985)]. (d) V. G. Mishakov, A. S. Tibilov, and A. M. Shukhtin, Opt. Spectrosc. 31, 324 (1971) [Opt. Spectrosc. (USSR) 31, 176 (1971)]. (e) N. N. Bezuglov and A. B. Tsyganov, Opt. Spectrosc. 59, 195 (1985) [Opt. Spectrosc. (USSR) 59, 115 (1985)].
 33. I. Tanarro, F. Arqueros, and J. Campos, J. Chem. Phys. 77, 1826 (1982).
 34. J. W. Ager III, C. L. Talcott, and C. J. Howard, J. Chem. Phys. 85, 5584 (1986).
 35. J. R. Woodward, J. S. Hayden, and J. L. Gole, Chemical Physics 134, 395 (1989).
 35. Chemical Laser Experiments and Analysis, Directed Energy Devices Technology Support Delivery Order No. 0015 prepared by W. Smith, S. Taylor, J. Dansereau, J. Long, and W. Warren for U. S. Army Missile Command, Directed Energy Directorate, Redstone Arsenal, Alabama 35898.

Table I

Near Resonances of SiO^* ($a^3\Sigma^+$, $b^3\Pi-X^1\Sigma^+$) and Select Na and K Atomic Transitions in Energy Transfer Laser Pumping^a

Atom	Upper Atomic Level	$\text{SiO}(v',v'')$			
		a-X Trans. $\Delta E(\text{cm}^{-1})^b$		b-X Trans. $\Delta E(\text{cm}^{-1})^b$	
Na	$4d^2D_{5/2,3/2}$	--	--	(1,0) (2,1) (3,2)	294 45 -209
Na	$5s^2S_{1/2}$	(0,0)	200	(2,2) (3,3)	177 67
Na	$3d^2D_{5/2,3/2}$	(1,4)	180	(0,4)	-184
Na	$6s^2S_{1/2}$	(4,0)	155	(4,1)	137
Na	$4s^2S_{1/2}$	No near resonances			
K	$4d^2D_{5/2,3/2}$	(0,5)	-25	(2,7)	60
K	$5d^2D_{5/2,3/2}$	(0,3)	-420	(0,3)	20
K	$6s^2S_{1/2}$	(0,5)	-70	--	--
K	$6d^2D_{5/2,3/2}$	--	--	(0,2) (4,5) (3,4)	-286 40 264
K	$7s^2S_{1/2}$	--	--	(0,3)	-69

a. Listed potential resonances are meant to be indicative but not exhaustive.

b. Δ Molecular level energy - Atom level energy. Positive quantities denote exothermic energy transfer.

Table II

Near Resonances of GeO^* ($a^3\Sigma^+$, $b^3\Pi-X^1\Sigma^+$) and Select Na and K Atomic Transitions in Energy Transfer Laser Pumping^a

Atom	Upper Atomic Level	$\text{GeO}(v',v'')$			
		a-X Trans. $\Delta E(\text{cm}^{-1})^b$		b-X Trans. $\Delta E(\text{cm}^{-1})^b$	
Na	$3d^2D_{5/2,3/2}$	(2,0) (3,0)	-367 250	(0,3)	-73
Na	$4s^2S_{1/2}$	(0,2)	130	--	--
Na	$6s^2S_{1/2}$	--	--	(6,0)	-180
Na	$5s^2S_{1/2}$	--	--	(2,0)	245
Na	$4d^2D_{5/2,3/2}$	--	--	(3,0) (4,0)	-401 293
K	$4d^2D_{5/2,3/2}$	(0,0) (1,1)	160 -195	--	--
K	$5d^2D_{5/2,3/2}$	(4,0)	-149	(0,2)	-123
K	$6s^2S_{1/2}$	(0,0)	110	--	--
K	$6d^2D_{5/2,3/2}$	--	--	(2,2)	-185
K	$7s^2S_{1/2}$	(4,0)	-240	(0,2)	-110

a. Listed potential resonances are meant to be indicative but not exhaustive.

b. Δ Molecular level energy - Atom level energy. Positive quantities denote exothermic energy transfer.

Table III

Near Resonances of SiO^* ($a^3\Sigma^+, b^3\Pi-X^1\Sigma^+$) and Select Pb Atomic Transitions in Energy Transfer Laser Pumping.

Atom	Upper Atomic Level	$\text{SiO}(v', v'')$			
		$a-X$		$b-X$	
		Trans. $\Delta E(\text{cm}^{-1})^a$		Trans. $\Delta E(\text{cm}^{-1})^a$	
Pb	$6p^2 \ ^1D$	(0,10)	192	---	---
Pb	$6p^2 \ ^1S$	(0,3)	282	---	---
		(1,4)	-42		
		(2,5)	-436		
Pb	$6p7s \ ^3P_0$	(2,0)	24	(1,0)	-117
				(2,1)	366
Pb	$6p7s \ ^3P_1$	(3,0)	474	(2,0)	529
				(3,1)	269
				(4,2)	6
				(5,3)	-260

a. \sim Molecular level energy - Atomic level energy. Positive quantities denote exothermic energy transfer.

Table IV

Near Resonances of GeO^* ($a^3\Sigma^+, b^3\Pi-X^1\Sigma^+$) and Select Pb Atomic Transitions in Energy Transfer Laser Pumping.

Atom	Upper Atomic Level	$\text{GeO}(v', v'')$			
		$a-X$		$b-X$	
		Trans. $\Delta E(\text{cm}^{-1})^a$		Trans. $\Delta E(\text{cm}^{-1})^a$	
Pb	$6p^2 \ ^1D$	(0,6)	366	---	---
		(1,7)	69		
		(2,8)	-225		
Pb	$6p^2 \ ^1S$	(3,0)	-43	(2,4)	122
				(3,5)	-117
Pb	$6p7s \ ^3P_0$	---	---	(4,0)	-120
				(5,1)	415
Pb	$6p7s \ ^3P_1$	---	---	(5,0)	235
				(6,1)	-70

a. \sim Molecular level energy - Atomic level energy. Positive quantities denote exothermic energy transfer.

Table V

Near Resonances of SiO^* , GeO^* ($a^3\Sigma^+$, $b^3\Pi \rightarrow X^1\Sigma^+$) and Select Cu Atomic Transitions in Energy Transfer Laser Pumping

Atom	MO*	Upper Atomic Level	MO*(v',v'')			
			a-X		b-X	
			Trans.	E(cm ⁻¹) ^a	Trans.	E(cm ⁻¹) ^a
Cu	GeO	$4p^2P_{3/2}$	--	--	(0,1)	247
					(1,2)	3
					(2,3)	-233
Cu	GeO	$4p^2P_{1/2}$	--	--	(1,2)	251
					(2,3)	15
					(3,4)	-243
Cu	SiO	$4p^2P_{3/2}$	(0,2)	171	(2,4)	198
					(3,5)	-15
					(4,6)	-229
Cu	SiO	$4p^2P_{1/2}$	--	--	(2,4)	446
					(3,5)	233
					(4,6)	19
					(5,7)	-202

a. Molecular level energy - Atom level energy. Positive quantities denote exothermic energy transfer.

Table VI

Near Resonances of SiO^* , GeO^* ($a^3\Sigma^+$, $b^3\Pi \rightarrow X^1\Sigma^+$) and Select Sn Atomic Transitions in Energy Transfer Laser Pumping.

Atom	MO*	Upper Atomic Level	MO*(v',v'')			
			a-X		b-X	
			Trans.	$\Delta E(\text{cm}^{-1})^a$	Trans.	$\Delta E(\text{cm}^{-1})^a$
Sn	SiO	$6s5p^3P_0$	(2,0)	343	(1,0)	202
					(2,1)	-47
					(3,2)	295
Sn	GeO	$6s5p^3P_0$	---	---	(4,0)	199
					(5,1)	-96
Sn	SiO	$6s5p^3P_1$	(2,0)	70	(1,0)	-71
					(2,1)	320
Sn	GeO	$6s5p^3P_1$	---	---	(4,0)	-74
					(5,1)	369

No near resonances of SiO, GeO metastables with Sn 1D_2 @ 8613.0 and Sn 1S_0 @ 17162.6 cm⁻¹

a. Molecular level energy - Atomic level energy. Positive quantities denote exothermic energy transfer.

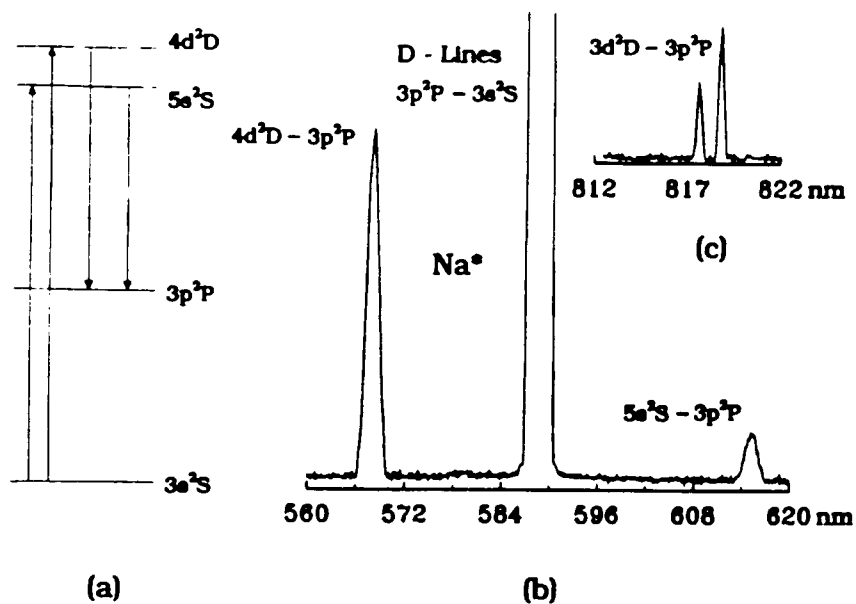


Figure 1(a): Na atom energy level scheme and pumping cycles to produce $4d^2D$ and $5s^2S$ excited states.
 Figure 1(b): Typical energy transfer pumping spectrum for Na $4d^2D - 3p^2P$ and $5s^2S - 3p^2P$ transitions and $3p^2P - 3p^2S$ sodium D-line emission. The D-line emission results both from direct energy transfer pumping from ground state NaO and from subsequent fluorescence following emission to the $3p^2P$ level.
 Figure 1(c): Energy transfer pumping spectrum corresponding to Na $3d^2D - 3p^2P$ transition.

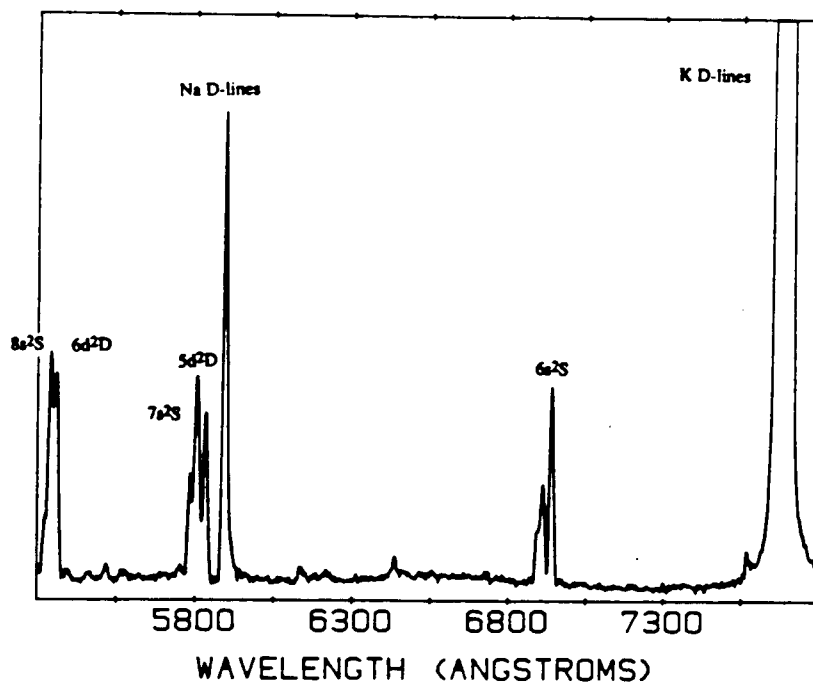


Figure 2: Potassium - SiO ($a^3\Sigma^+$, $b^3\Pi$) near resonant energy transfer spectrum showing the potassium D lines, and atomic emissions corresponding to the $6s-4p$, $5d-4p$, $7s-4p$, $6d-4p$ and $8s-4p$ transitions.

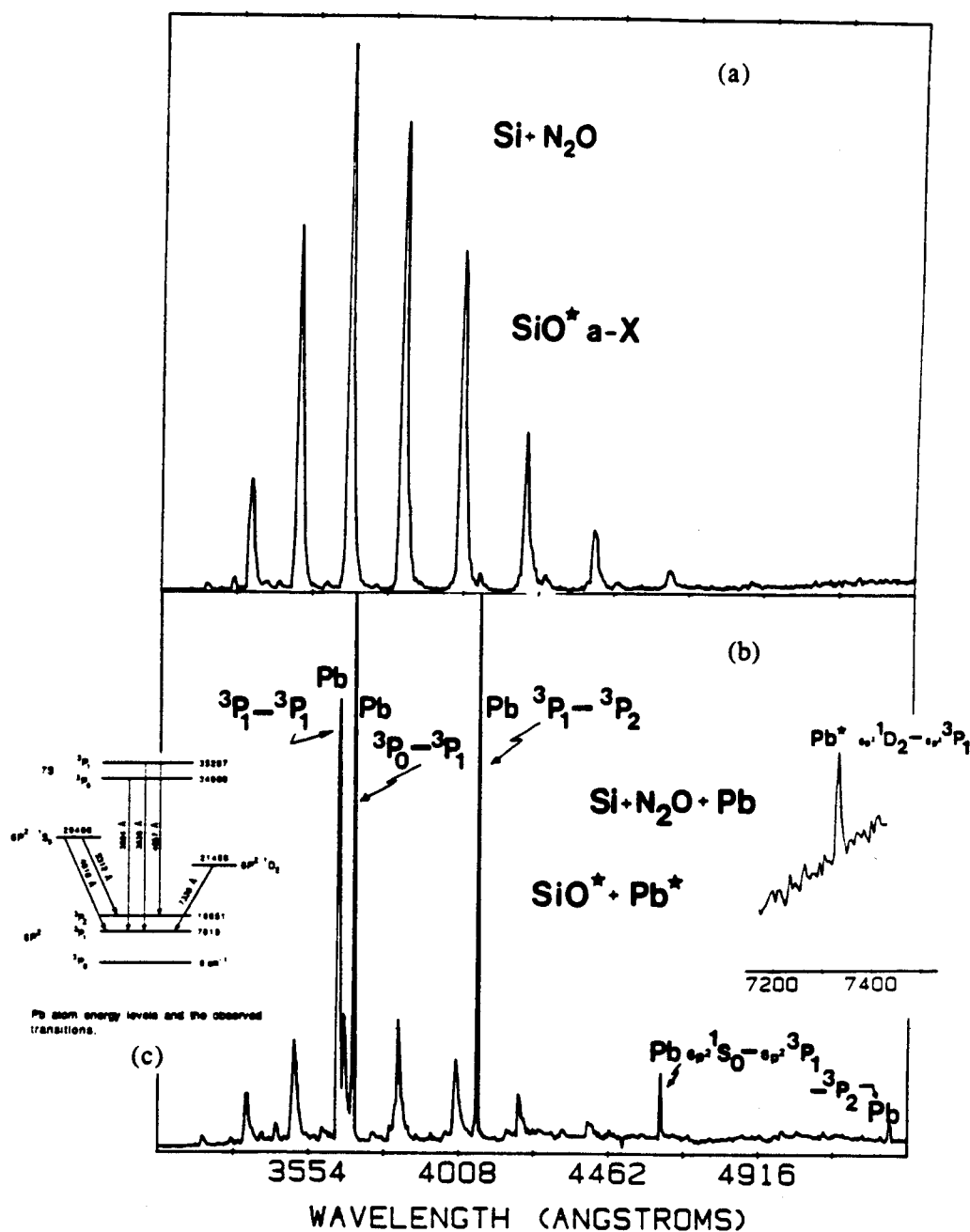


Figure 3: Comparison of lead - SiO ($\text{a}^3\Sigma^+$, $\text{b}^3\Pi$) near resonant energy transfer spectra. Metastable SiO molecules were created in the reaction $\text{Si} + \text{N}_2\text{O} \rightarrow \text{SiO}^* + \text{N}_2$. (a) The spectrum corresponds to a portion of the SiO metastable emission spectrum before lead atoms are brought into the reaction zone. (b) Spectrum recorded with high Pb Flux (~ 1 torr vapor pressure) showing the manifestation of energy transfer pumping to produce electronically excited $^3\text{P}_0$, $^3\text{P}_1$, $^1\text{S}_0$, and $^1\text{D}_2$ levels of the lead atom. (c) Energy levels for the lead atom with observed transitions as indicated in (b). See text for discussion.

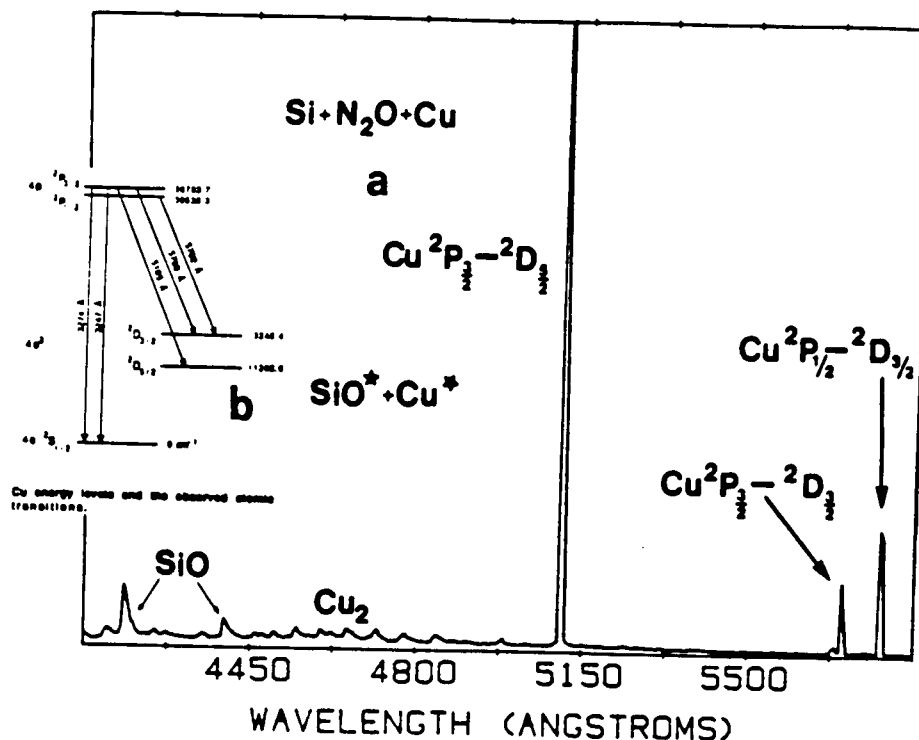


Figure 4: Copper - SiO ($a^3\Pi^+$, $b^3\Pi$) near resonant energy transfer spectra generated from a "premixed" Si-Cu mixture subsequently oxidized with N₂O. (a) Spectrum showing a portion of the SiO metastable emission, the Cu $^2P_{3/2}-^2D_{5/2}$ blue green emission line (copper vapor laser) and the Cu $^2P_{3/2}, 1/2-^2D_{3/2}$ yellow-orange emission features. (b) Energy levels for the copper atom with observed transitions as indicated in (a). See text for discussion.

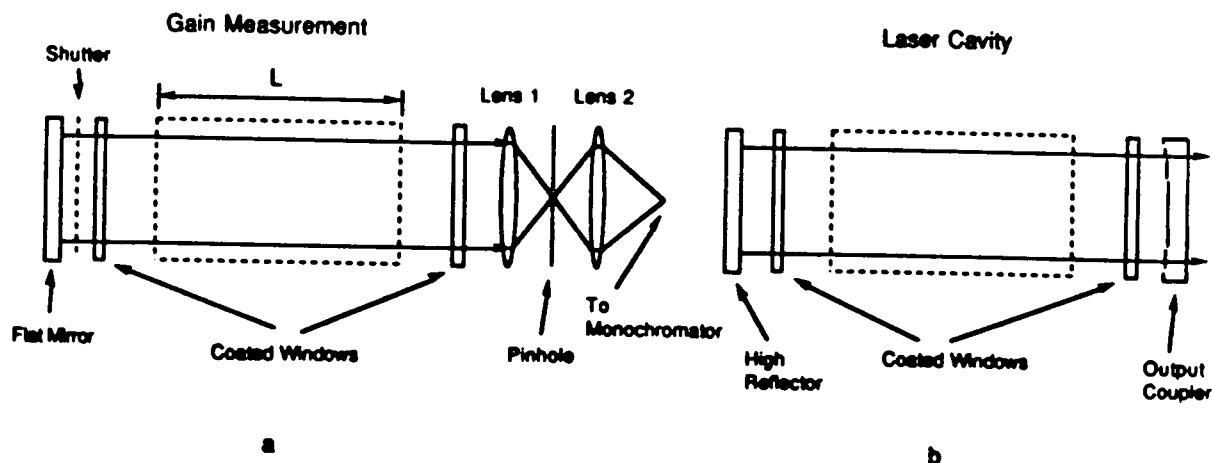


Figure 5(a): Gain measurement configuration after Roll and Mantel (ref. 27). The region marked L in the figure corresponds to the reaction - amplification zone.

Figure 5(b): Laser cavity configuration to characterize potential oscillation in the Si-SiO-Na system at 569 nm.

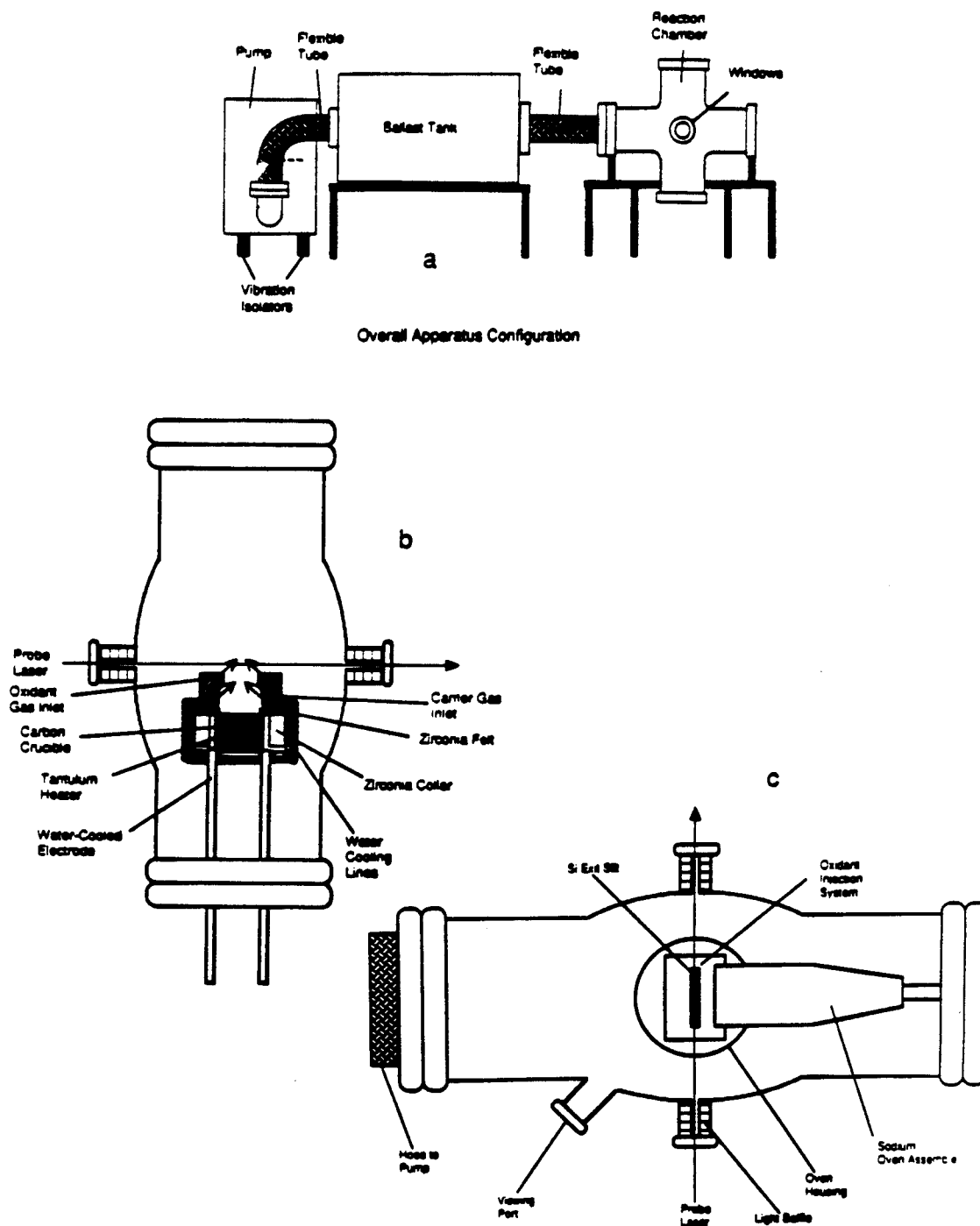


Figure 6: (a) Schematic of reaction chamber and windows defining optical train, ballast tank to moderate pumping fluctuations, and pumping configuration, for extended path length Si-SiO (Si-N₂O)-Na reaction amplification zone. (b),(c) Side and overhead views of reaction chamber showing positioning of Si oven source, relative locations of Si and Na oven sources, oxidant injection system, and relative positions of these devices with respect to the optical train.

Sodium Atomic Emissions
SiO-Na Energy Transfer

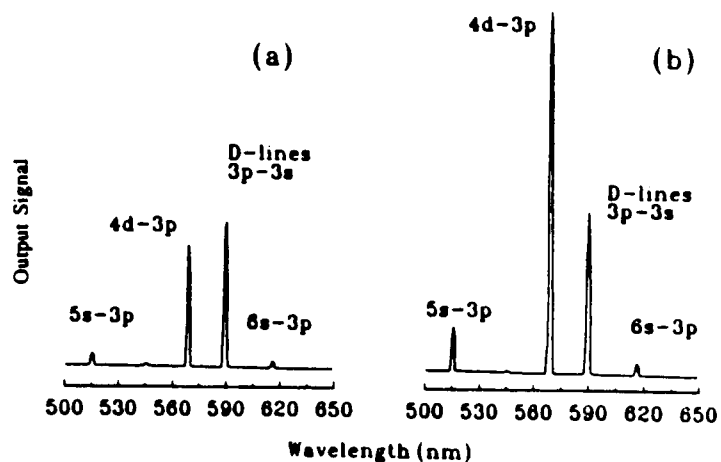


Figure 7(a): Single pass continuous amplified spontaneous emission (ASE) intensity (I_1) measured using a Spex 1 meter spectrometer and RCA 4840 phototube and the gain configuration depicted in Figure 3(a) for the Si-SiO-Na system. Spectral resolution is 1 nm. Because the figure is uncorrected for photo-tube response, decreasing from 510 to 630 nm, or grating blaze (500 nm), the emission associated with the $6s^2S - 3p^2P$ transition appears more intense than that associated with the $5s^2S - 3p^2P$ transition.

Figure 7(b): Double pass continuous amplified spontaneous emission (ASE) intensity (I_2) measured using the gain configuration depicted in Fig. 3(a) for the Si-SiO-Na system. The Na D-line intensity is comparable to that in Fig. 5(a). The ratio of the I_2/I_1 intensity for the 569 nm Na emission feature is 2.6/1 for this individual study and can approach 3.8/1 under optimal conditions for the system. Spectral resolution is ~ 1 nm (see (a)).

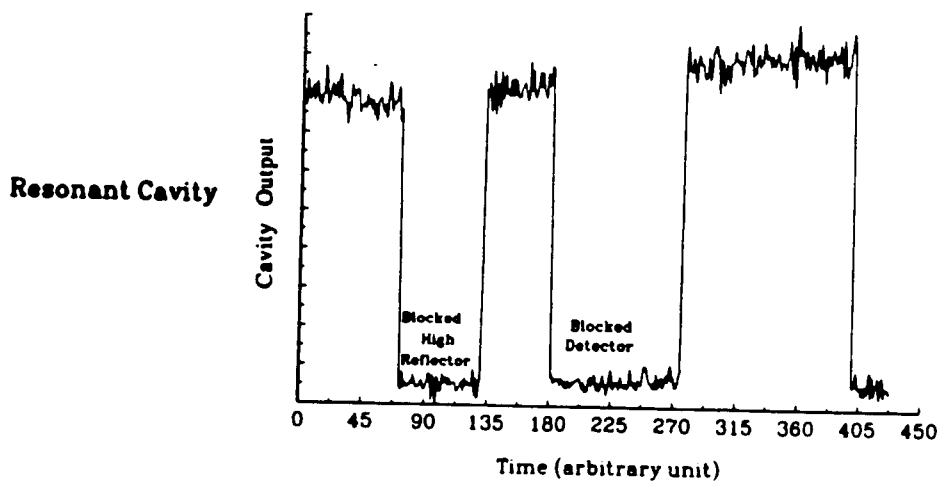


Figure 8: Full cavity output created with $\sim 0.2\%$ output coupling for the continuous Si-SiO(Si-N₂O)-Na amplifier at $\lambda = 569$ nm. These measurements were taken in continuous flow with the cavity configuration depicted in Fig. 6(b). The full cavity output is compared to the obtained with both a blocked high reflector and with the entire cavity isolated from the signal detection system. The ratio of the output obtained for the full cavity to that obtained with a blocked high reflector exceeds $10^3/1$.

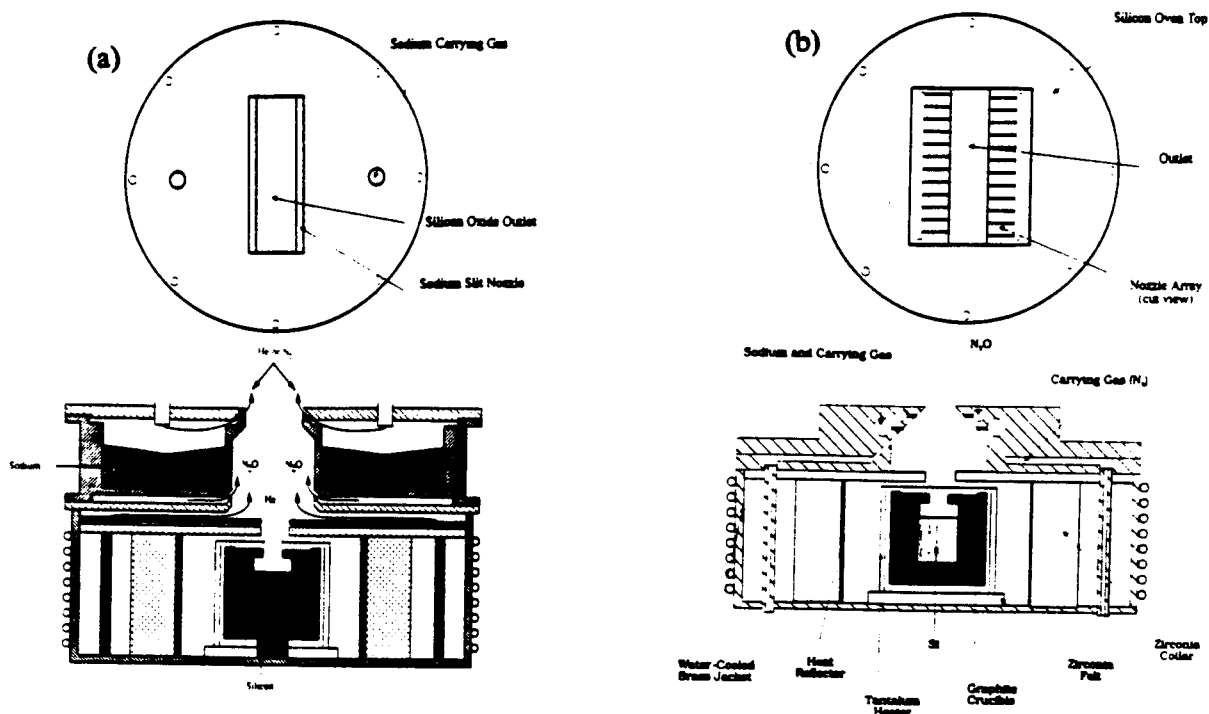


Figure 9(a): Concentric configuration for energy transfer pumping. The sodium oven is placed above the silicon oven. The oxidant N_2O is introduced into the silicon flow to form SiO^* which then interacts with sodium vapor. The energy transfer zone is approximately 1" above the silicon oven.

Figure 9(b): Concentric configuration for energy transfer pumping with a sodium and N_2O injector nozzle array placed above the silicon oven. In this configuration the sodium and silicon are mixed before the oxidant is introduced to initiate the energy transfer process.

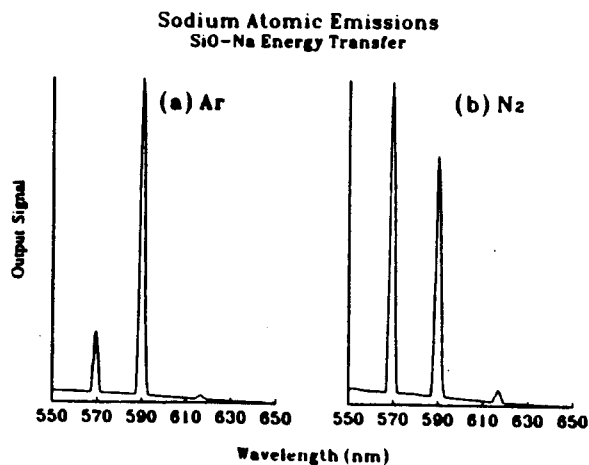


Figure 10: Energy transfer pumping spectra obtained for (a) Ar and (b) N_2 entrainment. The observed Na $4d^2D-3p^2P$ emission feature ($\sim 569\text{nm}$) is seen to increase precipitously in intensity relative to the Na $3p^2P-3s^2S$ D-line ($\sim 590\text{nm}$) with change of entrainment gas from argon to N_2 . See also Fig. 1.

APPENDIX XII

"Laser Induced Fluorescence and Radiative Lifetimes of the Low-Lying Electronic States of Gaseous AgF", H. Wang, and J. L. Gole, J. Mol. Spectros. 161, 28 (1993).

Laser induced fluorescence and radiative lifetimes of the low-lying electronic states of gaseous AgF

He Wang and James L. Gole

School of Physics, Georgia Institute of Technology, Atlanta, Georgia 30332

(Received 10 February 1993; accepted 12 March 1993)

At the fringes of the visible region, two low-lying $1 (\Omega=1)$ electronic states $A'\Omega 1$ and $a\Omega 1$ of gaseous AgF located $\sim 4300 \text{ cm}^{-1}$ below the previously known lowest excited $A0^+$ state have been excited for the first time in a silver vapor-fluorine reaction system. The $A'\Omega 1-X^1\Sigma^+$ and $a\Omega 1-X^1\Sigma^+$ band systems (also observed in chemiluminescence) have been excited and studied using pulsed laser induced fluorescence spectroscopy. The band system associated with the $A'\Omega 1-X^1\Sigma^+$ transition has been rotationally analyzed. The UV fluorescence of the $A0^+$ and $B0^+-X^1\Sigma^+$ transitions has also been excited. The radiative lifetimes of these four low-lying electronic states have been measured as $7.1 \mu\text{s}$ ($A'\Omega 1$), $9.1 \mu\text{s}$ ($a\Omega 1$), 240 ns ($A0^+$), and 21 ns ($B0^+$), respectively, revealing that the two $\Omega=1$ states are of triplet character, while the two 0^+ states are of singlet character. The observed low-lying states of AgF appear to dissociate adiabatically to neutral atoms in contrast to the apparent dissociation of the low-lying electronic states in CuF to ion pairs. The observation of the low-lying 1 states of AgF also indicates the existence of similar stable 1 states for the remaining silver halides, all of which should absorb visible photons. Major molecular constants of the newly observed $A'\Omega 1$ state of ^{107}AgF are $T_e=24\,950.71(10) \text{ cm}^{-1}$, $\Delta G_{1/2}=506.74(8) \text{ cm}^{-1}$, $B_e=0.281\,32(15) \text{ cm}^{-1}$, $D_e=0.116(60) \times 10^{-6} \text{ cm}^{-1}$, and $r_e=1.927 \text{ \AA}$.

I. INTRODUCTION

In contrast to atomic oxidation via $A+BC$ reactive encounters, the internal mode structure and dynamics associated with the kinetically controlled highly exothermic oxidation of metal molecules is largely unaddressed. However, the limited information which is available demonstrates that these metal molecules can undergo a unique and sometimes unexpected reactive branching.¹⁻³ The study of this reactive branching can provide information useful for the development of extrapolations from simple $A+BC$ reactions as well as detailed maps of the quantum level structure of product metal based oxides and halides formed in reaction.⁴⁻⁶

Recently, Devore *et al.*⁶ have begun a study of the silver molecule (Ag_x , $x \geq 2$)–ozone reactions, correlating the observed emission from these reactive encounters with AgO , Ag_2 , and Ag_xO ($x \geq 2$) excited state product formation. Here, we report an experimental study of the silver vapor–fluorine reaction system. We have obtained the first evidence for two stable $1 (\Omega=1)$ states of the gaseous silver monohalide AgF, which lie $\sim 4300 \text{ cm}^{-1}$ below the previously known lowest excited $A0^+$ state. The band systems associated with the $A'\Omega 1-X^1\Sigma^+$ (Ref. 7), $a\Omega 1-X^1\Sigma^+$, $A0^+-X^1\Sigma^+$, and $B0^+-X^1\Sigma^+$ transitions have been studied using a combination of chemiluminescence and pulsed laser induced fluorescence spectroscopy following fluoride formation from the four center $\text{Ag}_2\text{--F}_2$ reaction.

The silver halide molecules AgX ($X=\text{F}, \text{Cl}, \text{Br}$, and I) are potentially important in the photographic process.⁸ Their spectroscopic study has had a long albeit limited history.⁹⁻¹⁴ The halide ground states are highly ionic with AgCl and AgBr , respectively, of 52% (Ref. 15) and 47%

(Ref. 16) ionic character and the AgF ground state dipole moment being 6.22 D .¹⁷ The heavy halides follow primarily Hund's case (c) coupling. If we assume a covalent model, the ground state of AgF dissociates to $\text{Ag}^2S_{1/2} + \text{F}^2P_{3/2}$ ground state atoms whose combination generates five molecular states 0^+ , 0^- , 1 , 1 , and 2 . At slightly higher energy, the $\text{Ag}^2S_{1/2} + \text{F}^2P_{1/2}$ atoms can combine to yield 0^+ , 0^- , and 1 states. The ground state of AgF, identified with $^1\Sigma^+$ symmetry, has been well studied by Barrow and Clements^{18,19} using UV absorption and by Hoeft *et al.*¹⁷ using microwave spectroscopy. The absorption spectrum of AgF reported by Barrow and Clements in Ref. 19 consists of a continuum transition at about 303.0 nm and two band systems originating from the $A0^+$ ($T_e=29\,220 \text{ cm}^{-1}$) and the $B0^+$ ($T_e=31\,663 \text{ cm}^{-1}$) states, with the former dissociating to the $\text{Ag}^2S_{1/2} + \text{F}^2P_{1/2}$ atomic limit and the latter to the higher atomic dissociation products $\text{Ag}^2P_{1/2} + \text{F}^2P_{3/2}$. Predissociation has also been observed in high J rotational levels for both the $A0^+$ and $B0^+$ states. However, no transitions in the visible region or stable electronic states with $\Omega=1$ symmetry have been reported previously for any of the silver halides.

Furthermore, striking differences have been found between the observed spectra of AgF (Refs. 18 and 19) and CuF (Ref. 20) even though Cu and Ag have similar electron configurations as a result of their positions in the periodic table. All five observed low-lying electronic states of CuF are located between $14\,500$ and $22\,800 \text{ cm}^{-1}$, at much lower energy than the $A0^+$ state of AgF. The lowest CuF electronic state identified is of $^3\Sigma^+$ symmetry (with components $\Omega=0^-$ and 1). The radiative lifetimes of the CuF states have been found experimentally to be fairly long, of the order of one to several microseconds^{21,22} even for the reported singlet–singlet transitions. This behavior has been

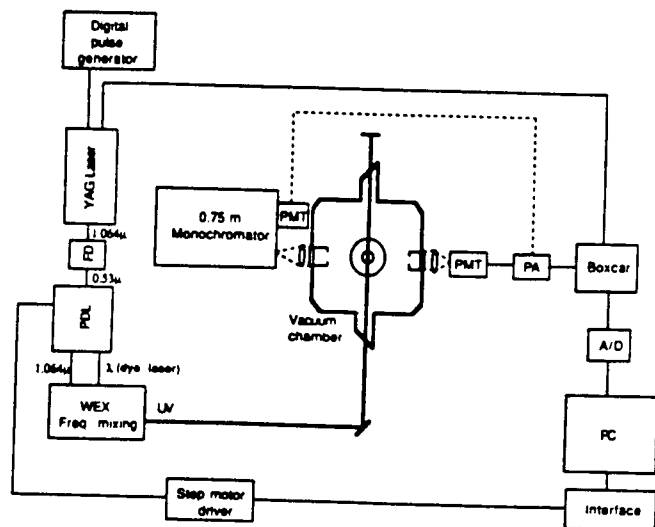


FIG. 1. Experimental setup for chemiluminescence and laser induced fluorescence spectroscopy.

explained with *ab initio* calculations²³⁻²⁵ within a framework in which all observed bands of CuF are assigned to transitions between the excited $\text{Cu}^+(3d^9 4s)F^-(2p^6)$ structure and the closed-shell $\text{Cu}^+(3d^{10})F^-(2p^6)X^1\Sigma^+$ ground state ion pair. These transitions correspond to forbidden $3d-4s$ electron transfers in the Cu^+ atomic limit.

It seems apparent that the observation of additional low-lying electronic states in AgF and the measurement of the radiative lifetimes for several of the low-lying states of the AgF molecule can provide key information which can be used to better understand differences and correlations in both the spectral and electronic properties of CuF and AgF. These lifetime measurements are also important as they characterize predissociations. In obtaining the first evidence for two stable $\Omega=1$ states of AgF, we have rotationally analyzed the $A'\Omega 1-X^1\Sigma^+$ transition.⁷ The radiative lifetimes of the four observed low-lying electronic states of AgF have also been measured. The spin characters and the dissociation limits of these low-lying states are discussed. The internal energy distribution of the reaction product AgF molecules and the possible reaction paths to produce excited and ground state AgF are also considered. Our spectroscopic analysis of the $A'\Omega 1-X^1\Sigma^+$ transition is presented in detail elsewhere.⁷

II. EXPERIMENT

AgF molecules were generated in reactive encounters under multiple collision conditions as a helium entrained silver flow was intersected by molecular fluorine. The overall experimental configuration is depicted schematically in Fig. 1. The entrainment flow device used in this study has been described in detail previously.² Briefly, silver metal was heated in a graphite crucible to temperatures in the range close to 1600 K. The silver flux emanating from the crucible was entrained in a flow of helium gas at a total pressure of 1 Torr. The fluorine gas was introduced into the entrained silver flow through a concentric ring inlet located ~ 1 cm above the crucible. A chemiluminescence

flame was generated in the reaction zone which could be dispersed by a 0.75 m Spex 1702 monochromator, operated in first order with a 1200 groove/mm grating blazed at 500 nm, and positioned at right angles to the reactant flow signals being detected with an RCA 1P28 photomultiplier. The photomultiplier (PMT) signal was fed to a Keithley 417 autoscale picoammeter and recorded with a personal computer.

In order to carry out the laser-induced fluorescence (LIF) experiments, the second harmonic of a Quanta-ray Nd:YAG laser (0.53μ) was used to pump a Spectra-Physics PDL-3 pulsed tunable dye laser system operated with DCM or LD698 dye. The output of the pulsed dye laser (with a linewidth of 0.07 cm^{-1} and a pulsewidth of 9 ns) was then either mixed with the fundamental output of the YAG laser or frequency doubled in a frequency mixer (Quanta-Ray WEX-1) to produce the UV (in the range 310–410 nm) coherent radiation which was introduced to the reaction chamber in a direction perpendicular to both the reactant flow and detector. The YAG laser was triggered by a digital pulse generator (SRS DG535) with a repetition rate of 15 Hz. The Q-switching signal of the YAG oscillator was used to trigger a boxcar integrator (SRS SR250) for better synchronization. The fluorescence induced by the UV laser pulse was collected with a RCA 1P28 photomultiplier (2.2 ns rise time) and, through a fast preamplifier (CLC 100 Video Amplifier, 500 MHz), sent to the gated integrator to record the spectrum as a function of the laser frequency. A fast digital oscilloscope (HP 54111D, 0.7 ns rise time) was used to real time monitor and record the fluorescence decay. The integration gate was set to a proper width in the range from 20 to 300 ns dictated by the nature of the monitored fluorescence decay with a delay timed such that the gate opens just after the short laser scattering pulse, thus reducing background noise. A personal computer drives the dye laser stepper motor, scanning the dye laser frequency and acquiring the averaged output data from the boxcar synchronously. In order to achieve a linear scan in wavelength when the dye laser frequency was mixed with the infrared, the scan step size of the dye laser was calculated in real time using the PC. The output frequency of the WEX-1 was calibrated using aluminum atom lines.⁷

III. SPECTROSCOPY AND RADIATIVE LIFETIMES

An overview of the chemiluminescent emission from the silver vapor-fluorine molecule reaction is depicted in Fig. 2(a). The peak at 342 nm is readily identified as the $(v',v'')=(0,0)$ band of the $A'\Omega 1-X^1\Sigma^+$ transition of AgF. However, the spectrum is dominated by intense vibrationally resolved structure due to the $A'\Omega 1-X^1\Sigma^+$ band system observed for the first time as a result of the silver molecule-molecular fluorine reaction. Figures 2(b) and 2(c) display two detailed views of the regions near 400 and 409 nm and reveal two of the weaker features associated with a second system which we label and correlate with an $a\Omega 1-X^1\Sigma^+$ transition. As Fig. 3(a) demonstrates, both the $A'\Omega 1-X^1\Sigma^+$ and $a\Omega 1-X^1\Sigma^+$ band systems can be excited with the output from a pulsed dye laser scanning

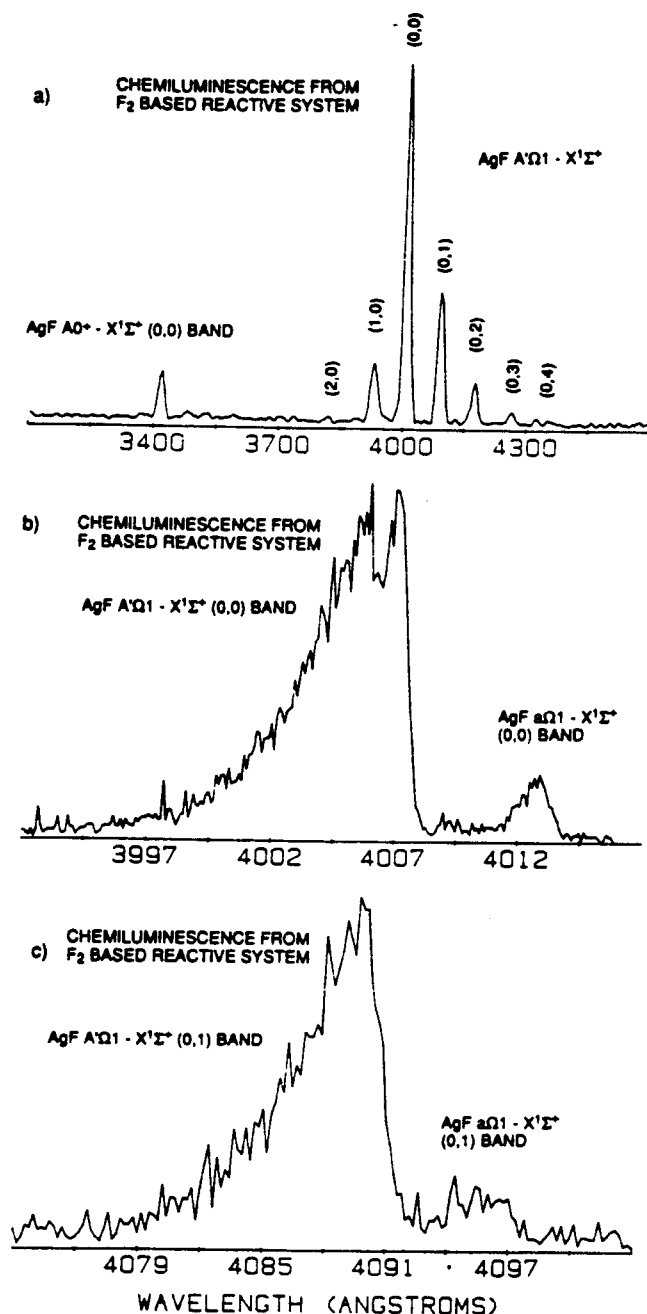


FIG. 2. (a) Overview chemiluminescence spectrum for the reaction $\text{Ag}_2 + \text{F}_2 \rightarrow \text{AgF}^* + \text{AgF}$ at a resolution of 5 Å. (b) Chemiluminescence spectrum for the reaction $\text{Ag}_2 + \text{F}_2 \rightarrow \text{AgF}^* + \text{AgF}$ in the region near 400 nm at a resolution of 0.1 Å. (c) Chemiluminescence spectrum for the reaction $\text{Ag}_2 + \text{F}_2 \rightarrow \text{AgF}^* + \text{AgF}$ in the region near 409 nm at a resolution of 0.1 Å.

through the region about 400 nm. Figure 3(b) depicts a simulation for the (0,0) band of the $A'-X$ system. Both the CL and LIF signals associated with the structure in Figs. 2 and 3 correlate with the Ag vapor concentration and fluorine gas pressure. These measured band separations agree well, within experimental error, with the known vibrational separations for the ground $X^1\Sigma^+$ state of ^{107}AgF given by Barrow and Clements.¹⁹ Based on this comparison, one can tentatively attribute the observed structure to a transition of the AgF molecule originating from a newly

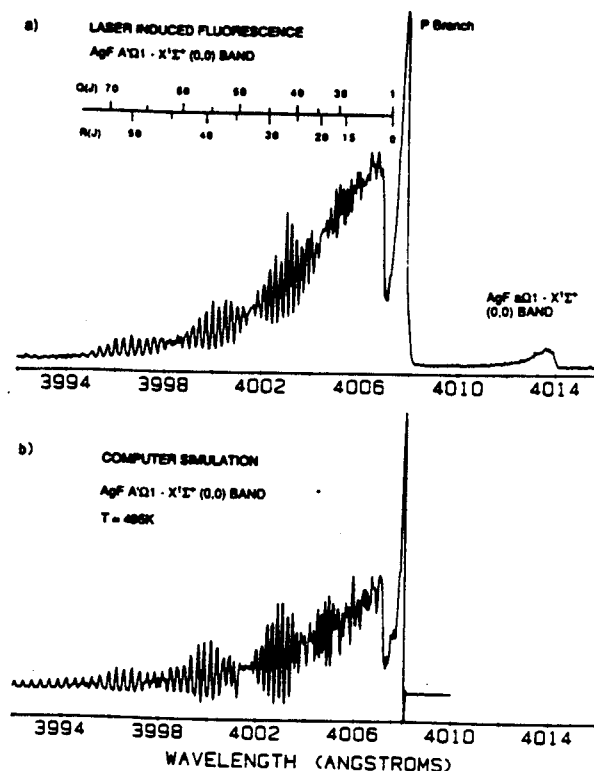


FIG. 3. (a) Pulsed laser induced fluorescence spectrum of the $A'\Omega_1-X^1\Sigma^+$ (0,0) band of AgF. The intensity anomalies are due to the superpositions of the R branch and the Q branch peaks. (b) Computer simulation of the $A'\Omega_1-X^1\Sigma^+$ (0,0) band of AgF.

observed A' electronic state. Using LIF, we identify this electronically excited state as an $\Omega=1$ state. The vibrational assignment, as listed in Table I and shown in Fig. 2(a), can be readily obtained and further confirmed with dispersed laser induced fluorescence.

A. Rotational analysis of the $A'\Omega_1-X^1\Sigma^+$ band system

Figure 3(a) corresponds to the rotationally resolved LIF spectrum for the $(v',v'')=(0,0)$ band of the $A'\Omega_1-X^1\Sigma^+$ band system which we computer simulate in Fig. 3(b). These features are considered in more detail elsewhere.⁷ The LIF spectrum corresponding to the (v',v'')

TABLE I. Measured vibrational separations of the ground $X^1\Sigma^+$ state of AgF observed by chemiluminescence and laser induced fluorescence. Also listed are the experimental data obtained by Barrow *et al.* in Ref. 19 (for ^{107}AgF).

v	ΔG (Ref. 19) (cm^{-1})	ΔG (Observed by CL) (cm^{-1})	ΔG (Observed by LIF) (cm^{-1})
0	508.26 ± 0.04	509.6 ± 6	508.14 ± 0.1
1	503.08 ± 0.04	500.7 ± 6	...
2	497.89 ± 0.04	491.6 ± 6	...
3	...	485.5 ± 6	...
4			

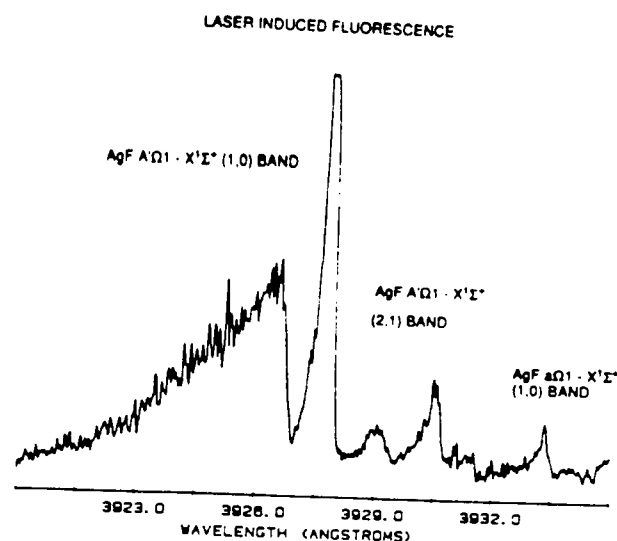


FIG. 4. Pulsed laser induced fluorescence spectrum of the $A'\Omega_1-X'\Sigma^+(1,0)$ band of AgF.

$= (1,0)$ and $(2,1)$ bands of the $A'-X$ system have also been observed and are depicted in Figure 4. The two weak peaks at 401.39 [also observed in CL in Fig. 2(b)] and 393.33 nm in Figs. 3(a) and 4 cannot be assigned to the $A'\Omega_1$ electronic state and are associated tentatively with a second $\Omega=1$ state based on the atomic-molecular correlations which we consider shortly. The rotational spectra for the A' system show typical blue degraded rotational progressions with clear P heads to the red, indicating that the upper electronic state has a larger rotational constant B_e than does the ground $X'\Sigma^+$ state. Two rotational branches (R and Q) have been identified from the blue degraded rotational structure labeled in Fig. 3.⁷ Apparent intensity anomalies result from the superposition of the R and Q branches with the latter progressing slightly behind the former. This conclusion is based on the analysis of the simulation calculation depicted in Fig. 3(b). In analyzing the dispersed fluorescence induced by pumping at the P head of the $(v',v'')=(0,0)$ band, we have confirmed the vibrational assignment for the dominant features of the chemiluminescent spectrum depicted in Fig. 2(a).⁷

The electronic assignment for the dominant $A'-X$ system has been made by considering the rotational transition patterns. In Hund's case (c), transitions with $\Delta\Omega=0$ and $\Omega=\Omega'=0$ are similar to $^1\Sigma-^1\Sigma$ transitions (with R and P branches), and transitions with $\Delta\Omega=1$ and $\Omega'=1$, $\Omega''=0$ have the pattern of $^1\Pi-^1\Sigma$ band systems (with R , Q , and P branches).²⁶ Rotational assignments for well-resolved R and Q peaks (Fig. 3 and Ref. 7) of the $A'-X$ system were easily determined using the following expressions and the previously known ground state rotational constants given in Ref. 19:

$$\nu_R = \nu_0 + (B'_v + B''_v)(J+1) + (B'_v - B''_v)(J+1)^2, \quad J > 0, \quad (1)$$

$$\nu_Q = \nu_0 + (B'_v + B''_v)J + (B'_v - B''_v)J^2, \quad J > 1, \quad (2)$$

$$\nu_P = \nu_0 - (B'_v + B''_v)J + (B'_v - B''_v)J^2, \quad J > 2, \quad (3)$$

TABLE II. Molecular constants of the $A'\Omega_1$ state of ^{107}AgF . The vibrational and rotational constants for ^{109}AgF are calculated from the ones of ^{107}AgF with the formulas given in the footnote. All numbers are in cm^{-1} except for r_e .^a

	^{107}AgF	$^{109}\text{AgF}^b$
T_e	24 950.71(10)	24 950.71(10)
$\Delta G_{1/2}$	506.744(80)	506.041
B_e	0.281 32(15)	0.280 54
α_e	$0.404 4(89) \times 10^{-2}$	$0.402 7 \times 10^{-2}$
D_e	$0.116(60) \times 10^{-6}$	0.115×10^{-6}
H_e	$-0.403(83) \times 10^{-10}$	-0.400×10^{-10}
r_e (Å)	1.927	1.927

^aThe numbers in parentheses are 1σ uncertainties.

^bThe following formulas are used: $B'_e = \rho^2 B_e$, $\alpha'_e = \rho^3 \alpha_e$, $D'_e = \rho^4 D_e$, $H'_e = \rho^5 H_e$, $\omega'_e = \rho \omega_e$, $\omega'_e x'_e = \rho^2 \omega_e x_e$, and $\rho^2 = \mu/\mu'$, where μ and μ' are the reduced masses of the two isotopes. For ^{107}AgF and ^{109}AgF , $\rho = 1.001 39$.

where ν_R , ν_Q , and ν_P are the peak positions of the R , Q , and P branches, respectively. J is the lower state rotational quantum number and B'_v and B''_v are the rotational constants of the upper and the lower states. The centers of the deep valleys near the P heads in Figs. 3(a) and 4 are very good approximations to the band origins ν_0 . With the vibrational and rotational assignments and the ground state molecular constants of ^{107}AgF given in Ref. 19, term values for the observed vibronic levels were calculated. A set of Dunham coefficients consistent with the assignment of an $A'\Omega_1$ state were obtained and are listed in Table II. The constants in Table II can reproduce all well-resolved R and Q branch levels with a standard deviation of 0.1 cm^{-1} . We note that, under the present experimental resolution, no Ω -type doubling has been observed for the $A'\Omega_1-X'\Sigma^+$ transition.

The vibrational and rotational constants of the isotope ^{109}AgF listed in Table II were calculated from those of ^{107}AgF using the well-known formula for isotope effect.²⁷ The isotope splittings of the $A'\Omega_1-X'\Sigma^+(0,0)$ band [also the $A0^+$, $B0^+-X'\Sigma^+(0,0)$ bands as depicted in Fig. 5] are too small to be resolved for those rotational levels observed under the current experimental resolution.⁷ Furthermore, in comparing Figs. 3(a) and 4, we find that the $(v',v'')=(1,0)$ band of the $A'\Omega_1-X'\Sigma^+$ system is not as well resolved as the $(v',v'')=(0,0)$ band due to the increasing isotope splittings for higher vibrational levels.

The rotational simulation for the $A'\Omega_1-X'\Sigma^+(0,0)$ band, depicted in Fig. 3(b), was carried out assuming a Boltzmann rotational distribution ($T=495 \text{ K}$) for the ground state and the $\Omega_1-^1\Sigma^+$ transition pattern (with R , Q , and P branches). The determined rotational temperature $T=495 \text{ K}$ may not be an accurate measure of the thermodynamic temperature since Hund's case (c) mixing effects have not been considered in the calculation. The molecular constants for ^{107}AgF given in Table II were used with no isotope effect taken into account in the calculation. The agreement of the intensity patterns for the simulation and the LIF spectrum further confirms the electronic assignment to a newly observed $A'\Omega_1$ state. From the molecular constants given in Table II, calculated Franck-

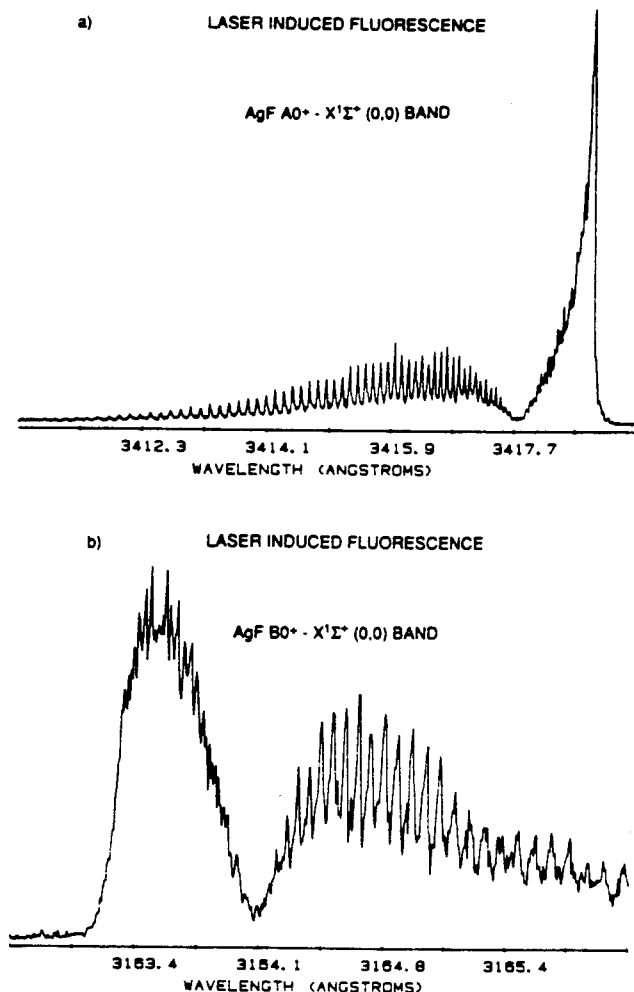


FIG. 5. Pulsed laser induced fluorescence spectra of (a) the $A0^+-X'\Sigma^+(0,0)$ band, and (b) the $B0^+-X'\Sigma^+(0,0)$ band of AgF.

Condon factors are found to be in excellent agreement with the CL intensity distribution.⁷

B. The $A\Omega 1-X'\Sigma^+$ band system

The three weak peaks which are located at 409.5, 401.39, and 393.33 nm as depicted in Figs. 2(b), 2(c), 3(a), and 4, cannot be identified as vibrational bands of the $A'\Omega 1-X'\Sigma^+$ system and are tentatively considered to originate from another electronic state. Since no rotational structure has been resolved for these features, the electronic symmetry of the emitting state is not clear. We can, however, make a suggested assignment based on correlations between the molecular states and their atomic limits (see the following). The three weak peaks, located 39, 38, and 36 cm^{-1} , respectively, to the red of the P heads of the (0,1), (0,0), and (1,0) bands of the $A'\Omega 1-X'\Sigma^+$ system, have a separation of 508 and 510 cm^{-1} . The former agrees closely with $\Delta\omega_{1/2}$ (508.26 cm^{-1}) of the ground $X'\Sigma^+$ state of AgF, while the latter is similar to the $\Delta\omega_{1/2}$ (506.7 cm^{-1}) of the $A'\Omega 1$ state. It is also noted that the 409.5 nm peak is observed only in emission (chemiluminescence). The 401.39 nm peak is observed both in emission (CL) and LIF excitation, while the 393.33 nm peak is recorded

TABLE III. Molecular constants associated with (A) the $A0^+-X'\Sigma^+(0,0)$ and (B) the $B0^+-X'\Sigma^+(0,0)$ bands of ^{107}AgF . The B_0 and D_0 values are for the upper states.

(A) $A0^+-X'\Sigma^+(0,0)$ band		
	This work	Ref. 19
ν_0 (cm^{-1})	29 250.20(1)	29 250.87
B_0 (cm^{-1})	0.272 543(21)	0.272 68
D_0 (cm^{-1})	$3.61(7) \times 10^{-7}$	3.71×10^{-7}
(B) $B0^+-X'\Sigma^+(0,0)$ band		
ν_0 (cm^{-1})	31 594.77(2)	31 594.13
B_0 (cm^{-1})	0.255 47(10)	0.255 486
D_0 (cm^{-1})	$6.5(\pm 2.0) \times 10^{-7}$	4.72×10^{-7}

only in LIF excitation. It appears, therefore, very likely that the peak at 401.39 nm corresponds to the (0,0) band of an $a\Omega 1-X'\Sigma^+$ transition. An electronic state with a potential energy curve very similar to that of the $A'\Omega 1$ state but located about 38 cm^{-1} below the $A'\Omega 1$ state is suggested. This $a\Omega 1$ state also has, as we outline shortly, a radiative lifetime similar to the $A'\Omega 1$ state.

C. The $A0^+$, $B0^+-X'\Sigma^+$ band systems

Laser induced fluorescence has also been observed for the AgF $A0^+-X'\Sigma^+(0,0)$ and $B0^+-X'\Sigma^+(0,0)$ bands in the UV region. Laser induced fluorescence spectra are depicted in Figs. 5(a) and 5(b), respectively. Both the $A-X$ and $B-X$ emission spectra show clear $^1\Sigma^+-^1\Sigma^+$ -like features. The $A-X$ (0,0) band is blue degraded, whereas the $B-X$ (0,0) band is red degraded. The molecular constants determined for these two bands are tabulated in Table III and compared with those given in Ref. 19. The LIF intensity for these two systems is considerably stronger than that for the $A'\Omega 1-X'\Sigma^+$ transition. Intense laser fluorescence could be observed for the $A-X$ and $B-X$ systems at oven temperatures just above the silver melting point (1234 K), while a considerably higher temperature (1600 K) was needed to observe both CL and LIF for the $A'\Omega 1-X'\Sigma^+$ transition. The $(v',v'')=(1,0)$ bands for both the $A0^+-X'\Sigma^+$ and $B0^+-X'\Sigma^+$ systems were not observed even with a sensitivity ten times higher than that necessary to record the (0,0) bands. This is partly due to unfavorable Franck-Condon factors and partly the result of the predisassociation of these two states as considered in Ref. 19.

D. Radiative lifetimes

Using a digital oscilloscope, we have recorded the exponential fluorescence decay with a laser pump frequency set at the intense P heads of the $A'\Omega 1-X'\Sigma^+(0,0)$ and $A0^+-X'\Sigma^+(0,0)$ bands and the R head of the $B0^+-X'\Sigma^+(0,0)$ band. Typical fluorescence decay waveforms (an average of ten laser shots) for the $A'\Omega 1-X'\Sigma^+(0,0)$, $A0^+-X'\Sigma^+(0,0)$, and $B0^+-X'\Sigma^+(0,0)$ transitions are shown in Fig. 6. Table IV lists the measured radiative lifetimes for the four low-lying electronic states characterized in this study (together with several of their other properties). The fluorescence decay of the long-lived $A'\Omega 1$ state has been found to be sensitive to the fluorine gas pressure.

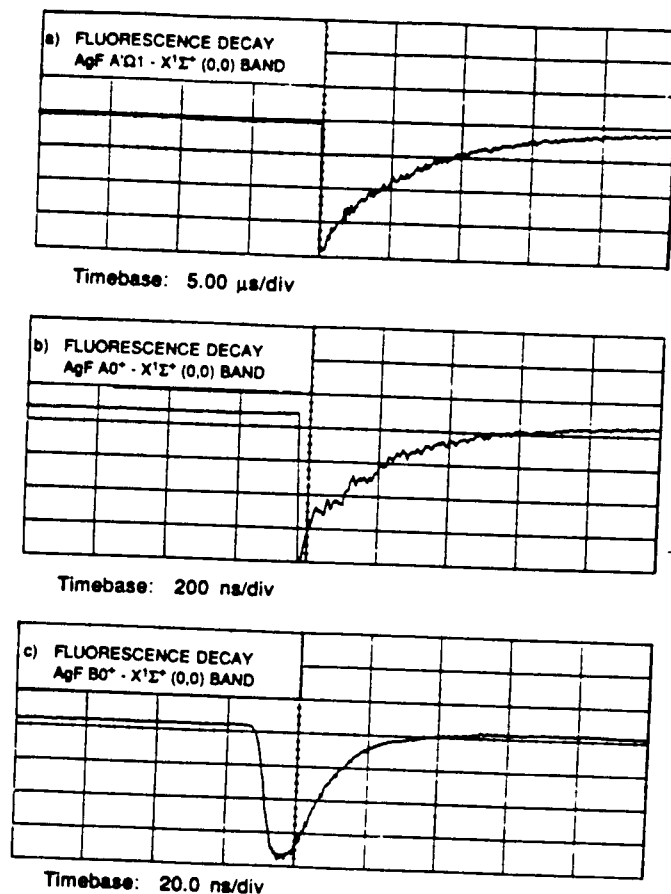


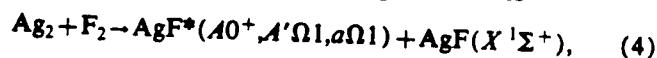
FIG. 6. Exponential fluorescence decay waveforms, each of which is an average of ten laser shots. The P or R heads of the following bands are excited: (a) the AgF $A'\Omega 1-X'\Sigma^+$ (0,0) band (5 μ s/division); (b) the AgF $A0^+-X'\Sigma^+$ (0,0) band (200 ns/division); and (c) the $B0^+-X'\Sigma^+$ (0,0) band (20 ns/division).

Under the optimal conditions for obtaining a LIF signal, fluorescence decays ranging from 12 to 4 μ s (with an averaged value of 7.1 μ s) were recorded when the fluorine gas pressure was increased. No quenching effects have been observed with increasing He entrainment gas pressure and no pressure dependence is found to be associated with the shorter-lived $A0^+-X'\Sigma^+$ and $B0^+-X'\Sigma^+$ transitions. With real-time monitoring of the fluorescence decay while

scanning the laser frequency, we find no apparent rotational dependence for the radiative lifetimes. Finally, we should note that since the laser pulse used to induce the fluorescence has a pulse duration of 9 ns [full width at half-maximum (FWHM)], the build-up process for LIF, which is virtually identical to the laser pulse rise time, cannot be detected on the 5 μ s/division and 200 ns/division time scales of Figs. 6(a) and 6(b). However, the build-up process is well resolved in Fig. 6(c) taken on a comparable time scale of 20 ns/division.

IV. DISCUSSION

Under the conditions of the present experiment, the four center silver dimer-fluorine molecule reaction is considered to be the dominant process for the formation of both excited and ground state AgF molecules



$$\Delta E = 2D_0^0(\text{Ag-F}) - D_0^0(\text{Ag-Ag}) - D_0^0(\text{F-F}) = 4.04 \text{ eV}. \quad (5)$$

The process (4) results in chemiluminescent emission dominated by the $A0^+-X'\Sigma^+$ and $A'\Omega 1-X'\Sigma^+$ band systems [Figs. 2(a) and 2(b)]. The AgF $A'\Omega 1-X'\Sigma^+$ emission system can also be excited employing the reaction of silver molecules Ag_x ($x \geq 3$) and fluorine atoms,⁷ a process which we consider elsewhere.⁷

The three major band systems observed in this study—the $A'\Omega 1$, $A0^+$, and $B0^+-X'\Sigma^+$ transitions—are Hund's case (c) allowed. However, as Table IV summarizes, they have clearly distinct and well-separated radiative lifetimes. We can divide the four low-lying electronic states into three classes, i.e., the long-lived $A'\Omega 1$ (7.1 μ s) and $a\Omega 1$ (9.1 μ s) states, the intermediate lifetime $A0^+$ (240 ns) state and the short-lived $B0^+$ (21 ns) state. We can attempt to understand this lifetime behavior by correlating these states to (1) the spin characters of their dominating Hund's case (a) components and (2) their dissociation limits.

The $\Omega = 1$ states have three components $^3\Pi_1$, $^3\Sigma^+_{(\Omega=1)}$, and $^1\Pi$, while the 0^+ states correspond to a mix of two $^3\Pi_0$ and $^1\Sigma^+$. The long lifetime of the $A'\Omega 1$ state apparently indicates that the triplet components [very likely the

TABLE IV. A summary of the major properties of the low-lying electronic states of gaseous AgF. The estimated dissociation energies are obtained from the thermochemical value $D^0 = 29\,600 \pm 1400 \text{ cm}^{-1}$ for the AgF ground state (Ref. 28).

State	T_e (cm^{-1})	r_e (\AA)	Spin character	Lifetime	Dissociation energy D_e (cm^{-1})	Atomic limits
$X'\Sigma^+$	0	1.983	Singlet	...	29 600	
$a\Omega 1$	(24 913) ^a	...	Triplet	9.1 \pm 3.3 μ s	(4 687)	
$A'\Omega 1$	24 950.71 ^a	1.927	Triplet	7.1 \pm 2.6 μ s	4 649	
$A0^+$	29 220 ^b	1.957(r_0)	Singlet	240 \pm 14 ns	784	$\text{Ag } ^2S_{1/2} + \text{F } ^2P_{3/2}$
$B0^+$	31 663 ^b	2.022(r_0)	Singlet	21 \pm 1.2 ns	27 489	$\text{Ag } ^2S_{1/2} + \text{F } ^2P_{1/2}$
Repulsive ($\Omega 1$)	$\text{Ag } ^2P_{1/2} + \text{F } ^2P_{3/2}$

^aThis work.

^bData taken from Ref. 31.

$^3\Pi_1$ component by comparison with the lifetimes of the low-lying electronic states of CuF (Refs. 21, 22, and 25)] dominate this state. Thus, the transition probability for emission terminating in the ground $X^1\Sigma^+$ state is (intensity) borrowed from the $^1\Pi$ state. Similarly, a dominant triplet character is also likely for the $a\Omega 1$ state with its long radiative lifetime (9.1 μ s) and weaker transition intensity. We suggest that this state is an $\Omega=1$ state by process of elimination. Two of the remaining possible transitions 0^- and $\Omega 2-X^1\Sigma^+$ are strictly forbidden electric dipole transitions and should be possessed of even longer radiative lifetimes and hence a much weaker emission intensity. For CuF, these lifetimes range from several hundred microseconds to milliseconds, the emission being 1000 times weaker than the $\Omega 1-X^1\Sigma^+$ system.^{21,22,25} A remaining possibility, the assignment to a 0^+ state, is readily eliminated by considering atomic asymptotic limits.

Ground state silver and fluorine atoms $Ag^2S_{1/2} + F^2P_{3/2}$ combine to generate one 0^+ ($X^1\Sigma^+$), one 0^- , two $\Omega=1$, and one $\Omega=2$ molecular state, whereas the $Ag^2S_{1/2} + F^2P_{1/2}$ combination, which lies 400 cm^{-1} above the ground atomic state, yields one 0^+ ($A0^+$), one 0^- , and only one $\Omega=1$ state. If the repulsive $\Omega 1$ state assigned by Barrow and Clements¹⁹ dissociates diabatically to the second atomic state as indicated in Fig. 2 of Ref. 19, the newly observed A' and a states can only dissociate to ground state atoms and must be the two $\Omega=1$ states generated by this atomic combination (note that the next possible neutral atomic asymptote $Ag^2P_{1/2} + F^2P_{3/2}$ is located approximately 30 000 cm^{-1} above the ground atomic state and is thus too energetic to correlate with these two lowest-lying states). If the repulsive $\Omega 1$ state correlates diabatically to the ground state atomic limit $Ag^2S_{1/2} + F^2P_{3/2}$, the $A'\Omega 1$ state must diabatically dissociate to the second atomic limit $Ag^2S_{1/2} + F^2P_{1/2}$ by crossing this repulsive potential. This possibility, which seems highly unlikely, would appear to be eliminated by the avoided crossing rule. The repulsive $\Omega 1$ state and the $A'\Omega 1$ state will adiabatically correlate to the same dissociation limits rather than undergo a curve crossing. Figure 7 illustrates correlation diagrams between the low-lying molecular states of silver fluoride and their corresponding atomic asymptotes, as proposed above and considered by other workers.¹⁹ The values of D_e for AgF are based on the thermochemical value $D^0 = 29\,600 \pm 1400$ cm^{-1} .²⁸ Note that the transitions $A'\Omega 1$, $a\Omega 1-X^1\Sigma^+$ also involve no change in angular momentum or electron configuration for the atoms, which must account, at least in part, for the long lifetimes of these two states.

The $A0^+$ state has an intermediate lifetime of 240 ns, which, on the one hand, suggests possible singlet character ($^1\Sigma^+$) upon comparison with the known transitions for CuF.^{21,22,25} However, this lifetime is certainly longer than that associated with a typical allowed singlet-singlet transition for diatomic molecules [e.g., 12 ns for the $A^1\Sigma_u^+ - X^1\Sigma_g^+$ system of Na_2 (Refs. 29 and 30)]. The observed lifetime for the $A0^+$ state might be explained by noting that the $A0^+-X^1\Sigma^+$ system corresponds to a weak $p-p$ ($\Delta l = 0$) F atom transition as indicated in Fig. 7. Using a similar argument, the short lifetime of the $B0^+$ state (21

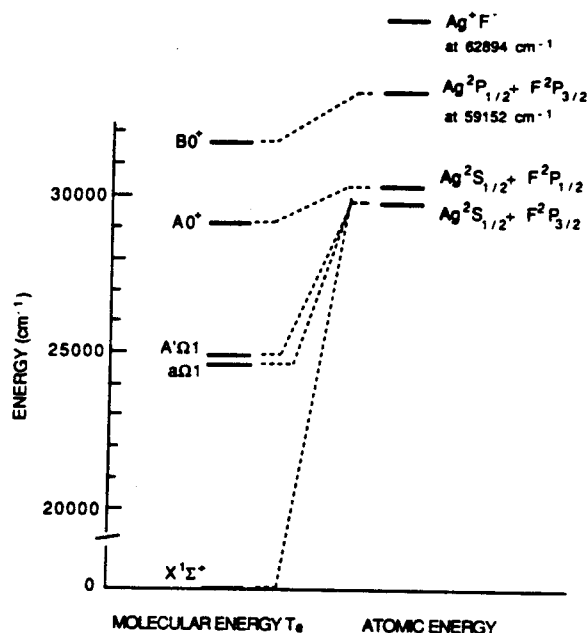


FIG. 7. Correlation diagram for the low-lying molecular states and the corresponding atomic asymptotic limits of the AgF system.

ns) can be readily understood from (1) its singlet character ($^1\Sigma^+$) and (2) the strongly allowed $p-s$ ($\Delta l = 1$) transition in atomic Ag. In summary, Table IV lists the T_e 's and r_e 's, spin character, measured lifetimes, dissociation energies, and proposed dissociation limits for the four low-lying electronic states of AgF.

Although copper and silver fluoride are isoelectronic, the five observed low-lying states of CuF lie at considerably lower energies ($\sim 14\,500$ – $22\,800$ cm^{-1}) than even the newly observed $A'\Omega 1$ and $a\Omega 1$ states of AgF. Furthermore, the radiative lifetimes of the low-lying CuF states considerably exceed those of AgF. We suggest that these differences may be attributed to a significantly different molecular electronic structure for these isoelectronic diatomics.

Using *ab initio* calculations as a guide, Dufour *et al.*²³ have developed a consistent model to account for the observed behavior of the CuF excited states assigning them to a single structure $Cu^+ (3d^9 4s) F^- (2p^6)$ with the manifold of observed emissions resulting from transitions between the states resulting from this structure and the closed shell, $Cu^+ (3d^{10}) F^- (2p^6)$, $X^1\Sigma^+$ ground state ion pair. The relatively long-lived CuF transitions are thought to correspond to electric dipole forbidden $3d-4s$ electron transfers in the Cu^+ atomic limit.

The situation in AgF is clearly different. This might be explained by considering the distinctly different energy level patterns for the copper and silver atoms and their ions as catalogued in Table V. We note that the lowest energy atomic transitions in silver (1) lie at considerably higher energy than those in atomic copper and (2) involve an allowed $p \rightarrow s$ electron transfer vs the Cu forbidden $d \rightarrow s$ transition. Furthermore, although the lowest energy excited states in Cu^+ and Ag^+ are both 3D and the lowest

TABLE V. The lowest electronic configurations and the corresponding energies of Cu and Ag atoms and Cu⁺ and Ag⁺ ions. All data are taken from Ref. 32.

Cu atom			Ag atom		
Electron configuration	<i>J</i>	Energy (cm ⁻¹)	Electron configuration	<i>J</i>	Energy (cm ⁻¹)
3d ¹⁰ 4s ² S	1/2	0.0	4d ¹⁰ 5s ² S	1/2	0.0
3d ⁹ 4s ² 2D	5/2	11 202.565	4d ⁹ 5p ² P ^o	1/2	29 552.05
	3/2	13 245.423		3/2	30 472.71
3d ¹⁰ 4p ² P ^o	1/2	30 535.302	4d ⁹ 5s ² 2D	5/2	30 242.26
	3/2	30 783.686		3/2	34 714.16

Cu ⁺ ion			Ag ⁺ ion		
Electron configuration	<i>J</i>	Energy (cm ⁻¹)	Electron configuration	<i>J</i>	Energy (cm ⁻¹)
3d ¹⁰ 1S	0	0.0	4d ¹⁰ 1S	0	0.0
3d ⁹ 4s ¹ D	3	21 928.60	4d ⁹ 5s ¹ D	3	39 163.9
	2	22 847.03		2	40 741.0
	1	23 998.31		1	43 738.7

energy atomic emissions in both ions correspond to electric dipole forbidden *d-s* transitions, these states lie at significantly higher energy for the silver ion, making correlation with the low-lying molecular states of AgF tenuous in an ionic model.

The combination of data in Table V, in fact, favors a model correlated more closely with the neutral silver atomic limits which we have considered in our previous discussion. In order to construct the correlation diagram of Fig. 7, we take the AgF bond energy to be $29\,600 \pm 1400$ cm⁻¹.²⁸ With this energy increment, we estimate *D_e* for the *X*¹Σ⁺ state as $\sim 29\,600$ cm⁻¹, for the *a*Ω1 state as ~ 4687 cm⁻¹, and for the *A'*Ω1 state as ~ 4649 cm⁻¹ as they dissociate to ground state silver and fluorine atoms. We estimate the *A*0⁺ state to be stable by only ~ 784 cm⁻¹ as it dissociates to Ag²S_{1/2} + F²P_{1/2} at 30 004 cm⁻¹. The *B*0⁺ state whose short radiative lifetime signals its correlation with Ag²P_{1/2} is, of course, predissociated.

V. CONCLUSION

We have observed the optical signatures for two low-lying Ω=1 states *A'*Ω1 and *a*Ω1 of AgF which dissociate to ground state atoms and lie about 4300 cm⁻¹ below the previously known lowest excited *A*0⁺ state. The measured radiative lifetimes reveal that the two Ω=1 states are of triplet character, while the two 0⁺ states *A*0⁺ and *B*0⁺ are singlet. It appears that all of the observed low-lying electronic states of AgF dissociate adiabatically to neutral atoms in contrast to the ion-pair dissociation attributed to the low-lying states of CuF. The observation of the two Ω=1 states suggests the probable existence of the similar stable low-lying electronic states for the remaining silver halides. The long-lived *A'*Ω1 state is also important because of its suitability as an intermediate state for studies of high-lying electronic states and photoionization using multiple resonance laser excitation.

Note added in proof. On the electronic assignment of the low-lying *a* state, we emphasize that it is almost impossible, at this time, to make an unambiguous electronic assignment for the weak *a* state because of the lack of either well resolved rotational structure for the *a*-*X*¹Σ⁺ bands or *ab initio* calculations of the radiative lifetimes for the low-lying electronic states of AgF. We have contemplated that the *A'*Ω1 and this *a* states might be the Ω=1 and Ω=0⁻ components of a Hund's case (a) ³Σ⁺ state which correlates with the *a*³Σ⁺ state observed in CuF.²⁰ However, we are troubled by the fact that (1) the *A'*-*a* separation in AgF (~ 38 cm⁻¹) is so similar to the separation of the Ω=1 and 0⁻ components in CuF (43.5 cm⁻¹),²⁰ and (2) that the radiative lifetime of the *a* state is virtually the same as that of the *A'*Ω1 state. For those reasons, we tentatively suggest that this weak *a* state be an Ω=1 state by process of elimination as described in the paper and do not rule out the possibility that this state might be assigned to another possible electronic symmetry.

ACKNOWLEDGMENTS

We are grateful to Professor R. F. Barrow for his valuable comments and suggestions on this work. H. Wang would like to thank Professor T. C. Devore for helpful discussions on the analysis of the spectrum and Mr. C. B. Winstead for his technical help in the pulsed laser system and the data acquisition system. This work was partially supported by the Army Research Office, the Eastman Kodak Company, and the Air Force Office of Scientific Research through the Strategic Defense Initiative.

- ¹ J. L. Gole, in *Advances in Metal and Semiconductor Clusters*, edited by M. A. Duncan (JAI, Greenwich, 1993), Vol. 1, p. 159.
- ² (a) R. W. Woodward, P. N. Le, M. Temmen, and J. L. Gole, *J. Phys. Chem.* **91**, 2537 (1987); (b) J. L. Gole, *AIP Conf. Proc.* **160**, 439 (1987); (c) T. C. Devore, R. W. Woodward, and J. L. Gole, *J. Phys. Chem.* **92**, 6919 (1988); (d) T. C. Devore, J. R. Woodward, and J. L. Gole, *ibid.* **93**, 4920 (1989); (e) M. J. McQuaid and J. L. Gole, *AIP Conf. Proc.* **191**, 687 (1988).
- ³ T. C. Devore and J. L. Gole, *Proc. Sixth Int. Conf. High Temp. Mater., High Temp. Sci.* **27**, 49 (1989).
- ⁴ (a) *Metal Clusters*, edited by M. Moskovits (Wiley-Interscience, New York, 1986); (b) ACS Symp. Ser. **179**, edited by J. L. Gole and W. C. Stwalley (1982); (c) M. Morse, *Chem. Rev.* **86**, 1049 (1986).
- ⁵ (a) M. J. McQuaid, K. Morris, and J. L. Gole, *J. Am. Chem. Soc.* **110**, 5280 (1988); (b) J. L. Gole, *NATO ASI Ser.* **374**, 1025 (1992); (c) in *Gas Phase Metal Reactions*, edited by A. Fontijn (Elsevier, Amsterdam, 1992), pp. 573-604.
- ⁶ T. C. Devore, J. R. Woodward, P. N. Le, J. L. Gole, and D. A. Dixon, *J. Phys. Chem.* **94**, 756 (1990).
- ⁷ H. Wang and J. L. Gole, *J. Mol. Spectrosc.* (in press).
- ⁸ (a) *The Physics of Latent Image Formation in the Silver Halides*, edited by A. Baldeschwi, W. Czaja, E. Tosatti, and M. Tosi (World Scientific, Singapore, 1984); (b) *The Theory of the Photographic Process*, edited by T. H. James (MacMillan, New York, 1977); (c) A. Marchetti and J. Deaton (private communication).
- ⁹ B. A. Brice, *Phys. Rev.* **35**, 960 (1930).
- ¹⁰ B. A. Brice, *Phys. Rev.* **38**, 658 (1931).
- ¹¹ F. A. Jenkins and G. D. Rochester, *Phys. Rev.* **52**, 1141 (1937).
- ¹² R. S. Mulliken, *Phys. Rev.* **51**, 310 (1937).
- ¹³ N. Metropolis, *Phys. Rev.* **55**, 636 (1939).
- ¹⁴ N. Metropolis and H. Beutler, *Phys. Rev.* **55**, 1113 (1939).
- ¹⁵ L. C. Krisher and W. G. Norris, *J. Chem. Phys.* **44**, 391 (1966); **44**, 974 (1966).
- ¹⁶ E. Pearson and W. Gordy, *Phys. Rev.* **152**, 42 (1966).

- ¹⁷J. Hoefft, F. J. Lovas, E. Tiemann, and T. Topping, *Z. Naturforsch. Teil A* **25**, 35 (1970).
- ¹⁸R. M. Clements and R. F. Barrow, *Chem. Commun.* **1254**, 27 (1968).
- ¹⁹R. F. Barrow and R. M. Clements, *Proc. R. Soc. London Ser. A* **322**, 243 (1971).
- ²⁰F. Ahmed, R. F. Barrow, A. H. Chojnicki, C. Dufour, and J. Schamps, *J. Phys. B* **15**, 3816 (1982).
- ²¹R. E. Steele and H. P. Broida, *J. Chem. Phys.* **69**, 2300 (1978).
- ²²J. M. Delaval, Y. Lefebvre, H. Bocquet, P. Bernage, and P. Niay, *Chem. Phys.* **111**, 129 (1987).
- ²³C. Dufour, J. Schamps, and R. F. Barrow, *J. Phys. B* **15**, 3819 (1982).
- ²⁴J. M. Delaval and J. Schamps, *Chem. Phys.* **100**, 21 (1985).
- ²⁵J. Schamps, J. M. Delaval, and O. Faucher, *Chem. Phys.* **145**, 101 (1990).
- ²⁶G. Herzberg, *Molecular Spectra and Molecular Structure, I Spectra of Diatomic Molecules*, 2nd ed. (Krieger, Malabar, 1989).
- ²⁷J. L. Dunham, *Phys. Rev.* **41**, 721 (1932).
- ²⁸K. F. Zmbov and J. L. Margrave, *J. Phys. Chem.* **71**, 446 (1967).
- ²⁹T. W. Ducas, M. G. Littman, M. L. Zimmerman, and D. Kleppner, *J. Chem. Phys.* **65**, 842 (1976).
- ³⁰W. T. Zemke, K. K. Verma, T. Vu, and W. C. Stwalley, *J. Mol. Spectrosc.* **85**, 150 (1981).
- ³¹K. P. Huber and G. Herzberg, *Molecular Spectra and Molecular Structure IV. Constants of Diatomic Molecules* (Van Nostrand-Reinhold, New York, 1979).
- ³²Charlotte E. Moore, *Atomic Energy Levels* (U.S. Government Printing Office, Washington, D.C., 1949), Vols. 2 and 3.

APPENDIX XIII

"A Chemiluminescent and Laser Induced Fluorescent Probe Of A New Low-Lying $A'^{\Omega}1$ State of Gaseous AgF", H. Wang and J. L. Gole, J. Mol. Spectros, 161, 28 (1993).

A Chemiluminescent and Laser-Induced Fluorescent Probe of a New Low-Lying $A' \Omega = 1$ State of Gaseous AgF

HE WANG AND JAMES L. GOLE

School of Physics, Georgia Institute of Technology, Atlanta, Georgia 30332

A new $A' 1 (\Omega = 1)$ state of AgF at the fringes of the visible region has been excited and analyzed. The chemiluminescence from this state, which is located $\sim 4300 \text{ cm}^{-1}$ below the previously known lowest excited $A 0^+$ state, is observed for the first time in a beam-gas reaction where silver molecules, Ag_x , are reacted with either atomic or molecular fluorine. Using pulsed laser-induced fluorescence, two vibrational bands $(v', v'') = (0, 0)$ and $(1, 0)$ have been rotationally resolved and electronic and rotational assignments have been obtained. Molecular constants which can reproduce the observed data with a standard deviation of 0.1 cm^{-1} , the RKR potential energy curve, and the Franck-Condon factors for the $A' 1-X' \Sigma^+$ transition have been determined. The internal energy distributions of the reaction product AgF molecules are studied by vibrational intensity analysis and rotational simulation calculations. The possible reaction paths to produce the excited A' state from either the four-center $\text{Ag}_2 + \text{F}_2$ or $\text{Ag}_x (x \geq 3) + \text{F}$ reactions and the formation of ground state AgF molecules are discussed through consideration of reactant-product correlations and energetics. The dissociation energy of the newly observed $A' 1$ state is $4649 \pm 1400 \text{ cm}^{-1}$. The observation of this low-lying $\Omega = 1$ state indicates the existence of similar stable $\Omega = 1$ states for the remaining silver halides, all of which should readily absorb visible photons. Their existence, which may have implications for the detailed understanding of the photographic process, provides intermediate states for multiple-resonance laser excitation and multiphoton laser ionization. © 1993 Academic Press, Inc.

INTRODUCTION

The study of the highly exothermic kinetically controlled oxidation of metal molecules not only provides a means to extrapolate and modify concepts which govern simple $A + BC$ reactive encounters (1-3), but also, through a unique reactive branching, facilitates the formation of previously inaccessible reaction products. The analyzed quantum level structure of the product metal-based oxides and halides formed in highly exothermic oxidation processes can provide useful information on molecular structure and bonding (4-6) especially when detailed chemiluminescent (CL) studies can be used to pinpoint regions which will be accessible to a laser-induced fluorescent (LIF) probe.

In developing such studies, we have observed particularly intriguing groups of metal cluster oxidations. For example, the sodium trimer-halogen atom reactive interactions signal a surprising chemistry (7-9) as the high cross section $\text{Na}_n (n = 2, 3) - X (\text{Cl}, \text{Br}, \text{I})$ encounters create a continuous electronic population inversion based on the chemical pumping of sodium dimer (Na_2). While this unusual reactive behavior has potential for extension to other alkali trimers, we also realize that the Group IB dimers and trimers constitute direct analogs of the alkali systems, suggesting that additional insight might be gained through the study of the $\text{Ag}_n - X$ oxidation reactions. Further, the oxidation behavior of small silver agglomerates is of significance in both the photographic process (10) and catalysis (11).

Recently, Devore *et al.* (6) have reported and analyzed the chemiluminescent emission from silver cluster-ozone reactions, correlating a portion of these emissions with Ag_xO ($x \geq 2$) emitters. Here, we report an experimental study of the silver vapor-fluorine reaction system. We have obtained the first evidence for a stable $\Omega = 1$ state of the gaseous silver monohalide AgF, which lies 4300 cm^{-1} below the previously known lowest excited $A\ 0^+$ state. The band system associated with the $A' 1-X' 1\Sigma^+$ transition has been studied using a combination of CL and LIF spectroscopy.

Spectroscopic studies of the silver monohalides, AgX ($X = \text{F}, \text{Cl}, \text{Br}$), have a long, albeit limited, history (12-17). The halide ground states are highly ionic, with AgCl and AgBr respectively 52 (18) and 46% (19) ionic character, and the AgF ground state dipole moment determined to be 6.22 D (20). The heavy halides follow primarily Hund's case (c) coupling. The ground state of AgF dissociates to $\text{Ag } ^2S_{1/2} + \text{F } ^2P_{3/2}$ ground state atoms whose combination generates five molecular states, 0^+ , 0^- , 1, 1, and 2. At slightly higher energy the $\text{Ag } ^2S_{1/2} + \text{F } ^2P_{1/2}$ atoms can combine to yield 0^+ , 0^- , and 1 states. From the manifold of states resulting from these two atomic combinations, only the $A\ 0^+ (^2S_{1/2} + ^2P_{1/2})$ and $X' 1\Sigma^+ (^2S_{1/2} + ^2P_{3/2})$ states had been identified before the current study. Joshi and Sharma (21) first reported the near UV absorption spectrum of the $\text{AgF } B\ 0^+-X' 1\Sigma^+$ system. They also reported the observation of some features due to the $A\ 0^+-X' 1\Sigma^+$ transition. Barrow and Clements (22, 23) carried out a rotational analysis of these two ultraviolet systems and Hoeft *et al.* studied the rotational spectrum of the AgF ground state using microwave absorption (20). Until the present study no visible absorption spectrum and no transition involving a stable $\Omega = 1$ state has been reported for the silver halides.

EXPERIMENTAL DETAILS

Both chemiluminescence and pulsed laser-induced fluorescence were generated under multiple-collision conditions as a stream of silver entrained in helium was intersected by molecular or atomic fluorine. The overall experimental configuration is depicted schematically in Fig. 1. The entrainment flow device used in this study has been described previously (2). Briefly, silver metal was heated in a specially designed graphite crucible to temperatures in the range of 1600 K. The silver, emanating from the crucible, was entrained in a flow of helium gas at a total pressure of 1 Torr. For those experiments employing molecular fluorine, fluorine gas was introduced into the entrained silver flow through a concentric ring inlet located $\sim 1\text{ cm}$ above the crucible. For those experiments which used atomic fluorine as an oxidant, fluorine atoms were formed by electric discharge through SF_6 and used in a manner previously applied to studies of the $\text{Bi}_2 + \text{F}$ (24) and $\text{Mg}_x + \text{F}$ (25) reactive systems. Entrained fluorine atoms exited a directed-flow channel perpendicular to the direction of the entrained silver and about 1.5 cm above the silver source crucible. For both the fluorine atom and the fluorine molecule oxidation studies a chemiluminescent flame was generated in the reaction zone. However, this flame was considerably more intense for the fluorine molecule-based reactive encounters. The chemiluminescence from the reaction zone was observed at right angles to the reactant flows using a 0.75-m Spex 1702 monochromator operated in first order with a 1200 groove/mm grating blazed at 500 nm and an RCA 1P28 photomultiplier. The PMT signal was fed to a Keithley 417 autoscale picoammeter and recorded with a computer.

The pulsed LIF studies were performed employing only the fluorine molecule-based reactions. The second harmonic of a Quanta-ray Nd:YAG laser ($0.53\ \mu$) was used to pump a Spectra Physics PDL-3 pulsed tunable dye laser system operated with DCM

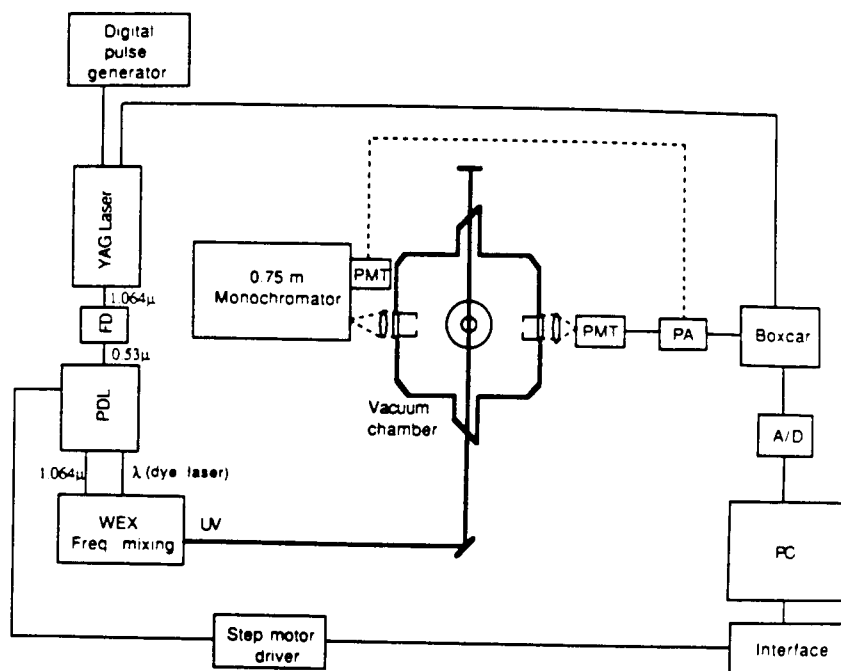


FIG. 1. Experimental setup for chemiluminescence and laser-induced fluorescence spectroscopy.

dye. The output of the pulsed dye laser (with a linewidth of 0.07 cm^{-1} and a pulse width of 9 nses) was then mixed with the fundamental output of the YAG laser in a frequency mixer (Quanta-Ray WEX-1) to produce the near-UV coherent radiation which was introduced to the reaction chamber in a direction perpendicular to the reactant flow. The YAG laser was triggered by a digital pulse generator (SRS DG535) with a repetition rate of 15 Hz. The Q-switching signal of the YAG oscillator was used to trigger a Boxcar integrator (SRS SR250) for better synchronization. The pulsed laser-induced fluorescence was collected with a 1P28 photomultiplier (2.2 nsec rise time) and sent to the gated integrator through a fast preamplifier (CLC 100 Video Amplifier, 500 MHz). The integration gate was set to a width of 300 nsec with a time delay such that the gate opens just after the short laser scattering pulse, thus reducing background noise. A computer drives the laser stepper motor, scans the dye laser, and acquires the averaged output data from the Boxcar synchronously. In order to achieve a linear scan in wavelength with the frequency mixer, the scan step size of the dye laser was calculated in real time using the PC. The output frequency of the WEX-1 was calibrated using aluminum atomic lines.

RESULTS AND ANALYSIS

Chemiluminescent spectra characterizing the entrained silver-fluorine atom and silver-fluorine molecule reactive encounters are depicted in Figs. 2a and 2b, respectively. The chemiluminescence from the fluorine atom-based system is considerably weaker than that obtained in the fluorine molecule reactive environment. It appears that the available energy corresponding to those processes which involve fluorine molecule reactions exceeds the energy available from the fluorine atom system. This sug-

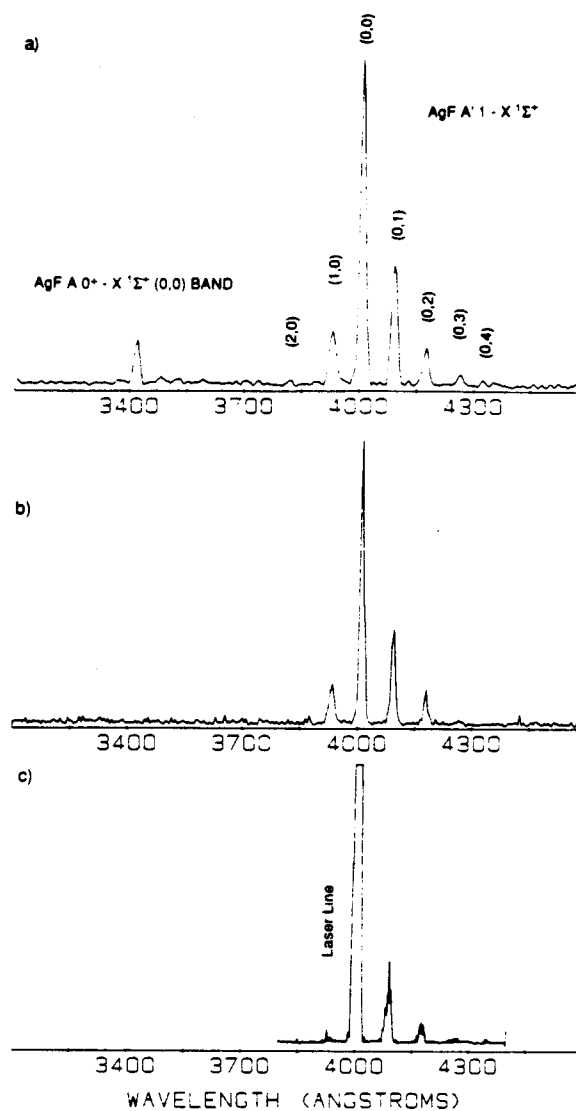


FIG. 2. (a) Chemiluminescence spectrum from the fluorine molecule-based reactive system at a resolution of 5 Å. (b) Chemiluminescence spectrum from the fluorine atom-based reactive system at a resolution of 5 Å. (c) The dispersed fluorescence induced by laser pumping at the P head of the $A' 1-X' 1\Sigma^+ (0,0)$ band of AgF.

gests the possibility of multicentered fluorine molecule-silver molecule reaction dynamics which produces two metal fluoride molecules. The situation, which is also apparent in several metal molecule-based oxidative environments, certainly represents a departure from $A + BC$ reaction dynamics (1-6). The peak at 342 nm, present only when fluorine molecules are used as reactants, is readily identified as the $(v', v'') = (0,0)$ band of the $A 0^+ - X' 1\Sigma^+$ transition of AgF. However, the spectrum is dominated by an intense vibrationally resolved structure around 400 nm observed for the first time in these silver-fluorine-based reactive systems. The CL signals associated with

this newly observed structure correlate with both the silver vapor concentration and the fluorine gas pressure. Table I catalogs the peak separations from the strongest CL peak to longer wavelengths. These separations agree well, within experimental error, with the known vibrational separations for the ground $X^1\Sigma^+$ state of ^{107}AgF given by Barrow and Clements (23). Based on this comparison, we can tentatively attribute the observed structure to a transition of the AgF molecule originating from a newly observed electronic state. We use LIF to identify the newly monitored electronically excited state as an $\Omega = 1$ state (LIF to the ground $^1\Sigma^+$ state). The vibrational assignment, as listed in Table I (note also Fig. 2a), can also be readily obtained and further confirmed by dispersed laser-induced fluorescence as exemplified in Fig. 2c.

Figures 3a and 3b present representative rotationally resolved LIF spectra corresponding to the $(v', v'') = (0, 0)$ and $(1, 0)$ bands, respectively. The $(v', v'') = (2, 1)$ band was also observed as depicted in Fig. 3b. Two detailed scans of the rotational structure of the $(0, 0)$ band are shown in Figs. 4a and 4b. The rotational spectra show typical blue degraded rotational progressions with clear P heads to the red, indicating that the upper state has a larger rotational constant, B_v , than does the lower state. Two rotational branches (R and Q) have been identified from the blue degraded rotational structure as labeled in Figs. 3 and 4. The apparent intensity anomalies are attributed to the superposition of the R branch and the Q branch. This argument is proved with a simulation calculation described below. The observed P head positions are listed in Table II. Figure 2c depicts the dispersed fluorescence induced by laser pumping at the P head of the $(v', v'') = (0, 0)$ band. The apparent disappearance of the $(v', v'') = (1, 0)$ band, which is otherwise clearly seen in the CL emission spectrum (Figs. 2a and 2b), confirms our vibrational assignment.

The electronic assignment has been made by considering the rotational transition patterns. In Hund's case (c), we have the electronic selection rule $\Delta\Omega = 0, \pm 1$ since Λ and Σ are no longer good quantum numbers. Furthermore, case (c) coupling may be regarded as case (a) coupling with very large multiplet splittings, the band structures in case (c) being quite similar to those in case (a). That is, transitions with $\Omega = 0$ and $\Omega' = \Omega'' = 0$ are similar to $^1\Sigma-^1\Sigma$ transitions (with R and P branches), and transitions with $\Omega = 1$ and $\Omega' = 1, \Omega'' = 0$ are similar to $^1\Pi-^1\Sigma$ transitions (with R, Q , and P branches) (26). Based on the above arguments, our newly observed electronic state can be assigned as a $\Omega = 1$ state without ambiguity. To match the previous nomenclature, we will call this newly observed state the $A'1$ state.

TABLE I
Vibrational Separations of the Ground $X^1\Sigma^+$ State of AgF Observed by Chemiluminescence and Laser-Induced Fluorescence

v	$\Delta G_{\text{Ref. 23}}$ (cm^{-1})	$\Delta G_{\text{Obs. by CL}}$ (cm^{-1})	$\Delta G_{\text{Obs. by LIF}}$ (cm^{-1})
0			
1	508.26 \pm 0.04	509.6 \pm 6	508.14 \pm 0.1
2	503.08 \pm 0.04	500.7 \pm 6	-
3	497.89 \pm 0.04	491.6 \pm 6	-
4	-	485.5 \pm 6	-

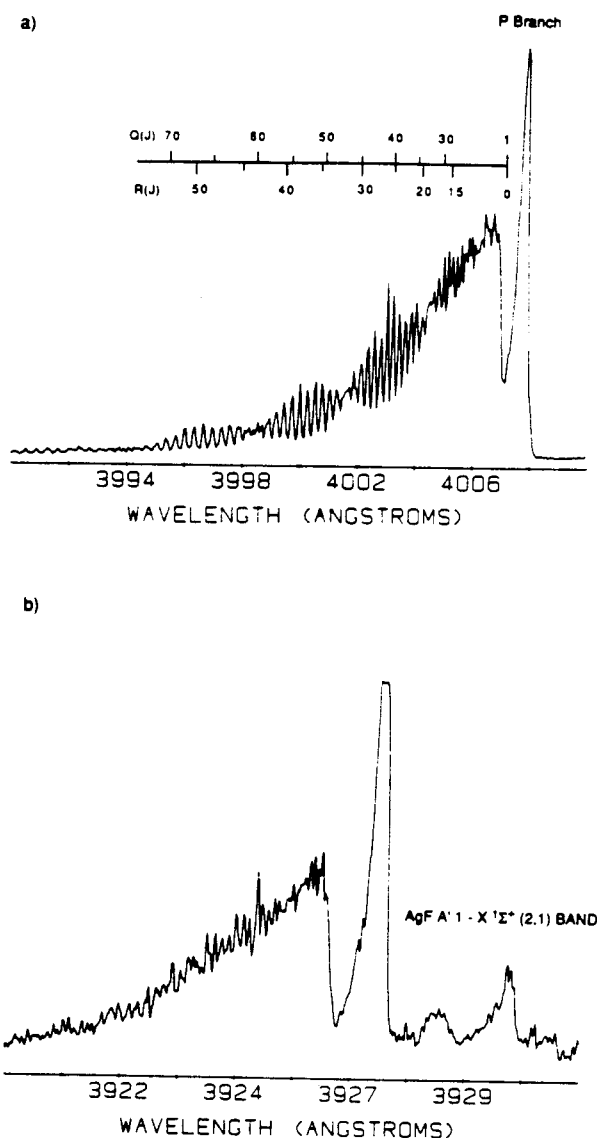


FIG. 3. Pulsed laser-induced fluorescence spectra of the $A' 1-X' 1\Sigma^+$ system of AgF. (a) $(v', v'') = (0, 0)$ band and (b) $(v', v'') = (1, 0)$ band. The intensity anomalies are due to the superposition of the R -branch and the Q -branch peaks.

The rotational assignment for the R , P , and Q branches was easily determined using the following equations and the previously known ground state rotational constants given in Ref. (23):

$$\nu_R = \nu_0 + (B'_v + B''_v)(J+1) + (B'_v - B''_v)(J+1)^2 \quad J \geq 0, \quad (1)$$

$$\nu_Q = \nu_0 + (B'_v - B''_v)J + (B'_v - B''_v)J^2 \quad J \geq 1, \quad (2)$$

$$\nu_P = \nu_0 - (B'_v + B''_v)J + (B'_v - B''_v)J^2 \quad J \geq 2, \quad (3)$$

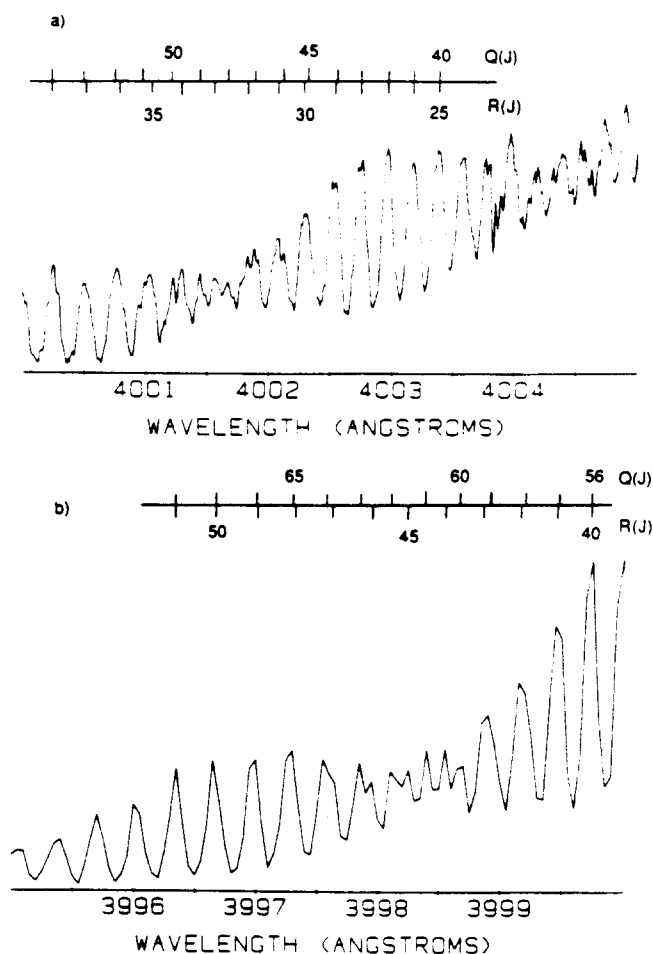


FIG. 4. Two detailed LIF scans (laser scan step size, 0.01 cm^{-1}) for the R and Q branches of the $(v', v'') = (0, 0)$ band of AgF .

where ν_R , ν_Q , and ν_P are the peak positions of the R , Q , and P branches, respectively. J is the lower state rotational quantum number, and B'_v and B''_v are the rotational constants for the upper and the lower state. The centers of the deep valleys near the P heads in Figs. 3a and 3b are very good approximations of the band origins ν_0 . With the vibrational and rotational assignments and the ground state molecular constants of ^{107}AgF given by Barrow and Clements (23), a total of 71 well resolved R and Q lines have been fit to the well-known Dunham formula (27)

$$T(v, J) = \sum Y_{jk}(v + 1/2)^j [J(J + 1) - 1]^k, \quad (4)$$

where $T(v, J)$ are the vibronic energy levels and Y_{jk} are the Dunham coefficients. Tables III, IV, and V tabulate the observed and the calculated spectral lines and the differences between them for the R and Q branches of the $(v', v'') = (0, 0)$ band and the R branch of the $(v', v'') = (1, 0)$ band, respectively. Table VI gives the molecular constants for the newly observed $A' 1$ state of ^{107}AgF and ^{109}AgF . The constants listed

TABLE II

P Bandhead Positions of the $A'1-X'1\Sigma^+$ System Observed by Laser-Induced Fluorescence

(v', v'')	<i>P</i> Head
	λ (Å)
(0,0)	4007.76
(0,1)	4090.90
(1,0)	3927.81
(2,1)	3930.82

TABLE III

Observed and Calculated *R*-Branch Vibronic Transitions for the $(v', v'') = (0, 0)$ Band of the $A'1-X'1\Sigma^+$ System of ^{107}AgF

Assignment J	<i>R</i> (J) (cm^{-1})		ΔV (cm^{-1}) Obs. - Cal.
	Observed	Calculated	
15	24960.234	24960.165	0.069
16	24961.168	24961.192	-0.024
17	24962.356	24962.249	0.107
18	24963.352	24963.335	0.017
23	24969.148	24969.210	-0.062
24	24970.522	24970.475	0.047
25	24971.772	24971.769	0.003
26	24973.080	24973.093	-0.013
27	24974.389	24974.447	-0.058
28	24975.699	24975.830	-0.131
30	24978.570	24978.687	-0.117
32	24981.502	24981.662	-0.160
33	24983.127	24983.195	-0.068
34	24984.813	24984.757	0.057
35	24986.500	24986.348	0.152
36	24988.121	24987.969	0.152
37	24989.744	24989.619	0.125
38	24991.367	24991.299	0.068
39	24992.930	24993.007	-0.077
41	24996.367	24996.511	-0.144
42	24998.242	24998.306	-0.064
44	25001.992	25001.981	0.011
45	25003.869	25003.860	0.009
46	25005.744	25005.766	-0.022
48	25009.813	25009.661	0.152
49	25011.688	25011.649	0.039
50	25013.879	25013.662	0.217
51	25015.756	25015.701	0.055
52	25017.949	25017.766	0.183
53	25019.826	25019.855	-0.029

TABLE IV

Observed and Calculated Q -Branch Vibronic Transitions for the $(v', v'') = (0, 0)$ Band of the $A' 1-X' 1\Sigma^+$ System of ^{107}AgF

Assignment J	$Q(J)$ (cm^{-1})		ΔV (cm^{-1}) Obs. - Cal.
	Observed	Calculated	
30	24961.418	24961.391	0.027
31	24962.356	24962.308	0.048
32	24963.352	24963.255	0.097
39	24970.522	24970.718	-0.196
40	24971.772	24971.903	-0.131
41	24973.080	24973.116	-0.036
42	24974.389	24974.359	0.030
43	24975.699	24975.631	0.068
44	24977.010	24976.931	0.079
47	24981.066	24981.001	0.065
48	24982.502	24982.413	0.089
49	24983.940	24983.853	0.087
50	24985.313	24985.319	-0.006
53	24989.744	24989.875	-0.131
54	24991.367	24991.445	-0.078
55	24992.930	24993.038	-0.108
56	24994.492	24994.656	-0.164
57	24996.367	24996.297	0.070
61	25002.932	25003.080	-0.148
62	25004.807	25004.827	-0.020
63	25006.369	25006.592	-0.223
64	25008.248	25008.375	-0.127
67	25013.879	25013.819	0.060
68	25015.756	25015.662	0.094

in Table VI can reproduce all well resolved experimental R - and Q -branch levels with a standard deviation of 0.1 cm^{-1} . We note that, under the present experimental resolution, no Ω -type doubling has been observed for the $A' 1-X' 1\Sigma^+$ transition.

The vibrational and rotational constants of the isotope ^{109}AgF were calculated from those of ^{107}AgF using the well-known formula for isotope effect (27). The isotope splittings of the R and Q branches for the $(v', v'') = (0, 0)$ band have been estimated from the molecular constants given in Table VI (for the $A' 1$ state) and in Ref. (23) (for the $X' 1\Sigma^+$ ground state) and plotted as a function of J in Fig. 5. The electronic isotope shift has been ignored in first-order approximation. Apparently, for the rotational spectral lines which we have observed, the isotope splittings for the lowest vibrational band are too small to be resolved under our experimental conditions. This is due primarily to the similarity of the vibrational and rotational constants for the upper and the lower states. It is also obvious in comparing Figs. 3a and 3b that the $(v', v'') = (1, 0)$ band is not as well resolved as the $(v', v'') = (0, 0)$ band due to the increasing isotope splittings for higher excited state vibrational quantum levels.

A comparison between the CL spectrum, the LIF spectrum, and a computer simulation of the $A' 1-X' 1\Sigma^+$, $(v', v'') = (0, 0)$ band is shown in Fig. 6. The rotational simulation was carried out assuming a Boltzman rotational distribution ($T = 495 \text{ K}$)

TABLE V

Observed and Calculated R -Branch Vibronic Transitions for the $(v', v'') = (1, 0)$ Band of the $A' 1-\Sigma^+$ System of ^{107}AgF

Assignment J	R(J) (cm^{-1})		ΔV (cm^{-1}) Obs. - Cal.
	Observed	Calculated	
14	25465.174	25464.945	0.229
15	25466.082	25465.813	0.269
16	25466.731	25466.702	0.029
17	25467.770	25467.613	0.157
18	25468.549	25468.546	0.003
19	25469.457	25469.500	-0.043
21	25471.402	25471.473	-0.071
22	25472.441	25472.492	-0.051
23	25473.350	25473.532	-0.182
28	25479.193	25479.060	0.133
29	25480.232	25480.231	0.001
30	25481.531	25481.423	0.108
31	25482.699	25482.637	0.062
32	25483.740	25483.873	-0.133
33	25484.908	25485.130	-0.222
34	25486.338	25486.409	-0.071
35	25487.768	25487.710	-0.058

for the ground state and the $1-\Sigma^+$ transition pattern (with R , Q , and P branches). The molecular constants for ^{107}AgF given in Table VI were used and no isotope effect was taken into account in the calculation. The agreement of the intensity patterns for the simulation and the LIF spectrum further confirms our electronic assignment to

TABLE VI

Dunham Coefficients for the $A' 1$ State of ^{107}AgF

Y_{jk}	^{107}AgF	$^{109}\text{AgF}^*$
T_e	24950.71(10)	24950.71(10)
$Y_{10} (\Delta G_{1/2})$	506.744(80)	506.041
$Y_{01} (B_e)$	0.28132(15)	0.28054
$Y_{11} (-\alpha_e)$	$-0.4044(89) \times 10^{-2}$	-0.4027×10^{-2}
$Y_{02} (-D_e)$	$-0.116(60) \times 10^{-6}$	-0.115×10^{-6}
$Y_{03} (H_e)$	$-0.403(83) \times 10^{-10}$	-0.400×10^{-10}
$R_e (\text{\AA})$	1.927	1.927

Note. All numbers are in cm^{-1} except for R_e . The numbers in parentheses are 1σ uncertainties.

* The following formulas are used: $B_e' = \rho^2 B_e$, $\alpha_e' = \rho^3 \alpha_e$, $D_e' = \rho^4 D_e$, $H_e' = \rho^6 H_e$, $\omega_e' = \rho \omega_e$, $\omega_e' \chi_e' = \rho^2 \omega_{exe}$, $\rho^2 = \mu/\mu'$, where μ and μ' are the reduced masses of the two isotopes. For ^{107}AgF and ^{109}AgF $\rho = 1.00139$.

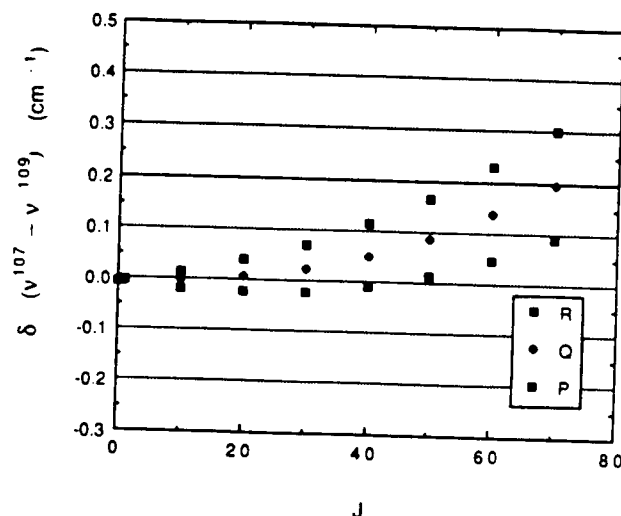
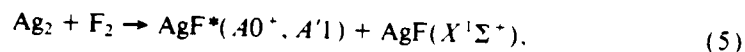


FIG. 5. Isotope splittings of the spectral lines of the $A'1-X^1\Sigma^+(0,0)$ band of ^{107}AgF and ^{109}AgF calculated from the constants given in Table VI and Ref. (23).

the newly observed $A'1$ state. From the Dunham coefficients given in Table VI, an RKR potential energy curve for the $A'1$ state and hence the Franck-Condon factors for the $A'1-X^1\Sigma^+$ system have been calculated. Table VII tabulates the RKR potential energy curve and Fig. 7 indicates the very good agreement between the calculated FCFs and the CL intensity distribution.

DISCUSSION

Since the silver atom-fluorine molecule reaction process $\text{Ag} + \text{F}_2 \rightarrow \text{AgF} + \text{F}$ ($\Delta E = 2.03$ eV) is not exothermic enough to excite the chemiluminescence that we observe in this study, the reactions of silver molecules must lead to the observed emission. For the $\text{Ag}_2\text{-F}_2$ system, the four-center silver dimer-fluorine molecule reaction is considered to be the dominant process.



with an exothermicity of $\Delta E = 2D_0^0(\text{Ag-F}) - D_0^0(\text{Ag-Ag}) - D_0^0(\text{F-F}) = 4.04$ eV (26, 28, 29), producing chemiluminescence corresponding to the $A0^+ \rightarrow X^1\Sigma^+$, $(v', v'') = (0, 0)$ band with a photon energy of ~ 3.62 eV. The much weaker chemiluminescence from the $\text{Ag}_2\text{-F}$ system, observed under considerably more stringent agglomeration conditions, must result from the reaction of a polyatomic silver molecule, the most likely candidate being silver trimer (Ag_3) with its 0.99 eV bond dissociation energy (30). The silver trimer-fluorine atom reaction, with an exothermicity of $\Delta E = D_0^0(\text{Ag-F}) - D_0^0(\text{Ag}_2\text{-Ag}) = 2.65$ eV is not sufficiently energetic to populate the $A'1$ state based strictly on its reaction exothermicity. However, the hot F atom translational energy easily exceeds 0.5 eV (24), the extra energy needed to form the $A'1$ state at 3.10 eV. Finally, it is worth noting that additional silver cluster reactions such as the multicentered

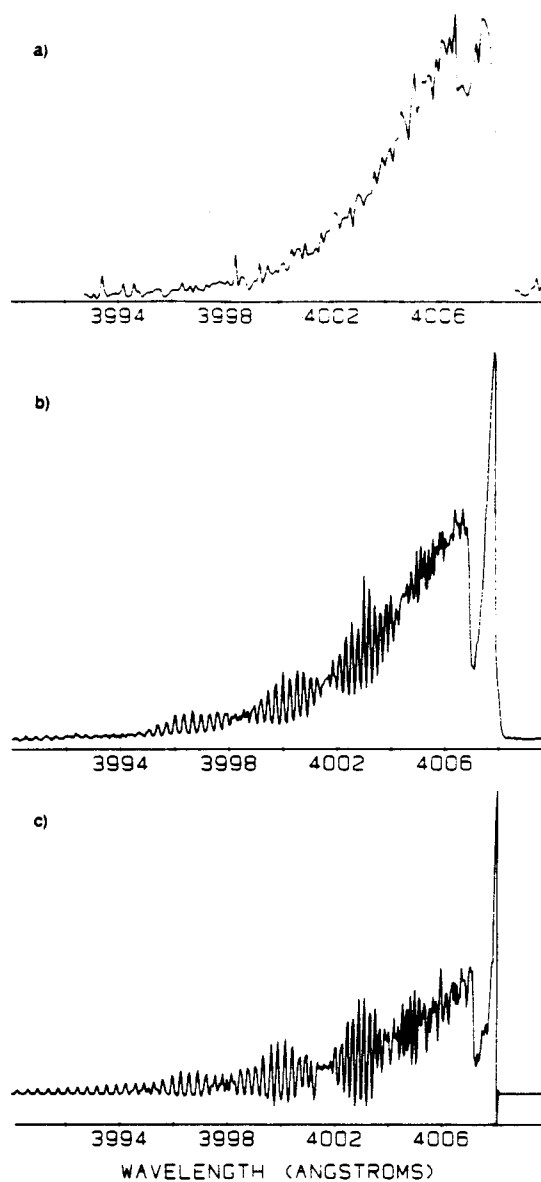
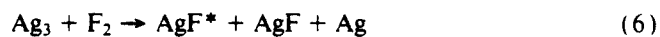


FIG. 6. Comparison between (a) chemiluminescence, (b) laser-induced fluorescence, and (c) computer simulation ($T = 495$ K) of the $A' 1-X' 1\Sigma^+ (0, 0)$ band of AgF.



and



may also be considered as possible precursors to excited AgF products.

By comparing the blue degraded CL spectrum of the $A' 1-X' 1\Sigma^+ (0, 0)$ band given in Fig. 6a with the LIF spectrum in Fig. 6b, we observe that the excited state and the

TABLE VII
RKR Potential Energy Curve of the $A' 1$ State of AgF Derived from the Molecular Constant of ^{107}AgF

v	$B_v (\text{cm}^{-1})$	$G_v (\text{cm}^{-1})$	$R_{v-} (\text{\AA})$	$R_{v+} (\text{\AA})$
0	0.27930	253.372	1.869	1.997
1	0.27525	760.115	1.833	2.056
$R_e = 1.927 \text{\AA}$				

ground state have similar rotational population distributions. This suggests that the product AgF molecules are nearly fully relaxed under our multiple-collision conditions. The rotational simulation shown in Fig. 6c corresponds to a rotational temperature of 495 K and $J_{\text{MAX}} = 25$. The determined rotational temperature, $T = 495$ K, may not be an accurate measure of the thermodynamic temperature since Hund's case (c) mixing effects have not been considered in the calculation. The vibrational temperature is roughly estimated to be 415 K from the LIF intensity ratio of the $(v', v'') = (1, 0)$ and $(2, 1)$ bands shown in Fig. 3b and the calculated Franck-Condon factors.

As we have indicated in the Introduction, the lowest atomic limit of the AgF system ($\text{Ag } ^2S_{1/2} + \text{F } ^2P_{3/2}$) generates two $\Omega = 1$ molecular states, whereas the ($\text{Ag } ^2S_{1/2} + \text{F } ^2P_{1/2}$) combination couples to produce only one $\Omega = 1$ state. In Ref. (23), Barrow and Clements report the observation of a continuum transition centered at 303.0 nm as well as predissociation in the vibronic levels of the $B 0^+$ state of AgF. They attribute the predissociation to the potential curve crossing of the $B 0^+$ state by a repulsive $\Omega = 1$ state, which seems to dissociate to the second atomic limit (Fig. 2 of Ref. (23)). Therefore the newly observed $A' 1$ state reported in this paper can only dissociate to the ground atomic limit. Figure 8 outlines the correlation diagram for the $X^1\Sigma^+$, $A' 1$, $A 0^+$, and $B 0^+$ molecular states and their corresponding atomic dissociation asymptotes. A value of the dissociation energy of the $A' 1$ state, D_e , can be estimated

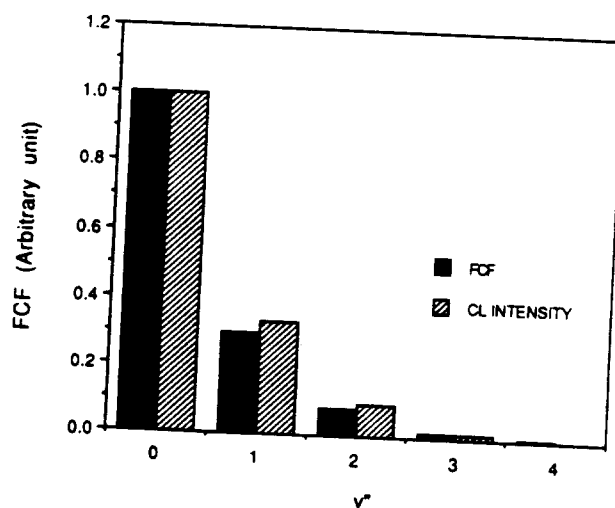


FIG. 7. Comparison between the calculated Franck-Condon factors and the CL intensity distribution for the $A' 1 v' = 0 - X' 1 \Sigma^+ v'' = x$ transitions of AgF.

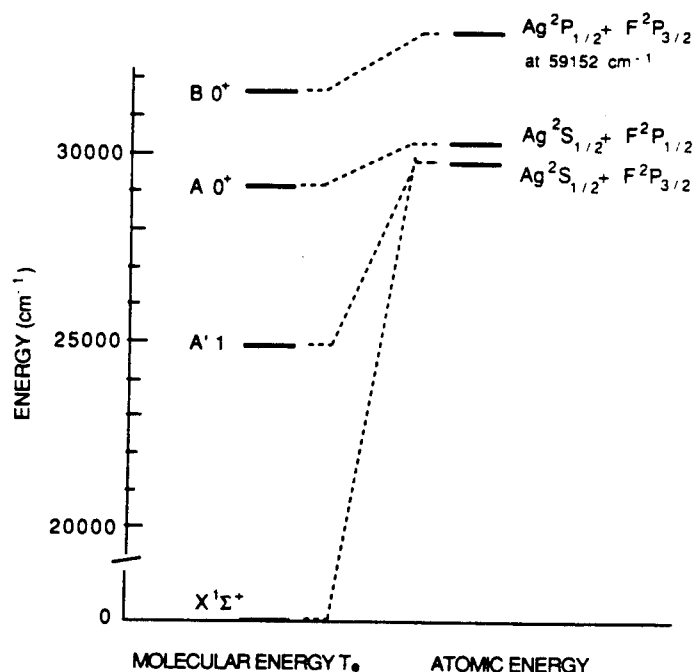


FIG. 8. Correlation diagram of the low-lying molecular states and the corresponding atomic asymptotic limits of the AgF system.

to be $4649 \pm 1400 \text{ cm}^{-1}$ from the thermochemical value, $D^0 = 29\,600 \pm 1400 \text{ cm}^{-1}$ (29) for the AgF ground state.

The observation of the $A' 1$ state of AgF indicates that there may exist similar stable $\Omega = 1$ states for the remaining silver monohalides located a few thousand wavenumbers below the previously known lowest excited $A 0^+$ states. Table VIII summarizes the observed T_e values for the low-lying electronic states of the silver monohalides. In addition to the ground state, the $B 0^+$ state is the only excited state well studied for

TABLE VIII

Summary of the Observed T_e Values of the Low-Lying Electronic States of the Silver Monohalides

	AgF	AgCl	AgBr	AgI
X ¹ Σ ⁺	0	0	0	0
A' 1	24950.71 ^a	-	(-23810 ^d)	-
A 0 ⁺	29220 ^b	-	-	23906 ^c
B 0 ⁺	31663 ^b	31602.65 ^b	31280.43 ^b	31194.06 ^b

^a This work.

^b Data taken from reference 28.

^c Electronic symmetry is not clear.

^d Transitions around 420nm mentioned by Metropolis and Beutler in reference 17. No electronic symmetry is assigned.

the remaining silver monohalide molecules with T_e values smoothly shifted to the red from AgF to AgI. No corresponding stable $A 0^+$ states have been observed for AgCl and AgBr. It should be noted that the electronic symmetry of the A state of AgI listed in Table VIII is unclear (28). This state seems to more closely correlate with the $A' 1$ state rather than the $A 0^+$ state of AgF. With no electronic symmetry assigned, Metropolis and Beutler (17) also mention transitions around 420 nm ($23\,810\text{ cm}^{-1}$) for AgBr which we tentatively associate with the $A' 1$ state in Table VIII. The experimental search for the similar $A' 1$ states of AgCl, AgBr, and AgI is in progress in our laboratory.

CONCLUSION

The $A 0^+$ state has been found not to be the lowest excited electronic state of the AgF molecule as previously indicated in Ref. (28). About 4300 cm^{-1} below the $A 0^+$ state, a stable $A' 1$ state has been observed and rovibrationally analyzed for the first time using the combination of chemiluminescence and pulsed laser-induced fluorescence. The possible existence of similar stable $\Omega = 1$ states for other silver monohalides is predicted. The observation of this $A' 1$ state is also of importance for its possible role as an intermediate state in multiple-resonance laser spectroscopy and multiphoton laser ionization experiments.

ACKNOWLEDGMENTS

We are grateful to Professor R. F. Barrow for his valuable comments and suggestions on this work. H. Wang would like to thank Professor T. C. Devore for helpful discussions on the analysis of the spectrum and Mr. C. B. Winstead for his technical help in the pulsed laser system and the data acquisition system. This work was partially supported by the Army Research Office, the Eastman Kodak Company, and the Air Force Office of Scientific Research through the Strategic Defense Initiative.

RECEIVED: February 12, 1993

REFERENCES

1. J. L. GOLE, in "Advances in Metal and Semiconductor Clusters," Vol. I, "Spectroscopy and Dynamics" (M. A. Duncan, Ed.), pp. 159-209, Jai Press, Greenwich, CT, 1993.
2. (a) R. W. WOODWARD, P. N. LE, M. TEMMEN, AND J. L. GOLE, *J. Phys. Chem.* **91**, 2637-2645 (1987); (b) J. L. GOLE, *Opt. Sci. Eng. Ser.* **8**, 439; (c) T. C. DEVORE, R. W. WOODWARD, AND J. L. GOLE, *J. Phys. Chem.* **92**, 6919-6923 (1988); (d) T. C. DEVORE, J. R. WOODWARD, AND J. L. GOLE, *J. Phys. Chem.* **93**, 4920-4923 (1989); (e) M. J. MCQUAID AND J. L. GOLE, *Opt. Sci. Eng. Ser.* **10**, 687.
3. T. C. DEVORE AND J. L. GOLE, *High Temp. Sci.* **27**, 49-59 (1989).
4. (a) M. MOSKOVITS (Ed.), "Metal Clusters," Wiley-Interscience, New York, 1986; (b) J. L. GOLE AND W. C. STWALLEY, *ACS Symp. Ser.* **179** (1982); (c) J. L. GOLE AND W. C. STWALLEY, *Symp. Faraday Soc.* **14** (1980); (d) M. MORSE, *Chem. Rev.* **86**, 1049-1109 (1986).
5. (a) M. J. MCQUAID, K. MORRIS, AND J. L. GOLE, *J. Am. Chem. Soc.* **110**, 5280-5285 (1988); (b) J. L. GOLE in "Proceedings of the International Symposium on the Physics and Chemistry of Finite Systems: From Clusters to Crystals," NATO ASI Series C: Mathematical and Physical Sciences, Vol. 374, p. 1025, Kluwer Academic, Norwell, MA, 1992; (c) J. L. GOLE, in "Gas Phase Metal Reactions" (A. Fontijn, Ed.), pp. 573-604, Elsevier/North-Holland, Amsterdam/New York, 1992.
6. T. C. DEVORE, J. R. WOODWARD, P. N. LE, J. L. GOLE, AND D. A. DIXON, *J. Phys. Chem.* **94**, 756-760 (1990).
7. S. H. COBB, J. R. WOODWARD, AND J. L. GOLE, *Chem. Phys. Lett.* **143**, 205-213 (1988); **156**, 197-203 (1989).
8. (a) W. H. CRUMLEY, J. L. GOLE, AND D. A. DIXON, *J. Chem. Phys.* **76**, 6439-6441 (1982); (b) W. H. CRUMLEY, Ph.D. Thesis, Georgia Institute of Technology, 1985; (c) S. H. COBB, Ph.D. Thesis, Georgia Institute of Technology, 1988.

9. (a) K. K. SHEN, J. R. WOODWARD, S. H. COBB, J. R. DOUGHTY, AND J. L. GOLE, *SPIE Vol. 1397*, 125-135 (1991). (b) K. K. SHEN, H. WANG, D. GRANTIER, AND J. L. GOLE, in "Proceedings of the 23rd AIAA Plasma-Dynamics and Laser Science Conference," Nashville, TN, pp. 92-2994, 1992.
10. (a) A. BALDERESCHI, W. CZAJA, E. TOSATTI AND M. TOSI, (Eds.), "The Physics of Latent Image Formation in the Silver Halides," World Scientific, Singapore, 1984. (b) T. H. JAMES, Ed., "The Theory of the Photographic Process," MacMillan, New York, 1977. (c) A. MARCHETTI AND J. DEATON, private communication.
11. S. A. MILLER AND E. BENN (Eds.), "Ethylene and Industrial Derivatives," MacMillan, New York, 1977.
12. B. A. BRICE, *Phys. Rev.* **35**, 960-972 (1930).
13. B. A. BRICE, *Phys. Rev.* **38**, 658-669 (1931).
14. F. A. JENKINS AND G. D. ROCHESTER, *Phys. Rev.* **52**, 1141-1143 (1937).
15. R. S. MULLIKEN, *Phys. Rev.* **51**, 310-332 (1937).
16. N. METROPOLIS, *Phys. Rev.* **55**, 636-638 (1939).
17. N. METROPOLIS AND H. BEUTLER, *Phys. Rev.* **55**, 1113-1113 (1939).
18. L. C. KRISHER AND W. G. NORRIS, *J. Chem. Phys.* **44**, 391-394, 974 (1966).
19. E. PEARSON AND W. GORDY, *Phys. Rev.* **152**, 42-45 (1966).
20. J. HOEFT, F. J. LOVAS, E. TIEMANN, AND T. TORRING, *Z. Naturforsch., A* **25**, 35-39 (1970).
21. M. M. JOSHI AND D. SHARMA, *Indian J. Pure Appl. Phys.* **1**, 86 (1963).
22. R. M. CLEMENTS AND R. F. BARROW, *Chem. Comm. No. 1254*, 27-28 (1968).
23. R. F. BARROW AND R. M. CLEMENTS, *Proc. R. Soc. London A* **322**, 243-249 (1971).
24. T. C. DEVORE, L. BROCK, R. KAHLSCHEUER, K. DULANEY, AND J. L. GOLE, *Chem. Phys.* **155**, 423-433 (1991); T. C. DEVORE AND J. L. GOLE, submitted for publication.
25. T. C. DEVORE, R. KAHLSCHEUER, D. A. DIXON, AND J. L. GOLE, submitted for publication.
26. G. HERZBERG, "Molecular Spectra and Molecular Structure." Vol. I. "Spectra of Diatomic Molecules," Second ed., Robert E. Krieger, Malabar, 1989.
27. J. L. DUNHAM, *Phys. Rev.* **41**, 721-731 (1932).
28. K. P. HUBER AND G. HERZBERG, "Molecular Spectra and Molecular Structure IV: Constants of Diatomic Molecules," Van Nostrand-Reinhold, New York, 1979.
29. K. F. ZMBOV AND J. L. MARGRAVE, *J. Phys. Chem.* **71**, 446-448 (1967).
30. K. HILPERT AND K. A. GINGERICH, *Ber. Bunsenges. Phys. Chem.* **84**, 739-745 (1980).

APPENDIX XIV

"Raman Pumping in the Absence of an External Light Source", D. Grantier, and J. L. Gole, J. Phys. Chem. Letters, 98, 7427 (1994).

Raman Pumping in the Absence of an External Light Source

David R. Grantier and James L. Gole*

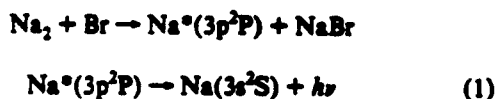
School of Physics, Georgia Institute of Technology, Atlanta, Georgia 30332

Received: April 4, 1994*

The first observation of a chemically enhanced resonance Raman pumping process, observed in the absence of an external light source, is reported. In an extended path length reactive environment, sodium dimer molecules are Raman pumped by radiation from the Na D-line produced by the reaction of additional dimer molecules with bromine atoms. The observed Raman spectrum would appear to result from much more than a simple light scattering process.

Introduction

Recently, we have been concerned with the reactions of small supersonically cooled sodium molecules with halogen atoms ($\text{Na}_2 + \text{X} \rightarrow \text{Na}^*_{n-1} + \text{NaX}$; $\text{X} = \text{Cl}, \text{Br}, \text{I}, n = 2, 3$).^{1,2} These reactions have been shown to demonstrate gain on transitions involving the electronically excited Na_2 products of the $\text{Na}_2 + \text{Br}$ reaction.^{3,4} In an extension of these experiments, focused on the development of a long path length amplifying medium employing slit source based supersonic expansions, we have observed the first resonance Raman pumping generated in a purely chemical reactive environment. The observations made in the present study bear a close analogy to those of Wellegehausen,^{5,6} Bergmann,⁷ and co-workers in their analysis of optically pumped sodium dimer lasers operative on a stimulated Raman scattering process. Here, however, we observe a series of Raman-like Stokes and anti-Stokes features which (1) are associated with the lowest vibrational levels of Na_2 , (2) correlate with a scattering process involving the Na D-line components ($\text{Na } 3p^2P_{3/2,1/2} \rightarrow 3s^2S_{1/2}$) created in the chemical reaction sequence



(3) are not readily generated by light scattering due to an external laser light source, and (4) appear to be enhanced by the environment of the reaction zone itself. The D-line emission is scattered by cooled sodium dimers (Na_2) formed, as a result of supersonic expansion, in the lowest vibrational levels of the Na_2 ground electronic state. Multiple Stokes and anti-Stokes features assigned as resonance Raman progressions are well simulated on the basis of the resonance Raman theory outlined by Rousseau and Williams⁸ and others.⁹ The results of initial gain studies, in which amplification has been observed on many of the Stokes and anti-Stokes components of the Raman spectrum, are suggestive of a stimulated Raman scattering process similar to that associated with optically pumped alkali dimer lasers. However, the scattering line width Γ associated with the present process is determined to be close to 4 cm^{-1} . These results suggest an unusually fast resonance Raman scattering process which appears to be chemically enhanced.

Experimental Section

The apparatus which we have used to generate high sodium fluxes in supersonic expansion from an extended slit source is described in detail elsewhere.^{10,11} A dual oven (large capacity ($\sim 350 \text{ g}$) stagnation chamber and frontal nozzle expansion channel) system has been designed to produce a supersonic flux

of alkali vapor through a slit nozzle approximately 0.003 in. wide by 2 in. in length. The slit is formed from two sheets of 0.005 in. tantalum prepared, mounted, and sandwiched between frontal and rear nozzle sections. The precise width of the created tantalum slit is adjusted to 0.003 in. under a Vickers microscope and verified for accuracy (across the length of the slit) using single slit diffraction techniques.

The rear stagnation chamber (850–900 K) and frontal nozzle expansion channel (900–950 K) are heated independently. Expansion from the slit source produces a near planar flux (slight divergence) at the reaction region consisting primarily of sodium atoms and internally cooled dimers.¹¹ In the reaction region, the sodium flux is intersected at variable angles from above and below by two diverging but nearly planar bromine atom flows emerging also from slits machined into graphite tube furnaces^{10,11} operated at temperatures¹² $T > 1700 \text{ K}$ necessary to ensure a greater than 95% conversion of bromine molecules to bromine atoms. At the significant reactant fluxes necessary to generate a strong Raman scattering signal, the absolute number density of bromine atoms in the reaction zone is conservatively estimated¹⁰ at between 10^{14} and 10^{15} cm^{-3} whereas the absolute number density of sodium dimers in the reaction zone may exceed 10^{16} cm^{-3} .

The optical signature of the long path length sodium molecule-bromine atom reaction zone is focused onto the entrance slit of a SPEX 1704 scanning monochromator coupled to an RCA 1P28 photomultiplier tube (PMT). The PMT is maintained at $\sim 1000 \text{ V}$, and the response current is sent through an IEEE interfaced autoranging picoammeter (Keithley) to an IBM compatible AT class microcomputer.

We have also attempted, unsuccessfully, to reproduce the Raman signal created following the reaction sequence (1) by resonantly pumping the supersonically expanded sodium dimers with external laser light. Intensity stabilized broad-band (multimode) laser light ($\sim 1 \text{ W}$) from an argon ion laser (Spectra Physics, Model 171) at 4765 and 4880 Å and dye laser light ($\sim 100 \text{ mW}$) at 5890 and 5896 Å (argon ion pumped R6G) was frequency chopped and passed through the reaction zone in an effort to generate a Raman scattering signal similar to that observed from the chemical reaction pumping. The frequency content of the emergent beam was again monitored with a monochromator-PMT combination. The PMT response, detected with a phase-sensitive amplifier, was digitized and stored in an IBM AT class microcomputer.

In addition to those experiments outlined, an optical configuration similar to the ingenious design of Roll and Mentel¹³ was constructed about the extended Na_2 -Br reaction zone and used to measure optical gain on several of the observed features depicted in Figure 1. These gain measurements are discussed in more detail elsewhere.¹⁰

* Abstract published in *Abstracts ACS Abstracts*, July 15, 1994.

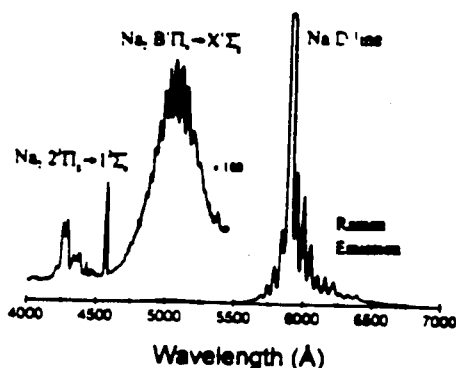


Figure 1. Survey spectrum of chemiluminescent emission and Raman scattering from various electronic states of diatomic sodium. The Na_2 $2^1\Pi_g \rightarrow 1^1\Sigma_g^+$ transition corresponds to a triplet-triplet bound-free excimer-like emission process (resolution ~ 12 Å, $T_{\text{exc}} \sim 875$ K, $T_{\text{trans}} \sim 935$ K).

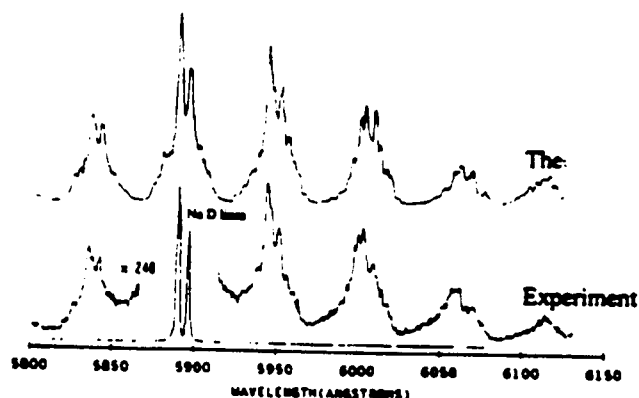


Figure 2. Raman-like spectrum taken at a resolution of ~ 1.5 Å ($T_{\text{exc}} \sim 875$ K, $T_{\text{trans}} \sim 935$ K) depicting the two Na D-line components and the satellite Raman structure. The spin-orbit frequency difference of the two Na D-line components is reproduced in the scattered radiation. A simulated spectrum (calculated from eq 2) is presented for comparison ($T_{\text{rot}} \sim 400$ K, $\Gamma = 4$ cm $^{-1}$). See text for discussion.

Results and Analysis

There are several near-resonant rovibronic transitions associated with the $X^1\Sigma_g^+$ and the $A^1\Sigma_g^+$ states of Na_2 ,¹⁰ and the atomic emission from the Na D-lines, ω_{P1} and ω_{P2} ($2P_{3/2} \rightarrow 2S_{1/2}$ at 16 973.379 cm $^{-1}$ and $2P_{1/2} \rightarrow 2S_{1/2}$ at 16 936.183 cm $^{-1}$).¹⁴ We suggest that these near resonances are responsible, in large part, for the unusually intense optical signature depicted in Figure 1.

The spectrum in Figure 1 was taken at a resolution of ~ 12 Å. The relative intensity of the strong sodium dimer $B \rightarrow X$ chemiluminescence to the even stronger Raman-like emission features symmetrically surrounding the Na D-line is readily apparent. The frequency separation between adjacent Stokes (anti-Stokes) features corresponds closely to 155 cm $^{-1}$, correlating with the separations between the lowest sodium dimer ground-state vibrational levels. Despite considerable effort, we have found that these features cannot be made to fit a resonance fluorescence series but can be readily assigned to Stokes and anti-Stokes bands associated with a resonance Raman progression.¹⁰

Additional evidence suggestive of a Raman process is presented in Figure 2. The spectrum depicted in Figure 2 was taken under equivalent reaction zone conditions to those of the spectrum depicted in Figure 1. The intermediate resolution, ~ 1.5 Å, at which this spectrum was obtained is sufficient to clearly resolve the atomic sodium $2P_{3/2} \rightarrow 2P_{1/2}$ component splitting (~ 17.2 cm $^{-1}$) while leaving individual rotational lines unresolved. The relative intensities of each of the sodium D-line components are clearly evident in the scattered Raman emission. Furthermore, the frequency separation of the atomic line component splitting is clearly reproduced (within the experimental resolution of the scan) for both the vibrational Stokes and anti-Stokes components of the scattering.

We have successfully modeled the group of features symmetrically surrounding the Na D-line with the resonant Raman intensity expression⁸⁻¹⁰

$$I_s(\nu_G, \nu_G; \nu_P, \nu_P) = \frac{32\pi^2 \omega_i^4 I_P}{9c^4 \hbar^2} M(\xi_0)^4 e^{-\Delta E_0(J_0 + 1)\hbar c/kT} N(\nu_G) \times \sum_{\alpha, \beta} \left(3S_{J_\alpha} S_{J_\beta} \frac{|\langle \nu_P | p_1 \rangle \langle \nu_P | p_0 \rangle|^2}{(\omega_{G1} - \omega_{P1})^2 + \Gamma^2} + 2S_{J_\alpha} S_{J_\beta} \frac{|\langle \nu_P | p_1 \rangle \langle \nu_P | p_0 \rangle|^2}{(\omega_{G1} - \omega_{P2})^2 + \Gamma^2} \right) \quad (2)$$

where I_s is the total intensity for a scattered Stokes or anti-Stokes line as a function of frequency, ω , and pump intensity, I_P , and c is the speed of light. We consider transitions from an initial rovibrational ground electronic state of the Na_2 molecule labeled G to some final rovibrational electronic ground state labeled F through an intermediate excited electronic state labeled I where ω_{G1} and ω_{P1} represent the rovibronic energy difference between the G and I and I and F levels, and Γ refers to the line width arising from all damping phenomena. The S_J terms correspond to the appropriate Hönl-London factors for the Na_2 $A^1\Sigma_g^+ \rightarrow X^1\Sigma_g^+$ transition.¹⁰ $M(\xi_0)$ represents the electronic matrix element, expressed as a function of the normalized nuclear coordinate, $\xi = R(\mu\omega/\hbar)^{1/2}$, and $\langle \nu_P | p_1 \rangle$ and $\langle \nu_P | p_0 \rangle$ represent Franck-Condon overlap integrals. We have included a thermalized ground-state rotational distribution and a ground-state weighting function $N(\nu_0)$, which represents the deviation from a Boltzmann distribution. We also allow pumping due to each component of the sodium D-line ($\omega_{P1}(2P_{3/2})$ and $\omega_{P2}(2P_{1/2})$) to contribute to the scattered emission intensity, I_s . Here, the $2P_{3/2} \rightarrow 2P_{1/2}$ intensity weighting resulting from the reaction populated D-line components is 3:2, as determined from the experimental spectrum.

Numerical calculations¹⁰ were carried out by allowing the near-resonant atomic sodium transitions, ω_{P1} and ω_{P2} , appropriately broadened, to pump the first 30 levels in the Na_2 $X^1\Sigma_g^+$ state to the first 70 levels of the Na_2 $A^1\Sigma_g^+$ state. Deexcitation from the upper electronic state was allowed to proceed to the first 30 levels of the ground state. Rotational levels $J'', J' = 0-120$ were included with each vibrational level of both the excited electronic $A^1\Sigma_g^+$ state and the ground electronic $X^1\Sigma_g^+$ state of the sodium dimer scatterer. Each simulated spectrum produced in the modeling program was convolved with a Gaussian function to approximate the effects of a finite spectrometer slit width.¹⁰

The data in Figure 3 depict the fit to the vibrational structure surrounding the Na D-line under conditions of pure sodium expansion. All attempts to extract a vibrational temperature through comparison of the observed and calculated Raman spectra were unsuccessful. The low-resolution (~ 12 Å) vibrational Raman spectrum depicted in Figure 3 does not correspond to a thermalized vibrational distribution. The calculated spectrum in Figure 3, corresponding to a non-Boltzmann vibrational distribution, closely matches the experimental scan and also provides a consistent fit to higher resolution spectra. Although the rotational population distribution may also be non-Boltzmann, we find that with an effective rotational temperature of 400 K we are able to obtain a close agreement between the experimental and calculated spectrum depicted in Figure 4. This suggests that only slight modifications from a thermalized distribution will be necessary to exactly fit the rotational features. We need consider elsewhere that there are several possible sources for the deviation of the Raman scattering features, depicted in Figure 3, from a thermalized vibrational distribution.¹⁰

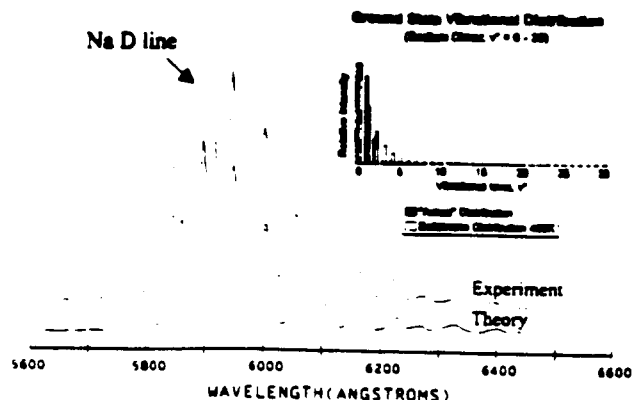


Figure 3. Comparison of experimental spectrum with computer-modeled distribution (resolution ~ 5 Å, $T_{\text{exc}} \sim 875$ K, $T_{\text{amb}} \sim 935$ K). Optimum agreement between calculation and experiment was found for the slightly nonthermal distribution depicted in the upper right-hand corner of the figure. A Boltzmann distribution at 400 K is included for comparison. See text for discussion.

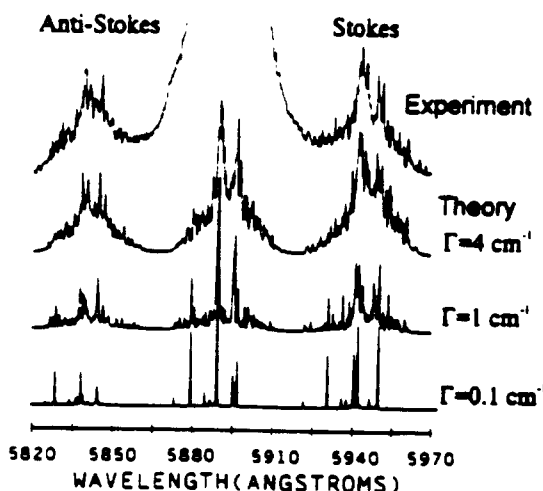


Figure 4. High-resolution spectrum (~ 0.5 Å) and simulated spectra for $\Gamma = 0.1$, 1, and 4 cm^{-1} demonstrating the marked improvement in the fit to the experimental Raman-like features for increasing values of Γ . See text for discussion.

A still higher resolution scan (~ 0.4 Å) of the first Stokes and anti-Stokes features is depicted and computer simulated in Figure 4. The computer simulation is again based on the application of eq 2. In a surprising result, we find that a line width $\Gamma \sim 4$ cm^{-1} is required to provide optimum agreement between the simulated and experimental results with correlation coefficients exceeding 0.92 for the anti-Stokes and 0.89 for the Stokes features, respectively. A further confirmation of the required line width is also indicated in Figure 4 where we compare the experimental spectrum to $\Gamma = 4$ -, 1-, and 0.1- cm^{-1} simulations based on eq 2.

While there are improvements that can be made in the simulations depicted in Figure 4, it is unlikely that simple power broadening can be responsible for the large effective line width indicated by our spectral simulations. On the basis of the required power broadening for a two-level quantum system driven at resonance, we estimate that an electric field of ~ 1.3 kV/cm and an absolute power density of ~ 0.215 MW/ cm^2 are necessary to produce the requisite spectral broadening of 4 cm^{-1} .

The apparent ~ 4 - cm^{-1} spectral broadening suggests the possibility of a scattering lifetime of order 10^{-11} s, implying a process which is considerably more efficient than would be expected on the basis of resonance Raman pumping involving the Na_2 A-X transition ($\sim 10^{-8}$ s based on the radiative lifetime¹⁵). Several additional experiments involving the direct pumping of the sodium expansion in the absence of bromine atom reactant at the Na D-line frequencies (argon ion pumped R6G) and at 4765 and 4880 Å using a multimode argon ion laser failed to

reveal optical signatures corresponding to those depicted in Figures 1–4. In fact, while it was possible to excite laser-induced fluorescence corresponding to the Na_2 A-X and B-X band systems analogous to that observed previously,¹⁶ although at somewhat higher temperatures in the present experiments, no clear Raman features were generated. This result also suggests a more efficient process than that associated with resonance Raman pumping.

These results suggest that we have observed more than a "simple" Raman-like scattering process. We might consider a further long-range interaction of the electronically excited sodium $3p^2P$ atoms with those Na_2 molecules which are Raman pumped, an interaction of the Na_2 molecules with the Br atoms that induces a time-varying enhancement of the dimer polarizability (hyperpolarizability) or (less likely) the presence of a large electric field created due to the reactive environment in the vicinity of the reaction zone. It would appear that this interaction or perturbation leads to a much more efficient Raman-like scattering process and appears to demonstrate a stimulated Raman gain condition.¹⁰

While further experiments will be necessary to clarify the mechanism for the scattering process, the long path length reaction zone employed in these experiments appears to have revealed the manifestation of a significant cooperative phenomena. The moderate Rydberg character of the Na $3p^2P$ excited state, with its diffuse electron density, may, in fact, lend itself to a considerable long-range interaction inducing cooperative effects. The assessment of these cooperative effects awaits further study.

Acknowledgment. The authors gratefully acknowledge the helpful comments of Professors Ron Felton and Michael Heaven and Dr. Kangkang Shen. Helpful comments and technical assistance from Mr. C. B. Winstead is also greatly appreciated. The support of the Georgia Tech Foundation through a grant from Mrs. Betty Peterman Gole, the Army Research Office through the Short Term Innovative Research Program, the Air Force Office of Scientific Research, and the Army Research Office and AFOSR/SDIO is greatly appreciated.

References and Notes

- (1) Cramley, W. H.; Gole, J. L.; Dixon, D. A. *J. Chem. Phys.* 1982, 76, 6439.
- (2) (a) Gole, J. L. The Unique Nature of Metal Cluster Oxidation. In *Physics and Chemistry of Finite Systems: From Clusters to Crystals*; Jena, P.; Khanna, S. N.; Rao, B. K., Eds.; NATO ASI Ser. Vol. II; 1992; p 1025. (b) Gole, J. L. Toward the Modeling of the Oxidation of Small Metal and Metalloid Molecules. In *Gas Phase Metal Reactions*; Fontijn, A., Ed.; North-Holland: Amsterdam, 1992; pp 578–604. (c) Gole, J. L. The Unique Complexation and Oxidation of Metal-Based Clusters. In *Advances in Metal and Semiconductor Clusters*; Duncan, M. A., Ed.; JAI Press: London, 1993; Vol. 1, pp 159–209.
- (3) Cobb, S. H.; Woodward, J. R.; Gole, J. L. *Chem. Phys. Lett.* 1989, 156, 197.
- (4) "Chemically Driven Pulsed and Continuous Visible Laser Amplifiers and Oscillators", with K. K. Shen, H. Wang, and D. Grantier; Invited Talk, Proceedings of the 23rd AIAA Plasma Dynamics and Laser Science Conference, Nashville, Tennessee, AIAA 92-2594, 1992.
- (5) Wellenhausen, B. *IEEE J. Quantum Electron.* 1979, 15, 1108.
- (6) Wellenhausen, B. In *Metal Bonding and Interactions in High Temperature Systems with Emphasis on Alkali Metals*; ACS Symp. Ser. 179; Gole, J. L.; Stwalley, W. C., Eds.; American Chemical Society: Washington, DC, p 462.
- (7) Gushatz, U.; Menantz, H.; Heftner, U.; Colomb de Daunant, I.; Bergmann, K.; Jonas, P. L. *J. Opt. Soc. Am.* 1989, 6, 1386.
- (8) Rousseau, D. L.; Williams, P. F. *J. Chem. Phys.* 1976, 64, 3519.
- (9) See, for example: Tang, J.; Albrecht, A. C. In *Raman Spectroscopy*; Szymanski, H. A., Ed.; Plenum: New York, 1970; Vol 2, pp 33–68. Albrecht, A. C. *J. Chem. Phys.* 1961, 34, 1476.
- (10) Grantier, D. R.; Gole, J. L. Chemically Enhanced Raman Scattering, to be submitted for publication.
- (11) Grantier, D.; Wang, H.; Winstead, C. B.; Gole, J. L. Proceedings of the 24th AIAA Plasma Dynamics and Lasers Conference, Orlando, FL, AIAA 93-3207, 1993.
- (12) Cobb, S. Ph.D. Thesis, Georgia Institute of Technology, Atlanta, GA, 1988.
- (13) Rall, G.; Mental, J. *J. Phys. D: Appl. Phys.* 1989, 22, 483.
- (14) Moore, C. E. *Atomic Energy Levels*; National Bureau of Standards: Washington, DC, 1949.
- (15) Zemlin, W. T.; Verma, K. K.; Vu, T.; Stwalley, W. C. *J. Mol. Spectrosc.* 1981, 85, 150.
- (16) Gole, J. L.; Green, G. J.; Pace, S. A.; Preuss, D. R. *J. Chem. Phys.* 1982, 76, 2247.

APPENDIX XV

"The Expansion of Small Molecule Configuration Space: Highly Efficient Long Range Stabilization and Energy Transfer Involving Electronically Excited States", D. R. Grantier, and J. L. Gole, High Temp. Science, in press.

The Expansion of Small Molecule Configuration Space:
Highly Efficient Long Range Stabilization and Energy Transfer Involving
Electronically Excited States

James L. Gole and David R. Grantier

School of Physics
Georgia Institute of Technology
Atlanta, Georgia 30332

Abstract

Highly efficient long range interactions in high temperature reactive environments are exemplified with two studies. A combination of single and multiple collision chemiluminescent studies has been used to (1) demonstrate the highly efficient collisional stabilization of electronically excited Group IIA dihalide collision complexes formed in direct $M + X_2 \rightarrow MX_2$ reactive encounters, (2) delineate the first direct evidence for symmetry constraints associated with dihalide formation in the $M + X_2$ insertion process, and (3) obtain the first discrete emission spectra for these dihalide complexes. A demonstrated collisional stabilization not readily explained within the RRKM framework suggests that new models will be necessary to explain the efficient interaction of electronically excited states. Information provided on the efficient stabilization of excited state intermediate complexes defines a much broader range of interaction than has typically been associated with collisional stabilization phenomena. The importance of long range interactions is further demonstrated by the first observation of a chemically enhanced stimulated resonance Raman pumping process, observed in the absence of an external light source. In an extended path length reactive environment, sodium dimer molecules are Raman pumped by radiation from the Na D-line produced by the reaction of additional dimer molecules with bromine atoms. The observed Raman spectrum would appear to result from much more than a simple light scattering process. The demonstrated interaction ranges and the enhanced interaction of high temperature molecules in general have direct implication for the understanding of molecular formation and energy transfer in the high stress environments which include combustors and high impulse propulsion systems.

INTRODUCTION

It is a pleasure to contribute this paper to the Margrave Symposium Volume of High Temperature Science. John Margrave has demonstrated an amazing versatility in the scientific problems with which he has been involved. In a very strong sense this is reflected in the diversity of students both graduate and undergraduate which have matriculated in his laboratory and whose interests and pursuits range from inorganic synthesis to fundamental problems in chemical physics. The symposium in his honor at Rice University on April 29, 1994 brought together many old friends and produced some very interesting tales.

This paper discusses topics which relate to the enhanced interactions characteristic of high temperature reactive environments. The storage and efficient conversion of the energy generated in (1) the products of highly exothermic reactive processes, (2) highly dense plasma-like reactive environments, and (3) the non-equilibrium laser based stimulated emission process can be influenced by similar although sometimes complex mechanisms. The realization of the potential conversion efficiency of these systems requires that we identify overriding factors associated not only with chemical reactivity but also with poorly understood energy transfer and stabilization processes.

Through a series of unique coupled experiments¹⁻⁸ spanning a seven decade pressure range from the near "single collision" pressure regime associated with the nascent products of chemical reaction to the moderate pressure diffusion flame environment, we observe the clear manifestation of long range energy transfer and stabilization. We suggest that the processes of interest may influence the dynamics of reactive interaction and energy pooling in combustion, propulsion, plasma, and laser environments, by utilizing the substantial configuration space encompassed by a diffuse excited state electron density. There have been few concerted efforts to assess and model these efficient pathways which we exemplify by outlining two ongoing studies involving (1) an evaluation of the extremely efficient radiative three body collisional stabilization of Group IIA atom (Ca, Sr, Ba)-halogen molecule reactive encounters leading to dihalide excited state formation and (2) the first chemically induced Raman pumping of a diatomic molecule in the absence of an external light source.

SYMMETRY CONSTRAINED DYNAMICS OF GROUP IIA DIHALIDE FORMATION

The transformation from covalent to ionic bonding and its influence on molecular electronic structure and reaction dynamics has long been fundamental to our understanding of chemistry, attracting the interest of chemists and chemical physicists alike.⁹ The reactions which form the Group IIA dihalides can be studied to provide insights for our understanding of these transformations and the nature of intermediate complex formation as strong ionic chemical bonds are formed. Through a series of selected preliminary experiments, we have obtained a wealth of evidence which casts new light on the dynamics of Group IIA dihalide formation via Group IIA metal-halogen molecule reactions. Further, we identify a symmetry constrained dynamics associated with the electron jump harpooning process and the formation of long-lived MX_2 ionic complexes where M corresponds to the Group IIA metal ($M=Ca, Sr, Ba$) and X to a halogen atom ($X=Cl, Br, I$). These complexes, while forming via a direct $M + X_2$ insertion reaction, are subject to a highly efficient collisional stabilization which may well exemplify the extended range of interaction (cross section) characteristic of many high temperature molecules.²⁻⁵ The controlled collisional relaxation of the Group IIA dihalide excited states has now produced the first discrete spectroscopic data on the low-lying and ground states of these highly ionic high temperature molecules, greatly aiding mechanistic interpretation. The results which we outline suggest that the study of these systems will provide an abundance of both dynamic and spectroscopic information, providing an opportunity for the systematic study of chemical and structural properties as they influence both reactivity and molecular electronic structure and leading to detailed periodic correlations which are basic to chemistry.

The Group IIA dihalides have been studied extensively by Hildenbrand¹⁰ who has used an astute combination of mass spectrometric data and a variety of structural estimates to evaluate the validity of ionic models. As Table I demonstrates, the IIA halides are unusual in that the strength of the second halogen bond is at least comparable to or considerably greater than that of the first. In other words, the atomization energy, especially of the heavier halogen dihalides, is at least twice the dissociation energy of the metal monohalide. This bonding characteristic suggests that the Group IIA-halogen molecule reactions might present ideal systems in which to study few body

complexation processes and hence the efficient collisional stabilization of intermediate complexes. Further, any spectroscopic data obtained on the dihalides, in combination with a firm thermochemical base, furnishes an important link to further refine the extent and validity of the ionic models which Hildenbrand¹⁰ and others¹¹ have developed to aid our understanding of high temperature chemistry. Within the framework of modeling reactivity and structure, the Group IIA metal reactions offer a wide range of atomic size as well as change in ionization potential and electron affinity. Their diversity far exceeds that of the much simpler alkali metals, yet they are sufficiently simple so as to render detailed modeling both useful and definitive.

A Clarification of Historical Perspective

The reactions of Group IIA metal atoms and halogen molecules have been studied under near single collision conditions in low pressure (10^{-6} - 10^{-4} Torr) beam-gas or beam-beam environments by a number of researchers. The analysis of their experimental results has been both controversial and ever-evolving. As first observed by Jonah and Zare¹², for the Ba + Cl₂ reaction (Fig. 1), the Group IIA metal (M=Ca,Sr,Ba)-halogen molecule ($X_2 = \text{Cl}_2, \text{Br}_2, \text{I}_2$) reactions produce a broad structureless emission feature (see Figs. 1,2) spanning the near ultraviolet and visible regions. Jonah and Zare initially attributed this feature to a two-body ($M + X_2$) radiative association viz.



first order in the Group IIA metal and halogen molecule. However, Wren and Menzinger¹³ soon revealed a quadratic dependence of the light emission on oxidant pressure. This second order oxidant pressure dependence, dominating at pressures as low as 3×10^{-6} Torr, appeared to signal the presence of a three-body radiative recombination process.



under conditions generally identified with the single collision pressure regime. Here the dagger signifies that the MX_2 species is formed at energies above its dissociation limit, however, the partitioning of the available energy into internal excitation and product translational motion is not

specified.⁷

In invoking mechanism (2), Wren and Menzinger¹³ thus suggested a very efficient collisional stabilization process operative in the micro-torr region, involving a collision complex of some considerable extent. The viability of an enhanced interactive range of electronically and/or highly vibrationally excited species is supported by recent studies of energy transfer collisions with the excited states of high temperature molecules.²⁻⁵ However, Rosano and Parson¹⁴ noted that (within an RRKM framework), in order for step (2b) to be significant, the quasibound MX_2 would have to have an unusually long lifetime, $\sim 10^{-5}$ s at 10^{-5} Torr; if its lifetime is estimated to be on the order of a molecular vibration, $\sim 10^{-13}$ s, the pressure would have to be on the order of an atmosphere. The results which we outline in following sections would suggest that these arguments, while soundly based, require modification as the reactions of interest are characterized by a much broader range of complex interaction.

In the absence of additional information, the considerations outlined above lead Menzinger,¹⁵ Rosano and Parson,¹⁴ and Engelke¹⁶ to conclude that the third order dependence for MX_2^* formation must be due exclusively to two sequential harpooning processes



involving¹⁵ highly vibrationally excited ground state $MX(X^2\Sigma^+)$. To support this mechanism these authors have noted the small amount of product recoil for step (3a))¹⁴ and the "apparent" insensitivity of the MX_2^* emission to addition of a nonreactive buffer gas.¹⁵ Further, in pointing out the established "known" validity of mechanism 2, Menzinger¹⁵ has also argued that the low ionization potential for $MX(X^2\Sigma^+)$ (slightly below that of the metal atom¹⁷ and decreasing for vibrationally excited MX) establishes that reaction (3(b)) corresponds to a more efficient electron jump process than reaction (3(a)).

Although the arguments of Rosano and Parson favoring mechanism (3), focused on the MX_2 excited state radiative lifetime, can be compelling, they result, in large part, from a misconception¹⁶ concerning the nature of the lowest energy dihalide excited electronic states. It is likely that at least the lowest-lying dihalide transition (A-X band system) does involve a long-

lived, $\tau_{\text{rad}} \geq 10^{-5}$ sec, excited electronic state.⁷ Therefore, provided that bound excited state levels are populated (which the extent of the emission continua in Figures 1 and 2 suggest and which multiple collision relaxation studies confirm), the collisional stabilization of a long-lived electronically excited dihalide emitter is possible. However, this is a requirement which becomes less stringent if the formed Group IIA dihalide complex is capable of interaction over a much longer range.⁷

Periodicity of Group IIA Dihalide States

Klemperer et al.¹⁸, using the technique of electric quadrupole deflection of molecular beams, determined the grid of dihalide geometries outlined in Table II. This table demonstrates clear trends as linear geometries are favored by the light metal-heavy halogen combination whereas bent structures are favored by the heavy metal-light halogen combination. These geometric trends can be explained¹⁹⁻²² on the basis of a modification of Walsh's correlation diagrams for AB_2 type molecules to take into account the influence of normally unfilled d orbitals on the metal atom. The IIA-dihalides are predicted to be strictly linear if described using only s and p orbitals within the Walsh framework. The strongly ionic character of the Group IIA dihalides also leads to important modifications of the Walsh-type diagram.²³

Figure 3 corresponds to a molecular orbital correlation diagram for BeF_2 .²³ Here we plot valence orbital energy as a function of bond angle. The orbital occupation for the ground state of BeF_2 is complete through the π_g orbital (16 valence electrons). It is clear that the sum of the valence orbital energies leads to the prediction of greatest stability for a bond angle of 180° .

The makeup of the valence molecular orbitals in BeF_2 has been discussed²³ and comparisons of the BeF_2 correlation diagram (Figure 3) with Walsh's valence molecular orbital diagram for CO_2 have been made. For our purposes, it is important to note that the lowest energy excited states in BeF_2 are predicted to result from transitions involving the highest occupied $\pi_g(b_2)$ and $\pi_g(a_2)$ molecular orbitals of the ground state to the lowest unoccupied $\sigma_g(a_1)$ molecular orbital. This is in contrast to the case of CO_2 where experiments have confirmed Walsh's prediction that the lowest energy transitions are from the $\pi_g(b_2)$ and $\pi_g(a_2)$ molecular orbitals to the $\pi_u(a_1)$

molecular orbital. This predicted change in the ordering of the $\pi_u(a_1)$ and $\sigma_g(a_1)$ orbitals for BeF_2 and CO_2 suggests that the lowest energy transitions in BeF_2 and, for that matter, several of the remaining Group IIA dihalides, should be quite weak in absorption since a $(g \rightarrow g)$ transition is electric dipole forbidden for the linear molecule. In fact, the lowest energy HOMO-LUMO transition (analog of $A^1\pi_g - X^1\Sigma_g^+$ for the linear dihalide) has not been observed even in attempted studies of the absorption spectrum for the highly bent BaF_2 molecule. Researchers have been lead to believe²⁴ that the absorption spectra for these inherently high temperature molecules cannot be obtained and studied; however, the experimental results which we discuss in the following sections demonstrate otherwise and fingerprint regions for studying this spectroscopy.

In emission, one might expect to observe reasonably intense transitions from a 1B_2 state [electron configuration ... $(1a_2)^2 (4b_2)(6a_1)$ for the highest three valence orbitals] as the spectrum is expected to involve long progressions in the bending mode of the upper and lower states. However, as can be noted in the pressure dependence of the multiple collision relaxed chemiluminescent emission,⁷ these transitions will also feel the effect of the $g-g$ selection rule. Transitions from the 1A_2 state [electron configuration ... $(1a_2) (4b_2)^2(6a_1)$ for the highest three valence orbitals] would be expected to be very weak due to the electric dipole selection rules for a C_{2v} molecule. Transitions from the 3B_2 states are "spin forbidden" and are therefore also expected to be weak. We anticipate the change in bond angle which accompanies these lowest energy transitions to be so pronounced that the observed emission spectrum can be expected to extend over several hundred angstroms. This is evidenced by an emission system tentatively ascribed to the $^1B_2 - X^1A_1$ (A-X) transition (see Figures 4 and 5) observed under multiple collision conditions, and resulting from Ca-Cl_2 , Ca-Br_2 , Sr-Cl_2 (Figs. 5,6), and Sr-Br_2 (Figs. 4,6) reactive encounters. At elevated pressures, the A-X band system feature (Figs. 4,5) which extends from the fringes of the ultraviolet to considerably longer wavelength is efficiently quenched relative to the B-X band systems indicated in Figs. 4 and 6, as would be expected for a long-lived excited state.⁷

Transitions which involve excitation from the π_g to the π_u valence molecular orbital (Fig. 3) are expected to occur at higher energy. These electric dipole allowed transitions should be characterized by both a strong

absorption and emission spectrum, the latter of which has tentatively been identified for the Ca-Cl₂, Ca-Br₂, Sr-Cl₂ (Fig. 6), Sr-Br₂ (Figs. 4,6) and Sr-ICl (Fig. 6) (SrICl-transition is π to π) systems at the fringes of the ultraviolet. The bond angle change accompanying this transition will not be as pronounced as that accompanying the lowest energy band system, however the change from π -nonbonding to π -antibonding character should result in a progression in the dihalide stretching frequency. Features ascribed to this mode have tentatively be associated with the observed emission spectra (see also Figures 6 and 7).

Periodicity of Group IIA Dihalide Formation

"Near 'Single Collision' Studies and Symmetry Effects"

The Group IIA metal-halogen molecule reactions involve the interaction of metals with reasonably low ionization potentials²⁵ and halogen molecules of high electron affinity.²⁶ They are therefore expected to proceed via an electron jump process whereby the Group IIA atom throws out an electron to harpoon the halogen molecule, forming an $M^+ X_2^-$ complex. The data presented in Figures 1 and 2 obtained under near single collision conditions^{1,7} (10^{-4} - 10^{-6} Torr) for the Ba-Cl₂, Ba-Br₂, and Ba-I₂ reactions, exemplifies the "continuum" emissions observed for the Ca, Sr, and Ba reactions with Cl₂, Br₂, and I₂. The spectra are dominated by dihalide emission features extending from ~ 3000 to 6000 \AA . The apparatus used to obtain these experimental results has been discussed elsewhere.^{1,7} In contrast to the Ca, Sr, and Ba reactions with the chlorides, bromides, and iodides which yield a spectrum dominated by Group IIA dihalide emission, the reactions involving F₂ are strongly dominated by emission from the monofluorides. Only a weak emission continuum is observed ($3500\text{-}5000 \text{ \AA}$) for the magnesium system and this emission is found to be quadratic in the fluorine molecule concentration. This clearly represents an important periodic trend in dihalide formation. In retrospect, the lack of a notable difluoride emission for the Mg, Ca, Sr, and Ba reactions casts suspicion on the double harpoon mechanism (3) since this reaction sequence easily supplies the energy necessary (see Table I) to access difluoride excited states. We suggest⁷ that these characteristics may result, at least in part, because the fluorine molecule negative ions produced in the electron jump process dissociate much more rapidly than do the

corresponding Cl_2^- , Br_2^- , or I_2^- ions. However, we must also note that, whereas $D_0^0(\text{MF}_2) \approx 2D_0^0(\text{MF})$, the atomization energies of the chlorides, bromides, and iodides well exceed twice the metal monohalide bond energy.

An important symmetry constraint is signaled by the intensity of the emission from the dihalides formed in the reactions of Ca, Sr, and Ba with the mixed halogen molecules IBr and ICl. This is illustrated in Figure 2 where we compare total scans for the Ba + I_2 , Ba + IBr, and Ba + Br_2 reaction systems. These scans, which demonstrate a much weaker emission for heteronuclear halogen molecule reaction, were taken under the same resolution and with nearly identical halogen pressures and metal beam fluxes. Similar, if not more pronounced, results have been observed when comparing the tri-groupings Ba + Cl_2 , ICl, and I_2 . We will suggest that the dominant intensity for the Cl_2 , Br_2 , and I_2 reactions results because of the C_{2v} reaction path available to the homonuclear but not accessible to the heteronuclear halogen reactions. The availability of this C_{2v} reactive geometry (conical intersection) promotes excited state dihalide formation for $\text{M} + \text{X}_2$ but not $\text{M} + \text{XY}$ reactive encounters. These effects can certainly be manifest in the collisional stabilization mechanism (2) but not in the two step harpoon mechanism (3). While the difference in continuum intensity is quite pronounced for the barium reactions, this difference decreases for the strontium reactions and is almost muted for calcium. This behavior is consistent with the electron jump model and an increasing characteristic velocity at the curve crossing region associated with an $\text{M} + \text{X}_2 \rightarrow \text{M}^+ + \text{X}_2^-$ "outer harpooning" process (see also following) which diminishes the coupling (cross section) for the interaction of the $\text{M} + \text{X}_2$ and $\text{M}^+ + \text{X}_2^-$ curves.

"Multiple Collision Relaxation Studies"

The successful extension of the low pressure studies outlined above, in a controlled manner, using primarily helium buffer gas, provides the means to collisionally relax the dihalide continuum so as to reveal what appear to be three discrete band systems. This is a key step in the unraveling of the dynamics of these systems. Thusfar, we have successfully relaxed the continuous emission features associated with the Ca- Cl_2 , Ca- Br_2 , Sr- Cl_2 , Sr- Br_2 , Sr- I_2 , and Sr-ICl reactive encounters. The overview spectrum depicted in Fig. 4 for the Sr + Br_2 combination is exemplary. The lower energy system

(feature), which extends from the fringes of the ultraviolet through the visible, is dominated by a long progression in the SrX_2 bending mode. This is clearly apparent in the SrCl_2 emission spectrum depicted in Figure 5. The observed feature most likely corresponds to a ${}^1\text{B}_2((1a_2)^2(4b_2)(6a_1)) \rightarrow X {}^1\text{A}_1((1a_2)^2(4b_2)^2)$ transition which correlates in linear configuration to the ${}^1\Pi_g - {}^1\Sigma_g^+$ transition involving the σ_g and π_g molecular orbitals (Fig. 3). For all of the reactive combinations studied thusfar, we find that both Group IIA metal and halogen molecule collisions effectively quench this feature, a fact which is not surprising in view of the anticipated longer lifetime ($\tau_{\text{radiative}}$) associated with the excited state emitter. We will want to improve our methods for exciting and observing this band system while expanding the grid of collision partners considered to barium based reactive encounters. This will require some considerable care as the increased density of states associated with the barium halides certainly can lead to a more efficient quenching process even with the decreasing radiative lifetime expected for the lowest-lying barium dihalide states ($\tau_{\text{rad}}(\text{BaF}_2) < \tau_{\text{rad}}(\text{BaCl}_2) < \tau_{\text{R}}(\text{BaBr}_2) < \tau_{\text{R}}(\text{BaI}_2)$). It should be noted that the expected trends in the barium dihalide radiative lifetimes appear manifest in the pressure dependent behavior of the observed low pressure ($10^{-4} - 10^{-6}$ torr) emission continua.⁷

The more clearly resolved higher energy band system depicted in Figure 4, and displayed in greater detail for the $\text{Sr} + \text{Cl}_2$, $\text{Sr} + \text{Br}_2$, and $\text{Sr} + \text{ICl}$ reactive encounters in Figure 6, would seem to correspond to one of the allowed ${}^1\text{B}_2((1a_2)(4b_2)^2(2b_1))$ or $(1a_2)^2(4b_2)(7a_1)) \rightarrow X {}^1\text{A}_1$ transitions which correlate in linear configuration to the allowed ${}^1\Pi_u - {}^1\Sigma_g^+$ transition involving the π_u and π_g molecular orbitals (Fig. 3). This transition, which in absorption would involve primarily a change from Sr-X nonbonding to Sr-X antibonding character, should be dominated by progressions in the SrX_2 or SrXY stretching modes. The frequency separations between the observed features are consistent with this suggestion.⁷

Support for a Collisionally Stabilized Dihalide Complex

The results we have obtained in our study of the Sr-ICl system (Fig. 6) and the mixed $\text{Sr} - \text{Br}_2 + \text{Cl}_2$ system (Figure 7) are particularly significant for they demonstrate that the observed dihalide emission results, in large

part, from the collisional stabilization process (2). If the two step double harpooning mechanism (3) were to be operative, the combination of Sr-ICl and SrX-ICl reactive encounters should produce SrCl₂, SrICl, and SrI₂ emission with the dichloride emission clearly dominating that for the mixed halide and SrI₂. If the collisional stabilization mechanism is operative, the observed emission spectrum will correspond to the SrICl complex formed in a dynamically constrained (see following) electron jump process.

The reaction of strontium with Cl₂ + Br₂ mixtures of varying relative chlorine and bromine concentration should produce emission from SrCl₂, SrBrCl, and SrBr₂ if the two step double harpooning mechanism (3) is operative. If the highly efficient collisional stabilization process (2) is operative, the observed spectra should consist of the sum of only SrCl₂ and SrBr₂ emissions varying with relative Cl₂ and Br₂ concentration.

A study of the Sr-ICl reaction, with its attendant symmetry based dynamic constraint, can be difficult for vibrationally excited SrCl molecules produced from the relaxation of emitting SrCl electronically excited products which can react with ICl in a sufficiently exothermic process to produce an SrCl₂ emission feature. In fact, under certain conditions, the observed spectral signature can be contaminated by SrCl₂ (A-X Fig. 5) formed via the reaction of a thermalized ground state SrCl product with ICl. It is also relevant that ultraviolet spectrum in Figure 6 corresponds to one of the "allowed" SrX₂ B¹B₂ - X¹A₁ transitions and therefore should display a minimal difference between the transition moments for the SrX₂ (X=Cl,Br) and corresponding SrXY (XY=ICl) emitters. We have observed a dominant emission corresponding to the SrICl complex both in the B-X region depicted in Fig. 6 and at higher energies corresponding to a C-X band system which can be populated by the more exothermic ICl reaction. The spectrum in Fig. 6 does show some Cl₂ contamination for the higher temperature conditions (higher Sr flux) under which the three spectra in the figure were obtained however, the dominance of the SrICl emission system is apparent. This dominance demonstrates the probable formation of SrICl in a collisionally stabilized direct reactive encounter.

The collage of spectra in Fig. 7 which are obtained for varying mixtures of Br₂ and Cl₂ correspond to sums of emission features resulting exclusively from the dichloride and dibromide with no evidence for the mixed halogen (SrBrCl) emitter. This is especially significant when we note that the sum of

both SrCl and SrBr emission features characterize the monohalide emissions for all of the chlorine - bromine mixtures (compare to Sr+Cl₂ (top) and Sr+Br₂ (bottom)) considered in Fig. 7.

These results, which demonstrate the utility of combining near single collision and multiple collision chemiluminescent studies, are fundamental to our assessment of the electron jump process leading to excited state dihalide formation. They strongly suggest the probability that the extremely efficient collisional stabilization mechanism (2) is the dominant means of forming the dihalide excited state. This conclusion is also further supported by the lack of a continuum emission associated with the fluorine based reactions which should also yield dihalide emission if the two step double harpooning mechanism (3) is operative.

The implication of these results is broader for it suggests that the extent of interaction of these high temperature molecular complexes, as they form, considerably exceeds that which we normally associate with collisional stabilization and energy transfer processes. High temperature molecules in electronically excited states or in high vibrational levels of their ground electronic states simply are capable of much longer range interactions. It is important that we understand the formation and interaction of these species for this must, in the final analysis, contribute strongly to the behavior of systems operating under extreme conditions. A neglect of these phenomena in models of combustion or propulsion systems renders these models unrealistic.

A Symmetry Constrained Electron Jump Process

As we have noted, the low Group IIA metal ionization potentials and the high halogen electron affinities suggest that the Group IIA-halogen molecule reactions proceed via an electron jump process wherein the metal atom, M, throws out an electron and harpoons the halogen molecule, X₂, to initiate reaction. The relative intensities of the continuum emissions observed for homo- and heteronuclear halogen reactions can be understood within the model⁷ using the correlations outlined in Table III and extrapolating on the simple, yet elegant, (Fig. 8) arguments of Menzinger¹⁵ used to explain metal monohalide chemiluminescent emissions from the fluorine and chlorine molecule reactions.

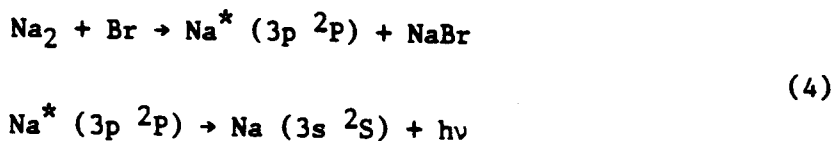
Reactions to produce the dihalide are thought to proceed⁷ through an

electron jump "outer harpooning" process involving the interaction of the $M + X_2$ ($|1\rangle$ in Fig. 8) covalent and $M^+ + X_2^-$ ($|3\rangle$ in Fig. 8) ionic curves. For a C_s or $C_{\infty v}$ collision geometry, this process involves the strong coupling of $^1A'$ or $^1\Sigma$ covalent and ionic potentials (Table III) of the same symmetry leading to an avoided crossing, harpooning, and formation of the ground state metal halide. However, if the collision geometry is of C_{2v} symmetry, the symmetry species of the covalent and ionic curves (Table III) are 1A_1 and 1B_2 respectively and the curves for the two states intersect. It is through this intersection and a range of approach angles within a cone of acceptance around the X_2 bisector²⁷ that the system slips past the "outer harpooning" region corresponding to the $|1\rangle|3\rangle$ crossing (Fig. 8) and gains access to the "inner harpooning" region. The crossing involving the ionic configuration $|3\rangle$ and the doubly ionic configuration $|5\rangle$ (Table III and Fig. 8) will be avoided as the $|3\rangle|5\rangle$ interaction between these curves, of the same symmetry, is thought to be significant. Access to the "inner harpooning" region thus promotes an avoided crossing leading to the chemiluminescent channels.^{7,12} The low statistical weight of the near C_{2v} collisions is partly responsible for the low chemiluminescent quantum yields in these systems. For the $M+XY$ reactive encounters, which cannot access a C_{2v} collision trajectory, the outer harpooning process must always correspond to an avoided crossing which shields the channel for chemiluminescent product formation.²⁸ However, as the characteristic velocity at the ionic-covalent crossing region increases in traversing the Group IIA metals from Ba to Ca, the symmetry effect which is clearly apparent in Fig. 2 diminishes.

Although this model qualitatively explains the observed trends in dihalide emission intensity, further detailed calculations of the couplings at the avoided crossing regions will be needed to place these arguments on a more quantitative base. These calculations, which will also rely on the spectroscopic parameterization obtained from the dihalide spectra exemplified in Figures 5-7. The calculations are, of course, best accomplished following some initial effort to parameterize dihalide electronic and vibronic structure from our observations of the optical signatures associated with the dihalides (energy levels, radiative lifetimes, differential bond angle changes) all of which also serves an important purpose for the refinement of ionic models.

CHEMICALLY INDUCED RAMAN PUMPING

In studying the reactions of small supersonically cooled sodium molecules (Na_n , $n=2,3$)^{29,30} with halogen atoms ($X=\text{Cl}, \text{Br}, \text{I}$), we have recently demonstrated the existence of population inversions associated with the electronically excited Na_2 products of the $\text{Na}_3 + \text{Br}$ reaction. In an extension of these experiments to develop a long path length amplifying medium, we discern, for the first time, the Raman pumping of Na_2 in the absence of an external light source. We observe a series of Raman-like Stokes and anti-Stokes features which (1) are associated with the lowest vibrational levels of Na_2 , (2) correlate with a scattering process involving the Na D-line components ($\text{Na } 3p^2P_{3/2,1/2} - 3s^2S_{1/2}$) created in the chemical reaction sequence



(3) are not readily generated by light scattering due to an external laser light source, and (4) appear to be enhanced by the environment of the reaction zone itself. The D-line emission is scattered by cooled sodium dimers (Na_2) formed, as a result of supersonic expansion, in the lowest vibrational levels of the Na_2 ground electronic state. Multiple Stokes and anti-Stokes features, assigned as resonance Raman progressions are well simulated on the basis of the resonance Raman effect.^{31,32} However, the scattering linewidth, Γ , associated with the present process is determined to be close to 4 cm^{-1} . This result suggests an unusually fast resonance Raman scattering process which appears to be chemically enhanced.

Outline of Extended Slit Source Sodium Expansion Configuration

We have generated high sodium atom and dimer fluxes using an extended slit source configuration which is described in detail elsewhere.^{8,33} Using a dual oven configuration, we produce a supersonically expanded flux of alkali vapor through a tantalum slit nozzle 0.003" wide by two inches in length. With an independently heated stagnation chamber (850-900K) and frontal nozzle

expansion channel (900-950K), we produce a near planar flow of primarily sodium atoms and internally cooled sodium dimers.^{8,33} This sodium flux is intersected at variable angles from above and below by two nearly planar but diverging bromine atom flows, emerging from slits machined into graphite tube furnaces, operated at temperatures in excess of 1700K to insure a 95+% conversion of bromine molecules to bromine atoms. At the significant reactant fluxes necessary to generate a strong Raman scattering signal, the absolute number density of bromine atoms in the reaction zone is conservatively estimated⁸ at between 10^{14} and 10^{15} cm⁻³ whereas the absolute number density of sodium dimers may exceed 10^{16} cm⁻³.

The optical signature of the long path length sodium molecule-bromine atom reaction zone is focused onto the entrance slit of a SPEX 1704 scanning monochromator coupled to an RCA 1P28 photomultiplier tube (PMT). The PMT is maintained at ~1000 volts and the response current is sent through an IEEE interfaced autoranging picoammeter (Keithley) to an IBM compatible AT class microcomputer.

We have attempted to reproduce the Raman signal created following the reaction sequence (4) by resonantly pumping the sodium expansion with external laser light. Intensity stabilized broadband (multimode) laser light (~1 W) from an argon ion laser (Spectra Physics, model 171) at 4765 Å and 4880 Å and dye laser light (~100 mW) at 5890 Å and 5896 Å (argon ion pumped R6G) was frequency chopped and passed through the expansion zone in an unsuccessful effort to generate a Raman scattering signal similar to that observed from the chemical reaction pumping. The frequency content of the emergent beam was again monitored with a monochromator-PMT combination. The PMT response, detected with a phase sensitive amplifier, was digitized and stored in an IBM AT-class microcomputer.

Chemically Induced Resonance Raman Pumping

There are several near-resonant rovibronic transitions associated with the $X^1\Sigma_g^+$ and the $A^1\Sigma_u^+$ states of Na₂^{8,33} and the atomic emission from the Na D-lines, ω_{P1} and ω_{P2} ($2P_{3/2} \rightarrow 2S_{1/2}$ @ 16973.379 cm⁻¹ and $2P_{1/2} \rightarrow 2S_{1/2}$ @ 16956.183 cm⁻¹) which may be responsible, in large part, for the unusually intense optical signature depicted in Figure 9. The spectrum in Figure 9 was taken at a resolution of ~12 Å. The relative intensity of the strong sodium

dimer $B \rightarrow X$ chemiluminescence to the even stronger Raman-like emission features symmetrically surrounding the Na D-line is readily apparent. The frequency separation between adjacent Stokes (anti-Stokes) features corresponds closely to 155 cm^{-1} , correlating with the separations between the lowest sodium dimer ground state vibrational levels. We have found that these features cannot be made to fit a resonance fluorescence series but can be confidently assigned to Stokes and anti-Stokes bands associated with a resonance Raman progression.^{8,33}

Evidence suggestive of a Raman process is also detailed in the spectrum of Figure 10 taken under equivalent reaction zone conditions. The intermediate resolution, $\sim 1.5 \text{ \AA}$, at which this spectrum was obtained is sufficient to clearly resolve the atomic sodium $2P_{3/2}-2P_{1/2}$ D-line splitting ($\sim 17.2 \text{ cm}^{-1}$) and the relative intensities of each of the sodium D-line components are clearly evident in the scattered Raman emission. Furthermore, the frequency separation of these atomic line components is clearly reproduced (within the experimental resolution of the scan) in both the vibrational Stokes and anti-Stokes features of the scattering.

We have successfully modeled the group of features symmetrically surrounding the Na D-line with the resonant Raman intensity expression.^{8,31-33}

$$I_S(v_G, J_G; v_F, J_F) = \frac{32\pi^3 \omega_s^4 I_p}{9c^4 h^2} M(\xi_0)^4 e^{-\frac{B J_G(J_G+1)hc}{kT}} N(v_G) \quad (5)$$

$$\times \sum_{v_I, J_I} \left(3 S_{J_{ex}} S_{J_{tr}} \frac{|\langle v_F | v_I \rangle \langle v_I | v_G \rangle|^2}{(\omega_{GI} - \omega_{FI})^2 + \Gamma^2} + 2 S_{J_{ex}} S_{J_{tr}} \frac{|\langle v_F | v_I \rangle \langle v_I | v_G \rangle|^2}{(\omega_{GI} - \omega_{FI})^2 + \Gamma^2} \right)$$

where I_s is the total intensity for a scattered Stokes or anti-Stokes line as a function of frequency, ω , and pump intensity, I_p , and c is the speed of light. We consider transitions from an initial rovibrational ground electronic state of the Na_2 molecule labeled G to some final rovibrational electronic ground state labeled F through an intermediate excited electronic state labeled I where ω_{GI} and ω_{IF} represent the rovibronic energy difference between the G and I and I and F levels and Γ refers to the linewidth arising from all damping phenomena. The S_J terms correspond to the appropriate Honl-London factors for the Na_2 $A^1\Sigma_u^+ - X^1\Sigma_g^+$ transition,^{8,33} $M(\xi_0)$ represents the electronic matrix element, expressed as a function of the normalized nuclear coordinate, $\xi = R(\mu\omega/h)^{1/2}$, and $\langle v_F | v_I \rangle$ and $\langle v_I | v_G \rangle$ represent Franck-Condon overlap integrals. We have included a thermalized ground state rotational distribution and a ground state weighting function $N(v_G)$, which represents the deviation from a Boltzmann distribution. We also allow pumping due to each component of the sodium D line, ($\omega_{P1}(^2P_{3/2})$ and $\omega_{P2}(^2P_{1/2})$), to contribute to the scattered emission intensity, I_s . Here, the $^2P_{3/2}:^2P_{1/2}$ intensity weighting resulting from the reaction populated D-line components is 3:2, as determined from the experimental spectrum.

Numerical calculations were carried out by allowing the near-resonant atomic sodium transitions, ω_{P1} and ω_{P2} , appropriately broadened, to pump the first thirty levels in the Na_2 $X^1\Sigma_g^+$ state to the first seventy levels of the Na_2 $A^1\Sigma_u^+$ state. De-excitation from the upper electronic state was allowed to proceed to the first thirty levels of the ground state. Rotational levels $J'', J' = 0$ to 120 were included with each vibrational level of both the excited electronic $A^1\Sigma_u^+$ state and the ground electronic $X^1\Sigma_g^+$ state of the sodium dimer scatterer. Each simulated spectrum produced in the modelling program was also convolved with a gaussian function to approximate the effects of a finite spectrometer slit width.

The data in Figure 11 depicts the fit to the vibrational structure surrounding the Na D-line for reaction with a pure sodium expansion. This low resolution ($\sim 12 \text{ \AA}$) vibrational Raman spectrum does not correspond to a thermalized vibrational distribution but rather to a non-Boltzmann vibrational distribution. The modeled spectrum closely matches the experimental scan and also provides a consistent fit to higher resolution spectra. Although the rotational population distribution may be non-Boltzmann, we find that, with an effective rotational temperature of 400K, we are able to obtain close

agreement between experiment and calculation. This suggests that only slight modifications from a thermalized distribution will be necessary to exactly fit the rotational features. There are several possible sources for the deviation of the Raman scattering features from a thermalized vibrational distribution.^{8,33}

A higher resolution scan ($\sim 0.4 \text{ \AA}$) of the first Stokes and anti-Stokes features is depicted and computer simulated in Figure 12, based again on the application of Equation (5). In a surprising result, we find that a linewidth, $\Gamma \approx 4 \text{ cm}^{-1}$, is required to provide optimum agreement between the simulated and experimental results with correlation coefficients exceeding 0.92 for the anti-Stokes and 0.89 for the Stokes features, respectively. A further confirmation of the required linewidth is also indicated in Figure 12 where we compare the experimental spectrum to $\Gamma = 4, 1$, and 0.1 cm^{-1} simulations based on Equation (5).

While there are improvements that can be made in the simulations depicted in Figure 12, it is unlikely that simple power broadening can be responsible for the large effective linewidth indicated by our spectral simulations. Based on the required power broadening for a two level quantum system driven at resonance, we estimate that an electric field of $\sim 1.3 \text{ KV/cm}$ and an absolute power density of $\sim 0.215 \text{ MW/cm}^2$ is necessary to produce the requisite spectral broadening of 4 cm^{-1} .

The apparent spectral broadening suggests the possibility of a scattering lifetime on the order of $\sim 10^{-11}$ seconds, implying a process which is considerably more efficient than would be expected on the basis of resonance Raman pumping involving the $\text{Na}_2 \text{ A-X}$ transition ($\sim 10^{-8}$ seconds based on the radiative lifetime³⁴). Several additional experiments involving the direct pumping of the sodium expansion in the absence of bromine atom reactant at the Na D-line frequencies (argon ion pumped R6G) and at 4765 \AA and 4880 \AA using a multimode argon ion laser, failed to reveal optical signatures corresponding to those depicted in Figures 9-12. In fact, while it was possible to excite laser induced fluorescence corresponding to the $\text{Na}_2 \text{ A-X}$ and B-X band systems analogous to that observed previously,³⁵ although at somewhat higher temperatures in the present experiments, no clear Raman features were generated. This result also suggests a more efficient process than that associated with resonance Raman pumping.

These results suggest that we have observed more than a "simple" Raman-

like scattering process. We might consider a further long range interaction of the electronically excited sodium $3p^2P$ atoms with those Na_2 molecules which are Raman pumped, an interaction of the Na_2 molecules with the Br atoms that induces a time varying enhancement of the dimer polarizability (hyperpolarizability), or (less likely) the presence of a large electric field created due to the reactive environment in the vicinity of the reaction zone. It would appear that this interaction or perturbation is long range and leads to a highly efficient Raman-like scattering process.

While further experiments will be necessary to clarify the mechanism for the scattering process, the long path length reaction zone employed in these experiments appears to have revealed the manifestation of significant long range cooperative phenomena. The moderate Rydberg character of the Na $3p^2P$ excited state, with its diffuse electron density, may, in fact, lend itself to a considerable long range interaction inducing cooperative effects. The assessment of these cooperative effects awaits further study.

Acknowledgement

The authors gratefully acknowledge the helpful comments of Professors Ron Felton and Michael Heaven, and Dr. Kangkang Shen. Helpful comments and technical assistance from Mr. C. B. Winstead are also greatly appreciated. The support of the Georgia Tech Foundation through a grant from Mrs. Betty Peterman Gole, the Army Research Office through the Short Term Innovative Research Program, the Air Force Office of Scientific Research and the Army Research Office and AFOSR/SDIO is greatly appreciated.

References

1. See for example, L. H. Dubois and J. L. Gole, J. Chem. Phys. 66, 779 (1977), D. R. Preuss and J. L. Gole, J. Chem. Phys. 66, 880 (1977), 66, 2994 (1977); G. J. Green and J. L. Gole, Chem. Phys. 46, 67 (1980), 69, 357 (1982), 100, 133 (1985) and references therein. D. M. Lindsay, J. R. Lombardi, and J. L. Gole, Chem. Phys. 37, 333 (1979), S. B. Oblath and J. L. Gole, Combust. and Flame 37, 293 (1980), Joerg Pfeifer and J. L. Gole, J. Chem. Phys. 80, 565 (1984), D. F. Dever, B. Cardelino, and J. L. Gole, High. Temp. Sci. 18, 159 (1984), T. C. Devore, L. Brock, R. Kahlscheuer, and K. Dulaney, Chem. Phys. 155, 423 (1991). H. Wang and J. L. Gole, J. Chem. Phys. 98, 9311 (1993), J. Mol. Spectros. 161, 28 (1993). J. L. Gole, "The Unique Complexation and Oxidation of Metal-Based Clusters", in Advances in Metal and Semiconductor Clusters, Vol. 1, Spectroscopy and Dynamics, ed. M. A. Duncan, JAI Press (1993), pg. 159-209 and references therein. J. L. Gole, "Toward the Modeling of the Oxidation of Small Metal and Metalloid Molecules," in "Gas Phase Metal Reactions", edited by A. Fontijn, North Holland, Amsterdam (1992), pp. 578-604 and references therein.
2. J. L. Gole, "Probing Ultrafast Energy Transfer Among the Excited States of Small High Temperature Molecules", in "Gas Phase Chemiluminescence and Chemiionization", A. Fontijn (editor) - Elsevier Science Publishers, 1985, p. 253.
3. D. M. Lindsay and J. L. Gole, J. Chem. Phys. 66, 3886 (1977). M. J. Sayers and J. L. Gole, J. Chem. Phys. 67, 5442 (1977). J. L. Gole and S. A. Pace, J. Chem. Phys. 73, 836 (1980).
4. G. J. Green and J. L. Gole, Chemical Physics 100, 133 (1985). R. W. Woodward, J. S. Hayden, and J. L. Gole, Chemical Physics 100, 153 (1985).
5. A. W. Hanner and J. L. Gole, J. Chem. Phys. 73, 5025 (1980). J. L. Gole and S. A. Pace, J. Phys. Chem. 85, 2651 (1981). J. L. Gole, B. Ohlsson, A. W. Hanner, and E. J. Greene, unpublished.
6. J. R. Woodward, S. H. Cobb, K. K. Shen, and J. L. Gole, JQE 26, 1574 (1990) - invited paper. K. K. Shen, H. Wang, and J. L. Gole, JQE 29, 2346 (1993).
7. J. L. Gole, "The Symmetry Constrained Dynamics Associated with Group IIA Dihalide Complex Formation via $M + X_2$ Reactions - Evidence Suggesting the Highly Efficient Collisional Stabilization of Dihalide Excited State Complexes", in preparation. T. C. Devore, J. L. Gole, and H. Wang, "Controlled Relaxation of Group IIA Dihalide Excited State Complexes - Resolution of Low Pressure Continuum Emissions to Discrete Structure and Confirmation of Dihalide Complex Formation via Highly Efficient R3BR", in preparation.
8. D. Grantier and J. L. Gole, "Chemically Enhanced Raman Scattering", in preparation.

9. Linus Pauling, The Nature of the Chemical Bond, Cornell University Press, Ithaca, New York, 1960. R. D. Levine and R. B. Bernstein, Molecular Reaction Dynamics and Chemical Reactivity, Oxford University Press, New York, 1987.
10. D. L. Hildenbrand, "Model Calculations of Thermochemical Properties of Gaseous Metal Halides", in Proceedings of the Symposium on High Temperature Metal Halide Chemistry, Vol. 78-1, The Electro-Chemical Society, pg. 248.
11. M. C. Drake and G. M. Rosenblatt, "Trends in Structure and Vibrational Frequencies of MX_2 and MX_3 High Temperature Halide Vapors", in Proceedings of the Symposium on High Temperature Metal Halide Chemistry, Vol. 78-1, The Electrochemical Society, pg. 234.
12. C. D. Jonah and R. N. Zare, Chem. Phys. Lett. 9, 65 (1971).
13. D. J. Wren and M. Menzinger, Chem. Phys. Lett. 18, 431 (1973), 20, 471 (1973), and 27, 572 (1974).
14. W. J. Rosano and J. M. Parson, J. Chem. Phys. 84, 6250 (1986).
15. M. Menzinger, Adv. Chem. Phys. 42, 1 (1980). M. Menzinger, "The $M+X_2$ Reactions: A Case Study". In Gas Phase Chemiluminescence and Chemiionization; A. Fontijn, Editor; Elsevier Science Publishers: Amsterdam, 1985, pp. 25-66. M. Menzinger, "Chemiluminescent and Chemiionization Metal-Halogen Reactions as Paradigms of Diabatic Reaction Dynamics", Acta Physica Polonica A73, 85 (1988).
16. F. Engelke, Chem. Phys. 44, 213 (1979).
17. D. Wren, Ph.D. Thesis, U. of Toronto, 1978.
18. L. Wharton, R. A. Berg, and W. Klemperer, J. Chem. Phys. 39, 2023 (1966). A. Buchler, J. L. Stauffer, W. Klemperer, and L. Wharton, J. Chem. Phys. 39, 2299 (1963). A. Buchler, J. L. Stauffer, and W. Klemperer, J. Chem. Phys. 40, 3471 (1964); J. Am. Chem. Soc. 86, 4544 (1964).
19. Edward F. Hayes, J. Phys. Chem. 70, 3740 (1966).
20. D. R. Yarkony, W. J. Hunt, H. F. Schaefer, Molecular Physics 26, 941-952 (1973).
21. R. L. DeKock, M. A. Peterson, L. K. Timmer, E. J. Baerendo, and P. Vernooijs, Polyhedron 9, 1919 (1990).
22. James L. Gole, Albert K. Q. Siu, and Edward F. Hayes, J. Chem. Phys. 58, 857 (1973).
23. James L. Gole, J. Chem. Phys. 58, 869 (1973).
24. R. H. Hauge, private communication.

25. See for example, NBS Special Publication 505, Bibliography on Atomic Transition Probabilities (1914 through October 1977) and Supplement I (November 1977 through March 1980), U. S. Department of Commerce/National Bureau of Standards. C. E. Moore, "Atomic Energy Levels", (National Bureau of Standards, 1949).
26. See for example, R. S. Berry and C. W. Reimann, J. Chem. Phys. 38, 1540 (1963), R. S. Berry, J. Chem. Phys. 27, 1288 (1957), W. S. Struve, J. R. Krenos, D. L. McFadden, and D. R. Herschbach, J. Chem. Phys. 62, 404 (1975), R. C. Oldenborg, J. L. Gole and R. N. Zare, J. Chem. Phys. 60, 4032 (1974).
27. T. Carrington, Accts. Chem. Res. 7, 20 (1974).
28. Note that the radiative lifetimes associated with the lowest energy MXY emission band systems ($\sigma - \pi$ transitions) will be shorter than their MX₂ counterparts ($\sigma g - \pi g$ transitions). Thus the MXY* excited state production is considerably muted relative to that indicated in Fig. 2.
29. (a) J. L. Gole, "The Unique Nature of Metal Cluster Oxidation", J. L. Gole, in Physics and Chemistry of Finite Systems: From Clusters to Crystals, Volume II, Edited by P. Jena, S. N. Khanna, and B. K. Rao, NATO ASI Series, Vol. II, pg. 1025 (1992).
(b) J. L. Gole, "Toward the Modeling of the Oxidation of Small Metal and Metalloid Molecules", in "Gas Phase Metal Reactions", edited by A. Fontijn, North Holland, Amsterdam (1992) pp. 578-604.
(c) J. L. Gole, "The Unique Complexation and Oxidation of Metal-Based Clusters", in Advances in Metal and Semiconductor Clusters, Vol. 1, Spectroscopy and Dynamics, ed. M. A. Duncan, JAI Press (1993), pg. 159-209.
30. S. H. Cobb, J. R. Woodward, and J. L. Gole, Chem. Phys. Lett. 156, 197 (1989). "Chemically Driven Pulsed and Continuous Visible Laser Amplifiers and Oscillators", J. L. Gole, K. K. Shen, H. Wang, and D. Grantier, Invited Talk, Proceedings of the 23rd AIAA Plasma-Dynamics and Laser Science Conference, Nashville, Tennessee, AIAA 92-2994 (1992).
31. D. L. Rousseau and P. F. Williams, J. Chem. Phys. 64, 3519 (1976).
32. See, for example, J. Tang and A. C. Albrecht in "Raman Spectroscopy", edited by H. A. Szymanski (Plenum, New York, 1970), Vol. 2, pp. 33-68. A. C. Albrecht, J. Chem. Phys. 34, 1476 (1961).
33. D. Grantier, H. Wang, C. B. Winstead, and J. L. Gole, Proceedings of the 24th AIAA Plasma Dynamics and Lasers Conference, Orlando, Florida, AIAA 93-3207 (1993).
34. W. T. Zemke, K. K. Verma, T. Vu, and W. C. Stwalley, J. Mol. Spectrosc. 85, 150 (1981).
35. J. L. Gole, G. J. Green, S. A. Pace, and D. R. Preuss, J. Chem. Phys. 76, 2247 (1982).

TABLE I

Geometry of Group IIA Dihalides

Metal	<u>Halide</u>			
	F	Cl	Br	I
Be	<i>l</i> ^a	<i>l</i>	<i>l</i>	<i>l</i>
Mg	<i>l</i>	<i>l</i>	<i>l</i>	<i>l</i>
Ca	<i>b</i>	<i>l</i>	<i>l</i>	<i>l</i>
Sr	<i>b</i>	<i>b</i>	<i>l</i>	<i>l</i>
Ba	<i>b</i>	<i>b</i>	<i>b</i>	<i>b</i>

^a *l*, linear; *b*, bent

Table II

Experimentally Determined Bond Energies of Group IIA Mono- and Dihalides

	D_0° kcal/mole ^a			
	F	Cl	Br	I
Hg	109	75	(58)	(45)
Ca	126 266(140°)	94 214(180°)	73 186(180°)	62 155(180°)
Sr	129 260(120°)	96 211(140°)	79 189(180°)	64 155(180°)
Ba	139 271(100°)	104 220(120°)	85 197(150°)	72 166(180°)

^aFor each entry, the upper value corresponds to the metal monohalide bond energy and the lower value corresponds to that for the metal dihalide.

Table III

States Arising from $M + X_2$ Reactant Configurations

	\underline{C}_s	\underline{C}_{2v}	$\underline{C}_{\infty v}$
$M(1s) + X_2(1\Sigma_g^+)$	$1A'$	$1A_1$	1Σ
$M^+(2s) + X_2^-(2\Sigma_u^+)$	$1,3A'$	$1,3B_2$	$1,3\Sigma$
$M^{+2}(1s) + X_2^{--}(1\Sigma_g^+)$	$1A'$	$1A_1$	1Σ

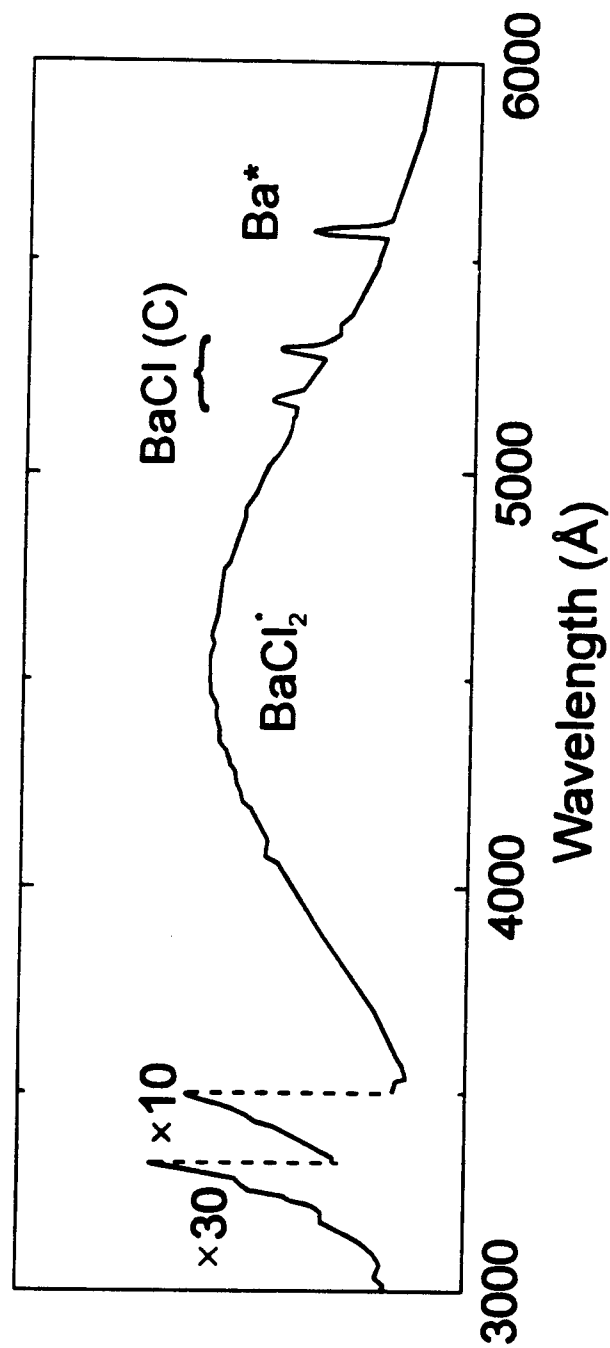
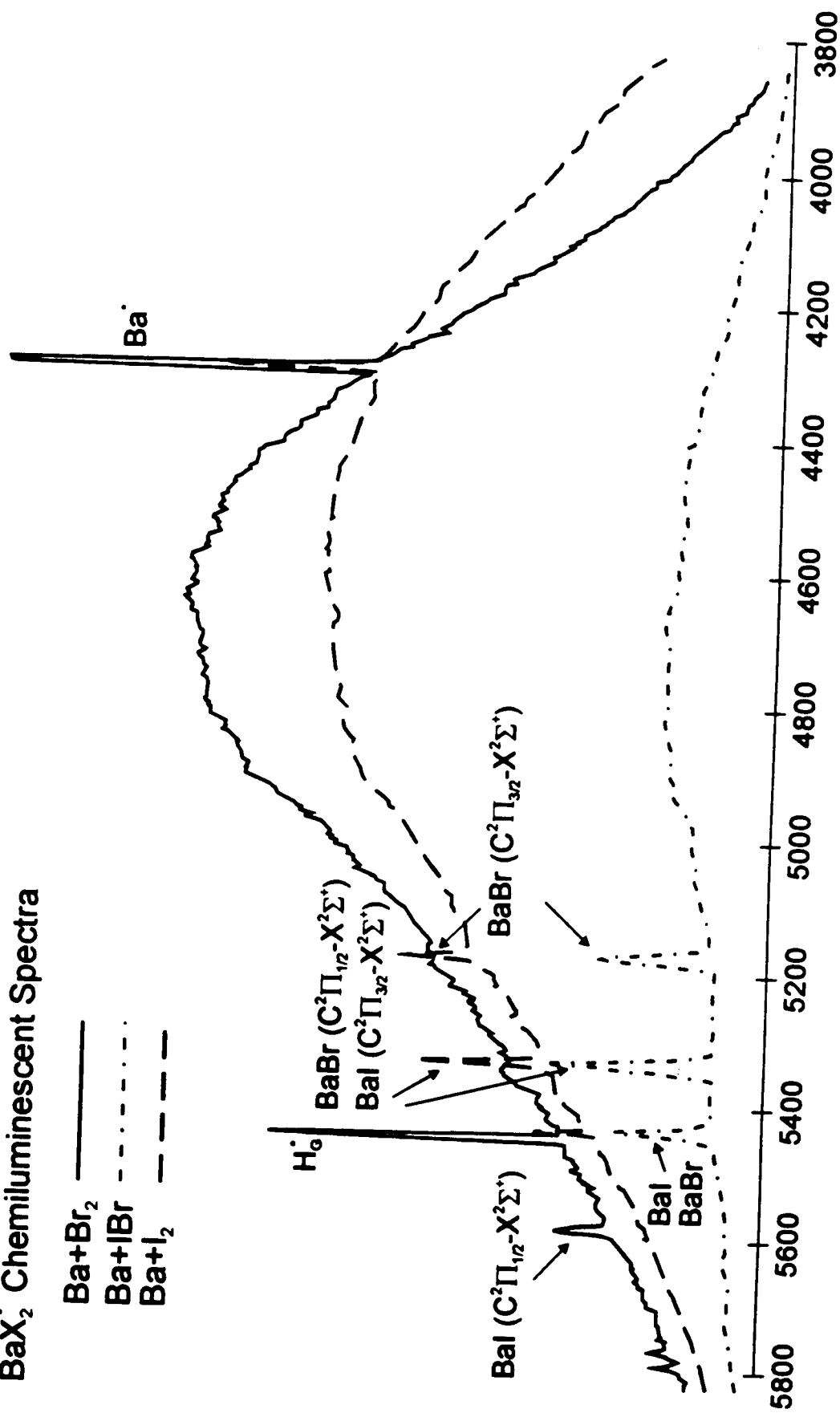


Figure 1

Chemiluminescent spectrum of the $\text{Ba}(\text{'s}) + \text{Cl}_2$ reaction

BaX_2 Chemiluminescent Spectra

$\text{Ba} + \text{Br}_2$ —————
 $\text{Ba} + \text{IBr}$ - - - - -
 $\text{Ba} + \text{I}_2$ - - - - -



Wavelength (\AA)

Figure 2

Chemiluminescent spectra for the $\text{BaX}_2(\text{XY})$ product of the $\text{Ba}({}^1\text{S}) + \text{I}_2$, IBr , and Br_2 reactions and the BaX products of the $\text{Ba}({}^1\text{D}) + \text{I}_2$, IBr , and Br_2 reactions.

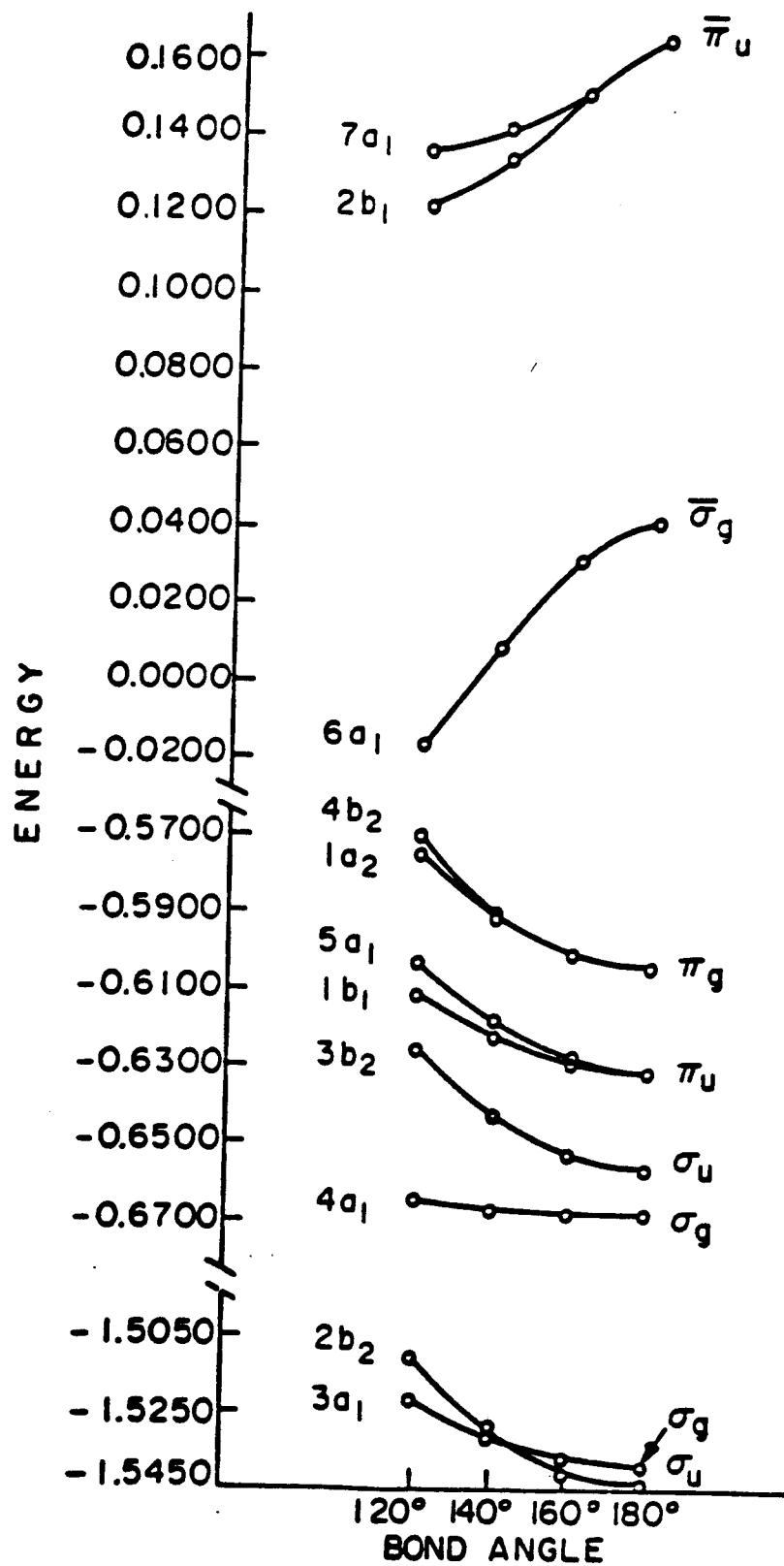


Figure 3: Correlation Diagram for BeF₂

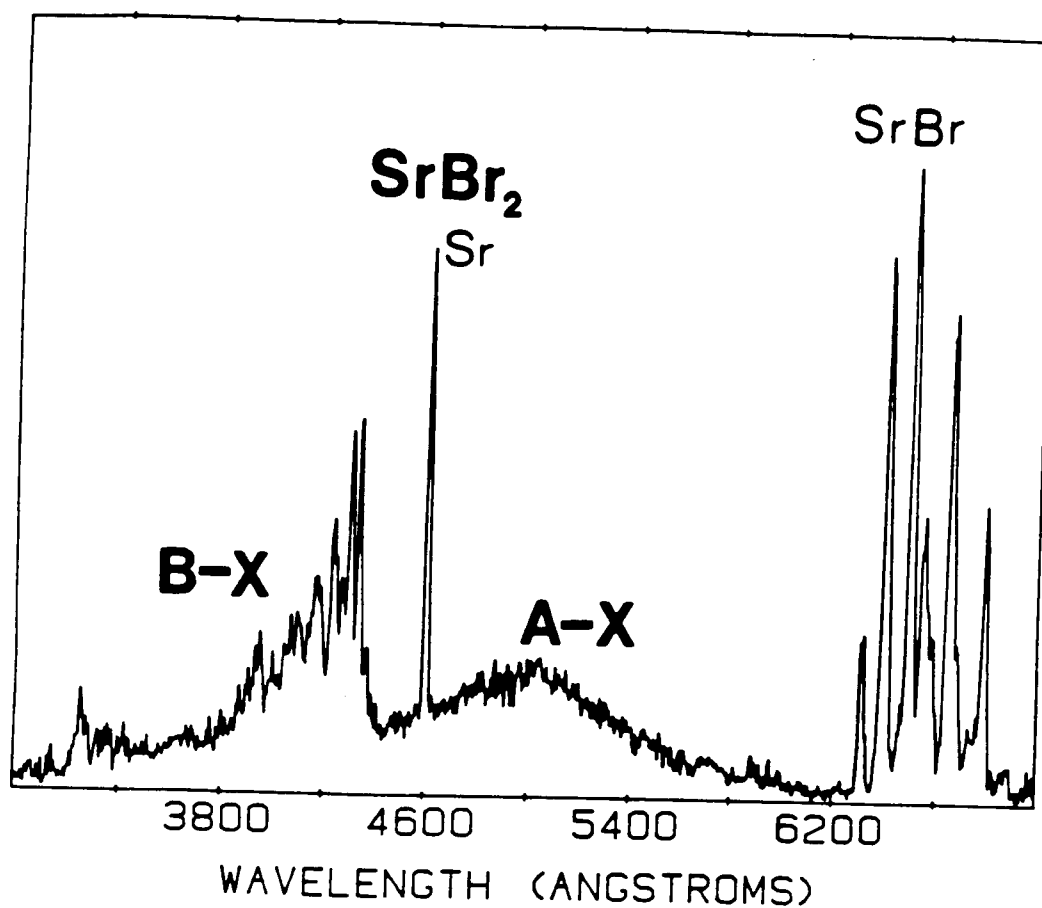
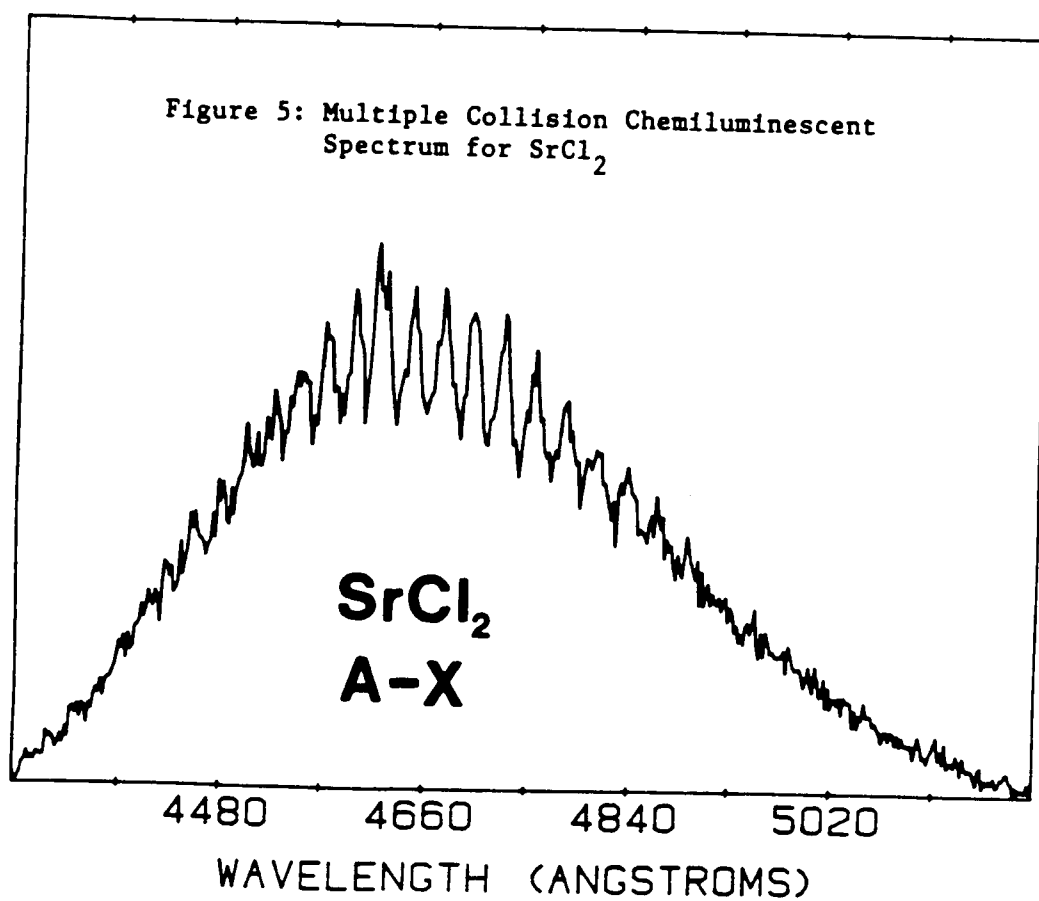


Figure 4: Multiple Collision SrBr₂ Chemiluminescent Spectrum



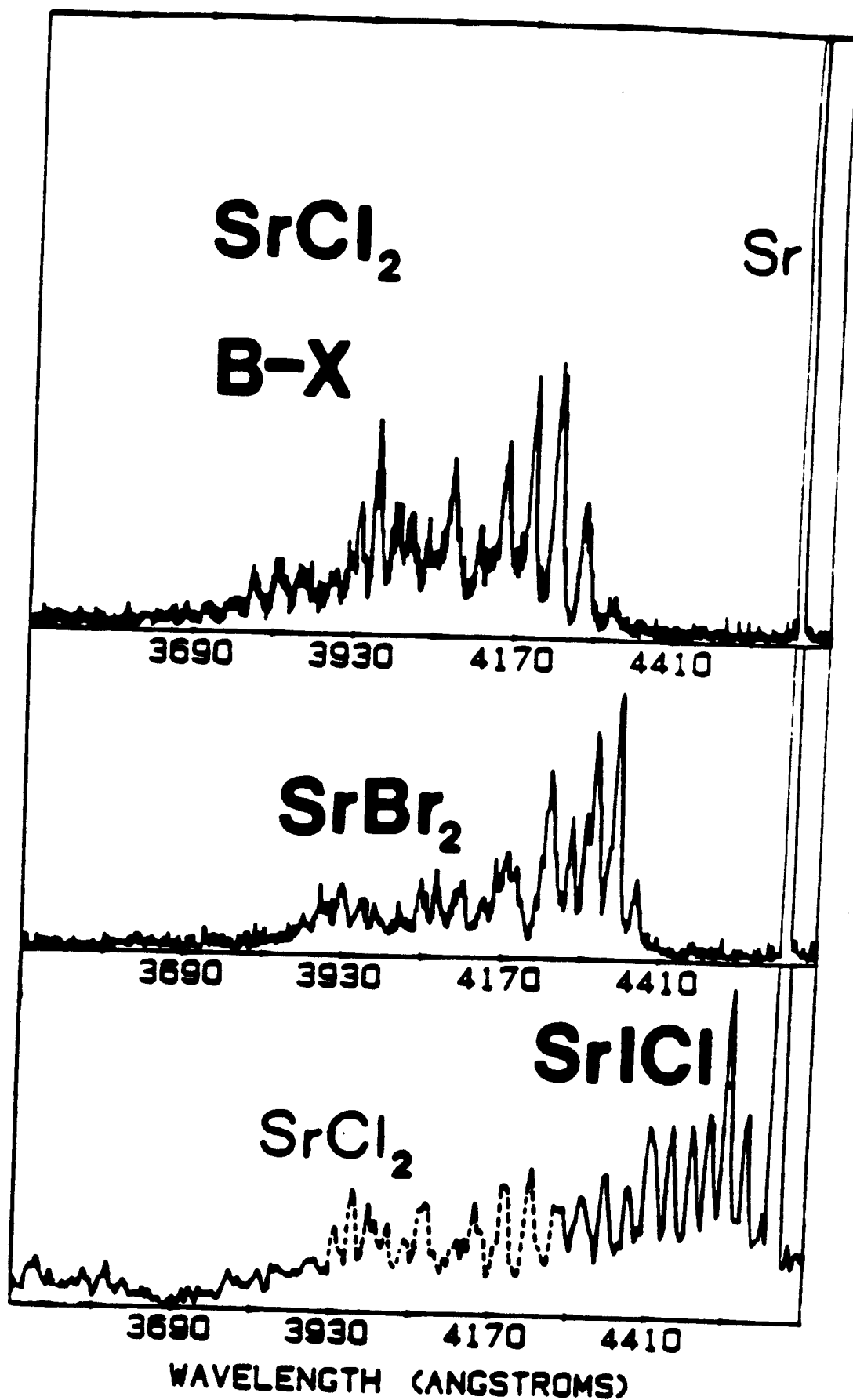


Figure 6: Multiple Collision Chemiluminescent Emission Spectra for SrCl_2 , SrBr_2 , and SrICl . See text for discussion.

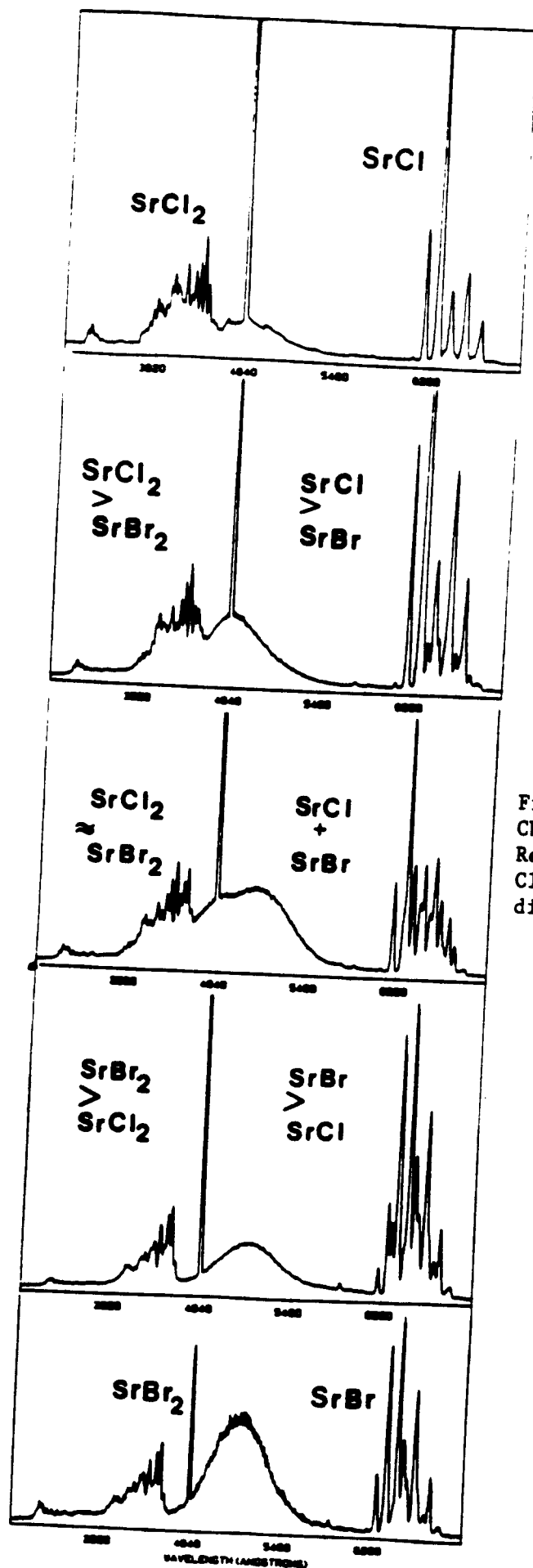


Figure 7: Multiple Collision Chemiluminescent Spectra for Reactive Mixtures of Sr Metal, Cl_2 and Br_2 . See text for discussion.

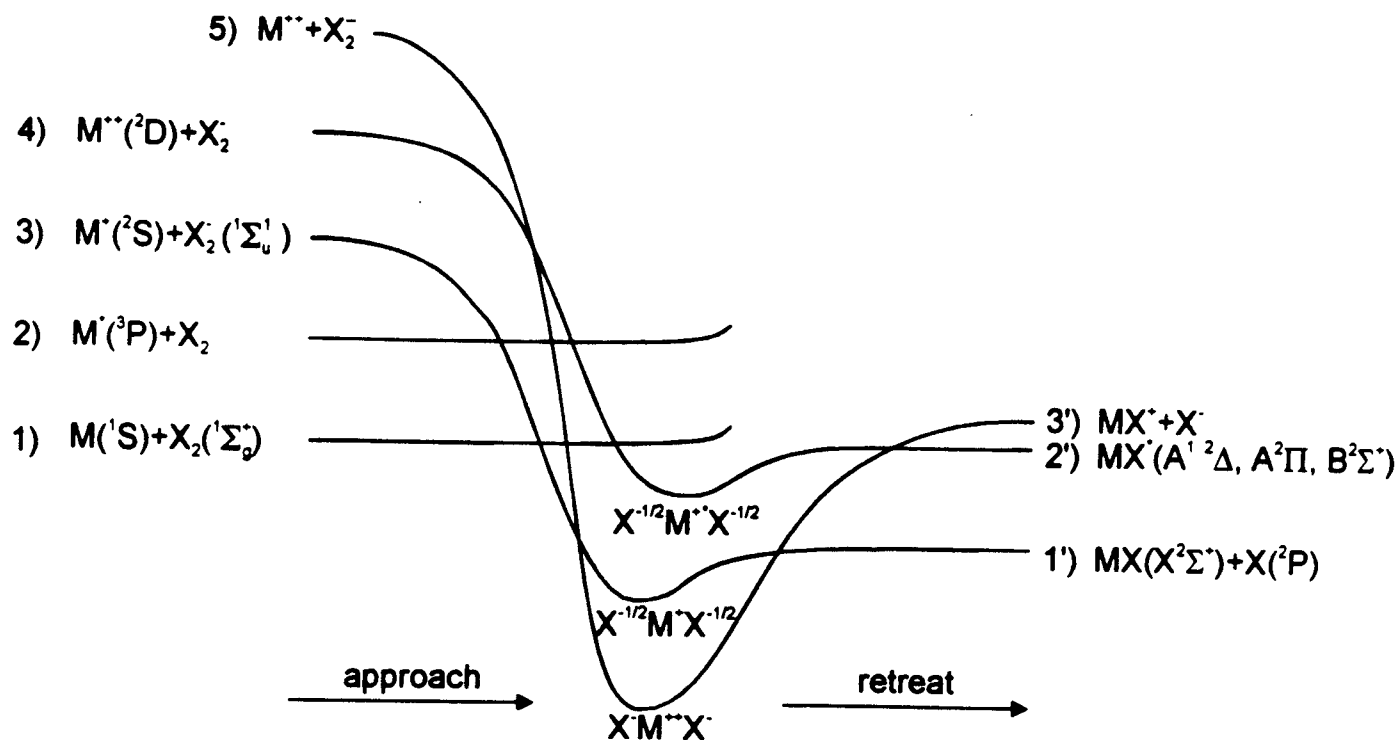


Figure 8

Correlation of electron configurations for Group IIA metal (M) - Halogen molecule (X_2) reactive encounters.

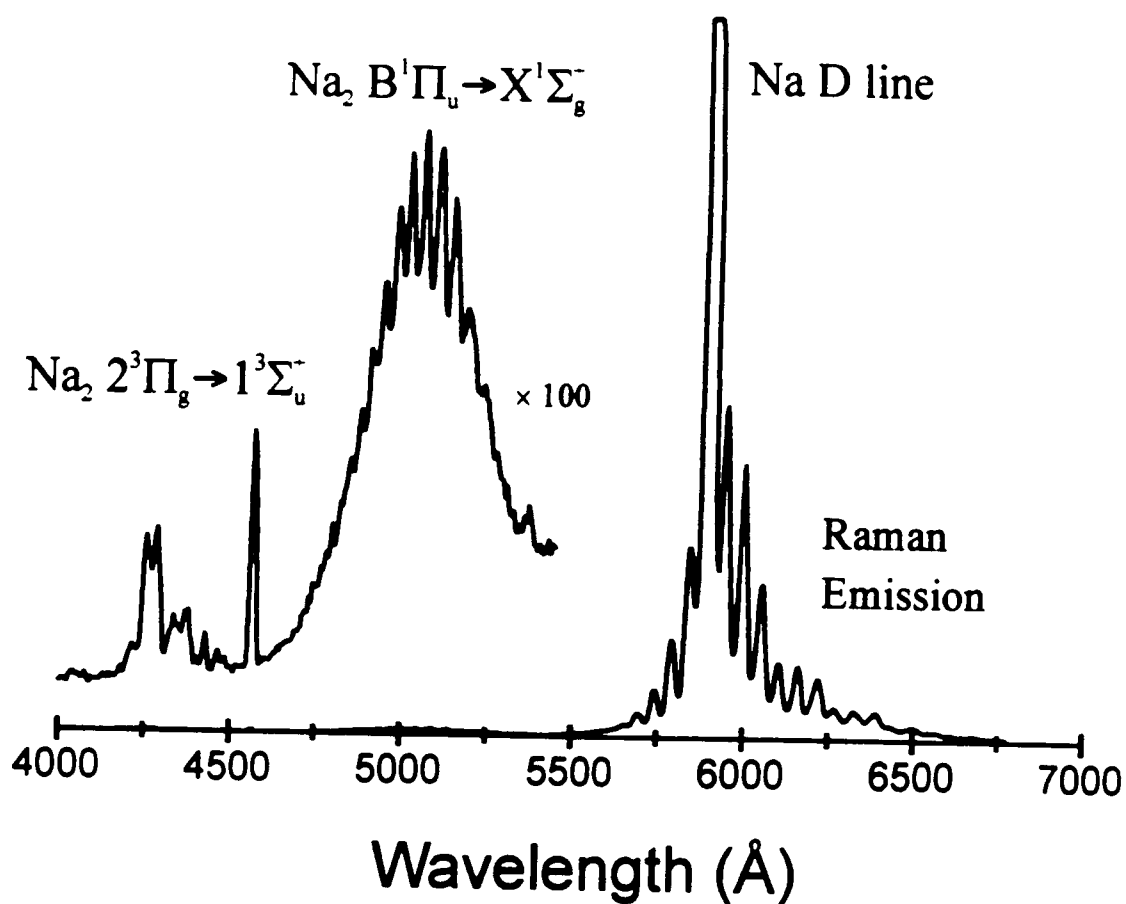


Figure 9

Survey spectrum of chemiluminescent emission and Raman scattering from various electronic states of diatomic sodium. The Na₂ 2³Π_g → 1³Σ_u⁺ transition corresponds to a triplet-triplet bound-free excimer like emission process. (Res. ~ 12 Å, T_{oven} ~ 875K, T_{meas} ~ 935K)

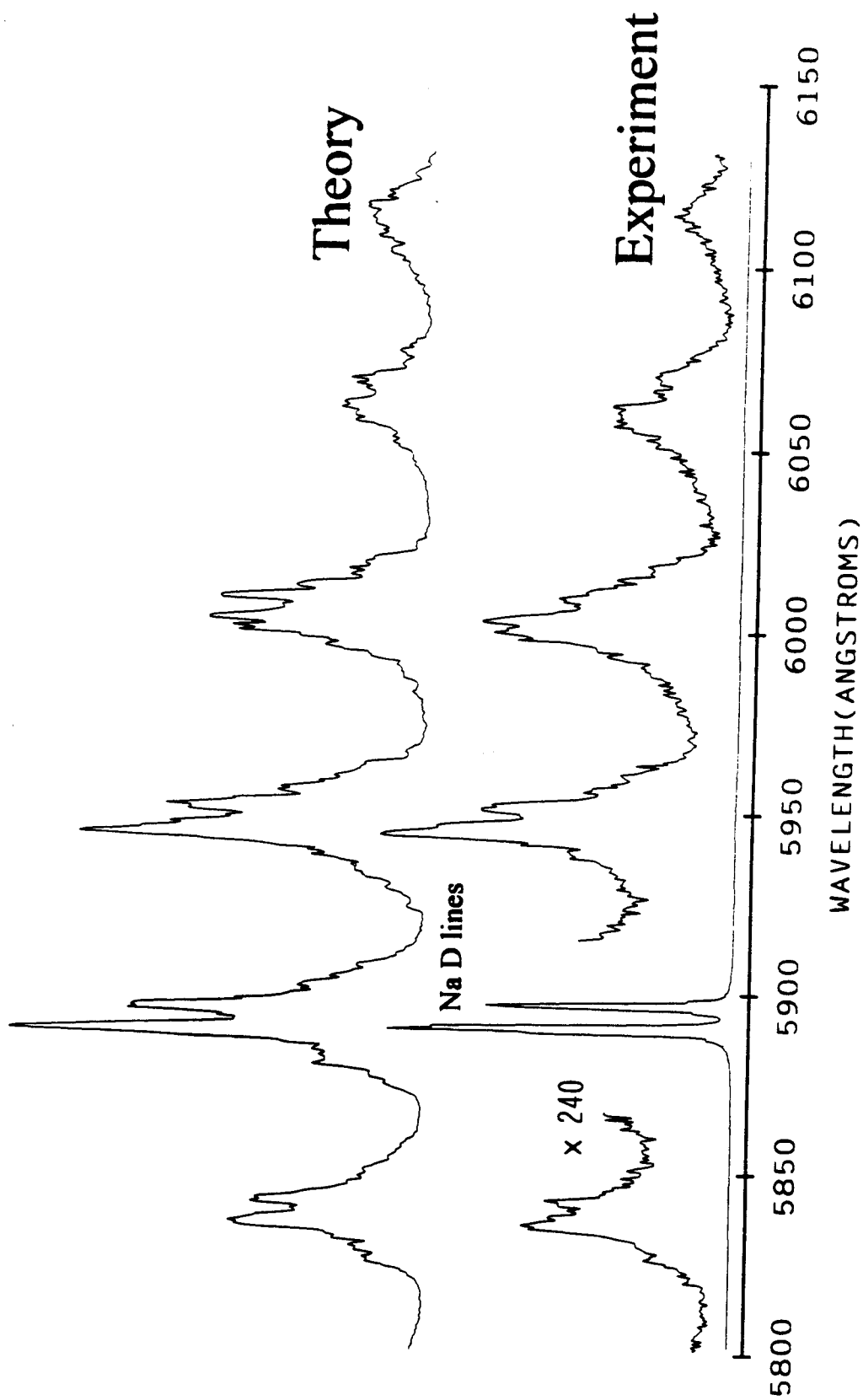


Figure 10

Raman-like spectrum taken at a resolution of $\sim 1.5 \text{ \AA}$ ($T_{\text{oven}} \sim 875\text{K}$, $T_{\text{nozzle}} \sim 935\text{K}$) depicting the two Na D-line components and the satellite Raman structure. The spin-orbit frequency difference of the two Na D-line components is reproduced in the scattered radiation. A simulated spectrum is presented for comparison ($T_{\text{rot}} \sim 400\text{K}$, $\Gamma = 4 \text{ cm}^{-1}$). See text for discussion.

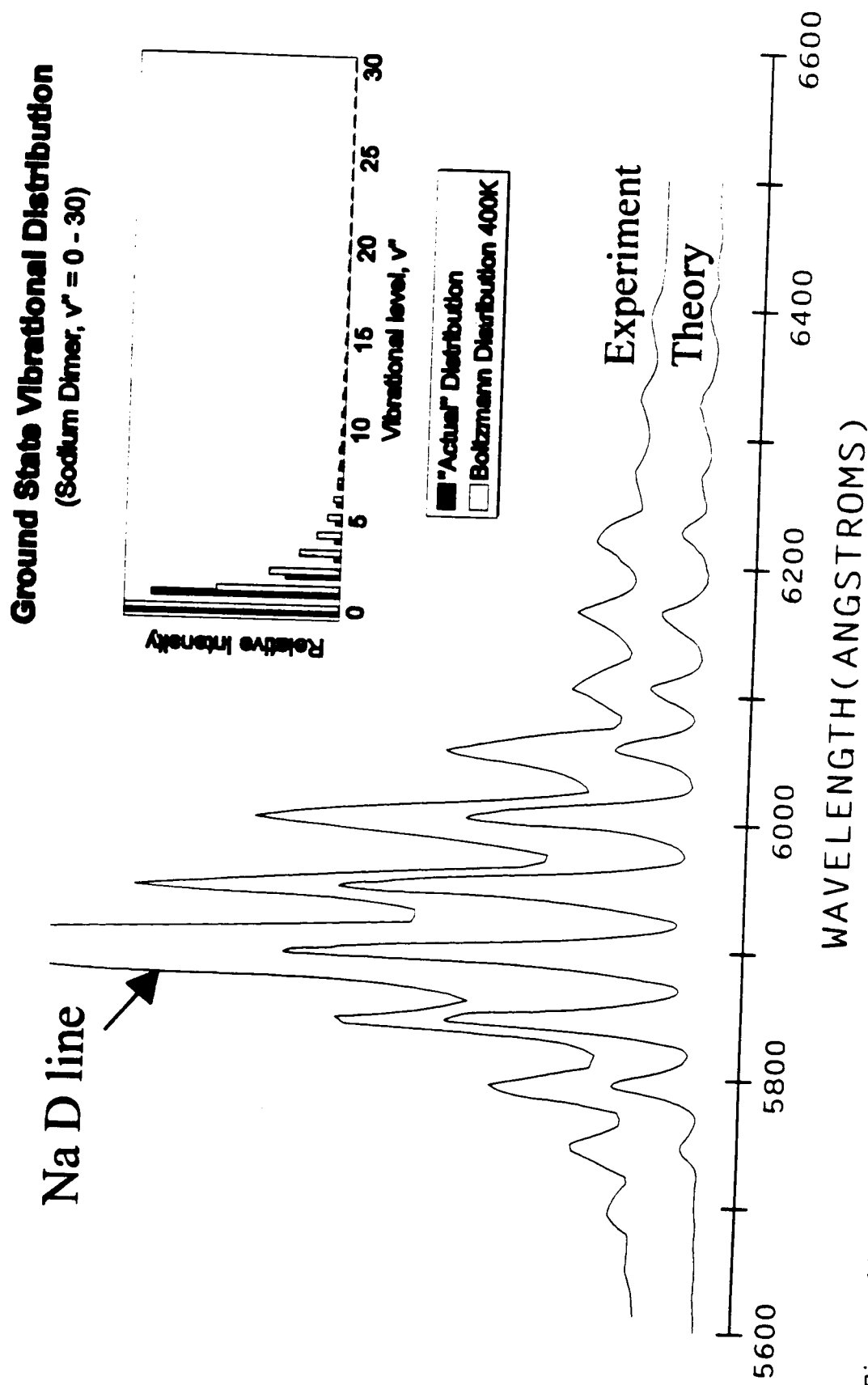


Figure 11

Comparison of experimental spectrum with computer modelled distribution (res. $\sim 5 \text{ \AA}$, T_{vib} $\sim 875 \text{ K}$, $T_{\text{nozzle}} \sim 935 \text{ K}$). Optimum agreement between calculation and experiment was found for the slightly nonthermal distribution depicted in the upper righthand corner of the figure. A Boltzmann distribution at 400K is included for comparison. See text for discussion.

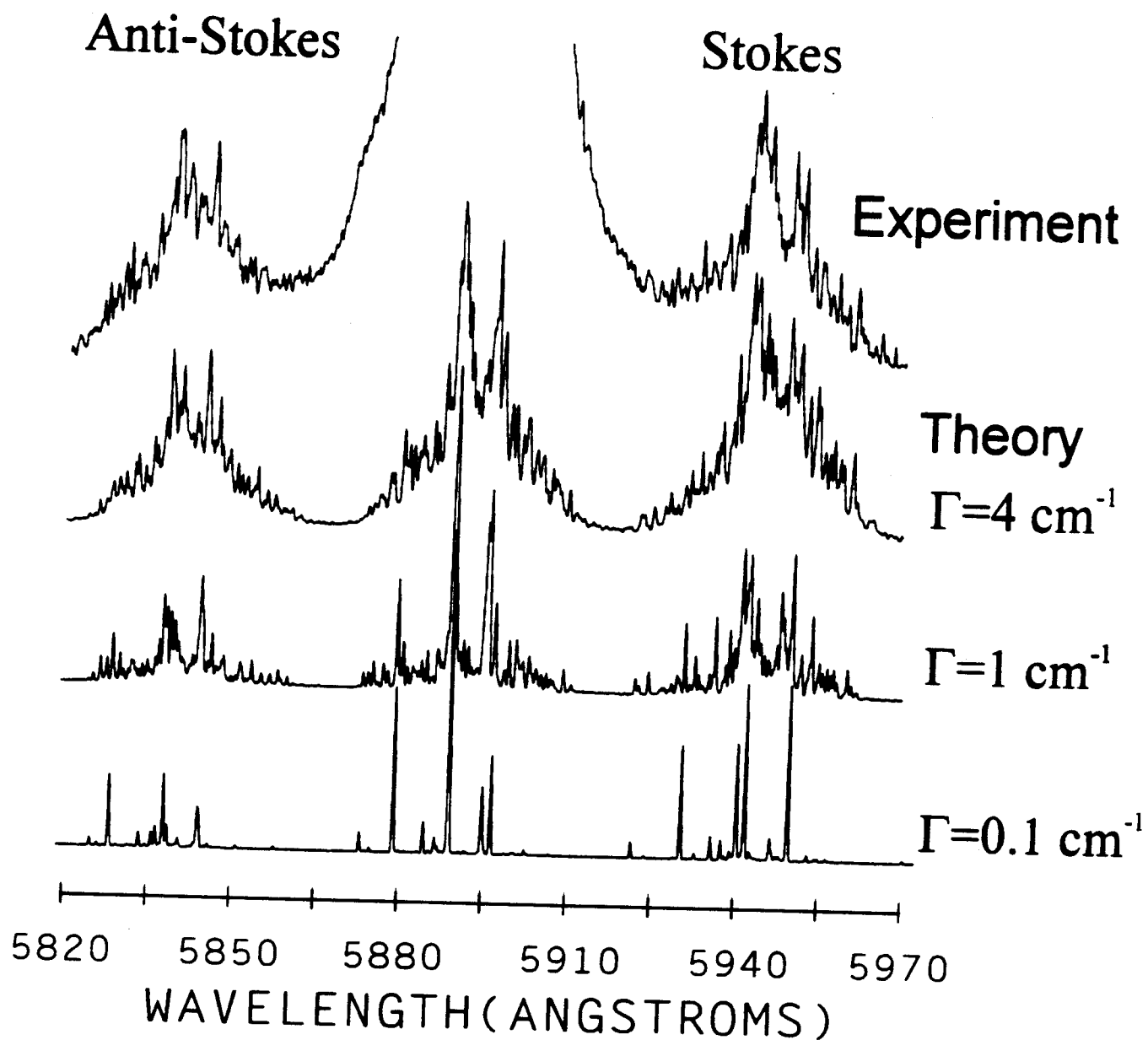


Figure 12

High resolution spectrum ($\sim 0.5 \text{ \AA}$) and simulated spectra for $\Gamma = 0.1$, 1, and 4 cm^{-1} demonstrating the marked improvement in the fit to the experimental Raman-like features for increasing values of Γ . See text for discussion

APPENDIX XVI

"Chemically Induced Processes Evidencing Raman Gain", D. R. Grantier, P. M. Medley, and J. L. Gole, Proceedings of the Tenth International Symposium on Gas Flow and Chemical Lasers, Friedrichshafen Germany, 1994, in press.

Chemically Induced Processes Evidencing Raman Gain

David R. Grantier,
Peter M. Medley,
and
James L. Gole

Georgia Institute of Technology, School of Physics
Atlanta, Georgia 30332

ABSTRACT

The highly selective $\text{Na}_2 + \text{X}$ (Cl, Br, I) reactions have been shown to create a continuous electronic population inversion based on the chemical pumping of Na_2 . Optical gain through stimulated emission has been demonstrated in regions close to 527, 492, and 460 nm ($\alpha = 8 \times 10^{-3} \text{ cm}^{-1}$ for an individual rotational level at $\sim 527 \text{ nm}$). A device has been constructed with a focus to increasing amplifier gain length and amplifying medium concentration based on the controlled intersection of supersonically expanded sodium and halogen atom sheaths. The interaction forms an extended reaction-amplification zone centered on-axis in an optical cavity, thus facilitating the conversion of the observed amplifiers to chemical laser oscillators. Initial results with this upscaled device, where the sodium metal expanded in both pure and seeded supersonic expansion is intersected by a bromine atom flow, provide the first example of chemically enhanced Raman scattering (CHERS). Unique Raman signals are induced by and correlate with emission from the Na D-line components formed in the chemical reaction zone primarily as a result of the $\text{Na}_2 + \text{Br} \rightarrow \text{Na}^* + \text{NaBr}$ reaction, cannot be readily generated by light scattering due to an external light source, and appear to be enhanced by the environment of the reaction zone itself. The Na D-line emitters interact with cooled sodium dimers in a resonance Raman scattering process, for which computer simulations suggest a scattering linewidth, $\Gamma \sim 4 \text{ cm}^{-1}$. These results suggest an unusually fast resonance Raman scattering process which appears to be chemically enhanced. The results of initial double pass gain measurements suggest that a stimulated Raman process, similar to that associated with optically pumped alkali dimer lasers, has been observed.

1. INTRODUCTION

Recently, we have been concerned with the reactions of small supersonically cooled sodium molecules and halogen atoms ($\text{Na}_n + \text{X} \rightarrow \text{Na}_{n-1}^* + \text{NaX}$, $\text{X} = \text{Cl}, \text{Br}, \text{I}$; $n = 2, 3$).^{1,2} These reactions have been shown to demonstrate gain on transitions involving the electronically excited Na_2 products of the $\text{Na}_3 + \text{Br}$ reaction.^{3,4} In an extension of these experiments, focused on the development of a long path length amplifying medium employing slit source based supersonic expansions, we have observed the first resonance Raman pumping generated in a purely chemical reactive environment in the absence of an external laser source. The observations made in the present study bear a close analogy to those of Wellegehausen,^{5,6} Bergmann,^{7,8} and others in their analysis of optically pumped sodium dimer lasers operative on a stimulated Raman scattering process. Here, we observe a series of Raman-like Stokes and anti-Stokes features which correlate strongly with a scattering process involving the Na D-line components ($\text{Na } 3p \text{ } ^2P_{3/2,1/2} - 3s^2S_{1/2}$) created in the chemical reaction sequence



but are not readily generated by light from an external laser tuned to the Na D-line resonance. The D-line emission generated in the above reaction sequence is scattered by supersonically cooled sodium dimers (Na_2) generating multiple Stokes and anti-Stokes features, which are assigned as resonance Raman progression and are well simulated on the basis of the resonance Raman theory outlined by Rousseau and Williams,⁹ and others.¹⁰ The results of initial gain studies, in which amplification has been observed on many of the Stokes and anti-Stokes components of the Raman spectrum, are suggestive of a stimulated Raman scattering process similar to that associated with optically pumped alkali dimer lasers. However, the scattering linewidth Γ , associated with the present process is determined to be close to 4 cm^{-1} . These results suggest the possibility of an unusually fast resonance Raman scattering process which appears to be chemically enhanced.

2. EXPERIMENTAL

The apparatus which we have used to generate high sodium fluxes in supersonic expansion is depicted schematically in Figure 1. Here, we provide only a brief description of the apparatus as more complete discussions can be found elsewhere.^{11,12}

A dual oven (stagnation and frontal nozzle) system has been designed to produce a supersonic flux of alkali vapor through a slit nozzle approximately $0.003''$ wide by two inches in length. The slit is formed from two sheets of $0.005''$ tantalum prepared, mounted, and sandwiched between frontal and rear nozzle sections. The precise width of the created tantalum slit is adjusted to $0.003''$ under a Vickers microscope and verified for accuracy across the length of the slit using single slit diffraction techniques.

The rear stagnation chamber (850-900K) and frontal nozzle expansion channel (900-950K) are heated independently. Expansion from the slit source produces a near planar flux at the reaction region consisting primarily of sodium atoms and vibrationally and rotationally cooled dimers. In the reaction region, the sodium flux is intersected from above and below at variable angles by two diverging near planar flows of monatomic bromine, emerging from slit sources, and produced by thermal dissociation in a graphite tube furnace ($T > 1700\text{K}$). In this temperature range, the bromine should be greater than 95% dissociated.¹³ At the significant reactant fluxes necessary to generate a strong Raman scattering signal, the absolute number density of bromine atoms in the reaction zone is conservatively estimated at between 10^{14} and 10^{15} cm^{-3} whereas the absolute number density of sodium dimers in the reaction zone may exceed 10^{16} cm^{-3} .

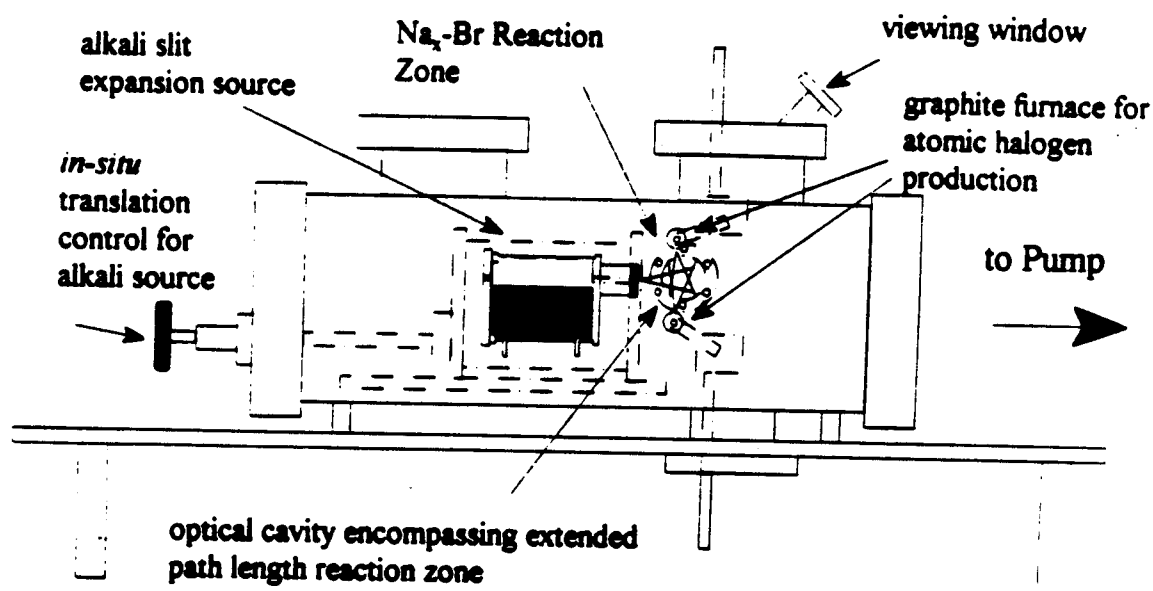


Figure 1

Schematic of slit supersonic alkali cluster source and associated atomic halogen delivery systems. See text for further discussion.

The emission resulting from the sodium molecule-bromine atom reactions is focussed onto the entrance slit of a SPEX 1704 scanning monochromator coupled to an RCA 1P28 photo-multiplier tube (PMT). The PMT is maintained at ~ 1000 volts and the response current is sent through an IEEE interfaced autoranging picoammeter (Keithley) to an IBM compatible AT class microcomputer.

We have also attempted to reproduce the Raman signal created following the reaction sequence (1) by resonantly pumping the supersonically expanded sodium dimers (in the absence of

the halogen reactant) with an external laser light. Intensity stabilized broadband (multimode) laser light (~ 1 W) from an argon ion laser (Spectra Physics, model 171) at 4765 Å and 4880 Å and dye laser light (~ 100 mW) at 5890 Å and 5896 Å (argon ion pumped R6G) was frequency chopped and passed through the reaction zone in an effort to generate a Raman scattering signal similar to that observed from the chemical reaction pumping. The frequency content of the emergent beam was again monitored with a monochromator-PMT combination. The PMT response, detected with a phase sensitive amplifier, was digitized and stored in an IBM AT-class microcomputer. However, no Raman-like features were generated.

Additionally, a double pass optical gain configuration¹⁴ constructed around the reaction region has been used to conduct several gain measurements on the Na₂-Br system. In these experiments, a laser beam from a He-Ne laser (used for alignment) is directed through a small adjustable aperture and the reaction zone, impinging on a flat high reflector. By adjusting the alignment of the reflector, the beam is subsequently reflected back through the aperture, thus insuring that the normal to the reflector is fixed parallel to the reaction zone. A light gathering lens of focal length 12 cm is placed between the reaction zone and the adjustable aperture in order to focus the reflected light from the He-Ne laser into the aperture. By establishing the geometry in this manner, we insure that the optical system rejects off-axis light rays while accepting only radiation parallel to the optic axis.

To further minimize the possibility of allowing off-axis radiation into the detection system, the distance between the high reflector and the aperture is extended to 1 meter while the aperture itself is narrowed to approximately a 1 mm diameter. Consequently, the observed output light intensities measured with the high reflector blocked can be compared with those intensities measured with the same reflector open to the reaction zone. Assuming that only on-axis radiation can be reflected from this flat mirror and subsequently detected, the maximum intensity observed with an unblocked mirror (I_u) to that observed with a blocked mirror (I_b) can be no greater than two (neglecting any amplification effects due to the active medium and any absorption/scattering losses caused by either the medium or optical elements present in the system). Therefore, the observation of ratios for I_u/I_b greater than 2:1 suggests the development of enough gain in the reaction medium to overcome losses due to absorption and/or scattering. As the simplest example of system losses, the windows which surround the reaction medium typically absorb about four percent of the incident radiation per pass.

3. RESULTS AND ANALYSIS

There are multiple near-resonant rovibronic transitions associated with the $X^1\Sigma_g^+$ and the $A^1\Sigma_g^+$ states of Na₂ and the atomic emission from the Na D lines, ($^2P_{3/2} - ^2S_{1/2}$ @ 16973.379 cm⁻¹ and $^2P_{1/2} - ^2S_{1/2}$ @ 16956.183 cm⁻¹). We suggest that these near resonances are responsible, in large part, for the unusually intense optical signature depicted in Figure 2.

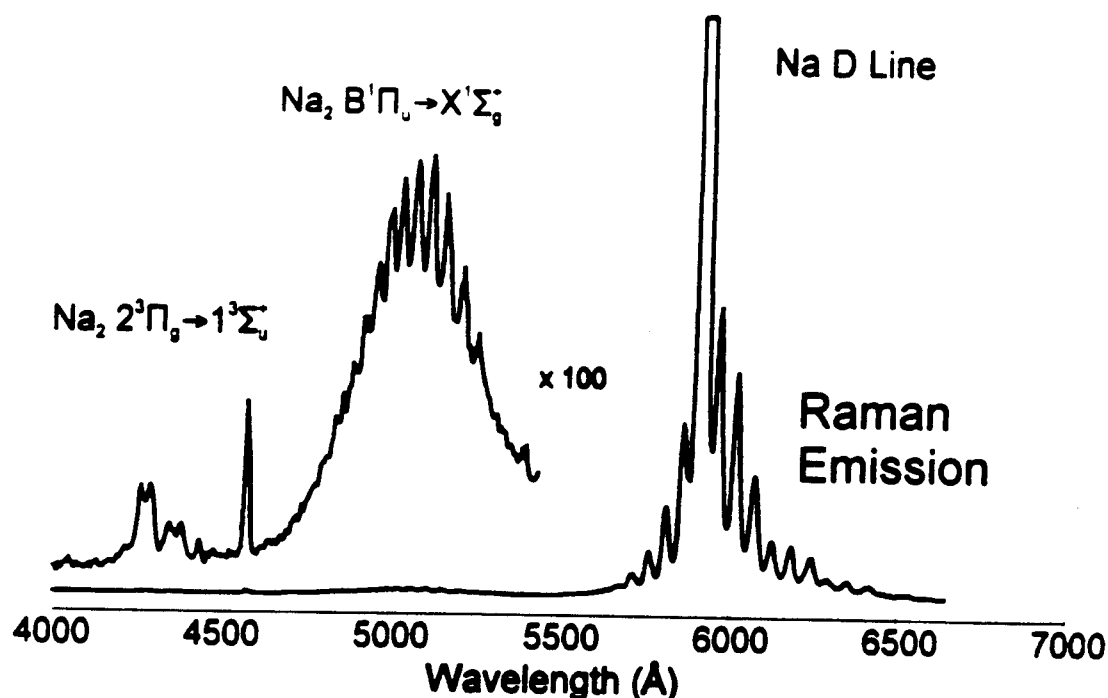


Figure 2

Survey spectrum of chemiluminescent emission and Raman scattering from various electronic states of diatomic sodium. The Na_2 $2^3\Pi_u \rightarrow 1^3\Sigma_u^-$ transition corresponds to a triplet-triplet bound-free excimer-like emission process. (Resolution - 12 Å, $T_{\text{oven}} \sim 875\text{K}$, $T_{\text{nozzle}} \sim 935\text{K}$)

The spectrum in Figure 2 was taken at a resolution of ~ 12 Å. The relative intensity of the strong sodium dimer B - X chemiluminescence to the even stronger Raman-like emission features symmetrically surrounding the Na D-line is readily apparent. The frequency separation between adjacent Stokes (anti-Stokes) features corresponds closely to 155 cm^{-1} , correlating with the separations between the lowest sodium dimer ground state vibrational levels. It should also be noted that the progression of Stokes and anti-Stokes bands cannot be made to fit a resonance fluorescence series but can be readily assigned to Stokes and anti-Stokes bands associated with a resonance Raman progression.¹³

Additional evidence suggestive of a Raman process is presented in Figure 3. The spectrum depicted in Figure 3 was taken under equivalent reaction zone conditions to those of the spectrum depicted in Figure 2. The intermediate resolution, ~ 1.5 Å, at which this spectrum was obtained is sufficient to cleanly resolve the atomic sodium $^2P_{3/2} - ^2P_{1/2}$ line splitting (17.2 cm^{-1}) while leaving individual rotational lines unresolved. The relative intensities of each of the sodium D-line components are clearly evident in the scattered Raman emission. Furthermore, the frequency separation of the sodium atomic splitting is clearly reproduced (within the experimental

resolution of the scan) for both the vibrational Stokes and anti-Stokes components of the scattering.

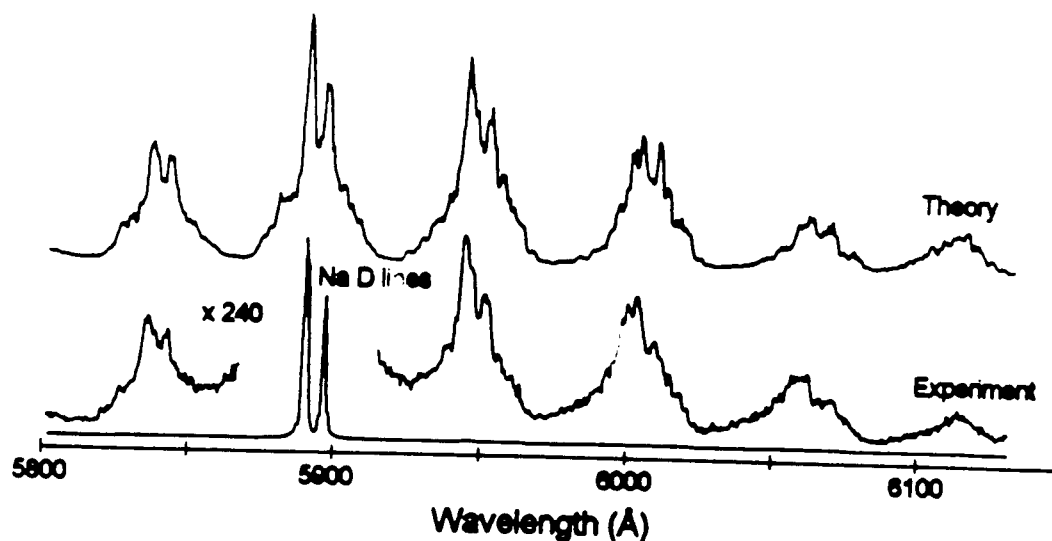


Figure 3

Raman-like spectrum depicting the two Na D-line components and accompanying satellite Raman structure. The $^2P_{3/2}$, $^2P_{1/2}$ - $^2S_{1/2}$ frequency difference of the two Na D-line components is reproduced in the scattered radiation. A simulated spectrum (calculated from Equation 2) is presented for comparison ($T_{\text{ROT}} = 400\text{K}$, $\Gamma = 4\text{ cm}^{-1}$).

We have successfully modeled the group of features symmetrically surrounding the Na D-line with the resonant Raman intensity expression^{9,10,12,13}

$$I_s(\nu_o, J_o; \nu_f, J_f) = \frac{32\pi^3 \omega_s^4 I_p}{9c^4 h^2} M(\xi_o)^4 e^{-\frac{8J_o(J_o+1)hc}{kT}} N(\nu_o) \times \sum_{J_f, J_i} \left(G(P_{3/2}) S_{J_o} S_{J_f} \frac{|\langle \nu_f | \nu_i \rangle \langle \nu_i | \nu_o \rangle|^2}{(\omega_{oi} - \omega_{P_{3/2}})^2 \Gamma^2} + G(P_{1/2}) S_{J_o} S_{J_f} \frac{|\langle \nu_f | \nu_i \rangle \langle \nu_i | \nu_o \rangle|^2}{(\omega_{oi} - \omega_{P_{1/2}})^2 \Gamma^2} \right) \quad (2)$$

where I_s is the total intensity for a scattered Stokes or anti-Stokes line as a function of frequency, ω , and pump intensity, I_p , and c is the speed of light. We consider transitions from an initial rovibrational ground electronic state (G) of the Na_2 molecule to some final rovibrational electronic ground state (F) via an intermediate excited electronic state (I) where ω_{oi} and ω_{if} represent the rovibronic energy differences for the G-I and I-F transitions. Γ is introduced to phenomenologically account for all damping effects. The S_J terms correspond to appropriate Hönl-London factors for the Na_2 $A^1\Sigma_u^+ - X^1\Sigma_g^+$ transition, $M(\xi_o)$ represents the normalized coordinate, $\xi = R/\sqrt{\mu\omega/\hbar}$, evaluated at the equilibrium internuclear distance, R_o , and $\langle \nu_f | \nu_i \rangle$ and

$\langle v_1, v_G \rangle$ represent Franck-Condon overlap integrals. We have included a thermalized ground state rotational distribution and a ground state weighting function $N(v_G)$, which allows for a non-Boltzmann vibrational distribution. We also allow pumping due to each component of the sodium D line, $\omega(P_{3,2})$ and $\omega(P_{1,2})$, to contribute to the scattered emission intensity, I_s . Here, the relative weighting of each component of the atomic emission (D-line) is accounted for by the weight factors, $G(P_{3,2})$ and $G(P_{1,2})$. In our simulations, we have taken the $G(P_{3,2}):G(P_{1,2})$ ratio to be 3:2, determined empirically from the experimental spectrum (see Figure 3).

The numerical calculations^{16,17} were carried out by allowing the near-resonant atomic sodium transitions, $\omega(P_{3,2})$ and $\omega(P_{1,2})$, to pump the first thirty levels in the Na_2 $X^1\Sigma_g^+$ state to the first seventy levels of the Na_2 $A^1\Sigma_u^+$ state. The absolute frequencies (in wavenumbers) of the two D-line components responsible for pumping the Raman-like features were taken from the National Bureau of Standard's compendium on atomic energy levels.¹⁸ A Doppler broadening of the Na D-line components by 0.08 cm^{-1} in our spectral simulations, corresponding to atomic sodium at 1000K, represents a conservative overestimate, and provides no observable correction to simulation spectra produced with narrower Doppler widths ($< 0.08 \text{ cm}^{-1}$). De-excitation from the upper electronic state was allowed to proceed to the first thirty levels of the ground state. Rotational levels $J'', J' = 0$ to 120 were included with each vibrational level of both the excited electronic $A^1\Sigma_u^+$ state and the ground electronic $X^1\Sigma_g^+$ state of the sodium dimer scatterer. Each simulated spectrum produced in the modelling program was convolved with a gaussian function to approximate the effects of a finite spectrometer slit width.

The data in Figure 4 depicts the fit to the vibrational structure surrounding the Na D-line under conditions of pure sodium expansion. All attempts to extract a vibrational temperature through comparison of the observed and calculated Raman spectra were unsuccessful. The low resolution ($\sim 12 \text{ \AA}$) vibrational Raman spectrum depicted in Figure 4 does not correspond to a thermalized vibrational distribution. The calculated spectrum in Figure 4, corresponding to a non-Boltzmann vibrational distribution, closely matches the experimental scan and will also provide a consistent fit to higher resolution spectra. Although the rotational population distribution may also be non-Boltzmann, we find that with an effective rotational temperature of 400K, we are able to obtain close agreement between the experimental and calculated spectrum depicted in Figure 4. This suggests that only slight modifications from a thermalized distribution will be necessary to exactly fit the rotational features.

A still higher resolution scan ($\sim 0.4 \text{ \AA}$) of the first Stokes and anti-Stokes features is depicted and computer simulated in Figure 5. The computer simulation is again based on the application of equation (2). In a surprising result, we find that a linewidth, $\Gamma = 4 \text{ cm}^{-1}$, is required to provide optimum agreement between the simulated and experimental results with correlation coefficients exceeding 0.92 for the anti-Stokes and 0.89 for the Stokes features, respectively. A further confirmation of the required linewidth is indicated in Figure 5 where we compare the experimental spectrum to $\Gamma = 4, 1$, and 0.1 cm^{-1} simulations.

While there are improvements that can be made in the simulations depicted in Figures 3, 4

and 5, it is unlikely that simple power broadening can be responsible for the large effective linewidth indicated by our spectral simulations. Based on the required power broadening for a two level quantum system driven at resonance, we estimate that an electric field of $\sim 1.3 \text{ KV/cm}$ and an absolute power density of $\sim 0.215 \text{ MW/cm}^2$ are necessary to produce the requisite spectral broadening of 4 cm^{-1} .

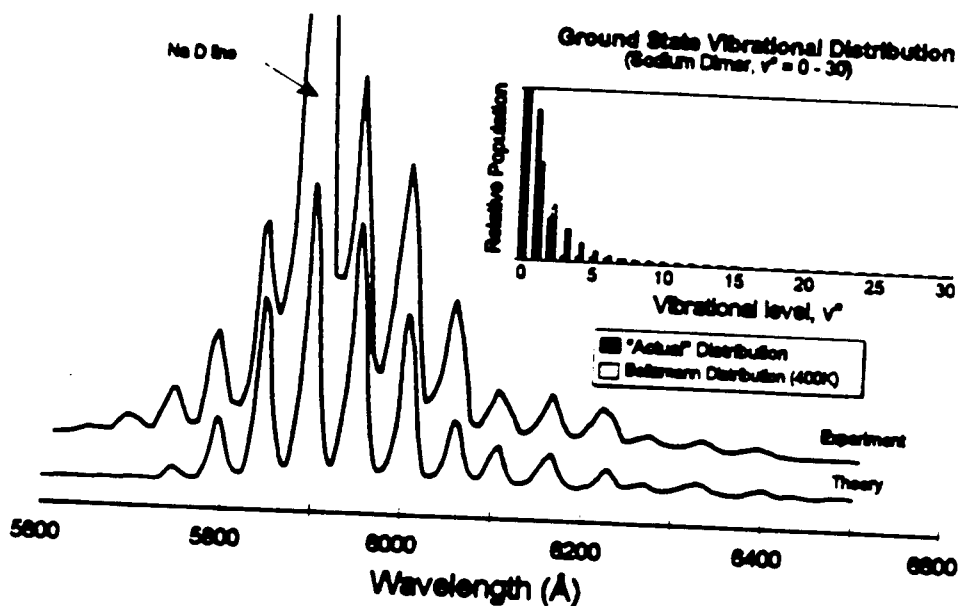


Figure 4
Comparison of experimental Raman spectrum with computer modelled distribution. Optimum agreement was found for the slightly nonthermal distribution depicted in the upper righthand corner of the figure. A Boltzmann distribution at 400K is included for comparison.

The apparent $\sim 4 \text{ cm}^{-1}$ spectral broadening suggests a scattering lifetime of order 10^{-11} seconds, implying a process which is considerably more efficient than would be expected on the basis of resonance Raman pumping involving the Na_2 A-X transition ($\sim 10^{-8}$ seconds based on the radiative lifetime¹⁶). Several additional experiments involving the direct pumping of the sodium expansion in the absence of bromine atom reactant at the Na D-line frequencies (argon ion pumped R6G) and at 4765 Å and 4880 Å using a multimode argon ion laser, failed to reveal optical signatures corresponding to those depicted in Figures 2-5. In fact, while it was possible to excite laser induced fluorescence corresponding to the Na_2 A-X and B-X band systems analogous to that observed previously,¹⁹ although at somewhat higher temperatures in the present experiments, no clear Raman features were generated. This result suggests a more efficient process than that associated with resonance Raman pumping and further demonstrates that halogen atoms must be present in the reactive environment for the Raman scattering to take place.

4. EVIDENCE FOR OPTICAL GAIN

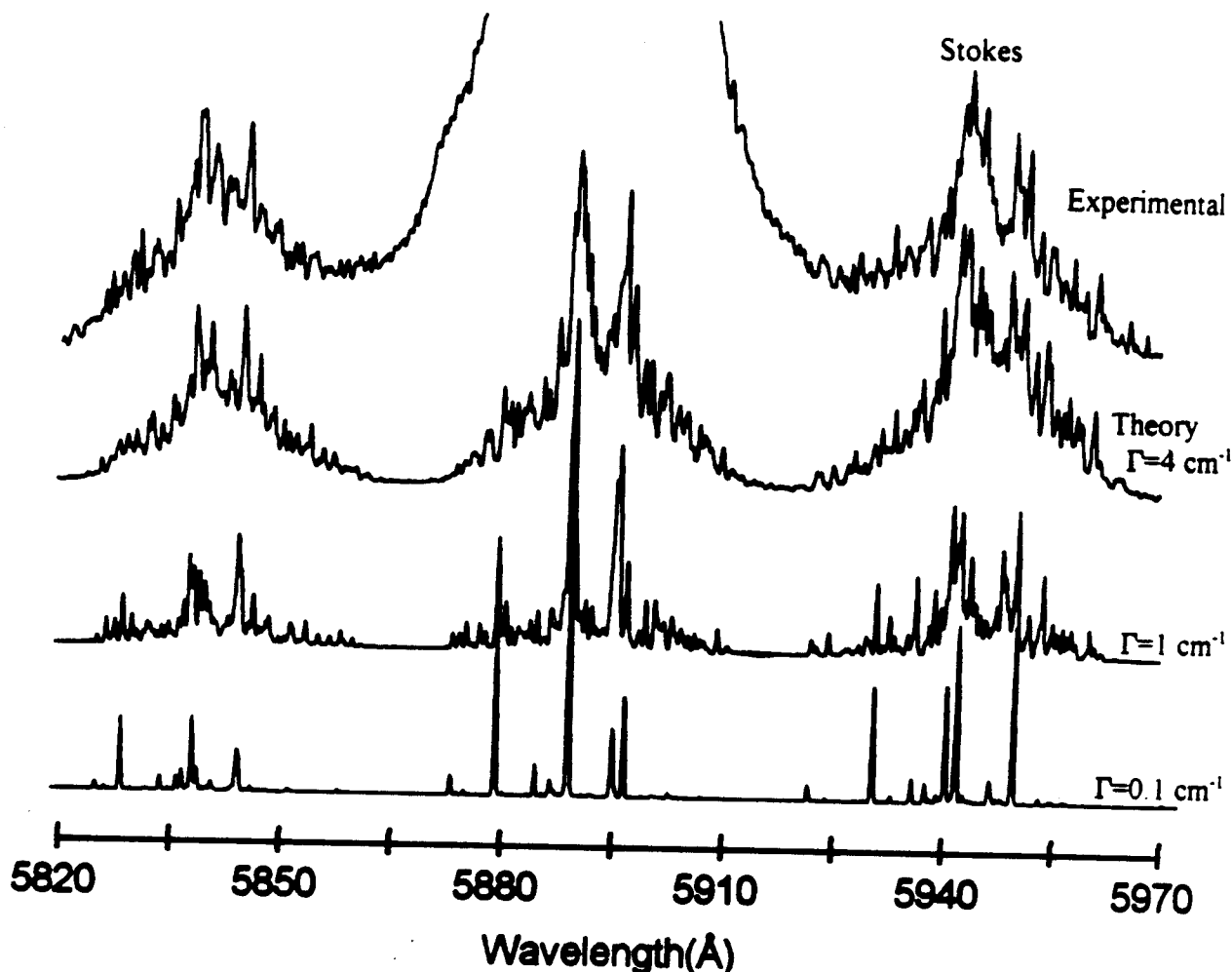


Figure 5
High resolution spectrum ($\sim 0.5 \text{ Å}$) and simulated spectra for $\Gamma = 0.1, 1$, and 4 cm^{-1} demonstrating the marked improvement in the fit to the experimental Raman-like features for increasing values of Γ . See text for discussion.

Using the optical configuration described in Figure 6, we have observed the manifestation of gain on several of the Stokes and anti-Stokes features depicted in Figure 4.

At a resolution of $\sim 12 \text{ Å}$, we have consistently observed a ratio of 2.3:1 for the double versus single pass light intensity ($I_a:I_b$) associated with the first Stokes feature located near 5940 Å. Apparent gain has also been monitored on several additional Raman features depicted in Figure 4. In monitoring the first anti-Stokes feature, for example, we determine a ratio for $I_a:I_b$ of 2.2:1. Ratios $I_a:I_b$ slightly greater than 2:1 were measured on all of the observable Stokes and

anti-Stokes features. For comparison, similar measurements were performed at 12 Å resolution on the center D-line frequency ($\lambda = 5892$ Å), where significant self-absorption is expected. At this frequency, a ratio close to 1.6:1 was measured for I_u/I_b . Other chemiluminescent features associated with the optical signature depicted in Figure 2, notably the emission corresponding to the thermalized Na_2 $B^1\Pi_u - X^1\Sigma_g^-$ transition, were also investigated and did not demonstrate gain. In fact, ratios I_u/I_b less than 1.5:1 were measured at the wavelengths associated with this transition. Further, no gain was monitored on the excimer-like Na_2 $2^3\Pi_g - 1^3\Sigma_u^-$ bound free transition.

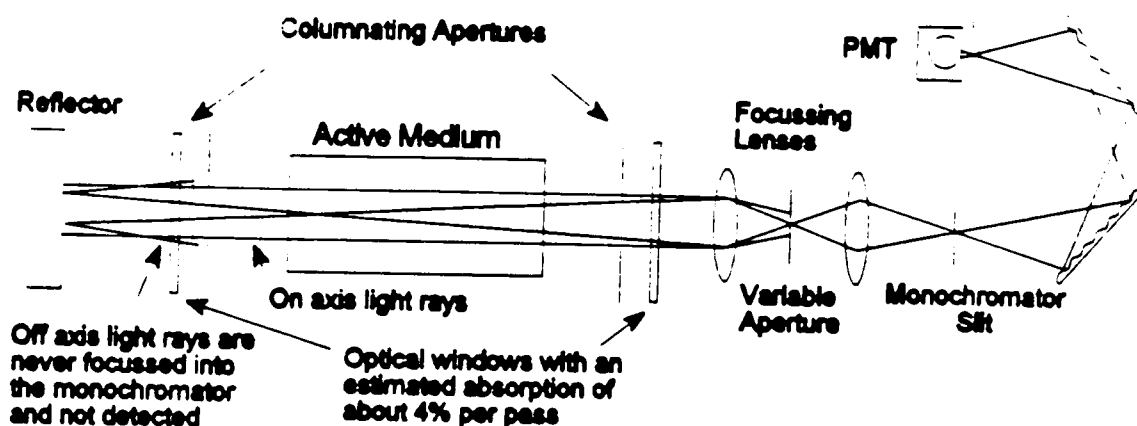


Figure 6

Schematic of gain measurement configuration. Intensities monitored with the PMT are measured with the high reflector blocked (I_b) and unblocked (I_u). In the absence of gain or loss, the maximum ratio of intensities that can be monitored can be no greater than two. This configuration accepts only light travelling parallel to the optical axis. See text for discussion.

While the results of these measurements are certainly valid for conventionally pumped gain media, care should be exercised in interpreting their meaning. In conventional stimulated emission, where a population inversion exists between two levels, a photon of the appropriate frequency can stimulate emission and the depopulation of the upper amplifier level, creating a coherent field of photons of intensity I and frequency ν . The simple gain detection scheme we have implemented here functions to reflect light of all frequencies present from the rear reflector back into the active medium. However, only photons of the appropriate frequency, ν , can contribute to an intensity increase in the light field. The monochromator-photomultiplier tube combination then detects the contribution of a narrow frequency range associated with the intensity of on-axis light both with and without the rear reflector operational. Absolute ratios of the measured light intensities can then be used to derive a double pass (or small signal) gain coefficient.

The situation in the present system, however, is slightly different. Under a Raman

scattering process, light of frequency ν_p (pump frequency) is reflected back into the active medium along with light of the scattering frequency ν_s (Stokes frequency). If gain is present in the system, light (I_s) at a frequency ν_s will increase in intensity as it propagates through the medium to the detector (monochromator + PMT). However, it must be remembered that the pump light, I_p , is also reflected back into the active medium by the broad band reflector, inducing a Raman scattering signal at a frequency ν_s . The observed increase in the intensity of the Stokes field, I_s , will necessarily represent contributions from Raman scattering as well as any amplification due to the existence of the gain condition.

This discussion suggests that one must be cautious in the interpretation of the I_s/I_p ratios. These initial gain measurements are important because they do not indicate the absence of gain associated with the Raman scattering. The measurements do, however, indicate the absence of gain on other chemiluminescent emission features (the Na_2 , $\text{B}^1\Pi_u - \text{X}^1\Sigma_g^+$ band, for example) since the I_s/I_p ratios, which are much less than 2:1, would suggest that no gain exists. Moreover, if we consider the losses associated with our measurements (1) at the high reflector ($\sim 1\%$) and (2) upon passage through the optical flats ($\sim 2 \times 4\%$), the determination of a ratio of 2.3:1 on the first Stokes feature may be indicative of substantial gain. However, for the reasons outlined above, it is premature to calculate a double pass gain coefficient for any of the Raman scattering features. Future studies involving the use of a probe laser will eventually resolve the gain question.

5. ACKNOWLEDGEMENTS

The authors gratefully acknowledge helpful discussions with Professors Ron Felton and Michael Heaven, and Dr. Kangkang Shen. Helpful comments and technical assistance from Mr. C. B. Winstead is also greatly appreciated. The support of the Georgia Tech Foundation through a grant from Mrs. Betty Peterman Gole, the Army Research Office through the Short Term Innovative Research Program, the Air Force Office of Scientific Research and the Army Research Office and AFOSR/SDIO is also greatly acknowledged.

6. REFERENCES

1. W.H. Crumley, J. L. Gole, and D. A. Dixon, *J. Chem. Phys.* vol. 76, pg. 6439, 1982.
2. (a) J. L. Gole, "The Unique Nature of Metal Cluster Oxidation," J. L. Gole, in Physics and Chemistry of Finite Systems: From Clusters to Crystals, Volume II, Edited by P. Jena, S. N. Khanna, and B. K. Rao, NATO ASI Series, Vol. II, pg. 1025 (1992).
 (b) J. L. Gole, "Toward the Modeling of the Oxidation of Small Metal and Metalloid Molecules," GasPhase Metal Reactions, edited by A. Fontijn, North Holland, Amsterdam 1992, pp. 578 - 604.
 (c) J. L. Gole, "The Unique Complexation and Oxidation of Metal-Based Clusters," Advances in Metal and Semiconductor Clusters, Vol. 1, Spectroscopy and Dynamics, ed. M. A. Duncan, JAI Press, 1993, pp. 159-209.
3. S. H. Cobb, J. R. Woodward, and J. L. Gole, *Chem. Phys. Lett.*, Vol. 156, pg 197, 1989.

4. J. L. Gole, K. K. Shen, H. Wang, and D. Grantier, "Chemically driven pulsed and continuous visible laser amplifiers and oscillators," Invited Talk, *Proceedings of the 23rd AIAA Plasma-Dynamics and Laser Science Conference*, AIAA 92-2994, Nashville, Tennessee, 1992.
5. B. Wellegehausen, *IEEE J. Q. E.*, Vol. 15, pg. 1108, 1979.
6. B. Wellegehausen, "Metal bonding and interactions in high temperature systems with emphasis on alkali metals," *Am. Chem. Soc. Symp. Ser. 179*, eds. J. L. Gole and W. C. Stwalley (Am. Chem. Society, Washington), pg. 462.
7. U. Gaubatz, H. Bissantz, U. Hefter, I. Colomb de Daunant, K. Bergmann, and P. L. Jones, *J. Opt. Soc. Am.*, Vol. 6, 1386, 1989.
8. I. Littler, S. Balle, and K. Bergmann, "Molecular beam Raman laser with a 250 nW threshold pump power," *Opt. Comm.*, Vol. 77, pp. 390-394, July 1990.
9. D. L. Rousseau and P. F. Williams, *J. Chem. Phys.*, Vol. 64, pg. 3519, 1976.
10. See, for example, J. Tang and A. C. Albrecht, "Raman Spectroscopy," edited by H. A. Szymanski (Plenum, New York, 1970), Vol. 2, pp. 33-68.
A. C. Albrecht, *J. Chem. Phys.*, Vol. 34, 1476, 1961.
11. D. Grantier, H. Wang, C. B. Winstead, and J. L. Gole, *Proceedings of the 24th AIAA Plasma Dynamics and Lasers Conference*, Orlando, Florida, AIAA 930-3207, 1993.
12. D. Grantier and J. L. Gole, "Chemically Enhanced Raman Scattering," in preparation.
13. S. H. Cobb, Ph.D. Thesis, Georgia Institute of Technology, Atlanta, Georgia, USA, 1988.
14. G. Roll and J. Mentel, *J. Phys. D. Appl. Phys.*, Vol. 22, pg. 483, 1989.
15. D. Grantier and J. L. Gole, "Raman Pumping in the Absence of an External Light Source", accepted for publication, *J. Phys. Chem. Lett.*, July 1994.
16. W. T. Zemke, K. K. Verma, T. Vu, and W. C. Stwalley, *J. Mol. Spectrosc.*, Vol. 85, pg. 150, 1981.
17. P. Kusch and M. M. Hessel, *J. Chem. Phys.*, Vol. 68, pg. 2591, 1978.
18. C. E. Moore, "Atomic Energy Levels," National Bureau of Standards, 1949.
19. J. L. Gole, G. J. Green, S. A. Pace, and D. R. Preuss, *J. Chem. Phys.*, Vol. 76, pg. 2247, 1982.

APPENDIX XVII

"Highly Efficient Collisional Stabilization and the Symmetry Constrained Dynamics of High Temperature Complex Formation", J. Chem. Phys., J. L. Gole submitted.

**HIGHLY EFFICIENT COLLISIONAL STABILIZATION AND THE SYMMETRY CONSTRAINED
DYNAMICS OF HIGH TEMPERATURE COMPLEX FORMATION**

James L. Gole
School of Physics
Georgia Institute of Technology
Atlanta, Georgia 30332

ABSTRACT

The highly efficient collisional stabilization of high temperature complexes of some considerable spatial extent is demonstrated. A series of near single collision and well defined multiple collision (following paper) chemiluminescent and laser induced fluorescent studies extending over six decades of pressure demonstrate the stabilization of electronically excited Group IIA dihalide collision complexes via a radiative three body recombination process (R3BR) operative at microTorr pressures. Over the pressure range 1×10^{-6} - 5×10^{-4} Torr, a comparative study of the emission from M (M=Ca,Sr,Ba) - X_2 (Cl_2, Br_2, I_2) and M-XY (ICl, IBr) reactive encounters identifies a symmetry constrained dynamics associated with the formation of the dihalide product complexes. The onset of the monitored R3BR process at 1×10^{-6} Torr signals an extremely large stabilization cross section ($\sigma_S > 3000 \text{ \AA}^2$) which may not be readily explained within the RRKM framework. Comparisons between the highly ionic dihalides and the isoelectronic CO_2 molecule are noted as they affect excited state dynamics. The pressure dependence of the light emission from these complexes in the near single collision pressure range displays a striking correlation with the periodicity of dihalide molecular electronic structure and the resultant nature of the low-lying dihalide electronic transitions. The absence of a difluoride emission associated with the M(Ca,Sr,Ba)- F_2 reactive encounters signals an important periodic trend in these systems. A simple first order model within the electron jump framework is presented to explain the qualitative trends inherent to these reactions.

INTRODUCTION

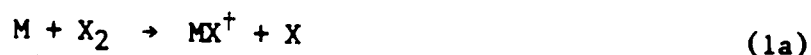
Collisions which lead to complex stabilization or rapid energy redistribution can play an important role in high temperature environments, including combustion and gasification streams,¹⁻³ as they influence energy storage and conversion. Further, they may play an important role in deposition processes whose inception is influenced by the formation of the gas phase constituency.³ Here we present evidence which suggests that a number of these interactions may be operative over a much broader region of configuration space than previously anticipated to the extent that a ready explanation of the present observations with existing models of recombination and energy transfer may be tenuous.

Typically, radiative association processes, which provide information on highly excited molecular states and dissociation limits,⁴ have been studied at sufficiently high pressures so as to allow collisional stabilization of the associating species and, consequently, the time necessary for a spontaneous radiative event. As these collisional stabilization processes can lead to some loss of dynamical information, it has been the province of the molecular beamist to extend their study, performing experiments which isolate and evaluate contributions from two-body radiative recombination.⁵⁻¹⁰ Thus, using crossed beams, Kasai et al.⁶ observed a binary reaction of NO and O, Parson⁵ obtained strong evidence for the Cr-O₂ association process, and Yoshimura et al.⁷ measured the HNO A-X emission from an associating H and NO.

The experiments of Yoshimura et al.⁷ are particularly intriguing with their emphasis on the study of a hydrogen based association as a means of monitoring discrete emission from a two-body association reaction. Their results, while carefully obtained, seem surprising for they indicate excited state relaxation under beam conditions before the emission of a photon from the lowest vibrational levels of the HNO A state (at energies well below ($\sim 3000 \text{ cm}^{-1}$) the HNO dissociation limit). Further, the observations under beam conditions seem counter to a pronounced A state vibrational excitation at somewhat higher pressures. This behavior, which might be explained by highly efficient - long range collisional events involving the forming HNO ground and low-lying A state, suggests that a much broader region of configuration space might be relevant to the description of several reactive environments. In fact, while the focus of the outlined molecular beam experiments has been

to isolate the two-body association process, it is of equal if not greater importance that they signal the efficiency of multicenter stabilization processes that are operative at extremely low pressures and can strongly influence system behavior over large pressure ranges. It is with this focus that we have carried out a detailed study of the formation, collisional stabilization, and relaxation of a set of periodically correlated collision processes involving the formation and interaction of complexes of considerable spatial extent.^{2,11,12}

The reactions of alkaline earth atoms with halogen molecules to form the Group IIA dihalides, MX_2^* , once thought to be bimolecular,^{8,9} have been shown to be termolecular and second order in the halogen concentration at micro-Torr pressures. On the basis of several considerations,¹³⁻¹⁷ it has been strongly suggested that the dihalide formation requires a two step mechanism involving a vibrationally excited ground state MX^+ intermediate viz.



This sequence involves two electron jump processes and produces the desired second order dependence on halogen concentration for the observed MX_2 emission.

While sequence (1) is quite appealing and would seem to be in accord with well established theoretical models and a number of experimental observations,¹³⁻¹⁷ an alternate mechanism, consistent with the halogen pressure dependence, centers on the collisional stabilization of a highly vibrationally excited MX_2^{*+} intermediate viz.



where the stabilization process, a radiative three-body recombination (R3BR), must overcome the propensity for a "rapid" dissociation of the highly excited MX_2^{*+} complex.

Through a series of near single collision¹⁸ and well defined multiple collision¹⁹⁻²¹ chemiluminescent and laser induced fluorescent studies

extending over six decades of pressure, we demonstrate the highly efficient stabilization of electronically excited Group IIA dihalide collision complexes via the R3BR process (mechanism 2). We identify a symmetry constrained dynamics associated with the formation of these complexes, obtaining the first vibrationally resolved emission spectra for the dihalides. The onset of the monitored R3BR process at 1×10^{-6} Torr signals an extremely large stabilization cross section ($\sigma_S > 3000 \text{ \AA}^2$) which may not be readily explained within the RRKM framework, suggesting that new models, adjusted to the interactions of electronically or highly vibrationally excited states, will be necessary to clarify these processes. The monitored complexations, which define a much broader range of interaction than has typically been associated with collisional stabilization phenomena, are best clarified by considering the periodicity inherent to a broad grid of Group IIA metal, $M(\text{Mg}, \text{Ca}, \text{Sr}, \text{Ba})$ -halogen molecule, $X_2(\text{F}_2, \text{Cl}_2, \text{ClF}, \text{Br}_2, \text{ICl}, \text{IBr}, \text{I}_2)$ reactions.

In this first paper, we demonstrate the symmetry constrained dynamics inherent to the Group IIA metal-halogen molecule reactions as it signals the highly efficient concerted and collisionally stabilized formation of Group IIA dihalide excited states. In the following paper, through the controlled extension and relaxation of the near single collision process under multiple collision conditions, we confirm the highly efficient R3BR mechanism as well as establishing discrete assignments for the near single collision emission continuum.

EXPERIMENTAL

The apparatus used to study the Group IIA-halogen molecule reactions under near single collision conditions represents a variant of one that has been described previously.¹⁸ Calcium, strontium, and barium metal were vaporized effusively from capped tantalum crucibles into a chamber whose background pressure was maintained at 5×10^{-7} Torr. The metals effuse from a hole $\leq 1/8$ " in diameter, $1/2$ " from the top of the capped crucibles. The crucibles were surrounded by a 1" diameter tantalum radiator which acted as a resistive heating element to produce uniform crucible temperatures in the range between 1000 and 1200K. The Group IIA metallic beams, passing through holes in the heating radiator, tantalum heat shields concentrically surrounding the radiator, and a water-cooled copper jacket surrounding the

entire grouping, entered a differentially pumped system. The beams then passed through an iris based adjustable orifice into a tenuous atmosphere of oxidant gas (reaction chamber) producing the chemiluminescent emissions recorded in Figures 1-3. There have been relatively few measurements of the calcium, strontium, and barium vapor pressures. Based on these studies,²² the vapor pressures in the crucibles ranged from 10^{-2} to 1 Torr.

Fluorine (Air Products Specialty Gases > 98% purity), ClF (K and K Laboratories 98%), Cl₂ (Matheson > 99.5%), Br₂ (Matheson > 99.9%, Fisher > 99.95%), ICl (Kodak > 99.9%, Alfa > 99.8%), IBr (Alfa > 99.8%), and I₂ (Fisher > 99.8%) were obtained commercially. The three oxidant gases F₂, ClF, and Cl₂ were allowed to bleed into the reaction chamber through a double micrometer needle valve assembly. In order to insure that the ClF was not contaminated, we purified the gas in two stages. The sample was placed in a glass ballast trap which was then placed in liquid nitrogen and evacuated in order to remove any possible fluorine contaminants. Subsequently, during the experimental run, the sample was placed in an n-amyl alcohol slush, thus insuring against Cl₂ contamination.

For studies involving Br₂, IBr, and I₂, the gas handling system was modified so that substances which are liquids or solids at room temperature could be introduced as gases into the reaction chamber. Small stainless steel or pyrex containers were attached to the first micrometer needle valve and a succession of pumping-freezing cycles was used to remove volatile impurities. The vapor pressure of Br₂ is sufficiently high to permit the production of a gas beam at room temperature. The same would appear to be true for IBr; however, as with I₂, it was necessary to increase the vaporization rate by heating the sample slightly in order to obtain a sufficient vapor pressure.

For these single collision studies, the oxidant gases were mildly collimated but filled the entire reaction chamber at pressures ranging from 1×10^{-6} to 5×10^{-4} Torr. The permanent gases were first partially transferred to a ballast tank which provides gas pressure stability during the course of an experiment. Background pressures were monitored primarily with an ionization gauge 25 cm from the reaction zone, however the majority of the in-situ pressure measurements were made with a capacitance manometer 3 cm from the reaction zone. If both gauges were used to monitor gas pressure, the values measured using the capacitance manometer were between 15 and 25% higher than those measured by the ionization gauge, depending upon the gas in use.

The pressure dependence plots presented in the following sections were obtained, using the capacitance manometer, by monitoring the light emission from the reaction zone. Corrections, which take into account slight pressure gradients across the chamber, have been made to these pressure dependence plots.

Metal source temperatures were measured with a Leeds and Northrup disappearing filament optical pyrometer focused on the back center of the crucible containing the metal of interest. The crucible was observed through a quartz window directly behind the oven and through a 5/16" diameter hole in the tantalum radiator. The pyrometer was calibrated during each run by comparison with a calibrated tungsten-5% rhenium vs. tungsten-25% rhenium thermocouple (Control Products Corp.). The thermocouple junction was sheathed in BeO and tantalum and protected by a tungsten well. This assembly was placed vertically through the base of the oven, between the crucible and the tantalum radiator, and located in its closest possible proximity to the crucible orifice.

The chemiluminescence from the reactions of interest was monitored at right angles to the metal flow. Spectral emissions were dispersed with a 1-m Spex scanning monochromator operated in first order with a Bausch and Lomb 1200 groove/mm grating blazed at 5000 Å. Either cooled RCA 1P28 or 4840 or a dry ice cooled EMI 9808 photomultiplier tube were used to detect the dispersed fluorescence and provide a signal for either a Keithley 417 fast picoammeter or a 417 autoranging picoammeter. The output signal from the picoammeters was then sent either to a Hewlett Packard chart recorder or to a personal computer for storage and subsequent analysis. All spectra were wavelength calibrated with a mercury arc lamp²³ or with respect to Group IIA metal atomic emissions.²³

RESULTS AND DISCUSSION - PERIODICITY OF GROUP IIA DIHALIDE FORMATION

Near "Single Collision" Chemiluminescence and Symmetry Constrained Product Formation

As Table I demonstrates, the strength of the second Group IIA metal halogen bond is at least comparable to or considerably exceeds that of the first. In other words the atomization energy, especially of the heavier

halogen dihalides, is at least twice the dissociation energy of the metal monohalide. This bonding characteristic suggests that the Group IIA-halogen molecule reactions might represent good candidates to study few body complexation processes.

The low Group IIA metal ionization potentials²³ and the high halogen electron affinities²⁴ signal that these reactions are expected to proceed via the electron jump process whereby the Group IIA metal throws out an electron and harpoons the halogen molecule forming an $M^+X_2^-$ complex. The data presented in Figures 1-3 summarizes the observed dihalide emission spectra generated for the reactions of Ca, Sr, and Ba with the homonuclear (Cl_2, Br_2, I_2) and mixed (ClF, ICl, IBr) halogens, under near single collision conditions (at pressures ranging from 10^{-6} - 10^{-4} Torr). The emission from the mixed halogen reactions with strontium and barium is distinctly weaker than that from the homonuclear metatheses.

In contrast to the $M = Ca, Sr, Ba-X_2$ ($X=Cl, Br, I$) reactions which yield a strong dihalide emission, the reactions of molecular fluorine with these metals leads only to monofluoride emission. In fact, only a weak emission continuum in the range $\sim 3500-5500 \text{ \AA}$ is observed for the magnesium system and this emission is found to be quadratic in the fluorine molecule concentration. This dichotomy represents an important periodic trend in the formation of the dihalides.

The lack of a notable difluoride emission for the Ca, Sr, and Ba reactions represents a serious challenge to the validity of the double harpoon mechanism (1). The data in Table I as well as periodic correlations with atomic dissociation products²⁵ suggest that the reaction sequence (1) easily supplies the energy necessary to access difluoride excited states. We suggest that the lack of a CaF_2 , SrF_2 , or BaF_2 emission results, at least in part, because the fluorine molecule negative ions produced in the electron jump process dissociate much more rapidly than do the corresponding Cl_2^- , Br_2^- , or I_2^- ions.²⁶ This results not only from the considerably smaller bond energy of the fluorine molecule but also from the nature of the vertical electron attachment process which creates the fluorine negative ion high on the repulsive wall of its ground state potential.²⁶ In contrast, the process for the more tightly bound, heavier halogens, whose size better accomodates electron attachment, can lead to the formation of a considerably longer-lived negative ion. While it is difficult to create a long-lived $M^+X_2^-$ complex in

those reactions with molecular fluorine, complex formation can be accommodated for the heavier halogens. The observation of both BaF monohalide and BaClF dihalide continuum emission for the reaction of barium with a strongly bound ClF (59.2 kcal/mole)²⁷ molecule (Fig. 1(c)) and the corresponding lack of a difluoride emission resulting from the Ba + F₂ reaction (Appendix A) support the outlined suggestions. However we must also note (Table I) that whereas the (MF₂) atomization energies are near to 2D₀⁰(MF), the atomization energies of the chlorides, bromides, and iodides well exceed twice the metal monohalide bond energy.

An important symmetry constraint is signaled by the intensity of the emission from the dihalides formed in the reactions of calcium, strontium, and barium with the mixed halogen molecules IBr and ICl. Figures 1(a) and 1(b) demonstrate a much weaker emission for the heteronuclear halogen molecule reactions with barium. The compared spectra were taken at the same resolution and with nearly identical halogen pressures and metal beam fluxes. We will suggest that the dominant intensity for the Cl₂, Br₂, and I₂ reactions results because of the C_{2v} reaction path available to the homonuclear (but not accessible to the heteronuclear) halogen reactions. The availability of this C_{2v} reactive geometry (conical intersection) promotes excited state dihalide formation for M + X₂ but not M + XY reactive encounters. The observed symmetry effects can be manifest by the collisional stabilization mechanism (2) but are highly unlikely for the two step harpoon mechanism (1). While the difference in continuum intensity is quite pronounced for the barium reactions, this difference decreases for the strontium reactions (Figure 2) and is almost muted for the calcium reactions (Figure 3). This behavior is consistent with the electron jump model and an increasing reactant relative velocity for the calcium and strontium reactions at the curve crossing region associated with the M+X₂ → M⁺ + X₂⁻ harpooning process.

Nature of Group IIA Dihalide Electronic States

The expected nature of the transitions responsible for the observed dihalide emission continua depicted in Figures 1-3 can be summarized using the data in Tables II²⁸ and III and the molecular orbital correlation diagram depicted in Figure 4.²⁹ We will discuss the contributing transition regions (Table III) in greater detail when considering the vibronically resolved

dihalide emission spectra observed under multiple collision conditions.³⁰ For our present purposes, however, it is relevant that we consider the grid of ground state dihalide geometries determined by Klemperer et al.²⁸ (electric quadrupole deflection of molecular beams) and outlined in Table II. A clear trend from linear to bent character, which has been discussed by several authors,³¹⁻³⁴ is apparent as linear geometries are favored by the light metal-heavy halogen combinations whereas bent structures are favored by the heavy metal-light halogen combinations.

The strongly ionic character of the Group IIA dihalides has important consequences as the BeF_2 valence correlation diagram of Figure 4 demonstrates. Here the orbital occupation for the ground state of BeF_2 is complete through the π_g orbital and the greater stability of the sum of valence orbital energies at 180° predicts a linear ground state geometry. However, in contrast to the strongly allowed transitions in the isoelectronic CO_2 molecule, the lowest energy excited states in BeF_2 are predicted to result from promotions involving the highest occupied π_g (a_2, b_2) molecular orbital of the ground state to the lowest unoccupied σ_g (a_1) orbital.²⁹ The resulting $A^1\Pi_g - X^1\Sigma_g^+$ transitions (which are electric dipole forbidden in absorption for the linear molecule) have not been observed even in attempted studies of the absorption spectrum for the highly bent BaF_2 molecule. In emission, $^1B_2 - ^1A_1$ transitions from a highly bent excited state (Table III, A-X region) should be of reasonable intensity, involving long progressions in the bending modes of the upper and lower states. However, even though the transition in emission is allowed (governed by the C_{2v} selection rules), the lack of any absorption data, even for BaF_2 , suggests that the observed emission spectra may manifest the influence of the $g \leftrightarrow g$ selection rule, resulting in a long-lived excited state emitter.

Transitions which involve excitation from the π_g to the π_u valence orbital are expected to occur at somewhat higher energy and to be characterized by allowed absorption and emission band systems which should be manifest of progressions in the dihalide stretching frequency (Table III).

Periodic Trends in the Pressure Dependence of Dihalide Emission Features

Collisional Stabilization of Dihalide Excited States

The behavior of the chemiluminescent intensity as a function of oxidant pressure follows a dependence of the form $p^\beta e^{-\alpha p}$ where β represents the order of the reaction relative to the constituents under study and $e^{-\alpha p}$ represents an attenuation factor proportional to the reaction cross section.³⁵ Reactions following first order bimolecular kinetics will display a linear increase in chemiluminescence intensity with increasing oxidant pressure until attenuation effects become significant. Faster than first order reactions will display a positive curvature since β is greater than one.³⁶ Both the collisional stabilization mechanism (2) and the two step double harpoon mechanism (1) should display a quadratic dependence in the oxidant pressure.

In Figure 5 we present plots of chemiluminescent intensity verses oxidant pressure for the $\text{Ba} + \text{Cl}_2$ and $\text{Ba} + \text{ClF}$ reactions. The plot for the $\text{Ba} + \text{Cl}_2$ reaction represents the compilation of two experimental runs at 4500 Å (res = 10 Å), whereas the data for the $\text{Ba} + \text{ClF}$ reaction were taken at 4000 Å. These plots indicate a second order dependence on oxidant pressure. They can be compared with the number density vs. light intensity plots of Wren and Menzinger¹⁰ for the $\text{Ba} - \text{F}_2$, Cl_2 , Br_2 and I_2 reactions depicted in Figure 6. While these authors interpret their data for the $\text{Ba} + \text{Cl}_2$, Br_2 and I_2 reactions as displaying a linear onset followed by a quadratic increase in light intensity as a function of pressure, we find no evidence for linearity at pressures as low as 1×10^{-6} Torr either for the $\text{Ba} + \text{Cl}_2$ reaction or for the $\text{Ba} + \text{I}_2$ reaction whose pressure dependence is depicted in Figure 7. Further insight into the behavior of the emission continuum is gained from Table IV where we plot relative intensities as a function of pressure and wavelength for the BaCl_2^* continuum. The data in Table IV suggest the collapse of intensity in the wings of the continuum with increasing pressure. We find that this pattern pervades as we extend these low pressure studies in a controlled manner to the multiple collision pressure regime.³⁰

If we consider more closely the pressure dependent behavior indicated by the data of Wren and Menzinger,¹⁰ we note a trend in the onset of the faster than first order pressure dependence. The onset of the nonlinear intensity increase with pressure is most pronounced for the $\text{Ba} + \text{I}_2$ continuum followed

by the continua for $\text{Ba} + \text{Br}_2$ and $\text{Ba} + \text{Cl}_2$, respectively. This trend might be explained by the increased density of states for the heavier product dihalides which promotes a more efficient collisionally stabilized emission. It might also result from the periodic interplay between the ground and low-lying electronic states of the dihalide.

For all of the dihalides which are linear in their ground electronic states, the $g \leftrightarrow g$ electric dipole forbidden nature of the lowest energy transition will lead to a very weak absorption. The results in Table II portend of a clear periodic trend. For the barium dihalides, all of which have bent configurations, BaI_2 will be influenced by the electric dipole forbidden $g \leftrightarrow g$ transition (for the linear configuration)³⁷ more than will BaBr_2 (which should then exceed BaCl_2 , and BaF_2 , respectively). The BaF_2 absorption cross section should exceed the cross sections of all the remaining Group IIA dihalides.

The emission spectra for the lowest energy transitions of the Group IIA dihalides should also be influenced by the nature of the $g \leftrightarrow g$ selection rule. The excited state radiative lifetimes for the barium halides will be expected to follow the trend $\tau_R(\text{BaI}_2) > \tau_R(\text{BaBr}_2) > \tau_R(\text{BaCl}_2) > \tau_R(\text{BaF}_2)$. The expected trend in the radiative lifetimes can be manifest in the observed pressure dependences (Figures 5-7) for the Group IIA-metal halogen reactions. The longer lived species are expected to display the effects of secondary stabilizing collisions at lower pressures. This appears manifest in Figure 6 where the BaI_2 pressure dependent emission intensity rises at a faster rate than that for BaBr_2 (whose rise is correspondingly faster than that for BaCl_2). A similar trend is manifest in Figure 7 for the CaI_2 , SrI_2 , and BaI_2 emission features where the "faster than first order" behavior onsets most sharply for the longer-lived CaI_2 followed by SrI_2 and then BaI_2 .

While it might be argued that the behavior observed for the barium halides corresponds to an enhanced stabilization cross section paralleling an increased density of states, this is an unlikely explanation for the trends observed in Figure 7 for the CaI_2 , SrI_2 , and BaI_2 pressure dependences. The data in Figure 5 for the BaCl_2 and BaClF emission features are also consistent with a dependence on radiative lifetime. Here the BaClF complex is expected to be shorter lived due to the lighter fluorine atom and the loss of symmetry relative to BaCl_2 .^{30,38} The parallel with the periodic trends observed in

Table II is striking.

The data presented in Figure 6 for the Ba + F₂ reaction seems inconsistent with this periodically based interpretation and with the observed pressure dependences of the remaining barium reactions. However, it can be demonstrated (Appendix A) that the observed linear pressure dependence which corresponds with the seemingly continuous emission feature observed to extend from 6000-7000 Å in the spectrum for the Ba + F₂ reaction (Fig. 1(d)) correlates not with BaF₂ but with a much shorter lived, highly vibrationally-rotationally excited, BaF molecule.

A Symmetry Constrained Electron Jump Process

The relative intensities of the Group IIA dihalide continuum emissions observed for homo- and heteronuclear halogen reactions can be understood within the electron jump harpoon model. Here we use the correlations outlined in Table V and extrapolate on the simple yet elegant arguments used by Menzinger¹⁴ to explain the metal monohalide chemiluminescent emissions from fluorine and chlorine molecule reactions.

The correlation diagram in Figure 8 provides a simple description of the reaction channels based upon electronic rearrangements along the reaction coordinate. This simple model, which reduces the four-dimensional hypersurface to two-dimensional energy profiles, can be used to provide a good first order description of the systems of interest because of the strongly covalent and ionic character of the relevant configurations. Within this framework, the location of the intersections, R_x, of the curves (configurations) of interest and the strength of their coupling¹⁴ can be estimated from Coulomb's law and empirical correlations.³⁹⁻⁴¹

We adopt the reasonable proviso that most of the electronic branching for these systems is governed by entrance channel interactions. We realize that at long range, where the Coulomb interaction of charge clouds dominates the multipole expansion of the interaction potential, the Harpooning model⁴² provides a reliable estimate of the covalent/ionic crossing radius

$$R_x = e^2 / \Delta E_{ci} \quad (3)$$

where $\Delta E_{ci} = IP - EA$ is the asymptotic separation of covalent |c> and ionic

$|i\rangle$ configurations and where IP and EA are the effective values of the reacting metal fragment ionization potential and halogen molecule electron affinity. Although the model is expected to fail at shorter range in proportion to the overlap of the fragment electron distributions, it can still provide a reasonable estimate of the inner crossing regions. The correlation diagram is constructed on this basis.

Reactions to produce the dihalide are thought to proceed through an electron jump "outer harpooning" process involving the interaction of the $M + X_2$ ($|1\rangle$ in Fig. 8) covalent and $M^+ + X_2^-$ ($|3\rangle$ in Fig. 8) ionic curves. For a C_s or $C_{\infty v}$ collision geometry, this process involves the strong coupling of $^1A'$ or $^1\Sigma$ covalent and ionic potentials (Table 8) of the same symmetry, leading to an avoided crossing, harpooning, and the formation of the ground state metal halide. However, if the collision geometry is of C_{2v} symmetry, the symmetry species of the covalent and ionic curves (Table 8) are 1A_1 and 1B_2 respectively, and the curves for the two states intersect. It is through this intersection and a range of approach angles within a cone of acceptance around the X_2 bisector⁴³ that the system slips past the "outer harpooning" region corresponding to the conical intersection of adiabatic states at the $|1\rangle|3\rangle$ crossing (Fig. 3) and gains access to the "inner harpooning" region.

The crossing involving the ionic configuration $|3\rangle$ and the doubly ionic configuration $|5\rangle$ will be avoided as the $|3\rangle|5\rangle$ interaction between these curves of the same symmetry is thought to be significant. Access to the "inner harpooning" region thus promotes an avoided crossing leading to the chemiluminescent channels. The low statistical weight of the near C_{2v} collisions is partly responsible for the chemiluminescent quantum yields in these systems. For the $M+XY$ reactive encounters, which cannot access a C_{2v} collision trajectory, the outer harpooning process must always correspond to an avoided crossing which shields the channel for chemiluminescent product formation.⁴⁴ As we compare the continua generated for the barium atom - mixed halogen reactions with ICl and IBr with those for the corresponding homonuclear Cl_2 , Br_2 , and I_2 reactions (Fig. 1), we observe a considerably weaker emission for the mixed halides vs. their homonuclear counterparts. However, this difference diminishes for the strontium system (Fig. 2) and is almost completely muted for the calcium system (Fig. 3).

We suggest that this behavior is again consistent with the electron jump process. The probability, P , that there is no change in electronic state

during passage through the "outer harpooning" crossing point, R_x , can be given approximately by

$$P = \exp(-v_m/v) \quad (4)$$

where v_m is the characteristic velocity (proportional to R_x^2 and ΔE_x^2 , the separation between the ionic and covalent curves at the crossing point) and v represents the initial relative velocity of the colliding alkaline earth metal and halogen molecule. In concert with the alkaline earth ionization potentials, we anticipate $R_x(\text{Ba}) > R_x(\text{Sr}) > R_x(\text{Ca})$ for a given halogen molecule, implying $v_m(\text{Ba}) > v_m(\text{Sr}) > v_m(\text{Ca})$. With $v_{\text{Ca-X}_2} > v_{\text{Sr-X}_2} > v_{\text{Ba-X}_2}$ we have

$$(v_m/v)_{\text{Ba}} > (v_m/v)_{\text{Sr}} > (v_m/v)_{\text{Ca}} \quad (5)$$

suggesting that the probability of "outer harpooning" and the formation of the ground state metal halide is greatest for the barium reactions and decreases for the reactions of strontium and calcium respectively. As the characteristic relative velocities of the reactants at the ionic-covalent crossing increases in traversing the Group IIA metals from barium to calcium, the reactions now overcome or tunnel through the barrier to chemiluminescent product formation.

The singly ionic excited configurations $X^{-1/2}M^+X^{-1/2}$ and $X^{-1/2}M^{+*}(\text{nd})X^{-1/2}$ are expected to have a substantially reduced binding energy compared with the ground state of the dihalide. This alone should promote an intermediate of considerable spatial extent, facilitating the possibility of collisional stabilization. The symmetry constrained electron jump process signals a dynamic constraint which is not consistent with the two step double harpooning process (1). The dominant participation of this process would require (Table VI) that the highly vibrationally and rotationally excited MX product of an initial $M+X_2$ reactive encounter maintain axial alignment along the perpendicular bisector of the X_2 bond as the second electron jump process occurs. This is a highly unlikely possibility.

We suggest that the absence of difluoride emission spectra resulting from the calcium, strontium, and barium reactions and the weak difluoride emission continuum observed for the magnesium reaction can also be explained within the framework of the electron jump process. Because the ionization potential²³ of magnesium (7.644 eV) considerably exceeds those of calcium (6.111 eV), strontium (5.692 eV), and barium (5.210 eV), the $\text{Mg} + \text{F}_2$ reaction is expected to proceed more slowly as covalent forces come into play and the electron jump

process is less efficient. With a less efficient electron jump process and an interaction at closer range, the probability for fluorine molecule dissociation can be diminished to the extent that the difluoride complex can be formed and collisionally stabilized.

The electron jump model qualitatively explains the observed trends in dihalide emission intensity. More detailed calculations of the couplings at the avoided crossing regions will be needed to place these arguments on a more quantitative base however the framework of collision complex stabilization is established. Refinements will best be accomplished following an initial effort to parameterize dihalide electronic and vibronic structure from optical signatures (energy levels, radiative lifetimes, differential bond angle changes), all of which can also serve to refine ionic models.

ACKNOWLEDGEMENT

The author gratefully acknowledges the helpful comments of Professor T. C. Devore and Dr. Kangkang Shen and the helpful comments and technical assistance of Mr. C. B. Winstead. The assistance of Mr. David Grantier and Mr. Peter Medley in preparing the figures is gratefully appreciated. Mr. David Grantier provided the simulations presented in Appendix A. The support of the Georgia Tech Foundation through a grant from Mrs. Betty Peterman Gole, the Army Research Office through the Short Term Innovative Research Program, the Air Force Office of Scientific Research and the Army Research Office and AFOSR/SDIO is greatly appreciated.

References

1. J. L. Gole, Opt. Eng. 20 (1981) 546.
2. J. L. Gole and D. R. Grantier, "The Expansion of Small Molecule Configuration Space: Highly Efficient Long Range Stabilization and Energy Transfer Involving Electronically Excited States", High Temperature Science, in press.
3. "Gas-Phase Metal Reactions", A. Fontijn (editor) - North Holland Publishers, 1992.
4. G. Herzberg, Molecular Spectra and Molecular Structure I. Spectra of Diatomic Molecules, Van Nostrand: New York, 1950, p. 443.
5. J. M. Parson, J. Phys. Chem. 90 (1986) 1811.
6. T. Kasai, T. Masui, H. Nakane, I. Hanazaki, and K. Kuwata, Chem. Phys. Lett. 56 (1978) 84.
7. Y. Yoshimura, H. Ohyama, T. Humada, T. Kasai, and K. Kuwata, Chem. Phys. Lett. 106 (1984) 271.
8. C. D. Jonah and R. N. Zare, Chem. Phys. Lett. 9 (1971) 65.
9. C. A. Mims and J. H. Brophy, J. Chem. Phys. 66 (1977) 1378.
10. D. J. Wren and M. Menzinger, Chem. Phys. Lett. 27 (1974) 572.
11. D. R. Grantier and J. L. Gole, "Raman Pumping in the Absence of an External Light Source", J. Phys. Chem. Letters, in press. "Chemically Enhanced Raman Scattering", J. Chem. Phys, submitted.
12. T. C. Devore, R. Kahlscheuer, D. A. Dixon, H. Wang, and C. B. Winstead, "Electronically Excited Charge Transfer Complex Formation in Magnesium Molecule - Halogen Atom Reactions", in preparation.
13. W. J. Rosano and J. M. Parson, J. Chem. Phys. 84 (1986) 6250.
14. M. Menzinger, Adv. Chem. Phys. 42 (1980) 1. M. Menzinger, "The $M+X_2$ Reactions: A Case Study", in "Gas Phase Chemiluminescence and Chemi-ionization", A. Fontijn, editor, Elsevier Science Publishers, Amsterdam, 1985, pp. 25-66. M. Menzinger, "Chemiluminescence and Chemiionization: Metal-Halogen Reactions as Paradigms of Diabatic Reaction Dynamics", Acta Physica Polonica A73 (1988) 85.
15. F. Engelke, Chem. Phys. 44 (1979) 213.
16. D. Wren, Ph.D. Thesis, U. of Toronto, 1978.
17. H. C. Brayman, D. R. Fischell, and T. A. Cool, J. Chem. Phys. 73 (1980) 4247.

18. See for example, L. H. Dubois and J. L. Gole, J. Chem. Phys. 66 (1977) 779; D. R. Preuss and J. L. Gole, J. Chem. Phys. 66 (1977) 880; 66 (1977) 2994; G. J. Green and J. L. Gole, Chem. Phys. 46 (1980) 67; 69 (1982) 357, and references therein.
19. J. L. Gole, "Probing Ultrafast Energy Transfer Among the Excited States of Small High Temperature Molecules", in "Gas Phase Chemiluminescence and Chemiionization", A. Fontijn (editor) - Elsevier Science Publishers, 1985, p. 253.
20. D. M. Lindsay and J. L. Gole, J. Chem. Phys. 66 (1977) 3886. M. J. Sayers and J. L. Gole, J. Chem. Phys. 67 (1977) 5442. J. L. Gole and S. A. Pace, J. Chem. Phys. 73 (1980) 836.
21. A. W. Hanner and J. L. Gole, J. Chem. Phys. 73 (1980) 5025. J. L. Gole and S. A. Pace, J. Phys. Chem. 85 (1981) 2651. J. L. Gole, B. Ohlsson, A. W. Hanner, and E. J. Greene, unpublished.
22. An. N. Nesmeyanov, Vapor Pressures of the Elements (Academic Press, N. Y., 1963).
23. See for example, NBS Special Publication 505, Bibliography on Atomic Transition Probabilities (1914 through October 1977) and Supplement I (November 1977 through March 1980), U. S. Department of Commerce/National Bureau of Standards. C. E. Moore, "Atomic Energy Levels", (National Bureau of Standards, 1949).
24. See for example, R. S. Berry and C. W. Reimann, J. Chem. Phys. 38 (1963) 1540; R. S. Berry, J. Chem. Phys. 27 (1957) 1288; W. S. Struve, J. R. Krenos, D. L. McFadden, and D. R. Herschbach, J. Chem. Phys. 62 (1975) 404; R. C. Oldenborg, J. L. Gole and R. N. Zare, J. Chem. Phys. 60 (1974) 4032.
25. T. C. Devore and J. L. Gole, "Formation and Characterization of Group IIA Dihalide Complexes - Bond Energy Determination from Chemiluminescence Spectra", in preparation.
26. For F_2^- see (a) J. A. Ayala, W. E. Wentworth, and E. C. M. Chen, J. Phys. Chem. 85 (1981) 768, (b) W. A. Chupka, J. Berkowitz, and D. Gutman, J. Chem. Phys. 55 (1971) 2724, (c) for ClF^- H. Dispert and K. Lacmann, Int. Jour. Mass. Spectrom. Ion Physics 28 (1978) 49, (d) for Cl_2^- see (a) and H. Dispert and K. Lacmann, Chem. Phys. Lett. 45 (1977) 311, (e) A. P. M. Baeda, Physica 59 (1972) 541, (f) for Br_2^- see D. L. Baulch, R. A. Cox, P. J. Crutzen, R. F. Hampson, Jr., J. A. Kerr, J. Troe, and R. T. Watson, J. Phys. Chem. Ref. Data 11 (1982) 327 and ref. (e) above, (g) for I_2^- A. P. M. Baeda, J. Averbach, and D. J. Los, Physica 64 (1973) 134.
27. J. A. Coxon and N. F. Ramsey, Can. J. Phys. 54 (1976) 1034.

28. L. Wharton, R. A. Berg, and W. Klemperer, J. Chem. Phys. 39 (1966) 2023. A. Buchler, J. L. Stauffer, W. Klemperer, and L. Wharton, J. Chem. Phys. 39 (1963) 2299. A. Buchler, J. L. Stauffer, and W. Klemperer, J. Chem. Phys. 40 (1964) 3471; J. Am. Chem. Soc. 86 (1964) 4544.
29. James L. Gole, J. Chem. Phys. 58 (1973) 869.
30. J. L. Gole, H. Wang, J. S. Joiner, and D. E. Dawson, "Confirmation of Long-Range Collision Complex Stabilization Through the Controlled Relaxation of High Internal Excitation" - following paper.
31. Edward F. Hayes, J. Phys. Chem. 70 (1966) 3740.
32. D. R. Yarkony, W. J. Hunt, H. F. Schaefer, Molecular Physics 26 (1973) 941-952.
33. R. L. DeKock, M. A. Peterson, L. K. Timmer, E. J. Baerendo, and P. Vernooijs, Polyhedron 9 (1990) 1919.
34. James L. Gole, Albert K. Q. Siu, and Edward F. Hayes, J. Chem. Phys. 58 (1973) 857.
35. P. J. Dagdigian, H. W. Cruse, and R. N. Zare, J. Chem. Phys. 60 (1974) 2330.
36. D. R. Preuss, C. L. Chalek and J. L. Gole, J. Chem. Phys. 66 (1977) 548.
37. Rapid vibrational motion corresponding to a bending mode for the MF_2 molecule will produce an "effective" linear molecule whose dipole moment may be near zero. Similarly rapid rotation produces an effective zero dipole moment.
38. The BaClF bond angle should also be smaller than that for the BaCl_2 , this further increasing the transition moment.
39. R. E. Olson, F. T. Smith, E. Bauer, Appl. Optics 10 (1970) 1848.
40. R. Grice, D. R. Herschbach, Mol. Phys. 27 (1974) 159.
41. J. Los, A. W. Kleyn, in: Alkali Halide Vapors, eds., P. Davidovits and D. L. McFadden (Academic Press, New York, 1979).
42. R. B. Bernstein, R. D. Levine, Molecular Reaction Dynamics, (Oxford University Press, New York, 1974).
43. T. Carrington, Accts. Chem. Res. 7 (1974) 20.
44. Note that the radiative lifetimes associated with the lowest energy MXY emission band systems ($\sigma - \pi$ transitions) will be shorter than their MX_2 counterparts ($\sigma_g - \pi_g$ transitions). Thus the MXY^* excited state production is considerably muted relative to that indicated in Figs. 1-3.

Table I

Experimentally Determined Bond Energies of Group IIA Mono- and Dihalides

	D_0^0 kcal/mole ^a			
	I	Cl	Br	I
Mg	109	75	(58)	(45)
Ca	126 266(140°)	94 214(180°)	73 186(180°)	62 155(180°)
Sr	129 260(120°)	96 211(140°)	79 189(180°)	64 155(180°)
Ba	139 271(100°)	104 220(120°)	85 197(150°)	72 166(180°)

^aFor each entry, the upper value corresponds to the metal monohalide bond energy and the lower value corresponds to that for the metal dihalide.

TABLE II

Geometry of Group IIA Dihalides

Metal	<u>Halide</u>			
	F	Cl	Br	I
Be	<i>l</i> ^a	<i>l</i>	<i>l</i>	<i>l</i>
Mg	<i>l</i>	<i>l</i>	<i>l</i>	<i>l</i>
Ca	<i>b</i>	<i>l</i>	<i>l</i>	<i>l</i>
Sr	<i>b</i>	<i>b</i>	<i>l</i>	<i>l</i>
Ba	<i>b</i>	<i>b</i>	<i>b</i>	<i>b</i>

^a *l*, linear; *b*, bent

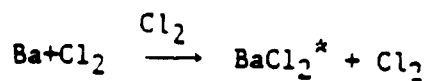
Table III

Group IIA Dihalide Low-Lying Electronic States
Potential Electronic Transitions in Emission

Electron Configuration ^a	State Designation	Comments ^b
$\dots(xa_2)^2(yb_2)^2$	X^1A_1 Ground State	
$\dots(xa_2)^1(yb_2)^2(za_1)^1$	$1,3A_2$	A-X region transitions ^b will produce large change in bond angle
$\dots(xa_2)^2(yb_2)^1(za_1)^1$	$1,3B_2$	
$\dots(xa_2)^1(yb_2)^2(mb_1)^1$	$1,3B_2$	B-X region will produce significant change in bond length
$\dots(xa_2)^2(yb_2)^1(mb_1)^1$	$1,3A_2$	
$\dots(xa_2)^1(yb_2)^2(na_1)^1$	$1,3A_2$	C-X region transitions ^b will produce significant change in bond length
$\dots(xa_2)^2(yb_2)^1(na_1)^1$	$1,3B_2$	

- a. Highest occupied orbitals (x,y) and lowest promotion orbitals (z,m,n).
 b. $^1B_2 - X^1A_1$ transition is electric dipole allowed, $^1A_2 - X^1A_1$ transition is vibronically allowed through coupling with the ground or excited state asymmetric stretch of b_2 symmetry. The corresponding triplet-singlet transitions will be weaker.

Table IV
BaCl₂^{*} Continuum



Relative Intensities as a Function of Pressure

Pressure \ λ (Å)	3000	3553	4327	4659	5000	5765	6318
3 x 10 ⁻⁵	.26	.58	1.0	.97	.68	.41	.34
4 x 10 ⁻⁵	.13	.51	1.0	.89	.57	.26	.18
4 x 10 ⁻⁵	.14	.46	1.0	.89	.60	.25	.18
5 x 10 ⁻⁵	.17	.50	1.0	.83	.58	.25	.18
5 x 10 ⁻⁵	.16	.52	1.0	.92	.63	.30	.19
6 x 10 ⁻⁵	.13	.50	1.0	.91	.59	.25	.16
6 x 10 ⁻⁵	.12	.49	1.0	.89	.58	.25	.16
7 x 10 ⁻⁵	.11	.49	1.0	.89	.58	.24	.14
7 x 10 ⁻⁵	.10	.50	1.0	.90	.60	.23	.15
8 x 10 ⁻⁵	.08	.50	1.0	.88	.56	.22	.13
8 x 10 ⁻⁵	.09	.51	1.0	.88	.55	.23	.13
9 x 10 ⁻⁵	.08	.50	1.0	.90	.54	.23	.11
9 x 10 ⁻⁵	.08	.47	1.0	.85	.53	.20	.11
10 x 10 ⁻⁵	.08	.49	1.0	.86	.55	.21	.16
10 x 10 ⁻⁵	.07	.49	1.0	.86	.53	.20	.11
2 x 10 ⁻⁴	.07	.51	1.0	.86	.54	.21	.10
2 x 10 ⁻⁴	.07	.52	1.0	.87	.55	.21	.10
3.1 x 10 ⁻⁴	.07	.49	1.0	.84	.53	.20	.10
3.1 x 10 ⁻⁴	.07	.49	1.0	.85	.54	.19	.10
4 x 10 ⁻⁴	.07	.52	1.0	.86	.54	.20	.10
4 x 10 ⁻⁴	.08	.51	1.0	.87	.55	.20	.10
5 x 10 ⁻⁴	.08	.52	1.0	.86	.55	.20	.11
5 x 10 ⁻⁴	.09	.53	1.0	.85	.55	.20	.10

Table V

States Arising from $M + X_2$ Reactant Configurations

	\underline{C}_s	\underline{C}_{2v}	$\underline{C}_{\infty v}$
$M(^1S) + X_2(^1\Sigma_g^+)$	$^1A'$	1A_1	$^1\Sigma$
$M^+(^2S) + X_2(^-2\Sigma_u^+)$	$1,3A'$	$1,3B_2$	$1,3\Sigma$
$M^{+2}(^1S) + X_2(^-1\Sigma_g^+)$	$^1A'$	1A_1	$^1\Sigma$

Table VI

States Arising from $MX + X_2$ Reactant Configurations with the MX Molecular Axis Along the Perpendicular Bisector of the X_2 Bond

	\underline{C}_s	\underline{C}_{2v}	$\underline{C}_{\infty v}$
$MX(^2\Sigma^+ + X_2(^1\Sigma_g^+))$	$^2A'$	2A_1	$^2\Sigma$
$MX^+(^1\Sigma^+) + X_2^-(^2\Sigma_u^+)$	$^2A'$	2B_2	$^2\Sigma$

Figure Captions

Figure 1: Chemiluminescent spectra for (a) the BaX_2 (XY) product of the $\text{Ba} (^1\text{S}) + \text{Cl}_2$, ICl , I_2 reactions at comparable Group IIA metal beam flux and comparable halogen pressures over the range 5×10^{-6} - 1×10^{-4} Torr as measured by a capacitance manometer. On the scale of the figure, the emission from a BaICl complex is negligible and the optical signature of the $\text{Ba} + \text{ICl}$ reaction consists almost exclusively of emission from the $\text{BaCl } C^2\Pi - X^2\Sigma^+$ transition. (b) the BaX_2 (XY) product of the $\text{Ba} (^1\text{S}) + \text{Br}_2$, IBr , I_2 reactions at comparable Group IIA metal beam flux and halogen pressures over the range 5×10^{-6} - 1×10^{-4} Torr as measured by capacitance manometer; the BaX products of the $\text{Ba} (^3\text{D}) + \text{I}_2$, IBr , and Br_2 reactions are also evident in the figure, (c) the BaX_2 (XY) product of the $\text{Ba} (^1\text{S}) + \text{Cl}_2$, ClF reactions at comparable Group IIA metal beam flux and halogen pressures over the range 5×10^{-6} - 1×10^{-4} Torr as measured by capacitance manometer; the BaF^* emission features resulting from the $\text{Ba} (^1\text{S}) + \text{ClF} \rightarrow \text{BaF}^* + \text{Cl}$ reaction are also indicated in the figure, (d) the BaF^* products of the $\text{Ba} + \text{F}_2 \rightarrow \text{BaF}^* + \text{F}$ reaction over the pressure range 5×10^{-6} - 1×10^{-4} Torr as measured by capacitance manometer. All spectra were taken at a resolution of 12 Å. See text for discussion.

Figure 2: Chemiluminescent spectra for (a) the SrX_2 (XY) product of the $\text{Sr} (^1\text{S}) + \text{Cl}_2$, ICl , I_2 reactions at comparable Group IIA metal beam flux and halogen pressures over the range 1×10^{-5} - 1×10^{-4} Torr as measured by a capacitance manometer; observed SrX emission features are also identified in the figure. The relative intensity of the SrIBr continuum chemiluminescence from the $\text{Sr} (^1\text{S}) + \text{IBr}$ reaction verses that for the $\text{Sr} (^1\text{S}) + \text{I}_2$, Br_2 reactions is similar to that for the $\text{Sr} (^1\text{S}) + \text{ICl}$ reaction versus the $\text{Sr} (^1\text{S}) + \text{I}_2$, Cl_2 reactions. All spectra were taken at a resolution of 12 Å. See text for discussion.

Figure 3: Chemiluminescent spectra for (a) the CaX_2 (XY) product of the $\text{Ca} (^1\text{S}) + \text{Cl}_2$, ICl , I_2 reactions at comparable Group IIA metal beam flux and halogen pressures over the range 3×10^{-5} - 2×10^{-4} Torr as measured by a capacitance manometer; observed CaX emission features are also identified in the figure, (b) the CaX_2 (XY) product of the $\text{Ca} (^1\text{S}) + \text{Br}_2$, IBr , I_2 reactions at comparable Group IIA metal beam flux and halogen pressures over the range 4×10^{-5} - 2×10^{-4} Torr as measured by capacitance manometer. All spectra were taken at a resolution of 12 Å. See text for discussion.

Figure 4: Bond angle variation valence correlation diagram for the highly ionic BaF_2 molecule. Energy is in Hartrees. See reference 29 and text for discussion.

Figure 5: Chemiluminescent intensity versus oxidant pressure for the reactions $\text{Ba} + \text{Cl}_2 \rightarrow \text{BaCl}_2^*$ and $\text{Ba} + \text{ClF} \rightarrow \text{BaClF}^*$. The results were obtained at wavelengths of 4500 Å and 4000 Å, respectively, and at a resolution of 10 Å. Pressures were measured with a capacitance manometer. See text for discussion.

Figure 6: Chemiluminescent intensity versus oxidant pressure for the reactions $\text{Ba} + \text{F}_2$, Cl_2 , Br_2 , and I_2 from the data of Wren and Menzinger (Ref. 9). As reinterpreted in the text, dihalide emission is monitored in the Cl_2 , Br_2 , and I_2 studies whereas monohalide emission is monitored in the F_2 study. See text and Appendix A for discussion.

Figure 7: Chemiluminescent intensity versus oxidant pressure for the reactions Ca, Sr, Ba + I₂ run at temperatures to give near matching Group IIA metal source fluxes. The results were obtained at a wavelength of 4700 Å and at a resolution of 10 Å. Pressures were measured with a capacitance manometer. See text for discussion.

Figure 8: Correlation of electron configurations for Group IIA metal (M) - halogen molecule (X₂) reactive encounters.

BaX^* Chemiluminescent Spectra

$\text{Ba}+\text{Cl}_2$ ---
 $\text{Ba}+\text{I}_2$ ____

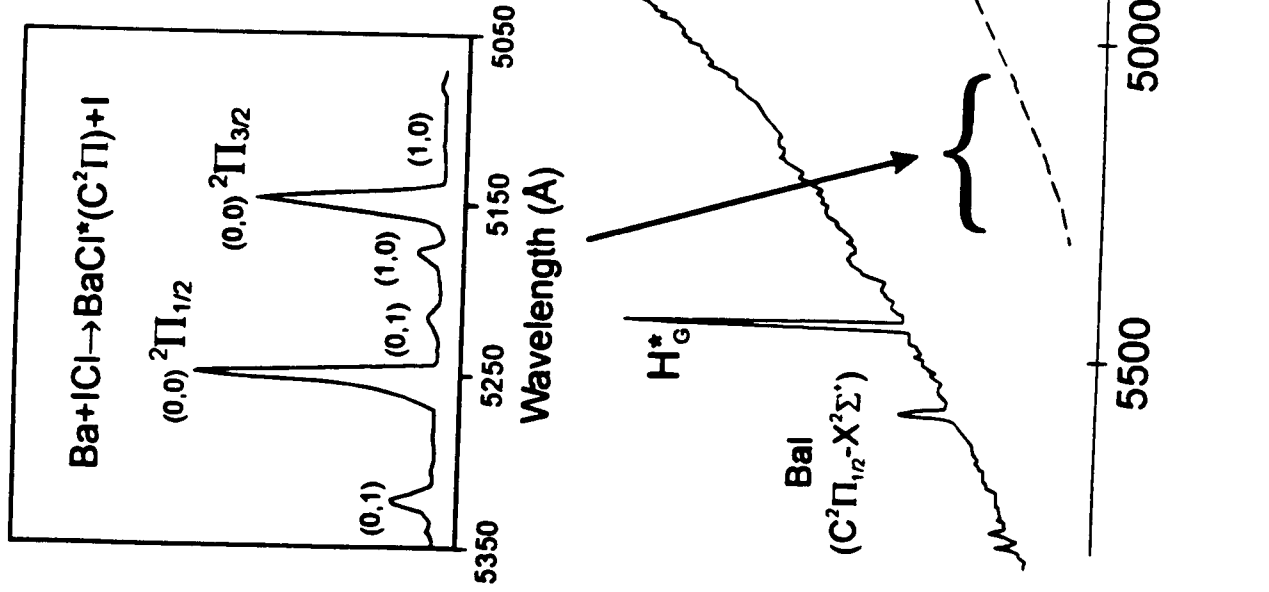


Figure 1(a)
 Wavelength (Å)

BaX_2 Chemiluminescent Spectra

$\text{Ba}+\text{Br}_2$ ---
 $\text{Ba}+\text{IBr}$ - - -
 $\text{Ba}+\text{I}_2$ _____

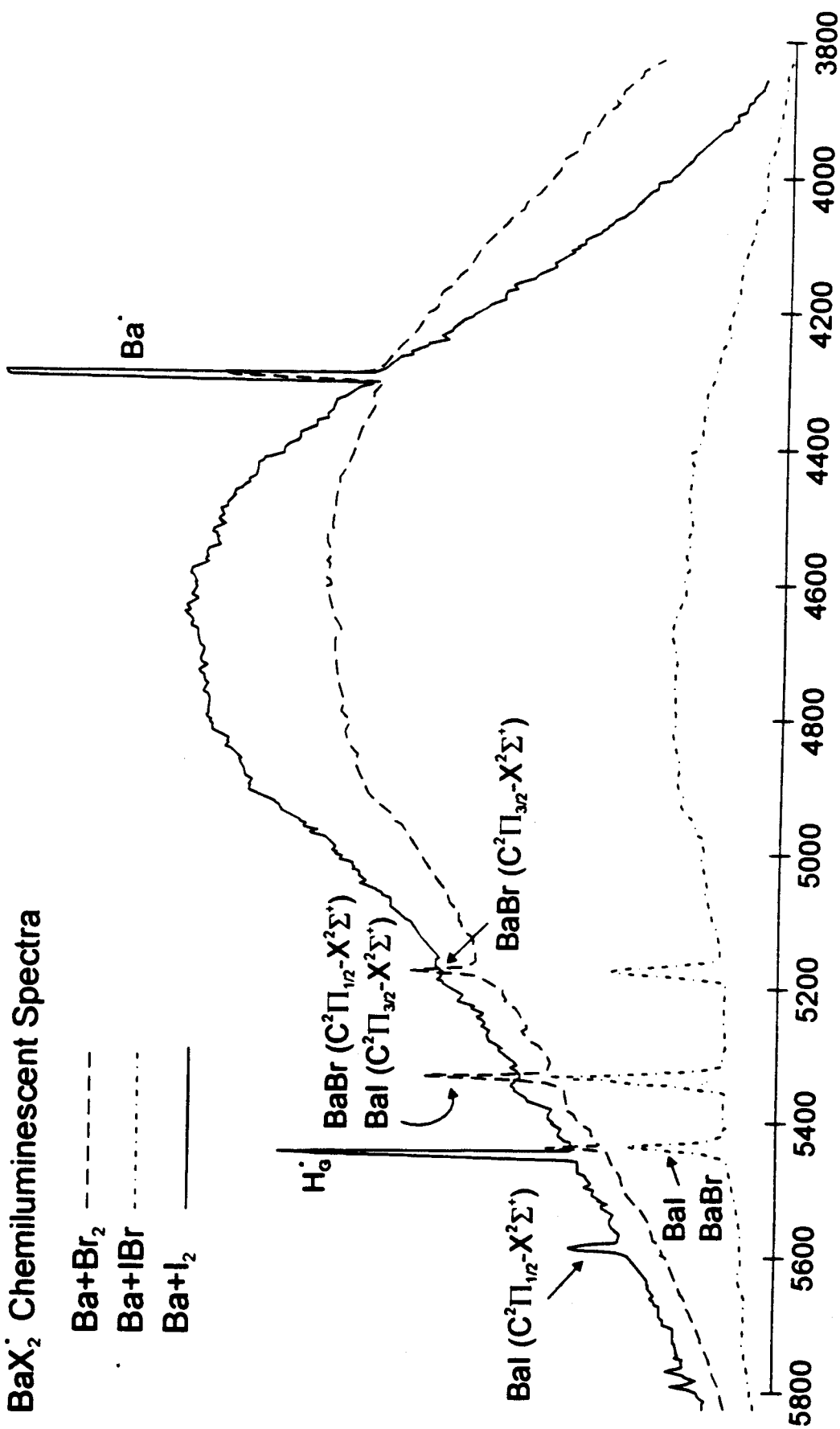


Figure 1(b)

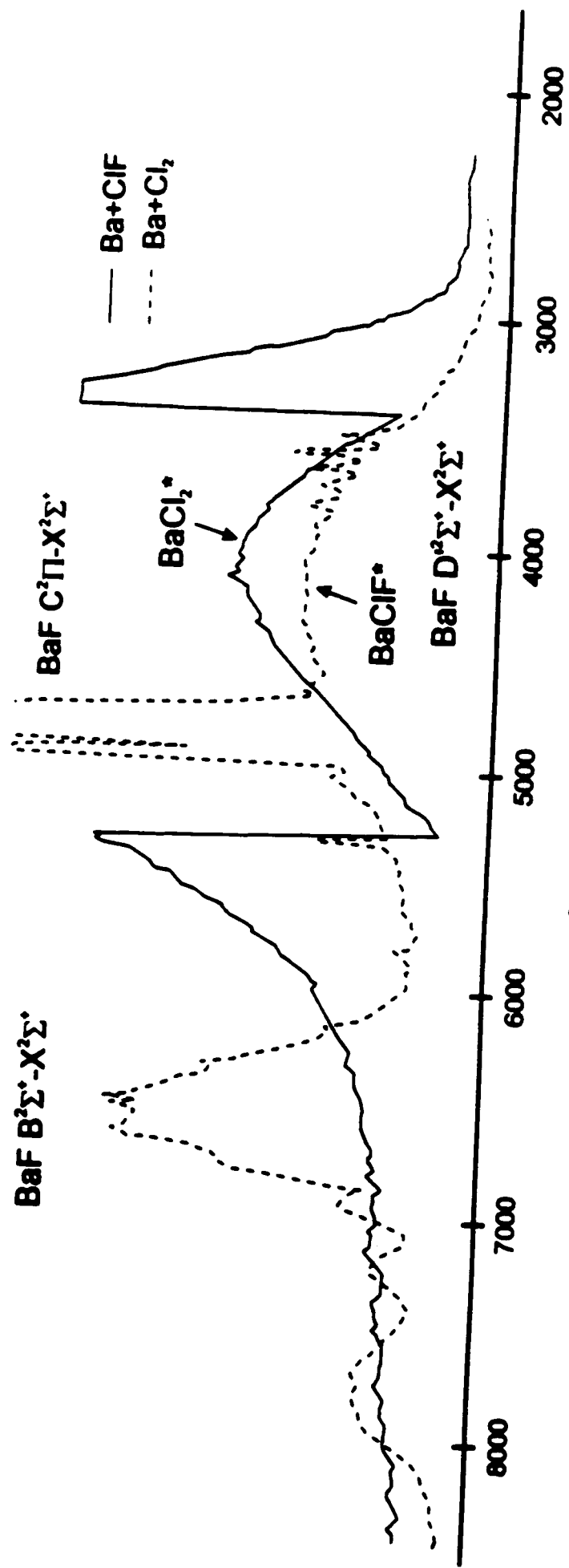
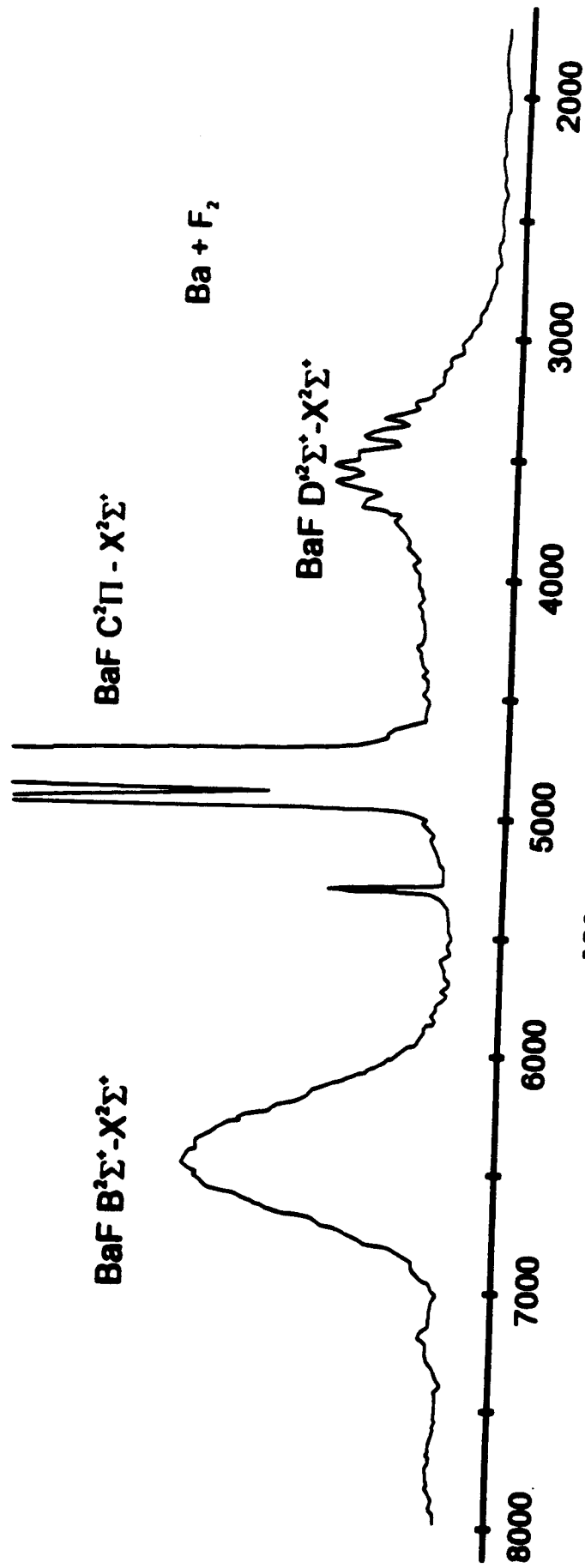


Figure 1(c)



Wavelength (Å)

Figure 1(d)

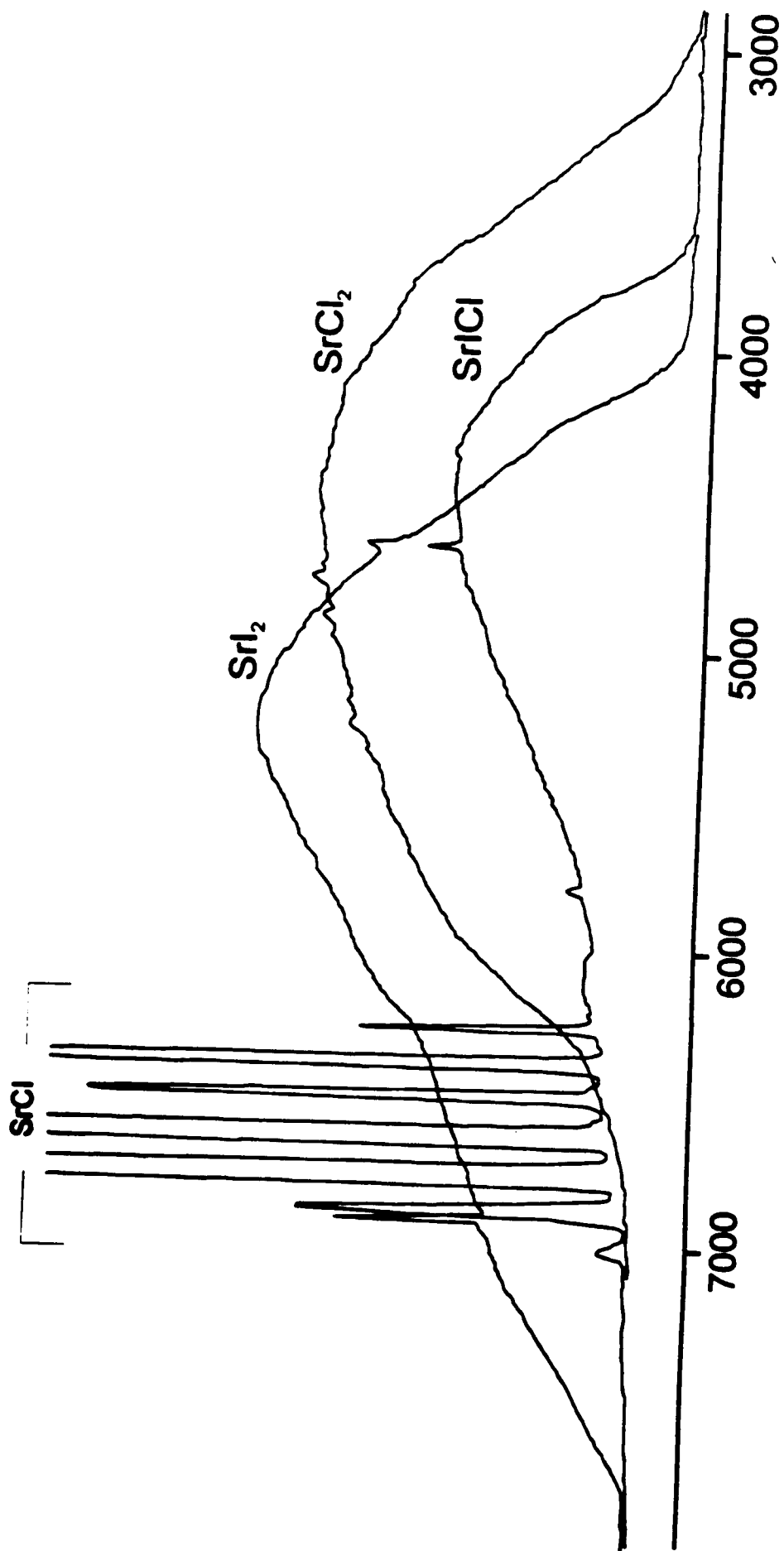
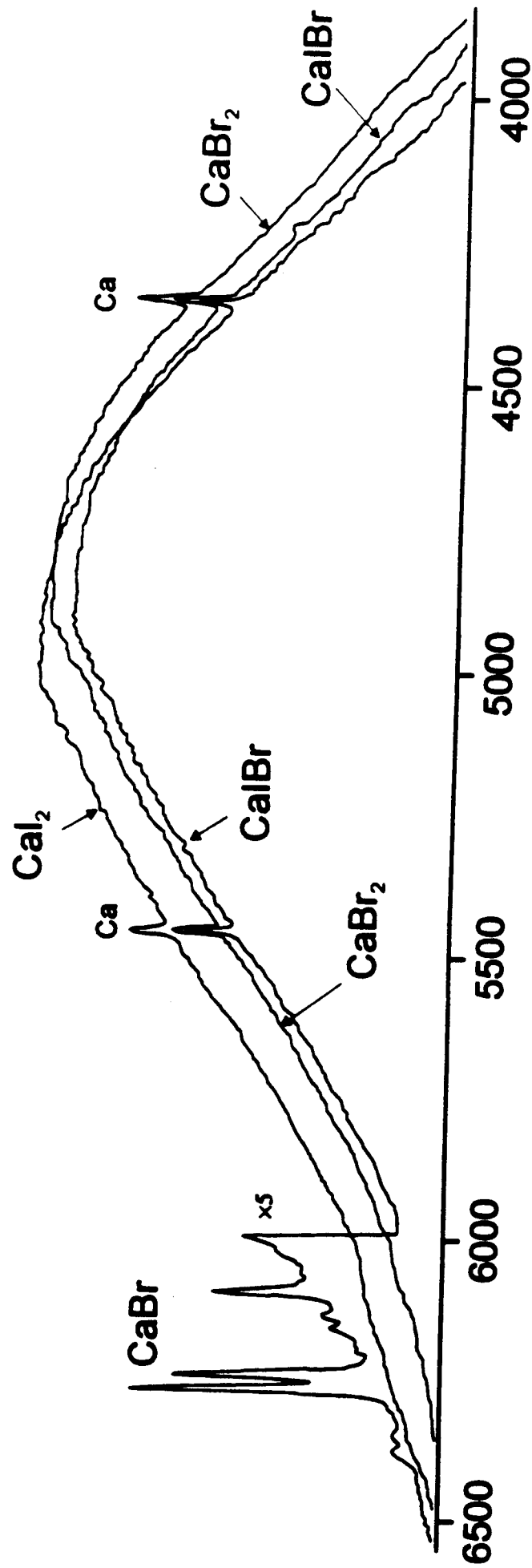
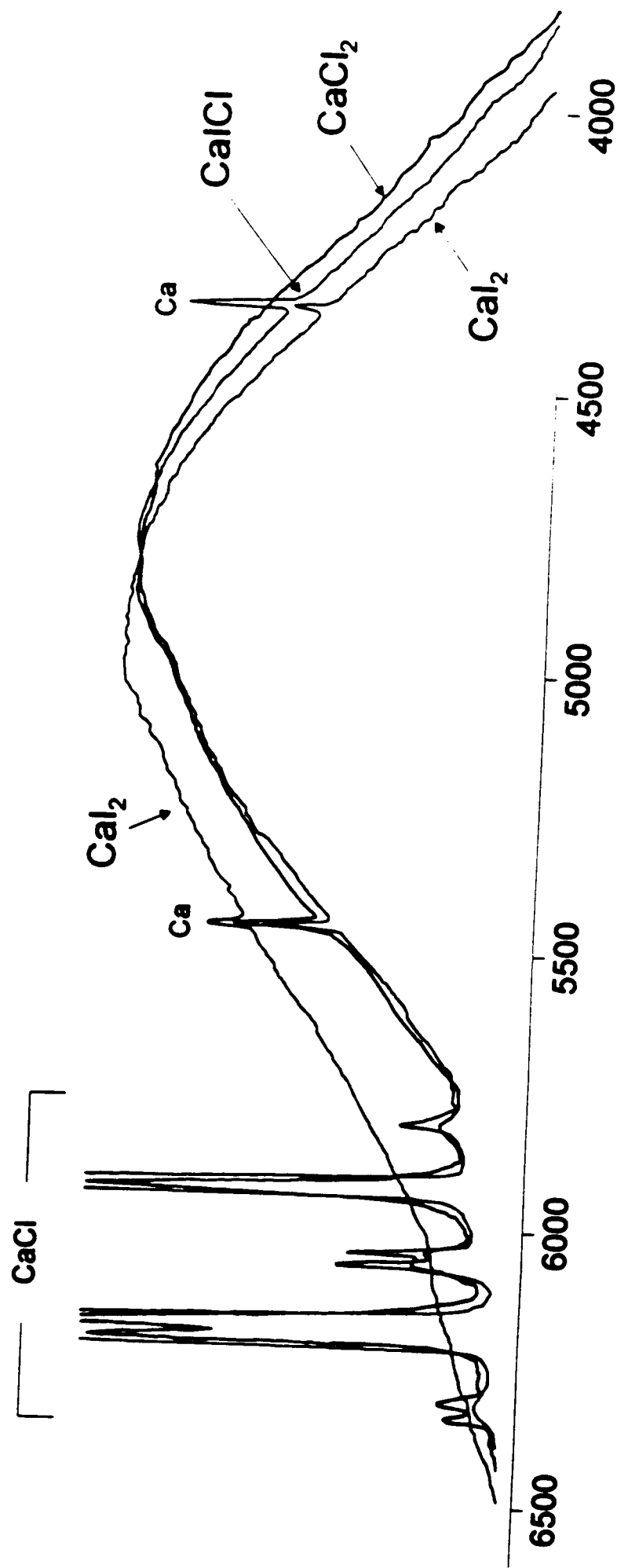


Figure 2
Wavelength (Å)



Wavelength (Å)

Figure 3(a)



Wavelength (Å)

Figure 3(b)

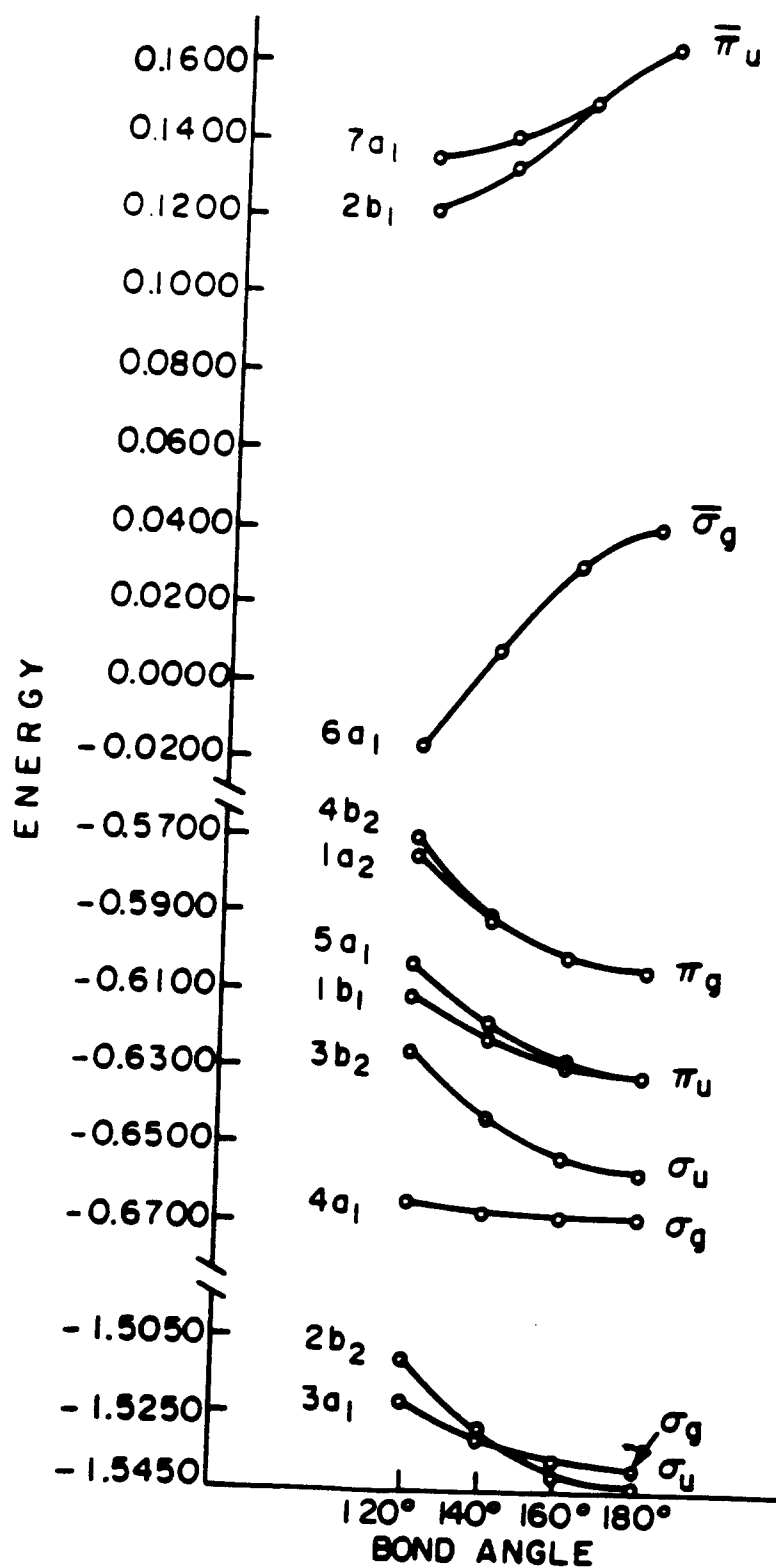


Figure 4

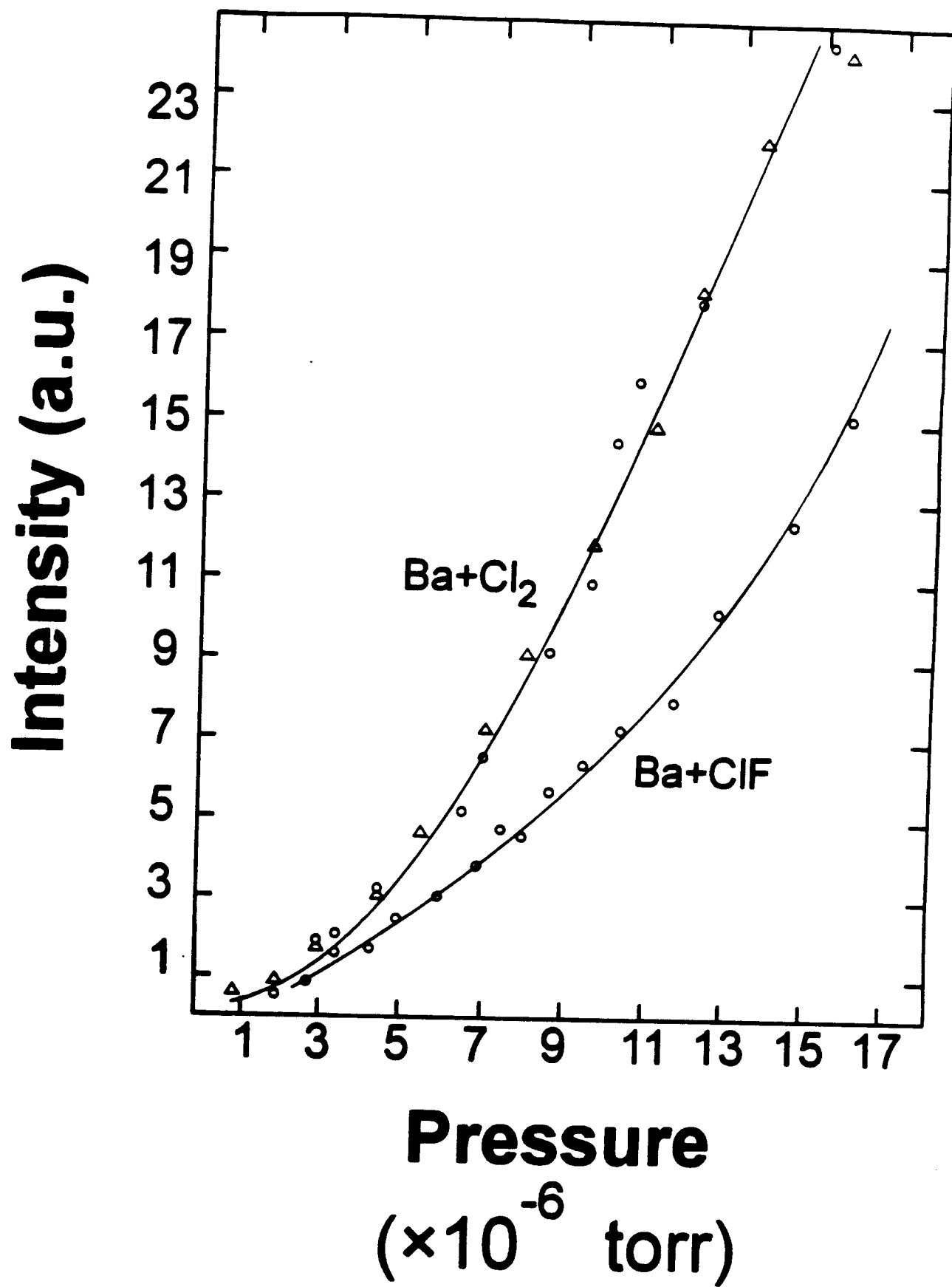


Figure 5

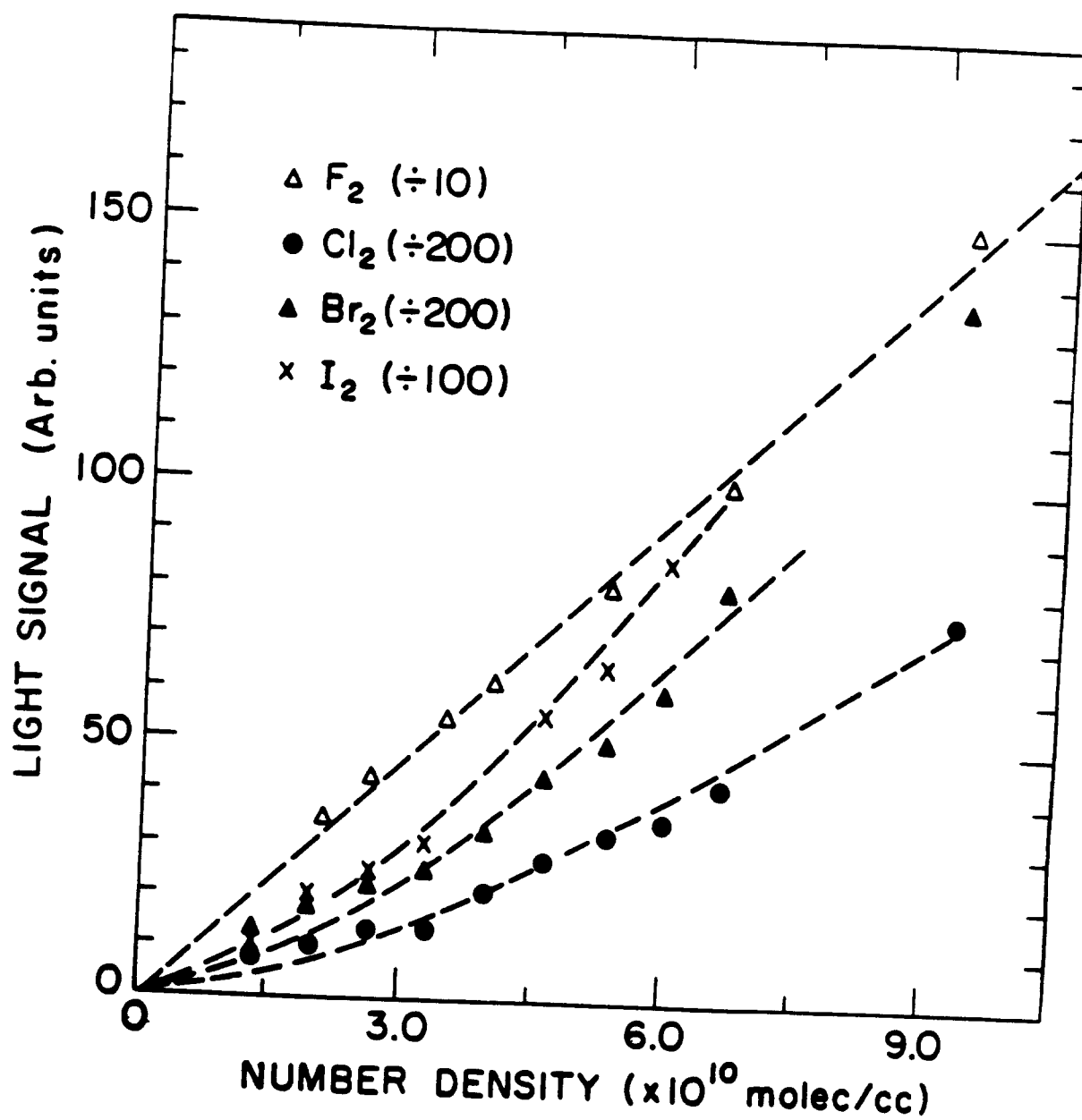


Figure 6

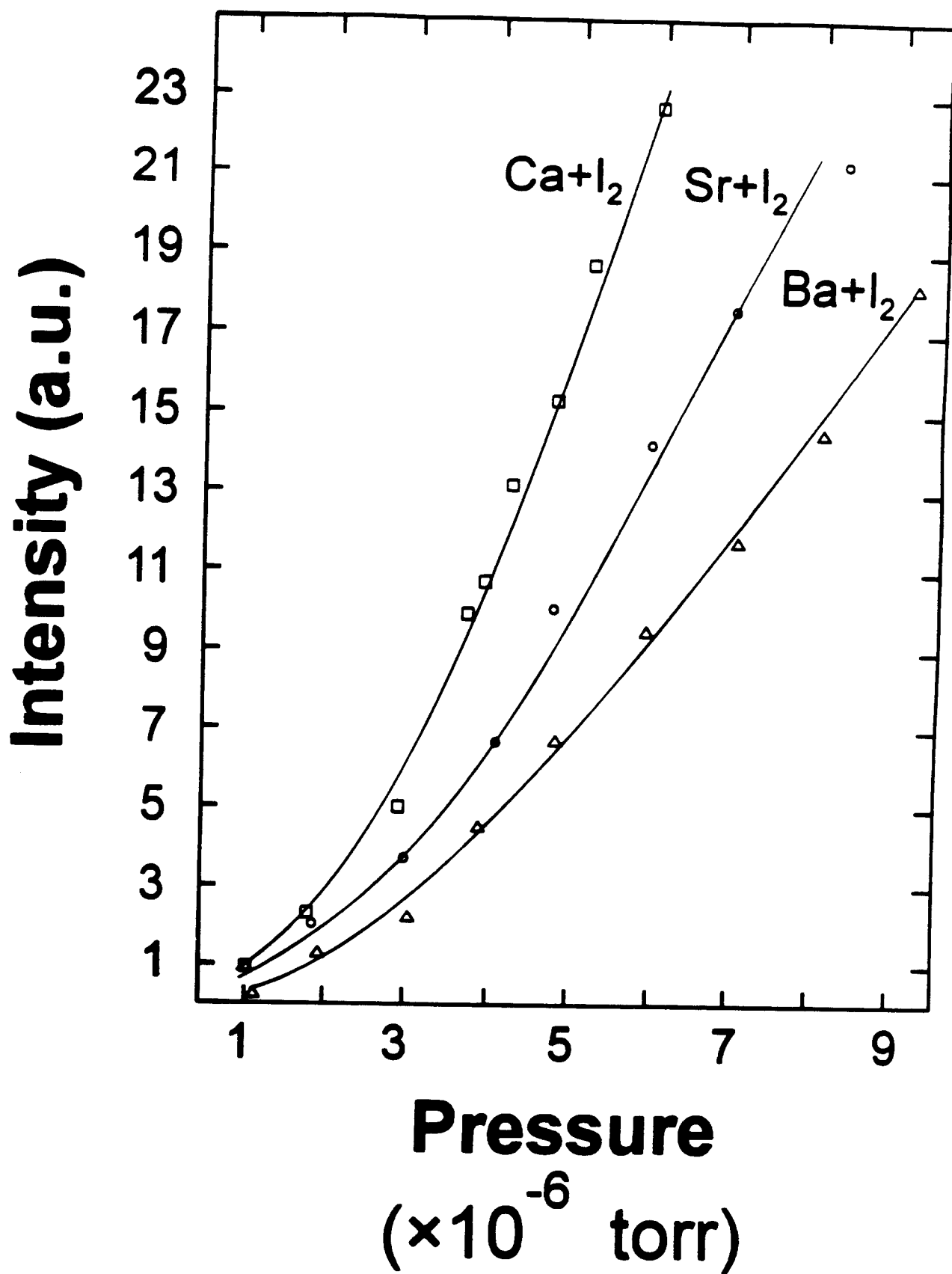
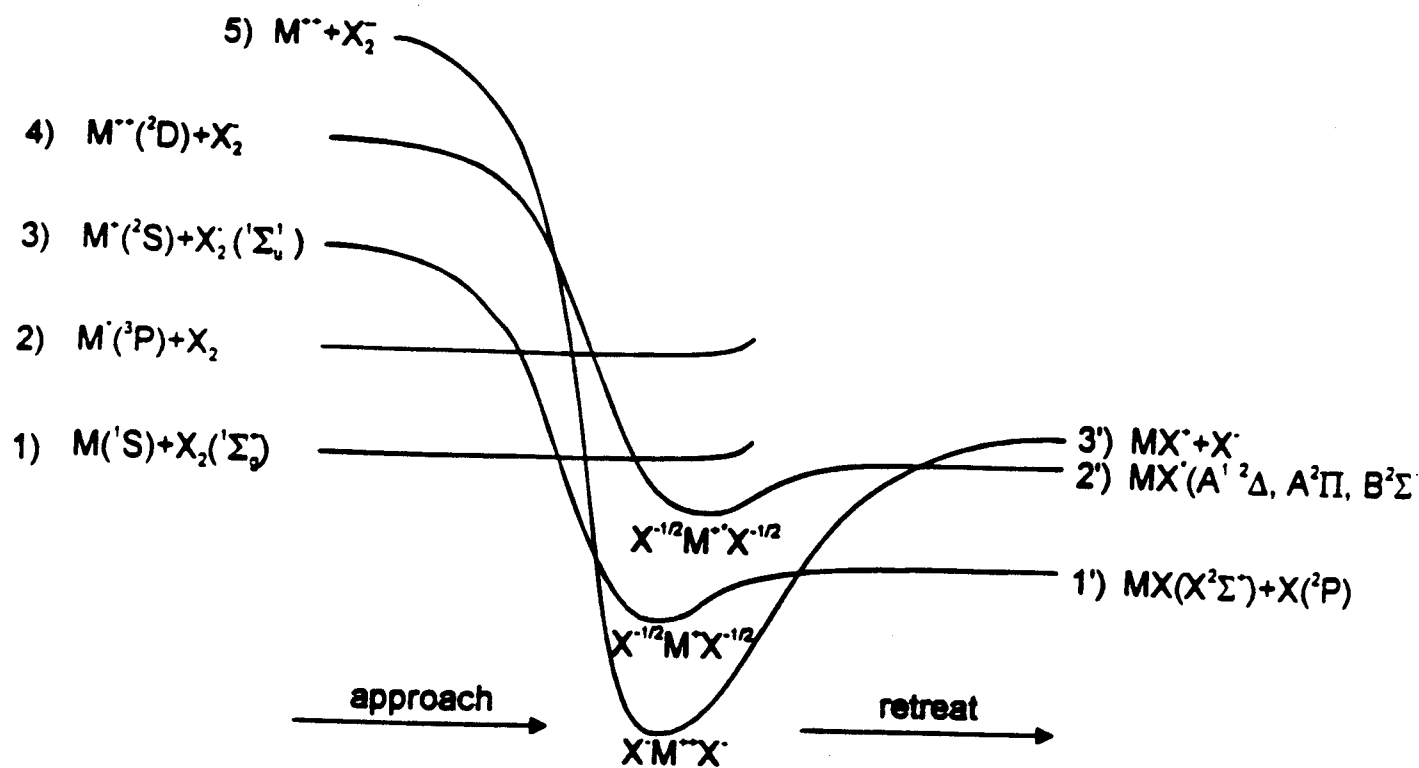


Figure 7



Correlation of electron configurations for Group IIA metal (M) - Halogen molecule (X_2) reactive encounters.

Figure 8

APPENDIX A

Formation of Highly Vibrationally Excited $\text{BaF}^* \text{B}^2\Sigma^+$ from the $\text{Ba} + \text{ClF}, \text{F}_2$ Reactions

Some confusion in the interpretation of the dynamics of the Group IIA-halogen molecule reactions has resulted from the assignment of monofluoride emission features to the difluorides. Menzinger,¹ in studying the reactions of calcium, strontium, and barium with molecular-fluorine, assigned an observed 6000-7500 Å feature, resulting from the $\text{Ba} + \text{F}_2$ reaction, to a BaF_2 continuum emission on the basis of a conceived minimal correlation with the $\text{BaF}^* \text{B}^2\Sigma^+ - \text{X}^2\Sigma^+$ emission system. He noted also the virtual absence of CaF_2 and SrF_2 emission features. Engelke^{2,3} identified the $\text{B}^2\Sigma^+ - \text{X}^2\Sigma^+$ (~ 6000 -7000 Å) and $\text{A}^2\Pi - \text{X}^2\Sigma^+$ (~ 7500 -8800 Å) band systems of BaF resulting from the "crossed beam" $\text{Ba}(^3\text{D}_1) + \text{F}_2$ reaction at pressures less than 10^{-5} Torr.

The $\text{Ba} + \text{ClF}$ reaction (Fig. 1(c)), like the $\text{Ba} + \text{F}_2$ system, is characterized by an emission feature extending from 6000 to 7000 Å. It is apparent even in the fast scan of Fig. 1(c) that this is a structured feature; the higher resolution scan depicted in Figure A1 demonstrates that the observed spectrum corresponds to the $\text{B}^2\Sigma^+ - \text{X}^2\Sigma^+$ band system of BaF . While this correspondence can be established, the chemiluminescence spectrum differs notably from previously observed emission features for the B-X system. The chemiluminescence spectrum is dominated by $\Delta v = +2$ to $\Delta v = +5$ sequences whereas all previous spectra are dominated by the $\Delta v = 0$, $\Delta v = +1$, and $\Delta v = -1$ sequence groupings. The reason for this discrepancy can be discerned from the simulation for the $\text{BaF} \text{B}^2\Sigma^+ - \text{X}^2\Sigma^+$ transition presented in Figure A2.

To generate the simulation of Figure A2, we used the BaF molecular constants of Effantin et al.⁴ A suitable set of Franck-Condon factors was calculated, using standard techniques,⁵ from the rotationless RKR potentials of the $\text{B}^2\Sigma^+$ and $\text{X}^2\Sigma^+$ electronic states of the BaF molecule. We considered transitions between the lowest fifty vibrational levels of each state. A Boltzmann rotational temperature close to 800K was imposed on each upper state vibrational level and chemiluminescent transitions were allowed from populated B state vibrational levels to the lowest fifty vibrational levels of the ground electronic state. Λ -type doubling, appropriate for a $^2\Sigma - ^2\Sigma$ transition,⁵ was included in the simulation for both the upper and lower electronic

states. The resulting spectrum was appropriately smoothed to simulate a finite bandwidth instrument response in order to facilitate comparison with experimental observations. The upper state vibrational population distribution is clearly non-Boltzmann in character. We find that the BaF spectrum of Figure A1 is well represented by a strongly inverted vibrational distribution peaking at $v' = 38$. Transitions involving the lower vibrational levels are strongly diagonal, however, high vibrational excitation fosters the observed sequence deviations.

Because the impact parameter for the electron jump reactions of barium is quite high, we also considered the possibility that the effective potential

$$U_{\text{eff}}(R) = U(R) + \hbar^2 J(J+1)/2\mu R^2$$

for the previous and present spectroscopic studies differs substantially, promoting a deviation from diagonal $\Delta v = 0$ sequence structure. While a greatly increased rotational excitation causes some deviation, this is by no means sufficient to explain the clear $\Delta v = +2, +3$ sequence domination depicted and simulated in Figs. A1 and A2.

The results obtained for the Ba + ClF reaction portend of the rovibrational distribution we expect for the Ba + F₂ reaction which is considerably more exothermic. From a scan (Fig. A3) taken at the long wavelength onset of the dominant continuous emission (Fig. 1(d)), we recognize features corresponding to the $\Delta v = +1$ sequence,⁶ however, the identification of these features is greatly aided by our knowledge of the observed trends in the Ba + ClF ($B^2\Sigma^+ - X^2\Sigma^+$) emission spectrum. With a larger reaction exoergicity and a comparable if not greater impact parameter, the Ba + F₂ reaction should display (1) a more pronounced off-diagonal shift in the BaF $B^2\Sigma^+ - X^2\Sigma$ emission system as considerably higher vibrational levels are populated and (2) a significant increase in rotational excitation. Experiments confirm this result as the rotational excitation is so pronounced that the resolution of vibrational structure is difficult. At wavelengths shorter than 6900 Å, the overlap of vibrational-rotational structure leads to a spectrum of such density that resolution is precluded. There is, however, a clear trend toward emission from the $\Delta v = +N$ sequences.

The linear pressure dependence reported by Wren and Menzinger⁷ for the Ba + F₂ reaction is not surprising. Because a BaF $B^2\Sigma^+ - X^2\Sigma^+$ fluorescent feature is monitored, the observed pressure dependence with halogen concentration is linear since the radiative lifetime for the $B^2\Sigma^+$ state of

BaF is of order 10^{-8} seconds.⁸ The collision frequency at 10^{-4} Torr, the upper limit of the pressure dependent plot, is of order 10^3 /sec; therefore, those BaF* B² Σ^+ molecules formed in bimolecular reaction radiate well before suffering secondary collisions.

References

1. M. Menzinger, Can. J. Chem. 52 (1974) 1688.
2. F. Engelke, Chem. Phys. 44 (1979) 213.
3. Engelke also observes a mildly structured emission associated with the Mg - F₂ reaction; however, he correlates 260 cm⁻¹ separations in the observed chemiluminescence with a 277 cm⁻¹ frequency assigned to the bending mode of MgF₂ in rare gas matrices. The bending mode of MgF₂ is now thought to be considerably lower ($\sim 150 - 160$ cm⁻¹) casting doubt on the assigned chemiluminescent features.
4. C. Effantin, A. Bernard, J. d'Incan, J. Verges, and R. F. Barrow, J. Molec. Spectrosc. 145 (1991) 456.
5. See for example, R. N. Zare, J. Chem. Phys. 40 (1964) 1934.
6. These features have also been observed by Engelke and correlated incorrectly with the BaF₂ bending mode.
7. D. J. Wren and M. Menzinger, Chem. Phys. Lett. 27 (1974) 572.
8. H. Wang and J. L. Gole, unpublished.

Figure Captions (Appendix A)

Figure 1: $\text{BaF}^* \text{B}^2\Sigma^+ - \text{X}^2\Sigma^+$ chemiluminescent emission spectrum for the reaction $\text{Ba} + \text{ClF} \rightarrow \text{BaF}^* + \text{Cl}$ over the pressure range 1×10^{-5} to 1×10^{-4} Torr corresponding to "single collision" conditions. The spectrum is characterized by off-diagonal sequence structure. Bandheads are designated by the excited state vibrational quantum number and all identified sequences correspond to a larger quantum number for the excited state than that for the ground state.

Figure 2: Simulation of the $\text{BaF}^* \text{B}^2\Sigma^+ - \text{X}^2\Sigma^+$ chemiluminescent emission spectrum for the $\text{Ba} + \text{ClF} \rightarrow \text{BaF}^* + \text{Cl}$ reaction (Fig. 1). The simulated spectrum suggests the vibrational distribution inset in the figure peaking at the high excited state vibrational quantum level $v' = 38$.

Figure 3: Section of the $\text{BaF}^* \text{B}^2\Sigma^+ - \text{X}^2\Sigma^+$ chemiluminescent emission spectrum for the reaction $\text{Ba} + \text{F}_2 \rightarrow \text{BaF}^* + \text{F}$. Based on comparison with Figures 1 and 2, the excited state distribution is expected to peak at very high vibrational quantum level, v' . Bandheads are designated (v', v'') .

BaF^* CHEMILUMINESCENT SPECTRUM

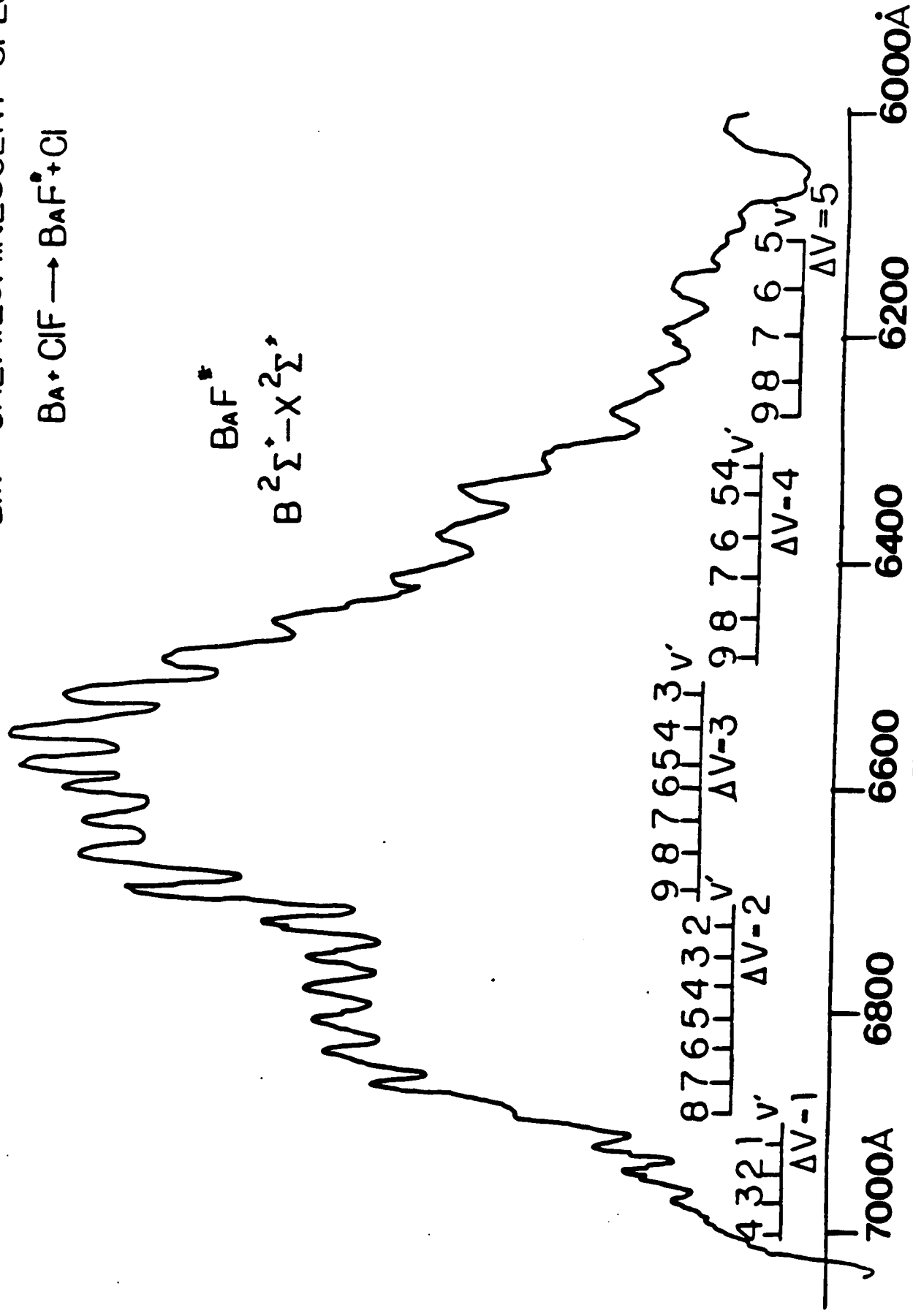


Figure A1

BaF Simulation

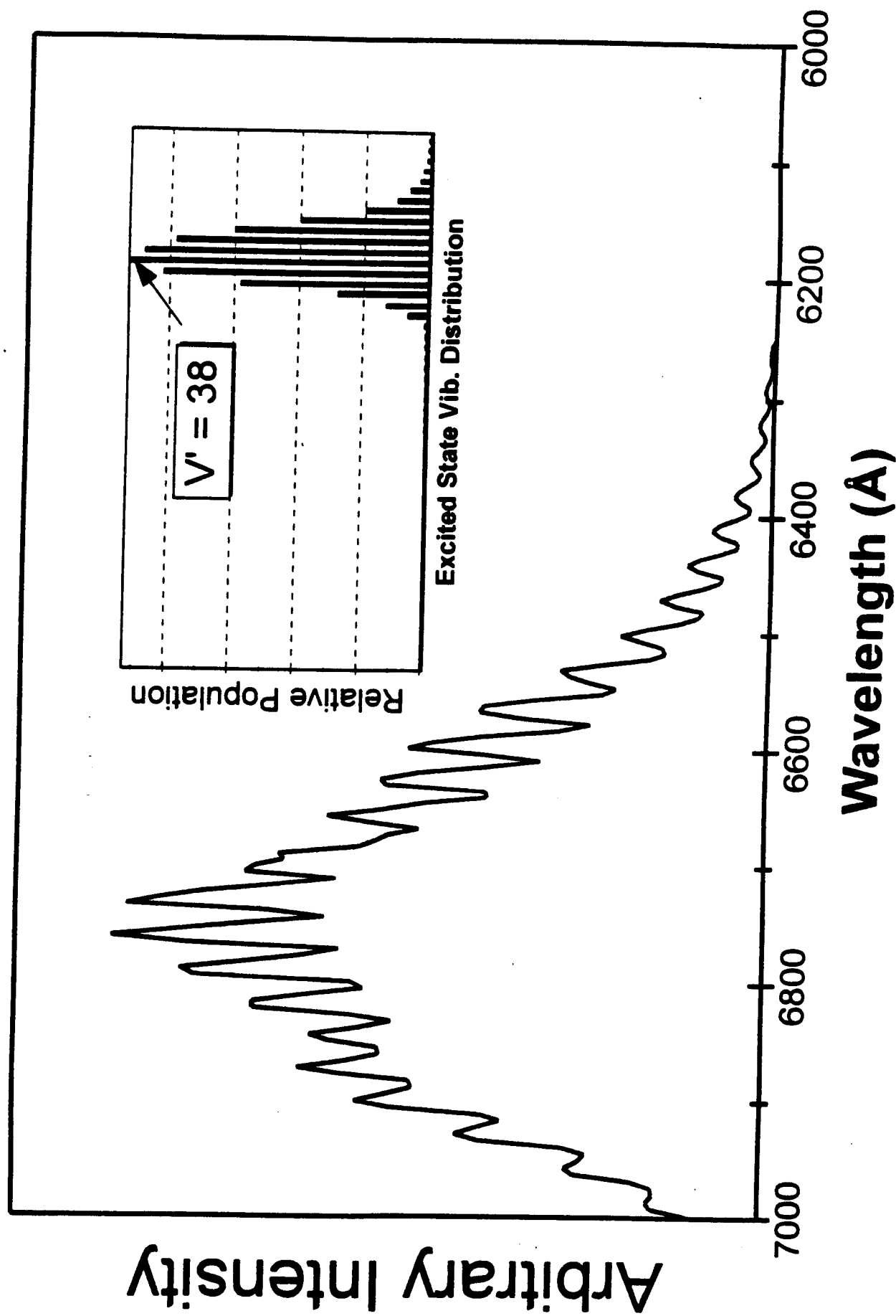


Figure A2

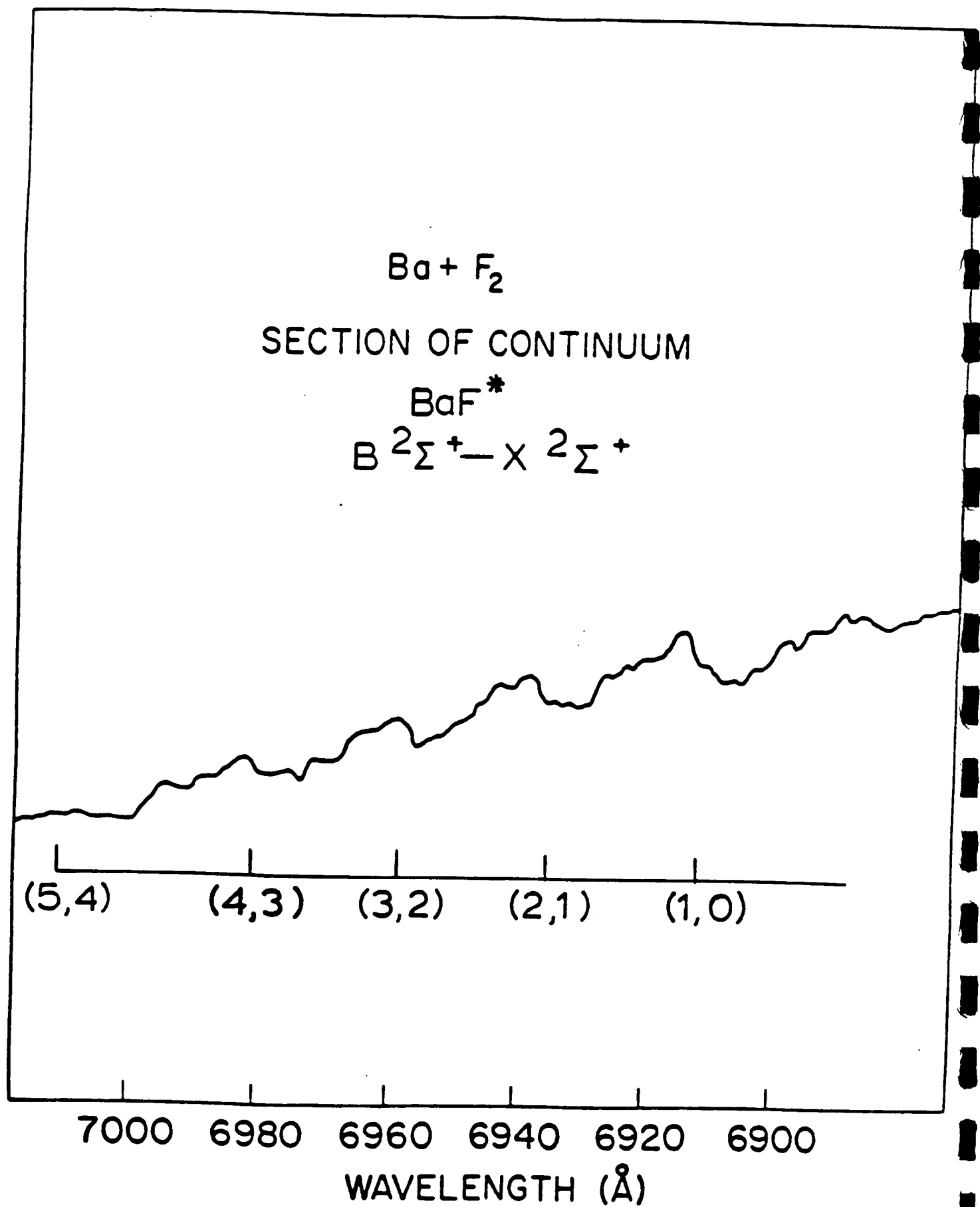


Figure A3

APPENDIX XVIII

"Confirmation of Long-Range Collision Complex Stabilization Through The Controlled Relaxation of High Internal Excitation", H. Wang, J. S. Joiner, D. E. Dawson, and J. L. Gole, J. Chem. Phys., submitted.

CONFIRMATION OF LONG-RANGE COLLISION COMPLEX STABILIZATION THROUGH THE
CONTROLLED RELAXATION OF HIGH INTERNAL EXCITATION

James L. Gole, H. Wang, J. S. Joiner, and Douglas E. Dawson

School of Physics

Georgia Institute of Technology

Atlanta, Georgia 30332

ABSTRACT

A series of controlled multiple collision chemiluminescent and laser induced fluorescent studies confirm the long-range collisional stabilization of high temperature Group IIA dihalide complexes of some considerable extent. The relaxation process demonstrates that the near continuous emissions observed under near single collision conditions (previous paper) correspond to the overlap of a closely spaced, highly excited, rovibronic distribution and reveals the first vibrationally resolved electronic emission for the dihalides. The vibronic structure of the observed emission spectra correlates well with expectations based on the molecular electronic structure of the ground and low-lying electronic states of the dihalides. The vibronically resolved emission from the $\text{Sr} + \text{ICl} \xrightarrow{\text{He}} \text{SrICl}^*$ and mixed halogen $\text{Sr} + \text{Cl}_2, \text{Br}_2 \xrightarrow{\text{He}} \text{SrCl}_2^* + \text{SrBr}_2^*$ reactions provides strong support for the formation of a collisionally stabilized dihalide complex. These results, correlated with the near single collision studies, form a basis for the discussion of the kinetics of formation of the dihalide complexes. The influence of dihalide complex formation on the discrepancies between those bond strengths determined by mass spectrometry and chemiluminescence are discussed.

INTRODUCTION

In the previous paper¹ we considered a series of nearly continuous emission features, generated from Group IIA metal-halogen molecule reactions and extending across the visible and ultraviolet regions of the spectrum. We assigned these continua to highly excited Group IIA dihalide emitters. These emission features, studied under near single collision conditions in a beam-gas environment, might be attributed to the overlap of a closely spaced highly excited ro-vibronic distribution. Alternatively they might correspond to a predissociating and broadened level structure or even the manifestation of a fly-by collision. By extending single collision chemiluminescent and laser induced fluorescent studies in a controlled manner to the multiple collision pressure regime² we wish to employ the relative rates of R-R and V-V relaxation processes. We wish to relax, if possible, the high degree of rotational excitation characteristic of the single collision environment while still preserving the degree of vibrational excitation. Not only does this approach elucidate the single collision process, but also it greatly aids the identification of the chemiluminescent emitter and simplifies laser induced fluorescent evaluations of the reactive environment.

The controlled extension of the study of highly exothermic processes to the multiple collision regime also reveals unexpected efficiencies for the rates of energy transfer among the electronically and highly vibrationally excited states of high temperature molecules.³⁻⁵ Collision induced intramolecular energy transfer proceeds at rates which for certain levels may approach 500 times gas kinetic with cross sections well in excess of 4000 \AA^2 . It appears that both the low-lying electronic states and high vibrational levels of the ground state of simple high temperature molecules interact with a collision partner as if strong interactions are present over a much larger region of configuration space than might have been previously anticipated.³⁻⁵

If the single collision dihalide continuum observed at low pressures¹ results from an extremely high rotational excitation, and if this excitation can be relaxed selectively, the identity of the contributing dihalide excited states might be established. Here we demonstrate the successful relaxation of the continuous dihalide emission features (considered previously) and determine that these continua correspond to the overlap of emission from three transition regions. We establish the discrete nature of the dihalide

emissions which contribute to the single collision continuum, obtain the first vibrationally resolved emission spectra for the Group IIA dihalides, and confirm the highly efficient R3BR mechanism for their formation.

EXPERIMENTAL

Sources

The multiple collision studies outlined here were carried out in an entrainment device similar to that used previously.^{6,7} The Group IIA metals calcium, strontium, and barium, were vaporized from specially designed and capped c.s. grade graphite crucibles at temperatures between 900 and 1200K producing a vapor pressure between $\sim 10^{-3}$ and 10^{-1} Torr for most of the experiments considered in the present study. The crucibles were machined to fit inside a commercial tungsten basket heater (R. D. Mathis, Long Beach, CA) which was lightly wrapped with zirconia cloth (Zircar Products, Florida, N. Y.). The Group IIA metal flux was entrained in a helium (Holox 99.998%) or argon (Holox 99.99%) buffer gas and transported to the reaction zone. At a suitable point above the flow the halogen molecule oxidants intersected the entrained Group IIA metals, entering from a concentric ring injector inlet. Typical operating pressures ranged from 10 to 80 mTorr of oxidant and between 1 and 2 Torr of helium buffer gas.

"Detection Systems and Laser Induced Fluorescence Studies"

Both chemiluminescent and laser induced fluorescent techniques⁸ were used to monitor reaction products in the multiple collision pressure regime. The chemiluminescence for the reactions of interest was monitored at right angles to the metal flow. Spectral emissions were dispersed with a 1-m Spex scanning monochromator operated in first order with a Bausch and Lomb 1200 groove/mm grating blazed at 5000 Å. Either cooled RCA 1P28 or 4840 or a dry ice cooled EMI 9808 photomultiplier tube was used to detect the dispersed fluorescence and provide a signal for either a Keithley 417 fast picoammeter or a 417 autoranging picoammeter. The output signal from the picoammeters was then sent either to a Hewlett Packard chart recorder or to a personal computer for storage and subsequent analysis. All spectra were wavelength

calibrated with a mercury arc lamp⁹ or with respect to the Group IIA metal atomic emissions.⁹

In order to carry out the laser-induced fluorescence (LIF) experiments, the second harmonic of a Quanta-ray Nd:YAG laser (0.53μ) was used to pump a Spectra-Physics PDL-3 pulsed tunable dye laser system operated with DCM or LDS698 dye. The output of the pulsed dye laser (with a linewidth of 0.07 cm^{-1} and a pulsewidth of 9 ns) was then either mixed with the fundamental output of the YAG laser or frequency doubled in a frequency mixer (Quanta-Ray WEX-1) to produce UV (in the range 310-410 nm) coherent radiation. The laser beam was introduced to the reaction chamber in a direction perpendicular to both the reactant flow and detector. The YAG laser was triggered by a digital pulse generator (SRS DG535) with a repetition rate of 15 Hz. The Q-switching signal of the YAG oscillator was used to trigger a boxcar integrator (SRS SR250) for better synchronization. The fluorescence induced by the UV laser pulse was collected with an RCA 1P28 photomultiplier (2.2 ns rise time) and, through a fast preamplifier (CLC 100 Video Amplifier, 500 MHz), sent to the gated integrator to record the spectrum as a function of the laser frequency. A fast digital oscilloscope (HP 54111D, 0.7 ns rise time) was used to real time monitor and record the fluorescence decay. The integration gate was set to a proper width in the range from 20 to 300 ns, dictated by the nature of the monitored fluorescence decay, with a delay timed such that the gate opened just after the short laser scattering pulse, thus reducing background noise. A personal computer (PC) drove the dye laser stepper motor, scanning the dye laser frequency and acquiring the averaged output data from the boxcar synchronously. In order to achieve a linear scan in wavelength when the dye laser frequency was mixed with the infrared, the scan step size of the dye laser was calculated in real time using the PC. The output frequency of the WEX-1 was calibrated using aluminum atom lines.⁹

A GROUP IIA DIHALIDE CORRELATION DIAGRAM

The BeF_2 correlation diagram presented in the previous paper¹, while oriented to the energetics of the BeF_2 valence orbitals as a function of bond angle¹⁰, carries the essence of the bonding trends in these highly ionic AB_2 type molecules. Even with a modification of this diagram to encompass changes associated with the transition from light metal-heavy halogen linear

configurations to heavy metal-light halogen bent configurations, the important considerations relate to the nature and ordering of the π_g HOMO and σ_g and π_u LUMO orbitals of the linear configuration. In contrast to CO_2 where the lowest lying LUMO is of π_u symmetry, the highly ionic character of the BeF_2 molecule facilitates a switch such that the σ_g LUMO lies lowest. The corresponding lowest energy transitions, which are electric dipole forbidden for the linear dihalides in absorption, should also be quite weak for the heavier bent dihalides because of their very low bending mode frequencies and floppy nature.¹¹ Transitions involving the π_g HOMO and π_u LUMO orbitals are electric dipole allowed, representing the analogs of the lowest energy allowed transitions in CO_2 ; however, the specific nature of the orbital makeup in BeF_2 suggests that the oscillator strength of these transitions will be smaller than that of CO_2 .

In emission, the lowest energy "allowed" dihalide transitions should be from a highly bent $^1\text{B}_2$ excited state and the $\text{A}^1\text{B}_2 - \text{X}^1\text{A}_1$ band system should be dominated by long progressions in the bending modes of the upper and (near linear) ground electronic states. We have observed this emission system for Ca-Cl_2 , Ca-Br_2 , Sr-Cl_2 , and Sr-Br_2 , reactive encounters. Even though we monitor an allowed transition in emission which is governed by the selection rules for a C_{2v} molecule, a ready pressure dependent quenching of the relaxed chemiluminescent spectrum for the A-X system would appear to manifest the g-g selection rule in absorption (Table I). In this same spectral region, transitions from a $^1\text{A}_2$ excited state would be expected to be weak due to the electric dipole selection rules for a C_{2v} molecule. However, the vibronically coupled transition involving the asymmetric stretch (b_2) mode is allowed. This might produce a band system of moderate strength characterized by an alternating intensity pattern with frequency intervals indicative of the asymmetric stretch. We find little evidence for this vibronically allowed emission in the observed relaxed multiple collision spectra for the dihalides. Transitions involving the $^3\text{B}_2$ state (corresponding to the spin unpaired electron configuration which is the analog of the $^1\text{B}_2$ state) are "spin forbidden" and are therefore also expected to be weak. We anticipate the change in bond angle which accompanies these lowest energy transitions to be so pronounced that the observed emission spectrum can be expected to extend over several hundred angstroms. We summarize our conclusions on the lowest energy transitions for the dihalides in Table I.

At somewhat higher energies in emission (Table I) we expect to observe transitions from excited states which result from promotion to the $b_1(\pi_u)$ and at somewhat higher energies, the $a_1(\pi_u)$ orbital. We associate the resulting electron configurations and transitions with the B and C state regions summarized in Table I, the electric dipole allowed transitions corresponding to $B^1B_2 - X^1A_1$ and $C^1B_2 - X^1A_1$ respectively. The bond angle change accompanying these transitions is not as pronounced as that accompanying the lowest energy A-X band system, however a change from π nonbonding to π -anti-bonding character should result in a spectrum dominated by progressions in the dihalide stretching frequency. Emission corresponding to the B-X system has been observed for Ca-Cl₂, Ca-Br₂, Sr-Cl₂, Sr-Br₂, and Sr-ICl reactive encounters, whereas the C-X system is excited only as a result of the strontium reactions.

MULTIPLE COLLISION RELAXED DIHALIDE EMISSION SYSTEMS

A successful and controlled extension from the near single collision pressure regime to the multiple collision condition, using primarily helium buffer gas entrainment, provides the means to collisionally relax the dihalide continuum so as to reveal what appear to be three discrete band systems. We obtain the first clear indication that the low pressure continua correspond to a profound rotational excitation associated with bound excited state levels and not with the free-bound transition of a very weakly bound dihalide excited state.¹² The overview spectrum depicted in Figure 1 for the Sr + Br₂ reaction combination is exemplary. From the figure, it is apparent that collisional relaxation produces a collapse in the wings of the near single collision SrBr₂ dihalide continuum, analogous to that noted previously for BaCl₂,¹ and leads to the observed relaxed spectrum in Figure 1.

In the SrBr₂ overview spectrum, the lower energy system (feature), which extends from the fringes of the ultraviolet through the visible, is dominated by a long progression in the bending mode of the SrX₂ complex. This is clearly apparent in the SrCl₂ emission spectrum depicted in Figure 2. The observed feature, catalogued in Table II, would appear to correspond to the analog of the $^1B_2((1a_2)^2(4b_2)(6a_1)) \rightarrow X^1A_1((1a_2)^2(4b_2)^2)$ transition in BeF₂ correlating in linear configuration to a $^1\Pi_g - ^1\Sigma_g^+$ transition involving σ_g and π_g molecular orbitals. For all of the reactive combinations studied thus

far, we find that both Group IIA metal and halogen molecule collisions very effectively quench this feature, a fact which is not surprising in view of the anticipated longer lifetime ($\tau_{\text{radiative}} \geq 10^{-5}$ seconds) for the excited state emitter.

The more clearly resolved, higher energy, B-X band system depicted in Figure 1 is displayed in greater detail for the $\text{Sr} + \text{Cl}_2$, $\text{Sr} + \text{Br}_2$ and $\text{Sr} + \text{ICl}$ reactive encounters in Figures 3-5, (catalogued in Table III). A weaker, higher energy, C-X emission system which appears energetically accessible only to the $\text{Sr} + \text{Cl}_2$, Br_2 , and ICl reactions is displayed in greater detail in Figure 6. The B-X and C-X band systems for SrCl_2 and SrBr_2 would seem to correspond to the analogs of the electric dipole allowed $^1\text{B}_2 \dots (1a_2)(4b_2)^2(2b_1)$ and $\dots (1a_2)^2(4b_2)(2b_1) - X^1\text{A}_1$ transitions in BeF_2 (Table I) which correlate in linear configuration to the allowed $^1\Sigma_u - ^1\Sigma_g^+$ transition involving the π_u and π_g molecular orbitals of the linear dihalide. This transition, which in adsorption involves primarily a change from M-X (M-X and M-Y for SrICl) nonbonding to M-X antibonding character, should be dominated by progressions in the MX_2 (or MXY for SrICl) stretching modes. The frequency separations between the observed features are consistent with short progressions in the dihalide stretching modes in agreement with this suggestion.

The tentative assignments which we give for the A-X, B-X, and C-X emission band systems are all consistent with the lowest electric dipole allowed transitions associated with the Group IIA dihalide correlation diagram. We favor these assignments over possible vibronically allowed transitions since we find little evidence for alternating intensity patterns associated with the dihalide asymmetric stretching mode. However, it is to be noted that there may be evidence for Fermi resonances in the observed emission patterns. This possibility is now the subject of further study.¹³

SUPPORT FOR A COLLISIONALLY STABILIZED DIHALIDE COMPLEX

The Energetics of Metal Monohalide Formation

We have suggested¹ that (1) the periodicity of Group IIA dihalide formation, (2) the lack of a difluoride emission associated with the calcium, strontium, and barium systems, and (3) the symmetry effects which are manifest in the mixed versus homonuclear halogen molecule reactions all support the validity of a collisional stabilization mechanism and cast doubt on a two step

harpooning mechanism for the formation of the dihalide emitter. The ability to relax while not quenching the near single collision dihalide emission continua, revealing discrete emission features, provides a means for supporting these conclusions.

The results we obtain in a comparative study of the Sr-Cl₂, Sr-Br₂, and Sr-ICl systems (Fig. 7) and in a study of the mixed Sr - Br₂ + Cl₂ system (Figure 8) are significant for they demonstrate that the observed dihalide emission results, in large part, from a collisional stabilization process. If dihalide formation occurs via the two step double harpooning mechanism strongly suggested by Menzinger¹⁴ and others the combination of Sr-ICl and SrX-ICl reactive encounters should produce SrCl₂, SrICl, and SrI₂ emission with the strong possibility that the dichloride emission dominates that for the mixed halide and SrI₂. If the collisional stabilization mechanism is operative, the observed emission spectrum will correspond to the SrICl complex formed in a dynamically constrained electron jump process.

The reactions of strontium with Cl₂ + Br₂ mixtures of varying relative chlorine and bromine concentration should produce emission from SrCl₂, SrBrCl, and SrBr₂ (Table IV) if the two step double harpooning mechanism is operative. If the highly efficient R3BR collisional stabilization process is operative, the observed spectra should consist of the sum of only SrCl₂ and SrBr₂ emission features, varying with the relative Cl₂ and Br₂ concentration.

A study of the Sr-ICl reaction, with its attendant symmetry based dynamic constraint,¹ must be cautiously pursued for SrCl molecules with moderate vibrational excitation, produced from the relaxation of rapidly emitting SrCl electronically excited products, can react with ICl in a sufficiently exothermic process to produce SrCl₂ emission features. In fact, under certain conditions, the observed spectral signature for the Sr-ICl reaction can be contaminated by SrCl₂ emitters (both A-X and B-X systems) formed via the reaction of a thermalized ground state SrCl product with ICl.

It is relevant that we choose to evaluate the ultraviolet spectra in the B-X region corresponding to one of the strongly allowed SrX₂ ¹B₂ - X¹A₁ transitions. The band systems in this region should display a minimal difference between the transition moments for the SrX₂ (X=Cl,Br) and corresponding SrXY (XY=ICl) emitters. In monitoring the Sr-ICl reaction, we observe a dominant emission corresponding to the SrICl complex both in the B-X region (Figs. 5,7) and at higher energies corresponding to a C-X band system (Fig. 6) which can

be easily populated by the more exothermic ICl reaction. The spectrum in Fig. 7 does show some SrCl_2 contamination at the higher temperatures (higher Sr flux) over which the three spectra in the figure were obtained. However the dominance of the SrICl emission system, especially as it results from a symmetry constrained process, is clearly apparent. This dominance signals the formation of SrICl in a collisionally stabilized reactive encounter (R3BR) where the formed excited state complex is stabilized by a long range interaction with a second ICl molecule.

The collage of dihalide spectra in Fig. 8, which have been obtained for varying mixtures of Br_2 and Cl_2 , correspond to sums of emission features resulting exclusively from the dichloride and dibromide with no evidence for the mixed halogen (SrBrCl) emitter. This represents a strong confirmation of the highly efficient collisional stabilization mechanism. The comparison which we make is based primarily on the B-X stretching mode region, again avoiding the possibility of comparing transitions with distinctly different oscillator strengths in the A-X emission region. We also note that the formation of an SrBrCl emitter should lead to a stronger A-X emission feature compared to those for SrCl_2 and SrBr_2 . The resultant SrBrCl emission should appear approximately central to the dichloride and dibromide features in the three intermediate panels of Figure 8. We find no evidence for this emission.

The lack of an SrBrCl emission feature in Figure 8 would appear to be especially significant when we note that the sum of both SrCl and SrBr emission features also characterize the monohalide emissions for all of the chlorine - bromine mixtures (compare to $\text{Sr}+\text{Cl}_2$ (top) and $\text{Sr}+\text{Br}_2$ (bottom)) depicted in Fig. 8. This implies that both SrCl and SrBr are available to react with Br_2 and Cl_2 to produce the mixed SrBrCl dihalide. However, the fast bimolecular $\text{Sr} + \text{X}_2 \rightarrow \text{SrX} + \text{X}$ reactions are not sufficiently exothermic¹ to populate the electronically excited states of SrCl or SrBr . Likewise, a collision induced transfer from the high vibrational levels of the ground state of SrCl or SrBr , to form the excited state emitters, can be eliminated as a possibility¹⁵ in the multiple collision environment of the present study not only on energetic grounds, but also on the basis of an expected thermalization of the ground state rovibrational distribution. The data displayed in Figures 9 and 10 correspond to laser induced fluorescence spectra for SrCl and SrBr obtained using a Nd:YAG pumped dye laser system. Fits to the LIF spectra, exemplified by that for the $\text{SrCl } C^2\Pi - X^2\Sigma^+$ band

system in Figure 11, suggest a thermalized distribution ($T_{\text{vib}} = 450\text{K}$, $T_{\text{rot}} = 450\text{K}$ - Appendix A) among the lowest vibrational levels of the ground electronic state of the monochloride and monobromide. As the LIF spectra are taken in the wavelength regions characterized by strong dihalide emission they indicate that either the radiative lifetimes of the dihalide excited states are considerably longer than those of the monohalide or the population of ground state dihalide levels is not significant.

We find a close interplay between the growth of the metal dihalide and metal monohalide emission features displayed in Figure 8. The considerable increase in the metal dihalide bond energy relative to that of the monohalide, combined with the data displayed in Figures 9-11, suggests that electronically excited SrCl and SrBr are formed via the dissociation of a dihalide complex.

The considerations which we outline demonstrate the utility of extrapolating near single collision chemiluminescence studies in a controlled manner to the multiple collision pressure regime. This allows an assessment of the electron jump process which leads to excited state dihalide formation. The results obtained under multiple collision conditions support the conclusions reached in the analysis of the low pressure data and they strongly suggest the probability that an extremely efficient collisional stabilization mechanism represents the dominant means of forming the dihalide excited state. This conclusion is also further supported by the lack of a continuum emission associated with the fluorine based reactions.

DISCUSSION

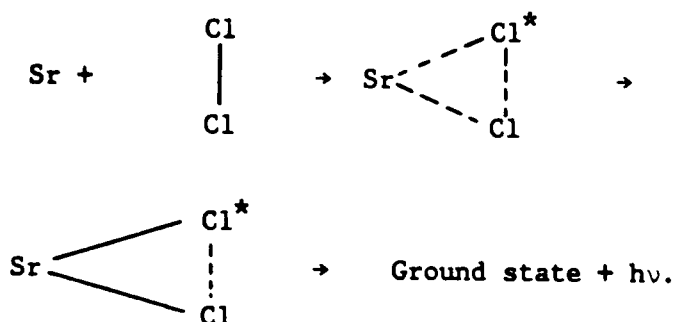
Relaxed (Discrete) Emission from the MX_2 Collision Complex

There have been numerous studies¹⁶⁻²² of the Group IIA dihalides, both experimental and theoretical, which suggest the ground state vibrational frequency ranges summarized in Table V for the SrCl_2 and SrBr_2 molecules. There are several comparisons which can be made with the data of Table V. It is apparent, as we have suggested previously, that the SrCl_2 and SrBr_2 B-X (Table III) and C-X band systems, which most likely involve a change from M-X nonbonding to M-X antibonding character, are dominated by progressions in the stretching modes of the dihalide. A precise interpretation of the level structure for these systems must consider higher order interactions including

Fermi resonances and possible vibronic couplings, although the latter do not appear to be strongly manifest in the observed emission features. Of equal importance may be the dynamics of the forming emitting complex and its relation to the molecular electronic structure of that excited state in which it is formed.

The resolved features for the SrCl_2 A-X band system in Figure 2 are certainly consistent with a long progression in the bending mode of the SrCl_2 emitter. However, the observed frequency separations for this readily quenched emission feature, which are on the order of $110\text{-}120\text{ cm}^{-1}$ (Table II), considerably exceed the bending mode frequency for the IIA dihalide, measured as $\sim 44\text{ cm}^{-1}$ ¹⁸ in rare gas matrices (calculated to be between 13 and 27 cm^{-1} ^{16,19}). The observed features cannot be attributed to a dihalide stretching mode. A series of relaxation studies suggest that the features associated with the A-X emission system correspond primarily to a progression in the ground state bending mode associated with the emitting complex. The ease with which this band system is quenched is consistent with its anticipated long lifetime.²³ These observations are consistent with previous studies of the chemiluminescent emission from long-lived excited electronic states in that the relaxed emission appears localized to the lowest vibrational levels of the upper electronic state.²

We suggest that the apparent discrepancy between the determined frequency separations and the expected dihalide bending mode frequency may reflect the remnants of bonding between the two chlorine atoms. The observed A-X band system may correspond to emission from an intermediate complex formed via the approach of strontium to Cl_2 viz.



The emitting complex would appear to correlate with a local minimum on the SrCl_2 potential surface^{24,25} which has not yet completely rearranged to the

final product dihalide.

If we have observed emission from a highly bent intermediate complex, this further complicates the analysis of the B-X and C-X emission features. As Table V demonstrates for the normal dihalide ground state geometries, the asymmetric stretch frequency considerably exceeds that of the symmetric stretch, both of which greatly exceed the bending mode. A preliminary normal mode analysis can be used to suggest that, as the dihalide bends to angles smaller than the equilibrium bond angle, its symmetric stretch frequency increases as the asymmetric stretch frequency decreases.²⁴ Because the symmetric stretch frequency can approach and exceed the asymmetric stretch frequency for an SrCl_2 complex formed as a local minimum on the Sr-Cl_2 reaction surface, the analysis of the observed features associated with the B-X and C-X emission systems becomes more complex. In fact, the nature of the bonding in those excited states formed in reaction may also strongly influence the formation of the dihalide in one or more local minima which subsequently emit radiation. These considerations are the subject of ongoing collaborative study.^{24,25}

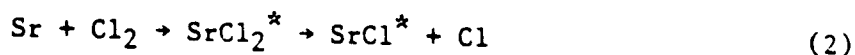
"Bond Energy Determinations"

The formation of a long-lived dihalide complex via the reaction of the Group IIA metals with chlorine, bromine, and iodine also may have implications for the determination of bond energies using chemiluminescent techniques.²⁶

The population of the electronically excited states of SrCl and SrBr from the Sr-Cl_2 and Sr-Br_2 reactions (Figs. 1,8) at first seems puzzling¹⁵ until we note the strong synergism between the development of the dihalide emission features and the subsequent increase in intensity of the monohalide emission features. We also realize that the exothermicity of a reactive process forming the dihalide provides sufficient energy to produce the excited states of the monohalide via a dissociative process. For example, under multiple collision conditions, the exothermicity of the reaction



given closely by the difference in the SrCl and Cl_2 molecule²⁷ bond energies is 39.8 Kcal/mole ($\sim 13920 \text{ cm}^{-1}$).¹ This is not a sufficient energy to produce the monochloride emission recorded in Fig. 8. The energy available through the process

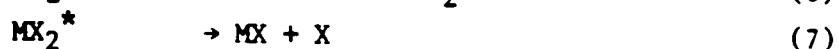
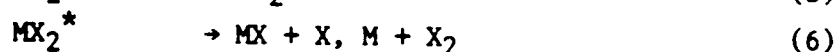


corresponds closely to an increment of order 49.3 Kcal/mole ($\sim 17243 \text{ cm}^{-1} = 1/2 \text{ AE}(\text{SrCl}_2) - D_0^0(\text{Cl}_2)$)²⁷ where $\text{AE}(\text{SrX}_2)$ is the dihalide atomization energy.¹ The significant differential in energy which can be manifest to pump electronically excited monohalide states results from a substantially larger dihalide bond energy. For the Sr-Br₂ system, the energetics¹ yield 33.5 Kcal/mole ($\sim 11717 \text{ cm}^{-1}$) and of order 49 Kcal/mole ($\sim 22600 \text{ cm}^{-1}$) for direct metal monohalide formation and dihalide complex dissociation, respectively.

The considerations above might account for the prediction of bond energies significantly higher than those determined from mass spectrometry²⁸ as one uses chemiluminescent techniques to evaluate the chlorides, bromides, and iodides. In contrast, the bond energies determined for the calcium, strontium, and barium fluorides, evaluated from direct fluorine molecule reactions which are believed not to proceed through a long-lived complex, are in good agreement with those obtained from mass spectroscopy.²⁸

"Kinetics of Formation of the Dihalide Complex"

Based on the combination of observations made under both single¹ and multiple collision conditions, the pressure dependent behavior monitored under near single collision conditions is indicative of the formation of a readily stabilized Group IIA dihalide complex of some considerable extent. A kinetic sequence consistent with both the single and multiple collision data is



where $\text{MX}_2^{*\dagger}$ represents the nascent dihalide formed in reaction and MX_2^* the collisionally stabilized complex.

The potential energy along the reaction coordinate for a general $\text{M} + \text{X}_2 \rightarrow \text{MX}_2^{*\dagger}$ association process certainly requires that the complexes formed via reaction (4) must possess low excess energy and/or high angular momentum in order to survive long enough to emit a photon or suffer a stabilizing collision. We suggest that these criteria may indeed be fulfilled for the

Group IIA dihalides as they may also be for many other high temperature constituents.

A comparison of the near single collision and multiple collision spectra for the dihalides suggests that a profound rotational excitation may play an important role in the observation of the near continuous emission observed in a beam-gas environment. The energy of the overall rotation for the complex

$$E_R = \hbar^2 (J)(J+1)/2\bar{I}, \quad (9)$$

where J is the total angular momentum quantum number and \bar{I} is the average moment of inertia, does not contribute to the non-fixed energy that facilitates the decay of the complex via a return through the $M + X_2$ entrance channel. Therefore, the funneling of energy into rotation may represent an important aspect of the observed behavior for these systems, lengthening the complex lifetime and enhancing the possibility for stabilization.

The importance of a stabilized "long-lived" MX_2^* intermediate complex is certainly evidenced in the chlorine, bromine, and iodine systems where it can lead to an enhanced excitation of the metal monohalide over and above that which would be obtained in a direct fast bi-molecular reactive encounter (metal monofluoride formation). Because the dihalide atomization energy more than doubles the metal monohalide bond energy, the conditions exist which we believe also facilitate complex formation and stabilization. It is relevant that these conditions may also be present in several other high temperature systems.

The observation of an R3BR process at pressures as low as 1×10^{-6} Torr is surprising.^{29,30} A steady state treatment of the mechanism (Eqs. (4)-(8)) gives an expression for the chemiluminescence signal as a function of X_2 density ($X_2 = Q$) which can be shown^{31,32} to be consistent with a significant stabilization cross section of order, $\sigma_S \approx 3000-5000 \text{ \AA}^2$, and a long excited state radiative lifetime ($\tau \sim 10^{-2}$ seconds). A long radiative lifetime can be consistent with the Group IIA dihalide A-X transition region (Table I and previous discussion). However, it is to be emphasized that in employing comparisons of the Group IIA dihalide B-X emission region to demonstrate strong evidence for the formation of the dihalides in a collisionally stabilized reactive encounter (R3BR), we have considered transitions which are electric dipole allowed in both absorption and emission. These allowed transitions should be characterized by radiative lifetimes much shorter than 10^{-2} seconds. The collisional stabilization mechanism (Eqs. (4)-(8)), within

an RRKM framework, requires a radiative lifetime well in excess of 10^{-5} seconds³¹ in order that emission from the complex compete favorably with excited state dihalide loss mechanisms. However, the collisional stabilization process would appear to be operative for much shorter lived excited states. If we eliminate the requirement of a long-lived electronic state, this implies a considerably larger stabilization cross section than that conceived by Wren and Menzinger³¹ and an extremely long range interaction involving the Group IIA dihalide excited states and their relaxing collision partner. It is clear that the stabilization process competes favorably with unimolecular decomposition for which RRKM calculations suggest a unimolecular lifetime (averaged over the distribution of energy and angular momentum) on the order of $\tau_D \sim 10^{-7}$ seconds.

A large stabilization cross section provides the route for dissipating the energy increments³¹ which must be funneled from the freshly forming Group IIA MX_2 complex. The facilitating inelastic events may not be surprising in view of the high level density and large geometrical cross section presented by the strongly vibrating complex. Present studies, strongly dependent on the effective transfer of energy, suggest that the configuration space associated with collisional stabilization and energy transfer far exceeds that which would be associated with rotationally averaged hard sphere collision cross sections. This, of course, raises the question of whether association processes in these systems can be treated in a satisfactory fashion employing some variant of unimolecular rate theory.³³ The key question must be whether dissociative processes, well characterized by RRKM theory, or highly efficient energy transfer dominates the system. The present results, in conjunction with the highly efficient V-E and E-E transfers characterizing high temperature molecules in general³, would suggest that it is appropriate to consider the expansion of small molecule configuration space to account for a significantly enhanced energy transfer efficiency.

Addendum

We have outlined the nature of an extremely efficient collisional stabilization process involving intermediate complexes of some considerable extent. We suggest that complexes which might be characterized by a diffuse excited state electron density, may be present in several environments. The

implication of the present results may be broader. The extent of interaction of high temperature molecular complexes, as they form, can considerably exceed that which we normally associate with collisional stabilization and energy transfer processes. High temperature molecules in electronically excited states or in high vibrational levels of their ground electronic states simply are capable of much longer range interactions. An understanding of the formation and interaction of these species must contribute to our ability to control the behavior of systems operating under extreme conditions. A neglect of these phenomena in models of combustion or propulsion systems renders these models unrealistic.

ACKNOWLEDGEMENT

The authors gratefully acknowledge the helpful comments of Dr. Kangkang Shen and the helpful comments and technical assistance of Mr. C. B. Winstead. The assistance of Mr. David Grantier and Mr. Peter Medley in preparing the figures is gratefully appreciated. Mr. David Grantier provided the simulations presented in Appendix A. The support of the Georgia Tech Foundation through a grant from Mrs. Betty Peterman Gole, the Army Research Office through the Short Term Innovative Research Program, the Air Force Office of Scientific Research, the Army Research Office, the National Science Foundation, and AFOSR/SDIO is greatly appreciated.

References

1. J. L. Gole, "Highly Efficient Collisional Stabilization and the Symmetry Constrained Dynamics of High Temperature Complex Formation", previous paper.
2. G. J. Green and J. L. Gole, *Chemical Physics* 100 (1985) 133. R. W. Woodward, J. S. Hayden and J. L. Gole, *Chemical Physics* 100 (1985) 153.
3. J. L. Gole, "Probing Ultrafast Energy Transfer Among the Excited States of Small High Temperature Molecules", in "Gas Phase Chemiluminescence and Chemiionization", A. Fontijn (editor) - Elsevier Science Publishers, 1985, p. 253.
4. D. M. Lindsay and J. L. Gole, *J. Chem. Phys.* 66 (1977) 3886. M. J. Sayers and J. L. Gole, *J. Chem. Phys.* 67 (1977) 5442. J. L. Gole and S. A. Pace, *J. Chem. Phys.* 73 (1980) 836.
5. A. W. Hanner and J. L. Gole, *J. Chem. Phys.* 73 (1980) 5025. J. L. Gole and S. A. Pace, *J. Phys. Chem.* 85 (1981) 2651. J. L. Gole, B. Ohlsson, A. W. Hanner, and E. J. Greene, unpublished.
6. See reference 2 and 3, and M. McQuaid, K. Morris, and J. L. Gole, *J. Am. Chem. Soc.* 110 (1988) 5280.
7. J. R. Woodward, S. H. Cobb, K. K. Shen, and J. L. Gole, *JQE* 26 (1990) 1574 - invited paper. K. K. Shen, H. Wang, and J. L. Gole, *JQE* 29 (1993) 2346.
8. See references 16, 28 and H. Wang and J. L. Gole, *J. Chem. Phys.* 98 (1993) 9311; *J. Mol. Spectros.* 161 (1993) 28.
9. See for example, NBS Special Publication 505, Bibliography on Atomic Transition Probabilities (1914 through October 1977) and Supplement I (November 1977 through March 1980), U. S. Department of Commerce/National Bureau of Standards. C. E. Moore, "Atomic Energy Levels", (National Bureau of Standards, 1949).
10. James L. Gole, *J. Chem. Phys.* 58 (1973) 869.
11. Rapid vibrational motion corresponding to a bending mode for the MF_2 molecule will produce an "effective" linear molecule whose dipole moment may be near zero. Similarly rapid rotation produces an effective zero dipole moment.
12. J. M. Parson, *J. Phys. Chem.* 90 (1986) 1811.
13. T. C. Devore and James L. Gole, "Formation and Characterization of Group IIA Dihalide Complexes - Bond Energy Determination from Chemiluminescence Spectra", in preparation.

14. M. Menzinger, Adv. Chem. Phys. 42 (1980) 1. M. Menzinger, "The $M+X_2$ Reactions: A Case Study", in "Gas Phase Chemiluminescence and Chemi-ionization", A. Fontijn, editor, Elsevier Science Publishers, Amsterdam, 1985, pp. 25-66. M. Menzinger, "Chemiluminescence and Chemiionization: Metal-Halogen Reactions as Paradigms of Diabatic Reaction Dynamics", Acta Physica Polonica A73 (1988) 85.
15. We have found that the careful and controlled extension of chemiluminescent studies from single to multiple collision conditions (see ref. 3) preserves the maximum internal excitation observed under single conditions with no exceptions. While we observe rotational followed by vibrational relaxation and thermalization, no enhanced excitation is manifest due to energy transfer collisions.
16. L. Seijo, Z. Barandiaran, and S. Huzinaga, J. Chem. Phys. 94 (1991) 3762.
17. J. L. Gole and D. A. Dixon, unpublished results.
18. F. Ramondo, L. Bencivenni, C. Nunziante, and K. Hilpert, J. Molec. Struct. 192 (1989) 83.
19. M. Kaupp, P. R. Schleyer, H. Stoll, and H. Preuss, J. Am. Chem. Soc. 113 (1991) 6012.
20. D. White, G. V. Calder, S. Hemple, and D. E. Mann, J. Chem. Phys. 59 (1973) 6645.
21. V. Calder, D. E. Mann, K. S. Seshadri, M. Alleva, and D. White, J. Chem. Phys. 51 (1969) 2093.
22. D. E. Mann, G. V. Calder, K. S. Seshadri, D. White, and M. J. Linevsky, J. Chem. Phys. 46 (1967) 1138.
23. R. B. Bernstein, R. D. Levine, Molecular Reaction Dynamics, (Oxford University Press, New York, 1974).
24. T. C. Devore and J. L. Gole, work in progress.
25. K. Morokuma, J. Bowman, D. A. Kabysh, and J. L. Gole, work in progress.
26. M. Menzinger, Can. J. Chem. 52 (1974) 1688.
27. $D_0^0(Cl_2) = 2.479367$ eV (57.2 Kcal/mole) from R. J. Leroy in "Molecular Spectroscopy", Volume 1, pg. 113, The Chemical Society, 1973. $D_0^0(Br_2) = 1.971$ eV (45.5 Kcal/mole) from J. A. Horsley and R. F. Barrow, Transactions Faraday Society 63 (1967) 32. $D_0^0(ICl) = 2.152$ eV (49.6 Kcal/mole) from W. E. Eberhardt, W. C. Cheng, and H. Renner, J. Molec. Spectros. 3 (1959) 664.
28. D. L. Hildenbrand, "Model Calculations of Thermochemical Properties of Gaseous Metal Halides", in Proceedings of the Symposium on High Temperature Metal Halide Chemistry, Vol. 78-1, The Electro-Chemical Society, pg. 248.

29. W. J. Rosano and J. M. Parson, J. Chem. Phys. 84 (1986) 6250.
30. F. Engelke, Chem. Phys. 44 (1979) 213.
31. D. J. Wren and M. Menzinger, Chem. Phys. Lett. 27 (1974) 572.
32. D. Wren, Ph.D. Thesis, U. of Toronto, 1978.
33. P. J. Robinson and K. A. Holbrook: Unimolecular Reactions, Wiley - Interscience (London 1972).

Table I

Group IIA Dihalides - Low-Lying Electronic States Electronic Transitions in $D_{\infty h}$ (Absorption) or C_{2v} (Emission) Symmetry

Electron Configuration ^a (Absorption)	State Designation (Absorption)	Electron Configuration ^a (Emission)	State Designation (Emission)	Comments ^b
$\dots(x,y,\pi_g)^4$ c linear	$X^1\Sigma_g^+$ Ground State	$\dots(xa_2)^2(yb_2)^2$	X^1A_1 Ground State	
$\dots(x,y,\pi_g)^3(\pi\sigma_g)^c$ linear	$1,3\Pi_g$ A-X region	$\dots(xa_2)^1(yb_2)^2(\pi a_1)^1$ $\dots(xa_2)^2(yb_2)^1(\pi a_1)^1$	$1,3A_2$ $1,3B_2$ A-X region ^e	A-X region transitions ^f will produce large change in bond angle
$\dots(x,y,\pi_g)^3(\pi\pi_u)^c$ linear	$1,3\Sigma_u$ B-X region $1,3\Pi_u$ C-X region	$\dots(xa_2)^1(yb_2)^2(mb_1)^1$ $\dots(xa_2)^2(yb_2)^1(mb_1)^1$	$1,3B_2$ $1,3A_2$ B-X region ^f	B-X region transitions ^f will produce significant change in bond length
		$\dots(xa_2)^1(yb_2)^2(na_1)^1$ $\dots(xa_2)^2(yb_2)^1(na_1)^1$	$1,3A_2$ $1,3B_2$ C-X region ^g	C-X region transitions ^f will produce significant change in bond length

- a. Highest occupied orbitals (x,y) and lowest promotion orbitals (l,m,n).
 b. $1B_2 - X^1A_1$ transition is electric dipole allowed, $1A_2 - X^1A_1$ transition is vibronically allowed through coupling with the ground or excited state asymmetric stretch of b_2 symmetry. The corresponding triplet-singlet transitions will be weaker.
 c. For MX_2 ($SrCl_2, \dots$) we have $(x,y,\pi)^4$, $(x,y,\pi)^3(\pi\sigma)$, and $(x,y,\pi)^3(\pi\pi')$.
 d. For MX_2 ($SrCl_2, \dots$) we have (for example) $(xa'')^2(ya')^2(\pi a')$, $1,3A'$, in the A-X region.
 e. For the A-X region see Figures 1 and 2.
 f. For the B-X region see Figures 3-5.
 g. For the C-X region see Figure 6.

Table II

Vibronic Bands Observed for SrCl_2 in the Dihalide "A-X" Transition Region^a

Band Number (see Fig. 10)	Wavelength (Angstroms)	Frequency ^b (Vacuum - cm^{-1})	Δ (Frequency) (cm^{-1})
1	4387	22788.2	
2	4411	22664.2	124
3	4434	22546.7	117.5
4	4456	22435.4	111.3
5	4480	22315.2	120.2
6	4500	22216.0	99.2
7	4524	22098.2	117.8
8	4548	21981.6	116.6
9	4572	21866.2	115.4
10	4596	21752.0	114.2
11	4620	21639.0	113.0
12	4646	21517.9	121.1
13	4672	21397.2	119.7
14	4700	21277.7	127.5
15	4726	21153.7	117.0
16	4754	21029.1	124.6
17	4782	20905.9	123.2
18	4806	20801.5	104.4
19	4836	20672.5	119.0
20	4862	20561.9	111.6
21	4891	20440.0	121.9

a. See Table I and Figure 2.

b. Frequencies are $\pm 5 \text{ cm}^{-1}$. Additional poorly resolved features to shorter and longer wavelength.

Table III

Vibronic Bands Observed for SrX_2 , SrXY ($\text{X}=\text{Cl}, \text{Br}$; $\text{Y}=\text{I}$) in the Dihalide "B-X" Transition Region^a

Molecule/ Band Number	Wavelength (Angstroms)	Frequency ^b (Vacuum - cm^{-1})	Δ (Frequency) (cm^{-1})
SrCl_2 (Figure 13)			
1	3687	27114.6	
2	3715	26910.2	204.4
3	3750	26659.1	251.1
4	3782	26433.5	225.6
5	3818	26184.3	249.2
6	(3831)	26099.4	84.9
7	3852	25953.2	146.2
8	3900	25633.8	319.4
9	3923	25483.5	150.3
10	3940	25373.5	110
11	3964	25219.9	153.6
12	3994	25030.5	189.4
13	4015	24899.6	130.9
14	4038	24757.7	141.9
15	4076	24526.9	230.8
16	4117	24282.7	244.2
17	4156	24054.8	227.9
18	4196	23825.5	229.3
19	4233	23617.2	208.3
20	4275	23385.2	232.0
21	4318	23152.4	232.8

Table III (continued)

Molecule/ Band Number	Wavelength (Angstroms)	Frequency ^b (Vacuum - cm^{-1})	Δ (Frequency) (cm^{-1})
SrBr ₂ (Figure 14)			
1	3873	25812.5	
2	3898	25646.9	165.6
3	(3905)	25600.9	46.0
4	3928	25451.0	149.0
5	3959	25251.8	199.2
6	3981	25112.2	139.6
7	4017	24887.2	225.0
8	4049	24690.5	196.7
9	4071	24557.1	133.4
10	4099	24389.3	167.8
11	4109	24330.0	59.3
12	4141	24141.9	188.1
13	4161	24025.9	116.0
14	4176	23939.6	86.3
15	4191	23853.9	85.7
16	4239	23583.8	270.1
17	4273	23396.2	187.6
18	4295	23276.3	119.9
19	4309	23200.7	75.6
20	4341	23029.7	171.0
21	4373	22861.2	168.5

Table III (continued)

Molecule/ Band Number	Wavelength (Angstroms)	Frequency ^b (Vacuum - cm^{-1})	Δ (Frequency) (cm^{-1})
SrICl (Figure 15)			
1	4347	22997.9	
2	4381	22819.5	178.4
3	4417	22633.5	186.0
4	4451	22460.5	173.0
5	4483	22300.3	160.2
6	4505	22191.4	108.9
7	4535	22044.6	146.8
8	4561	21918.9	125.7

a. See Table I and Figures 3, 4, and 5.

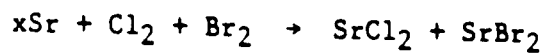
b. Frequencies are $\pm 10 \text{ cm}^{-1}$.

Table IV

Mechanisms for Mixed $\text{Cl}_2 + \text{Br}_2$

Reactions with Strontium Metal

Collisional Stabilization Mechanism



Two Step Harpooning Mechanism

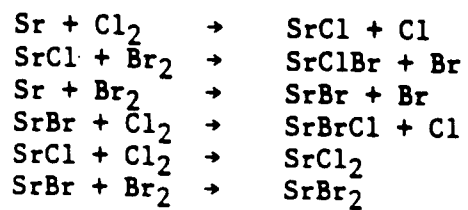


Table V
Ground State Vibrational Frequencies
for
SrCl₂, SrBr₂

Dihalide (vibrational mode)	Vibrational Frequencies (cm ⁻¹)
SrCl ₂ (ν ₁) (ν ₂) (ν ₃)	251 ^a , 256 ^b , 270 ^c 19 ^a , 20 ^b , 44 ^d 337 ^a , 307 ^b , 300 ^c
SrBr ₂ (ν ₁) (ν ₂) (ν ₃)	160 ^a , 152 ^b , 157 ^f 13 ^a , 11 ^b , 37 ^a 267 ^a , 242 ^b , 263 ^f , 223-269 ^d

- a. Reference 16,18-22.
b. Reference 17.
c. M. W. Chase, C. A. Davies, J. R. Downey, Jr., D. J. Frurip, R. A. McDonald, and A. N. Syverd; JANAF Thermochemical Tables. J. Phys. Chem. Ref. Data 14 (1985) Suppl. No. 1.
d. Reference 18.

Figure Captions

Figure 1: $\text{SrBr}_2 + \text{SrBr}$ multiple collision chemiluminescent spectrum taken at a resolution of 10 \AA . Formation of the di- and monobromide results from the reactive process $\text{Sr} + \text{Br}_2 \xrightarrow{\text{He}} \text{SrBr}_2^* \rightarrow \text{SrBr}_2 + h\nu_1$ or $\text{SrBr} + \text{Br} + h\nu_2$ at a background helium pressure of 0.8 - 1.2 Torr. The dihalide A-X, B-X, and C-X emission regions (see Table I) are indicated in the figure. The near single collision SrBr_2 spectrum (dashed line) is included for comparison. See text for discussion.

Figure 2: Multiple collision chemiluminescent spectrum for SrCl_2 in the dihalide A-X emission region (see Table I) taken at a resolution of 10 \AA . The emission corresponds to a long progression in the dihalide bending mode. The dihalide emitter is formed via a collisionally stabilized $\text{Sr} + \text{Cl}_2 \xrightarrow{\text{He}} \text{SrCl}_2^*$ reactive encounter. The helium gas background pressure ranges from 0.8 to 1.2 Torr. The labeled emission features are catalogued in Table II. See text for discussion.

Figure 3: Multiple collision chemiluminescent spectrum for SrCl_2 in the dihalide B-X emission region (see Table I) taken at a resolution of 10 \AA . The dihalide emitter is formed via a collisionally stabilized $\text{Sr} + \text{Cl}_2 \xrightarrow{\text{He}} \text{SrCl}_2^*$ reactive encounter. The helium background gas pressure ranges from 0.8 to 1.2 Torr. The spectrum appears to be dominated by dihalide stretching modes. The labeled emission features are catalogued in Table III. See text for discussion.

Figure 4: Multiple collision chemiluminescent spectrum for SrBr_2 in the dihalide B-X emission region (see Table I) taken at a resolution of 10 \AA . The dihalide emitter is formed via a collisionally stabilized $\text{Sr} + \text{Br}_2 \xrightarrow{\text{He}} \text{SrBr}_2^*$ reactive encounter. The helium background gas pressure ranges from 0.8 to 1.2 Torr. The spectrum appears to be dominated by dihalide stretching modes. The labeled emission features are catalogued in Table III. See text for discussion.

Figure 5: Multiple collision chemiluminescent spectrum for SrICl in the dihalide B-X emission region (see Table I) taken at a resolution of 10 \AA . The dominant dihalide emitter is formed via a collisionally stabilized $\text{Sr} + \text{ICl} \xrightarrow{\text{He}} \text{SrICl}^*$ reactive encounter (some SrCl_2^* contamination is also evident due to the $\text{SrCl} + \text{ICl} \rightarrow \text{SrCl}_2^* + \text{I}$ reaction). The helium background gas pressure ranges from 0.8 to 1.2 Torr. The spectrum appears to be dominated by dihalide stretching modes. The labeled emission features are catalogued in Table III. See text for discussion.

Figure 6: Collage of multiple collision chemiluminescent emission spectra for SrCl_2 , SrBr_2 , and SrICl in the dihalide C-X emission region (see Table I) taken at resolutions of 10 \AA . The dihalide emitters were formed via the collisionally stabilized $\text{Sr} + \text{Cl}_2$, Br_2 , $\text{ICl} \xrightarrow{\text{He}} \text{SrCl}_2^*$, SrBr_2^* , SrICl^* reactive encounters. The helium background gas pressure ranges from 0.8 to 1.2 Torr. The spectrum appears to be dominated by dihalide stretching modes although some evidence for short bending mode progressions may be manifest.

Figure 7: Comparison of multiple collision chemiluminescent spectra for SrCl_2 , SrBr_2 , and SrICl in the dihalide B-X emission region. The homo- and heteronuclear dihalide emitters are formed via the collisionally stabilized $\text{Sr} + \text{Cl}_2$, Br_2 , $\text{ICl} \xrightarrow{\text{He}}$ SrCl_2^* , SrBr_2^* , SrICl reactive encounters. The helium pressure ranges from 0.8 to 1.2 Torr. The spectra appear to be dominated by short progressions in the dihalide stretching modes. Note also Figures 3, 4 and 5 and Table III. See text for discussion.

Figure 8: (a) Collage of multiple collision chemiluminescent emission spectra for reactive mixtures of strontium metal and varying relative concentrations of Cl_2 and Br_2 reactants. The spectra correspond to the sum of metal dihalide and metal monohalide emitters. The dihalide emission features represent combinations of only SrCl_2 and SrBr_2 emitters with no evidence obtained for SrBrCl emission (see Table IV). The monohalide emission features represent combinations of SrCl and SrBr formed via the collisionally stabilized process $\text{Sr} + \text{X}_2 \xrightarrow{\text{He}}$ $\text{SrX}_2^* \xrightarrow{\text{He}}$ $\text{SrX}^* + \text{X}$ where the dihalide is formed as a precursor intermediate to the monohalide. (b) Closeup of inner three panels in (a). See text for discussion.

Figure 9: Laser induced fluorescence spectrum for SrCl obtained by pumping ground state SrCl to the $\text{SrCl } C^2\Pi$ state. The range of the laser induced fluorescent scan is correlated with a portion of the SrCl_2 chemiluminescent emission in the B-X region as indicated in the inset of the figure. All features in the LIF spectrum are to be associated with the monochloride suggesting a much higher oscillator strength for the monochloride versus the dichloride B-X (Table III) transitions. Note also Figure 3 and Table III. See text for discussion.

Figure 10: Laser induced fluorescence spectrum for SrBr obtained by pumping ground state SrBr to the $\text{SrBr } C^2\Pi$ state. The range of the laser induced fluorescent scan is correlated with a portion of the SrBr_2 chemiluminescent emission in the B-X region as indicated in the inset of the figure. All features in the LIF spectrum are to be associated with the monobromide suggesting a much higher oscillator strength for the monobromide versus the dibromide B-X (Table III) transitions. Note also Figure 4 and Table III. See text for discussion.

Figure 11: Fit of $\text{SrCl } C^2\Pi - \text{X}^2\Sigma^+$ laser induced fluorescence spectrum with known ground state and adjusted excited state constants. The vibrational and rotational temperatures are set at 450 K for the simulation. See text for discussion.

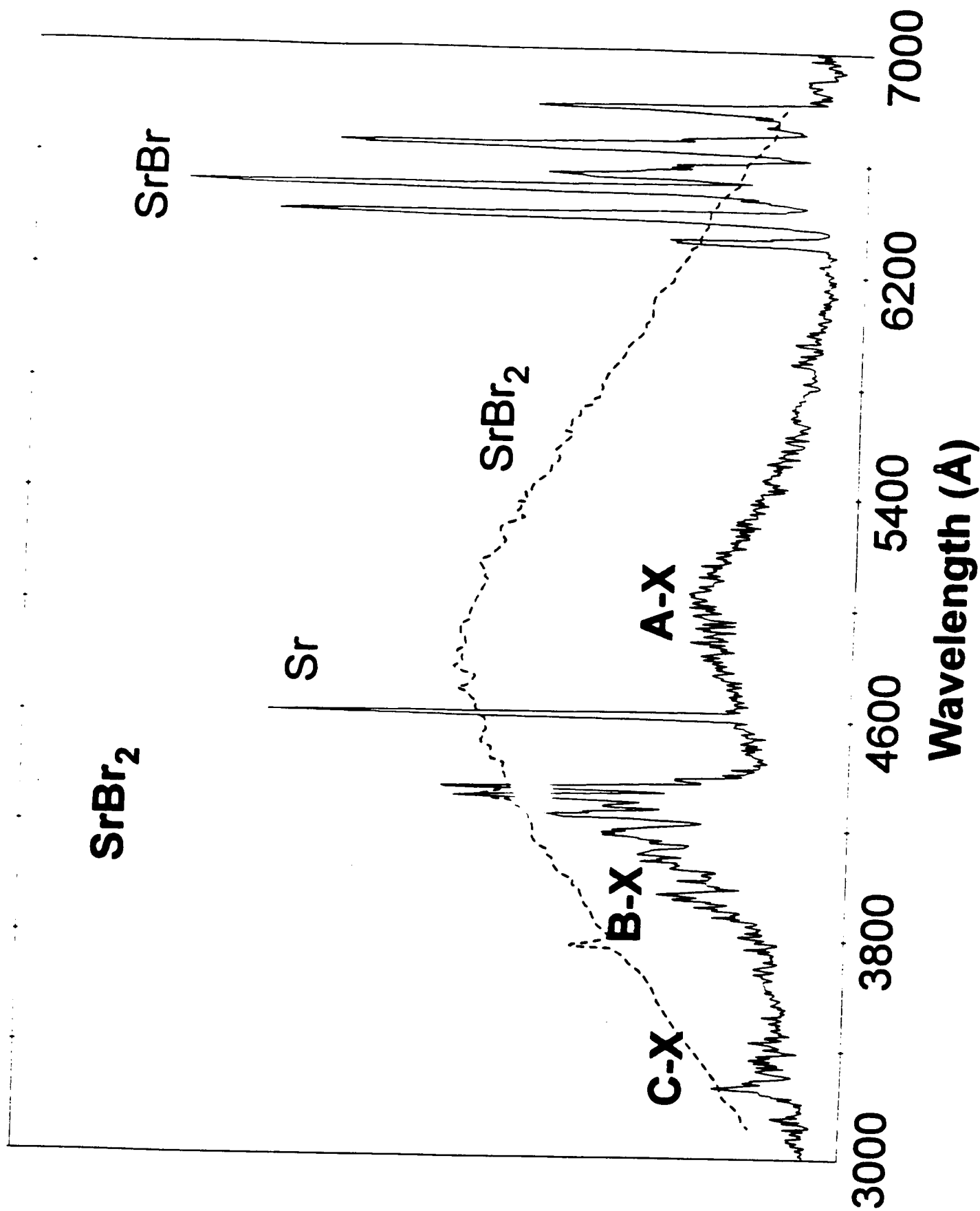
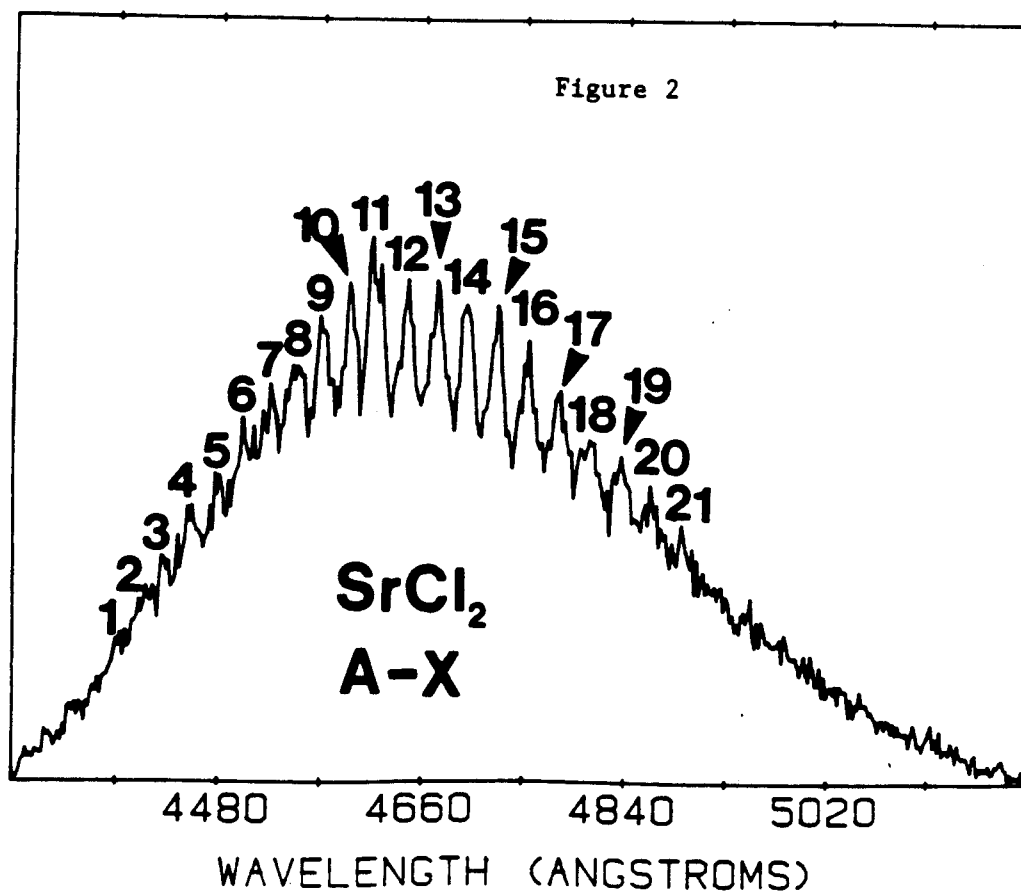
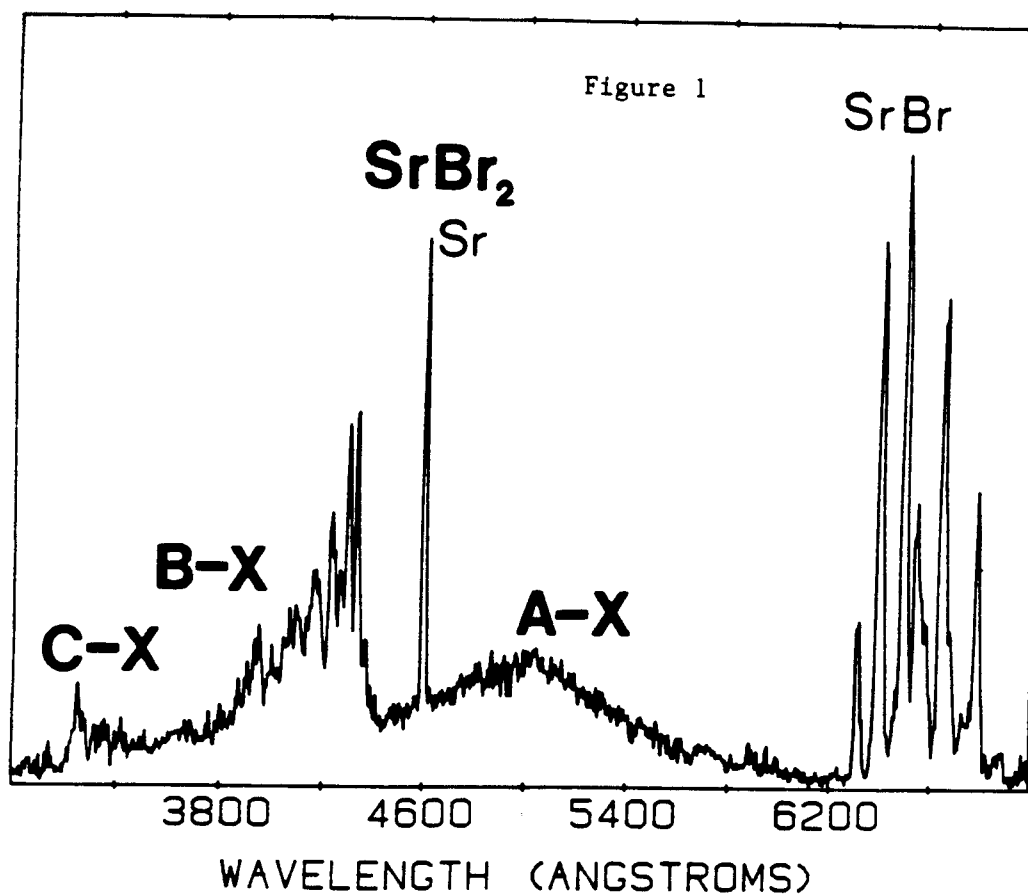
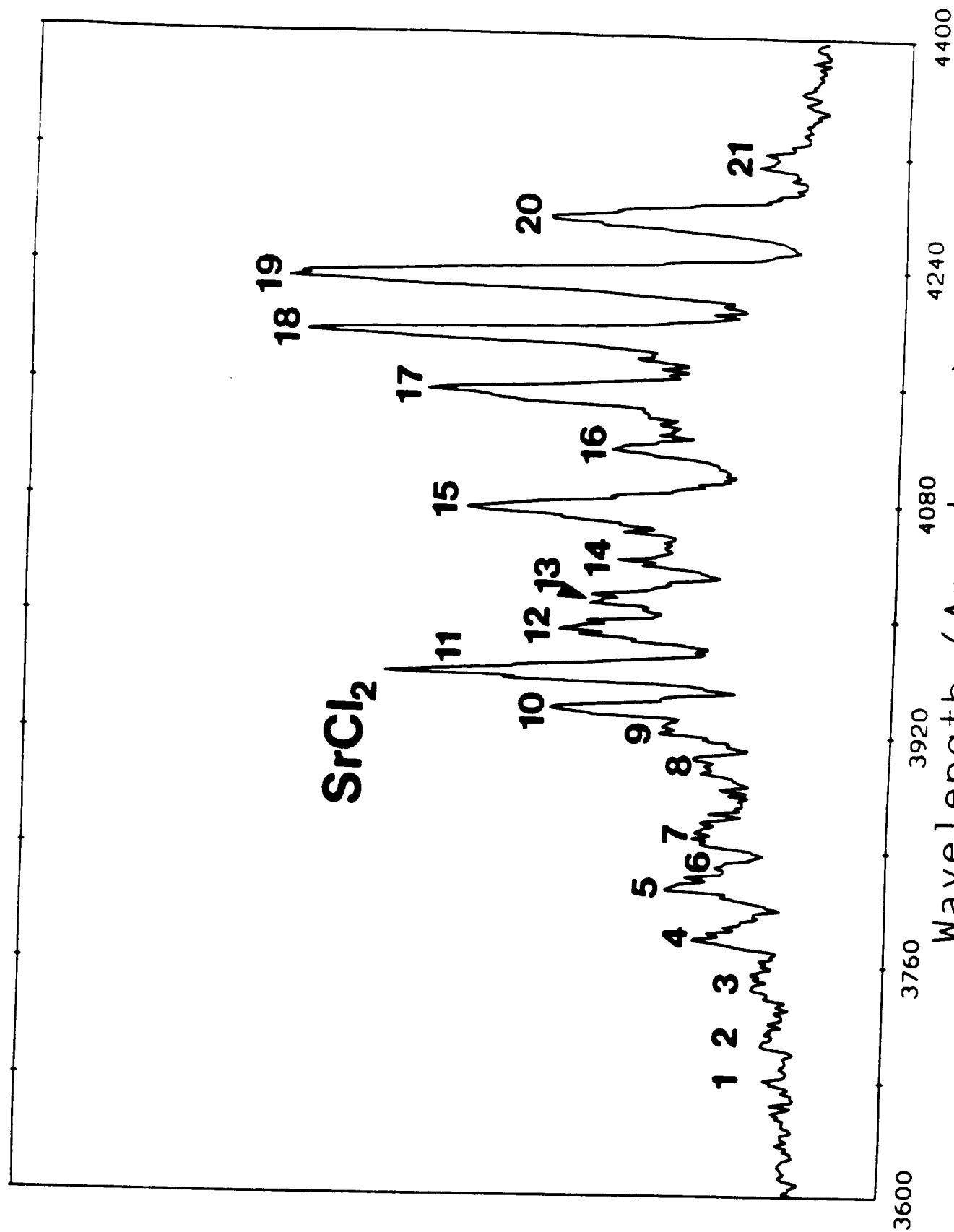


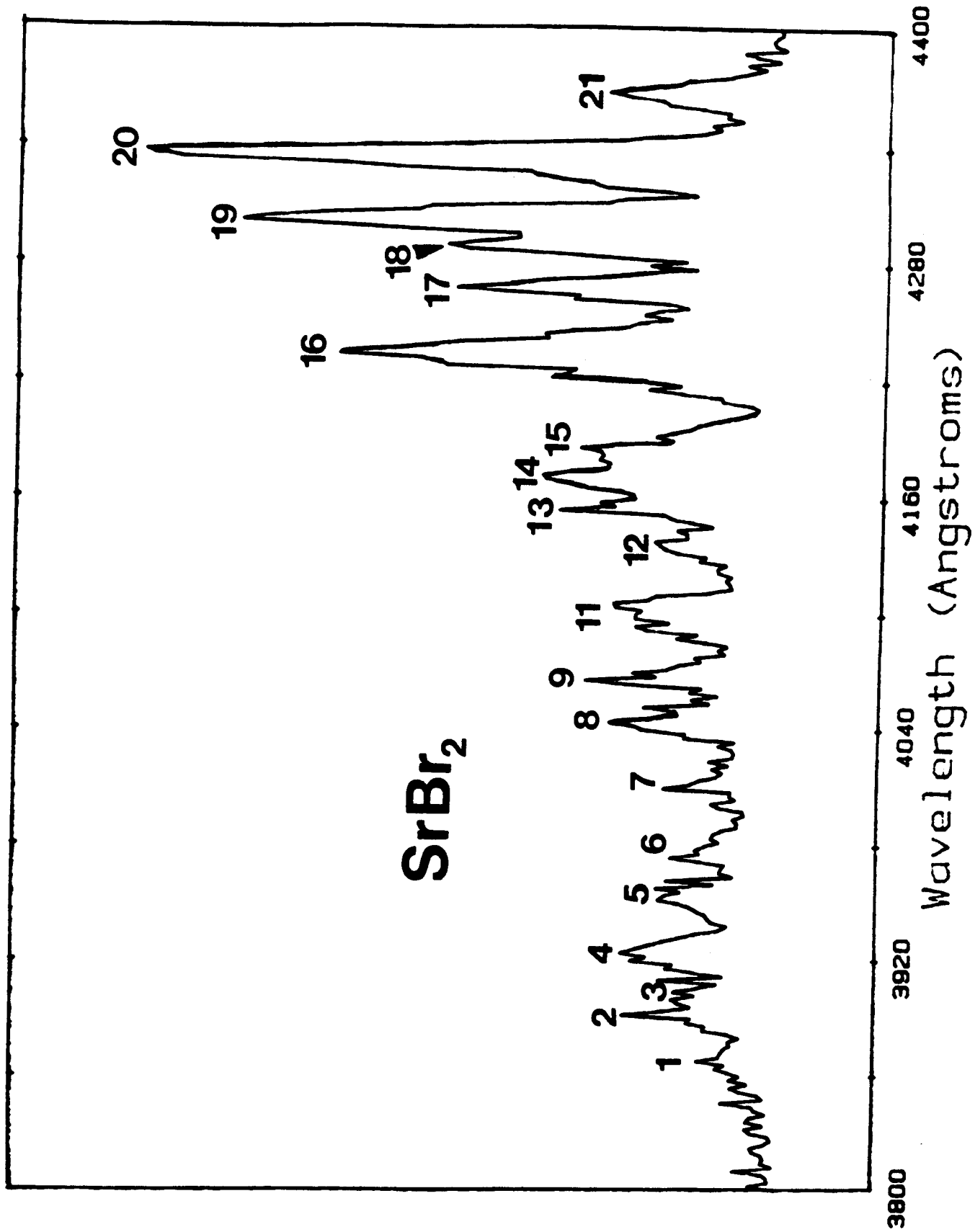
Figure 1





Wavelength (Angstroms)

Figure 3



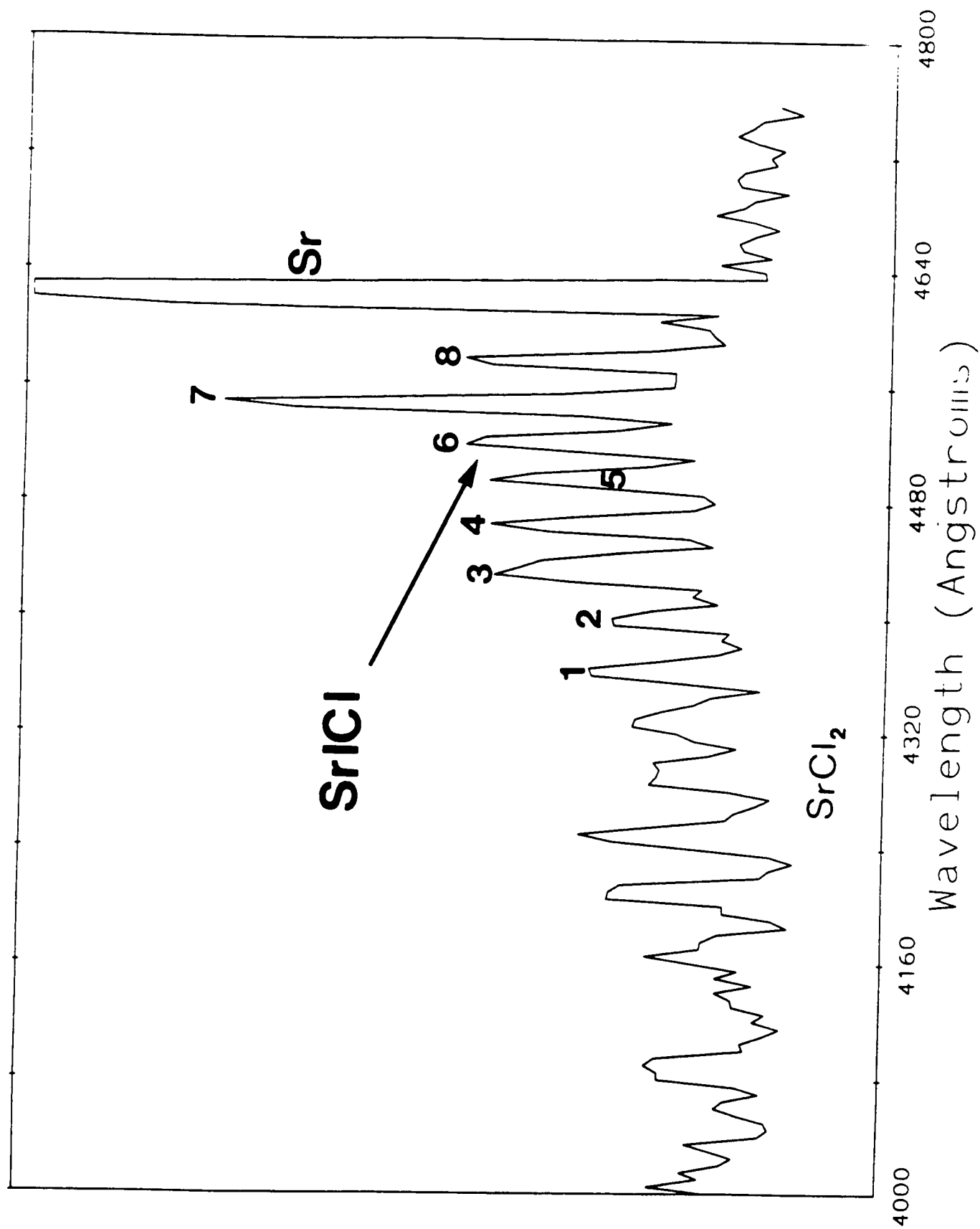


Figure 5

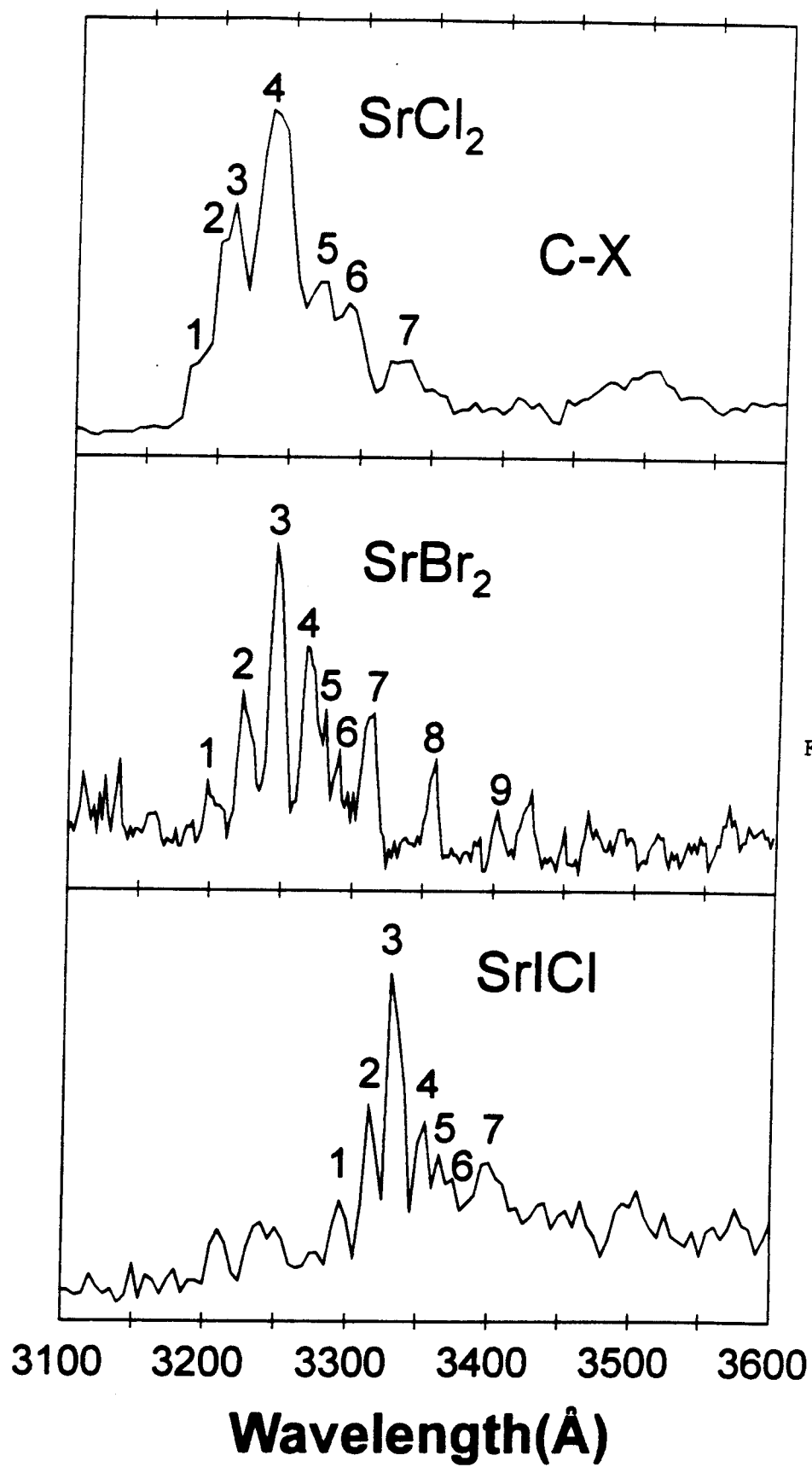
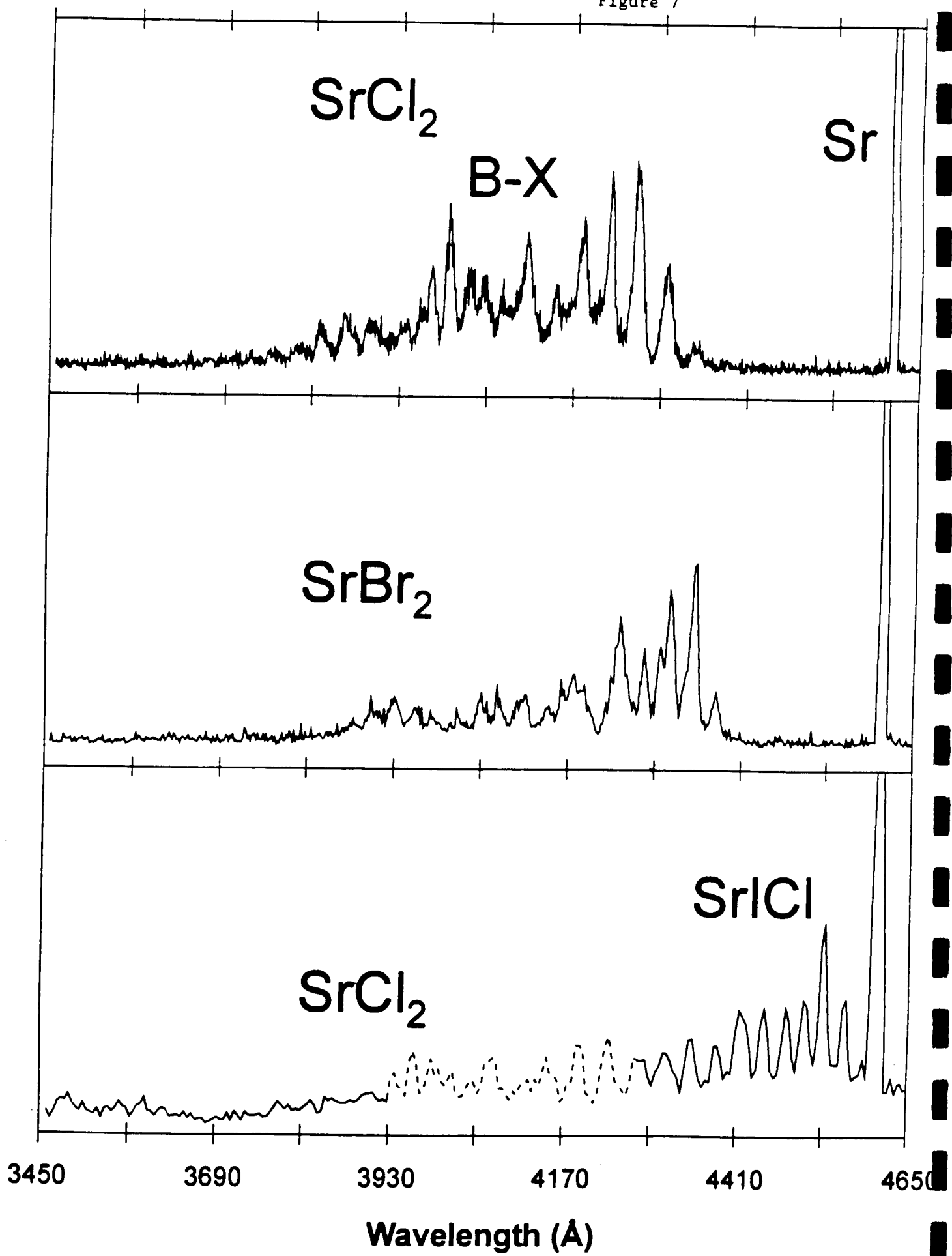


Figure 6

Figure 7



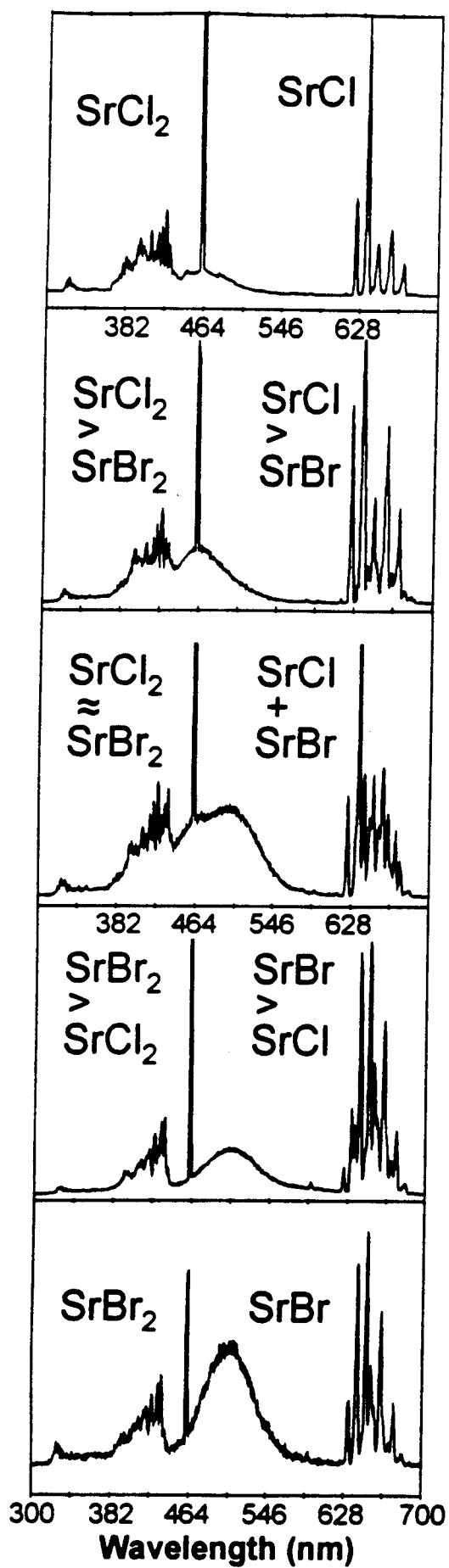


Figure 8(a)

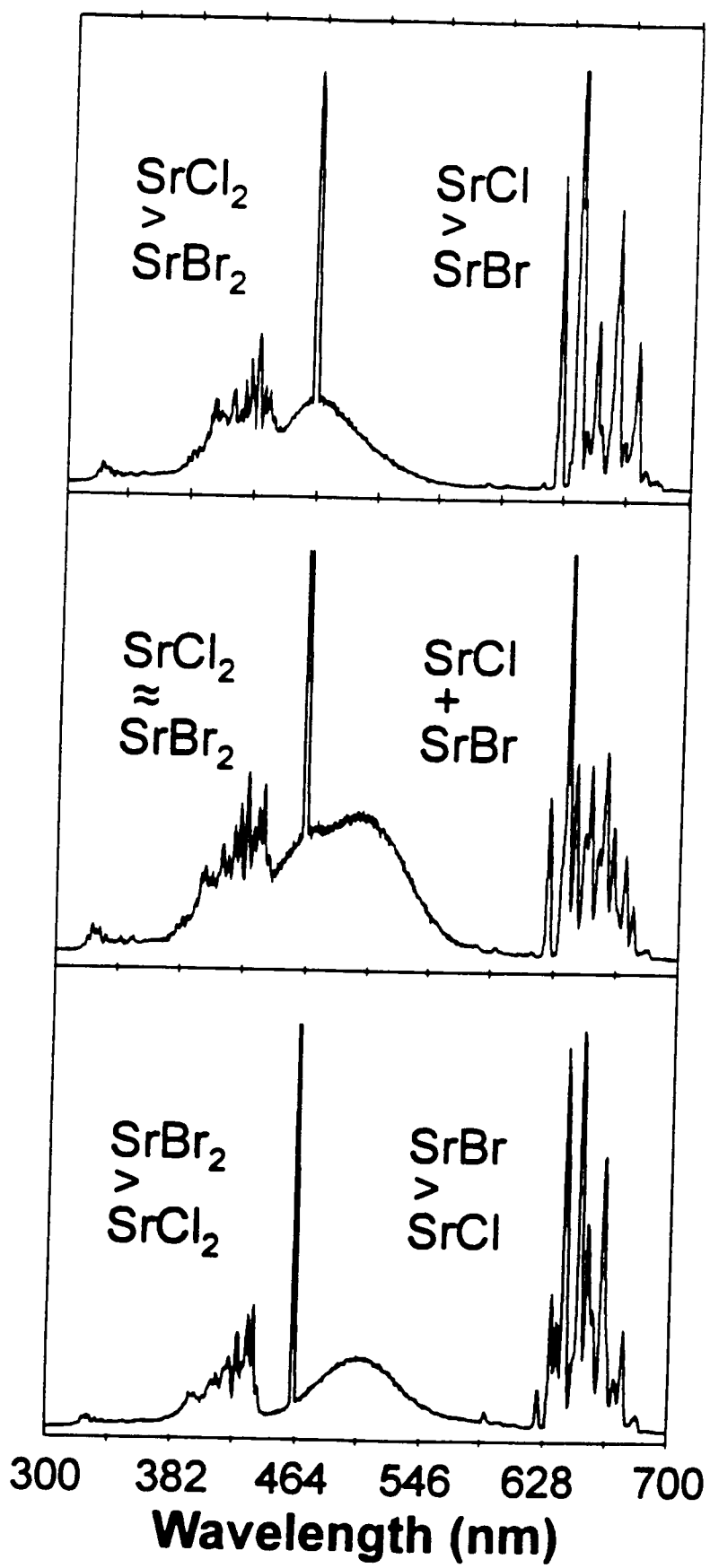


Figure 8(b)

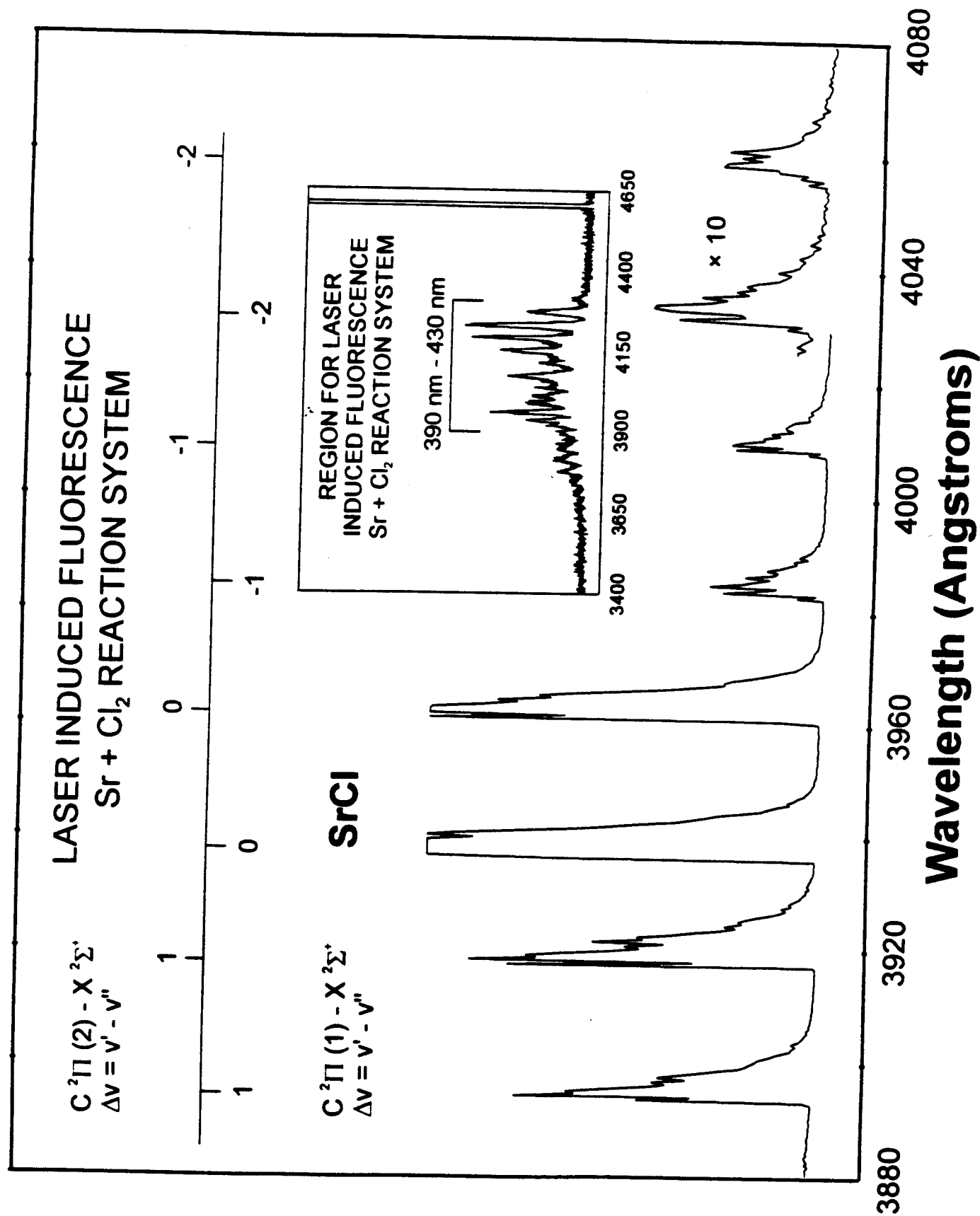
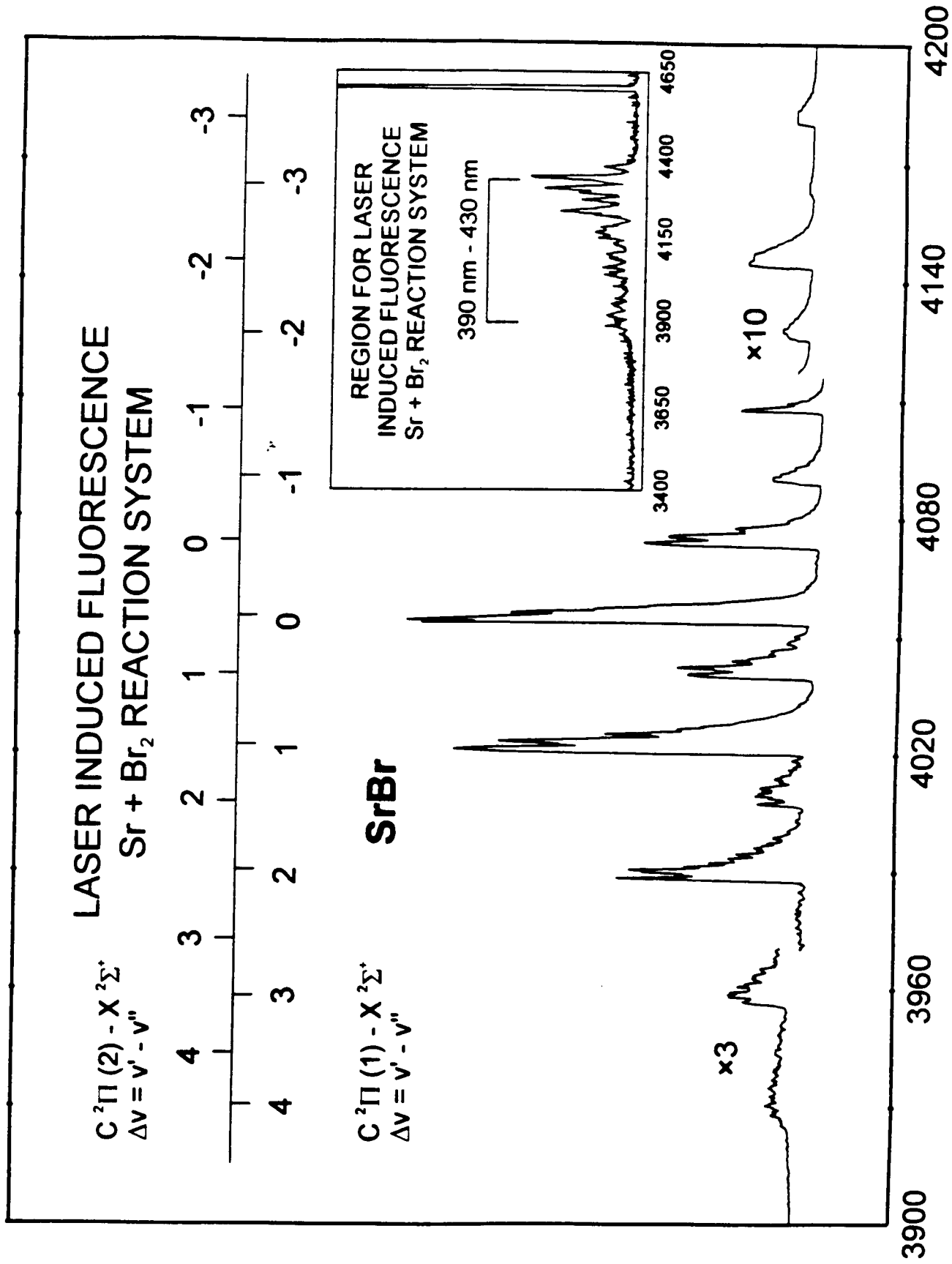


Figure 9



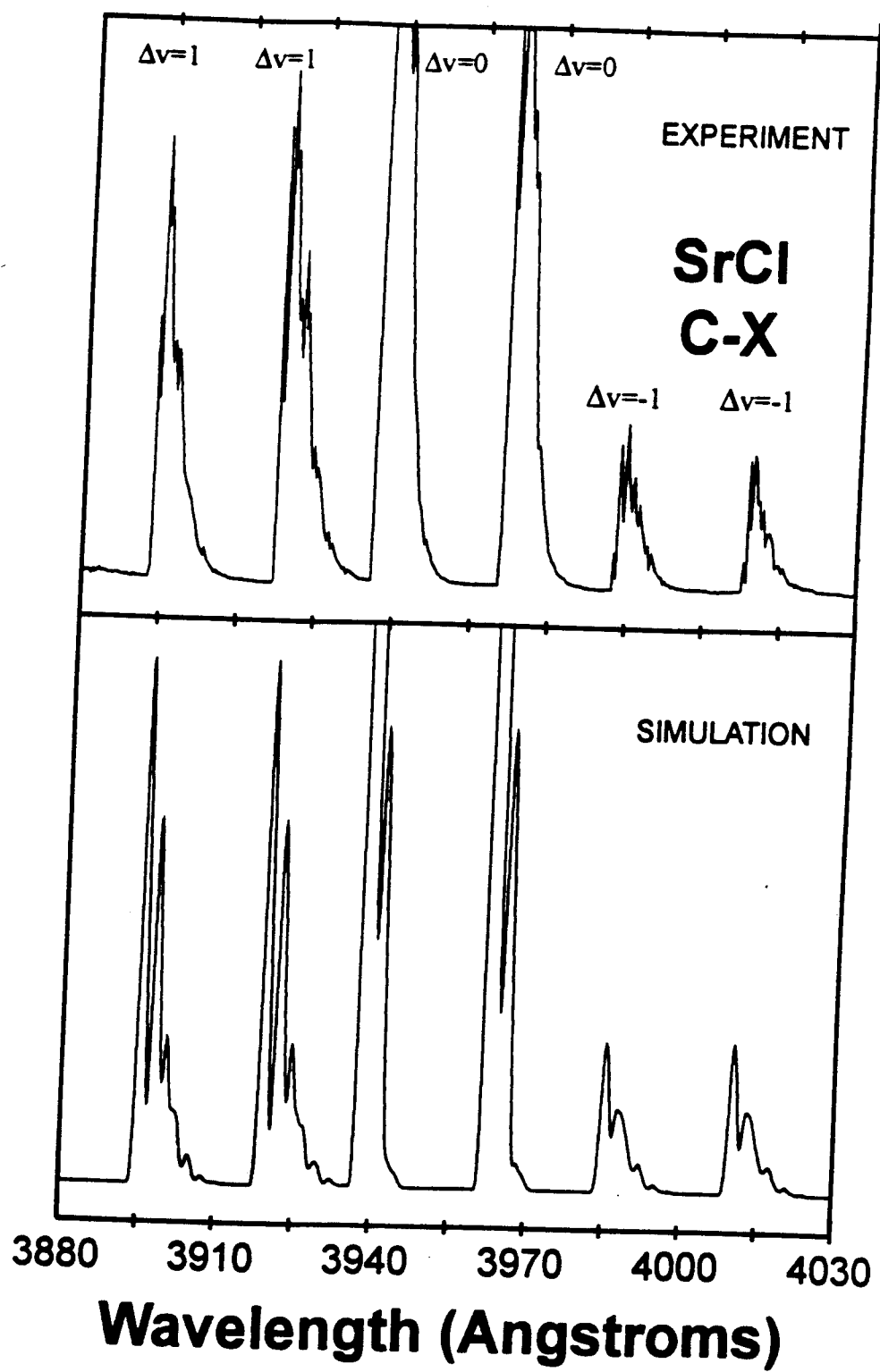


Figure 11

APPENDIX A

Estimation of Vibrational and Rotational Temperatures for the SrCl $X^2\Sigma^+$ Ground Electronic State (Figure 9)

Using molecular constants from Huber and Herzberg,¹ a suitable set of Franck-Condon factors was calculated, using standard techniques,² for the rotationless RKR potentials of the $C^2\Pi_{3/2} - X^2\Sigma_{1/2}$ and the $C^2\Pi_{1/2} - X^2\Sigma_{1/2}$ electronic transitions of the SrCl molecule. We considered only the first ten vibrational levels of each state. The rotational constants, B_e , were extrapolated for the upper and lower states ($B_e' \sim 0.098$, $B_e'' \sim 0.102$) from known data on the well characterized Group IIA monohalides. Vibrational ($v', v'' = 0-9$) and rotational distributions ($J', J'' = 0-19$) corresponding to temperatures of 450K were imposed on the ground and electronic state components of the doublet and all transitions to the ten lowest ground state vibrational levels were considered. The resulting simulated spectrum was also smoothed to simulate a finite bandwidth instrument response and facilitate comparison with the experimental results.

References

1. K. P. Huber and G. Herzberg, Constants of Diatomic Molecules, Van Nostrand, Princeton, 1979. See also reference 3.
2. See for example, R. N. Zare, J. Chem. Phys. 40 (1964) 1934.